Methods in Molecular Biology 1678

Springer Protocols

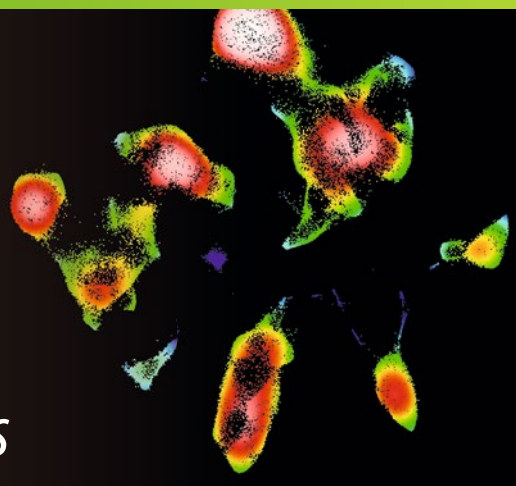

Teresa S. Hawley
Robert G. Hawley *Editors*

Flow Cytometry Protocols

Fourth Edition

EXTRAS ONLINE

Humana Press

METHODS IN MOLECULAR BIOLOGY

Series Editor
John M. Walker
School of Life and Medical Sciences
University of Hertfordshire
Hatfield, Hertfordshire, AL10 9AB, UK

For further volumes:
http://www.springer.com/series/7651

Flow Cytometry Protocols

Fourth Edition

Edited by

Teresa S. Hawley

Flow Cytometry Section, Research Technologies Branch, National Institute of Allergy and Infectious Diseases, National Institutes of Health, Bethesda, MD, USA

Robert G. Hawley

Department of Anatomy and Regenerative Biology, School of Medicine and Health Sciences, George Washington University, Washington, DC, USA

Humana Press

Editors
Teresa S. Hawley
Flow Cytometry Section
Research Technologies Branch
National Institute of Allergy
and Infectious Diseases
National Institutes of Health
Bethesda, MD, USA

Robert G. Hawley
Department of Anatomy and Regenerative Biology
School of Medicine and Health Sciences
George Washington University
Washington, DC, USA

ISSN 1064-3745 ISSN 1940-6029 (electronic)
Methods in Molecular Biology
ISBN 978-1-4939-7344-6 ISBN 978-1-4939-7346-0 (eBook)
DOI 10.1007/978-1-4939-7346-0

Library of Congress Control Number: 2017954575

Printed on acid-free paper

This Humana Press imprint is published by Springer Nature
The registered company is Springer Science+Business Media, LLC
The registered company address is: 233 Spring Street, New York, NY 10013, U.S.A.

Dedicated to our loving parents

Wing Han Chan, Sheung Tak Lam, Vietta Ruth Hawley, and George Robert Hawley

Preface

In the last edition, we noted that we were riding the crest of remarkable advances in innovative technologies. We did not anticipate that 6 years later we would still be in the midst of groundbreaking innovations that push the field of cytometry to new heights. Established as well as emerging methodologies are taking advantage of the availability of a plethora of cytometers, reagents, and analysis software. The development of new instrumentation has been greatly facilitated by compact and affordable solid-state lasers providing excitation wavelengths spanning the ultraviolet, violet, and near-infrared spectra. Accessibility to new fluorochromes covering the aforementioned spectra allows flexibility in panel design. It is now possible to perform measurements of increasing complexity in an attempt to answer questions proposed to unravel intricate communication networks in multicellular organisms. The ability of cytometry to simultaneously measure multiple aspects of cellular mechanisms down to the single cell/nucleus level holds promise for a profound understanding of homeostasis versus perturbation, the latter often leading to human diseases.

In the introductory chapter, Howard Shapiro, a pioneer in the field as well as a historian with an encyclopedic mind, recounts the landmark discoveries leading to the birth of flow cytometry. His insightful and philosophical account of the journey, both historical and personal, reveals how this enabling technology has made it possible to answer questions that no one even knew how to ask a few decades ago. In the concluding chapter, Howard reiterates the view that he expounded in the last edition on "The Cytometric Future: It Ain't Necessarily Flow." In it, he discusses alternative technologies that can also be used in the quest to improve human health.

The current edition aims to present established as well as emerging methodologies in cytometry. Each chapter explains the principles behind the methodology, presents step-by-step protocols, and highlights tips for successful execution. Quantitative fluorescence measurement is a well-established but underutilized technique that can benefit from a standardized procedure independent of instrument platforms and reagent differences. Hence, one chapter provides a detailed procedure for quantifying surface and intracellular protein biomarkers by calibrating the output of a multicolor flow cytometer in units of antibodies bound per cell. Other well-established methodologies include intracellular cytokine staining, apoptosis analysis, cell cycle analysis, tracking cell proliferation by dye dilution, and monitoring protein–protein interactions using Förster (fluorescence) resonance energy transfer (FRET). The utility of flow cytometry in basic science and clinical diagnosis is illustrated in the study of normal developmental stages of hematopoiesis and the detection of immune abnormality in peripheral blood cells of primary immunodeficiency patients, respectively. Additionally, two chapters provide the groundwork for designing and performing conventional flow cytometry. One of these chapters reviews current lasers available for flow cytometry, and provides guidance in matching laser wavelengths and characteristics to specific assays. The other chapter discusses strategies in panel design and optimization for simultaneous detection of more than 20 markers.

Some emerging methodologies, such as mass cytometry, vesicle flow cytometry, time-resolved flow cytometry, and real-time label-free deformability cytometry evolve around new or modified instrumentation. Mass cytometry, unlike conventional flow cytometry which uses a flow cytometer to analyze cells labeled with antibodies attached to fluorescent

tags, employs a mass spectrometer to analyze cells labeled with antibodies attached to heavy-metal isotopes. This novel technology enables simultaneous detection of more than 40 markers without significant signal spillover between detector channels. Vesicle flow cytometry, a challenge for conventional flow cytometers due to the small size of extracellular vesicles, can now be performed on flow cytometers equipped with high quantum efficiency avalanche photodiode array-based detectors. Extracellular vesicles are objects of interest as disease biomarkers and therapeutic targets. Fluorescence-triggered vesicle flow cytometry provides a general approach to the quantitative measurement of extracellular vesicle number, size, and surface marker expression. Time-resolved flow cytometry, an old concept dating back to 1992, is feasible with modifications to conventional flow cytometers. Time-resolved flow cytometry is broadly defined as the ability to measure the timing of fluorescence decay from excited fluorophores that pass through the flow cytometer. Because fluorescence lifetime is proportional to the quantum yield and independent of expression level, it measures the intrinsic brightness of a fluorophore. Fluorescence lifetime can also be used as a quantitative metric for FRET which is a nonradiative energy transfer event between a fluorescent donor and fluorescent acceptor molecule. Lifetime-based FRET measurements obviate the need to quantitate the acceptor and provide absolute FRET efficiencies based on the decrease of donor lifetime when it is quenched by energy transfer to the acceptor. Real-time label-free deformability cytometry leverages microfluidics to measure cell elasticity in engineered channel geometries of micrometer size. Appealing aspects of this technique include the possibility to characterize cells, and sensitively detect physiological and pathological changes in cell function without any external markers.

Other emerging methodologies involve new assaying techniques such as high-throughput cell surface profiling, single nuclei isolation and detection, and mRNA measurement. High-throughput cell surface profiling represents a rapid, simple, and cost-effective method to characterize the cell surfaceome. This monoclonal antibody-based screen is composed of 368 fluorochrome-conjugated cell surface protein-targeted antibodies arrayed into 96-well plates. Used in combination with a plate-based sample loading device for flow cytometers, it enables high-throughput analysis of an unprecedentedly large number of cell surface proteins in a single assay. The well-established method of direct isolation of nuclei from tissue and organ homogenates of plants has been extended to nuclei within homogenates produced from animal tissues and organs. The value of nuclear sorting for characterization of nuclear state has been recently enhanced by the development of molecular methods of RNA manipulation and amplification, allowing whole genome transcriptional analyses from single nuclei. Measurement of mRNA at the single cell level has been achieved recently with the branched DNA platform that is compatible with the detection of surface and intracellular antigens using monoclonal antibodies conjugated to fluorochromes, thus permitting simultaneous detection of mRNAs and proteins.

Data analysis is an integral and critical aspect of cytometry. High-dimensional data are generated as a result of combining a large number of measurements. Analysis of high-dimensional data incorporates dimensionality reduction algorithms and modeling. Unlike gating approaches, modeling lends itself to automation and accounts for measurement overlap among cellular populations. Designing models is greatly enhanced by a new technique called high-definition t-SNE mapping that can be used to visualize high-dimensional data as simple dot-plot displays. The chapter on data analysis introduces the concept behind building robust models and uses an example to illustrate how to build complex models that involve more than 35 correlated measurements.

We would like to thank John Walker for his invitation to participate once again in this exciting endeavor, his patience, and his expert editorial guidance. We are indebted to all of the contributors for their enthusiasm and generosity. Their willingness to impart their knowledge exemplifies the spirit of cooperation that is pervasive in the cytometry community.

Bethesda, MD, USA ***Teresa S. Hawley***
Washington, DC, USA ***Robert G. Hawley***

Contents

Contributors

Laurie E. Ailles • *Princess Margaret Cancer Centre, University Health Network, Toronto, ON, Canada*

C. Bruce Bagwell • *Verity Software House, Topsham, ME, USA*

David Bryder • *Division of Molecular Hematology, Institution for Laboratory Medicine, Lund University, Lund, Sweden*

Alexis N. Conway • *Roswell Park Cancer Institute, Buffalo, NY, USA*

Erika Duggan • *Scintillon Institute, San Diego, CA, USA*

Adolfas K. Gaigalas • *National Institute of Standards and Technology (NIST), Gaithersburg, MD, USA*

David W. Galbraith • *School of Plant Sciences, Bio5 Institute, University of Arizona, Tucson, AZ, USA*

Jochen Guck • *Biotechnology Center, Technische Universität Dresden, Dresden, Germany*

Maik Herbig • *Biotechnology Center, Technische Universität Dresden, Dresden, Germany*

Jessica P. Houston • *Department of Chemical & Materials Engineering, New Mexico State University, Las Cruces, NM, USA*

James W. Jacobberger • *Case Comprehensive Cancer Center, Case Western Reserve University, Cleveland, OH, USA*

Martin Kräter • *Universitätsklinikum Carl Gustav Carus, Technische Universität Dresden, Dresden, Germany*

Wenyan Li • *Department of Chemical & Materials Engineering, New Mexico State University, Las Cruces, NM, USA*

Dongxia Lin • *Fluidigm Corporation, South San Francisco, CA, USA*

Patricia Lovelace • *Human Immune Monitoring Center, Institute for Immunity, Transplantation, and Infection, Stanford University, Stanford, CA, USA*

Paul Müller • *Biotechnology Center, Technische Universität Dresden, Dresden, Germany*

Holden T. Maecker • *Human Immune Monitoring Center, Institute for Immunity, Transplantation, and Infection, Stanford University School of Medicine, Stanford, CA, USA*

Katherine M. McKinnon • *Vaccine Branch Flow Cytometry Facility, Center for Cancer Research, National Cancer Institute, National Institutes of Health, Bethesda, MD, USA*

Katharine A. Muirhead • *SciGro, Inc., Middleton, WI, USA*

Péter Nagy • *Department of Biophysics and Cell Biology, Faculty of Medicine, University of Debrecen, Debrecen, Hungary*

Kapil Nichani • *Department of Chemical & Materials Engineering, New Mexico State University, Las Cruces, NM, USA*

John P. Nolan • *Scintillon Institute, San Diego, CA, USA*

Maurice R.G. O'Gorman • *Department of Pathology and Pediatrics, Children's Hospital of Los Angeles and the Keck School of Medicine, University of Southern California, Los Angeles, CA, USA*

Oliver Otto • *Zentrum für Innovationskompetenz: Humorale Immunreaktionen bei Kardiovaskulären Erkrankungen, Universität Greifswald, Greifswald, Germany*

Joshua Paterson • *Princess Margaret Cancer Centre, University Health Network, Toronto, ON, Canada*

Katarzyna Plak • *Biotechnology Center, Technische Universität Dresden, Dresden, Germany*
Cornelis J.H. Pronk • *Division of Molecular Hematology, Institution for Laboratory Medicine, Lund University, Lund, Sweden; Department of Pediatric Oncology/ Hematology, Skane University Hospital, Lund, Sweden*
Partha Samadder • *School of Plant Sciences, Bio5 Institute, University of Arizona, Tucson, AZ, USA*
Jesse Sambrano • *Department of Chemical & Materials Engineering, New Mexico State University, Las Cruces, NM, USA*
Howard M. Shapiro • *One World Cytometry, Inc., West Newton, MA, USA*
Elwira Sliwinska • *Laboratory of Molecular Biology and Cytometry, Department of Plant Genetics, Physiology and Biotechnology, UTP University of Science and Technology, Bydgoszcz, Poland*
Kah Teong Soh • *Department of Flow and Image Cytometry, Roswell Park Cancer Institute, Buffalo, NY, USA*
R. Michael Sramkoski • *Case Comprehensive Cancer Center, Case Western Reserve University, Cleveland, OH, USA*
Tammy Stefan • *Case Comprehensive Cancer Center, Case Western Reserve University, Cleveland, OH, USA*
János Szöllősi • *Department of Biophysics and Cell Biology, MTA-DE Cell Biology and Signaling Research Group, Faculty of Medicine, University of Debrecen, Debrecen, Hungary*
Joseph D. Tario Jr. • *Department of Flow and Image Cytometry, Roswell Park Cancer Institute, Buffalo, NY, USA*
William G. Telford • *Flow Cytometry Core Facility, Experimental Transplantation and Immunology Branch, Center for Cancer Research, National Cancer Institute, National Institutes of Health, Bethesda, MD, USA*
László Ujlaky-Nagy • *Department of Biophysics and Cell Biology, MTA-DE Cell Biology and Signaling Research Group, Faculty of Medicine, University of Debrecen, Debrecen, Hungary*
Giacomo Vacca • *Kinetic River Corp., Mountain View, CA, USA*
György Vereb • *Department of Biophysics and Cell Biology, MTA-DE Cell Biology and Signaling Research Group, Faculty of Medicine, Faculty of Pharmacy, University of Debrecen, Debrecen, Hungary*
Paul K. Wallace • *Department of Flow and Image Cytometry, Roswell Park Cancer Institute, Buffalo, NY, USA*
Lili Wang • *National Institute of Standards and Technology (NIST), Gaithersburg, MD, USA*
James Wood • *Wake Forest University School of Medicine, Winston-Salem, NC, USA*
Philip G. Woost • *Case Comprehensive Cancer Center, Case Western Reserve University, Cleveland, OH, USA*
Zhihua Yang • *Department of Chemical & Materials Engineering, New Mexico State University, Las Cruces, NM, USA*

Chapter 1

Flow Cytometry: The Glass Is Half Full

Howard M. Shapiro

Abstract

Accompanied by a historical perspective of the field of cytometry, this introductory chapter provides a broad view of what flow cytometry can do; hence, the glass is half full.

Key words Micrographia, Cells, Blood cells, Dyes, Fluorescence, Microscopy, Hemacytometry, Flow cytometry, Electrostatic sorting, Coulter volume, Poisson statistics

1 Introduction

This book presents ample evidence that flow cytometry has provided the means for developing an armamentarium of reagents and measurements that make it possible to answer questions about cells that nobody even knew how to ask when the field got started. The technology now accounts for a multibillion-dollar market, with tens of thousands of instruments, most of which cost at least tens of thousands of U.S. dollars, now in use worldwide. Most of the annual expenditure is aimed, directly or indirectly, at improving the overall health of our species, which may require suppressing or eliminating cells from other species and rogue elements from our own. A recent PubMed search on "flow cytometry" returned 180,038 references, dating back to the 1960s; over 75,000 have been added since I wrote a chapter for the previous edition of this compendium in 2010.

There are almost certainly not tens of thousands of people who know how to make optimal use of the full range of capabilities of any state-of-the-art flow cytometer; books such as this one are designed to help the users keep up with the apparatus and the methodology, both of which make demands on the user. This chapter and those that follow, except for the last one, will provide a broad view of what flow can do. At the end of the book, I will focus on what flow cannot do, and on what can now be done using

Teresa S. Hawley and Robert G. Hawley (eds.), *Flow Cytometry Protocols*, Methods in Molecular Biology, vol. 1678, DOI 10.1007/978-1-4939-7346-0_1,

alternative methods, both elaborate and simple, in hopes of improving readers' perspectives.

I remember strolling through Glasgow in 2015 with Bob and Teresa Hawley and some other folks, during the CYTO meeting of the International Society for the Advancement of Cytometry (ISAC), an organization with which I would guess most readers of this piece are acquainted. The major lecture of an ISAC meeting is the Robert Hooke lecture, given that year by Carl June, who has been doing flow cytometry since 1986, and who has attracted worldwide attention in recent years by engineering T cells to fight cancer, a project in which flow cytometry has been and is expected to be critical. It was impressive to hear him speak and even more impressive to hear the discussion that followed, with several members of the audience who had also ventured into cancer immunotherapy comparing notes on their respective successful treatment methods.

The Hooke lecture was named because Robert Hooke had given cells their name in a book written before he had actually seen what we would today recognize as cells. Hooke's classic "Micrographia: or some Physiological Descriptions of Minute Bodies made by Magnifying Glasses with Observations and Inquiries thereupon," impressively illustrated by the author, was commissioned by the Royal Society of London, for which he was a curator of experiments, and appeared in January 1665. In it, Hooke, citing their similarity to cells in a honeycomb, called the spaces visible in thin longitudinal and transverse slices of cork "cells," with no inkling that they had been formerly occupied by living components of the tree.

Lenses (so named because they were lentil-shaped) had been used to start fires since ancient times (the "focus" is where the fire starts) and correct vision since around 1300, but it was not until about 1600 that Italian and Dutch spectacle makers combined them to bring faraway objects closer, thereby inventing the telescope, and to bring objects otherwise too small to see into view, inventing the microscope. Hooke conceived these devices as extending the sense of vision.

Although there is no evidence of his having provided a jacket blurb, Samuel Pepys, the famous diarist, noted then that he had sat up until 2 a.m. reading *Micrographia*, and described it as "the most ingenious book that ever I read in my life." An even better indication of the book's popularity is given in the writings of Jonathan Swift, born two years after *Micrographia* was published. In the 1726 novel Gulliver's Travels, Swift's surgeon protagonist, Gulliver, describes an encounter with giant Brobdingnagian beggars:

> There was a woman with a cancer in her breast, swelled to a monstrous size, full of holes, in two or three of which I could have easily crept, and covered my whole body. There was a fellow with a wen in his neck, larger than five wool-packs. . . But the most hateful sight of all, was the lice crawling on their

> clothes. I could see distinctly the limbs of these vermin with my naked eye, much better than those of a European louse through a microscope, and their snouts with which they rooted like swine.

Gulliver's last two sentences make it clear that Swift had some familiarity with Hooke's book; the drawings of the louse undoubtedly attracted more attention from the lay audience than did those of the cork slices.

Although I didn't get around to it until after I wrote my cytometry book [1], I've been through *Micrographia* at least a couple of times. When I have asked how many people in audiences listening to Hooke Lectures at ISAC meetings have read it, however, I haven't seen a lot of hands go up. That may explain why there are so many places on the Internet in which it is erroneously claimed the analogy was made to cells in a monastery or prison. This cytometric urban legend, like the notion that forward scatter measures cell size, is harder to kill than Dracula. *Micrographia* is fascinating for many reasons, written in understandable English, and available free online; I modestly propose you read it if you haven't.

Hooke did not actually see living cells until years after "Micrographia" was published, when the Royal Society asked him to check up on reports from a self-taught Dutch fabric merchant, Antoni van Leeuwenhoek, who used simple microscopes of his own design that provided much higher magnification than was available from the compound microscopes then used by Hooke and others. The property van Leeuwenhoek used to distinguish "animate" particles, now known as cells, from "inanimate" ones was motility, which kept him obsessively interested in bacteria, protozoa, sperm, and other "animalcules" and largely indifferent to yeast and the considerable contributions it had made to humanity over the millennia.

Many early microscopists anticipated that improvements in optics would quickly enable them to visualize atoms; they also tended to attribute morphological and biological characteristics of humans and other vertebrates to microorganisms, in which Van Leeuwenhoek notably estimated the sizes of livers, kidneys, and other internal organs he expected would eventually be discernible. The expectation that the parts would scale as did the wholes was incorrect. A real Gulliver might have known what a microscope was; he would not have known what a cell was. What we now call cells were known by many other names until the mid-1800s, by which time improvements in microscopy including substage condensers and achromats and other lenses that reduced aberrations and increased resolution had made it easier to distinguish biologic structures from artifacts. Both Matthias Schleiden and Theodor Schwann, prime movers of but hardly sole contributors to what has been known since that time as the cell theory [1], used and favored the term. Whereas Hooke had used it to describe an empty

space, it now referred to the membrane-bounded "elementary particle" of biology.

Swift's 1726 narrative speaks of a breast cancer and a wen (sebaceous cyst) at a time when no one had yet conceived of them as representative of two types of abnormal growth, or that an infected and inflamed wen also exemplified bacterial growth and a proliferative response by the patient's immune cells. By the late 1800s, both the metabolic versatility and pathogenic capability of microorganisms had been revealed by Louis Pasteur, Robert Koch, and others, The cell theory had become accepted, and Rudolf Virchow's famous quote, "Omnis cellula e cellula," embodied the efforts of many pathologists to understand disease at the cellular level.

Human blood cells had come to microscopists' attention; they were relatively easy to procure, and could provide some information about patients' overall state of health. Although anemias and leukemias had been described by this time, their causes were unclear; there were no known treatments for either, but their diagnosis and prognosis could be indicated by changes in the numbers of morphologically different cell types in the blood over time. The term "cytometer," coined around 1880, described a device in which cells within a defined volume of specimen could be counted. "Cytometry" described the process. The cells most often came from blood, giving us the "hemacytometer" and "hemacytometry." "Flow" and "cytometry" would not be combined until the 1970s; there could be no instrumental alternatives to microscopy until the 1950s.

A fascinating account of the development of cell biology from medieval times until the twentieth century is given by the late Sir Henry Harris in *The Birth of the Cell* [2]. I have written at length on the history, technology, and philosophy of cytometry in my book [1] and, more recently, in a chapter in the previous edition of this compendium [3], a review/overview [4], and two additional book chapters [5, 6]. A detailed retrospective view of the origins of analytical flow cytometry, among other things, was also presented by the late Leonard Ornstein [7].

Because light scattering and absorption by most cells were insufficient to permit visual discrimination of internal details, synthetic dyes began to be used by the 1860s to stain specimens, with Paul Ehrlich providing much leadership. As a medical student in the 1870s, he recognized that different colored organic dyes with different chemical affinities would be bound to different degrees to different parts of different cells. This provided a basis for identifying cells within mixed populations; Ehrlich's first practical success was in classifying the different types of white blood cells using dye samples provided by manufacturers. By 1880, he had experimented with several stains containing mixtures of acidic and basic dyes, the

former tending to stain cytoplasm and the latter to stain nuclei. He had also used the blue basic dye methylene blue to stain bacteria.

In 1882, Ehrlich joined forces with Koch, and developed a stain that identified *Mycobacterium tuberculosis* (Mtb), newly discovered by Koch, by its ability ("acid-fastness") to retain stains after being washed in strongly acidic alcohol solutions. Slight modifications by others yielded the Ziehl-Neelsen (ZN) stain, which has remained the standard for detecting Mtb by transmitted light microscopy since 1883, with over 50 million slides analyzed annually. Ehrlich's work also inspired Christian Gram's initial work on staining bacteria.

Ironically, Europe's burgeoning dye industry had had its beginnings in the 1850s; a British chemistry student's failed attempt to synthesize quinine, which could be used to treat malaria and was much in demand, serendipitously yielded the dye mauve, made fashionable by Queen Victoria. Quinine itself had been isolated in 1820 from cinchona bark; it had been known as an antimalarial (and one of the only effective drugs against any disease) since the 1600s.

In the 1630s, after European invaders and their African slaves brought malaria to the Americas, Jesuits brought cinchona, a native Peruvian folk remedy for chills back to Rome, based on the unscientific but correct suspicion that it might cure malaria, a disease known since ancient times and common enough in Rome to have killed several popes. "Jesuit Powder" became an effective, though scarce and expensive, remedy for the disease, which until the 1950s was a problem in Northern as well as Southern regions of the world. No similarly effective treatment for any other infectious disease appeared before 1890.

The discovery of malaria parasites by Alphonse Laveran in 1880 motivated an intensive search for dyes which facilitated identification of these organisms in the blood of infected patients, who could then be treated with quinine. Laveran, a French military physician in Algeria, had examined the unstained blood of a malaria patient and found motile particles containing a blackish-brown pigment (now called hemozoin) known to be associated with the disease, but his findings would not be widely accepted until the pathogen's morphology was better characterized by staining. It took over 20 years to come up with "the new black" for parasites. Gustav Giemsa's stain, developed in 1904 and containing the red acid dye eosin, methylene blue, and the blue basic dye azure B, quickly became and has remained the "gold standard" for blood smear microscopy.

Noting in 1891 that methylene blue by itself stained malaria parasites, Ehrlich had procured a supply from a dye company and successfully treated two malaria patients with it, anticipating his later success in curing syphilis with two of the over 900 compounds he tested against that disease. Ehrlich coined the term chemotherapy and his demonstrations of it prompted many dye companies to

expand into pharmacologic research. The company from which he obtained methylene blue is still in business, and is now known as Hoechst.

The year 1891 also saw the emergence of diphtheria antitoxin, the first successful immunotherapy, developed by Emil Behring (von Behring after he won the first Nobel Prize in medicine, in 1901), a longtime colleague of Ehrlich. Immunoprophylaxis had been around longer. Variolation, which intentionally infected its subject with what was hoped would be a mild case of smallpox in hopes of preventing infection with the virulent natural form, had been known for centuries but often proved fatal. Beginning around 1800, it was replaced by vaccination, introduced by Edward Jenner, who had noted that milkmaids who had contracted cowpox, which rarely caused serious illness, were thereafter immune to smallpox. Pasteur decided to honor Jenner by calling the immunoprophylaxes for anthrax and rabies he himself later developed "vaccines." The list of vaccine targets continues to increase.

It was not until the 1890s that it was accepted that eukaryotic cells gave rise to new cells only by mitotic division, and the role of the chromosomes (the name of which provides the clue that they were not readily visible without staining) in heredity was not elucidated until the next century. By 1900, the chemistry of proteins was beginning to be understood, but the two types of nucleic acid then recently found to comprise "nuclein" had not yet been named and would not be called DNA and RNA for decades. Although photography permitted more objective recording of microscope images than did drawing, the enhanced visual sense given to observers only allowed them to describe the sizes, shapes, colors, and textures of cells and their components, and motility and growth in culture offered the only indications of viability. Most microscopists still relied on sunlight as an illumination source; electric light and bright mantle lamps fueled by oil or gas only arrived on the scene late in the nineteenth century. Detection, characterization, and counting of cells were dependent on fallible human observers who in almost all cases had no objective means to confirm their findings and no alternative to manual data input and analysis.

Advanced darkfield microscopy techniques requiring only sunlight illumination had, by the early 1900s, permitted visual observation of light scattered by particles below the resolution limit; "ultramicroscopes" documented the Brownian motion of large colloid molecules and confirmed Einstein's predictions. Fluorescence microscopy, introduced around 1915, allowed observation of viruses stained with fluorescent dyes decades before the physicochemical bases of the phenomenon were clarified. By the 1930s, the development of photoelectric sensors and electronics allowed spectrophotometers and microspectrophotometers to be built. There were already cytometric problems for them to solve.

What we now know as the "rare event" problem arose almost as soon as it became necessary to examine sputum slides looking for TB and blood slides looking for malaria. In both diseases, it is likely that a slide taken from a patient with active disease will contain only a few pathogens. Clinicians needed to know how much of a sample needed to be analyzed to detect these. In 1907, William Sealy Gossett, writing under the pseudonym "Student," had published a paper on the error of counting cells in a hemacytometer. The cells of interest to him were yeast; the pseudonym was necessary because his employers at the Guinness brewery feared their competitors might discover the utility of statistics in brewing.

The statistical distribution involved had been discovered by Poisson a century earlier and is now known to be useful in determining sample sizes needed for determining a selected level of precision of counts of just about anything. Gossett's methodology was adopted by Ronald Ross in 1910 to determine how much blood needed to be analyzed to get accurate estimates of the number of malaria parasites contained in the sample, which led to his introduction of the now-standard "thick smear." Poisson statistics are now widely used in cytometry not only for cell counting, but also in the context of photon counting, which determines the precision of fluorescence measurements.

By the 1930s, when at least some types of anemia had become treatable, Maxwell Wintrobe defined "red cell indices," obtained by dividing bulk measurements of cell volume and blood hemoglobin by cell counts. Although these could, in principle, be used to distinguish normal and anemic blood and define types of anemia, visual counting of thousands red cells to obtain the required precision was impractical. It was suggested in a 1934 article in *Science* that a photocell could be used to detect and count cells in suspension as they passed through an illuminated region of a capillary tube under a microscope, but the text suggested that the author's initial experiments had not succeeded.

The first working flow cytometer was built at the US Army's Camp Detrick during World War II, and designed to detect anthrax spores in aerosols using dark-field illumination to measure light scattering. Although it could capture signals from almost 60% of bacteria resembling anthrax, it could not distinguish one species of bacterium from another or a bacterium from an organic or inorganic particle of approximately the same size. It could hardly be expected to do the job for which it was designed on a dusty battlefield.

In 1951, an apparatus optically similar to the anthrax machine was demonstrated to be able to detect red blood cells in saline suspension, and eventually produced in England as a hematology counter. It could distinguish between the scatter signals from red cells and those from platelets; white cells were counted as red cells, which in normal blood and most abnormal blood would not

significantly affect the results. Competitive optical blood cell counters were soon developed by several companies.

Wallace Coulter, an American engineer who had attempted to produce a similar instrument, instead found it easier to build a counter that detected the increase in electrical impedance produced as blood cells in saline flowed through a small orifice. It was soon established that impedance measurements accurately reflected particle volume. Both optical and Coulter counters were on the market by 1960; the latter could use small orifices to detect platelets, and white cell counts could be obtained from both types of counters after red cells were chemically lysed. A German group showed in 1964 that staining whole blood with acridine orange allowed white cells to be discriminated from red cells by a modified scatter-based counter using their nuclear or cytoplasmic fluorescence signals. This paper apparently represents the first instance of both fluorescence measurement and multiparameter analysis in flow cytometry.

I had not run across any of the early work described above, by 1964, but I had had some introduction to cytometry. I was a "science brat"; my father was an M.D. interested in cancer treatment, and my mother, who had first studied microbiology, ran an electron microscope, and was working on her Ph.D. thesis in structural biology. Dinner table talk was frequently about science. I would hang out in her lab after school and help her stain slides, at least some of which involved stains for DNA, probably to distinguish developmental stages of the trematode sperm she studied.

I did my first cytometry experiment in 1957, as a high school senior. It involved counting mitoses in sections of rapidly proliferating tissues fixed at varying intervals after animals were sacrificed, and showed that mitosis could be completed in cells after death. It would be unacceptable and probably illegal to do the same experiment under the same circumstances today. In college, I studied biochemistry, taking a lab course in which we duplicated the experiments of Jacob and Monod et al. as they were published. I also learned about computers, and built a mathematical model of metabolic fluxes in *E. coli*. I went on to medical school at NYU, where a mainframe computer had been fitted with an analog-to-digital converter to process EKGs recorded on tape; that gave me both computer time for my model-building and reasonable compensation for writing EKG analysis software.

By 1965, I was a surgical intern at Bellevue Hospital in New York, where the researchers had Coulter Counters and routine clinical blood cell counting was done by third-year medical students using microscopes and the classical Giemsa and Wright's stains that had been around since the early 1900s. I had learned to do differential white blood counts from my mother when I was around 12 years old, and initially was sure that hematologists and pathologists must learn some secret handshake that allowed them to identify unusual white cells correctly.

As an intern, I should have had no time to do so, but I still managed to sneak a glimpse at *Science* magazine every week when it came out. I realized that the October report by Louis Kamentsky et al at IBM, who incorporated Caspersson's UV nucleic acid measurements and a scatter-based size measurement into the first analytical flow cytometer, described something about which I had heard rumors the year before. In November, *Science* published Mack Fulwyler's paper on electrostatic sorting of cells based on Coulter volume, which I also found of great interest.

There were not a lot of new MDs with computer experience in those days; mine helped me get a job at NIH. I would be joining the National Cancer Institute (NCI) in July 1967 and working on building an automated microscope to study DNA synthesis in leukemic cells in children using thymidine autoradiography. NCI sent me to a meeting in early June at which Kamentsky described the current version of his instrument, which was measuring four parameters, including fluorescence, had acquired fluidic sorting capability, and was about to be equipped with a minicomputer. Even before my colleagues at NIH and the National Bureau of Standards and I started to build what was for a time the fanciest automated microscope around, I was solidly sold on flow cytometry.

By the time I left NIH in 1971, having both helped build and used the minicomputer-controlled microscope and gotten some experience looking at leukemic blood with conventional stains, I knew there were no magic handshakes. I also realized that doing most serious cell-based diagnostic tasks were likely to require measurement of more parameters than could be done by the flow cytometers then in existence. Since there did not seem to be an available opportunity for me to make that happen, I had to shelve my empty glass for a couple of years.

By 1976, I had access to a completely computer-controlled, three-laser, eight-parameter flow cytometer, which did not have a sorter because it had been designed for clinical blood cell counting and which would never be used for that because we found, using it, that a single-laser, four-parameter instrument could do the job, be more reliable, and cost much less. I, at least, thought it would be great for research, and be a much better front end for a cell sorter than was available for the two such instruments then available. At the 1976 Engineering Foundation meeting on Automatic Cytology, in Pensacola, Florida, manufacturers of sorters assured me that nobody would ever need all those beams and all those parameters, and would not pick up the project, so we scrounged some grants and stumbled on. Also at that meeting, it was decided that what the participants were doing would thereafter be known as "flow cytometry." Happy Hour had begun.

We can now measure dozens of parameters with huge libraries of specific reagents and generate terabytes of data with a dozen or

more lasers, most of which plug into the wall and do not cost more than a few thousand dollars. Detectors have gotten better, smaller, and, in some cases cheaper.

But there are problems. Flow has made it too easy to continue working at the single cell level, or at the level of aggregates of too few cells to relate meaningfully to what happens in extremely multicellular organisms like us. Human sperm can be analyzed in flow cytometers, and sorted according to their sex chromosome content to minimize the likelihood that an embryo produced by in vitro fertilization (IVF) will be affected by a sex-linked disease. Human oocytes are a bit large for standard flow cytometers, and the 5- or 6-day old blastocysts implanted in IVF, which have already differentiated to form about 40 trophoectoderm cells and 40 inner cell mass cells, have diameters of over 200 μm, allowing the transfer process to be monitored by nothing fancier than a light microscope. Most cytometry can be done without flow, but it is not as easy as it should be to get started doing it that way.

So some people's glasses are full, and others' are empty. And, on average. . . stay tuned.

References

1. Shapiro HM (2003) Practical flow cytometry, 4th edn. Wiley-Liss, Hoboken, NJ
2. Harris H (1999) The birth of the cell. Yale University Press, New Haven, CT
3. Shapiro HM (2011) The cytometric future: it ain't necessarily flow! Methods Mol Biol 699:471–482. doi:10.1007/978-1-61737-950-5_23
4. Shapiro HM, Apte SH, Chojnowski GM, Hanscheid T, Rebelo M, Grimberg BT (2013) Cytometry in malaria—a practical replacement for microscopy? Curr Protoc Cytom Chapter 11:Unit 11.20. doi:10.1002/0471142956.cy1120s65
5. Shapiro HM (2015) Microbial cytometry: what it was, is, and may be. In: Wilkinson MG (ed) Flow cytometry in microbiology: technology and applications. Caister Academic Press, Norfolk, pp 1–16
6. Shapiro HM (2017) Cytometry. In: Rifai N, Horvath AR, Wittwer CT (eds) Tietz textbook of clinical chemistry and molecular diagnostics, 6th edn. Elsevier, Amsterdam
7. Ornstein L (1987) Tenuous but contingent connections. Electrophoresis 8:3–13

Chapter 2

High-Dimensional Modeling for Cytometry: Building Rock Solid Models Using GemStone™ and Verity Cen-se'™ High-Definition t-SNE Mapping

C. Bruce Bagwell

Abstract

This chapter outlines how to approach the complex tasks associated with designing models for high-dimensional cytometry data. Unlike gating approaches, modeling lends itself to automation and accounts for measurement overlap among cellular populations. Designing these models is now easier because of a new technique called high-definition t-SNE mapping. Nontrivial examples are provided that serve as a guide to create models that are consistent with data.

Key words Probability state model, t-SNE, Cen-se' mapping, High-dimensional modeling

1 Introduction

I can think of no analysis activity for cytometry that is as difficult yet fulfilling as high-dimensional modeling. It is very satisfying watching a well-designed model automatically analyzing hundreds of list mode files. In the past few years a number of models for various cytometry applications have been published [1–4], but many are proprietary and will never be published. In developing these models, a long list of practical steps, tricks, and tips has accumulated and it is the purpose of this chapter to organize and describe these hard-learned concepts in order that you do not need to waste time relearning them.

A new analysis tool called "t-SNE" was introduced to cytometry a few years ago. The t-SNE dimensionality reduction algorithm [5–7] is arguably the most exciting addition to the cytometry analysis arsenal in the last 5–10 years. A new high-resolution variant of the SNE method called Verity Cen-se'™ will be used to visualize high-dimensional data as simple dot-plot displays. This visualization process helps in the design of models that reflect the real biology of one or more populations in a sample.

Teresa S. Hawley and Robert G. Hawley (eds.), *Flow Cytometry Protocols*, Methods in Molecular Biology, vol. 1678, DOI 10.1007/978-1-4939-7346-0_2, © Springer Science+Business Media LLC 2018

This chapter will describe an approach for building rock solid models that can automate very complex cytometry applications. The approach involves the building and refining of probability state models [8] by leveraging published results and critically examining high-definition Cen-se' data patterns. Analyzing PBMC samples derived from the Helios^{tm} mass cytometer will serve as an example of how to approach building complex models that involve 35+ correlated measurements.

2 Modeling vs. Gating

2.1 Gating

Gating is a data partitioning methodology that separates one population from another via one or more measurement boundaries. Typically, gating involves drawing closed polygons around clusters of dots on two dimensional surfaces commonly called "dot-plots." Gating can also be performed with defined ranges over one-dimensional frequency distributions. Figure 1a shows two gating regions for one measurement, M1, which happens to have a bimodal distribution containing two populations labeled as "PopA" and "PopB." The ranges are placed to enumerate as much of their encompassed populations as possible without involving too many overlapping events. Because the underlying populations are not defined mathematically, the decisions for placing gates are often subjective and therefore difficult to reproduce and automate. Gates usually result in false positive and negative populations that can become confounding as gated event states cascade into other gates.

2.2 Frequency-Based and Probability-Based Modeling

Models on the other hand usually define the theoretical shape of one or more distributions and then "fit" the distributions to the data by optimizing a set of model parameters. As its name implies, a model attempts to describe one or more biological processes. Figure 1b shows a modeling approach to enumerating the "PopA" and "PopB" populations. A key attribute of a modeling approach is that it accounts for overlap between populations. Another key attribute of many models is that once it has fit data, it has the capability of synthesizing similar data. We will take advantage of that attribute in Subheading 5 when we discuss the synergistic relationships between modeling and Cen-se' mapping.

There are two fundamentally different approaches to modeling cytometry data. One approach represents data by fitting frequency on the *y*-axis and the measurement intensity on the *x*-axis as shown in panel b. Most early modeling theory and software packages were frequency-based [9] as depicted in panel b. The "best" parameters for the model are found by either minimizing or maximizing objective functions.

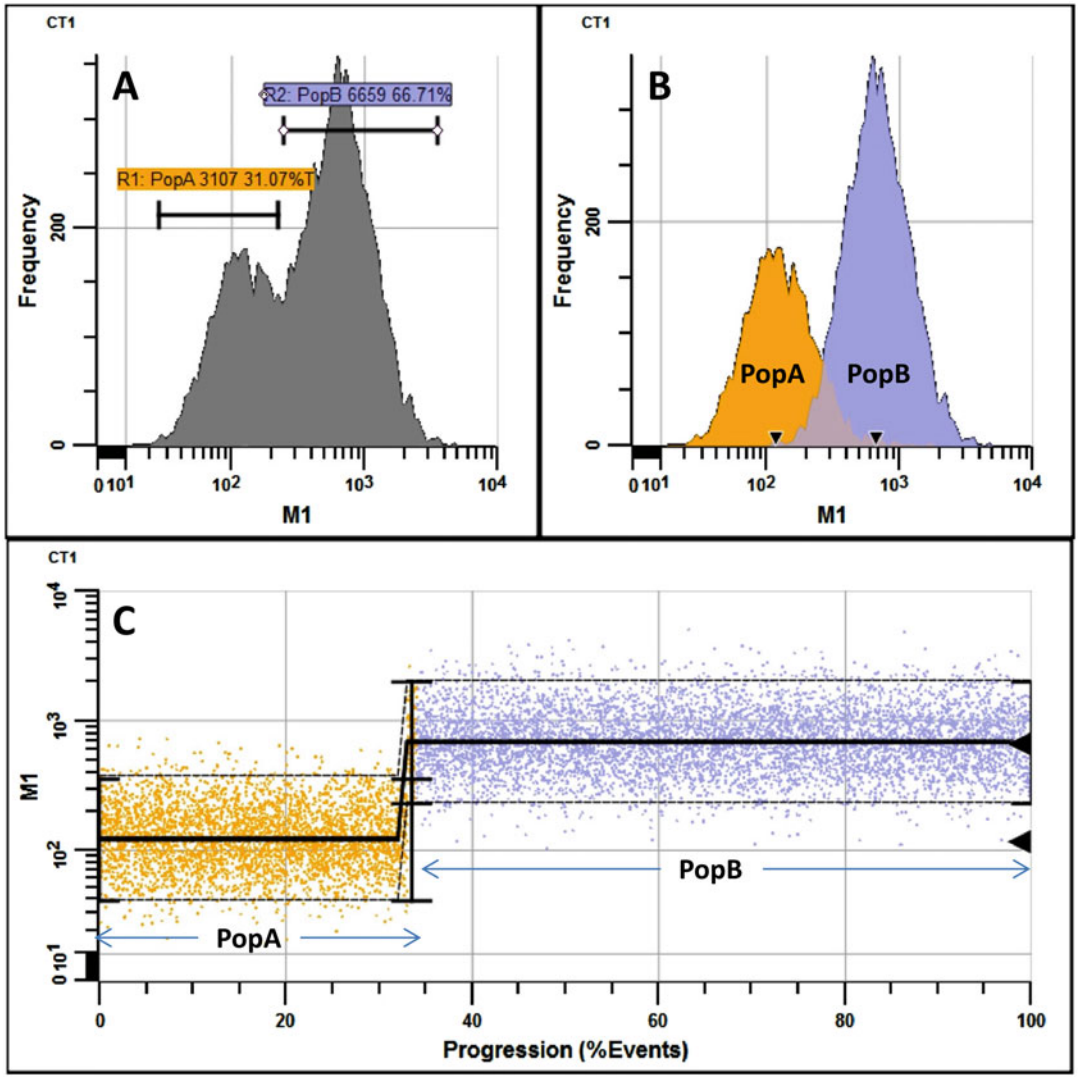

Fig. 1 Gating vs. modeling. (**a**) It shows two gating regions encompassing populations "PopA" and "PopB" for one measurement, *M1*. Ranges are placed to enumerate as much of their encompassed populations as possible without involving too many overlapping events. (**b**) It shows the two populations accounting for overlap. (**c**) It shows the same data in a probability state format where the *x*-axis is cumulative percent or "Progression" and the *y*-axis is *M1* intensity

Another type of data representation is shown in panel c. In this case, measurement intensity is the *y*-axis and cumulative percent is the *x*-axis. This type of configuration is used in probability state modeling (PSM, [4, 8, 10–12]). There are two major advantages for this type of data representation. The first is that process directions can be assigned to PSM models. For example, "PopA" in panel C can be interpreted as marking the beginning of a cellular progression and "PopB," the ending, since "PopA" appears first

and "PopB" appears last. The second advantage is that if cellular processes are defined by many different measurements, they all can be overlaid since they have the same cumulative percent *x*-axis (*see* Subheading 5.1). Since cumulative percent has many of the same characteristics as time, such as being nondecreasing, it can act as a surrogate for time and therefore represent cellular kinetic progressions defined by many measurements.

Whether models are frequency-based or probability-based, they can account for overlap between populations, which is a fundamental improvement over gating. Because models use nonsubjective objective functions to optimize their "parameters," they also tend to be able to automate complex cytometric analyses.

3 The Anatomy of Probability State Models

3.1 Cell Types

A model cell type roughly corresponds to a particular population of cells. Bone marrow $CD19^+$ B cells and $CD3^+CD4^+$ T cells are examples of different cell types. When defining cell types, one or more measurements are chosen to select for specific events. These selection measurements normally have relatively constant levels of measurement intensities. The selection can be based on positive or negative measurement intensity levels. T cells, for example, are positively selected with $CD3^+$, but negatively selected with $CD33^-$. Model cell types not only define selection measurements but also the order in which they are applied to the data. Cell types usually have unique signatures in high-dimensional space and appear well separated in high-dimensional Cen-se' maps (Subheading 5.2 and refs. 5–9).

Probability state modeling works out the mixture of cell types in a sample using probabilistic algorithms [8]. Some cell types such as B cells, T cells, NK cells, and Monocytes modulate key gene products as they differentiate [13, 14]. The appearance and disappearance of these gene products can stratify events into specific stages. For example as B cells develop in the bone marrow, proteins such as CD34, CD10, CD20, CD38, and CD45 modulate as they differentiate and form at least four stages [12]. A GemStone™ (Verity Software House, Topsham, ME) model can contain any number of cell types but typically the number of cell types ranges between 2 and 10.

3.2 Expression Profiles

An expression profile describes the general type of modulation that a measurement has in a cell type. It is important not to use cytometry slang that refers to measurements as parameters since the word, "parameter," has a very specific meaning in the context of modeling and statistics. Expression profiles are composed of a set of control definition points (CDPs) that describe the important

modulations of specific measurements. The CDPs also define the degree of heterogeneity in data as a function of a progression.

3.2.1 Constant

Constant expression profiles are typically used for cell type selections. The modeling notation used for these expression profiles mimics standard gating notations. For example, $CD3^{-}$, CD3d, $CD3^{+}$, and $CD3^{++}$ indicate the relative intensity of CD3 measurements (negative, dim, positive, bright). CDPs can be adjusted to combine different intensities. For example $CD3^{-}$, *d* indicates that the expression profile is designed to encompass both the negative and dim intensities. Inverse expression profiles are also available to the modeler for these types of expression profiles. For example, since live/dead measurements, L/D, usually have discrete peaks for the live cells, but complex set of peaks for dead cells; dead cells can be selected by using the inverse of the low L/D measurement, Inv (L/D^{-}).

3.2.2 Variable

Variable expression profiles describe how measurements change with progressions. In many cases, a measurement of a gene product can downregulate or upregulate, which is represented with step-down or step-up expression profiles. In other cases, expression profiles may be more complex and have three or more levels of expression. The job of a modeler is to choose the simplest set of expression profiles that are consistent with both the data and the literature. The notation used in this chapter to denote this type of modulation is to separate the intensities with the symbol, ">." For example, $CD10^{++} > CD10^{+} > CD10^{-}$ indicates that the CD10 expression profile has three decreasing intensity levels. The first level is bright for CD10, the second level decreases to a positive state, and the third level is negative or very low intensity. In some cases, progressions can branch. The notation for a branch will look similar to the following: $CD57^{-}$ > Br(+,−). This notation indicates that CD57 is initially negative and then some fraction of events upregulate to a positive state while others will remain negative.

3.2.3 Stages/Zones

If there are multiple measurements that have variable expression during a progression, many times it is advantageous to use the points of modulation to describe boundaries and labels for specific stages of progressions. For example, staging B cells in bone marrow [12] may be represented as, (B1) $CD34^{+}CD45^{+}CD10^{+} >$ (B2) $CD34^{-}CD45^{+}CD10^{+} >$ (B3)$CD34^{-}CD45^{++}CD10^{+} >$ (B4) $CD34^{-}CD45^{++}CD10^{-}$. The identification of these stages can be error prone with conventional dot-plot displays since phenotypic transitions are many times difficult to visualize. Modeling and HD Cen-se' maps have made it much easier to visualize these stages and often show that some published stages do not exist and other stages are present but have yet to be recognized as valid stages. When faced with a situation where the data is not consistent with the

literature, it is incumbent on the modeler to try to come up with a reasonable compromise where model stages are enumerated by the model as closely as possible to published stages.

3.2.4 Line-Spreads

An important aspect of expression profiles is the degree of heterogeneity in the data at each point along the expression profile. This heterogeneity is quantified as line-spreads or standard deviations (sds) associated with specific CDPs. Graphically, line-spreads are shown as 95% confidence limits (*see* Fig. 1c), which represent + and – 1.96 sds from measurement means. Line-spreads represent both biologic heterogeneity and measurement uncertainty.

3.2.5 Matching/Un-matching Expression Profiles

Each expression profile can be in either an "un-matched" or "matched" state. If it is un-matched, then the expression profile is not involved in the classification process. When building models, it is common to turn on and off the match status option to better understand how to approach modeling tasks.

3.3 TriCOMs

In some cases, it is important to perform a combinatory analysis of subpopulations within one or more stages within a specific cell type. Expression profiles naturally divide measurements into three partitions: 0: within some defined confidence limit (CL, e.g., 95%), 1: lower than CL, and 2: greater than CL. By applying these three states to each involved expression profile, specific combinations can form identifying trinary numbers. For example, the trinary number, 021, for CXCR3, CXCR5, and CCR6, represents events that are within the defined CL for CXCR3, greater than the CL for CXCR5, and less than the CL for CCR6. Expression profiles used in TriCOMs are set to not participate in the classification process. Cell types can contain any number of TriCOMs.

3.4 Model Documents

All cell types, reports, and database entries are stored as a model document. There are two important types of model documents. A template model generally contains everything in a model except for model data. Also, in the process of saving a template model, the program will automatically un-match or inactivate all expression profiles. This document format is designed to be loaded into GemStone™ and then processed by Auto Analysis. The other type of model document has all the modeled data and reflects the state of the system after modeling. Typically, batch systems are programmed to automatically save the model document in this format after an analysis has been performed.

4 HD t-SNE or Cen-se' Mapping

In 2002 at the Neural Information Processing Systems Conference, Geoffrey Hinton and Sam Roweis presented a novel set of

algorithms, called "SNE" that attempted to place events or objects defined in high-dimensional space into low-dimensional space that preserve much of their "neighborhood identity" [15]. Since then, there have been many published variants of their method where currently the most popular is t-SNE.

The t-SNE algorithms were first described in 2008 by Laurens van der Maaten [5] and later made more efficient with the Barnes Hut approximation [6, 7]. The algorithms use a *t*-distribution with one degree of freedom, and are *s*tochastic, involving *n*earest neighbor events that *e*mbed or map high-dimensional data to low-dimensions. It is a mapping process that attempts to preserve local and regional high-dimensional data relationships in low-dimensional space.

The original algorithms have been heavily modified and improved in GemStone™ to optimize resolution of mapped data, minimize random placement of populations, run at reasonably high speeds, and require far less memory. Because these changes result in higher resolution t-SNE maps than originally published, they will be referred to as "high-definition" or HD t-SNE maps or Cen-se'™ maps. Although a detailed description of how and why this algorithm works as well as it does for high-dimensional cytometry data it is outside the scope of this chapter, the major involved algorithms for SNE mapping are described below.

4.1 Normalization and Nearest Neighbor Distances

The SNE process begins with data normalization. This process attempts to eliminate any scaling differences among involved measurements while preserving their variance differences. Figure 2a shows a simple nine-event example. The events or points are defined in high dimensions and form three clusters of three points where two clusters are closer together than the other pairs of clusters. A high-speed vantage point tree [16] then finds nearest neighbor events for each event. The number of nearest neighbor events is an important free parameter of the system. Figure 2b depicts this neighborhood about event 0 with an ellipse encompassing six neighboring events. In the original t-SNE implementation, this value was determined from the parameter, perplexity, by multiplying it by three.

4.2 Similarities and Symmetrizing

Euclidean distances between events and their nearest neighbors are then converted to probabilities by employing a suitable probability density function (*see* Fig. 2c). These probabilities determine the "similarity" of the neighboring events to each event. Note that distant events outside the neighborhood end up having similarities of zero which is why the algorithm does not preserve distant data relationships. A symmetrizing algorithm then ensures that these similarities are symmetric for all participating events. The events and their nearest neighbor similarities are encoded in the matrix $\mathbf{p}_{i,j}$ (*see* lower-left corner of Fig. 2c). In the original implementation,

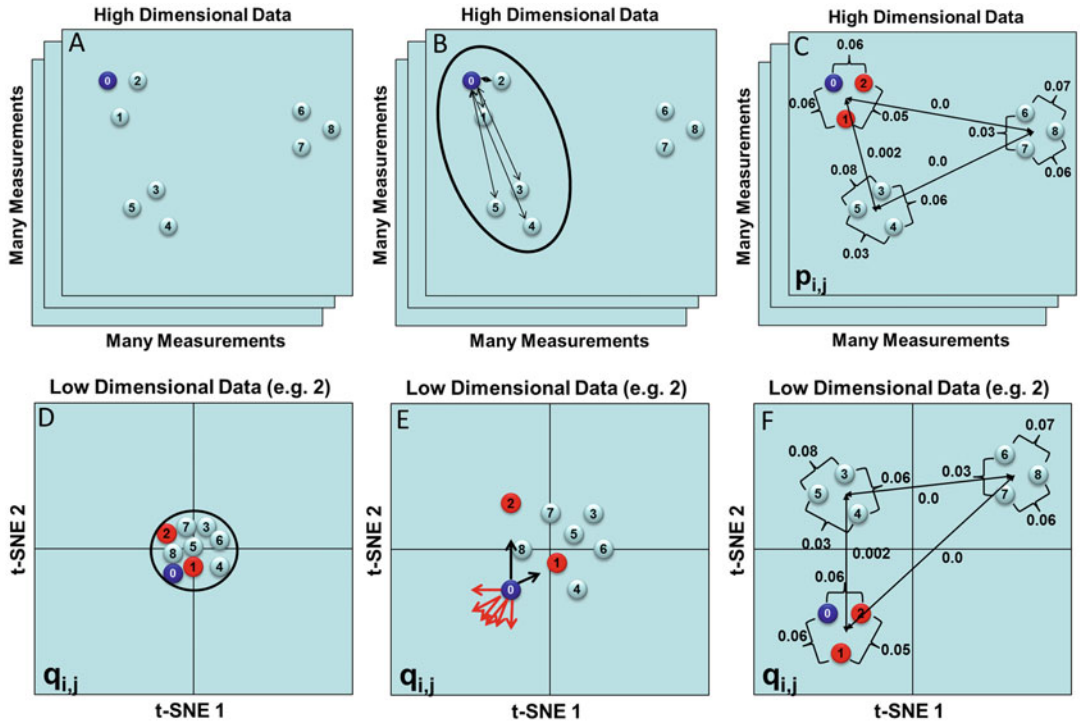

Fig. 2 HD t-SNE mapping (Cen-se'). (**a**) It schematizes a nine-point example of some high-dimensional data. (**b**) It shows a six-point neighborhood around event 0. The other events have similar nearest neighborhoods. The distance between each neighboring event is then converted to similarity probabilities by the use of a suitable probability density function. (**c**) These similarity probabilities define local structures (e.g., the three neighboring events) and regional structures (the two closest pairs of clusters) at the expense of more distant clusters. (**d**) Corresponding points are randomly placed in a small spot in t-SNE space. The distances are converted to similarity probabilities, q_{ij}, using the Cauchy probability distribution. (**e**) Positive and negative forces are computed on each event in t-SNE space. (**f**) As the events expand, the positive forces bring similar events together forming structures that preserve the local and regional structures defined in high-dimensional space

the corresponding mapped points are randomly placed in a very small spot in t-SNE space (*see* Fig. 2d). This random placement normally results in t-SNE maps with random population locations. GemStone™ Cen-se'™ mapping employs a more structured initialization that mitigates much of this randomness.

4.3 Force-Directed Solution

The t-SNE mapped points are converted to a similarity matrix much like the one described above for the high-dimensional points. A Cauchy distance distribution [17], which is equivalent to the Student's *t*-distribution with one degree of freedom, is used to convert the low-dimensional distances to probabilities, $\mathbf{q_{ij}}$. All the preceding steps have been to prepare the data for the final force-directed step in the mapping process. At this point, the system has a

high-dimensional nearest neighbor matrix of event similarities, $\mathbf{p_{i,j}}$, and a corresponding matrix of low-dimension t-SNE event similarities, $\mathbf{q_{i,j}}$. The purpose of this last stage is to move the t-SNE points in such a way that the difference between the two sets of probabilities is minimized. The Kullback-Leibler Divergence formula [18] quantifies differences between the two sets of probabilities with a single unit less number, D_{KL}.

$$D_{\mathrm{KL}} = \sum_i \sum p_{i,j} \cdot \ln\left(\frac{p_{i,j}}{q_{i,j}}\right), \quad i,j \in 1 \ldots n.$$

Lower D_{KL} values are associated with sets of probabilities that are more similar. Note that as $\mathbf{q_{i,j}}$ approaches $\mathbf{p_{i,j}}$, the ratio approaches unity. Since the log of unity is zero, D_{KL}, approaches zero as the two probabilities approach each other. Also note that distant pairs of points where $\mathbf{p_{i,j}}$ values are near zero will have little contribution to the D_{KL} value, thus making the method resistant to the effects of outlier populations.

By appropriately differentiating the D_{KL} function, gradient equations provide a means for calculating positive and negative forces on each event (*see* Fig.2e, red are the negative forces and black arrows are the positive forces on event 0). The positive and negative force equations are given as.

$$\mathrm{pos}F_{i,d} = \sum_{N_j} p_{i,j} q_{i,j} Z\left(\Upsilon_{i,d} - \Upsilon_{j,d}\right),\ i \in 1 \ldots n, j \in N_i,$$

$$\mathrm{neg}F_{i,d} = \sum_j {q_{i,j}}^2 Z\left(\Upsilon_{i,d} - \Upsilon_{j,d}\right), i,j \in 1 \ldots n,$$

where,

$$q_{i,j} = \frac{\left(1 + \sum_d \left(\Upsilon_{i,d} - \Upsilon_{j,d}\right)^2\right)^{-1}}{Z},$$

$$Z = \sum_k \sum_{l \neq k} \left(1 + \sum_d \left(\Upsilon_{k,d} - \Upsilon_{l,d}\right)^2\right)^{-1}.$$

Note that as $\mathbf{q_{i,j}}$ approaches $\mathbf{p_{i,j}}$ the positive and negative forces will cancel out for all event pairs within the *i*th event's neighborhood, N_i. What is fascinating about this system is that the negative forces are computed between all events using the Barnes Hut approximation [7, 19], not just the neighborhood events. As a consequence, the events will have a net repelling force that continually expands the collection of points on the t-SNE map. As the points expand, the positive or attractive forces between neighborhood events form domains of similar events. The patterns eventually stabilize as the two forces cancel and the result is a dot plot pattern that closely represents local and regional structures defined in high-dimensional space (*see* Fig. 2f).

4.4 Very High-Definition t-SNE Maps

For most applications, the ability of the HD t-SNE map to distinguish populations defined in high dimensions is more than adequate. However, if maximum resolution is desired, there are a few additional strategies that can be employed. The first strategy is to leverage the program's enriching option to only examine a single cell type. By not including all cell types, the t-SNE algorithms will optimally separate all the subpopulations within the enriched cell type. Also, the enriching process ensures that every selected cell type event in the file is available for the mapping process. Another important strategy is to not include measurements in the t-SNE that are not relevant for the cell type. Care should be taken with this strategy since the mapping process normally leverages noncanonical measurements for separating subpopulations. When defining staging expression profiles within a cell type, a useful strategy is to create a HD t-SNE map that involves only those measurements that are known to modulate at stage boundaries.

5 Synergistic Relationships Between Modeling and HD t-SNE Maps

A good way of initially evaluating the relevancy of HD t-SNE maps is to generate relatively simple data of known characteristics with probability state models and then render the associated t-SNE maps. A detailed comparison between the two is often illuminating on how best to leverage t-SNE maps for designing models.

5.1 Two Cell Type Model

Figure 3a shows an expression overlay for the first example cell type, CT1, and Fig. 3b shows an expression profile overlay for the second cell type, CT2. Both the cell types are defined with six hypothetical measurements: M1–M6.

The first cell type, CT1, is selected with $M1^{+}$ $M2^{+}$ $M3^{-}$. M4 downregulates ($M4^{+} > M4^{-}$) and M5 slightly upregulates and then downregulates ($M5^{+} > M5^{++} > M5^{-}$). M6 is initially negative and then some of the events upregulate while others do not ($M6^{-} >$ Br ($M6^{-}$,$M6^{+}$)). CT1 has three stages defined by M4 downregulating and M5 downregulating later.

The second cell type, CT2, is selected with $M1^{+}M2^{-}M3^{+}M6^{-}$. The progression begins with M4 downregulating, $M4^{+} > M4^{-}$, and ends with M5 downregulating, $M5^{+} > M5^{-}$. CT2 also has three stages defined by M4 downregulating and then M5 downregulating. Note that all stages have transitions with intermediate intensity events except for the first to second stage in CT1 where it has little or no transitional events.

5.2 Associated HD t-SNE Maps

Figure 3c shows the associated t-SNE map with dots colored by the associated stages and appropriately labeled from the model. Since CT1 and CT2 have different selection phenotypes, they appear well separated in the HD t-SNE map. Because of this separation t-SNE

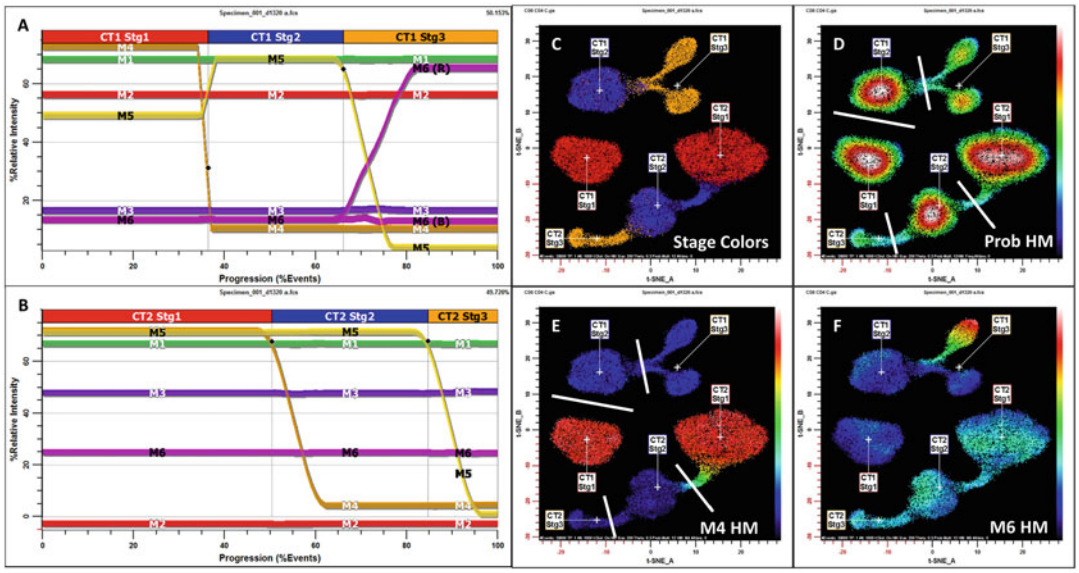

Fig. 3 Modeling and HD t-SNE. (**a**) It shows an expression overlay for the first example cell type, CT1. (**b**) It shows an expression profile overlay for the second cell type, CT2. Both cell types are defined with six hypothetical measurements: M1–M6. (**c**) It shows a HD t-SNE map of simulated data derived from the model. The *dot colors* are the same as the stage colors shown in (**a**) and (**b**). (**d**) It shows a probability heat map of the same data demonstrating that the cell types as well as the stages can be easily delineated (see *white lines*). (**e**) It shows a M4 heat map of the data demonstrating that the initial stage demarcations correspond to M4 expression levels. (**f**) It shows the variable intensity levels of the branched marker, *M6*

maps can help modelers create selection criteria that optimally define cell types. The transition from CT1 stage 1–2 is abrupt and as a consequence, a clear gap is present between these stages; whereas, the other stage transitions have a thin isthmus of transitional events connecting them. Not shown in this example is the tendency for stages to be separated by gaps with high-dimensional data. Examples of this characteristic will be demonstrated with the CD8 cell type (*see* Subheading 8).

Because of the nature of t-SNE mapping, progressions like the ones shown here will normally have sequential stages next to each other and nonsequential stages distal to each other. One exception to this rule occurs if the t-SNE map is inappropriately configured to only look at local structure. In the original implementation, this exception frequently occurred when the entropy and/or perplexity parameters were set too low (e.g., perplexity <= 50). Another exception to the adjacency rule occurs if a stage has no intermediate events as with CT1, stage 1. This stage can act like a different cell type and can be positioned anywhere since distant structures are not preserved in the mapping. Fortunately, this problem is very rare when examining high-dimensional data since there are usually intermediate events in other dimensions. Also, redoing the map

with random event starting positions is a valuable technique that can rule in or out this particular problem.

A good way of approaching the proper staging of a cell type is initially to draw lines through the gaps and valleys of the map without being biased by any additional information (*see* Fig. 3d for probability heat map). As demonstrated in this panel, the probability heat map is a good graphic option to use to better visualize peaks and valleys. Spot regions before and after the lines or heat maps will reveal which markers are modulating (*see* Fig. 3e for M4 heat map). Heat maps generally use heat-related colors to denote measurement intensity or event frequency/probability. A common sequence of colors is black- > blue (cold)- > Cyan- > Green- > Yellow > Red (hot) > White. Although heat maps are quite convenient, they can be tedious to interpret and they are qualitative in nature. The best way of examining marker transitions is with animated regions. Animated regions blink dots in all other graphics with a specified color.

Look at other samples to make sure the boundaries and marker transitions are consistent. If there are multiple measurements changing at the same time, choose the one where the transition is greatest with the least degree of variability. In order to assign a direction to the stages, it is necessary to know at least one part of a progression's directional information. For example, to know that CT1's progression moves left to right and CT2's moves right to left, the stage that contains high-intensity M4 needs to be known.

One major advantage of HD t-SNE maps is that branched progressions can be directly inferred from the dot patterns. A close examination of the CT1 stage 3 heat map of M6 in Fig. 3f shows transitional events forming a fork in the progression where some events upregulate M6 while others do not. This ability to detect branched progressions is difficult if not impossible using conventional dot-plot displays and is important in properly designing models.

If measurement expression profiles are branched as shown for M6, then they will not work well to identify stages of progression. One of the reasons for this is that other marker transitions will appear much more complicated than they really are. For example, if M6 were not known to be branched and were modeled as a non-branched expression profile, then M5 would inappropriately appear branched. This problem progressively worsens with higher numbers of correlated measurements. In the gating world, using branched measurements to define stages can result in subsets with overly complicated phenotypes.

Once the appropriate measurements are chosen for staging, they can be introduced into the model as step-up, step-down, or multiple level expression profiles. After ensuring that all the validation data are consistent with the model stages, the literature can be consulted to determine how best to label the stages. If a model

stage and the literature are consistent with each other, then use literature-determined label for the stage; otherwise, use simple labels such as "early," "int," "late," or just a sequence such as "B1," "B2," etc. Model and literature determined stages may be very different. If they are different, it is always possible to output data that is equivalent to literature-determined stage phenotypes using the TriCOM combinatory system. The mistake a modeler can make is to force literature-determined stages onto data that are not consistent with those stages.

5.3 Error Analysis

All analysis methods have some degree of error. It is important to attempt to evaluate this error for all designed models. There are a few strategies that can be employed to perform error analyses on your models. All these strategies require that you have some estimates that represent "truth."

5.3.1 Synthesized Data

Since models can synthesize data, it is possible to produce or synthesize data as shown in this section where all information is known and therefore can act as a "truth" set. For example, the number of CT1 events synthesized from the data shown in Fig. 3 was exactly 14,906 and the number of CT2 events was 15,094. After Auto Analysis, the actual numbers of events classified as CT1 and CT2 events were 14,892 and 14,916. The error of model classification is the percentage of the number of misclassified events to the number of "truth" events. For CT1, the error is $(14{,}906–14{,}892) \times 100/14{,}906 = 0.13\%$ and for CT2 it is 1.2%. Because probability state modeling defines cell type boundaries probabilistically, there will always be some unclassified events if the probability of exclusion property is set to some positive fraction. By default, it is set to 0.001 or 0.1%. For some applications such as rare event detection, the probability of exclusion can be set to 0 to force the system to categorize every event. The same %error can then be calculated when in this mode.

5.3.2 HD t-SNE Cell Types

Since HD t-SNE maps can separate cell types based on many measurements, a truth set can be approximated by enclosing the cell type events shown in the map with polygonal boundaries (not shown). For this example, the numbers of events reported by the regions are 15,071 and 14,929 for CT1 and CT2, which are quite close to the synthesized numbers. Keep in mind that regions will enumerate all the enclosed events including the unclassified events. To find the number of classified and unclassified events enclosed by a region use Information equations. For example, if region 4 is used to encompass CT1 events, the number of events classified as CT1 is given by GSUM(C1,R4) and the number of unclassified events is given by GSUM(C0,R4). For many applications such as the ones discussed in Subheading 8, this is a very practical method for assessing model classification error.

Another important calculation that is possible using this technique is to calculate the % specificity of a model's cell type. % Specificity is defined as the percent of cell type events that are appropriately classified. For example, the % specificity equation that returns the percent of CT1 events that are properly classified is GSUM(C1,R4) × 100/GSUM(C1).

5.3.3 Legacy Method

Another strategy for assessing the merits of a model is to compare it against some legacy method. A legacy method could be a gating method or it could be a previous version of a model. Since gating is highly inaccurate, the best that normally can be done is to perform correlations with the gated results. The degree of correlation is usually enumerated as a correlation coefficient. Keep in mind that a probabilistic model will normally capture more cell type events than gating.

5.3.4 Measurement Intensities

All the above strategies involve estimating numbers or percentages of events. Another type of error analysis is to examine the veracity of measurement intensities. For high-dimensional data sets, this kind of analysis can be quite tedious and rarely justified. If the application does require an accurate assessment of one or more measurement intensities, use medians and robust standard deviations to estimate central tendencies and variabilities. There are two largely equivalent methods for measuring intensity variability, rSD and qSD. If X is a set of values for measurement X, then the equations for rSD and qSD are

$$\begin{aligned}
&\text{median} = \text{Median}(X),\\
&\text{rSD} = \text{Median}(|X_i - \text{median}|) \times 1.4826,\\
&\text{IQR} = Q3(X) - Q1(X),\\
&q\text{SD} = \frac{\text{IQR}}{1.34898}.
\end{aligned}$$

6 Initial Preparations and General Considerations

6.1 Computer System

Before beginning to model, make sure the computer and display systems work well with the computationally intensive demands of high-dimensional modeling. Keep in mind that performance will be directly proportional to the computer's clock speed, the amount of RAM, and number of core processors. Since this type of analysis is especially graphics intensive, consider using two or more high-resolution color monitors.

6.2 Organize Folders and Files

Organizing your work before beginning a modeling project has a lot of personal preference elements, but there are some basics that should be followed. Create folders for analysis, batch system, files, images, models, and templates for your modeling project. Most of

these are self-explanatory; however, the analysis folder should use something like PowerPoint to document your progress as you develop models. As the template model develops, save it to the templates folder identified with different version numbers. It is very important to be able to go back to specific versions of the model as it is developed with different strategies.

As mentioned earlier, a template model differs from a regular model in that it does not contain any data and all the expression profiles are unmatched in order that Auto Analysis can enable them in a specific order. If you intend on eventually moving all the folders to different drives, consider using a virtual drive for your project folders. Since the paths for files, models, images, and other key documents contain the drive letter, you can save time moving the system if you use a virtual drive letter for the drive containing you project.

6.3 Test Feasibility and Create Test Data Sets

Gather an adequate number of validation files. Quickly determine the feasibility of a modeling project with a few example files. After feasibility is assured, then use 50 to 100 sample files for initial testing purposes. Many times, it is necessary for these files to be carefully analyzed by manual gating with key results databased. The databased results can later be compared with the automated modeling results. Another approach to validation is to create a set of contextual plots that can be inspected after modeling to determine if event classifications are reasonable. For fluorescence cytometers, all files need to be properly compensated.

6.4 Optimize Measurement Transforms

Each model measurement must have a valid transformation. Transformations mathematically convert raw linear measurements to scales that appropriately stabilize population variabilities [20]. Both t-SNE maps and modeling results are affected by transforms. Inappropriate transforms can render measurements useless or even worse, deceiving; therefore, it is very important to take time to evaluate each measurement's transformation using either dot-plot or histogram displays. Once a measurement transform has been optimized, rarely is it desirable to have the software modify the transform's parameters with subsequent sample files.

6.5 Start Simply and Document as You Go

There is a strong tendency to want to build the complete model in one step. The problem with this approach is that if something fails, it is hard to determine reasons the model failed. A better approach is to inspect models against validation files at key steps in their evolution. Once a cell type is designed, do not go to the next step in model building until it is tested for all validation files. It is important to remember that since models support automation, it is relatively easy to make small changes to them and retest against validation sample files. Use the batch system to automatically analyze files with specific model versions and generate useful sets of contextual images and databased results.

6.6 Organize a Study with the Batch System

The batch system contains not only pathways to FCS data files but also sets of actions to apply to these files. It also contains a complete database that is normally hidden from view. Each level of the batch can have a different set of actions assigned to it. Usually, the first level is left in its default state, which is to read a FCS file into the system. Higher batch levels are used to open a model template, read the associated FCS files, Auto Analyze the data with the template, save the analyzed model, and also save images. There is a rich set of other actions that can also be assigned to batch levels. For most applications, after the template model is loaded into the system, another batch level simply resets the model back to its previous loaded state and then does all the same analyses as the preceding batch level. This technique of resetting the model before subsequent analyses is important for advanced analysis techniques such as creating averaged models.

7 General Approach to Modeling

Fig. 4 shows the general iterative process for developing probability state models.

7.1 Background Investigation

Before beginning any modeling project, relevant literature should be obtained and studied. Also, it is important to have on hand any relevant manual gating strategies. Keep an open mind during the modeling process. Because cell type stages, branches, and subsets are difficult to visualize with traditional dot plots, literature descriptions may not be completely consistent with data analysis results.

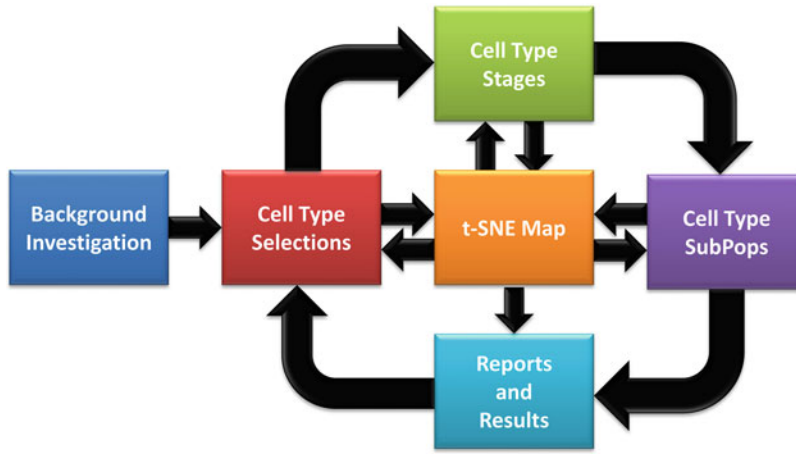

Fig. 4 General approach to modeling. This figure shows the general iterative process for developing probability state models

7.2 HD t-SNE Maps

An early step in modeling is creating high-definition t-SNE maps of all relevant measurements for a typical sample file. Using one representative file at the start makes it easier to see branched measurements and stage separations. Once you have t-SNE maps defined for a typical sample file, it can be useful to sample a number of files and create t-SNE maps of composite files. Keep in mind that composite files will inevitably have less resolution than single representative files.

7.3 Cell Type Selections

Usually, there are a number of equivalent choices for the first cell type to model. Pick the easiest and most prevalent cell type first. Since cell types compete probabilistically for events, they often serve to "clean up" events for subsequently defined cell types. Add negative selection measurements to the cell type first and then, add the best positive selection measurements. Start with canonical antibody-based measurements and then clean up selections with measurements like side-scatter, if available.

Measurements that modulate within the cell type can be added at this point, but do not create expression profiles for them yet. Populate the cell type reports with graphs that provide contextual information on the validity of cell type selections. Use HD t-SNE maps to make sure cell type selections do not include other cell types. Examine unclassified events in t-SNE maps to ensure that the model is not excluding valid cell type events.

An often overlooked modeling step is to produce a set of graphs that assess the quality of the data. On at least one cell type include a plot of time or chronology versus some positive intensity measurement to check for acquisition drifting. For fluorescence cytometers, ninety-degree light-scatter is a good choice since it is highly influenced when bubbles are present in the nozzle. A selected set of median intensity measurements is also important to report since it may indicate a problem with antibody staining or modeling. For fluorescence cytometers, always include a peak versus integral or equivalent side-scatter dot plots since the presence of aggregates is another kind of quality assessment for a sample.

Continue adding cell types in this manner until all the desired cell types are modeled with selection expression profiles. Do not begin modeling the cell type stages until all cell types have been added to the model and events have been appropriately selected for each one. Validate the selection of cell types by analyzing all test files and suitably examining their contextual plots and perhaps comparing the results with some predicate method. Usually, additional refinements of selection expression profiles are necessary after evaluating a collection of files. Always put the complete phenotypic description of the selection on the cell type report.

7.4 Cell Type Stages

This step can be skipped if the cell type does not have measurements that modulate with progression or the cell type does not have a progression. For complex cell types such as peripheral blood CD8 T

cells, the t-SNE system should be put into very high-resolution mode where the t-SNE map is restricted to a single cell type. As mentioned in Subheading 5, try first to develop the stages in an unbiased manner. Test the model stages on all the validation files. For large panels, it is advantageous to examine t-SNE maps derived from just those measurements that are involved or could be involved in staging.

Begin staging with those measurements that have simple up- or downregulating patterns that also have low line-spreads that clearly separate the different levels of measurement intensity. Model simple expression profiles first and then progress to more complex multi-level expression profiles. Use small animation regions before and after the stages or heat maps to validate stage boundaries. Choose the appropriate beginning and ending CDPs for defining stages and label them as close to the literature as possible.

If published stages are not consistent with the data, use TriCOMs to enumerate them. Create a table on the cell type report that enumerates the stage percentages and also describes them phenotypically. Archive cell types as individual files in order that future models can quickly be created by assembling appropriate cell type files.

7.5 Cell Type Subsets

In some cell type stages, there may be cellular subpopulations or subsets that have varied measurement phenotypes. Use TriCOM graphs to enumerate the phenotypically defined subpopulations. Try to use labels that are consistent with the literature and always show the phenotypic signature for each subpopulation. As mentioned above, the TriCOM system can also be used to enumerate published stages that are not consistent with model-defined stages.

7.6 Reports, Database Entries, and Alerts

The final edits to models should be to create clear and relevant graphics on generated reports. This last stage of model building is also a convenient time to select which analysis results to database. Consider storing event counts instead of percentages since they can always be used later to form percentages in programs like Excel. Finally, decide which results are capable of detecting either failures in data integrity or modeling. These databased results can be turned into alerts that inform users when something went wrong.

8 Specific Example

The following example describes model development that enumerates and displays most known populations in human peripheral blood mononuclear preparations, PBMCs. Although all the steps described in Subheading 7 were followed, this Subheading describes only a sampling of noteworthy modeling decisions for some cell types. The panel was developed by the Human Immune

Monitoring Center at Stanford University and was composed of the following antibodies and rare-earth isotope labels: (1) CD45RA Dy162, (2) CD20 Dy164, (3) CD33 Er166, (4) CD28 Er167, (5) CD24 Er168, (6) CD161 Er170, (7) CD38 Eu151, (8) CD11b Eu153, (9) CCR6 Gd155, (10) CD94 Gd156, (11) CD86 Gd157, (12) CXCR5 Gd158, (13) CCR7 Gd160, (14) CD127 Ho165, (15) CD57 In113, (16) Live/Dead In115, (17) DNA1, (18) DNA2, (19) HLA-DR Lu175, (20) CD19 Nd142, (21) CD4 Nd143, (22) CD8 Nd144, (23) IgD Nd146, (24) CD11c Nd148, (25) CD3 Nd150, (26) CD85j Sm147, (27) CD16 Sm149, (28) CD27 Sm152, (29) CD14 Sm154, (30) CXCR3 Tb159, (31) ICOS Tm169, (32) TCRgd Yb171, (33) PD-1 Yb172, (34) CD123 Yb173, (35) CD56 Yb174, and (36) CD25 Yb176. The data shown in this section were obtained from a Helios™ mass cytometer (Fluidigm Corporation).

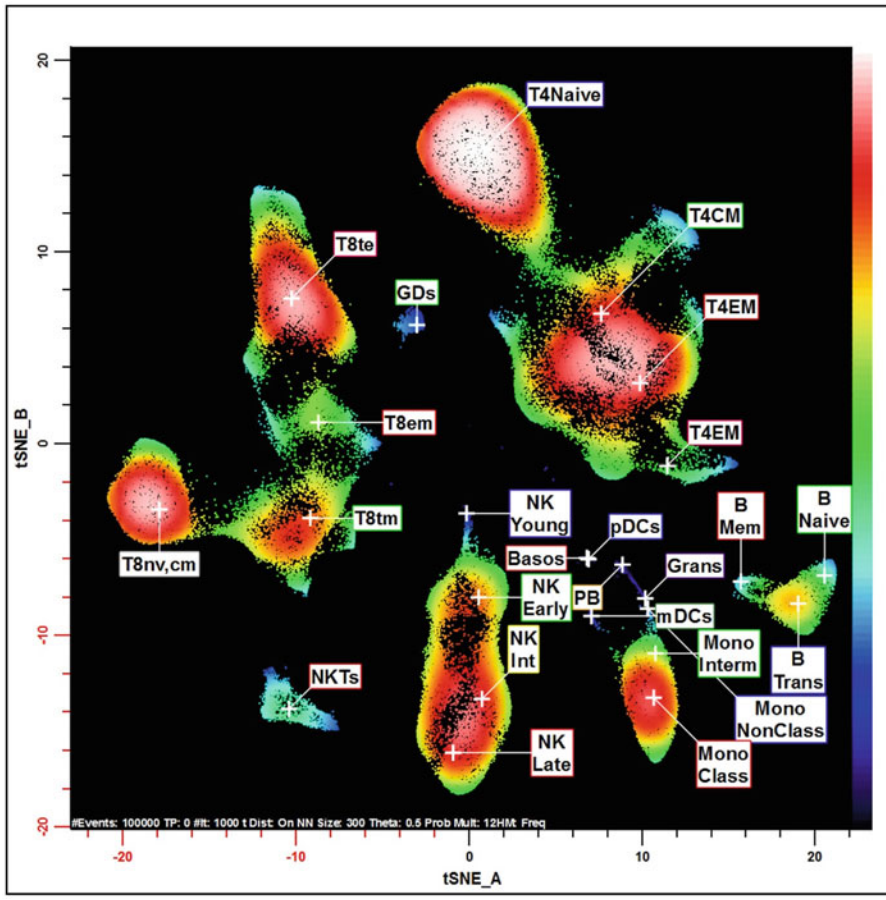

Fig. 5 PBMC HD t-SNE overview map. This figure shows a HD t-SNE map of a PBMC sample involving 36 measurements displayed as a probability heat map. All the major cell types are well separated. Many of the cell type stages are also labeled

Figure 5 shows an overview t-SNE map involving all the measurements listed above. The map separates a PBMC sample into the major cell types: CD8 T, CD4 T, NKTs, γδ (GDs), NK, Monocytes (Mono), Grans, and B cells. Many of the cell type stages are also labeled. Minor populations such as plasmacytoid dendritic cells (pDCs), myeloid dendritic cells (mDCs), and plasmablasts (PB) are not well shown with this view because their frequency is so low. Event colors are drawn from a probability heat map that is designed to allow easy inspection of cell type frequency topographies.

8.1 CD8 T Cells

Modeling CD8 T cells exemplifies the importance of validating selection and staging against high-definition t-SNE maps.

8.1.1 Selection

CD8 T cells were initially selected as $CD33^{-}CD14^{-}CD3^{+}CD8^{+}CD4^{-}$ [4, 21, 22]. A good technique for assessing cell type specificity is to only look at events classified for a specific cell type and evaluate how contained these events are within the t-SNE cell type boundary. When CD8 T cells were selected and evaluated on the HD t-SNE map, some events were inappropriately positioned in the NKT and γδ (GDs) map domains (*see* Fig. 6a, white arrows). We used colored regions to explore these NKT and γδ events in a number of expression profiles and found that CD161 and TCRgd allow for better differentiation between CD8 T cells and the NKT and γδ cell types (*see* Fig. 6b, c). This inspection only takes a few minutes since you are searching for expression profiles where blue dots, the CD8 T cells, are separated from red and green dots, the NKT and γδ events respectively.

By adding the expression profiles, Inv($CD161^{+}$) and $\gamma\delta^{-}$, to the selection phenotype, these false CD8 events were greatly reduced (*see* Fig. 6d). When HD t-SNE maps unambiguously separate cell types as in this example, this kind of selection refinement can be employed to reduce model false negatives and positives.

8.1.2 Staging

Before beginning to stage the CD8 T cells, make sure that all cell types are properly selected for all validation files. Figure 7a shows a HD t-SNE map of CD8 T cells for one donor sample using all 36 measurements. Although most of the staging information can be inferred from this map, a good technique for validating staging is to redo the t-SNE map with a limited set of measurements that appear to modulate on either side of the gaps in the overview t-SNE map. Heat map and region color analyses show that the key staging measurements are CD45RA, CCR7, CD28, CD27, and CD56 (data not shown). Figure 7b shows the same sample as shown in Fig. 7a with this limited set of involved measurements. White lines separate the map's obvious similarity domains and labels indicate the domain's key phenotypes.

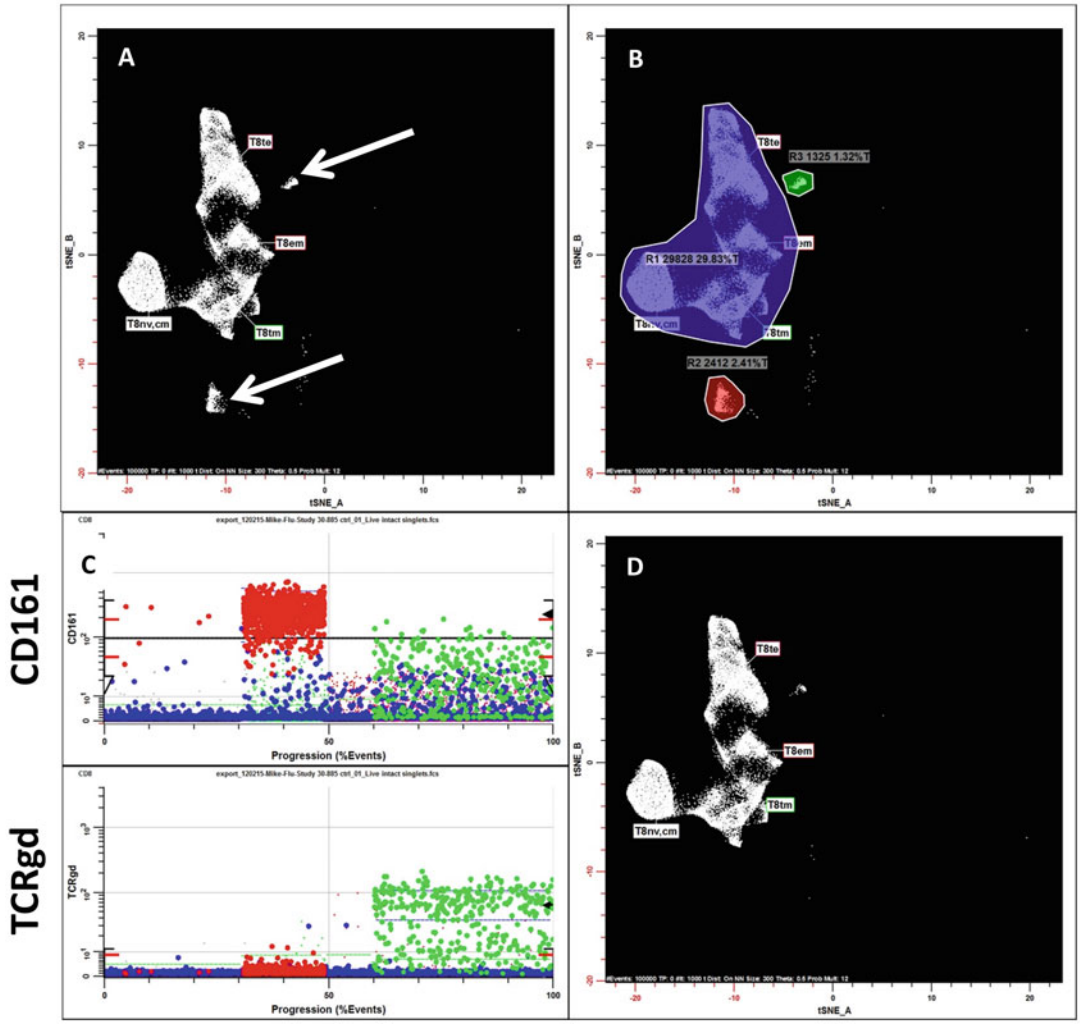

Fig. 6 Optimizing CD8 T cell type selection. (**a**) It shows CD8 T cells (*white dots*) that were selected as $CD33^{-}CD14^{-}CD3^{+}CD4^{-}$. The *white arrows* indicate areas where the CD8 T cells are inappropriately positioned within the GD and NKT domains. (**b**) It shows three different colored regions that encompass the CD8 T (*blue*), NKT (*red*), and TCRgd (*green*) t-SNE map regions. (**c**) The CD8 T cell expression profiles for CD161 and TCRgd are shown, and demonstrate that the selection phenotype can be improved by including $CD161^{-}$,d and $TCRgd^{-}$ to CD8 T cell selection phenotype. (**d**) It shows the improved specificity results by adding these additional measurements

Figure 7c–f show the associated CCR7, CD28, CD27, and CD56 heat map displays. The CD28, CD27, and CD56 measurements are clearly delineated by the gaps in the t-SNE map, whereas $CCR7^{+}$ portion of the heat map only partially fills the contained domain. The progressive nature of the heat maps confirms that they are demarcating a valid progression.

A surprising and significant finding is the gradient of CD45RA expressions (*see* Fig. 8a) through each t-SNE similarity domain.

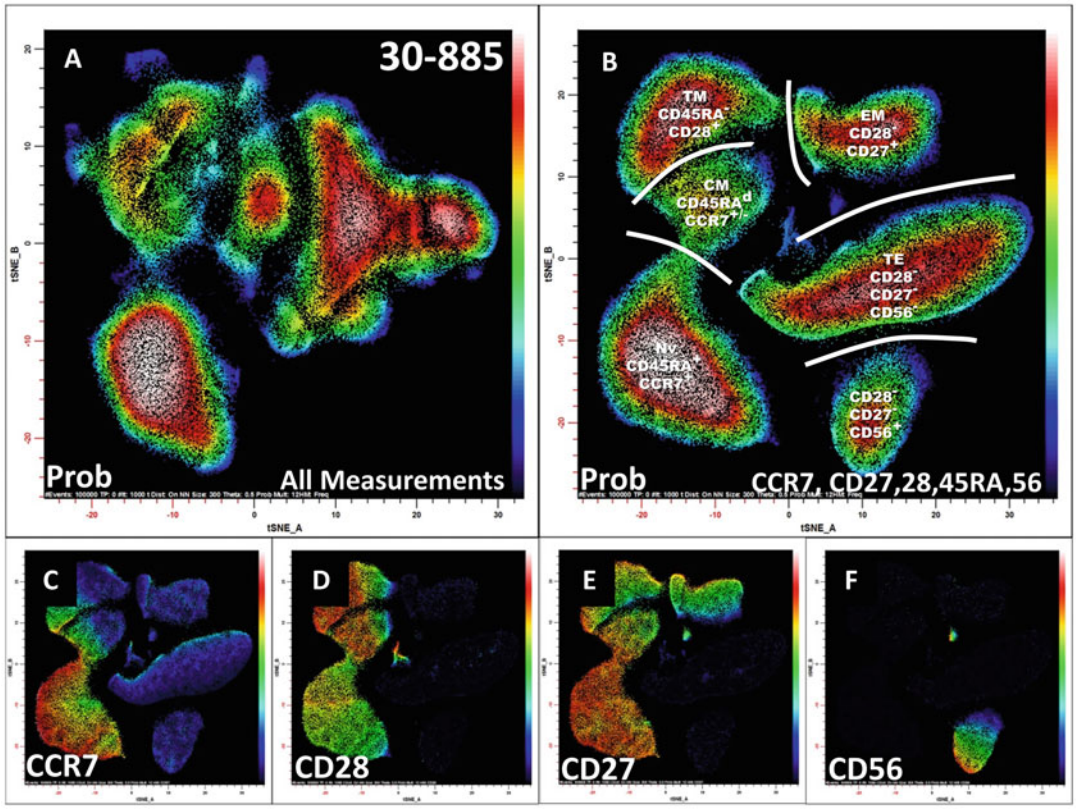

Fig. 7 Optimizing CD8 T cell staging. (**a**) It shows a HD t-SNE map of CD8 T cells for one donor sample using all 36 measurements. (**b**) It shows the same sample as shown in (**a**) with only CCR7, CD28, CD27, CD45RA, and CD56 involved in the t-SNE mapping. *White lines* separate the map's obvious similarity domains and labels indicate the domain's key phenotypes. (**c**–**f**) These show the associated CCR7, CD28, CD27, and CD56 heat map displays. The CD28, CD27, and CD56 measurements are clearly delineated by the gaps in the t-SNE map, whereas $CCR7^{+}$ portion of the heat map only partially fills the contained domain. The progressive nature of the heat maps confirms that they are demarcating a valid progression

This pattern suggests that CD45RA is complex and branched which makes it undesirable to use as a staging marker as discussed in Subheadings 2 and 5. A reasonable question to ask is what would happen if CD45RA were used as a staging marker? Most of the negative (blue and cyan) events in the TE domain would end up being re-categorized into the CM and EM stages and the positive EM domain events (red and white) would end up being in the TE stage. Because of this shuffling of events, both CD28 and CD27 would then appear branched when modeled. Also, the stages would end up crossing the t-SNE determined domains. One of the tenants of modeling is to use the simplest model that is consistent with the data. In this case, the simplest model is to not stage with CD45RA and stage with CD28 and CD27 instead. When these two markers are used as stages, the model fit is excellent (not shown) and the

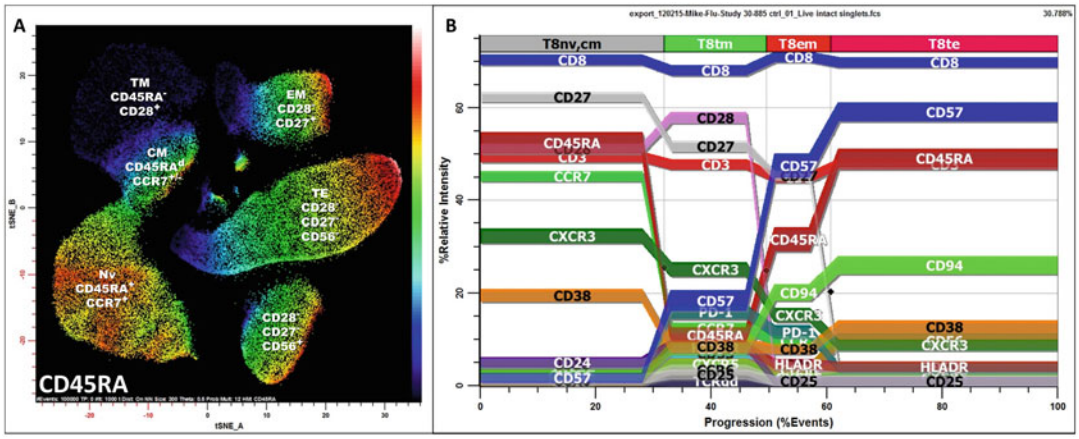

Fig. 8 Appropriate CD8 T cell type staging. (**a**) It shows a gradient of CD45RA expressions through each t-SNE similarity domain. This pattern suggests that CD45RA is complex and branched which makes it undesirable to use as a staging marker as discussed in Subheadings 2 and 5. (**b**) It shows the end result of using CCR7, CD28, and CD27 to properly stage CD8 T cells

final set of expression profiles are very similar to those presented by Appay et al. ([22]; *see* Fig. 8b).

Since the CM stage is defined as $CD45RA^{-}CCR7^{+}$ in most publications, this relatively small population can be enumerated by a TriCOM within the Nv-CM stage. The last decision that needs to be made is whether to use a step-up expression profile for CD56 or to use TriCOM to enumerate the $CD56^{+}$ population within the EM stage. If a step-up were used for CD56, then we would need to rename these stages since they would no longer be compatible with many literature-determined labels. In this case, it is best to enumerate the $CD56^{+}$ population as a TriCOM determined subpopulation.

At this point, the model needs to be tested against all validation files to make sure there was not something unusual with this single sample. Often when evaluating cell type stages and subsets as in this example, there is a discovery component to the process. A good approach to take is to be conservative in staging assessments and to use the TriCOM combinatory system as a means of enumerating these subsets. Only generalize when a reasonably large number of samples have been evaluated.

8.2 NK Cells

Traditionally, NK cells are simply $CD3^{-}CD56^{+}$ but examining the HD t-SNE in Fig. 9a shows that NK cells are far more interesting and complex than that.

8.2.1 Selection

The selection for the NKs was found to be $CD33^{-}CD14^{-}CD3^{-}CD123^{-}$Inv($CD56^{-}$).

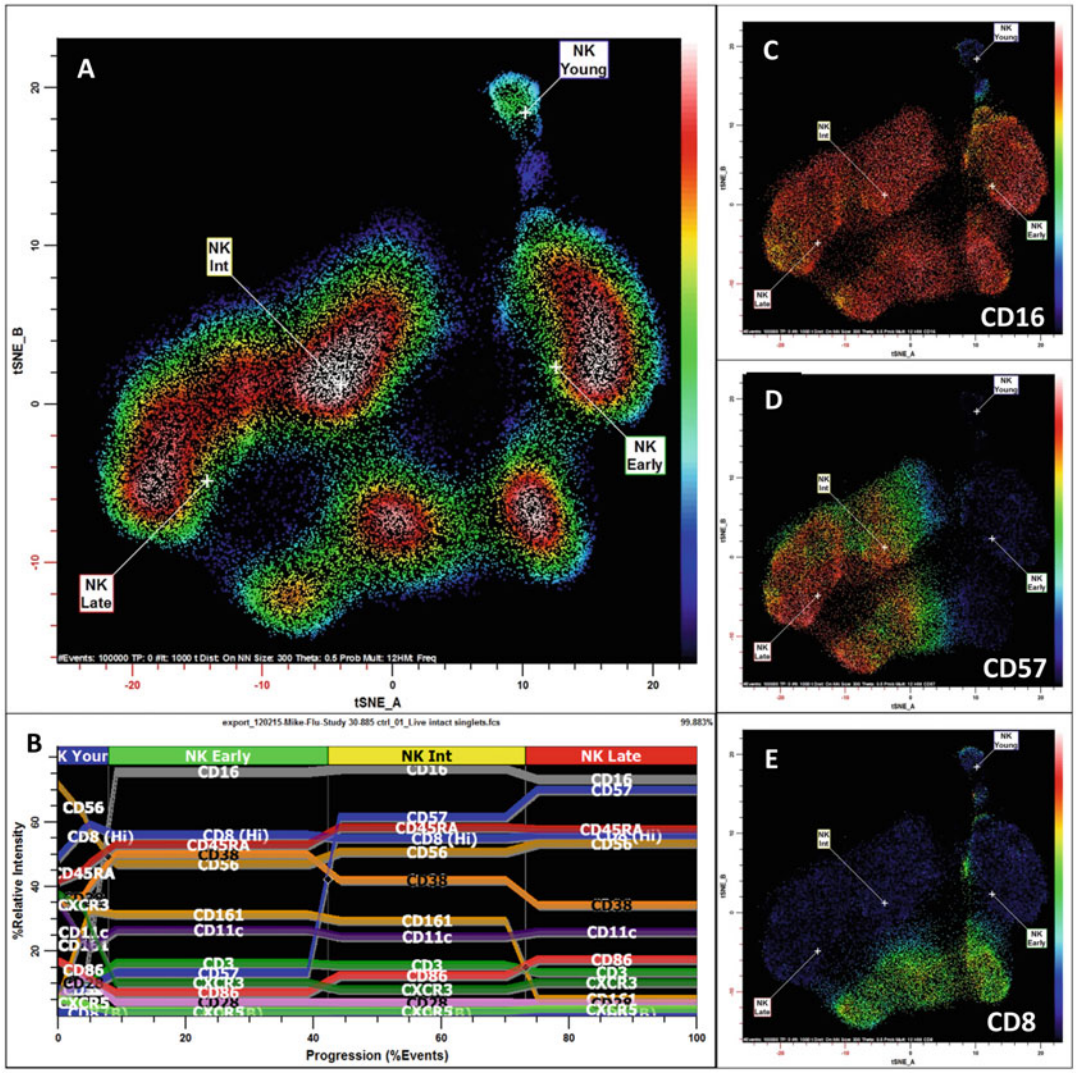

Fig. 9 Modeling NK cells. (**a**) It shows a HD t-SNE map based on all 36 measurements of NK cells. Selection of the NK cell type is $CD33^{-}CD14^{-}CD3^{-}CD123^{-}$Inv($CD56^{-}$). The population labeled as NK Young is $CD16^{-}CD56^{++}$ (*see* (**b**) for expression profile overlays and (**c**) for CD16 heat map). The next stages are (Early) $CD16^{+}CD57^{-}CD161^{+}$>(Int) $CD16^{+}CD57^{+}CD161^{+}$ and (Late) $CD16^{+}CD57^{+}CD161^{+}$ and the other stage-related marker intensities are summarized in (**b**). This sample has a biphasic expression of CD8 forming two bands in the HD t-SNE map (*see* (**a**) and (**e**))

8.2.2 Staging

The population labeled as "Young NK" is $CD16^{-}CD56^{++}$ and is thought to be immature NKs [23, 24]. Figure 9c heat map demonstrates that this population is $CD16^{-}$. CD57 then upregulates as shown by Fig. 9d. For many samples, there appears to be a branch in CD8 expression where one side of the t-SNE defined population is $CD8^{-}$ and the other $CD8^{+}$ (*see* Fig. 9e). The last stage is determined by a downregulation of CD161. The stages are therefore

defined as (Young) $CD16^{-}CD57^{-}$ > (Early) $CD16^{+}CD57^{-}CD161^{+}$ > (Int) $CD16^{+}CD57^{+}$ $CD161^{+}$ > (Late) $CD16^{+}CD57^{+}CD161^{-}$ and the other stage-related marker intensities are summarized in Fig. 9b.

9 Summary

As you no doubt noticed, modeling complex cellular populations defined by cytometry's correlated single-cell measurements is not easy. Hopefully, the framework provided will help those interested in building automated systems using modeling principles. I hope you enjoyed reading this chapter and if you ever have questions about any part, please send me emails.

Disclaimer

This author works for the company that develops and sells GemStone™. Every effort has been made to discuss general modeling concepts that would be applicable to other modeling packages if and when they become available.

References

1. Miller D, Hunsberger B, Bagwell C (2012) Automated analysis of GPI-deficient leukocyte flow cytometric data using GemStone. Cytometry B Clin Cytom 82B:319–324
2. Wong L, Hunsberger BC, Bruce Bagwell C, Davis BH (2013) Automated quantitation of fetomaternal hemorrhage by flow cytometry for HbF-containing fetal red blood cells using probability state modeling. Int J Lab Hematol 35(5):548–554. doi:10.1111/ijlh.12060
3. Wong L, Hill BL, Hunsberger BC, Bagwell CB, Curtis AD, Davis BH (2014) Automated analysis of flow cytometric data for measuring neutrophil CD64 expression using a multi-instrument compatible probability state model. Cytometry B Clin Cytom. doi:10.1002/cyto.b.21217
4. Inokuma MS, Maino VC, Bagwell CB (2013) Probability state modeling of memory CD8(+) T-cell differentiation. J Immunol Methods 397 (1-2):8–17. doi:10.1016/j.jim.2013.08.003
5. van der Maaten L, Hinton G (2008) Visualizing data using t-SNE. J Mach Learn Res 9:2579–2605
6. van der Maaten L (2009) Learning a parametric embedding by preserving local structure. Paper presented at the AISTATS, TiCC, Tilburg University P.O. Box 90153, 5000 LE Tilburg, The Netherlands
7. van der Maaten L (2014) Accelerating t-SNE using tree-based algorithms. J Mach Learn Res 15:1–21
8. Bagwell CB, Hunsberger BC, Herbert DJ, Munson ME, Hill BL, Bray CM, Preffer FI (2015) Probability state modeling theory. Cytometry A. doi:10.1002/cyto.a.22687
9. Bagwell C (2001) Data analysis through modeling. Curr Protoc Cytometry Chapter 10:Unit 10.17. doi:10.1002/0471142956.cy1007s01
10. Bagwell C (2010) Probability state modeling: a new paradigm for cytometric analysis. In: Litwin V, Marder P (eds) Flow cytometry in drug discovery and development. John Wiley and Sons Inc, Hoboken, NJ, p 281
11. Bagwell CB (2011) Breaking the dimensionality barrier. Methods Mol Biol 699:31–51. doi:10.1007/978-1-61737-950-5_2
12. Bagwell C, Hill B, Wood B, Wallace P, Alrazzak M, Kelliher A, Preffer F (2015) Human B-cell and progenitor stages as determined by probability state modeling of multidimensional

cytometry data. Cytometry B Clin Cytom 88 (4):214–226
13. Loken M, Shah V, Dattilo K, Civin C (1987) Flow cytometric analysis of human bone marrow II: normal lymphocyte development. Blood 70:1316–1324
14. Loken M, Wells D (2000) Normal antigen expression in hematopoiesis. In: Stewart C, Nicholson J (eds) Immunophenotyping. Wiley-Liss Inc, Hoboken, NJ, pp 133–160
15. Hinton G (2002) Roweis S Stochastic neighbor embedding. NIPS, In, pp 833–840
16. Yianilos PN (1993) Data structures and algorithms for nearest neighbor search in general metric spaces. Proceedings of the ACM-SIAM symposium on discrete algorithms, pp 311–321
17. Meyer SL (1975) Data analysis for scientists and engineers. John Wiley & Sons, New York, NY
18. Kullback S, Leibler RA (1951) On information and sufficiency. Ann Math Stat 22(1):79–86
19. Barnes J, Hut P (1986) A hierarchical O(N log N) force-calculation algorithm. Nature 324 (4):446–449
20. Bagwell CB, Hill BL, Herbert DJ, Bray CM, Hunsberger BC (2016) Sometimes simpler is better: VLog, a general but easy-to-implement log-like transform for cytometry. Cytometry A 89(12):1097–1105. doi:10.1002/cyto.a.23017
21. Maecker HT, McCoy JP, Nussenblatt R (2012) Standardizing immunophenotyping for the Human Immunology Project. Nat Rev Immunol 12(3):191–200. doi:10.1038/nri3158
22. Appay V, van Lier RA, Sallusto F, Roederer M (2008) Phenotype and function of human T lymphocyte subsets: consensus and issues. Cytometry A 73(11):975–983. doi:10.1002/cyto.a.20643
23. Blom B, Spits H (2006) Development of human lymphoid cells. Annu Rev Immunol 24:287–320. doi:10.1146/annurev.immunol.24.021605.090612
24. Poli A, Michel T, Theresine M, Andres E, Hentges F, Zimmer J (2009) CD56bright natural killer (NK) cells: an important NK cell subset. Immunology 126(4):458–465. doi:10.1111/j.1365-2567.2008.03027.x

Chapter 3

Mass Cytometry Assays for Antigen-Specific T Cells Using CyTOF

Dongxia Lin and Holden T. Maecker

Abstract

T Cells specific for a single antigen tend to be rare, even after expansion of memory cells. They are commonly detected by in vitro stimulation with peptides or protein, followed by staining for intracellular cytokines. In this protocol, we use CyTOF® mass cytometry to collect single-cell data on a large number of cytokines/chemokines, as well as cell-surface proteins that characterize T cells and other immune cells. We also include a method for magnetic bead enrichment of antigen-stimulated T cells, based on their expression of CD154 and CD69. Coupling magnetic enrichment with highly multi-parameter mass cytometry, this method enables the ability to dissect the frequency, phenotype, and function of antigen-specific T cells in greater detail than previously possible. Rare cell subsets can be examined, while minimizing run times on the CyTOF.

Key words Antigen-specific, Intracellular staining, Cytokines, T Cells, CyTOF, Magnetic enrichment

1 Introduction

Mass cytometry, CyTOF (Fluidigm Corporation), is based on the concept of using heavy-metal isotopes to label antibodies for flow cytometry, rather than fluorescent tags [1–3]. The isotopes are attached to the antibodies via a metal-chelating polymer, and the labeled cells are introduced sequentially into a mass spectrometer for the quantitative detection of the metal labels associated with each cell. This novel technology affords the ability to combine many more specific antibodies in a single experiment without significant spillover between detector channels.

Like conventional flow cytometry, CyTOF can be used for intracellular as well as cell-surface staining. Intracellular cytokine staining (ICS) can be done to look at the intersection of cell phenotype and function, and is often used with multiparameter flow cytometry to dissect antigen-specific T-cell responses to infection or vaccination [4]. ICS was first adapted to the CyTOF platform by Newell et al. [5], who showed the diversity of CD8+ T cell

Teresa S. Hawley and Robert G. Hawley (eds.), *Flow Cytometry Protocols*, Methods in Molecular Biology, vol. 1678, DOI 10.1007/978-1-4939-7346-0_3,

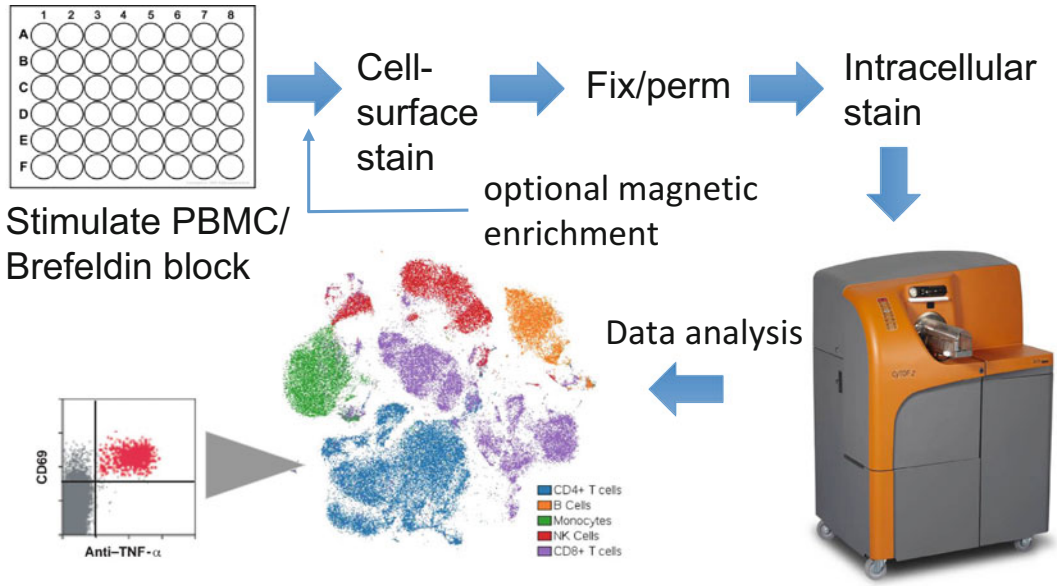

Fig. 1 Workflow for CyTOF with intracellular cytokine staining (ICS)

functions and phenotypes, which nevertheless were biased based on pathogen specificity. A general protocol for CyTOF ICS has also been published [6].

As the throughput on the CyTOF is lower than conventional flow cytometry, magnetic enrichment of target population is helpful for the analysis of rare antigen-specific T cells. The principal steps of enrichment are as follows: first, cells are activated for 4 h using specific peptides in the presence of monensin, CD107a-metal conjugate (if analyzing for CD107a in the assay [7, 8]), and either CD40 or CD154-biotin antibody [9–11]. Anti-CD28 and CD49d costimulatory monoclonal antibodies (mAbs) can be used to enhance the T-cell stimulation if desired [12]. During the first 4 h of stimulation, CD69 and CD154 accumulate on the surface of activated (antigen-responsive) cells. The addition of brefeldin A after 4 h further blocks the secretion of cytokines to allow their intracellular detection. After stimulation, EDTA is added to dislodge adherent cells from the culture plates. Next, cells are labeled with CD154-biotin (if not already in the stimulation cocktail) and CD69-biotin antibodies, followed by anti-biotin microbeads and magnetic enrichment on MS MACS columns (Miltenyi Biotec) [13]. After washing, the enriched cells are stained with antibodies to cell surface markers. The cells are then fixed in paraformaldehyde and permeabilized. We use a gentle detergent, saponin, as the permeabilization buffer because it is less destructive to surface and intracellular epitopes compared to harsh detergents or methanol. After permeabilization, the metal-conjugated anti-cytokine antibodies are added to the cell suspension. The stained cells are analyzed by the mass cytometer. A schematic of these steps is shown in Fig. 1.

2 Materials

2.1 Reagents (See Note 1)

1. Peripheral blood mononuclear cells (PBMCs).
2. Complete RPMI medium: RPMI-1640, 10% FBS, 1× Pen-strep-Glutamine.
3. ≥ 250 units/μL Benzonase® Nuclease.
4. 0.5 M EDTA.
5. PBS.
6. 5 mg/mL Brefeldin A: dissolved in dimethyl sulfoxide (DMSO) and frozen in small aliquots at −80 °C.
7. 5 mg/mL Monensin: dissolved in ethanol and stored at −20 °C (no need to aliquot since it will not freeze at −20 °C).
8. Anti-Human CD28/CD49d Costimulatory Reagent (BD Biosciences, San Jose, CA).
9. Anti-Human CD40 pure (Miltenyi Biotec, San Diego, CA).
10. Anti-Human CD154-Biotin (Miltenyi Biotec).
11. Anti-Human CD69-Biotin (Miltenyi Biotec).
12. Anti-Biotin Multisort kit (Miltenyi Biotec).
13. Cell-ID™ Cisplatin (Fluidigm Corporation, South San Francisco, CA).
14. Maxpar® Metal Conjugated Antibodies (Fluidigm Corporation) filtered with 0.1 μm spin filters (Millipore, Temecula, CA).
15. Maxpar® Cell Staining Buffer (Fluidigm Corporation).
16. 5× Maxpar® Fix I Buffer (Fluidigm Corporation).
17. Maxpar® Perm-S Buffer (Fluidigm Corporation).
18. 125 μM or 500 μM Cell-ID™ Intercalator–Ir (Fluidigm Corporation).
19. Maxpar® Fix and Perm Buffer (Fluidigm Corporation).
20. Maxpar® Water (Fluidigm Corporation).
21. (Optional) Dead Cell Removal Kit (Miltenyi Biotec).
22. (Optional) Human Fc-receptor Blocking Solution (BioLegend, San Diego, CA).

2.2 Equipment and Supplies

1. Multiwell plates: 24-well tissue culture plates, 2 mL deep well v-bottom 96-well plates (Corning Life Science, Corning, New York).
2. Pipettors: calibrated pipettors, multichannel pipettor.

3. Cell strainers: 70 μm cell strainers, tubes with cell strainer caps.
4. 30 μm Pre-separation filters (Miltenyi Biotec).
5. Biosafety cabinet.
6. CO_2 incubator at 37 °C.
7. Water bath at 37 °C.
8. Centrifuge.
9. Vi-CELL counter (Beckman Coulter, Brea, CA) or equivalent, or a microscope with hemocytometer.
10. MiniMACS separator (Miltenyi Biotec).
11. MS MACS columns (Miltenyi Biotec).
12. CyTOF®mass cytometer (Fluidigm Corporation).

3 Methods

3.1 Thawing of PBMC

1. Warm complete RPMI medium to 37 °C in water bath. Each sample will require 22 mL of medium with benzonase. Calculate the amount needed to thaw all samples, and prepare a separate aliquot of warm medium with 1:10,000 dilution of benzonase (final concentration at 25 units/mL). Benzonase is added to prevent cell aggregation. Thaw not more than three samples at a time.
2. Remove samples from liquid nitrogen and transport to a lab on dry ice.
3. Place 10 mL of warm medium with benzonase into a 15 mL tube, making a separate tube for each sample.
4. Thaw frozen vials in 37 °C water bath.
5. When cells are nearly completely thawed, carry to the biosafety cabinet.
6. Add 1 mL of warm medium with benzonase from appropriately labeled centrifuge tube slowly to the cells, and then transfer the cells to the centrifuge tube. Rinse vial with more medium from the centrifuge tube to retrieve all of the cells.
7. Continue with the rest of the samples as quickly as possible.
8. Centrifuge cells at 473 × *g* for 8 min at room temperature.
9. Remove the supernatant from the cells and resuspend the pellet by tapping the tube.
10. Gently resuspend the pellet in 1 mL of warm medium with benzonase. Filter cells through a 70 μm cell strainer if needed. Add 9 mL more warm medium with benzonase to the tube.

11. Centrifuge cells at 473 × *g* for 8 min at room temperature. Remove the supernatant from the cells and resuspend the pellet by tapping the tube.
12. Resuspend cells in 1 mL of warm medium.
13. Count cells with Vi-CELL (or hemocytometer). To count, take 20 μL of cells and dilute with 480 μL of PBS in a Vicell counting chamber. Load onto Vi-CELL as PBMC with a 1:25 dilution factor.
14. Adjust the cell concentration to 5–10 × 10^6 cells/mL with warm medium (no more benzonase at this point).
15. Using a multichannel pipettor, add 200 μL of cells (for at least 1 × 10^6 cells) into each well of a 2 mL deep-well v-bottom 96-well plate. If more cells are needed for enrichment, 24-well tissue culture plates are used for 10^7 cells in 1 mL of medium. Split each sample equally into two or more wells keeping one as an unstimulated control and the others for different types of stimulation.
16. Rest overnight (6–18 h) at 37 °C in a CO_2 incubator.

3.2 Cell Activation

For stimulation without cell enrichment, proceed to Subheading 3.2.1; for stimulation with antigen-specific T-cell enrichment, proceed to Subheading 3.2.2.

3.2.1 Without Enrichment

1. After overnight rest at 37 °C, add the activation reagents and secretion inhibitor (brefeldin A or monensin) to the well for stimulation (*see* Table 1) (*see* **Notes 2** and **3**). Add only the secretion inhibitor to the unstimulated control well. If doing CD107a staining, add CD107a antibody during the stimulation.
2. Add stimuli as directed in Table 2 (*see* **Note 4**). Incubate the cells for 4 h (PMA + ionomycin stimulation, PHA + ionomycin stimulation) or 6–8 h (SEB, anti-CD3/CD28, peptide stimulation) at 37 °C, in a CO_2 incubator (*see* **Note 5**).
3. Proceed to Subheading 3.3.

Table 1
Protein secretion inhibitors

Reagent	Stock concentration	Intermediate dilution	Final concentration
Brefeldin A	5 mg/mL in DMSO (stored in aliquots at −20 °C)	1:10 in PBS	10 μg/mL (1:50) or 5 μg/mL (1:100) with monensin
Monensin	5 mg/mL in ethanol (stored at −20 °C)	1:10 in PBS	10 μg/mL (1:50) or 5 μg/mL (1:100) with brefeldinA

Table 2
Activators

Reagent	Stock concentration	Intermediate dilution	Final concentration
Phorbol 12-myristate 13-acetate (PMA)	1 mg/mL in DMSO (stored in aliquots at −20 °C)	1:1000 in PBS	10 ng/mL
Ionomycin	1 mg/mL in DMSO (stored in aliquots at −20 °C)	1:10 in PBS	1 μg/mL
Phytohemagglutinin (PHA)	1 mg/mL in DMSO (stored at 4 °C)	1:10 in PBS	1 μg/mL
SEB	50 μg/mL in PBS	None	1 μg/mL (1:50)
Anti-CD3/CD28	Follow manufacturer instruction	–	–
Peptide mixes (JPT, Acton, MA)	0.5–1 mg/mL/pep in DMSO (stored in aliquots at −20 °C)	1:10 in PBS	1 μg/mL/peptide (1:50–1:100)

3.2.2 With Enrichment

1. After overnight rest of cells, spin down cells and remove the supernatant. Make a cocktail of the following: 1000 μL medium +1 μL monensin stock solution (final concentration at 5 μg/mL) + 10 μL CD28/CD49d co-stimulatory reagent + optimal concentration of CD107a-metal conjugate (if analyzing for CD107a) + either 20 μL CD40 Ab or optimal concentration of CD154-Biotin. Add 1 mL of this cocktail to resuspend each cell pellet. Add antigens (e.g., peptides from JPT at 1 μg/mL final concentration) or other stimuli to respective wells for stimulation (*see* **Note 6**).
2. 4 h later, add 1 μL of brefeldin A stock solution (final concentration at 5 μg/mL) to each well, mix well by pipetting, and continue to incubate for 4 h.
3. To enrich for antigen-specific cells, transfer cells from a 24-well plate to a 2 mL deep-well v-bottom 96-well plate. Spin down at 473 × *g* for 10 min at 4 °C. The same volume and centrifuge conditions are used in additional wash steps for enrichment. Flick or aspirate to remove the supernatant. Gently resuspend the pellet in 1 mL of cold Maxpar Cell Staining Buffer with pipette. Repeat wash step and centrifugation with 1 mL of cold Maxpar Cell Staining Buffer.
4. An optional dead cell removal step can be included at this step by using, for example, Dead Cell Removal Kit.
5. Make cocktail of the following: 20 μL CD69-biotin +20 μL CD154-biotin +60 μL Maxpar Cell Staining Buffer. Incubate cells with this cocktail at 4 °C for 20 min, and then wash with 1 mL of cold Maxpar Cell Staining Buffer. Spin and discard the supernatant.

6. Make cocktail of 20 μL anti-biotin microbeads +80 μL Maxpar Cell Staining Buffer. Incubate cells with this cocktail at 4 °C for 20 min, and then wash with 1 mL of cold Maxpar Cell Staining Buffer. Spin and discard the supernatant.
7. Set up magnetic columns: Use a cooled MiniMACS separator, and pre-wet pre-separation filters and MS MACS columns with 500 μL of cold Maxpar Cell Staining Buffer.
8. Resuspend cells in 1 mL of Maxpar Cell Staining Buffer, apply cell suspension through the pre-separation filters and columns at 500 μL twice; wash wells with 1 mL of Maxpar Cell Staining Buffer, and pass through the columns at 500 μL twice again.
9. Collect the flow-through containing unlabeled cells in a 15 mL tube and pass through a new column if desired. To check for carry over in the negative fraction, spin down the flow-through at 473 × *g* for 10 min at 4 °C, and proceed to later staining steps.
10. Remove the column from the magnet, put above the well of a 2 mL deep well v-bottom 96-well plate, add 500 μL of Maxpar Cell Staining Buffer into the column, and immediately flush out the magnetically labeled cells as the positive fraction by firmly pushing the plunger into the column. Repeat with 500 μL of Maxpar Cell Staining Buffer into the same or another well.
11. Spin down the cells at 473 × *g* for 10 min at 4 °C. Combine the two wells into one well (if applicable) in 1 mL of Maxpar Cell Staining Buffer. Add 20 μL of Release Reagent to dissociate the beads from cells, and incubate for 10 min at 4 °C.
12. Pass the dissociated beads and cells over a second magnetic column, collecting the flow-through (cells without beads). For details, see: https://www.miltenyibiotec.com/~/media/Images/Products/Import/0001100/IM0001122.ashx?force=1 (*see* **Note 7**).

3.3 Viability Dye and Cell-Surface Staining

1. At the end of stimulation, add EDTA to a final concentration of 2 mM and incubate for 15 min at room temperature.
2. Wash cells 2× with 500 μL of PBS per well, spin at 473 × *g* for 10 min at room temperature, and discard the supernatant. The same volume and centrifuge conditions are used in additional wash steps before fixation with PFA.
3. Resuspend cells to 1×10^7 mL^{-1} in PBS and add Cell-ID Cisplatin to a final concentration of 5 μM (1000× dilution of 5 mM stock solution).
4. Incubate at room temperature for 5 min.
5. Wash with Maxpar Cell Staining Buffer using 5× the volume of the cell suspension. Spin and discard the supernatant.

6. An optional step of Fc-blocking can be done by using, for example, Fc-Receptor Blocking Solution. Incubate for 10 min at room temperature. Without washing off Fc-Receptor Blocking solution continue to the next steps.
7. Make surface antibody cocktail in Maxpar Cell Staining Buffer and filter with 0.1 μm spin filter, 100 μL per reaction. Incubate on ice for 45 min. Use Fluidigm recommended concentration (or optimal titer as determined for self-made conjugates) for each antibody.
8. Wash 3× in Maxpar Cell Staining Buffer. Spin and discard the supernatant.

3.4 Fixation and Permeabilization

1. Resuspend cells in 1 mL of 1× Maxpar Fix I buffer (diluted in PBS) to each well. Incubate at room temperature for 10–30 min or 4 °C overnight.
2. Wash 2× with 1 mL of Maxpar Perm-S Buffer. Spin at 787 × *g* for 10 min at 4 °C and discard the supernatant. The same volume and centrifuge conditions are used in the following wash steps.

3.5 Intracellular Staining

1. Make intracellular staining cocktail in Maxpar Perm-S Buffer and filter with 0.1 μm spin filter, 100 μL per reaction. Incubate on ice for 45 min.
2. Wash 3× in Maxpar Cell Staining Buffer. Spin and discard the supernatant.
3. Resuspend cells in 1 mL of 125 nM Cell-ID Intercalation-Ir (a 1000× dilution of the 125 μM stock solution in Fix and Perm Buffer). Incubate for 1 h at room temperature or leave overnight at 4 °C.
4. Wash 2× in Maxpar Cell Staining Buffer. Spin and discard the supernatant.
5. Wash 3× in Maxpar Water. Spin and discard the supernatant.
6. Resuspend cells in Maxpar Water to a concentration of 2.5–5 × 10^5 mL^{-1}. Filter cells into tubes with cell strainer caps.
7. Acquire data on CyTOF. *See* Fig. 2 for representative data and gating.

4 Notes

1. *See* ref. 6 for suppliers and catalogue numbers of reagents used in this chapter.
2. It is important to avoid solvent toxicity. Final DMSO + ethanol concentration from all sources (peptides, brefeldin A, monensin) should not exceed 0.5%.

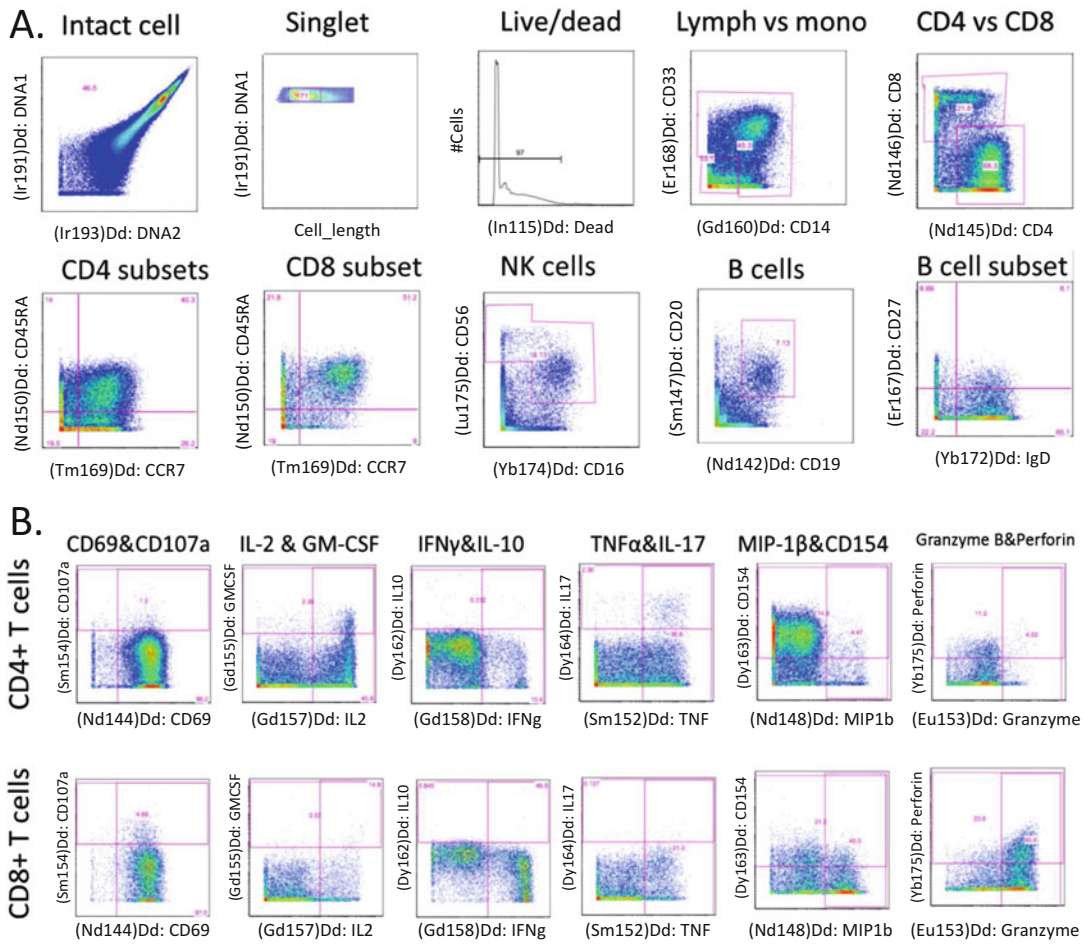

Fig. 2 Representative CyTOF ICS data. (**a**) Initial gating on intact cells, singlets, and live cells, followed by gating of major cell subsets and T-cell differentiation markers. (**b**) Representative data from intracellular cytokines, after PMA + ionomycin stimulation

3. For most cytokines: Use brefeldin A at 10 μg/mL final concentration (*see* the stock preparation table). For CD107 and CD154: Use monensin at 10 μg/mL final concentration. For assays combining cytokines and CD107 or CD154: Use brefeldin A and monensin at 5 μg/mL final concentration each.
4. Addition of costimulatory antibodies is optional. These antibodies can increase the frequency of cells responding to specific antigen. Add 1 μg/mL final concentration of CD28 and/or CD49d (labeled antibody can be used if analysis of the marker is desired).
5. For most cytokines, 6–12 h incubation at 37 °C is sufficient. For IL-10, optimal incubation time is 12–24 h, but detection in 6 h is possible.

6. The addition of staining antibodies for CD107a and CD154 allows these targets to be stained despite being only transiently expressed on the cell surface during activation. Metal-labeled antibodies are titrated in separate experiments for their optimal concentration. The amount of staining antibody should be scaled up to account for the larger (1 mL) incubation volume. Alternatively, CD40 antibody can be used during stimulation to block the interaction of CD154 with CD40, which triggers the re-uptake of CD154. The addition of monensin prevents the acidification of vesicles that might contain these stained complexes and that would otherwise lead to their degradation. *See* refs. 1–6 for details.
7. Milltenyi beads may contain barium and other heavy metals, which could interfere with detection of certain mass channels, and which could shorten detector life. We therefore recommend cleaving and separating cells from beads as described in Subheading 3.2.2 **steps 11** and **12**.

Acknowledgments

This work was supported by grants # 5U19AI057229 and S10RR027582 from the National Institutes of Health, and SFB 650 and the BCRT (FKZ 13GW0099).

References

1. Tanner SD, Bandura DR, Ornatsky O, Baranov VI, Nitz M, Winnik MA (2008) Flow cytometer with mass spectrometer detection for massively multiplexed single-cell biomarker assay. Pure Appl Chem 80(12):2627–2641. doi:10.1351/pac200880122627
2. Bandura DR, Baranov VI, Ornatsky OI, Antonov A, Kinach R, Lou X, Pavlov S, Vorobiev S, Dick JE, Tanner SD (2009) Mass cytometry: technique for real time single cell multitarget immunoassay based on inductively coupled plasma time-of-flight mass spectrometry. Anal Chem 81(16):6813–6822. doi:10.1021/ac901049w
3. Ornatsky O, Bandura D, Baranov V, Nitz M, Winnik MA, Tanner S (2010) Highly multiparametric analysis by mass cytometry. J Immunol Methods 361(1–2):1–20. doi:10.1016/j.jim.2010.07.002
4. Lovelace P, Maecker HT (2011) Multiparameter intracellular cytokine staining. Methods Mol Biol 699:165–178. doi:10.1007/978-1-61737-950-5_8
5. Newell EW, Sigal N, Bendall SC, Nolan GP, Davis MM (2012) Cytometry by time-of-flight shows combinatorial cytokine expression and virus-specific cell niches within a continuum of CD8+ T cell phenotypes. Immunity 36(1):142–152. doi:10.1016/j.immuni.2012.01.002
6. Lin DGS, Maecker HT (2015) Intracellular cytokine staining on PBMCs using CyTOF mass cytometry. Bioprotocol 5(1):1–7. doi:10.21769/BioProtoc.1370
7. Betts MR, Brenchley JM, Price DA, De Rosa SC, Douek DC, Roederer M, Koup RA (2003) Sensitive and viable identification of antigen-specific CD8+ T cells by a flow cytometric assay for degranulation. J Immunol Methods 281(1–2):65–78
8. Betts MR, Koup RA (2004) Detection of T-cell degranulation: CD107a and b. Methods Cell Biol 75:497–512
9. Chattopadhyay PK, Yu J, Roederer M (2005) A live-cell assay to detect antigen-specific CD4+ T cells with diverse cytokine profiles.

Nat Med 11(10):1113–1117. doi:10.1038/nm1293

10. Chattopadhyay PK, Yu J, Roederer M (2006) Live-cell assay to detect antigen-specific CD4+ T-cell responses by CD154 expression. Nat Protoc 1(1):1–6. doi:10.1038/nprot.2006.1
11. Frentsch M, Arbach O, Kirchhoff D, Moewes B, Worm M, Rothe M, Scheffold A, Thiel A (2005) Direct access to CD4+ T cells specific for defined antigens according to CD154 expression. Nat Med 11(10):1118–1124. doi:10.1038/nm1292
12. Bitmansour AD, Douek DC, Maino VC, Picker LJ (2002) Direct ex vivo analysis of human CD4(+) memory T cell activation requirements at the single clonotype level. J Immunol 169(3):1207–1218
13. Miltenyi S, Muller W, Weichel W, Radbruch A (1990) High gradient magnetic cell separation with MACS. Cytometry 11(2):231–238. doi:10.1002/cyto.990110203

Chapter 4

RNA Flow Cytometry Using the Branched DNA Technique

Kah Teong Soh and Paul K. Wallace

Abstract

The systematic modulation of mRNA and proteins governs the complicated and intermingled biological functions of our cells. Traditionally, transcriptomic technologies such as DNA microarray and RNA-Seq have been used to identify, characterize, and profile gene expression data. These are, however, considered bulk methods as they are unable to measure gene expression at the single-cell level, unless the cells are pre-sorted. Branched DNA is a flow cytometry-based detection platform that has been developed recently to measure mRNA at the single-cell level. Originally adapted from microscopy, the current system has been modified to achieve compatibility with the detection of surface and intracellular antigens using monoclonal antibodies conjugated to fluorochromes, thus permitting simultaneous detection of mRNAs and proteins. The Branched DNA method offers a variety of advantages when compared to traditional or standard methods used for the quantification of mRNA, such as (a) the detection of specific mRNA on a per cell basis, (b) an alternate detection tool when the measurement of a protein is technically infeasible (i.e., no quality antibody exists) or the epitope is not assessable, and (c) correlate the analysis of mRNA with protein. Compared to earlier attempts at measuring nucleic acid by flow cytometry, the hybridization temperature applied in the Branched DNA assay is much lower, thus preserving the integrity of cellular structures for further characterization. It also has greatly increased specificity and sensitivity. Here, we provide detailed instruction for performing the Branched DNA method using it in a model system to correlate the expression of CD8 mRNA and CD8 protein by flow cytometry.

Key words RNA flow cytometry, Branched DNA, CD8 protein and mRNA correlation, In-situ hybridization, Peripheral blood mononuclear cells

1 Introduction

The relationship between the expression of mRNAs and proteins during the homeostatic regulation of physiological processes and clinical manifestations of disease, such as cancer and inflammation, cannot be separated. Following the transcription of DNA, the stability and eventual translation of mRNA are regulated through a series of modifications including its exportation to the cytoplasm, splicing, capping, and the addition of poly(A) tails, serving as a switch to control the abundance of protein in cells at any given time [1, 2]. Studies by separate investigators have shown that

Teresa S. Hawley and Robert G. Hawley (eds.), *Flow Cytometry Protocols*, Methods in Molecular Biology, vol. 1678, DOI 10.1007/978-1-4939-7346-0_4,

the expression levels of mRNA and protein can be utilized as independent prognostic indicators to unravel interesting and important information associated with malignancy and viral diseases. For instance, Patterson and his group found that while both infected CD4+ T lymphocytes and CD14+ monocytes sheltered HIV, transcriptional activity was only observed in monocytes, even during late stage disease progression [3, 4]. Another example is the detection of IFN-γ mRNA in activated lymphocytes, in which the mRNA expression was found to precede protein expression by approximately 90 min [5].

There are several methods to profile gene expression including next-generation sequencing, reverse transcription polymerase chain reaction (RT-PCR), Northern blotting, and nuclease protection assays which have been historically employed for mRNA measurements. A significant limitation of these methods lies in the fact that an average value is generated. Measuring gene expression with a multiparametric technology such as flow cytometry is an attractive alternative to bulk methods because it can be used to study the intricacies within the sample. For example in neoplasia, it is extremely challenging if not impossible without cell sorting to determine if the detected mRNA originated from the tumor cells, associated stroma, or from infiltrating leukocytes as soon as the biopsy sample is homogenized. Consequently, not only can the characteristics of collected cells be distinguished on a cell-by-cell basis, but a flow-cytometric approach, being quasi-quantitative, permits the investigator to examine heterogeneity within related and unrelated cells. In addition, large number of events can be reliably collected by flow cytometry, thus generating the appropriate statistical sampling power which is especially important in rare cell event analysis.

Barbara Trask and her colleagues were the first to detect DNA by flow cytometry [6]. They cross-linked nuclear proteins using dimethylsuberimidate to prevent nuclei disintegration during denaturation and hybridization. These stabilized mouse nuclei were then hybridized with a probe specific for mouse satellite DNA sequences, which comprise approximately 10% of the total DNA in mouse nuclei. The probe had been treated with N-acetoxy-2-acetylaminofluorene (AAF) which modified approximately 20% of the guanine bases to N-(guanine-8-yl)-AAF. This was followed by an indirect immunofluorescent labeling procedure (rabbit anti-AAF followed with goat anti-rabbit Ig conjugated with rhodamine) to quantify both the amount of hybridized probe and DNA content (using Hoechst 33258) at the single-cell level. Other investigators subsequently integrated PCR with flow cytometry to improve signals by amplifying the target sequence [7, 8]. These investigators also developed a biotin-streptavidin detection system to detect surface antigens, labeling before the PCR a cell surface epitope with a biotinylated antibody and then detecting with a fluorescently

labeled streptavidin after the PCR. Early efforts to detect RNA used a fluorescence in situ hybridization (FISH) approach. Patterson et al. employed a cocktail of different 5-carboxyfluorescein-labeled oligonucleotide probes which in aggregate hybridized to the majority of expressed HIV RNAs [4]. They combined this with the previously mentioned biotin-streptavidin detection system to phenotype the cells. Studies from Alan Waggoner's lab [9] were the first to detect multiple RNA species using three different 5′ cyanine-labeled oligodeoxynucleotides probes (e.g., Cy5.18, Cy3.18, and OCy3) to simultaneously detect Histone H4 mRNA, 18S rRNA, and 28S rRNA in HeLa cells.

Unfortunately, these early successes to measure nucleic acid by flow cytometry presented several impediments to progress. First, success was limited to the detection of nucleic acids that were highly abundant and repetitive in nature. A second major problem with this approach was the increased autofluorescence caused by the high temperatures required for annealing and hybridization and then the subsequent loss of scatter characteristics. Third, the PCR protocol compromised the fluorochromes used for detection of surface antigens. Finally, the use of the biotin-streptavidin detection system restrained the immunophenotyping to just one antigenic determination at a time.

In early 2010, two microscopy-based mRNA detection platforms were adapted to flow cytometry allowing a correlated determination of mRNA and protein. The SmartFlare™ (EMD Millipore) system employs gold nanoparticles conjugated to oligonucleotides with specificity complementary to an mRNA of interest. Bound to the complementary oligonucleotide strand is a short fluorescently labeled reporter strand whose fluorescence is quenched by the gold nanoparticle. When placed into culture with cells, the gold nanoparticles are taken into the cytoplasm, a process dependent entirely on the endocytic machinery of the cell. If the mRNA of interest is present inside the cell, it will displace the lower-affinity fluorescently tagged reporter strand from the complementary oligonucleotide. Consequently, the reporter oligonucleotide is no longer quenched and the emitted fluorescence can be detected by the flow cytometer. To date, the SmartFlare™ system is the only methodology known to work with live cells for sorting and subsequent downstream assay but it is limited to only Cy3 and Cy5 fluorescent probes.

Alternatively, PrimeFlow™ (Thermo Fisher Scientific), generically referred to here as the "Branched DNA" method, can be used to determine the differential mRNA expression within a heterogeneous population of cells. Originally adapted from microscopy, the current system has been modified to achieve compatibility with the detection of selected antigens using monoclonal antibodies (mAb) conjugated to fluorochromes, thus permitting simultaneous detection of mRNA and protein at the single-cell level. In brief, cells are

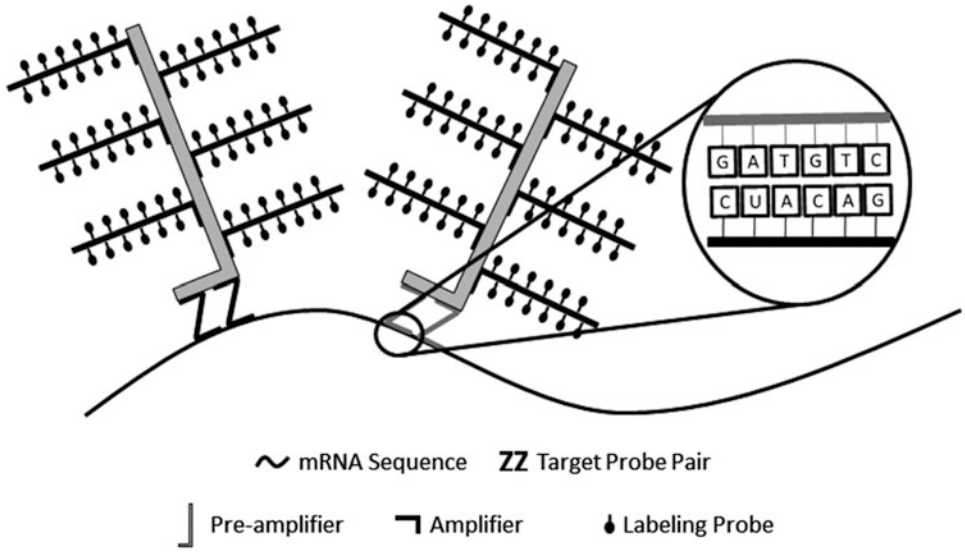

Fig. 1 Target Probes hybridization and signal amplification of mRNA using the Branched DNA assay. Fixed and permeabilized cells are sequentially exposed to and hybridized with Target Probe Pairs, Pre-Amplifiers, Amplifiers, and Labeling Probes at 40 ± 1 °C. Washing steps are performed in between each of the hybridization steps to remove un-hybridized material. In order for signal amplification to occur, each pair of Target Probes must first hybridize adjacent to one another on the mRNA sequence, so that the Pre-Amplifier can anneal stably. Each individual Target Probe consists of approximately 18–25 DNA bases with unique specificity for the mRNA sequence to be detected. A targeted mRNA sequence with 1,000 bases can accommodate up to 20 different pairs of Target Probes, thus serving as the foundation for the initial signal amplification. The un-hybridized sequence of each Target Probe Pair is complementary to the Pre-Amplifier sequence, adding another layer of specificity. Next, approximately 20 Amplifier sequences hybridize to each Pre-amplifier sequence, followed by the hybridization of multiple fluorescent Label Probes to each Amplifier molecule. An optimally assembled Branched DNA complex provides a theoretical 8000- to 16,000-fold signal amplification of the targeted mRNA

initially fixed and permeabilized using a proprietary "Fixation Buffer" to preserve mRNA transcripts (Fig. 1). The sample is then exposed to the first hybridization step, during which a pair of mRNA-specific oligonucleotide Target Probes are annealed to a sequence, approximately 50 base pairs in length, on the target mRNA of interest. An mRNA sequence with 1,000 bases can accommodate up to 20 different pairs of Target Probes, which serve as the foundation for signal amplification. To increase the specificity of the assay, each pair of Target Probes must hybridize in close proximity to each other before signal amplification can occur. The specificity is insured by the addition of "Pre-Amplifiers", as these molecules will only form a stable complex when both Target Probes have hybridized appropriately. The detection system is further magnified using "Amplifiers", which hybridize to multiple sites on each "Pre-Amplifier". Finally, multiple "Label Probe" oligonucleotides conjugated to either Alexa Fluor® 488, Alexa Fluor®

647, or Alexa Fluor® 750 are hybridized to multiple sites on each "Amplifier". An optimally assembled Branched DNA complex can provide a theoretical 8,000- to 16,000-fold signal amplification of the targeted mRNA.

The advent of these flow cytometry-based mRNA detection platforms allows for many determinations that were previously unachievable. Notably, this technology enables the correlation of measurements between mRNA transcripts and antigen expression at the single-cell level, as well as to label cell targets for which antibody reagents do not exist. In this chapter, we detail the instruction for performing the Branched DNA method to correlate the expression of CD8 mRNA and protein by flow cytometry as our model system. We discuss extensively within the "Notes" section tips and techniques for a successful experiment, including the basics of sample preparation, quality control, analysis strategies, and precautions that must be considered to prevent adverse experimental outcomes.

2 Materials

2.1 Supplies and Reagents

1. Suitable biological specimens such as a cell line, EDTA, or sodium heparin anti-coagulated human peripheral blood or bone marrow. Store blood/bone marrow samples at room temperature for not more than 48 h before use.
2. Unless otherwise specified, all of the following reagents are a component of the PrimeFlow RNA kit (Affymetrix/eBioscience, Division of Thermo Fisher Scientific, Santa Clara, CA).
   (a) 1.5-mL Branched DNA Microcentrifuge Labeling Tubes (*see* **Note 1**).
   (b) Branched DNA Fixation Buffer 1A (2×) and Branched DNA Fixation Buffer 1B (2×). Store at 2–8 °C until use. Prepare fresh 1× Fixation Buffer by mixing equal volume of Fixation Buffer 1A and Fixation Buffer 1B. Gently mix the solution by inverting the dilution container and avoid vortexing. Diluted buffer solution is stable at 2–8 °C for not more than 1 day.
   (c) Molecular Grade DNase-, RNase-, and Protease-Free Water (Corning, Manassas, VA).
   (d) Branched DNA Permeabilization Buffer (10×). Store at 2–8 °C until use. Dilute 10× Permeabilization Buffer with Molecular Grade DNase-, RNase-, and Protease-Free Water to yield a final concentration of 1× Permeabilization buffer. Store diluted buffer at 2–8 °C. Diluted buffer solution is stable at 2–8 °C for 1 day.

(e) Branched DNA Wash Buffer.

(f) Branched DNA Fixation Buffer 2 (8×). Store at 2–8 °C until use. Before use, warm 8× Fixation Buffer 2 and Branched DNA Wash Buffer to room temperature. Prepare 1× Fixation Buffer 2 by diluting 8× Fixation Buffer 2 with per-warmed Branched DNA Wash Buffer to yield a 1× Fixation Buffer. Diluted buffer is stable at room temperature for up to a day.

(g) Branched DNA Target Probe Diluent. Store at 2–8 °C until use.

(h) Branched DNA PreAmp Mix. Store at 2–8 °C until use.

(i) Branched DNA Amp Mix. Store at 2–8 °C until use.

(j) Branched DNA Label Probe Diluent. Store at 2–8 °C until use.

(k) Branched DNA Storage Buffer. Store at 2–8 °C until use.

(l) RNase Inhibitor 1 (1,000×). Store at −20 °C until use. Dilute the stock solution using either 1× Permeabilization Buffer or Wash Buffer, depending on the step to a final concentration of 1× RNase Inhibitor. Keep the diluted RNase Inhibitor at 2–8 °C for no longer than 1 day.

(m) RNase Inhibitor 2 (100×). Store at −20 °C until use. Dilute the stock solution using either 1× Permeabilization Buffer or Wash Buffer, depending on the step to a final concentration of 1× RNase Inhibitor. Keep the diluted RNase Inhibitor at 2–8 °C for no longer than 1 day.

(n) Branched DNA Label Probe (100×). Store at −20 °C until use and minimize exposure to light (*see* **Note 2** for a discussion on available detection probes).

(o) Positive Control Target Probe Sets (20×) for the detection of RPL13A housekeeping gene using AX488, AX647, or AX750 fluorescence probes. Store at −20 °C until use.

(p) Target Probe(s) specific to CD8a mRNA (100×) (*see* **Note 3**).

3. PrimeFlow™ Compensation Kit (Affymetrix/eBioscience).
4. 12 × 75 mm Polystyrene Tubes compatible with flow cytometer used for sample acquisition.
5. Appropriate 15- and 50-mL Conical Centrifuge Tubes as required for the preparation of biological specimens and buffers.
6. Lymphocyte Separation Medium (LSM) (GE Healthcare, Mississauga, ON) or equivalent Ficoll Hypaque reagent.

Table 1
Fluorochrome-conjugated mAbs utilized in this study

Antibody Specificity	Murine isotype	Format	Clone	Source
CD3	$IgG_{1,k}$	PE	SK7	BD Biosciences
CD8	$IgG_{1,k}$	BUV395	RPA-T8	BD Biosciences
CD8	$IgG_{1,k}$	BV421	RPA-T8	BioLegend
CD8	$IgG_{1,k}$	BV510	RPA-T8	BioLegend
CD8	$IgG_{1,k}$	BV605	RPA-T8	BioLegend
CD8	$IgG_{1,k}$	AX488	SK1	BioLegend
CD8	$IgG_{1,k}$	PE	RPA-T8	BioLegend
CD8	$IgG_{1,k}$	PECy5	RPA-T8	BD Biosciences
CD8	$IgG_{1,k}$	PECy7	RPA-T8	BioLegend
CD8	$IgG_{1,k}$	AX647	SK1	BioLegend
CD8	$IgG_{1,k}$	APCH7	SK1	BD Biosciences
CD28	$IgG_{1,k}$	PE	CD28.2	BD Biosciences
CD45RA	$IgG_{2b,k}$	PE	HI100	BioLegend
CD197	$IgG_{2a,k}$	PE	G043H7	BioLegend
T-bet	$IgG_{1,k}$	PE	eBio4B10	eBioscience

7. Hanks' Balanced Salt Solution (HBSS; magnesium, calcium, and phenol free).
8. Fluorochrome-conjugated monoclonal antibody (mAb). *See* Table 1 for a complete list of mAb used in this chapter.
9. Flow Cytometry (FCM) buffer: Phosphate-Buffered Saline with 5 g/L Bovine Serum Albumin, 1 g/L sodium azide, and 0.04 g/L disodium ethylenediaminetetraacetate. Store at 2–8 °C until use.
10. 10% Formaldehyde, methanol free, Ultra Pure. To prepare 2% formaldehyde, dilute 1 part of 10% formaldehyde with 4 parts of Dulbecco's Phosphate Buffered Saline (calcium and magnesium free).
11. Human IgG Fc Block Solution: 12 mg/mL γ-Globulins from human blood (Sigma Aldrich, St. Louis, MO) diluted in RPMI 1640.

2.2 Equipment

1. Flow Cytometer equipped with excitation lasers and detector configurations used for collecting fluorescence signals emitted by Alexa Fluor® 488, Alexa Fluor® 647, Alexa Fluor® 750, as well as for the detection of fluorochromes conjugated to the mAb of interest. In our experiments, an LSRFortessa (BD Biosciences) flow cytometer equipped with 355 nm (60 mW) UV laser, 405 nm (50 mW) violet laser, 488 nm (50 mW) blue laser, and 640 nm (40 mW) red laser was utilized for the acquisition of all the experiments in this chapter. Performance of the instrument is monitored daily using Cytometer Setup and Tracking Beads (BD Biosciences).
2. Horizontal Air Flow or Hybridization Oven capable of achieving and maintaining a temperature of 40 ± 1 °C (Affymetrix/eBioscience).
3. Digital NIST-traceable thermometer capable of accurately measuring temperatures at 40 °C (Affymetrix/eBioscience).
4. Modular Heat Sink for Microcentrifuge Tubes (VWR, Radnor, PA).
5. Vacuum or other aspiration devices.
6. Manual or automated cell counting device. In our experiments, an AcT Diff (Beckman Coulter, Miami, FL) was used.
7. Centrifuge with swinging bucket for 1.5-mL microcentrifuge tubes (e.g., Sorvall™ Legend™ XT/XF Centrifuge Series, Thermo Fisher Scientific).

3 Methods

Using the Branched DNA assay, the expression of any mRNA transcript produced by a cell can be detected by conventional flow cytometer. A Branched DNA Target Probe set is typically designed to detect a 1,000 base pair sequence using at least 20 oligonucleotide pairs that hybridize to the target mRNA transcript. As discussed in the introduction there are currently three Alexa-conjugated fluorochromes available for detection. When a new Target Probe is being designed, it is desirable to use Alexa Fluor® 647 which has the best signal-to-noise resolution on conventionally configured flow cytometers. Temperature optimization is another important step to be considered prior to the initiation of the experiments, as any temperature outside of 40 ± 1 °C will fail. In our experience, a typical full-length Branched DNA assay will require a minimum of 10 h to complete, and the length of time will increase as the number of experimental samples and variables are increased. The inclusion of cell surface and intracellular labeling steps will add an additional 1.5–2.5 h to the procedure. In this chapter, we describe two steps where the assay can be paused overnight.

3.1 Validation of Hybridization Oven

One of the major advantages of using the Branched DNA assay for the measurement of mRNA is the preservation of cellular architecture. This is accomplished by using a much lower annealing temperature (40 ± 1 °C) than typically required for traditional PCR hybridization methods. In order to achieve an optimal signal-to-noise ratio while reducing non-specific hybridization, it is extremely important to establish and maintain the temperature of the hybridization oven at 40 ± 1 °C (*see* **Note 4**). A milled aluminum heat sink should be used to facilitate the heat conduction to the microcentrifuge labeling tube, so that the reaction mixtures can equilibrate to the obligatory temperature as rapidly as possible. A NIST-traceable temperature probe is employed to allow for accurate monitoring of temperature during the calibration procedures.

3.1.1 Temperature Adjustment and Validation

1. Set the hybridization oven to 40 °C, and place the milled aluminum heat sink in the chamber center.
2. Allow the temperature to equilibrate overnight (*see* **Note 5**).
3. Drill a hole in the lid of a Branched DNA microcentrifuge tube to accommodate the temperature probe and add 200 μL of the Branched DNA Target Probe Diluent to the tube.
4. Insert the temperature probe through the hole and into the diluent sealing the microcentrifuge tube with laboratory parafilm.
5. After overnight temperature equilibration, insert the microcentrifuge tube into the pre-warmed heat sink and immediately close the door of the hybridization oven.
6. Record the temperature every minute for 10 min.
7. If the oven has not equilibrated to 40 °C, adjust the thermostat control and repeat **steps 5**–**7**.

3.1.2 Temperature Ramp-Up Time

1. After the temperature of the oven has been calibrated to maintain 40 ± 1 °C, use the 1.5-mL microcentrifuge tube prepared in **step 3** of Subheading 3.1.1 to assess the temperature ramp-up time.
2. Open the incubator door for 1 min, then place the 1.5-mL tube containing 200 μL of Target Probe Diluent at room temperature into the heat sink and close the door.
3. Record the temperature every minute for 10 min to determine the time required for the temperature to return and maintain 40 ± 1 °C.
4. Repeat this process at least one more time.
5. Do not use the hybridization oven if it takes longer than 5 min to return to 40 °C or if it overshoots the set point temperature by more than 2 °C during this process.

3.2 Preparation of Mononuclear Cells from Human Blood or Bone Marrow Specimens

Mononuclear cells are prepared by conventional Ficoll Hypaque density gradient centrifugation [10, 11]. It is important to keep in mind that the detection of mRNA in cells can be easily compromised if precaution is not taken, as the ubiquitous presence of RNases can readily degrade target mRNA of interest. For this reason, one should always be wearing gloves along with other suitable Personal Protection Equipment when working with mRNA. Commercially available RNase inactivating agents can be used to treat bench top surfaces and glassware to remove RNases and RNase-free reagents should be used throughout the procedure. When preparing biological specimens for experiments, fresh tissue samples are always preferred and should be kept cold (4–8 °C) or on ice to preserve the mRNA integrity.

1. Collect human peripheral blood or bone marrow into suitable blood collection tubes containing either EDTA or sodium heparin.
2. Combine equal volumes of HBSS and blood or bone marrow. Gently mix the tube by inversion.
3. Gradually overlay 2 parts of the diluted sample on top of 1 part of Ficoll. Be careful not to mix the layers (*see* **Note 6**).
4. Centrifuge the cells at 400 × *g* for 30 min with no brake applied.
5. Collect the mononuclear cells at the interphase between plasma and Ficoll into a separate conical tube, and add ice-cold HBSS to obtain a 5× final total volume.
6. Centrifuge the cells at 800 × *g* at 4–8 °C for 10 min and discard the supernatant. Resuspend the cells in ice-cold HBSS and centrifuge the cells at 800 × *g* at 4–8 °C for 5 min.
7. Discard the supernatant. Resuspend the cells to 1 mL with ice-cold HBSS.
8. Perform a cell count and adjust the cell density to 1–5 × 10^7 cells/mL by adding an appropriate amount of ice-cold HBSS.
9. Keep the cells on ice until use.

3.3 Measurement of Housekeeping β2M and RPL13A mRNAs in Human Peripheral Blood Mononuclear Cells

Housekeeping genes are essential for the maintenance of basal cellular functions and are therefore expected to be expressed at high levels in cells under normal and patho-physiological conditions. Since their expression is usually in a steady state, housekeeping mRNAs are convenient controls that can be used in the Branched DNA assay to verify if the procedure has been executed correctly. The expression level of a control candidate housekeeping gene should be validated prior to use, as their expression levels can vary (i.e., the expression of mRNA can increase or decrease) depending on tissue types and experimental conditions.

Table 2
Experimental layout for the measurement of housekeeping β2M and RPL13A in human peripheral blood mononuclear cells

Tube number	Tube description	488 nm laser AX488 B530/30	640 nm laser AX647 R670/14	640 nm laser AX750 R780/60
1	No target probe control[a]	–	–	–
Experimental tube				
2	Test articles	β2M (m)[b]	–	–
3		–	β2M (m)	–
4		–	–	β2M (m)
5		RPL13A (m)	–	–
6		–	RPL13A (m)	–
7		–	–	RPL13A (m)

– Denotes either mRNA target probes or fluorochrome-conjugated antibodies were not added
[a]Samples are processed through the Branched DNA procedure without addition of mAbs or target probes
[b](m): Denotes the detection of mRNA

In the Branched DNA assay, the expression of housekeeping mRNAs can be used as an internal control to circumscribe cells that have undergone successful hybridization. The specific staining of a housekeeping gene or any mRNAs is differentiated from background by establishing the cells autofluorescence using a No Target Probe Control, in which cells are treated with all Branched DNA reagents with the exclusion of Target Probes.

In the protocol below, we described a complete Branched DNA procedure to label the expression of housekeeping β2M and RPL13A mRNAs in human peripheral blood, as a model system and to contrast the Probe Sets. The experimental design can be found in Table 2. The results shown in Fig. 2 illustrate the Type 1 AX647 Probe Set intensity is brighter than either Type 4 AX488 or Type 6 AX750 Probe Set for β2M and RPL13A mRNAs.

3.3.1 Fixation, Permeabilization, Target Probes Hybridization, and Signal Amplification

1. Transfer 100 μL (1–5 × 10^6 cells) of the prepared cell suspension into pre-labeled microcentrifuge tubes.
2. Prepare 1× Fixation Buffer 1 by mixing equal volumes of 2× Fixation Buffer 1A with 2× Fixation Buffer 1B. Gently invert the suspension several times (*see* **Note 7**).
3. Add 1 mL of 1× Fixation Buffer 1 to each microcentrifuge tube, cap the tubes, and invert several times to mix. Incubate samples for 30 min on ice.
4. Centrifuge fixed samples at 800 × *g* for 5 min.

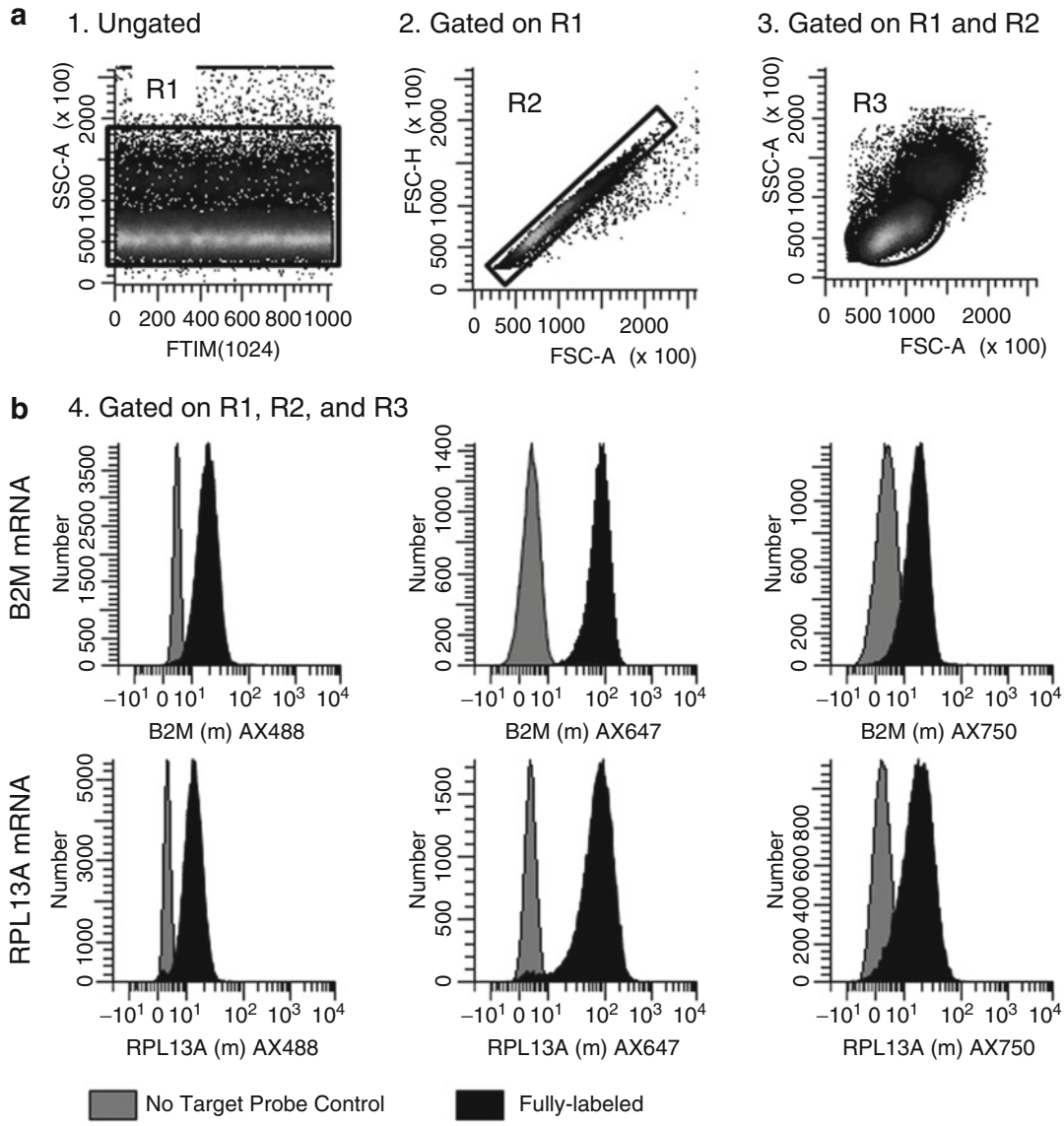

Fig. 2 Measurement of housekeeping B2M and RPL13A mRNAs in human lymphocytes comparing AX488, AX647, and AX750 detection systems. (**a**) Gating strategy used to identify lymphocytes. *A1*. A rectangular region (R1) is created on a bivariate plot of FTIM (event chronology) vs. SSC-A to review acquisition uniformity and to exclude air bubbles, clogs, etc. *A2*. A rectangular region (R2) is created on a gated (R1) bivariate plot of FSC-A vs. FSC-H to circumscribe the singlet-cell population. *A3.* An elliptical region (R3) is created on a gated (R1 and R2) bivariate plot of FSC-A vs. SSC-A to circumscribe cellular events with lymphocyte scatter characteristics. (**b**) Measurement of β2M and RPL13A mRNAs using AX488, AX647, or AX750 as the detection system. *B4*. Single-parameter histograms are gated on R1, R2, and R3. The positive expression (*black histograms*) and autofluorescence (*gray histograms*) of β2M and RPL13A are detected using AX488 (Type 4 probe set), AX647 (Type 1 probe set), or AX750 (Type 6 probe set). The tests articles used for the generation of autofluorescent signals were processed by exposing the cells to all Branched DNA reagents except the Target Probes

5. Remove the supernatant by careful vacuum aspiration leaving 100 µL of buffer. Resuspend the cells in residual buffer (*see* **Note 8**).
6. Prepare 1× Permeabilization Buffer with RNase Inhibitors. First dilute 10× Permeabilization Buffer to 1× with RNase-free water. Then add RNase Inhibitor 1 (1,000×) at a 1:1,000 dilution and RNase Inhibitor 2 (100×) at a 1:100 dilution. For example, to make 50 mL of 1× Permeabilization Buffer add: 5 mL of 10× Permeabilization Buffer, 45 mL of RNase-free water, 50 µL of 1,000× RNase Inhibitor 1, and 500 µL of 100× RNase Inhibitor 2. Gently mix the solution by inversion and store the Permeabilization Buffer on ice when not in use (*see* **Note 9**).
7. Add 1 mL of 1× Permeabilization Buffer with RNase Inhibitors to each sample. Cap and invert tubes several times to mix, centrifuge at 800 ×*g* for 5 min, aspirate the supernatant to the 100 µL mark, and resuspend cells in the residual fluid.
8. Repeat **step 7** for a total of two washes.
9. Prepare 1× Fixation Buffer 2 by combining 1 part of 8× Fixation Buffer 2 with 7 parts of Wash Buffer. Mix this suspension gently by inversion (*see* **Note 10**).
10. Add 1 mL of 1× Fixation Buffer 2 to each sample. Cap the tubes and invert several times to mix. Incubate the samples for 60 min in the dark at room temperature.
11. Centrifuge fixed samples at 800 × *g* for 5 min, and then aspirate all but 100 µL of the supernatant. Resuspend cells in the residual fluid.
12. Add 1 mL of Wash Buffer to each sample. Cap, invert to mix, centrifuge at 800 × *g* for 5 min, and aspirate all but 100 µL of supernatant and resuspend cells in the residual fluid.
13. Repeat **step 12** (Optional stopping point; *see* **Note 11**).
14. Thaw Target Probes, including Positive Control Probe, and maintain at room temperature.
15. Pre-warm Target Probe Diluent to 40 °C.
16. Dilute Target Probes 1:20 in Target Probe Diluent. Mix thoroughly by pipetting several times (*see* **Note 12**).
17. Add 100 µL of diluted Target Probe directly to the cell suspension for the appropriate samples and vortex briefly to mix. Incubate samples for 2 h at 40 ± 1 °C, inverting samples to mix after 1 h (*see* **Note 13**).
18. Add 1 mL of Wash Buffer to each sample. Cap, invert to mix, and centrifuge at 800 × *g* for 5 min. Aspirate all but 100 µL of supernatant and resuspend cells in the residual fluid (Optional stopping point; *see* **Note 14**).

19. Repeat **step 18** twice, for a total of three washes (*see* **Note 15**).
20. Pre-warm the PreAmp Mix, Amp Mix, and Label Probe Diluent to 40 ± 1 °C.
21. Add 100 µL of PreAmp Mix directly to the cell suspension in each tube, briefly vortex to mix, and incubate for 1.5 h at 40 ± 1 °C (*see* **Note 16**).
22. Add 1 mL of Wash Buffer to each sample. Cap, invert to mix, and centrifuge at 800 × *g* for 5 min. Aspirate all but 100 µL of supernatant and resuspend cells in the residual fluid.
23. Repeat **step 22** for a total of two washes.
24. Thaw Label Probes on ice and in the dark.
25. Add 100 µL of Amp Mix directly to the cell suspension in each tube, briefly vortex to mix, and then incubate for 1.5 h at 40 ± 1 °C (*see* **Note 16**).
26. Add 1 mL of Wash Buffer to each sample, invert to mix, and centrifuge at 800 × *g* for 5 min. Aspirate all but 100 µL of supernatant and resuspend cells in the residual fluid.
27. Repeat **step 26** for a total of two washes.
28. Dilute 1 part of 100× Label Probe (100×) with 99 parts of Label Probe Diluent.
29. Add 100 µL of diluted Label Probe directly to the cell suspension for each sample. Cap, briefly vortex to mix, and then incubate for 1 h at 40 ± 1 °C.
30. Add 1 mL of Wash Buffer to each sample. Cap, invert to mix, and centrifuge at 800 × *g* for 5 min. Aspirate all but 100 µL of supernatant and resuspend cells in the residual fluid.
31. Repeat **step 30** for a total of two washes.
32. Add 1 mL of FCM buffer or if storing overnight Branched DNA Storage Buffer to each sample. Cap, invert to mix, and centrifuge at 800 × *g* for 5 min. Aspirate all but 100 µL of the supernatant.
33. Resuspend cells in 500 µL of FCM buffer or Branched DNA Storage Buffer, transfer samples to 12 × 75 mm polystyrene tubes, and acquire samples on the flow cytometer (*see* **Note 17**).

3.3.2 Instrument Setup and Data Acquisition

1. Excite the fluorochrome Alexa Fluor® 488 using a 488 nm laser. Collect its emission using a suitable bandpass filter (e.g., 530/30 nm or equivalent). The peak emission of Alexa Fluor® 488 is at approximately 519 nm.
2. Excite the fluorochrome Alexa Fluor® 647 using a 633 nm (or 640 nm) laser. Collect its emission using a suitable bandpass filter (e.g., 670/14 nm or equivalent). The peak emission of Alexa Fluor® 647 is at approximately 668 nm.

3. The fluorochrome Alexa Fluor® 750 can be excited suboptimally when using a conventionally equipped red laser (e.g., 633 nm or 640 nm lasers). Collect its emission using a suitable bandpass filter (e.g., 780/60 nm or equivalent). For optimal excitation, a far-red laser with approximately 750 nm excitation is required.
4. For each detection channel, set the voltage such that the autofluorescence of the No Target Probe Control (e.g., cells that had been exposed to a complete Branched DNA assay, except no Target Probes are added to this control tube) should accumulate beyond the origin and within the first decade of the histogram.
5. Manually adjust the threshold value for forward scatter area prior to the acquisition of each sample to minimize the collection of debris and dead cells. For each sample, collect a minimum of 50,000 events. When setting the number of events to be recorded, consider the frequency of cellular subpopulation (s) of interest and adjust upward to ensure a meaningful statistical analysis (*see* **Note 18**).

3.3.3 Gating Strategy and Analysis

1. Generate the following bivariate plots and single-parameter histograms as per Fig. 2 using a flow cytometry data analysis software package such as WinList (Verity Software House, Topsham, ME), FlowJo (FlowJo, LLC, Ashland, OR), and FCS Express (De Novo Software, Glendale, CA):

   Figure 2a1 Time vs. SSC-A.

   Figure 2a2 FSC-A vs. FSC-H.

   Figure 2a3 FSC-A vs. SSC-A.

   Figure 2b4 Single-Parameter Histograms for AX488, AX647, and AX750.
2. To ascertain the quality of the data acquisition, place a rectangular region (R1) on the bivariate plot of FTIM vs. SSC-A to circumscribe the events collected in continuity. This dot plot can be used to eliminate any air bubbles or problems which occur during the run.
3. On the bivariate plot of FSC-A vs. FSC-H, create a rectangular region (R2) to include the singlet cell population. Gate this bivariate histogram on (R1).
4. On the bivariate plot of FSC-A vs. SSC-A, create an elliptical region (R3) to circumscribe the cell population of interest and exclude doublets, debris, and apoptotic events. Gate this bivariate histogram on (R1 and R2). For this example, a lymphocyte region is used.

Table 3
Experimental design testing different labeling strategies to create the Branched DNA compensation matrix

Compensation strategy	Single color	AX488	AX647	AX750
A. mRNA labeled by branched DNA procedure	Unlabeled	–	–	–
	AX488	RPL13A (m)[a]	–	–
	AX647	–	RPL13A (m)	–
	AX750	–	–	RPL13A (m)
B. PrimeFlow™ compensation kit	Unlabeled	–	–	–
	AX488	AX488 beads	–	–
	AX647	–	AX647 beads	–
	AX750	–	–	AX750 beads
C. mAbs and mRNA labeled by branched DNA procedure	Unlabeled	–	–	–
	AX488	CD8 (p)[b]	–	–
	AX647	–	CD8 (p)	–
	AX750	–	–	RPL13A (m)
D. mAbs labeled by standard immunophenotyping procedure & mRNA labeled by branched DNA procedure	Unlabeled	–	–	–
	AX488	CD8 (p)	–	–
	AX647	–	CD8 (p)	–
	AX750	–	–	RPL13A (m)

– Denotes either the mRNA target probes or fluorochrome-conjugated antibodies were not added
[a](m): Denotes the detection of mRNA
[b](p): Denotes the detection of protein

5. Analyze the expression of B2M mRNA and RPL13A mRNA for each detection channel (e.g., Alexa Fluor® 488, Alexa Fluor® 647, and Alexa Fluor® 750) using single-parameter histograms that are gated on (R1–R3).

3.3.4 Compensation of Fluorescence Signals Using PrimeFlow Compensation Kit

A proper compensation of fluorescence signal is an important aspect to be considered in virtually any multi-color flow cytometry experiment. Properly compensated data is important when determining the frequency of a cell population and is critical for the accurate measurement of antigen and mRNA densities (e.g., geometric mean fluorescence intensity). The compensation setup described below utilizes the bead-based PrimeFlow Compensation Kit (*see* **Note 19**). For a comparison of compensation matrices generated using different compensation strategies, *see* Tables 3 and 4.

Table 4
Compensation matrices values for the different compensation strategies tested in Table 3

Signal	Into B530/30	B575/26	R670/14	R730/45	R780/60
A. mRNA labeled by Branched DNA procedure					
RPL13A (m) AX488	100.00	21.18	15.87	7.09	10.01
RPL13A (m) AX647	1.69	0.12	100.00	44.11	42.21
RPL13A (m) AX750	3.86	1.40	13.31	11.33	100.00
B. PrimeFlow™ compensation kit					
Beads AX488	100.00	21.17	0.01	0.00	0.02
Beads AX647	0.00	0.01	100.00	45.30	41.13
Beads AX750	0.02	0.08	0.49	2.85	100.00
C. mAbs and mRNA labeled by branched DNA procedure					
CD8 (p) AX488	100.00	22.82	5.61	3.29	5.61
CD8 (p) AX647	0.49	0.53	100.00	42.70	38.36
RPL13A (m) AX750	0.28	0.00	8.69	6.24	100.00
D. mAbs labeled by standard immunophenotyping procedure & mRNA labeled by branched DNA procedure					
CD8 (p) AX488	100.00	21.54	0.10	0.03	0.13
CD8 (p) AX647	0.11	0.07	100.00	42.21	38.33
RPL13A (m) AX750	0.00	0.00	8.29	7.23	100.00

1. Separately label as many 12 × 75 mm polystyrene tubes as required for the compensation of each fluorochrome used in the experiment, for the detection of either mRNA or protein targets (*see* **Note 20**).
2. Vigorously mix the beads by vortexing for a few seconds.
3. Dispense 1 drop of the beads to each labeled tube.
4. For each mRNA target, add 5 μL of the appropriate RNA Compensation Control (as provided by the kit) to the appropriate tube. For each fluorochrome-conjugated mAb, add a saturating amount of mAb to the corresponding tube.
5. Vortex the tubes briefly to mix and incubate at 2–8 °C for 20 min. Protect the beads from prolonged exposure to light.
6. Add 2 mL of FCM buffer to each tube and centrifuge at 800 × *g* for 5 min.
7. Discard the supernatant and vortex briefly to resuspend beads in residual buffer.

8. Add 100 μL of fixation reagent to each tube and incubate at room temperature for 15 min. If desired, beads may be stored in fixation buffer at 2–8 °C for a maximum of 3 days.
9. Add 2 mL of FCM buffer to each tube and centrifuge at 800 × *g* for 5 min.
10. Discard the supernatant and resuspend the beads with 500 μL of FCM buffer.
11. After optimizing the flow cytometer's voltages (*see* Subheading 3.3.2), individually acquire each tube and create a compensation matrix using the software embedded in the acquisition program. *See* Table 4B for an example of a PrimeFlow Compensation Kit compensation matrix.

3.4 Simultaneous Measurement of mRNA and Protein Using the Branched DNA Method

Traditional strategies employed for the measurement of mRNA such as PCR will generate an average value because they are bulk methods unless the cells are pre-sorted. As a result, a direct correlation between mRNA and protein can be technically challenging, and the actual expression levels may be underestimated or obscured by contaminating and irrelevant cells. Originally adapted from microscopy, the current version of the Branched DNA assay has been modified to achieve compatibility with the detection of surface and intracellular proteins. This enables the correlation of mRNA and protein at the single-cell level. Before starting an experiment, caution should be taken to ensure that the phenotyping reagents and antibodies are compatible with the Branched DNA assay (*see* Subheading 3.5 for more details on the compatibility of fluorochrome choices with the Branched DNA assay).

3.4.1 Labeling of Surface Antigen Using the Branched DNA Assay

1. Prepare PBMCs using Ficoll Hypaque density gradient centrifugation or other suitable techniques as discussed in Subheading 3.2.
2. After adjusting the cell density to 1–5 × 10^7 cells/mL, transfer 100 μL of cell suspension into each microcentrifuge tube.
3. Add 10 μL of Human IgG Fc Block per 100 μL of sample volume to block unwanted binding of mAbs to Fc receptors and incubate cells on ice for 10 min.
4. Transfer saturating amounts of mAb to each sample tube and incubate on ice for 60 min. Protect the samples from exposure to light to minimize the potential effect of photo-bleaching.
5. Add 1 mL of FCM buffer to each microcentrifuge tube, cap the tubes, and invert several times to mix. Centrifuge the samples at 800 × *g* for 5 min. Carefully remove the supernatant to the 100 μL mark using a vacuum aspiration device. Resuspend the cell pellet in residual buffer.
6. Repeat **step 5**.
7. From this point onward, execute **steps 2–33** of Subheading 3.3.1.

3.4.2 Labeling of Intracellular Protein Using the Branched DNA Assay

1. Prepare PBMCs using Ficoll Hypaque density gradient centrifugation or other suitable techniques as described in Subheading 3.2. If desired, surface staining can be performed according to Subheading 3.4.1.
2. Perform Subheading 3.3.1, **steps 1–8** to fix and permeabilize the cells.
3. Add 10 μL of Human IgG Fc Block per 100 μL of sample volume to block unwanted binding of mAbs to Fc receptors and incubate cells at ambient temperature for 10 min.
4. Pipet saturating amounts of mAb to each sample tube, and incubate at ambient temperature for 30 min.
5. Prepare 1× Permeabilization Buffer with RNase Inhibitor. First dilute 10× Permeabilization Buffer to 1× with RNase-free water. Then add RNase Inhibitor 1 (1,000×) at a 1:1,000 dilution and RNase Inhibitor 2 (100×) at a 1:100 dilution. Gently mix the solution by inversion and store the Permeabilization Buffer on ice when not in use (*see* **Note 9**).
6. Add 1 mL of 1× Permeabilization Buffer with RNase Inhibitor to each sample, cap the tubes, invert several times to mix, and centrifuge at 800 × *g* for 5 min. Aspirate the supernatant to the 100 μL mark and resuspend cells in the residual buffer.
7. Repeat **step 6** for a total of two washes.
8. From this point onward, execute **steps 9–33** of Subheading 3.3.1.

3.4.3 Instrument Setup and Data Acquisition

1. Configure flow cytometer according to the recommendation suggested in **steps 1–3** of Subheading 3.3.2 for the detection of mRNA in each channel (e.g., Alexa Fluor® 488, Alexa Fluor® 647, and Alexa Fluor® 750).
2. Set the voltages for each detection channel and acquisition parameters according to **steps 4–5** of Subheading 3.3.2.

3.4.4 Gating Strategy and Analysis

To demonstrate the simultaneous measurement of mRNA and protein using the Branched DNA assay, the correlated expression pattern of CD8 mRNA and CD8 protein using human PBMCs was examined (Fig. 3). The experimental design can be found in Table 5. Briefly, Ficolled PBMCs were isolated as per Subheading 3.2, surface-labeled with an antibody to CD8 PE protein (p) as per Subheading 3.4.1, and hybridized with an AX647 Target Probe to CD8 mRNA (m) using the Branched DNA technique as per Subheading 3.3.1. The data were acquired on an LSRFortessa according to the procedure described in Subheading 3.4.3 and analyzed in WinList version 8.1 (Verity Software House) as follows:

1. Generate the following bivariate plots as per Fig. 2a using a flow cytometry data analysis software package such as WinList, FlowJo, and FCS Express:

   Figure 2a1 FTIM vs. SSC-A.

   Figure 2a2 FSC-A vs. FSC-H.

   Figure 2a3 FSC-A vs. SSC-A.

2. To ascertain the quality of the data acquisition, place a rectangular region (R1) on the bivariate plot of FTIM vs. SSC-A to circumscribe the events collected in continuity. This dot plot can be used to eliminate any air bubbles or problems which occur during sample collection.
3. On the bivariate plot of FSC-A vs. FSC-H, create a rectangular region (R2) to include the singlet-cell population. Gate this bivariate histogram on (R1).
4. On the bivariate plot of FSC-A vs. SSC-A, create an elliptical region (R3) to circumscribe the cell population of interest and exclude doublets, debris, and apoptotic events. Gate this bivariate histogram on (R1 and R2). In this example, a lymphocyte region is used.
5. As per Fig. 3, create a quadrant region on a bivariate plot of CD8 protein [CD8 (p)] PE vs. CD8 mRNA [CD8 (m)] AX647. This plot should be gated on (R1–R3). The boundary of the quadrant region should be constructed based upon "Fluorescence Minus One" controls, in which the FMO

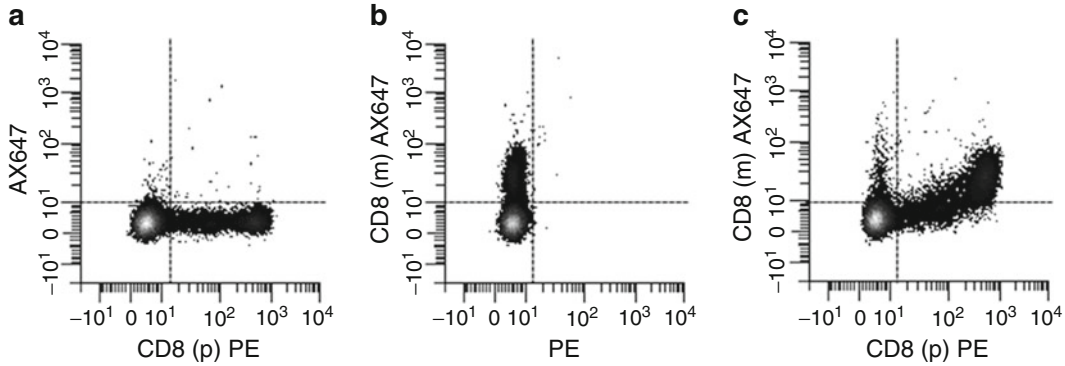

Fig. 3 Correlated measurement of CD8 protein and CD8 mRNA in human lymphocytes using the Branched DNA assay. Human PBMCs with lymphocytic scatter characteristic were identified using the gating strategy described in Fig. 2. (**a**) mRNA AX647 FMO control. The expression level of CD8 protein was measured using PE as the detection system. The cells were exposed to a complete Branched DNA procedure except Target Probes for CD8 mRNA were not added. (**b**) Protein PE FMO control. The expression level of CD8 mRNA was measured using AX647 as the detection fluorochrome. (**c**) The correlated expression levels of CD8 protein and CD8 mRNA were measured using PE and AX647 as the detection systems, respectively. Quadrant regions were set using the FMO controls

Table 5
Experimental layout for the simultaneous measurement of mRNA transcripts and cell surface proteins in PBMCs using the Branched DNA assay

Tube number	Tube description	488 nm laser PE B575/26	640 nm laser AX647 R670/14
1.	No target probe Control[a]	–	–
Compensation tubes (PrimeFlow™ compensation kit)			
2.	PE labeled beads	Beads with PE	–
3.	AX647 labeled beads	–	Beads with AX647
FMO[b] controls			
4.	Cells without PE label	–	CD8 (m)[c]
5.	Cells without AX647 label	CD8 (p)[d]	–
Experimental tube			
6.	Test article	CD8 (p)	CD8 (m)

– Denotes either mRNA target probes or fluorochrome-conjugated antibodies were not added
[a]Samples are processed through the Branched DNA procedure without mAbs or target probes
[b]FMO: Fluorescence minus one
[c](m): Denotes the detection of mRNA
[d](p): Denotes the detection of protein

tubes would be identical to the experimental tube; except the mAb/mRNA label probe is excluded in the fluorochrome channel that is being controlled (*see* **Note 21**).

3.5 Validation of Surface and Intracellular Labeling Reagent Compatibility

Early investigators who combined cell phenotyping via antibody labeling with PCR encountered poorly detectable antibody signals because fluorochromes exposed to the high thermal cycling temperatures required for nucleic acids amplification (e.g., in excess of 90 °C) were partially disintegrated and the cells became highly autofluorescent [7]. The temperatures employed in the Branched DNA assay are much lower (40 ± 1 °C) than those used in PCR, making it possible to detect most fluorochromes. Nevertheless, decreases in fluorochrome intensity and increases in autofluorescence remain as issues that need to be addressed when planning experiments. Fixative and permeabilization reagents used in the procedure may also have adverse effects. The following protocol

describes an experimental design that should be carried out to assess the effect of the Branched DNA procedure on the autofluorescence of unlabeled cells and fluorochrome intensity.

3.5.1 Sample Preparation

1. Label as many 12 × 75 mm polystyrene tubes and Branched DNA microcentrifuge tubes as is required for the experiment.
2. Prepare PBMCs using Ficoll Hypaque density gradient centrifugation technique or other suitable methods. *See* Subheading 3.2 for more information.
3. Wash the resultant cell suspension two times using FCM buffer.
4. Perform a cell count to adjust the cell density to 1–5 × 10^7 cells/mL.
5. Transfer 100 μL of cell suspension into each of the polystyrene tubes.
6. Add 10 μL of Human IgG Fc Block per 100 μL of sample volume to block binding of mAbs to Fc receptors. Incubate the cells on ice for 10 min.
7. Transfer a saturating amount of mAb to each of the sample tubes and incubate on ice for 60 min. From this step onward, protect the samples from exposure to light to minimize the potential effect of photo-bleaching.
8. Add 3 mL of FCM buffer to each sample, centrifuge at 800 × *g* for 5 min, and discard the supernatant to remove unbound mAb.
9. Resuspend the cell pellet in 1 mL of FCM buffer. Transfer 500 μL of this suspension to a microcentrifuge tube, which will be exposed to the entire Branched DNA assay. The polystyrene tube, which will be used for comparison, should be stored at 2–8 °C until acquisition.
10. Centrifuge the microcentrifuge tube prepared in **step 9** at 800 × *g* for 5 min. Aspirate all but 100 μL of supernatant and resuspend the pellet in residual buffer. From this step onward, execute **steps 2–33** of Subheading 3.3.1.

3.5.2 Instrument Setup, Data Acquisition, and Analysis

1. Set the voltages for each detection channel and acquisition parameters according to **steps 4–5** of Subheading 3.3.2.
2. Create the bivariate plots as described in Subheading 3.4.4.
3. In addition to the bivariate plots created in **step 2**, add a single-parameter histogram gated on (R1–R3) for each surface staining mAb. Create regions (R4) and (R5) to circumscribe the negative and positive cell populations, respectively, on the histogram.
4. Calculate the Stain Index for each mAb using the following formula:

$$\text{StainIndex} = \frac{(\text{gMFI of Positive Population}) - (\text{gMFI of Negative Population})}{2 \times (\text{Negative Population Robust Standard Deviation})}$$

5. For each mAb, compare its Stain Index using the standard immunophenotyping technique with its Stain Index measured using the complete Branched DNA assay (*see* **Note 22** for a discussion on the results comparing the effect of Branched DNA on fluorochrome selection).

4 Notes

1. Microcentrifuge tubes are provided by Affymetrix/eBioscience in the PrimeFlow RNA kit. The utilization of inappropriate microcentrifuge tube can result in severe cell loss and/or decrease in hybridization efficiency due to inefficient heat transfer, which can lead to low cell yield and poor signal detection. If an investigator wants to replace this component of the assay with alternative source of tubes, the tubes should be thoroughly tested for compatibility with the assay using relevant positive and negative controls.
2. Currently, the labeling probe formats for this Branched DNA assay are conjugated to either Alexa Fluor® 488, Alexa Fluor® 647, or Alexa Fluor® 750. When acquired on a conventionally configured flow cytometer (i.e., configured with 405, 488, and 640 nm lasers), the fluorescence intensity of Alexa Fluor® 647 labeled probe is the brightest option. Therefore, it is recommended that Alexa Fluor® 647 should be reserved for the detection of mRNA targets with lowest abundances or of highest priority. While optimally excited by a 488 nm laser, Alexa Fluor® 488 exhibits lower fluorescence yield than Alexa Fluor® 647. Also, the detection channel in which Alexa Fluor® 488 is measured is associated with a higher level of background fluorescence. Alexa Fluor® 750 is optimally excited at 750 nm, but on conventional flow cytometers it can be suboptimally excited by the 640 nm laser. Since it produces the lowest detectable fluorescence, mRNAs that are typically expressed at higher frequencies, such as the control or housekeeping mRNAs, are relegated to the Alexa Fluor® 750 probe set. These three detection probe sets are commercially referred to as Type 1 (Alexa Fluor® 647), Type 4 (Alexa Fluor® 488), or Type 6 (Alexa Fluor® 750). It is important to note that all of the amplification components found in the Branched DNA kit provided by Affymetrix/eBioscience (i.e., the Pre-Amplifiers, Amplifiers, and Label Probes) consist of an inseparable mixture of all three type-specific probe sets.

3. Commercially available Target Probe sets used for the detection of mRNA of interest can be found on Affymetrix's Website using the following link: <media.ebioscience.com/data/pdf/literature/quantigene-flowrna-available-probe-sets.pdf>. Alternatively, a customized Target Probe set can be constructed by Affymetrix for sequences that are not listed or to increase/decrease detection sensitivity.
4. The heat sink should be milled to fit the 1.5-mL microcentrifuge tubes, or any alternative and validated tubes that the investigators desire to use. A rapid, efficient, and consistent heat transfer from the heat sink to the tubes is an important consideration in order to reach and maintain 40 ± 1 °C, which is the the optimal temperature for hybridization of Target Probes and amplifiers in the Branched DNA assay. In addition, a small amount of water can be added into each well to facilitate heat transfer.
5. If the temperature of the hybridization oven fails to achieve 40 ± 1 °C after the overnight equilibration period, adjust the incubator's baseline temperature setting such that a 40 ± 1 °C temperature is achieved, and then repeat Subheadings 3.1.1 and 3.1.2.
6. For the best isolation of MNCs, the reagent should be equilibrated to and the separation procedure carried out at room temperature (18–22 °C) as per manufacturer's recommendation.
7. One milliliter of this buffer will be required per sample. Prepare this buffer in bulk to accommodate all samples. To prevent potential denaturation and degradation of the reagents, do not vortex or vigorously shake this buffer after mixing. This buffer should be prepared fresh at the time of use. Properly dispose of any unused buffer according to standard laboratory practice.
8. Due to the high number of washing steps involved in the Branched DNA assay, removing supernatant after centrifugation through the use of vacuum aspiration device is highly recommended to prevent or minimize cell loss. Use the 100 μL mark imprinted on the microcentrifuge tube as a volume reference each time a wash step is performed.
9. Two milliliter of the 1× Permeabilization Buffer is required for each sample. If intracellular staining is performed, an additional 1 mL is needed. For example, to make 50 mL of 1× Permeabilization Buffer add: 5 mL of 10× Permeabilization Buffer, 45 mL of RNase-free water, 50 μL of 1,000× RNase Inhibitor 1, and 500 μL of 100× RNase Inhibitor 2. Do not vortex or vigorously shake this buffer. To ensure consistency, prepare this

buffer fresh at the time of each use and in sufficient quantity to accommodate all samples. Dispose of any unused buffer.

10. Wash Buffer should be equilibrated to ambient temperature prior to use. According to our experience, purifying the Wash Buffer by running it through a 0.8 μM filtration unit can help reduce some nonspecific or background noises, and this will not adversely affect subsequent fixation and hybridization steps. For planning purposes, 1 mL of fresh Wash Buffer is needed per sample and the buffer should be prepared in bulk to accommodate all of the samples. Any unused buffer should be discarded properly at the end of each experiment.
11. This depicts an optional "Stopping Point" in the protocol for maintaining a more manageable workflow. Cells may be stored in Wash Buffer with 1× RNase Inhibitor 1 overnight and in the dark at 2–8 °C. To do this, add RNase Inhibitor 1 to Wash Buffer at a 1:1,000 dilution during the second wash step. For the best detection, it is recommended that first-time users do not stop at this point, in order to avoid the possibility of mRNA degradation.
12. The probes are incubated with the cells in a final volume of 200 μL. A volume of 100 μL should already be present in the tube from the previous washing step, leaving 100 μL for the probe dilution. If one Target Probe is employed per sample, combine 5 μL of Target Probe with 95 μL of Target Probe Diluent. If more than one Target Probe is employed per sample, adjust the volume of the Target Probe Diluent accordingly by subtracting the total volume of the Target Probe(s) from 100 μL to calculate the volume of Target Probe Diluent required.
13. When adding diluted Target Probes to each sample tube, it is important to ensure that the residual buffer be as close to 100 μL as possible. Diluted Target Probes should be pipetted directly into the 100 μL of residual buffer and then samples should be briefly vortexed before incubating at 40 ± 1 °C. Avoid pipetting the solutions onto the walls of the tubes. Maintaining the 40 ± 1 °C temperature is critical to the success of this procedure (*see* Subheading 3.1).
14. This represents an optional "Stopping Point" in the protocol for maintaining a more manageable workflow. For overnight storage, cells should be washed once in Wash Buffer with 1× RNase Inhibitor. Resuspend samples in 100 μL of residual volume and store in the dark at 2–8 °C. As per the previous suggestion (*see* **Note 11**), in order to avoid the possibility of mRNA degradation, it is recommended that first-time users consider not stopping at this point.

15. If samples were stored overnight at 2–8 °C, ensure that samples and Wash Buffer reagents are equilibrated to room temperature prior to next step.
16. PreAmp Mix and Amp Mix should be pipetted directly into the 100 μL of residual buffer and samples should be mixed well by vortexing before incubating at 40 ± 1 °C.
17. Samples may be stored for not more than 3 days at 2–8 °C in the dark before flow cytometric acquisition is performed. For best results, it is recommended that samples be acquired as soon as possible following the execution of the Branched DNA protocol, in order to preserve fluorescence and signal resolution.
18. The minimum number of events that should be acquired will depend on the precision required, as well as the frequency of targeted cell population in the sample. First, consider the amount of counting error that is deemed acceptable. As a rule of thumb, it is desirable to count a minimum of 100 target cell events. Counting 100 events will yield a counting error CV of 10%, which is likely the highest amount of error most investigators would accept. Counting error CV is determined by the following formula, where n represents the total number of acquired events for the population in question. For example, if a counting error of 1% is desired, then 10,000 target cell events must be counted.

$$\text{Counting Error CV} = \frac{\text{Sqrt}\,(n)}{n} \times 100\%$$

Consideration is next given to the percentage of targeted cells in the sample. If the target cell frequency ($\mathbf{f}$) is 5% and a 1% counting error is desired, then 200,000 total events must be collected.

$$\text{Number of Events to Collect} = \frac{n}{\mathbf{f}}$$

There are no hard and fast rules, but counting a minimum of 2500 target cell events, which can be easily done by drawing a stopping region around this population, will yield a 2% Counting Error CV.

19. Modifications are required when using cells to establish a compensation matrix, ensuring any channel used to detect an mRNA target should be compensated with cells labeled with a bright mRNA control. We recommend using the PrimeFlow Compensation kit because compensation using cells labeled with many mRNA detection probe sets (AX488, AX647, and AX750) has dim signals. Regardless of the strategies used for the compensation calculation, it is crucial to

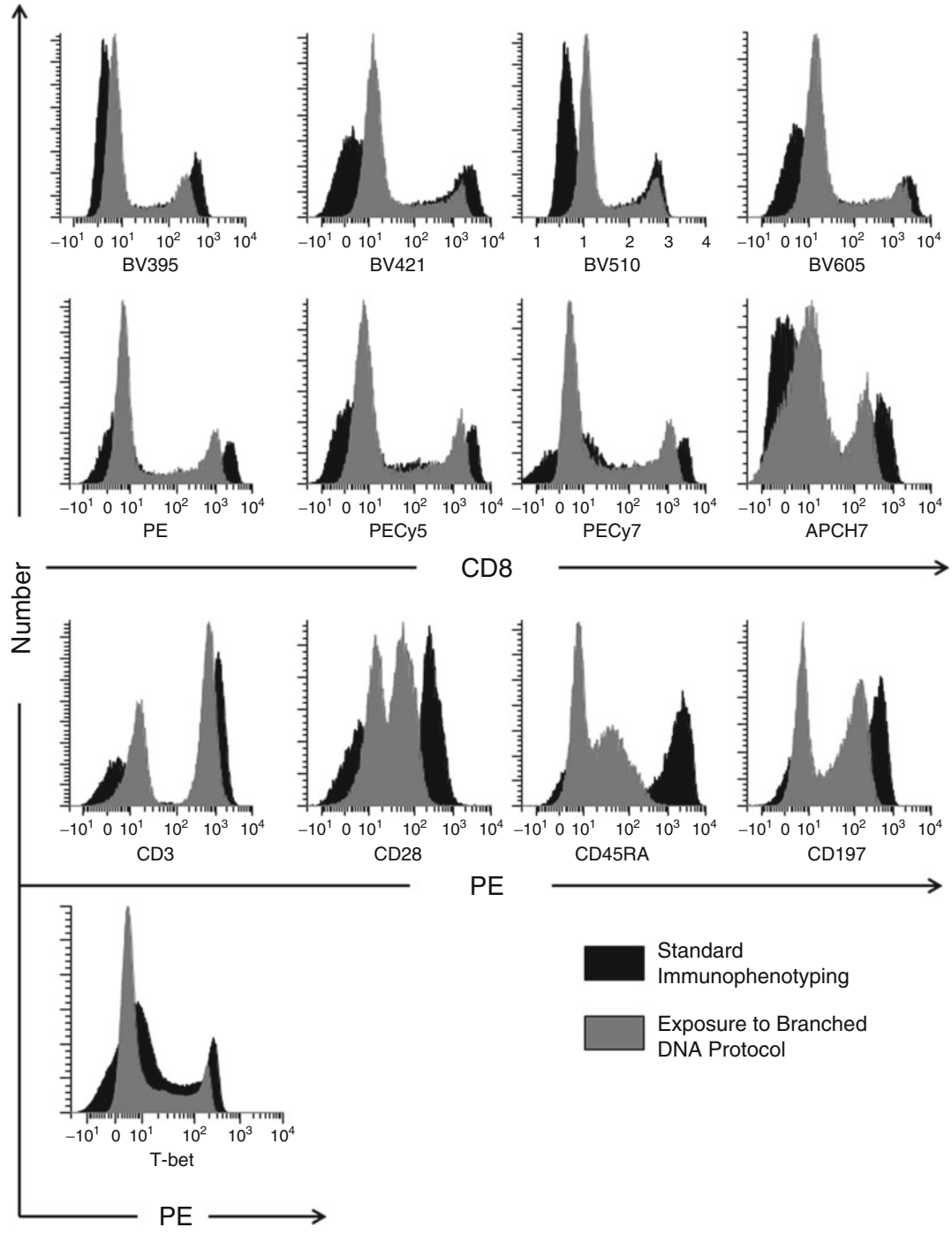

Fig. 4 Signal resolution for the detection and measurement of protein expression using the Branched DNA Assay is dependent upon the antigen and fluorochrome being evaluated. To assess the effects of the Branched DNA assay on fluorochromes (rows 1 and 2), CD8 mAbs labeled with eight different fluorochromes were processed through the complete protocol (*gray histograms*). The geometric mean fluorescence intensities (*data not shown*) and staining patterns for each of the fluorochromes were compared to a set of parallel

emphasize that an appropriate negative population should be used. The beads or cells should possess similar autofluorescence properties as the test article's negative events (e.g., cells that were exposed to all Branched DNA reagents excluding the Target Probe).

20. The beads are designed to be compatible with mouse, rat, or hamster fluorochrome-conjugated mAbs used for either surface or intracellular staining. Each drop of beads contains two separate populations; a positive population that will bind both mAb and the RNA Compensation Control (a product designed to mimic the spectral characteristic of the Label Probes used in the PrimeFlow RNA assay) and a negative population that will not bind either the mAb or the RNA Compensation Control. It is important to note that when these beads are being used for compensation, the negative population associated with each single-color control should be used to set the background fluorescence for that fluorochrome.
21. The Fluorescence Minus One control (FMO) is a type of control commonly included in a multi-color flow cytometry analysis to set boundaries between negative and positive populations. An FMO control contains all the fluorochromes used in a tube, except for one being controlled. It is used to control for fluorescence spreading from one channel into another. This is especially important when the accurate separation of dimly expressed antigens from negative is required [12].
22. The data shown in Fig. 4 indicated cells processed through the Branched DNA assay generally have higher autofluorescence and decreased staining intensity than those labeled using standard immunophenotyping procedure and not processed through the Branched DNA assay. This study emphasizes the importance of testing the suitability of fluorochrome choices prior to starting experiments with Branched DNA assay, as certain clones, antigens, or fluorochromes may be more susceptible; resulting in an overall decrease in the ability to resolve positive from negative populations [13].

Fig. 4 (continued) samples that were stained directly with mAbs based on standard immunophenotyping procedures (*black histograms*). The ability to resolve the staining for each of the surface antigens (i.e., CD3, CD28, CD45RA, and CD197) and intracellular marker (i.e., T-bet) were compared between samples that have been treated using the Branched DNA reagents and standard immunophenotyping procedure. All measured mAbs utilized PE as the detection fluorochrome (rows 3 and 4). In all the cases, the voltage gains applied in each of the detection channels were set based upon unstained samples processed using the standard immunophenotyping procedure

Acknowledgment

The authors acknowledge Dylan Malayter and Castle Funatake (both from Affymetrix/eBioscience) for their contributions to this chapter. Paul K. Wallace is partially supported by the Roswell Park Cancer Institute Ovarian SPORE NIH Grant 1P50CA159981-01A1. Flow cytometry was performed at Roswell Park Cancer Institute's Department of Flow and Image Cytometry, which was established in part by equipment grants from the NIH Shared Instrument Program, and receives support from the Core Grant (5 P30 CA016056-29) from the National Cancer Institute to the Roswell Park Cancer Institute.

References

1. Bentley DL (2014) Coupling mRNA processing with transcription in time and space. Nat Rev Genet 15(3):163–175. doi:10.1038/nrg3662
2. Hocine S, Singer RH, Grunwald D (2010) RNA processing and export. Cold Spring Harb Perspect Biol 2(12):a000752. doi:10.1101/cshperspect.a000752
3. Patterson BK, Till M, Otto P, Goolsby C, Furtado MR, McBride LJ, Wolinsky SM (1993) Detection of HIV-1 DNA and messenger RNA in individual cells by PCR-driven in situ hybridization and flow cytometry. Science 260 (5110):976–979
4. Patterson BK, Mosiman VL, Cantarero L, Furtado M, Bhattacharya M, Goolsby C (1998) Detection of HIV-RNA-positive monocytes in peripheral blood of HIV-positive patients by simultaneous flow cytometric analysis of intracellular HIV RNA and cellular immunophenotype. Cytometry 31(4):265–274
5. Van Hoof D, Lomas W, Hanley MB, Park E (2014) Simultaneous flow cytometric analysis of IFN-gamma and CD4 mRNA and protein expression kinetics in human peripheral blood mononuclear cells during activation. Cytometry A 85(10):894–900. doi:10.1002/cyto.a.22521
6. Trask B, van den Engh G, Landegent J, in de Wal NJ, van der Ploeg M (1985) Detection of DNA sequences in nuclei in suspension by in situ hybridization and dual beam flow cytometry. Science 230(4732):1401–1403
7. Mutty CE, Timm EA Jr, Stewart CC (1999) Effects of thermal exposure on immunophenotyping combined with in situ PCR, measured by flow cytometry. Cytometry 36(4):303–311
8. Patterson BK, Goolsby C, Hodara V, Lohman KL, Wolinsky SM (1995) Detection of CD4 (+) T-cells harboring human-immunodeficiency-virus type-1 DNA by flow cytometry using simultaneous immunophenotyping and PCR-driven in-situ hybridization - evidence of epitope masking of the CD4 cell surface molecule in-vivo. J Virol 69(7):4316–4322
9. Yu H, Ernst L, Wagner M, Waggoner A (1992) Sensitive detection of RNAs in single cells by flow cytometry. Nucleic Acids Res 20 (1):83–88
10. Boyum A (1968) Isolation of leucocytes from human blood. Further observations. Methylcellulose, dextran, and ficoll as erythrocyteaggregating agents. Scand J Clin Lab Invest Suppl 97:31–50
11. Fuss IJ, Kanof ME, Smith PD, Zola H (2009) Isolation of whole mononuclear cells from peripheral blood and cord blood. Curr Protoc Immunol Chapter 7:Unit7 1. doi:10.1002/0471142735.im0701s85
12. Roederer M (2001) Spectral compensation for flow cytometry: visualization artifacts, limitations, and caveats. Cytometry 45(3):194–205
13. Soh KT, Tario JD Jr, Colligan S, Maguire O, Pan D, Minderman H, Wallace PK (2016) Simultaneous, single-cell measurement of messenger RNA, cell surface proteins, and intracellular proteins. Curr Protoc Cytom 75:7.45.1–7.45.33. doi:10.1002/0471142956.cy0745s75

Chapter 5

Analysis of Individual Extracellular Vesicles by Flow Cytometry

John P. Nolan and Erika Duggan

Abstract

Extracellular vesicles (EVs) are released by cells and can be found in cell culture supernatants and biofluids. EVs carry proteins, nucleic acids, and other cellular components and can deliver these to nearby or distant cells, making EVs of interest as both disease biomarkers and therapeutic targets. EVs in biofluids are heterogeneous, coming from different cell types and from different sources with the cell, which limits the usefulness of bulk EV analysis methods that report the average features of all EVs present. Single-particle measurements such as flow cytometry would be preferred, but the small size and low abundance of surface antigens challenges conventional flow cytometry approaches, leading to the development of vesicle-specific assays and experimental design. Among the key issues that have emerged are: (a) judicious choice of detection (triggering) approach; (b) appropriate control experiments to confirm the vesicular nature of the detected events and the contribution of coincidence (aka swarm detection); and (c) the importance of fluorescence calibration to allow data to be compared over time and between laboratories. We illustrate these issues in the context of fluorescence-triggered Vesicle Flow Cytometry (VFC), a general approach to the quantitative measurement of EV number, size, and surface marker expression.

Key words Exosome, Microvesicle, Calibration, Standardization

1 Introduction

Extracellular vesicles (EV), which include exosomes produced and secreted by multivesicular bodies, ectosomes (aka microvesicles or microparticles) shed from the plasma membrane, as well as vesicles produced during apoptosis, cell death, and other processes, are produced by all cells as part of normal physiological processes [1]. They carry proteins, nucleic acids, and other molecules from their cell of origin and can deliver this cargo to nearby or distant cells and can be found in various biofluids including plasma, cerebrospinal fluid, urine, and saliva. There is significant interest in understanding the role of EVs in inter-cellular communication and exploiting them in "liquid biopsies" for diagnostics in cancer, cardiovascular, and infectious diseases [2]. Because EVs can be produced from different

Teresa S. Hawley and Robert G. Hawley (eds.), *Flow Cytometry Protocols*, Methods in Molecular Biology, vol. 1678, DOI 10.1007/978-1-4939-7346-0_5,

places within a cell and are released by many different cell types, EVs found in biofluids are very heterogeneous and bulk analysis methods, including most for genomic or proteomic analyses, that report only population average features have limited value, as the signal from EVs of interest can be lost in the background of irrelevant EVs. Single-particle analysis methods, including flow cytometry, are potentially powerful tools for understanding this heterogeneity, but EVs small size poses a significant challenge for conventional approaches [3]. Extracellular vesicles range in size from ~50 nm to >1 μm, although the vast majority are between ~70 nm and 200 nm in diameter [4]. As such, they are on the order of about 100 times smaller than a typical mammalian cell, with 10,000 times less surface area and 1,000,000 time less volume. Thus, a cell with 1,000,000 copies of a highly abundant cell surface receptor, easily detected by a commercial flow cytometer designed for lymphocyte analysis, might release EVs with only 100 copies of that surface molecule, challenging the detection limit of most instruments. Moderate or low abundance cell surface molecules would be expected to have even fewer antigens per EV [3].

Despite the challenges that the small size and low number of antigens of EVs present, the principles of flow cytometry are generally applicable to EV analysis and it is expected that as commercial instruments designed to measure small, dim particles become available, flow cytometry-based approaches will play an important role in understanding the origins, functions, and diagnostic and therapeutic significance of EVs in health and disease. This chapter describes some of the common sample preparation, experimental design, and calibration considerations that are relevant to EV analysis.

2 Sample Collection and Storage

Sample collection considerations vary with the type of biofluid being analyzed. For blood or plasma, studies conducted with support of the International Society for Thrombosis and Hemostasis (ISTH) have followed recommendations that include collection of blood into citrate as an anticoagulant, and two serial low speed (2500 x *g*, 10 min) spins to prepare cell-free plasma [5–7]. The International Society for Extracellular Vesicles (ISEV) has also produced several position papers on best practices for collection, isolation, and characterization of EVs [8, 9]. While a consensus is emerging on best practices, the final word on many aspects has yet to be written, so the reader is advised to keep this in mind. EV storage is one aspect on which there is a mixture of opinions, with some investigators advising that EVs be analyzed fresh, while others finding little detectable change after storage at –80 °C [10]. As a practical matter for longitudinal studies and sharing of samples across labs, storage of frozen samples is widely practised.

Enrichment, purification, or isolation of EVs from culture media or biofluids is often required for subsequent analysis or functional studies, but can also introduce unanticipated variables into an analysis. Differential centrifugation is a popular approach to fractionation of enrichment of EVs, but significant variation in procedures is observed in the literature. A common paradigm is to perform a first centrifugation at a moderate speed (10,000–20,000 x *g*, 30–60 min) to prepare a "microvesicle" pellet followed by the centrifugation of the supernatant at high speed (100,000 x *g*, 60 min) to prepare an "exosome" pellet [11]. While widely used in the literature, there is little consensus on what these different fractions represent and they appear similar in size and molecular content. Moreover, these centrifugation steps can induce aggregation of EVs that may impact downstream purification, analysis, or functional analyses [12]. Perhaps more useful, although time consuming, is density gradient centrifugation that can produce distinct populations of EVs, although the significance of differences in density in terms of EV biogenesis or function is not clear. It has been suggested that EVs prepared using iodoxanol (Optiprep) gradients retain greater functional activity than those prepared using sucrose gradients, but there is much to be learned about the molecular and functional properties of EVs fractionated by centrifugation.

Other approaches to EV isolation include precipitation methods involving polyethylene glycol (PEG) or other polymers. Commercially available "exosome isolation" kits based on this principal are widely used to concentrate EVs, though it is recognized that they will also precipitate other particles and bulk protein, so that their use as an isolation or purification method has limitations. Size-exclusion chromatography and ultrafiltration methods can be useful for separating EVs from proteins and other smaller molecules, but size itself has limited value for separating different classes of EV from each other or from other particles such as viruses or larger lipoproteins. Immuno-capture methods have the potential to isolate distinct molecular classes of EV from each other, but this depends on knowing what antigenic targets will provide the desired specificity. Immuno-capture targeting tetraspanin proteins (CD9, CD63, and CD81) are widely used in the literature and by commercial products for exosome-specific capture, but the molecules are also found on the cell surface and are presumably released in ectosomes shed from the plasma membrane, so the specificity of these targets is questionable. However, with appropriately validated antigenic targets, immune-isolation approaches have significant potential.

In summary, consensus on the appropriate sample collection, processing and storage methods is slowly emerging, but much remains to be settled. From an analysis standpoint, methods that can characterize EVs directly in biofluids without the need for

isolation and purification have significant advantages both in terms of accuracy, by avoiding the uncertainty associated with various fractionation methods, and in terms of workflow for large scale or clinical studies.

3 Flow Cytometry of EVs

There are several goals of a flow cytometric EV analysis including: (a) detecting individual EVs and measuring their concentration in a sample; (b) estimating the population size distribution; (c) detecting EVs bearing specific cargo molecules; and (d) measuring the amount of that cargo in individual EVs. These goals for EV analysis are similar to those in cell analysis, but EVs' small size and the dim signals they generate present significant challenges that result in departures from the standard operating procedures used in cell analysis.

3.1 EV Detection and Sizing

The first challenge is the choice of parameter to trigger EV detection by the flow cytometer, with the most common options presented in Table 1. In cell analysis, the trigger channel is generally light scatter, usually forward angle light scatter, which allows cells that are much larger than the laser wavelength to be reliably distinguished from debris. The vast majority of EVs are smaller than the laser wavelength, which results in much less light scatter, often producing signals smaller than the various sources of background in an instrument. Moreover, Mie light scattering theory predicts that light scatter decreases with the 4th–6th power of the radius,

Table 1
Choice of trigger parameters.

Trigger Parameter	Advantages	Disadvantages
Forward angle scatter	Strong scatter from particles larger than laser wavelength	High background; Difficult to estimate particle size from intensity; Nonspecific
Side scatter	Lower background compared to FSC	Difficult to estimate particle size from intensity; Nonspecific
Ligand fluorescence	High specificity for selected target; Quantitative, sensitive	Only detects particles bearing sufficient quantity of specific receptor
Membrane fluorescence	High specificity for membranous particles; Can be calibrated to estimate diameter	Some membrane dyes can result in unwanted background
Volume fluorescence	Can stain EVs	May also stain other particles; staining can be dependent on enzyme activity

depending on the laser wavelength and particle size, so that a twofold difference in vesicle size will result in as much as a sixty-four-fold difference in light scatter intensity [3, 13, 14]. Practically, these considerations restrict the user to measuring only the very largest EVs or to accepting a significant amount of noise (false triggers from background), both of which compromise estimates of EV concentration. Various approaches to standardizing or calibrating light scatter detection for EV analysis have been proposed [7, 15, 16]. These can be useful, provided one keeps in mind that beads differ from EVs in their refractive index and cannot be used to directly calibrate EV size.

An alternative approach is the use of fluorescence as a trigger, which can provide improved detection of EVs if the appropriate fluorescence markers are used. One variant on this approach is to use fluorescence-labeled antibodies to trigger detection of EVs bearing specific antigens [17]. This has the advantage of allowing specific detection of EV subpopulations, assuming that the antigen is abundant enough to detect using a particular fluorophore and instrument, but also the disadvantage of only detecting EVs bearing the antigen of interest. A more general approach is to use a surface or volume probe to stain vesicles [18–20]. Lipophilic dyes can intercalate into the membrane surface, allowing specific detection of membrane-bound particles. Similarly, membrane permeable reactive dyes can diffuse into the vesicle lumen to stain proteins or other content. In the former case, the staining may be proportional to vesicle surface area [19] while in the latter the staining may be proportional to vesicle volume, allowing the estimation of vesicle size using an appropriate calibration procedure. Either staining approach can result in high backgrounds, necessitating the addition of a wash step, although with careful experimental design such approaches can be implemented as homogeneous, no-wash assays [19, 21, 22].

3.2 EV Immunophenotyping

Regardless of the approach taken to detect and estimate the size of the EVs, immunostaining involves some common experimental design, calibration, and analysis issues that differ from those generally employed in cell immunofluorescence measurements.

First, because of their small size, the wash steps to remove unbound antibodies that are commonly used in staining protocols for cell immunofluorescence are impractical due to sample losses. Dilution of the stained sample to reduce the concentration of unbound antibodies is an acceptable alternative in most cases, and enables a homogeneous, no wash assay. Note that this approach requires direct immunofluorescence and generally precludes the use of indirect labeling with unlabeled primary antibodies and fluorescent secondary antibodies.

Second, in cell immunofluorescence, sensitivity is generally limited by cellular autofluorescence, which might be equivalent in

intensity to several thousand fluorophores. EVs, with ~ a million-times less volume, have very little autofluorescence, and sensitivity is limited by various background sources from the sample or instrument. Sample background may result from free dye, which can be decreased by dilution, as discussed above. Instrument background includes optical background from scattered laser light and other sources and electronic background from detectors and other components of the data acquisition system. Because of the differences between commercial instruments, and the importance of comparing data between labs and over time, as well as to benchmark new EV analysis systems, appropriate fluorescence calibration is essential.

3.3 Experimental Design and Controls

Another important difference between flow cytometry of cells and EVs is in the nature of the control experiments that are necessary to establish the specificity of single EV detection. Because the light scatter and fluorescence signals produced by EVs are near the detection limit of commercial flow cytometers, several types of control experiments are recommended to ensure that the events being detected are single EVs.

First, while filtering the buffers and sheath fluid used for flow cytometry of EVs can reduce particulate background, detection (trigger) thresholds are typically set near the background levels of the instrument, such that some minimal level of background events will be detected in a buffer-only sample, making this an essential control. Moreover, many commercial reagents, including fluorescent antibodies, may contain particulates, such as antibody aggregates. While these can often be reduced by centrifugation or filtration of the reagent, reagent-only controls should also be performed.

Second, because samples being analyzed can also contain non-vesicle particulates, it is important to demonstrate that the events being measured are vesicular in nature, which can be done with detergent treatment. Treatment of stained sample with a low concentration (for example, 0.05%) of Triton X-100 should result in lysis/solubilization of EVs, leaving only non-vesicular background. Such a control experiment is especially important when measuring samples prepared from crude biofluids that may contain significant amounts of protein aggregates such as immune complexes.

Finally, while in cell analysis doublet discrimination is readily performed by examining plots of pulse height vs pulse area or pulse width, such approaches cannot discriminate doublets of small, dim EVs. In fact, coincidence, the occurrence of more than one EV in the laser beam simultaneously, is a common artifact in the EV flow cytometry literature. EVs that are too dim to be detected as individual particles may trigger detection at high concentrations due to the presence of many particles. An important control experiment to demonstrate the absence of coincidence is to perform a series of

two-fold serial dilutions of the stained sample and show that event rate decreases in proportion to the dilution, but that the light scatter and fluorescence distributions do not change with dilution. If the population intensity distribution decreases with sample dilution, this suggests that the events being measured result from coincident measurement of multiple particles rather than single particles.

3.4 Calibration and Standards

As discussed above, while there are aspects of flow cytometry common to analysis of both cells and EVs, there are also significant differences that necessitate specific considerations for the analysis of EVs. In particular, standardization and calibration of EV size estimates, fluorescence measurements of EV cargo, and the confirmation of specificity for measuring single EVs require special attention.

A common misconception is that flow cytometry light scatter signals can be calibrated in terms of particle size using beads of different sizes. In fact, light scatter signals are highly dependent upon the illumination wavelength, angle of light collection (which can vary greatly between instruments), and the particle refractive index (which is very different among polystyrene, silica, synthetic vesicles, and EVs from biological sources) [3, 13, 23]. These issues have been discussed in depth elsewhere. Synthetic lipid vesicles (liposomes) can, however, be useful for calibrating fluorescence-based size measurements [19].

Because the fluorescence sensitivity of commercial flow cytometers can vary, even between different instruments of the same model, it is especially important to report fluorescence measurements in absolute units rather than relative intensity units produced by the flow cytometer. Calibration of fluorescence measurements of EV cargo using antibodies or other ligands bears many similarities of calibration of cell-based fluorescence measurements. In many cases, fluorescence measurements can be calibrated in units of mean equivalent soluble fluorochromes (MESF) using commercially available intensity standards [24], or hard-dyed beads that have been cross calibrated against MESF standards [25]. For fluorophores for which MESF standards are not available, beads calibrated in units of equivalent reference fluorophores (ERFs) can provide a useful traceable intensity standard [25, 26]. With knowledge of the absolute intensity of detected particles and the fluorescence properties of the ligands (antibody F/P and relative quantum yield), the number of bound ligands can be estimated [27, 28].

Antibody capture beads with calibrated binding capacities can provide an independent approach to estimating the number of bound antibodies per particle in a manner that can be used with any fluorophore. It is important to note that, at present, the commercially available fluorescence intensity standard and antibody capture beads are designed for cell analysis, and are thus significantly brighter than signals obtained from EVs. However, the

linearity of fluorescence signals is well established, and existing commercial standards are still a reasonable choice until EV-specific calibrators and standards become commercially available.

Finally, there is a critical need for stable and reproducibly manufactural biological EV reference materials that can be used to compare results across labs and over time, and also to support the development of new technologies for EV analysis. While there are some commercially available EV preparations, these have not been extensively characterized at the single vesicle level or validated for stability or reproducibility. Several different preparations have been proposed as reference materials, including EVs derived from urine and blood [4, 29, 30]. More broadly useful, perhaps would be EV preparations derived from well-characterized cell lines engineered to express defined cargo and that could be produced in a reproducible fashion at a large scale. The generation of such engineered systems is currently being pursued in many research labs.

4 Examples

To illustrate some of the points made in this article, we demonstrate the analysis of a red-blood cell (RBC)-derived EV preparation produced by treating washed erythrocytes with the calcium ionophore (A23187) to induce vesiculation, followed by centrifugation to pellet the RBCs and produce an EV-enriched supernatant, which was then aliquoted and frozen. We have developed an approach that uses a fluorogenic membrane probe (di-8-ANEPPS) to stoichiometrically stain membrane particles and enable them to be measured to estimate vesicle concentration and size without requiring a wash step. This approach, which we refer to as vesicle flow cytometry (VFC) [19], uses synthetic lipid vesicles (liposomes) whose size distribution has been determined using an independent method as standards for calibrating vesicle fluorescence in terms of size.

VFC was originally developed using a custom high sensitivity flow cytometer [21, 22, 19] but has more recently been adapted to a commercial flow cytometer, the Beckman Coulter CytoFlex, which has improved sensitivity compared to conventional PMT-based instruments, especially for red-emitting fluorophores, owing to its use of a high quantum efficiency avalanche photodiode array-based detector. Detection is triggered using blue (488 nm)-excited red fluorescence (690/50 nm bandpass), which is recorded along with other fluorescence parameters and violet side scatter (VSSC). The trigger channel threshold is set so that the event rate from a sample of clean buffer is low (1–2/s). Samples are run at high speed (60 μL/min) for a fixed amount of time so that events numbers can be expressed as a concentration after accounting for all dilution steps.

Presented in Fig. 1 are fluorescence histograms of samples of buffer plus vesicle stain (Fig. 1a), vesicles plus stain (Fig. 1b), and

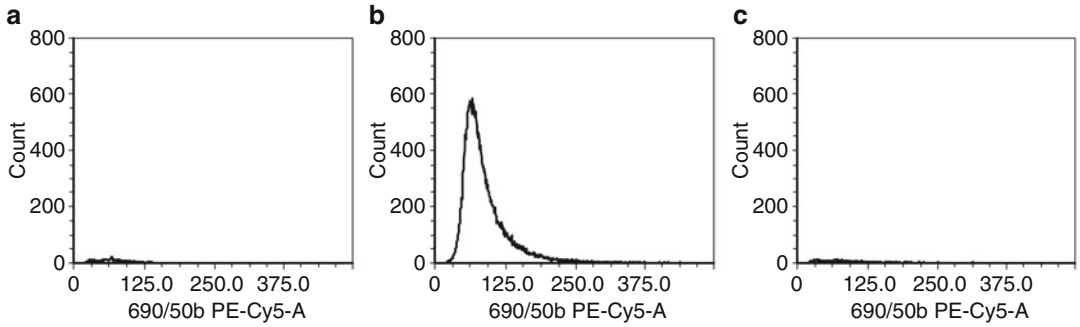

Fig. 1 Vesicle flow cytometry (VFC) of synthetic vesicle size standards. Fluorescence histograms of (**a**) buffer plus vesicle stain, (**b**) vesicles plus stain, and (**c**) vesicles plus stain plus detergent

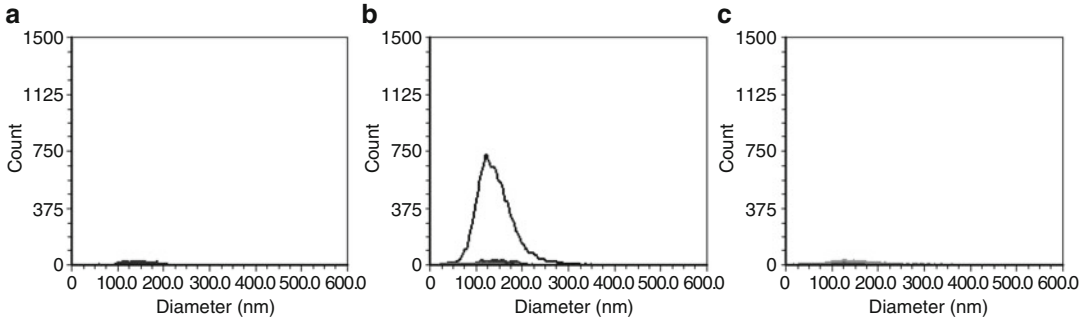

Fig. 2 VFC of RBC EVs. Fluorescence histograms of (**a**) buffer plus vesicle stain, (**b**) RBC EVs plus stain, and (**c**) RBC EVs plus stain plus detergent

vesicles plus stain plus detergent (Fig. 1c), showing the specificity of membrane staining. Presented in Fig. 2 are fluorescence histograms of buffer plus vesicle stain (Fig. 2a), RBC EVs plus stain (Fig. 2b), and RBC EVs plus stain plus detergent (Fig. 2c).

When the sample is stained to saturation, the fluorescence intensity is proportional to vesicle surface area and can be used to estimate vesicle size. Presented in Fig. 3d is the population size (diameter) distribution of the synthetic vesicle size standard as measured by nanoparticle tracking analysis (NTA) and the calibrated flow cytometry surface area (Fig. 3e) and diameter distributions (Fig. 3f). This calibration can be applied to the fluorescence distribution of the RBC EV preparation stained to saturation to calculate the estimated diameter distribution (Fig. 2b), which can be compared to the diameter distribution estimated using NTA.

Because EVs are small and dim, it can be difficult to know whether measured events are truly from individual EVs or the result of coincident occurrence of many sub-detection limit particles in the measurement volume at the same time. One measurement that can help demonstrate that the detected events are from single particles is to serially dilute a stained sample and show that the

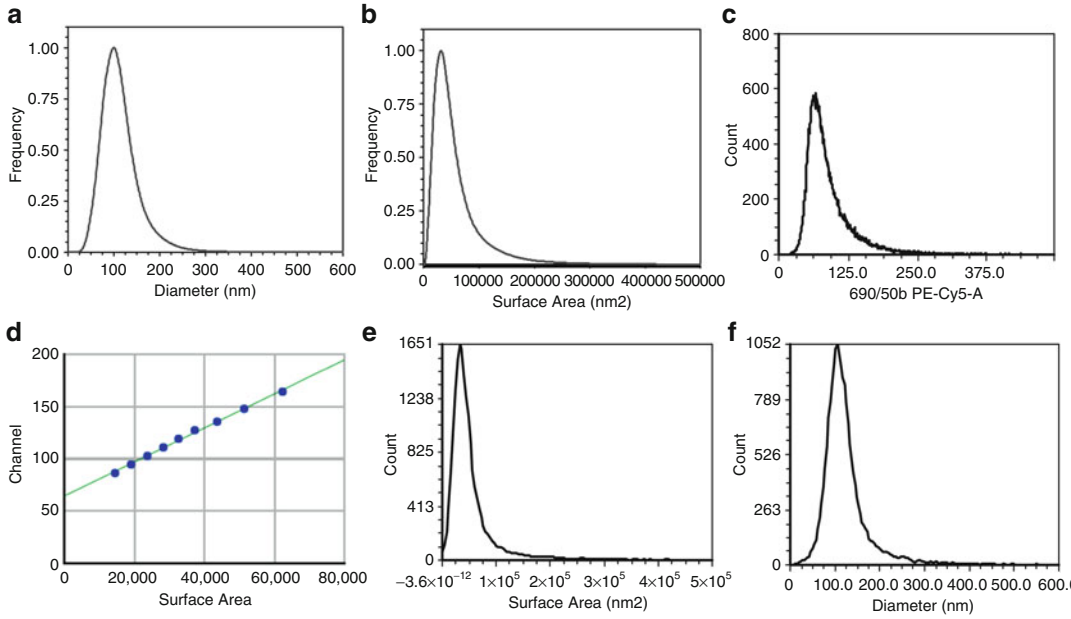

Fig. 3 VFC size calibration. (**a**) NTA-based diameter size distribution of synthetic vesicle size standard. (**b**) NTA-derived surface area distribution of synthetic vesicle size standard. (**c**) Fluorescence intensity distribution of stained vesicle size standard. (**d**) Regression of the surface area and fluorescence intensity distributions. (**e**) VFC-based surface area distribution of the vesicle size standard. (**f**) VFC-based diameter distribution of the vesicle size standard

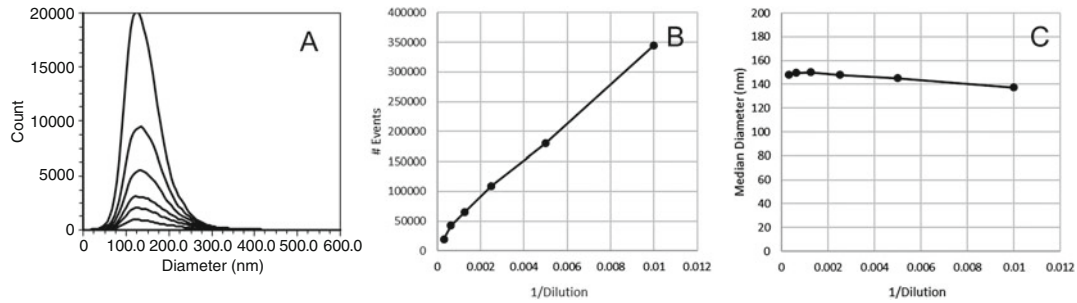

Fig. 4 Dilution of stained sample to demonstrate lack of coincidence. (**a**) Fluorescence intensity histograms of twofold serially diluted stained RBC EVs. (**b**) Plot of Event Number vs reciprocal dilution. (**c**) Plot of fluorescence Intensity-derived Median Diameter vs reciprocal dilution

number of events detected decreases in proportion to dilution but that the brightness of the detected events does not. Presented in Fig. 4a are overlaid histograms from an RBC EV preparation that has been stained and measured after repeated serial dilutions, showing the expected decrease in event number (Fig. 4b) with no significant change in event brightness (Fig. 4c), consistent with the analysis of single particles.

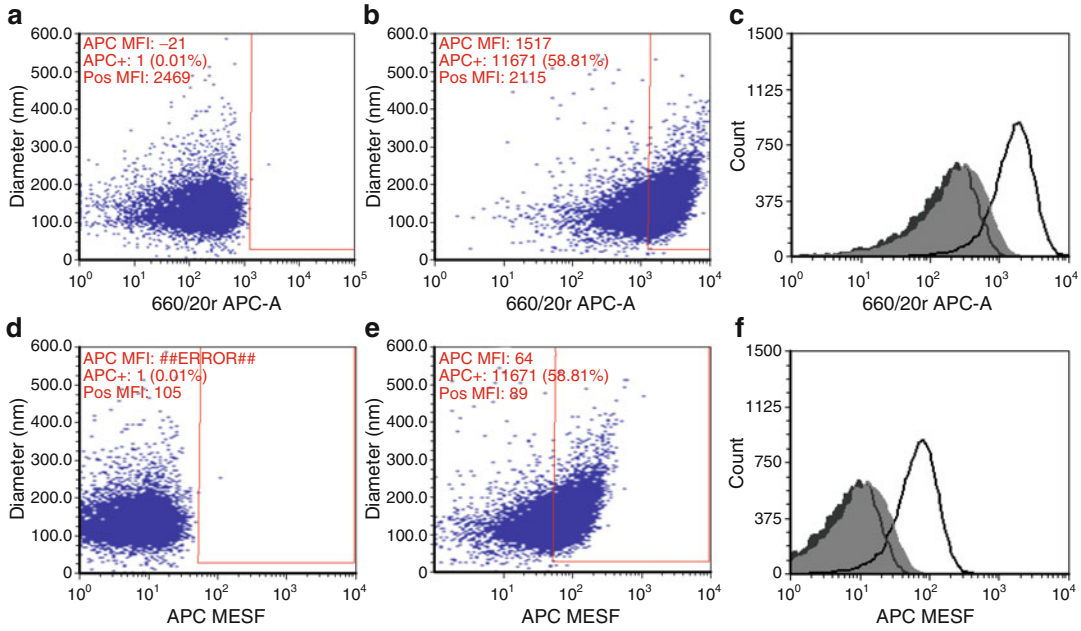

Fig. 5 Immunofluorescence of RBC EVs. Bivariate histograms of RBC EVs unstained (**a**) and stained (**b**) with APC-anti-CD235ab. (**c**) Overlay of unstained RBC EVs (dark gray), stained blank vesicles (light gray), and stained RBC EVs (no fill). (**d–f**) Versions of panels (**a–c**) with the immunofluorescence intensity calibrated in units of MESF

Antigens present on the EV surface can be measured using fluorescent antibodies. Presented in Fig. 5 is the red (640 nm)-excited red fluorescence (660/20 nm bandpass) from RBC EVs unstained (Fig. 5a) or stained with APC-anti-CD235ab (Fig. 5b), which shows that the entire EV population exhibits an increase in intensity (Fig. 5c) compared to unstained EVs (dark gray) or to liposomes (light gray), which have no CD235. The APC intensity can be calibrated and expressed in MESF units using intensity standard beads. In this case, we used multi-intensity Rainbow beads (Spherotech) and the manufacturer's MESF assignments (Fig. 5d–f), allowing results obtained on instruments with similar laser and filter configurations to be compared between labs and over time.

5 Summary and Prospects

Extracellular vesicles have attracted wide interest as an important new mechanism of inter-cellular communication and as potential biomarkers of disease. Most EV studies of protein expression have used bulk analyses such as Western blot, ELISA, or mass-spec proteomics, which report only average properties of an EV preparation. Single EV analysis methods such as flow cytometry have the

potential to reveal EV subpopulations via immunophenotyping, but this has been limited by a lack of sensitivity of most conventional instruments designed for lymphocyte analysis, as well as by a general lack of calibration and standardization of experimental design and data reporting. However, recent activities by the International Society for Extracellular Vesicles (ISEV), the International Society for Advancement of Cytometry (ISAC), and the International Society on Thrombosis and Hemostasis (ISTH) are helping to bring consensus to these issues. Notably, the ISTH has supported a number of studies to evaluate standardized approaches to light scatter-based detection of platelet microvesicles [5, 7, 16], while the ISEV and ISAC have published Minimum Information recommendations for EV isolation and characterization [8] and for general flow cytometry analysis [31], respectively. A consortium of labs recently published an analysis of methods reported in the EV literature [32], and found generally low compliance with MI recommendations and proposed steps to improve this. A joint working group of the three societies is currently evaluating approaches for standardized reporting of EV fluorescence measurements, with discussions and workshops being held at their annual conferences. Together, these activities will increase the rigor and reproducibility of EV analysis and provide a framework within which new, improved high-resolution analysis approaches can be developed.

Acknowledgments

Supported by: UH2TR000931 from the NIH Common Fund, through the Office of Strategic Coordination/Office of the NIH Director.

References

1. Colombo M, Raposo G, Théry C (2014) Biogenesis, secretion, and intercellular interactions of Exosomes and other extracellular vesicles. Annu Rev Cell Dev Biol 30(1)
2. Zaborowski MP, Balaj L, Breakefield XO, Lai CP (2015) Extracellular vesicles: composition, biological relevance, and methods of study. Bioscience 65(8):783–797. doi:10.1093/biosci/biv084
3. Nolan JP (2015) Flow Cytometry of extracellular vesicles: potential, pitfalls, and prospects. Curr Protoc Cytom 73:13.14.11–13.14.16. doi:10.1002/0471142956.cy1314s73
4. van der Pol E, Coumans FAW, Grootemaat AE, Gardiner C, Sargent IL, Harrison P, Sturk A, van Leeuwen TG, Nieuwland R (2014) Particle size distribution of exosomes and microvesicles determined by transmission electron microscopy, flow cytometry, nanoparticle tracking analysis, and resistive pulse sensing. J Thromb Haemost 12(7):1182–1192. doi:10.1111/jth.12602
5. Lacroix R, Judicone C, Mooberry M, Boucekine M, Key NS, Dignat-George F, the ISSCW (2013) Standardization of pre-analytical variables in plasma microparticle determination: results of the international society on thrombosis and Haemostasis SSC collaborative workshop. J Thromb Haemost 11(6):1190–1193. doi:10.1111/jth.12207
6. Lacroix R, Judicone C, Poncelet P, Robert S, Arnaud L, Sampol J, Dignat-george F (2012)

Impact of pre-analytical parameters on the measurement of circulating microparticles: towards standardization of protocol. J Thromb Haemost 10(3):437–446

7. Lacroix R, Robert S, Poncelet P, Kasthuri R, Key N, Dignat-George F (2010) Standardization of platelet-derived microparticle enumeration by flow cytometry with calibrated beads: results of the international society on thrombosis and Haemostasis SSC collaborative workshop. J Thromb Haemost 8(11):2571–2574
8. Lötvall J, Hill AF, Hochberg F, Buzás EI, Di Vizio D, Gardiner C, Gho YS, Kurochkin IV, Mathivanan S, Quesenberry P, Sahoo S, Tahara H, Wauben MH, Witwer KW, Théry C (2014) Minimal experimental requirements for definition of extracellular vesicles and their functions: a position statement from the International Society for Extracellular Vesicles. J Extracell Vesicles 3(1.) 3:10.3402/jev.v3403.26913). doi:10.3402/jev.v3.26913
9. Witwer KW, Buzás EI, Bemis LT, Bora A, Lässer C, Lötvall J, Nolte-'t Hoen EN, Piper MG, Sivaraman S, Skog J, Théry C, Wauben MH, Hochberg F (2013) Standardization of sample collection, isolation and analysis methods in extracellular vesicle research. J Extracell Vesicles, 2. 10.3402/jev.v3402i3400.20360. doi:10.3402/jev.v2i0.20360
10. Böing AN, van der Pol E, Grootemaat AE, Coumans FA, Sturk A, Nieuwland R (2014) Single-step isolation of extracellular vesicles by size-exclusion chromatography. J Extracell Vesicles 3:23430
11. Théry C, Amigorena S, Raposo G, Clayton A (2006) Isolation and characterization of exosomes from cell culture supernatants and biological fluids. Current Protocols Cell Biol Unit 3.22. 21-23.22. 29
12. Linares R, Tan S, Gounou C, Arraud N, Brisson AR (2015) High-speed centrifugation induces aggregation of extracellular vesicles. J Extracell Vesicles 4:29509
13. Chandler W, Yeung W, Tait J (2011) A new microparticle size calibration standard for use in measuring smaller microparticles using a new flow cytometer. J Thromb Haemost 9 (6):1216–1224
14. van der Pol E, Coumans FAW, Sturk A, Nieuwland R, van Leeuwen TG (2014) Refractive index determination of nanoparticles in suspension using nanoparticle tracking analysis. Nano Lett 14(11):6195–6201. doi:10.1021/nl503371p
15. Robert S, Poncelet P, Lacroix R, Arnaud L, Giraudo L, Hauchard A, Sampol J, Dignatgeorge F (2009) Standardization of platelet-derived microparticle counting using calibrated beads and a Cytomics FC500 routine flow cytometer: a first step towards multicenter studies? J Thromb Haemost 7(1):190–197
16. Cointe S, Judicone C, Robert S, Mooberry M, Poncelet P, Wauben M, Nieuwland R, Key N, Dignat-George F, Lacroix R (2016) Standardization of microparticle enumeration across different flow cytometry platforms: results of a multicenter collaborative workshop. J Thromb Haemost 15(1):187–193
17. Arraud N, Gounou C, Turpin D, Brisson AR (2016) Fluorescence triggering: a general strategy for enumerating and phenotyping extracellular vesicles by flow cytometry. Cytometry A 89(2):184–195. doi:10.1002/cyto.a.22669
18. Kormelink TG, Arkesteijn GJA, Nauwelaers FA, van den Engh G, Nolte-'t Hoen ENM, Wauben MHM (2016) Prerequisites for the analysis and sorting of extracellular vesicle subpopulations by high-resolution flow cytometry. Cytometry A 89(2):135–147. doi:10.1002/cyto.a.22644
19. Stoner SA, Duggan E, Condello D, Guerrero A, Turk JR, Narayanan PK, Nolan JP (2016) High sensitivity flow cytometry of membrane vesicles. Cytometry A 89(2):196–206. doi:10.1002/cyto.a.22787
20. van der Vlist EJ, Nolte EN, Stoorvogel W, Arkesteijn GJ, Wauben MH (2012) Fluorescent labeling of nano-sized vesicles released by cells and subsequent quantitative and qualitative analysis by high-resolution flow cytometry. Nat Protoc 7(7):1311–1326
21. Akers JC, Ramakrishnan V, Nolan JP, Duggan E, Fu C-C, Hochberg FH, Chen CC, Carter BS (2016) Comparative analysis of technologies for quantifying extracellular vesicles (EVs) in clinical cerebrospinal fluids (CSF). PLoS One 11(2):e0149866
22. Brooks MB, Turk JR, Guerrero A, Narayanan PK, Nolan JP, Besteman EG, Wilson DW, Thomas RA, Fishman CE, Thompson KL, Eliinger-Ziegelbauer H, Pierson JB, Paulman A, Chiang AY, Schultze AE (2016) Non-lethal endotoxin injection: a rat model for new biomarkers of hypercoagulability. PLoS One 12 (1):e0169976
23. Van Der Pol E, Hoekstra A, Sturk A, Otto C, Van Leeuwen T, Nieuwland R (2010) Optical and non-optical methods for detection and characterization of microparticles and exosomes. J Thromb Haemost 8(12):2596–2607
24. Wang L, Gaigalas AK, Abbasi F, Marti GE, Vogt RF, Schwartz A (2002) Quantitating fluorescence intensity from fluorophores: practical use of MESF values. J Res-Natl Inst Stand Technol 107(4):339–354

25. Hoffman RA, Wang L, Bigos M, Nolan JP (2012) NIST/ISAC standardization study: variability in assignment of intensity values to fluorescence standard beads and in cross calibration of standard beads to hard dyed beads. Cytometry A 81(9):785–796
26. Wang L, Gaigalas AK, Marti G, Abbasi F, Hoffman RA (2008) Toward quantitative fluorescence measurements with multicolor flow cytometry. Cytometry A 73(4):279–288
27. Nolan JP, Chambers JD, Sklar LA (1998) Cytometric approaches to the study of receptors. Phagocyte function: a guide for research and clinical evaluation. Wiley-Liss, New York, pp 19–45
28. Woods TA, Graves SW, Nolan JP (2005) Microsphere Surface Protein Determination Using Flow Cytometry. Current Protocols in Cytometry: Unit13.12. 11-13.12. 13
29. Coumans FAW, van der Pol E, Böing AN, Hajji N, Sturk G, van Leeuwen TG, Nieuwland R (2014) Reproducible extracellular vesicle size and concentration determination with tunable resistive pulse sensing. J Extracell Vesicles 3:25922
30. Valkonen S, van der Pol E, Böing A, Yuana Y, Yliperttula M, Nieuwland R, Laitinen S, Siljander P (2017) Biological reference materials for extracellular vesicle studies. Eur J Pharm Sci 98:4–16
31. Lee JA, Spidlen J, Boyce K, Cai J, Crosbie N, Dalphin M, Furlong J, Gasparetto M, Goldberg M, Goralczyk EM (2008) MIFlowCyt: the minimum information about a flow cytometry experiment. Cytometry A 73 (10):926–930
32. Van Deun J, Mestdagh P, Agostinis P, Akay Ö, Anand S, Anckaert J, Martinez ZA, Baetens T, Beghein E, Bertier L (2017) EV-TRACK: transparent reporting and centralizing knowledge in extracellular vesicle research. Nat Methods 14(3):228–232

Chapter 6

Quantitative Fluorescence Measurements with Multicolor Flow Cytometry

Lili Wang, Adolfas K. Gaigalas, and James Wood

Abstract

Multicolor flow cytometer assays are routinely used in clinical laboratories for immunophenotyping, monitoring disease and treatment, and determining prognostic factors. However, existing methods for quantitative measurements have not yet produced satisfactory results independent of flow cytometers used. This chapter details a procedure for quantifying surface and intracellular protein biomarkers by calibrating the output of a multicolor flow cytometer in units of antibodies bound per cell (ABC). The procedure includes the following critical steps: (a) quality control (QC) and performance characterization of the multicolor flow cytometer, (b) fluorescence calibration using hard dyed microspheres assigned with fluorescence intensity values in equivalent number of reference fluorophores (ERF), (c) compensation for correction of fluorescence spillover, and (d) application of a biological reference standard for translating the ERF scale to the ABC scale. The chapter also points out current efforts for implementing quantification of biomarkers in a manner which is independent of instrument platforms and reagent differences.

Key words Multicolor flow cytometry, Fluorescence calibration, Equivalent number of reference fluorophores (ERF), CD4+ lymphocytes, Antibodies bound per cell, Instrument quality control, Instrument sensitivity, Pulsed light-emitting diode (LED) light source, Compensation

1 Introduction

1.1 Background

Multicolor flow cytometers are used to monitor the level of expression of multiple cell receptors that are significant in disease diagnostics and immunotherapies. The complexity of the immune response necessitates the monitoring of as many cell receptors as practical. However, to determine the levels of expression of cell receptors requires quantitative measurements which at present are not very satisfactory and are instrument dependent. The purpose of this chapter is to detail procedures which can lead to quantitative multicolor flow cytometer measurements. These quantitative measurements rely heavily on the availability of fluorescence standards to characterize and calibrate the flow cytometer, and of biological cell reference controls that are known to possess a fixed number of a

Teresa S. Hawley and Robert G. Hawley (eds.), *Flow Cytometry Protocols*, Methods in Molecular Biology, vol. 1678, DOI 10.1007/978-1-4939-7346-0_6,

well characterized biomarker for ultimate quantification of unknown markers in the units of antibodies bound per cell (ABC).

In the past, quantitative measurements with single color flow cytometers were performed using microspheres with assigned units of MESF (molecules of equivalent soluble fluorophore) to calibrate the fluorescence signal. Reference standards were developed for the assignment of MESF values to microspheres with surface labeled FITC. The use of these microspheres was described in the Clinical and Laboratory Standards Institute (CLSI) guideline for fluorescence calibration and quantitative measurements [1]. However, the quantitation methodology developed for single color cytometers is not easily extended to multicolor flow cytometers. It is impractical to produce different standard reference fluorophore solutions, such as National Institute of Standards and Technology (NIST) fluorescein Standard Reference Material (SRM) 1932 [2], for every fluorophore label used in multicolor flow cytometry. An alternative approach to quantitative measurements with multicolor flow cytometers has been described [3]. This approach involves two major steps and provides a workable scheme for converting the detected fluorescence signals in various fluorescence channels of a multicolor flow cytometer into numbers of antibodies bound per cell (ABC). The ABC values are good indicators of the actual number of different receptors on the cell surface and intracellular antigens. In the following, we describe in detail the two major steps involved in the quantitation scheme.

1.2 Methodology for Quantitative Measurements

1.2.1 Fluorescence Calibration Using Hard Dyed Microspheres Assigned with Fluorescence Intensity Values in Equivalent Number of Reference Fluorophores

In the first major step, a unit of fluorescence intensity is assigned to a given population of hard dyed microspheres. The assignment is based on the equality of the fluorescence signals from the microsphere suspension and a solution of reference fluorophores. This fluorescence unit is defined as the equivalent number of reference fluorophores (ERF) that gives the same fluorescence signal as one microsphere. The ERF unit is different from MESF in that the fluorophores embedded in the microspheres and the fluorophores in the reference solution can be very different and may have very different molar absorptivities. Consequently, the ERF unit applies only to a specific excitation-detection scheme associated with a fluorescence channel (FC) in a multicolor flow cytometer. However, the ERF unit assignments can be performed using a fluorimeter that mimics the response of the flow cytometer.

The microspheres embedded with multiple fluorophores display a broad emission profile to cover many FCs of multicolor flow cytometers. These microspheres were traditionally used to monitor the daily performance of the flow instruments because of their superb stability. However, the microspheres with ERF assignments can also be used to define a linear scale for each FC as demonstrated in ref. 3. The scale is implemented by analyzing 5–6 different microsphere populations, each implanted with different amount

of fluorophores and each assigned with an ERF value. We emphasize again that the ERF values are assigned for a specified laser excitation and a specified range of wavelength in the fluorescence detection channel. For a given FC, the fluorescence signals associated with the different microsphere populations can be plotted versus the ERF values assigned to the different microsphere populations leading to the calibration curve shown in Fig. 1a. Such a calibration curve is obtained for each of the FCs yielding an estimate of linearity of response and dynamic range. To support the calibration of microspheres in terms of ERF, NIST has developed a standard reference material, SRM 1934 which includes four fluorophore solutions, Fluorescein, Nile Red, Coumarin 30 and Allophycocyanin (APC) [4]. The microspheres with assigned ERF values, using SRM 1934 enable the standardization of the fluorescence intensity scale in quantitative ERF unit. In addition, it will be possible to estimate detection sensitivity and background level. The detection sensitivity, Q, is defined as statistical photoelectrons per ERF molecule, and is an important measure of instrument sensitivity and can be predictive of the success of the multicolor flow cytometer assay panel design [5].

1.2.2 Application of a Biological Reference Standard for Translating the ERF Scale to the ABC Scale

In the second major step, a biological standard such as a lymphocyte with a known number of antibody binding sites (e.g., CD4 binding sites) is used to translate the linear ERF scale to an ABC scale. The biological reference marker, CD4 receptor protein on human T helper cells can come from either whole blood of normal healthy individuals or Cyto-Trol™ Control Cells, a commercially available lyophilized peripheral blood mononuclear cell (PBMC) preparation [6–8] depending on the preference of users and the accessibility of normal individual whole blood samples. The expression levels in antibodies bound per cell are approximately 45,000 for fixed normal whole blood samples and approximately 40,000 for Cyto-Trol cells, respectively [7]. Figure 1b shows the steps taken in the preparation of the biological standard. The upper part of Fig. 1b shows five containers each with a population of standard cells (dotted line) at the bottom of each container. The antibody specific to the receptor is divided into several lots and each lot is labeled with one of the fluorophores that will be detected in each FC. The symbols Y in the upper part of Fig. 1b denote the antibody and the subscripts denote the label (FITC, PE, APC, etc.) corresponding to the FC. Figure 1b shows the case of a flow cytometer with five FCs; however, the number of FC can vary with the application. The antibodies with different labels are placed in different containers holding the biological standard cells. The mixture of the biological cell standard and the antibodies is incubated. After the incubation, the cells stained with labeled antibodies are washed, concentrated and pooled. The single container at the bottom of Fig. 1b shows the final biological standard which

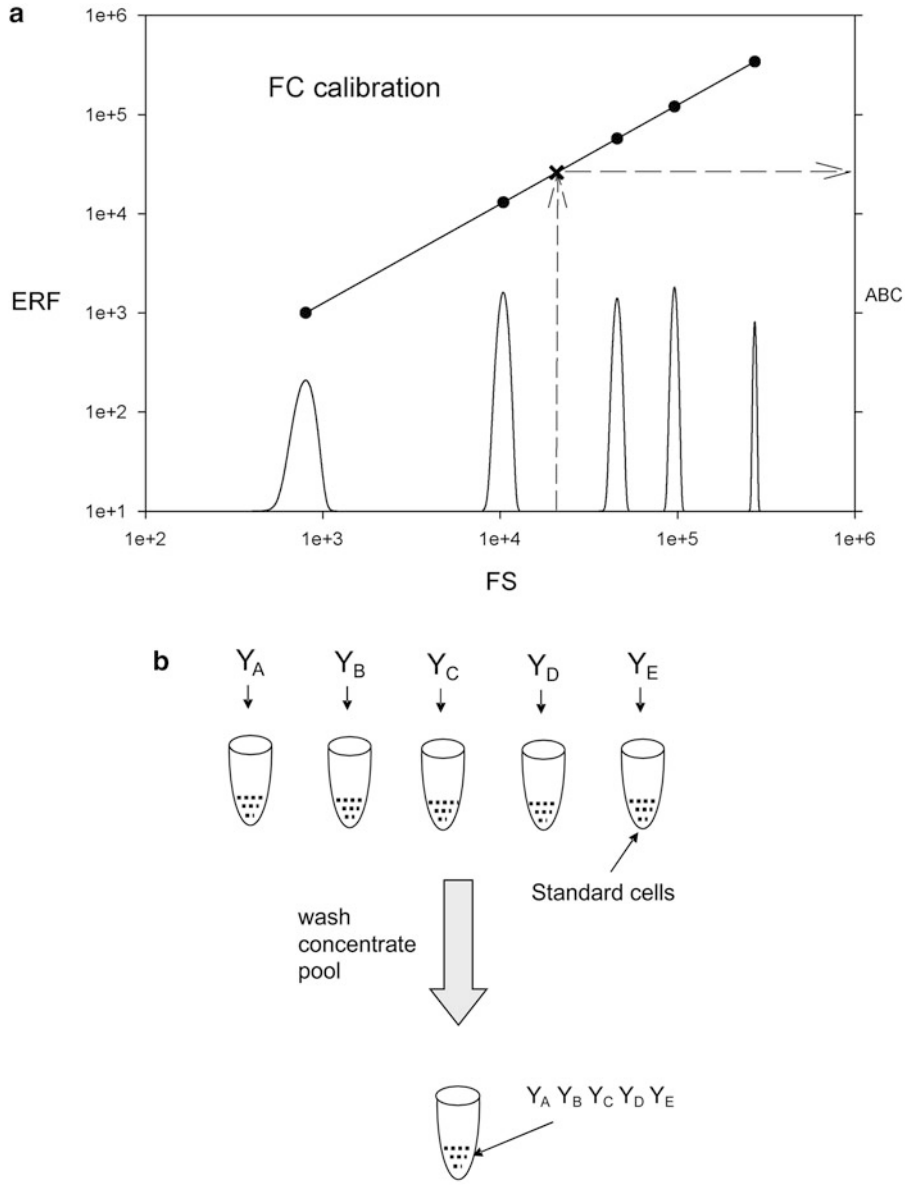

Fig. 1 (**a**) The solid circles represent a plot of the hypothetical numbers of equivalent reference fluorophores (ERF) assigned to the 5 populations of Ultra Rainbow microspheres as a function of the mean pulse height (fluorescence signal, FS) associated with the five simulated peaks in the fluorescence channel (FC). The solid line is a best linear fit to the log values of the five points and constitutes a calibration of the FC. (**b**) A schematic of the process used to produce a biological standard. Standard cells are incubated with the same antibody (Y) labeled with different fluorophores (A, B, C, D, E). After incubation, the labeled cells are washed, concentrated and pooled. The pooled cells constitute the biological sample. The vertical dashed line in Fig. 1a is drawn from the mean pulse height of the response associated with the biological standard. The point (x), where the dashed line crosses the calibration line, defines the ERF value which corresponds to the number of labeled antibodies on the biological standard. This point (as well as the zero point defined by a negative population) sets the antibodies bound per cell (ABC) scale on the right side of Fig. 1a

consists of the pooled antibody stained lymphocytes. Passing the labeled biological standard through the flow cytometer leads to a response in each of the FC. The dashed arrows in Fig. 1a show how the calibration line together with the response from the biological standard in that FC leads to the establishment of a scale for ABC (right hand axis in Fig. 1a). Subsequent to the calibration, flow cytometer measurements on the analyte cells can be reported in terms of ABC values. Examples of using CD4 reference biomarker on human T helper cells from whole blood of normal healthy individuals or Cyto-Trol™ Control Cells for the conversion of an ERF scale to an ABC scale have been provided recently for quantitative measurements of CD20 expression on normal human B lymphocytes [9].

The fluorescence spectra of most label fluorophores cover a wide range of wavelengths. Consequently, a given label fluorophore may give a large fluorescence signal in the FC assigned to that fluorophore and smaller fluorescence signals in FCs assigned to other label fluorophores. Clearly the fluorescence signal in the FC not assigned to a given label fluorophore is a bias and should be corrected. The correction procedure is called compensation and can be implemented using measurements with the individually labeled biological standard cells [10]. Using the present example, five individual measurements would be carried out on each population of cells stained with an antibody against a highly expressed receptor (e.g., CD45 or CD8) which is labeled with a specific fluorophore (Fig. 1b). Appropriate mathematical computation, so-called software compensation, on the data collected for each population would provide the necessary correction factors. Note that cells labeled with an antibody against CD4 might not be optimal for compensation correction. Compared to CD8 or CD45, the expression levels of CD4 are relatively weak so that spillover estimates are hampered by low signal levels.

2 Materials

2.1 Staining Fresh Whole Blood or Cyto-Trol™ Control Cells

1. Specimens: freshly drawn human whole blood or Cyto-Trol control cells kit including reconstitution buffer (Beckman Coulter, Miami, FL).
2. Phosphate-buffered saline (1× PBS), pH 7.4.
3. Buffer: 2% fetal bovine serum (FBS) in 1× PBS.
4. Lysing solution, fixative-free (e.g., ACK lysing buffer).
5. Fixative: 1% (w/v) paraformaldehyde (PFA) in 1× PBS.
6. Fluorescently labeled anti-CD4 antibodies (SK3 clone) covering every FC of a multicolor flow cytometer (*see* **Note 1**).
7. Fluorescently labeled anti-CD8 (or anti-CD45) antibodies covering every FC of a multicolor flow cytometer.

2.2 Quality Control, Fluorescence Calibration, and Characterization of Flow Cytometers

1. Microspheres for instrument quality control (QC) (e.g., BD™ Cytometer Setup and Tracking (CS&T) microspheres from BD Biosciences, San Jose, CA).
2. Microspheres for fluorescence calibration (e.g., Ultra Rainbow calibration microspheres from Spherotech Inc., Lake Forest, IL).
3. quantiFlash™ (A·P·E Angewandte Physik & Elektronik GmbH, Berlin, Germany).
4. Disposable 12 × 75-mm polystyrene tubes.
5. Flow cytometer.

3 Methods

In the following, we will use Ultra Rainbow microspheres with assigned ERF values to establish a linear scale for the fluorescence response. Fresh whole blood samples or Cyto-Trol control cells will be utilized to outline the procedure for converting the ERF scale to the ABC scale, which is used in reporting quantitative flow cytometry measurements. The procedure has been recently updated [9], and is applicable for flow cytometers operated with 405 nm, 488 nm, and 632 nm laser lines commonly used in most flow cytometers, and with appropriate dichroic mirrors and band pass filters to define the FCs. In addition to the Ultra Rainbow microspheres, we will also use quantiFlash™, a 2 μs pulsed light-emitting diode (LED) light source as another example for assuring instrument performance in terms of detection efficiency and optical background (as described in Subheading 3.2.2), and reference cell material with a known anti-CD4 antibody (SK3 clone) binding sites for converting the linear scale to a biologically relevant scale (as described in Subheading 3.4).

3.1 Staining Fresh Whole Blood or Cyto-Trol Control Cells

3.1.1 Fresh Whole Blood

1. Wash heparinized normal donor blood samples (6–8 mL) twice with buffer in 50-mL centrifugal tubes. After centrifugation at ~400 × *g* for 10 min, remove plasma portion of the blood by aspiration. Replenish the blood volume with buffer to the original blood volume.
2. Aliquot 100 μL of washed whole blood into individual tubes. Incubate the whole blood in each tube with differently labeled antibodies designated for each FC of a multicolor flow cytometer for 30 min at room temperature: one set of tubes with anti-CD4 antibody and another set of tubes with anti-CD8 (or anti-CD45) antibody. Protect from light during incubation. Users can either adopt the amount of antibody recommended by a manufacturer or perform their own antibody titration curve for the determination of an optimal amount of

each antibody used [11]. Start titrations with the amount of antibody recommended by the manufacturer, and do five 1.5-fold dilutions and one with 1.5-fold increase of the recommended amount of the antibody. Choose the lowest concentration that gives nearly maximal fluorescence.

3. Lyse the red blood cells in the cell suspensions for 10 min with 2 mL of a lysing solution. After centrifugation at ~400 × *g* for 10 min, remove the supernatant.
4. Wash once more with buffer. After centrifugation at ~400 × *g* for 10 min, remove the supernatant.
5. Add 100 μL of fixative in each tube, and combine white blood cells differently stained with anti-CD4 antibodies in different tubes into a single tube to make a final sample volume of no more than 1 mL with fixative.
6. Acquire samples immediately or store tubes at 4 °C and acquire within 2 h.

3.1.2 Cyto-Trol Control Cells

1. Reconstitute Cyto-Trol cells in a vial with 1 mL of reconstitution buffer provided in the Cyto-Trol kit and mix gently for 15–30 min.
2. Aliquot 100 μL of the reconstituted Cyto-Trol cells into individual tubes. Incubate Cyto-Trol cells in each tube with differently labeled anti-CD4 antibodies designated for each FC of a multicolor flow cytometer for 30 min at room temperature. Note that Cyto-Trol cells individually stained with anti-CD8 (or anti-CD45) antibody with high affinity can also be used for instrument compensation. Protect from light during incubation. Users should perform their own antibody titration curves to ensure that antibody staining is under saturation condition [11]. Start titrations based on the antibody amount recommended by the manufacturer and do five with 1.5-fold sequential dilutions and two with 1.5-fold sequential increase of the antibody amount. Choose the lowest concentration that gives nearly maximal fluorescence signal.
3. Wash cells with 2 mL of buffer. After centrifugation at ~400 × *g* for 10 min, aspirate the supernatant.
4. Add 100 μL of 1× PBS in each tube, and combine stained Cyto-Trol cells in different tubes into a single tube to make a final sample volume of no more than 1 mL with 1× PBS.
5. Acquire samples immediately or store tubes at 4 °C and acquire within 2 h.

3.2 Quality Control, Fluorescence Calibration, and Characterization of Flow Cytometers

Flow cytometer manufacturers generally provide QC microspheres and procedures for setting the instruments at optimal performance levels or at least qualifying the operation of the instrument. For instance, CS&T beads are used for QC of flow cytometers operated with FACS Diva acquisition software (BD Biosciences). These QC microspheres consist of two different hard-dyed fluorescent populations and an undyed blank population. The coefficient of variation (CV) of the brightest microsphere population is small enough to be used for the assessment of the laser alignment to the sample core stream of the flow cell in cytometer. By adjusting the photomultiplier tube (PMT) voltage of each FC, the linear response range for each FC is estimated using the brightest microsphere population. The other fluorescent microsphere populations are designed to measure cytometer performance such as the photon detecting efficiency (Q) and the optical background (B). Recall that Q is defined as the number of statistical photoelectrons (Spe) per fluorescence signal unit. However, there is currently no QC and calibration microspheres with formally assigned ERF values traceable to a reference fluorophore solution standard, such as SRM 1934 and/or through a NIST offered assignment service. Therefore, Q values measured by using various commercially available microspheres (with manufacturer-assigned fluorescence intensity values based on procedures developed by each manufacturer) are not comparable. In practice, Q and B can be evaluated by using hard-dyed microspheres or pulsed LED source [12, 13]. Due to variations of laser noise, illumination condition, and microsphere dye loading on the method using hard-dyed microspheres, the use of pulsed LED source provides more accurate assessment of Q and B. Accurate and reproducible Q values of fluorescence detectors within a flow cytometer or across different flow cytometers can further ensure successful design of staining panels and more accurate biomarker quantification.

A FACSAria II flow cytometer (BD Biosciences) is used below to illustrate a procedure for proper QC, fluorescence calibration and characterization. The procedure is applicable to any commercially available flow cytometers. Use microspheres recommended by the flow cytometer manufacturer for its instrument QC. Ultra Rainbow calibration microspheres with previously assigned ERF values are then used for instrument calibration. Lastly, quantiFlash™ is utilized for obtaining Q and B with cytometer fluorescence intensity scale in ERF units.

3.2.1 Quality Control and Fluorescence Calibration of Flow Cytometer

1. Prepare the CS&T microspheres suspension immediately before use. Add 3 drops of CS&T microspheres into a 12 × 75-mm tube with 1× PBS. Vortex the microsphere suspension thoroughly.
2. Run CS&T microspheres in suspension on a FACSAria II flow cytometer. Perform a baseline performance check followed by a daily performance check. The baseline performance check sets up basic performance parameters of the instrument accordingly

to the predefined properties of the CS&T bead lot used, and can be effective for up to 6 months as long as no major adjustment has been performed on the cytometer. A successful daily performance check assures the flow cytometer is operational with optimal PMT voltages on all fluorescence channels.

3. Add 2–3 drops of both blank and five fluorescent Ultra Rainbow calibration microspheres with assigned ERF values as described in ref. 3 in 0.5 mL of PBS. Acquire 20,000 events within a most populated microsphere gate on the FSC vs. SSC dot plot. Make sure that the brightest fluorescent microsphere population lies within the quantifiable cytometer scale. For analysis, use different gates in each FC histogram to obtain the five mean fluorescence intensity (MFI) values for the fluorescent calibration microspheres.
4. Construct a calibration curve of the calibration microspheres, mean intensity value (x-axis) vs. ERF value (y-axis). The ERF values for five microsphere populations are provided in Table 2 of ref. 3. The linear curve fitting results in a linear fitting equation, $Y_{\mathrm{ERF}} = a \cdot X_{\mathrm{mean\ channel}} + \mathrm{b}$, for every FC of the multicolor flow cytometer, where parameters, a and b, refer to slope and intercept of the linear fit in a given FC, respectively.

3.2.2 Cytometer Characterization

1. Block all laser beams and set laser delays to zero. Note that to process signals from a single event (particle/cell) passing through two or more lasers at different interrogation points, signal from the earlier laser has to be correlated to signal from the last laser once all signals from the single event are in the data queue. Laser delays must be established on the arrival times of the particle event at the interrogation point and are measured relative to the laser delay reference point.
2. Plug both trigger and fluorescence LED optic fibers into quantiFlash™ box and turn on quantiFlash™.
3. Mount the output of the trigger fiber optic firmly to the FACSAria II's side scatter filter location of the 488 nm laser detector array for triggering the flow cytometer [14] (*see* **Note 2**).
4. Generate a histogram of the trigger signal and reduce the PMT voltage of the side scatter so that the trigger signal is set on the left side of the histogram as shown in Fig. 2a.
5. Set the coarse attenuation on the quantiFlash™ to −20 dB and the variable fine adjustment knob to the middle position [14]. Place the fiber optic of the fluorescence LED firmly in the filter location of the fluorescence detector of interest.
6. Run a sample tube of either water or 1× PBS while collecting data of the fluorescence detector from the fluorescence LED.

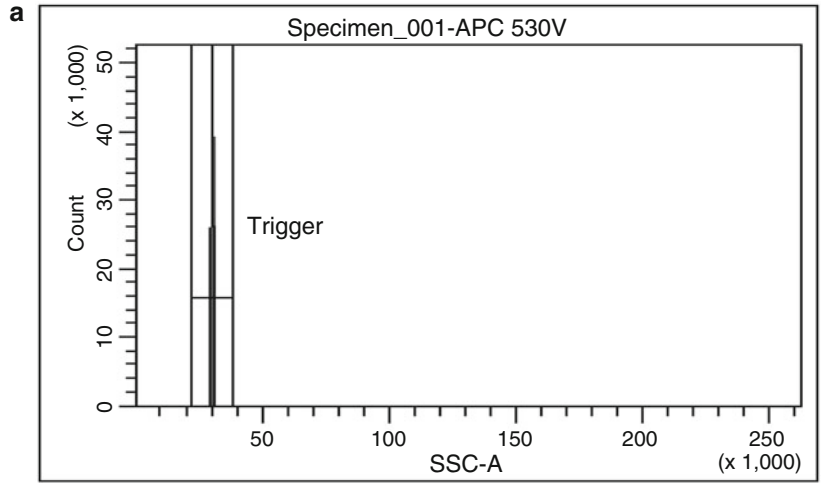

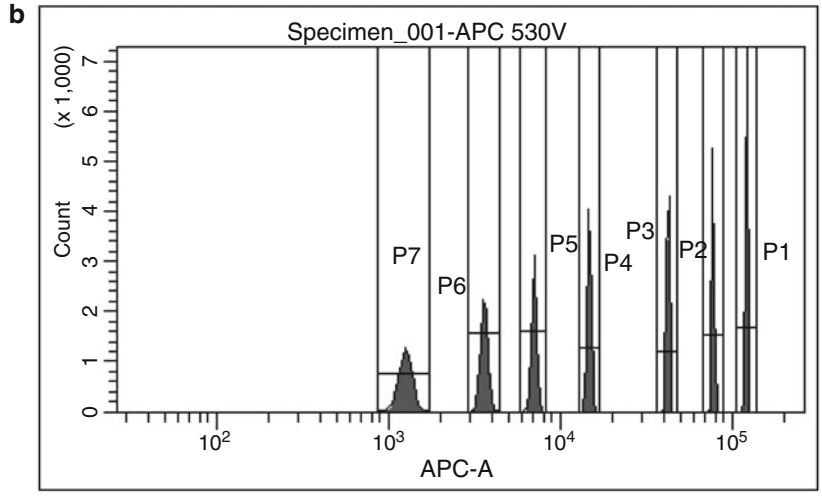

c

Population	APC-A Mean	APC-A SD
P1	124,529	933
P2	79,209	744
P3	43,181	559
P4	14,955	344
P5	7,161	228
P6	3,666	172
P7	1,273	112

Fig. 2 (**a**) A histogram of the trigger signal generated by the quantiFlash™ LED pulser and applied to the side scatter channel. (**b**) Concatenated fluorescence LED pulses from the quantiFlash™ collected in the APC channel. The gates with a gate drawn for each pulse peak are used to obtain the MFI value and associated SD. (**c**) The table summarizes the MFI values and respective SD of the fluorescence LED pulse peaks

7. Beginning with the PMT voltage set in Subheading 3.2.1, put the flow cytometer in setup mode and adjust the quantiFlash™ attenuation so signals are on scale but near the maximum value on the histogram. A good starting point would be at a signal level that gives a histogram CV of about 1%, corresponding to a signal level of about 10,000 Spes. Collect 10,000–20,000 counts per detector.
8. Adjust the quantiFlash™ attenuation to further collect signals covering the fluorescence intensity scale of the detector (over more than four decades in this case) and use "Append" in the save data window to save 5–10 individual histograms in a single histogram shown in Fig. 2b using APC detector as an example. The goal is to obtain data showing the broadening histogram populations from the light pulses as the signal is decreased. For example, at a Spe level of 100, the CV of the population would be about 10%.
9. Repeat the procedure above with each fluorescence detector.
10. After measurement completion of all detectors of interest, turn off the quantiFlash™ and remove the LED cable connections. Restore the laser delays to the standard operational setting values.
11. For data analysis, draw gates on concatenated LED pulses collected in APC detector in Fig. 2b, and obtain MFI values and associated SD of the LED pulses as shown in Fig. 2c and insert these values in the appropriate columns in the table on the top of Fig. 3.
12. Insert the MFI value of a fluorescent Ultra Rainbow bead population attained in Subheading 3.2.1 with a known ERF value as a reference bead in the line named as "Marker Beads" in the data table. This reference ERF value enables the conversion of MFI values of the LED pulses to the respective ERF values shown in the seventh column of the data table in Fig. 3.
13. Plot intensity value in ERF unit (x-axis) vs. SD^2 (y-axis) as shown on the up figure of Fig. 3, and click the "Calculate" button to compute the Q, B, and $CV_{intrinsic}$ using the following equation:

$$SD^2 = ERF^2 \times (CV_{intrinsic})^2 + ERF \times \left(\frac{1}{Q}\right) + \frac{B}{Q}$$

where $CV_{intrinsic}$ is associated with the accumulation of all the non-photonic errors occurred while measuring the fluorescence signal [13]. Non-photonic contributions to B are also possible. The contributions are from the electronics in the form of electronic noise and the base-line restorer. The contributions from the base-line restorer can be significant and

Fig. 3 An Excel worksheet for the computation of Q, B (background ERF), intrinsic CV and goodness of fit as described in the user manual of quantiFlash™ [14]. Insert the MFI values and associated SD of the LED pulses listed in Fig. 2c in the second and third columns of the table, respectively. The MFI value of a fluorescent calibration bead population attained in Subheading 3.2.1 was inserted in the second column on the last line of the table named with "Marker Beads". The known ERF value of the calibration bead population was inserted in the seventh column of the same line. Click the "Calculation" button besides the table. The automatic parameter calculation and fitting procedure are carried out according to the quadratic fit equation provided in Subheading 3.2.2. The resulted values of parameters are placed in the Excel sheet table under the columns named with either "Channels" and "ERFs", and the resulting fitting curves are displayed in the plots of ERF vs. SD^2 (ERF) and MFI (channel) vs. SD^2 (channel) below the table. Note that under the "ERFs" columns, the parameter values are in the units associated with ERF. The fitting results are shown on the right side of the table, e.g., a Q of 0.0691 Spe/ERF, a B of 7702.26 ERF, and a goodness of fit of 1.000. The quantiFlash™ LED has a specified intrinsic CV of 0.1%; an intrinsic CV of rounded 0.00% was obtained for this APC channel. On the basis of Q value obtained, Spe values can be computed by $\text{Spe} = Q \times ERF$ with fitted ERF values, and are shown in the last column of the table

result in higher than expected positive B values, as well as possible negative B values. More representative values for B without the effect of the base-line restorers can be obtained from the SDs collected described below in the absence of the fluorescence LED pulse. For the APC detector as shown in Fig. 3, the quadratic fit equation results in a Q value of 0.0691 Spe/ERF, a B value of 7702.26 ERF and a $CV_{intrinsic}$ of 0.00%, respectively (*see* **Note 3**).

The method described in Subheading 3.2.2 provides an estimate of Q value in Spe per ERF and an estimate of B in ERF units. The use of calibration microspheres with assigned ERF values for fluorescence detectors provides a calibration and standardization of the fluorescence intensity scale in quantitative ERF unit and will ensure the comparability of Q and B values across different instrument platforms. Knowing Q and B allows the prediction of the capacity of the flow cytometer under evaluation to resolve dim fluorescent populations by calculating the Separation Parameter, S, in normalized standard deviation units is given by the following [13, 15]:

$$S = \frac{\sqrt{Q \times f}}{\sqrt{1 + 2 \times \frac{B}{f}}}$$

If Q and B are in ERF units as mentioned above, then for a given fluorescence intensity, $f (f > 0)$, it is possible to calculate how many normalized standard deviation units separates the fluorescent population with intensity f from the background B. Using the Q and B values, it would be predicted with an $S > 2$ that a fluorescence level of 1000 ERF would be discernable from the background, B.

Additionally, using the trigger provided by quantiFlash™ without the accompanying fluorescence LED pulse, as described in Subheading 3.2.2, and keeping all lasers ON and laser delays at the standard operational settings, enable the assessment of the overall instrument background (expressed as SD) [14]. In the same manner, measurements with lasers OFF give an estimate of the instrument electronic noise of each detector. The assessment of the electronic noise profiles of flow cytometers is important for quantitative multiplexed flow cytometry measurements of biomarkers, particularly low expressed biomarkers across different instrument platforms [16].

3.3 Flow Cytometer Compensation

FC compensation can be carried out by using both an unstained control and individual samples of cells (either whole blood sample or Cyto-Trol cells) singly stained with different fluorochome-labeled anti-CD8 (or anti-CD45) [10]. Run stained and unstained samples following the cytometer manufacturer's compensation

protocol. It is assumed that cytometer acquisition software is able to compute the compensation matrix.

3.4 Quantitative Flow Cytometry Measurements in Antibodies Bound per Cell

1. Run the fluorescently anti-CD4 stained whole blood samples or Cyto-Trol cells in the quantitation channels and obtain the respective fluorescence histogram in every FC. Apply a double gating strategy: lymphocyte gate in the FSC vs. SSC dot plot with sufficient events, e.g., 25,000–50,000 events, and CD4+ gate in the fluorescence histogram. Note that a tight CD4+ gate should be drawn to exclude contribution from CD4+ monocytes or an anti-CD3 with a different fluorophore label could be added in the antibody staining panel for precise selection of CD3+CD4+ T cells. Obtain the geometric mean fluorescence intensity value of CD4+ lymphocyte population for every fluorescence channel. The expression levels in antibodies bound per cell are approximately 45,000 for fixed normal whole blood samples and approximately 40,000 for Cyto-Trol cells, respectively [7].
2. As illustrated in Fig. 1, one can draw a vertical dashed line from the geometric mean intensity value of CD4+ lymphocytes to the calibration curve obtain with the calibration microspheres in Subheading 3.2.1. The intersect point on the calibration line defines the ERF value corresponding to the ABC value for the reference marker CD4 on the reference cells (*see* **Note 4**). This point sets the ABC scale on the right side of y-axis of Fig. 1.
3. Run an unknown blood sample and obtain its geometric mean intensity value of the unknown antigen of interest. Determine the ABC value of the receptor of interest in the unknown sample by the following equation (also *see* **Note 4**):

$$\mathrm{ABC}_{\mathrm{unknown}} = \frac{(a * \mathrm{MFI}_{\mathrm{unknown}} + b)}{(a * \mathrm{MFI}_{CD4} + b)} * \mathrm{ABC}_{CD4}$$

where a and b are the slope and intercept of the linear fit in a given FC described in Subheading 3.2.1, and $\mathrm{MFI}_{\mathrm{unknown}}$ and $\mathrm{MFI}_{\mathrm{CD4}}$ are the geometric mean fluorescence intensity values of the unknown and CD4 reference marker, respectively. The above equation assumes that the autofluorescence of the calibration microspheres is the same as or similar to the autofluorescence of the reference cell. This assumption is currently under investigation.

4 Notes

1. It is recommended that fluorescently labeled anti-CD4 antibodies (e.g., SK3 clone from BD Biosciences) covering every FC of a multicolor flow cytometer are used to transform a linear

ERF scale to an ABC scale. The affinity binding dissociation constants of the eight off-the-shelf anti-CD4 antibodies (SK3 clone) labeled with different fluorophores have been measured, and are all in sub-nanomolar range [9], suggesting that fluorophore labeling does not significantly alter the binding of the antibodies to CD4 receptors on T cells. Assuming that different antibodies against different antigens, but labeled with the same fluorophore have similar average fluorescence per antibody bound, yields a direct measure of ABC. A basic factor to consider is whether the effective number of fluorophores per antibody (effective F/P) is the same for the calibration anti-CD4 antibody and test antibodies. Several published studies support the assumption that different antibodies against different antigens with the same fluorophore label can have similar effective F/P values if these antibodies are produced by the same manufacturer [16–18]. In principle, the effective F/P of antibodies can be measured by using a NIST monoclonal antibody reference material, RM 8671 with a known antibody concentration [19] to determine concentrations of these antibodies and by comparing their respective fluorescence intensities [20]. Due to changes in the microenvironment surrounding the fluorophore-antibody conjugates before and after the process of the cell staining, there could be further changes in the measured effective F/P [21]. The ideal situation would use antibody conjugates that consisted of only one fluorophore coupled to each antibody (e.g., unimolar PE antibody conjugate) in a location that did not interfere with the ability of the antibody to bind to antigen. Frequently a fluorophore-conjugated antibody will have lower affinity than unconjugated antibody, so both the calibration antibody and any test antibodies should be purified to exclude unconjugated antibody. Moreover, it is also possible that two different conjugates of the same antibody reagent conjugated with the same average number of fluorophores could give different effective F/P and different degrees of cell staining if the distribution of flurophores within antibody is different.

2. The specific measurement configuration of the quantiFlash™ used in this chapter for obtaining Q and B is only one of many configurations described in the User Manual [14]. Users can select their own choices of configurations while keeping in mind that if both trigger and fluorescence LED are placed under the same Laser detector array, but different fluorescence detectors, the laser delay does not have to be set at zero. Additionally, the quantiFlash™ fiber optic cables are terminated with an SMA (Sub-Miniature version A) fiber optic connector and can be attached directly to many manufacturers PMT blocks. Moreover, placement of both trigger and

fluorescence fiber optics must be physically stable over the duration of the measurements for valid data collection. Note that Q values can be affected by laser power and PMT voltages. The PMT voltages set during calibration should be used for the LED measurements. This will insure the Q value best represent instrument performance and detector sensitivity for quantitative cytometry measurements.

3. If generic least squares regression programs are used to fit the quadratic equation in Subheading 3.2.2, **step 13**, it is possible to obtain values for the $CV_{intrinsic}$ that may be negative, and are fitting artifacts. These don't have any physical meaning as the quantiFlash™ LED has a specified intrinsic CV of 0.1%. A negative $CV_{intrinsic}$ is most likely to occur when data points representing peak CVs of less than 1% are present and there is no weighting or improper weighting used for the fit. If the negative intrinsic CVs are small (<-0.2%) then they can be safely ignored. Alternatively, linear fits to the peaks with higher peak CVs can be used, effectively setting the $CV_{intrinsic}$ to zero.
4. Following the successful flow cytometers daily QC, the multiple gates of the calibration microsphere populations in the FC histograms in Subheading 3.2.1 can also be used to periodically track the stability of cytometer performance with the same PMT voltage setting. If the instrument performance is stable, users may transfer the CD4 reference biomarker expression in ABC to the calibration microspheres in their first experiment to subsequent experiments. Large deviations in the window of analysis of any FC would require attention for troubleshooting and/or instrument service. The equation for the determination of the ABC value of the unknown in Subheading 3.4 is appropriate for the measurements carried out under linear amplification which is highly recommended for quantitative cytometry measurements. In the case of measurements using logarithmic amplifier, the corresponding equation has been provided in ref. 9.

Acknowledgments

We are indebted to Steve Perfetto, Vaccine Research Center of NIH for his help with the troubleshooting the use of the quantiFlash™ LED pulser for the instrument sensitivity characterization. Authors are also thankful for Heba Degheidy, Fatima Abbasi, Howard Mostowski, Gerald Marti, and Steven Bauer all from FDA, and Robert Hoffman at Cytometry and Biophotonics Consulting, CA for their collaborative effort on quantitative flow cytometer measurements in the unit of antibodies bound per cell.

Disclaimer Certain commercial equipment, instruments, and materials are identified in this paper to specify adequately the experimental procedure. In no case does such identification imply recommendation or endorsement by the National Institute of Standards and Technology, nor does it imply that the materials or equipment are necessarily the best available for the purpose. One Author, James Wood declares a financial interest with A·P·E Angewandte Physik & Elektronik GmbH, Germany.

References

1. Fluorescence calibration and quantitative measurements of fluorescence instensity (2004) NCCLS (I/LA24-A)
2. Certificate of analysis, standard reference material 1932, fluorescein solution (2012) National Institute of Standards and Technology https://www-s.nist.gov/srmors/view_cert.cfm?srm=1932
3. Wang L, Gaigalas AK, Marti G, Abbasi F, Hoffman RA (2008) Toward quantitative fluorescence measurements with multicolor flow cytometry. Cytometry A 73(4):279–288. doi:10.1002/cyto.a.20507
4. Certificate of analysis, standard reference material 1934, fluorescent dyes for quantitative flow cytometry (visible spectral range) (2016). National Institute of Standards and Technology. https://www-s.nist.gov/srmors/view_cert.cfm?srm=1934
5. Perfetto SP, Chattopadhyay PK, Wood J, Nguyen R, Ambrozak D, Hill JP, Roederer M (2014) Q and B values are critical measurements required for inter-instrument standardization and development of multicolor flow cytometry staining panels. Cytometry A 85 (12):1037–1048. doi:10.1002/cyto.a.22579
6. Davis KA, Abrams B, Iyer SB, Hoffman RA, Bishop JE (1998) Determination of CD4 antigen density on cells: role of antibody valency, avidity, clones, and conjugation. Cytometry 33 (2):197–205
7. Wang L, Abbasi F, Ornatsky O, Cole KD, Misakian M, Gaigalas AK, He HJ, Marti GE, Tanner S, Stebbings R (2012) Human CD4+ lymphocytes for antigen quantification: characterization using conventional flow cytometry and mass cytometry. Cytometry A 81 (7):567–575. doi:10.1002/cyto.a.22060
8. Wang M, Misakian M, He HJ, Bajcsy P, Abbasi F, Davis JM, Cole KD, Turko IV, Wang L (2014) Quantifying CD4 receptor protein in two human CD4+ lymphocyte preparations for quantitative flow cytometry. Clin Proteomics 11(1):43. doi:10.1186/1559-0275-11-43
9. Wang L, Degheidy H, Abbasi F, Mostowski H, Marti G, Bauer S, Hoffman RA, Gaigalas AK (2016) Quantitative flow cytometry measurements in antibodies bound per cell based on a CD4 reference. Curr Protoc Cytom 75:1.29.1–1.29.14. doi:10.1002/0471142956.cy0129s75
10. Roederer M (2002) Compensation in flow cytometry. Curr Protoc Cytom 22:1.14.1–1.14.20. doi:10.1002/0471142956.cy0114s22
11. Stewart CC, Stewart SJ (2001) Titering antibodies. Curr Protoc Cytom 4:1.1–1.13. doi:10.1002/0471142956.cy0401s14
12. Chase ES, Hoffman RA (1998) Resolution of dimly fluorescent particles: a practical measure of fluorescence sensitivity. Cytometry 33 (2):267–279
13. Hoffman RA, Wood JC (2007) Characterization of flow cytometer instrument sensitivity. Curr Protoc Cytom 40:1.20.1–1.20.18. doi:10.1002/0471142956.cy0120s40
14. The quantiFlash™ User Manual (December 2015)
15. Wood JC (1998) Fundamental flow cytometer properties governing sensitivity and resolution. Cytometry 33(2):260–266
16. Degheidy H, Abbasi F, Mostowski H, Gaigalas AK, Marti G, Bauer S, Wang L (2015) Consistent, multi-instrument single tube quantification of CD20 in antibody bound per cell based on CD4 reference. Cytometry B Clin Cytom 90:159–167. doi:10.1002/cyto.b.21253
17. Wang L, Abbasi F, Gaigalas AK, Vogt RF, Marti GE (2006) Comparison of fluorescein and phycoerythrin conjugates for quantifying CD20 expression on normal and leukemic B-cells. Cytometry B Clin Cytom 70 (6):410–415. doi:10.1002/cyto.b.20140
18. Degheidy H, Bauer S, Marti GE, Wang L (2014) Flow cytometer performance characterization, standardization and calibration against CD4 on T lymphocytes enables quantification

of biomarker expression for immunological applications. J Biomed Sci Eng 7:756–768

19. Schiel JE, Mire-Sluis A, Davis D (2014) Monoclonal antibody therapeutics: the need for biopharmaceutical reference materials. In: Schiel JE, Davis DL, Borisov OV (eds) Monoclonal antibody therapeutics: structure, function, and regulatory space, vol 1. State-of-the-Art and Emerging Technologies for Therapeutic Monoclonal Antibody Characterization, ACS Symposium Series. doi:10.1021/bk-2014-1176.ch001
20. Wang L, Abbasi F, Gaigalas AK, Hoffman RA, Flagler D, Marti GE (2007) Discrepancy in measuring CD4 expression on T-lymphocytes using fluorescein conjugates in comparison with unimolar CD4-phycoerythrin conjugates. Cytometry B Clin Cytom 72(6):442–449. doi:10.1002/cyto.b.20354
21. Wang L, Gaigalas AK, Abbasi F, Marti GE, Vogt RF, Schwartz A (2002) Quantitating fluorescence intensity from Fluorophores: practical use of MESF values. J Res Natl Inst Stand Technol 107:339–353. doi:10.6028/jres.107.027

Chapter 7

High Throughput Flow Cytometry for Cell Surface Profiling

Joshua Paterson and Laurie E. Ailles

Abstract

Cell surface proteins are widely studied in the search for new biomarkers and therapeutic targets, but there is little information available about the surfaceome of individual cells, and this is difficult to obtain experimentally, especially in heterogeneous samples. Flow cytometry is a simple and robust tool for assessing cell surface protein expression on a single-cell level in a wide variety of cell types. However, due to the cost and relative scarcity of reagents, it is typically limited to interrogating known markers, screening small curated subsets of likely candidates, or validating targets obtained via other high throughput methods such as transcriptional profiling. Given recent advances in our understanding of stem cells, tumor-initiating cells, and other rare populations in seemingly homogenous samples, and the relative lack of correlation between the transcriptome and the surfaceome, large-scale flow cytometry screens have become an appealing option. A relatively exhaustive microarray-like flow cytometry screening platform can reveal unexpected markers or sub-populations that are not readily detected by other methods. The single-cell resolution, reliability, and simplicity of flow cytometry and the additional benefit of sub-population/heterogeneity discrimination with the addition of functional and/or phenotypic co-stains allow for the rapid generation of very reliable data from a wide variety of samples at a low cost per sample. These larger datasets can be used for more elaborate bioinformatics, such as hierarchical clustering. Here we describe a method for high throughput cell surface profiling using conventional single or multicolor flow cytometry, which can be adapted to an antibody panel of any size.

Key words High throughput, Cell surface markers, Stem cells, Antibody array, Biomarker, Surfaceome, Molecular profiling

1 Introduction

Cell surface proteins are of particular interest in biomedical research due to their utility as markers of cellular lineage or function, and because they are relatively amenable to targeted therapeutic intervention. The cell surfaceome consists of the subset of proteins (membrane-spanning or glycophosphatidylinositol (GPI)-anchored) with domains that extend into the extracellular space, such as integrins, receptor tyrosine kinases, G-protein coupled receptors, and ion channels. Collectively, these proteins mediate many important biological functions, including cell-cell

Teresa S. Hawley and Robert G. Hawley (eds.), *Flow Cytometry Protocols*, Methods in Molecular Biology, vol. 1678, DOI 10.1007/978-1-4939-7346-0_7,

communication and interaction, and responses to the external environment. Cell surface proteins can be used to very accurately define phenotypic and functional differences between cell types, and between normal and diseased cells, such as cancer cells. Cell surface proteins have therefore been the subject of much study in the search for novel phenotypic, diagnostic, prognostic, and therapeutic targets in oncology, immunology, and stem cell research. A method for rapid, simple, and cost-effective characterization of the cell surfaceome could not only lead to identification and development of new phenotypic or diagnostic markers and therapeutic targets, but also provide insights into basic biology.

One approach to cell surfaceome characterization is the use of genome-based methods to bioinformatically predict membrane-associated proteins and then measure the expression of these predicted genes in a given cell type using transcriptional profiling [1]. However, this approach lacks the ability to discern protein abundance, cellular distribution, and presence of isoforms, including post-translational modifications, factors which directly impact the signaling capacities or functions of these proteins and the overall functional impact of their expression. Furthermore, mRNA expression is not always correlated with protein expression [2, 3] and not all expressed membrane proteins are present on the cell surface. In fact, combined global gene expression and protein quantification studies have shown that correlation between mRNA levels and protein abundance is relatively low for cell surface proteins in particular [4]. Therefore, the presence of these proteins must be directly assessed on the cell surface.

A more direct method of assessing protein expression is to perform proteomics analysis using mass spectrometry to globally identify and quantify the entire proteome in a sample of interest [5]. However, identifying cell surface proteins with this approach is technically challenging due to their limited abundance and to the difficulty in resolving and identifying proteins with hydrophobic transmembrane domains [6]. Recent technical advances have allowed plasma membrane protein enrichment and "cell surface capturing" approaches for more accurate measurement of cell surface proteins by mass spectrometry [6, 7], but this method is still limited by the high number of cells required and the technical complexity of the method. Importantly, both transcriptomic and proteomic methods provide an average measure of the entire sample, making analysis of tumor heterogeneity and small cellular compartments within samples, such as stem cells or tumor-initiating cells, a challenge.

Monoclonal antibodies (MAbs) can provide extremely sensitive and reliable information about the expression of cell surface proteins, as well as the distribution of these proteins within a complex heterogeneous sample or discrete cellular compartments. Flow cytometry (FC) utilizes fluorescently-tagged MAbs to detect

proteins on large numbers of whole (typically live) cells. These assays are specific, sensitive, cost-effective, can exclude non-viable or other non-desirable cells from analysis, and importantly offer single-cell resolution. This resolution allows the identification of rare populations within samples that would appear homogenous with other approaches and easily allows the selective analysis of subpopulations within complex heterogeneous samples with the addition of stains for functional and/or phenotypic markers.

Given the general importance of cell surface proteins to a wide range of biological processes, their broad utility as biomarkers of disease, and their potential as therapeutic targets, as well as recent advances in our understanding of stem cells, tumor-initiating cells, and other rare populations, FC-based surfaceome analysis has become very appealing. We recently developed a MAb-based FC cell surface protein screen composed of 368 fluorochrome-conjugated cell surface protein targeted antibodies arrayed into 96-well plates. These are used with a high-speed plate-based sample loading device for flow cytometers, which allows high-throughput FC-based analysis of an unprecedentedly large number of cell surface proteins in a single assay [8]. This high throughput flow cytometry (HT-FC) screen can be used to rapidly generate highly reproducible cell surface protein profiles at a low cost per sample and can be used to answer a wide range of biological questions [8–11]. Since flow cytometry allows for multiple fluorochromes to be analyzed simultaneously co-stains for additional functional and/or phenotypic markers can be added (Global Co-staining), which allows for independent analysis of subpopulations of interest within complex cell mixtures (such as primary tumors), or for the discrimination of cells expressing specific functional markers from otherwise similar cell types. These large datasets are robust enough to allow for the application of standard microarray-like bioinformatics techniques such as hierarchical clustering and principal components analysis. The protocol we describe here was developed for a large antibody panel (Table 1), but would be useful for any panel greater than ~20 antibodies. Results are obtained rapidly, and the use of commercially available antibodies means that high quality reagents are immediately available for follow-up studies and/or development of more focused panels for specific applications.

2 Materials

2.1 Reagents

1. Fresh or cryopreserved primary or cultured cells in single-cell suspension.
2. Flow cytometry (FC) buffer: HBSS, 2 mM EDTA, 1% bovine serum albumin (BSA) (*see* **Note 1**).
3. Phosphate-buffered saline (PBS).

Table 1
Antibodies included in HT-FC panel

Antigen	Isotype	NCBI gene name	Entrez gene ID	Supplier	Clone
CD1a	Mouse IgG1, κ	CD1A	909	BD biosciences	HI149
CD1b	Mouse IgG1, κ	CD1B	910	BD biosciences	M-T101
CD1c	Mouse IgG1, κ	CD1C	911	BioLegend	L161
CD1d	Mouse IgG1, κ	CD1D	912	BD biosciences	CD1d42
CD2	Mouse IgG1, κ	CD2	914	BD biosciences	RPA-2.10
CD3	Mouse IgG2a, κ	CD3E	916	BD biosciences	HIT3a
CD3e	Mouse IgG1	CD3E	916	R&D systems	UCHT1
CD4	Mouse IgG1, κ	CD4	920	BD biosciences	RPA-T4
CD5	Mouse IgG1, κ	CD5	921	BD biosciences	UCHT2
CD6	Mouse IgG1, κ	CD6	923	BD biosciences	M-T605
CD7	Mouse IgG1, κ	CD7	924	BD biosciences	M-T701
CD8	Mouse IgG1, κ	CD8A	925	BD biosciences	HIT8a
CD8b	Mouse IgG2a, κ	CD8B	926	BD biosciences	2ST8.5H7
CD9	Mouse IgG1, κ	CD9	928	BD biosciences	M-L13
CD10	Mouse IgG1, κ	MME	4311	BD biosciences	HI10a
CD11a	Mouse IgG1, κ	ITGAL	3683	BD biosciences	HI111
CD11b	Mouse IgG1, κ	ITGAM	3684	BD biosciences	ICRF44
CD11c	Mouse IgG1, κ	ITGAX	3687	BD biosciences	B-ly6
CD13	Mouse IgG1, κ	ANPEP	290	BD biosciences	WM15
CD14	Mouse IgG2a, κ	CD14	929	BD biosciences	M5E2
CD15	Mouse IgM, k	FUT4	2526	BD biosciences	HI98
CD16	Mouse IgG1, κ	FCGR3A	2214	BD biosciences	3G8
CD16b	Mouse IgG2a, κ	FCGR3B	2215	BD biosciences	CLB-gran11.5
CD17	Mouse IgM	N/A	N/A	Lifespan biosciences	Not given
CD18	Mouse IgG1, κ	ITGB2	3689	BD biosciences	6.7
CD19	Mouse IgG1, κ	CD19	930	BD biosciences	HIB19
CD20	Mouse IgG2b, k	MS4A1	931	BD biosciences	2H7
CD21	Mouse IgG1, κ	CR2	1380	BD biosciences	B-ly4
CD22	Mouse IgG2b, k	CD22	933	BD biosciences	S-HCL-1

(continued)

Table 1
(continued)

Antigen	Isotype	NCBI gene name	Entrez gene ID	Supplier	Clone
CD23	Mouse IgG1, κ	FCER2	2208	BD biosciences	M-L233
CD24	Mouse IgG2a, κ	CD24	100133941	BD biosciences	ML5
CD25	Mouse IgG1, κ	IL2RA	3559	BD biosciences	M-A251
CD26	Mouse IgG1, κ	DPP4	1803	BD biosciences	M-A261
CD27	Mouse IgG1, κ	CD27	939	BD biosciences	M-T271
CD28	Mouse IgG1, κ	CD28	940	BD biosciences	CD28.2
CD29	Mouse IgG1, κ	ITGB1	3688	BD biosciences	MAR4
CD30	Mouse IgG1, κ	TNFRSF8	943	BD biosciences	BerH8
CD31	Mouse IgG1, κ	PECAM1	5175	BD biosciences	WM59
CD32	Mouse IgG1, κ	FCGR2A	2212	BD biosciences	3D3
CD33	Mouse IgG1, κ	CD33	945	BD biosciences	P67.6
CD34	Mouse IgG1, κ	CD34	947	BD biosciences	581
CD35	Mouse IgG1, κ	CR1	1378	BD biosciences	E11
CD36	Mouse IgM, k	CD36	948	BD biosciences	CB38 (NL07)
CD37	Mouse IgG1, κ	CD37	951	BD biosciences	M-B371
CD38	Mouse IgG1, κ	CD38	952	BD biosciences	HIT2
CD39	Mouse IgG2b, κ	ENTPD1	953	BD biosciences	TÜ66
CD40	Mouse IgG1, κ	CD40	958	BD biosciences	5C3
CD41a	Mouse IgG1, κ	ITGA2B/ ITGB3		BD biosciences	HIP8
CD41b	Mouse IgG3, κ	ITGA2B	3674	BD biosciences	HIP2
CD42a	Mouse IgG1, κ	GP9	2815	BD biosciences	ALMA.16
CD42b	Mouse IgG1, κ	GP1BA	2811	BD biosciences	HIP1
CD43	Mouse IgG1, κ	SPN	6693	BD biosciences	1G10
CD44	Mouse IgG2b, k	CD44	960	BD biosciences	G44-26
CD45	Mouse IgG1, κ	PTPRC	5788	BD biosciences	HI30
CD45RA	Mouse IgG2b, k	PTPRC	5788	BD biosciences	HI100
CD45RB	Mouse IgG1, κ	PTPRC	5788	BD biosciences	MT4
CD45RO	Mouse IgG2a, κ	PTPRC	5788	BD biosciences	UCHL1
CD46	Mouse IgG2a, κ	CD46	4179	BD biosciences	E4.3

(continued)

Table 1
(continued)

Antigen	Isotype	NCBI gene name	Entrez gene ID	Supplier	Clone
CD47	Mouse IgG1, κ	CD47	961	BD biosciences	B6H12
CD48	Mouse IgM, k	CD48	962	BD biosciences	TÜ145
CD49a	Mouse IgG1, κ	ITGA1	3672	BD biosciences	SR84
CD49b	Mouse IgG2a, κ	ITGA2	3673	BD biosciences	12F1
CD49c	Mouse IgG1, κ	ITGA3	3675	BD biosciences	C3 II.1
CD49d	Mouse IgG1, κ	ITGA4	3676	BD biosciences	9F10
CD49e	Mouse IgG1, κ	ITGA5	3678	BD biosciences	IIA1
CD49f	Rat IgG2a, κ	ITGA6	3655	BD biosciences	GoH3
CD50	Mouse IgG2b, k	ICAM3	3385	BD biosciences	TÜ41
CD51/CD61	Mouse IgG1, κ	ITGAV	3685	BD biosciences	23C6
CD52	Mouse IgG2b, k	CD52	1043	BioLegend	HI186
CD53	Mouse IgG1, κ	CD53	963	BD biosciences	HI29
CD54	Mouse IgG1, κ	ICAM1	3383	BD biosciences	HA58
CD55	Mouse IgG2a, κ	CD55	1604	BD biosciences	IA10
CD56	Mouse IgG1, κ	NCAM1	4684	BD biosciences	B159
CD57	Mouse IgM, k	B3GAT1	27087	BD biosciences	HNK-1
CD58	Mouse IgG2a, κ	CD58	965	BD biosciences	1C3
CD59	Mouse IgG2a, κ	CD59	966	BD biosciences	p282 (H19)
CD60b	Mouse IgM	N/A	N/A	Lifespan biosciences	Not provided
CD61	Mouse IgG1, κ	ITGB3	3690	BD biosciences	Vi-PL2
CD62E	Mouse IgG1, κ	SELE	6401	BD biosciences	68-5H11
CD62L	Mouse IgG2a, κ	SELL	6402	BD biosciences	Sk11
CD62P	Mouse IgG1, κ	SELP	6403	BD biosciences	AK-1
CD63	Mouse IgG1, κ	CD63	967	BD biosciences	H5C6
CD64	Mouse IgG1, κ	FCGR1A	2209	BD biosciences	10.1
CD65	Mouse IgM	N/A	N/A	Beckman coulter	88H7
CD65s	Mouse IgM	N/A	N/A	Abcam	VIM-2
CD66	Mouse IgG2a, κ	CEACAM1	109770	BD biosciences	B1.1/CD66
CD66b	Mouse IgM, k	CEACAM8	1088	BD biosciences	G10F5

(continued)

Table 1
(continued)

Antigen	Isotype	NCBI gene name	Entrez gene ID	Supplier	Clone
CD66c	Mouse IgG1, κ	CEACAM6	4680	BD biosciences	B6.2/ CD66c
CD66e	Mouse IgG1	CEACAM5	1048	R&D systems	487,618
CD69	Mouse IgG1, κ	CD69	969	BD biosciences	FN50
CD70	Mouse IgG3, κ	CD70	970	BD biosciences	Ki-24
CD71	Mouse IgG2a, κ	TFRC	7037	BD biosciences	M-A712
CD72	Mouse IgG2b, k	CD72	971	BD biosciences	J4-118
CD73	Mouse IgG1, κ	NT5E	4907	BD biosciences	AD2
CD74	Mouse IgG2a, κ	CD74	972	BD biosciences	M-B741
CD75	Mouse IgM, k	N/A	N/A	BD biosciences	LN1
CD77	Mouse IgM, k	N/A	N/A	BD biosciences	5B5
CD79a	Mouse IgG1, κ	CD79A	973	R&D	706,931
CD79b	Mouse IgG1, κ	CD79B	974	BD biosciences	CB3-1
CD80	Mouse IgG1, κ	CD80	941	BD biosciences	L307.4
CD81	Mouse IgG1, κ	CD81	975	BD biosciences	JS-81
CD82	Mouse IgG2a, κ	CD82	3732	BioLegend	ASL-24
CD83	Mouse IgG1, κ	CD83	9308	BD biosciences	HB15e
CD84	Mouse IgG1	CD84	8832	BioLegend	CD84.1.21
CD85A	Mouse IgG1	LILRB3	11025	BioLegend	MKT5.1
CD85D	Rat IgG2a	LILRB2	10288	BioLegend	42D1
CD85G	Mouse IgG1	LILRA4	23547	BioLegend	17G10.2
CD85H	Rat IgG2a, κ	LILRA2	11027	BioLegend	24
CD85J	Mouse IgG2b, k	LILRB1	10859	BD biosciences	GHI/75
CD86	Mouse IgG1, κ	CD86	942	BD biosciences	2331 (FUN-1)
CD87	Mouse IgG1, κ	PLAUR	5329	BD biosciences	VIM5
CD88	Rabbit IgG	C5AR1	728	BD biosciences	C85-4124
CD89	Mouse IgG1, κ	FCAR	2204	BD biosciences	A59
CD90	Mouse IgG1, κ	THY1	7070	BD biosciences	5E10
CD91	Mouse IgG1, κ	LRP1	4035	BD biosciences	A2MR-α2
CD92	Mouse IgG2b	SLC44A1	23446	Abcam	VIM-15b

(continued)

Table 1
(continued)

Antigen	Isotype	NCBI gene name	Entrez gene ID	Supplier	Clone
CDw93	Mouse IgG2b, k	CD93	22918	BD biosciences	R139
CD94	Mouse IgG1, κ	KLRD1	3824	BD biosciences	HP-3D9
CD95	Mouse IgG1, κ	FAS	355	e-bioscience	DX2
CD96	Mouse IgG1	CD96	10225	BioLegend	NK92.39
CD97	Mouse IgG1, κ	CD97	976	BD biosciences	VIM3b
CD98	Mouse IgG1, κ	SLC3A2	6520	BD biosciences	UM7F8
CD99	Mouse IgG2a, κ	CD99	4267	BD biosciences	TÜ12
CD100	Mouse IgM	SEMA4D	10507	e-bioscience	133-1C6
CD101	Mouse IgG1	IGSF2	9398	e-bioscience	BB27
CD102	Mouse IgG2a, κ	ICAM2	3384	BD biosciences	CBR-1C2/2.1
CD103	Mouse IgG1, κ	ITGAE	3682	BD biosciences	Ber-ACT8
CD104	Rat IgG2b, κ	ITGB4	3691	BD biosciences	439-9B
CD105	Mouse IgG1	ENG	2022	e-bioscience	SN6
CD106	Mouse IgG1, κ	VCAM1	7412	BD biosciences	51-10C9
CD107a	Mouse IgG1, κ	LAMP1	3916	BD biosciences	H4A3
CD107b	Mouse IgG1, κ	LAMP2	3920	BD biosciences	H4B4
CD108	Mouse IgG2a, κ	SEMA7A	8482	BD biosciences	KS-2
CD109	Mouse IgG1, κ	CD109	135228	BD biosciences	TEA 2/16
CD110	Mouse IgG2b, κ	MPL	4352	BD biosciences	1.6.1
CD111	Mouse IgG1, κ	PVRL1	5818	BioLegend	R1.302
CD112	Mouse IgG1, κ	PVRL2	5819	BD biosciences	R2.525
CD114	Mouse IgG1, κ	CSF3R	1441	BD biosciences	LMM741
CD115	Mouse IgG1	CSF1R	1436	R&D systems	61708
CD116	Mouse IgG1, κ	CSF2RA	1438	BD biosciences	hGMCSFR-M1
CD117	Mouse IgG1, κ	KIT	3815	BD biosciences	YB5.B8
CD118	Mouse IgG1	LIFR	3977	R&D systems	32953
CD119	Mouse IgG1, κ	IFNGR1	3459	BD biosciences	GIR-208
CD120a	Mouse IgG1	TNFRSF1A	7132	R&D systems	16803

(continued)

Table 1
(continued)

Antigen	Isotype	NCBI gene name	Entrez gene ID	Supplier	Clone
CD120b	Rat IgG2b, κ	TNFRSF1B	7133	BD biosciences	hTNFR-M1
CD121b	Mouse IgG1	IL1R2	7850	R&D systems	34141
CD122	Mouse IgG1, κ	IL2RB	3560	BD biosciences	Mik-β3
CD123	Mouse IgG2a, κ	IL3RA	3563	BD biosciences	7G3
CD124	Mouse IgG1, κ	IL4R	3566	BD biosciences	hIL4R-M57
CD125	Mouse IgG1	IL5RA	3568	R&D systems	26815
CD126	Mouse IgG1, κ	IL6R	3570	BD biosciences	M5
CD127	Mouse IgG1, κ	IL7R	3575	BD biosciences	hIL-7R-M21
CD129	Mouse IgG2b, k	IL9R	3581	BioLegend	AH9R7
CD130	Mouse IgG1, κ	IL6ST	3572	BD biosciences	AM64
CD131	Mouse IgG1, κ	CSF2RB	1439	e-bioscience	1C1
CD132	Mouse IgG1, κ	IL2RG	3561	BD biosciences	AG184
CD133	Mouse IgG1, κ	PROM1	8842	Miltenyi	AC133
CD134	Mouse IgG1, κ	TNFRSF4	7293	BD biosciences	ACT35
CD135	Mouse IgG1, κ	FLT3	2322	BD biosciences	4G8
CD136	Not given	MST1R	4486	Beckman coulter	ID1
CD137	Mouse IgG1, κ	TNFRSF9	3604	BD biosciences	4B4–1
CD137L	Mouse IgG1, κ	TNFSF9	8744	BioLegend	5F4
CD138	Mouse IgG1, κ	SDC1	6382	BD biosciences	MI15
CD140a	Mouse IgG2a, κ	PDGFRA	5156	BD biosciences	αR1
CD140b	Mouse IgG2a, κ	PDGFRB	5159	BD biosciences	28D4
CD141	Mouse IgG1, κ	THBD	7056	BD biosciences	1A4
CD142	Mouse IgG1, κ	F3	2152	BD biosciences	HTF-1
CD143 (R&D)	Mouse IgG1	ACE	1636	R&D systems	171417
CD143 (BD)	Mouse IgG1, κ	ACE	1636	BD biosciences	BB9
CD144	Mouse IgG1, κ	CDH5	1003	BD biosciences	55-7H1
CD146	Mouse IgG1, κ	MCAM	4162	BD biosciences	P1H12
CD147	Mouse IgG1, κ	BSG	682	BD biosciences	HIM6
CD148	Mouse IgG1	PTPRJ	5795	R&D systems	143-41
CD150	Mouse IgG1, κ	SLAMF1	6504	BD biosciences	A12

(continued)

Table 1
(continued)

Antigen	Isotype	NCBI gene name	Entrez gene ID	Supplier	Clone
CD151	Mouse IgG1, κ	CD151	977	BD biosciences	14A2.H1
CD152	Mouse IgG2a, κ	CTLA4	1493	BD biosciences	BNI3
CD153	Mouse IgG2B	TNFSF8	944	R&D systems	116,614
CD154	Mouse IgG1, κ	CD40LG	959	BD biosciences	TRAP1
CD155	Mouse IgG1	PVR	5817	e-bioscience	2H7CD155
CD156b	Mouse IgG1	ADAM17	6868	R&D systems	111,633
CD157	Mouse IgG1, κ	BST1	683	MBL	RF3
CD158A	Mouse IgM, κ	KIR2DL1	3802	BD biosciences	HP-3E4
CD158B1	Mouse IgG2b, k	KIR2DL2	3803	BD biosciences	CH-L
CD158B2	Mouse IgG2a, κ	KIR2DL3	3804	BD biosciences	DX27
CD158D	Mouse IgG2a	KIR2DL4	3805	R&D systems	181,703
CD158E2	Mouse IgG1, κ	KIR3DS1	3813	BD biosciences	DX9
CD158F	Mouse IgG1	KIR2DL5A	57292	BioLegend	UP-R1
CD158I	Mouse IgG1	KIR2DS4	3809	Miltenyi	JJC11.6
CD159a	Mouse IgG2a	KLRC1	3821	R&D systems	131411
CD159c	Mouse IgG1	KLRC2	3822	R&D systems	134591
CD160	Mouse IgM, κ	CD160	11126	BioLegend	BY55
CD161	Mouse IgG1, κ	KLRB1	3820	BD biosciences	DX12
CD162	Mouse IgG1, κ	SELPLG	6404	BD biosciences	KPL-1
CD163	Mouse IgG1, κ	CD163	9332	BD biosciences	GHI/61
CD164	Mouse IgG2a, κ	CD164	8763	BD biosciences	N6B6
CD165	Mouse IgG1	CD165	23449	e-bioscience	SN2 N56-D11
CD166	Mouse IgG1, κ	ALCAM	214	BD biosciences	3A6
CD167a	Mouse IgM, k	DDR1	780	BioLegend	51D6
CD169	Mouse IgG1	SIGLEC1	6614	BioLegend	7-239
CD170	Mouse IgG1	SIGLEC5	8778	R&D systems	194128
CD171	Mouse IgG2a	L1CAM	3897	e-bioscience	5G3
CD172a	Mouse IgG1, κ	SIRPA	140885	BioLegend	SE5A5
CD172b	Mouse IgG1, κ	SIRPB1	10326	BD biosciences	B4B6
CD172g	Mouse IgG1, κ	SIRPG	55423	BioLegend	LSB2.20

(continued)

Table 1
(continued)

Antigen	Isotype	NCBI gene name	Entrez gene ID	Supplier	Clone
CD175s	Mouse IgG1	N/A	N/A	Abcam	STn 219
CD177	Mouse IgG1	CD177	57126	Abcam	MEM-166
CD178	Mouse IgG1, κ	FASLG	356	BioLegend	NOK-1
CD179a	Mouse IgG1, κ	VPREB1	7441	BioLegend	HSL96
CD180	Mouse IgG1, κ	CD180	4064	BD biosciences	G28-8
CD181	Mouse IgG2b, k	IL8RA	3577	BD biosciences	5A12
CD182	Mouse IgG1, κ	IL8RB	3579	BD biosciences	6C6
CD183	Mouse IgG1, κ	CXCR3	2833	BD biosciences	1C6/ CXCR3
CD184	Mouse IgG2a, κ	CXCR4	7852	BD biosciences	12G5
CD185	Mouse IgG2b, k	BLR1	643	BD biosciences	RF8B2
CD186	Mouse IgG2b, k	CXCR6	10663	R&D systems	56811
CD191	Mouse IgG2b	CCR1	1230	R&D systems	53504
CD192	Mouse IgG2b, k	CCR2	729230	BD biosciences	48607
CD193	Mouse IgG2b, k	CCR3	1232	BD biosciences	5E8
CD194	Mouse IgG2b, k	CCR4	1233	BioLegend	TG6/CCR4
CD195	Mouse IgG2a, κ	CCR5	1234	BD biosciences	3A9
CD196	Mouse IgG1, κ	CCR6	1235	BD biosciences	11A9
CD197	Rat IgG2a, κ	CCR7	1236	BD biosciences	3D12
CDw198	Rat IgG2b	CCR8	1237	R&D systems	191704
CDw199	Mouse IgG2a, κ	CCR9	10803	BD biosciences	112509
CD200	Mouse IgG1, κ	CD200	4345	BD biosciences	MRC ox-104
CD201	Rat IgG1, k	PROCR	10544	BD biosciences	RCR-252
CD202b	Mouse IgG1, κ	TEK	7010	BioLegend	33.1 (Ab33)
CD203c	Mouse IgG1, κ	ENPP3	5169	BioLegend	NP4D6
CD204	Mouse IgG2B	MSR1	4481	R&D systems	351615
CD205	Mouse IgG2b, k	LY75	4065	BD biosciences	MG38
CD206	Mouse IgG1, κ	MRC1	4360	BD biosciences	19.2
CD207	Mouse IgG1	CD207	50489	R&D systems	343828
CD208	Mouse IgG1, κ	LAMP3	27074	BD biosciences	I10-1112
CD209	Mouse IgG2b, k	CD209	30835	BD biosciences	DCN46

(continued)

Table 1
(continued)

Antigen	Isotype	NCBI gene name	Entrez gene ID	Supplier	Clone
CDw210	Rat IgG2a, κ	IL10RA	3587	BD biosciences	3F9
CD212	Mouse IgG1, κ	IL12RB1	3594	BD biosciences	2.4e6
CD213a2	Mouse IgG1	IL13RA2	3598	Abcam	B-D13
CD215	Mouse IgG2B	IL15RA	3601	R&D systems	151303
CD217	Mouse IgG1	IL17RA	23765	BioLegend	BG/hIL17AR
CDw218a	Mouse IgG1, κ	IL18R1	8809	e-bioscience	H44
CD218b	Mouse IgG2b	IL18RAP	8807	R&D systems	132029
CD220	Goat IgG	INSR	3643	R&D systems	
CD221	Mouse IgG1, κ	IGF1R	3480	BD biosciences	1H7
CD222	Mouse IgG1, κ	IGF2R	3482	BioLegend	MEM-238
CD223	Goat IgG	LAG3	3902	R&D systems	Not given
CD226	Mouse IgG1, κ	CD226	10666	BD biosciences	DX11
CD227	Mouse IgG1, κ	MUC1	4582	BD biosciences	HMPV
CD229	Mouse IgG2a	LY9	4063	R&D systems	249936
CD230	Mouse IgG1, κ	PRNP	5621	e-bioscience	4D5
CD231	Mouse IgG1, κ	TSPAN7	7102	BioLegend	SN1a (M3-3D9)
CD234	Mouse IgG2A	DARC	2532	R&D systems	358307
CD235a	Mouse IgG2b, k	GYPA	2993	BD biosciences	GA-R2 (HIR2)
CD243 (BC)	Mouse IgG2a	ABCB1	5243	Beckman coulter	UIC2
CD243 (BD)	Mouse IgG2b, k	ABCB1	5243	BD biosciences	17F9
CD244	Mouse IgG2a, κ	CD244	51744	BD biosciences	2-69
CD245	Mouse IgG1, κ	NPAT	4863	BioLegend	DY12
CD249	Rat IgG1, k	ENPEP	2028	Lifespan bioscience	Not provided
CD252	Mouse IgG1, κ	TNFSF4	7292	BD biosciences	Ik-1
CD253	Mouse IgG1	TNFSF10	8743	BD biosciences	RIK-2
CD254	Mouse IgG2b, k	TNFSF11	8600	BioLegend	MIH24
CD255	Mouse IgG3	TNFSF12	8742	BD biosciences	CARL-1
CD256	Mouse IgG2a, κ	TNFSF13	8741	BioLegend	A3D8

(continued)

Table 1
(continued)

Antigen	Isotype	NCBI gene name	Entrez gene ID	Supplier	Clone
CD257	Mouse IgG1, κ	TNFSF13B	10673	BioLegend	T7-241
CD258	Mouse IgG1	TNFSF14	8740	R&D systems	115520
CD261	Mouse IgG1	TNFRSF10A	8797	BioLegend	DJR1
CD262	Mouse IgG2b	TNFRSF10B	8795	R&D systems	71908
CD263	Mouse IgG1	TNFRSF10C	8794	R&D systems	90906
CD264	Mouse IgG1	TNFRSF10D	8793	R&D systems	104918
CD267	Rat IgG2a, κ	TNFRSF13B	23495	BD biosciences	1A1-K21-M22
CD268	Mouse IgG1, κ	TNFRSF13C	115650	BD biosciences	11C1
CD269	Goat IgG	TNFRSF17	608	R&D systems	
CD270	Mouse IgG1, κ	TNFRSF14	8764	BioLegend	122
CD271	Mouse IgG1, κ	NGFR	4804	BD biosciences	C40-1457
CD272	Mouse IgG1, κ	BTLA	151888	BD biosciences	J168-540.90.22
CD273	Mouse IgG1, κ	PDCD1LG2	80380	BD biosciences	MIH18
CD274	Mouse IgG1, κ	CD274	29126	BD biosciences	MIH1
CD275	Mouse IgG2b, k	ICOSLG	23308	BD biosciences	2D3/B7-H2
CD276	Mouse IgG1, κ	CD276	80381	BioLegend	DCN.70
CD277	Mouse IgG1	BTN3A1	11119	e-bioscience	BT3.1
CD278	Mouse IgG1	ICOS	29851	BD biosciences	DX29
CD279	Mouse IgG1, κ	PDCD1	5133	BD biosciences	MIH4
CD281	Mouse IgG1, κ	TLR1	7096	BioLegend	TLR1.136
CD282	Mouse IgG1, κ	TLR2	7097	BD biosciences	11G7
CD283	Mouse IgG1, κ	TLR3	7098	e-bioscience	TLR3.7
CD284	Mouse IgG2a	TLR4	7099	R&D systems	610,015
CD286	Mouse IgG1, κ	TLR6	10333	BioLegend	TLR6.127
CD288	Mouse IgG1	TLR8	51311	Abcam	44C143
CD289	Rat IgG2a, κ	TLR9	54106	BD biosciences	eB72-1665
CD290	Mouse IgG1, κ	TLR10	81793	BioLegend	3C10C5
CD292	Goat IgG	BMPR1A	657	R&D systems	Polyclonal
CD294	Rat IgG2a, κ	GPR44	11251	BD biosciences	BM16
CD295	Mouse IgG2b	LEPR	3953	R&D systems	52263

(continued)

Table 1
(continued)

Antigen	Isotype	NCBI gene name	Entrez gene ID	Supplier	Clone
CD298	Mouse IgG2a	ATP1B3	483	BioLegend	LNH-94
CD299	Mouse IgG2b	CLEC4M	10332	R&D systems	120604
CD300a	Mouse IgG1	CD300A	11314	Abcam	MEM-260
CD300c	Mouse IgG1, κ	CD300C	10871	BioLegend	TX45
CD300e	Mouse IgG1, κ	CD300E	342510	BioLegend	UP-H2
CD301	Mouse IgG1	CLEC10A	10462	Imgenex	125A10.03
CD303	Mouse IgG1	CLEC4C	170482	Miltenyi	AC144
CD304	Mouse IgG1	NRP1	8829	Miltenyi	AD5-17F6
CD305	Mouse IgG1, κ	LAIR1	3903	BD biosciences	DX26
CD307e	Mouse IgG2a, κ	FCRL5	83416	BioLegend	509f6
CD309	Mouse IgG1	KDR	3791	R&D systems	89,106
CD312	Mouse IgG1	EMR2	30817	AbD Serotech	2A1
CD314	Mouse IgG1, κ	KLRK1	22914	BD biosciences	1D11
CD317	Mouse IgG1, κ	BST2	684	BioLegend	RS38E
CD318	Mouse IgG2a	CDCP1	64866	R&D systems	309,121
CD319	Mouse IgG2a	SLAMF7	57823	R&D systems	235,614
CD321	Mouse IgG1, κ	F11R	50848	BD biosciences	M.AB.F11
CD324	Mouse IgG2a, κ	CDH1	999	BD biosciences	67A4
CD325	Mouse IgG1, κ	CDH2	1000	e-bioscience	8C11
CD326	Mouse IgG1, κ	TACSTD1	4072	BD biosciences	EBA-1
CD328	Mouse IgG1, κ	SIGLEC7	27036	BD biosciences	F023-420
CDw329	Mouse IgG1, κ	SIGLEC9	27180	BD biosciences	E10-286
CD332	Mouse IgG1	FGFR2	2263	R&D systems	98725
CD333	Mouse IgG1	FGFR3	2261	R&D systems	136,334
CD334	Mouse IgG1, κ	FGFR4	2264	BioLegend	4FR6D3
CD335	Mouse IgG1, κ	NCR1	9437	BD biosciences	9E2/NKp46
CD336	Mouse IgG1, κ	NCR2	9436	BD biosciences	P44-8.1
CD337	Mouse IgG1, κ	NCR3	259197	BD biosciences	P30-15
CD338	Mouse IgG2b, k	ABCG2	9429	BioLegend	5D3
CD339	Mouse IgG2b	JAG1	182	R&D systems	188,331
CD340	Mouse IgG1, κ	ERBB2	2064	BD biosciences	Neu 24.7

(continued)

Table 1
(continued)

Antigen	Isotype	NCBI gene name	Entrez gene ID	Supplier	Clone
CD344	Mouse IgG1, κ	FZD4	8322	BioLegend	CH3A4A7
CD351	Mouse IgG1, κ	FCAMR	83953	BioLegend	TX61
CD352	Mouse IgG1, κ	SLAMF6	114836	BioLegend	NT-7
CD354	Mouse IgG1, κ	TREM1	54210	BioLegend	TREM-26
CD355	Mouse IgG2a, κ	CRTAM	56253	BioLegend	Cr24.1
CD357	Mouse IgG1, κ	TNFRSF18	8784	BioLegend	621
CD358/DR6	Mouse IgG1	TNFRSF21	27242	Abcam	DR-6-04-EC
CD360 (BL)	Mouse IgG1, κ	IL21R	50615	BioLegend	2G1-K12
CD360 (BD)	Mouse IgG1, κ	IL21R	50615	BD biosciences	17A12
CD362	Rat IgG2b	SDC2	6383	R&D systems	305515
CD363	Mouse IgG2b	S1PR1	1901	R&D systems	218713
β2-microglobulin	Mouse IgM, k	B2M	567	BD biosciences	TÜ99
BLTR-1	Mouse IgG1	LTB4R	1241	BD biosciences	203/14F11
CA9	Mouse IgG2a	CA9	768	R&D systems	303123
CDH11	Mouse IgG2a	CDH11	1009	R&D systems	667039
CDH3	Mouse IgG1	CDH3	1001	R&D systems	104805
CDH6	Mouse IgG1	CDH6	1004	R&D systems	427909
CLA	Rat IgM, κ	SELPLG	6404	BD biosciences	HECA-452
CLIP	Mouse IgG1, κ	N/A	N/A	BD biosciences	CerCLIP
DCIR	Mouse IgG1, κ	CLEC4A	50856	BD biosciences	I3–612
EGF-R	Mouse IgG2b, k	EGFR	1956	BD biosciences	EGFR1
FMC7	Mouse IgM, k	MS4A1	931	BD biosciences	FMC7
fMLP-R	Mouse IgG1, κ	FPR1	2357	BD biosciences	5F1
HLA-A2	Mouse IgG2b, k	HLA-A	3105	BD biosciences	BB7.2
HLA-ABC	Mouse IgG1, κ	ABCA1	19	BD biosciences	DX17
HLA-DM	Mouse IgG1, κ	HFE	3077	BD biosciences	MaP.DM1
HLA-DR	Mouse IgG2b, k	HFE	3077	BD biosciences	TU36
ITGB7	Rat IgG2a, κ	ITGB7	3695	BD biosciences	FIB504
LGR5	Rat IgG2b, κ	LGR5	8549	Miltenyi Biotec	DA03-22H2.8

(continued)

Table 1
(continued)

Antigen	Isotype	NCBI gene name	Entrez gene ID	Supplier	Clone
LTBR	Mouse IgG1, κ	LTBR	4055	BD biosciences	hTNFR-RP-M12
MIC A/B	Mouse IgG2a, κ	MICA/MICB	100507436/4277	BD biosciences	6D4
NOTCH1	Mouse IgG1	NOTCH1	4851	e-bioscience	MHN1-519
NOTCH2	Rat IgG1, k	NOTCH2	4853	e-bioscience	16F11
NOTCH3	Mouse IgG1, κ	NOTCH3	4854	e-bioscience	MHN3-21
NOTCH4	Mouse IgG1, κ	NOTCH4	4855	BioLegend	MHN4-2
PAC-1	Mouse IgM, k	DUSP2	1844	BD biosciences	PAC-1
Podoplanin	Rat IgG2a, λ	PDPN	10630	BioLegend	NC-08
SSEA-3	Rat IgM	FUT4		BD biosciences	MC631
SSEA-4	Mouse IgG3	FUT4		BD biosciences	MC813-70
Stro-1	Mouse IgM, λ	N/A	N/A	BioLegend	STRO-1
TCR αβ	Mouse IgM, k	TRA/TRB	6955/6957	BD biosciences	T10B9.1A-31
TCR γδ	Mouse IgG1, κ	TRG/TRD	6965/6964	BD biosciences	B1
TPBG	Mouse IgG1	TPBG	7162	R&D systems	524,744
Vβ8 TCR	Mouse IgG2b, k	N/A	N/A	BD biosciences	JR2
Vδ2 TCR	Mouse IgG1, κ	N/A	N/A	BD biosciences	B6

4. Blocking reagent: Purified IgGs matching the species of the antibodies in the screen and any co-staining antibodies, 1 mg/mL in sterile PBS; alternatively, BD Fc Block (BD Biosciences, San Jose, CA) can be used.
5. Panel of fluorophore-conjugated monoclonal antibodies (*see* **Note 2**).
6. Anti-immunoglobulin compensation beads.
7. Viability dye stock solution for unfixed cells: 1 mg/mL 4′,6-Diamidino-2-phenylindole dihydrochloride (DAPI) or propidium iodide (PI) dissolved in water.
8. (Optional) Fixative: 4% formaldehyde solution in PBS (*see* **Note 3**); alternatively, BD Cytofix (BD Biosciences) can be used.
9. (Optional) Viability dye for fixed cells: Amine reactive dye (e.g., LIVE/DEAD® Fixable Near-IR Dead Cell Stain Kit from ThermoFisher Scientific, Waltham, MA) (*see* **Note 3**).

2.2 Equipment

1. Working plates: 96-well U-bottom polystyrene non-tissue culture treated plates with lid.
2. (Optional) Master and Intermediary plates: 96-well polypropylene 1 mL deep-well plates (*see* **Note 4**).
3. Plate storage (if plates are to be prepared in advance): rubber sealing mats for 96-well plates, airtight container.
4. FACS tubes: 12 × 75 mm polystyrene round bottom tubes.
5. Nylon mesh filter: 70 μm or 40 μm (*see* **Note 5**).
6. (Recommended) Accessories for high-throughput sample processing: multichannel pipette reservoirs, 8 or 12 channel multichannel pipette, 8 or 12 channel vacuum manifold, plate shaker.
7. Centrifuge with plate adapters.
8. Flow cytometer with 96-well high-throughput sampler (HTS): equipped with suitable lasers, detectors, and filters for chosen fluorophore(s), and software compatible with flow cytometer (e.g., BD HTS with FACSDiva software from BD Biosciences).
9. Quality control beads for flow cytometer (e.g., CS&T beads from BD Biosciences).
10. Flow cytometry data analysis software.

3 Methods

3.1 HT-FC Plate Preparation

Select and purchase antibodies for screening (*see* **Note 2**). A schematic of HT-FC plate preparation is shown in Fig. 1.

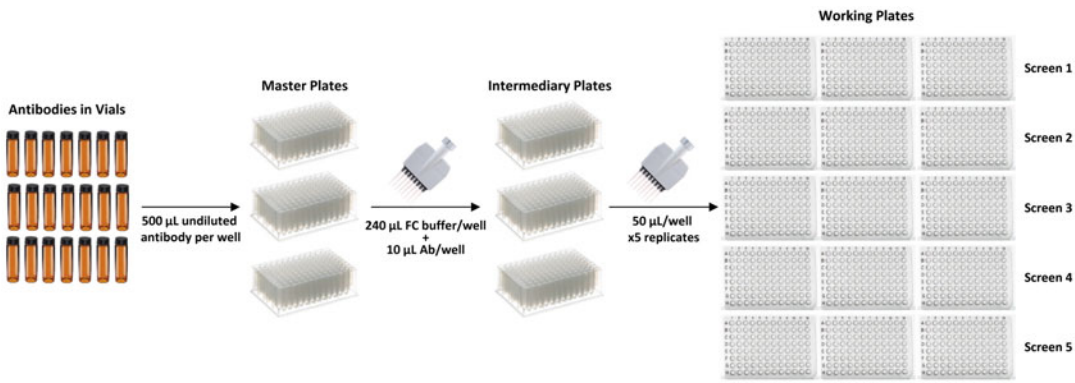

Fig. 1 Schematic of plate preparation. An example of how to prepare sufficient working plates to perform five screens is provided. Master plates are recommended for storage of antibodies, to allow for rapid generation of intermediary plates using a multi-channel pipette. Intermediary plates are recommended if more than one or two screens will be performed, as this increases the accuracy and uniformity of the assay

3.1.1 Preparation of Master Plates

If the screen will be run on an ongoing basis, master plates containing undiluted antibody should be prepared. If master plates are not required proceed to Subheading 3.1.2, **step 2**.

1. Pipette 500 μL of each antibody to be included in the screen into a separate well of a 96-well 1 mL polypropylene plate.
2. Add antibodies in the order in which you wish them run, or grouped logically otherwise (e.g., by fluorophore or antibody name/function) to facilitate analysis. Be sure to generate a "plate map" to keep track of antibody locations in the plates. Reserve multiple empty wells for unstained controls on every plate. This should be done in advance**.** Store plates sealed with 96-well rubber sealing mats in an airtight container containing moist paper towel at 4 °C in the dark. Always briefly centrifuge master plates in a centrifuge with plate adapters prior to opening to ensure antibodies are at the bottom of the wells.

3.1.2 Preparation of Intermediary Plates

Each sample to be screened requires 1 set of working plates. If multiple screens are to be run then intermediary plates should be prepared; otherwise proceed to Subheading 3.1.3, **step 2**. Intermediary plates increase the uniformity of working plates, and simplify the production workflow. Intermediary plates will contain antibodies at a 1:25 dilution in a volume sufficient for the number of screens planned (final volume 50 μL per screen).

1. If using master plates: Add 48 μL multiplied by the number of screens of FC buffer to each well of a 96-well 1 mL polypropylene plate (e.g., if doing 5 screens add 240 μL FC buffer per well; *see* **Notes 4** and **6**). Then, using a multichannel pipette, add 2 μL multiplied by the number of screens of undiluted antibody from the master plates to each well (e.g., if doing 5 screens add 10 μL of antibody per well, for a final dilution of 1:25 and a final volume of 250 μL), mirroring the layout of antibodies in the master plates in the intermediary plates. Include wells (2–3 per plate) with an equivalent volume of FC buffer, with no antibody, to be used as controls. Plates can be prepared in advance, sealed, and stored at 4 °C in the dark for up to 2 weeks.
2. If not using master plates: Add 48 μL multiplied by the number of screens of FC buffer to each well of a 96-well 1 mL polypropylene plate, then add 2 μL multiplied by the number of screens of undiluted antibody directly from antibody stock vials to each well (*see* **Notes 4** and **6**). Include wells (2–3 per plate) with an equivalent volume of FC buffer, with no antibody, to be used as controls. Plates can be prepared in advance, sealed, and stored at 4 °C in the dark for up to 2 weeks.

3.1.3 Preparation of Working Plates

Working plates will contain 50 μL per well of antibodies at a dilution of 1:25. If more than one screen is being run, then multiple identical working plates will be prepared.

1. If using intermediary plates: Briefly centrifuge intermediary plates prior to opening to ensure antibodies are at the bottom of the wells. Use a multichannel pipette to aliquot 50 μL/well from the intermediary plate into 96-well U-bottom polystyrene plates, mirroring the layout of antibodies in the intermediary plate in the working plates. Plates can be prepared in advance, sealed, and stored at 4 °C in the dark for up to 2 weeks. Proceed to Subheading 3.2.
2. If not using master and/or intermediary plates: For each intended screen add 48 μL of FC buffer to each well of a 96-well U-bottom polystyrene plate, then add 2 μL of undiluted antibody from antibody stock vials, for a final volume of 50 μL/well at 1:25 dilution. Add antibodies in the order in which you wish them run, or grouped logically otherwise (for example by fluorophore or antibody name/function) to facilitate analysis. Include wells (2–3 per plate) with an equivalent volume of FC buffer, with no antibody, to be used as controls. Plates can be prepared in advance, sealed, and stored at 4 °C in the dark for up to 2 weeks. Proceed to Subheading 3.2.

3.2 Cell Preparation

The screening platform/protocol we describe is meant to be as flexible as possible to allow a wide range of samples to be run. This can include, for example, peripheral blood mononuclear cells, adherently cultured cells that have been trypsinized, solid tumor tissues that have been dissociated by enzymatic digestion, etc. The investigator should follow the standard single-cell suspension preparation methods for their given cell type, and optimize if/as needed. It is also important to be aware of whether antigens that are recognized by antibodies used in the screen are affected by enzymes such as trypsin or collagenase. This must be assessed on an individual basis. We have identified several cell surface antigens that are negatively affected by commonly used enzymes, including trypsin and collagenase [8].

1. Prepare single cell suspension: The number of cells required will depend on the number of antibodies in the screen. Ideally, 50,000 cells per antibody should be used (*see* **Note 7**). Resuspend cells in 10 mL of FC buffer and mix gently, then filter through a 70 μm mesh filter (*see* **Note 5**). Centrifuge at 350 × *g* for 5 min. Aspirate supernatant, being careful not to disrupt the cell pellet.
2. Resuspend in 1–2 mL of FC buffer and mix gently. Count viable cells. Keep cells on ice and proceed to Subheading 3.3.

3.3 Cell-Surface Staining

3.3.1 Fixable Viability Staining (Optional)

If cells are to be fixed (*see* **Note 3**), they must be stained with a fixable viability dye prior to the other staining steps. If cells are not to be fixed, proceed to Subheading 3.3.2 (with Global Co-staining) or Subheading 3.3.3 (without Global Co-staining).

1. Prepare fixable viability dye of choice, as instructed by the manufacturer (*see* **Note 8**).
2. If using a LIVE/DEAD® Fixable Dead Cell Stain Kit, resuspend cells at 5×10^6–1×10^7 viable cells/mL in FC buffer without BSA.
3. Add prepared viability dye at a dilution of 1:1000; incubate on ice for 30 min in the dark.
4. Add 10 mL of FC buffer to cells and mix gently. Centrifuge at $350 \times g$ for 5 min. Aspirate, being careful not to disrupt the cell pellet.
5. Repeat **step 4** and resuspend cells at 5×10^6–1×10^7 viable cells/mL in FC buffer.
6. Keep cells on ice. Proceed to Subheading 3.3.2 (with Global Co-staining) or Subheading 3.3.3 (without Global Co-staining).

3.3.2 Global Co-staining (Optional)

It is possible to co-stain the cells being screened with antibodies that define specific cell subsets if so desired. For example, peripheral blood mononuclear cells can be co-stained for markers of T cells, B cells, myeloid cells, etc. Dissociated solid tumors can be stained with markers for stromal subpopulations, cancer stem cells, etc. This allows the cell surface profile of each individual subpopulation of cells within a sample to be obtained within a single screen. If global co-stains are not required, proceed to Subheading 3.3.3.

1. Resuspend cells at 5×10^6–1×10^7 viable cells/mL in FC buffer.
2. Add 1 mg/mL purified IgG(s) at a 1:100 dilution (*see* **Note 9**).
3. Gently pipette cells up and down several times, then filter through a nylon mesh filter. Incubate on ice for 5 min.
4. Retain approximately 5×10^5 cells in a FACS tube for unstained control. Retain approximately 1×10^5 cells in FACS tubes for each single-stain or fluorescence-minus-one (FMO) control, as needed (*see* **Note 10**).
5. Add co-stain antibodies to sample at predetermined dilutions, mix gently, and stain on ice for 30 min in dark (*see* **Note 11**).
6. Add 10 mL of FC buffer to cells and mix gently. Centrifuge at $350 \times g$ for 5 min. Aspirate, being careful not to disrupt the cell pellet.
7. Repeat **step 6**.
8. Proceed to Subheading 3.3.3.

3.3.3 HT-FC Panel Stain

1. Resuspend cells in FC buffer. Calculate the volume required to add 50 μL to each well of the working plates. Add an extra 500 μL for one tube of control cells.
2. Add 1 mg/mL purified IgG(s) at a 1:100 dilution (*see* **Note 9**). If IgG was added in Subheading 3.3.2, this step should be omitted.
3. Gently pipette cells up and down several times, then filter through a nylon mesh filter. Incubate on ice for 5 min.
4. Retain 500 μL in a FACS tube for control cells used for optimizing PMT voltage settings.
5. Add 50 μL of cell suspension/well to each working plate, for a final volume of 100 μL/well, giving a final antibody dilution of 1:50 (*see* **Note 12**). Mix on plate shaker or pipette up and down several times. Stain on ice for 30 min in dark.
6. Prepare 1 FACS tube of compensation beads for each color to be used in the screen (including those present in co-staining panel, if used). Add one drop of each bead type to 100 μL FC buffer per compensation control and add 1–5 μL of antibody (*see* **Note 13**).
7. Wash plates by adding 100 μL/well of FC buffer, for a final volume of 200 μL/well. Pipette up and down several times. Centrifuge plates at 350 × *g* for 5 min. Aspirate with a multichannel vacuum manifold, being careful not to disrupt the cell pellet.
8. Centrifuge control tubes at 350 × *g* for 5 min. Aspirate.
9. Add 200 μL/well of FC buffer to each working plate, and 500 μL of FC buffer to each control tube. Pipette up and down several times. Centrifuge at 350 × *g* for 5 min. Aspirate, being careful not to disrupt the cell pellet.
10. Repeat **step 9**.
11. If cells are to be fixed proceed directly to Subheading 3.3.4, otherwise continue to **step 12**.
12. Prepare FC buffer plus 1:1000 1 mg/mL DAPI, for a final concentration of 1 μg/mL (*see* **Note 14**). Calculate the volume required to add 50 μL to each well of the working plates. Calculate an extra 500 μL each for control tubes.
13. Add 50 μL/well of FC buffer plus DAPI to each working plate (*see* **Note 15**). Mix on plate shaker or pipette up and down several times. Keep on ice in dark for the duration of the experiment.
14. Resuspend unstained and FMO control cells in 300 μL FC buffer plus DAPI. Gently mix. Keep on ice in dark for the duration of the experiment.
15. Proceed to Subheading 3.4.

3.3.4 Fixation (Optional)

1. Prepare formaldehyde solution to give a final concentration of 1% (if using BD Cytofix dilute 1:4 in PBS). Calculate the volume required to add 100 μL to each well of the working plates. Calculate an extra 500 μL each for control tubes.
2. Add 100 μL/well of fixative to each working plate and 500 μL to each control tube. Mix on plate shaker or pipette up and down several times. Incubate on ice in the dark for 30 min.
3. Wash plates by adding 100 μL/well of PBS, for a final volume of 200 μL/well. Wash control tubes with 500 μL of PBS. Pipette up and down several times. Centrifuge plates at 350 × *g* for 5 min. Aspirate with a multi-channel vacuum manifold, being careful not to disrupt the cell pellet.
4. Centrifuge control tubes at 350 × *g* for 5 min. Aspirate.
5. Add 200 μL/well of PBS to each working plate, and 500 μL of PBS to each control tube. Pipette up and down several times. Centrifuge at 350 × *g* for 5 min. Aspirate, being careful not to disrupt the cell pellet.
6. Repeat **step 5**.
7. Resuspend in a final volume of 50 μL/well or 300 μL/control tube of PBS. Fixed cells can be kept at 4 °C in the dark for up to 1 week prior to analysis.

3.4 Data Acquisition and Analysis

At the end of the staining protocol the following should be ready for acquisition: 96-well plate(s) containing cells (±global co-stain) stained with individual antibodies and DAPI (or other viability dye); a tube of cells stained with DAPI alone; tubes of cells with FMO controls for global co-stains if applicable; tubes of compensation beads, one for each fluorochrome present in the screen, including any global co-stains.

3.4.1 Creation of Acquisition Templates

1. Create an acquisition template using dot plots to display all relevant parameters, including all colors used in the screen. Include plots for viability gating (always apply this gate first) and doublet discrimination.
2. Create an HTS acquisition template by adding plates to the experiment template and labeling to match the layout of your screen. Adjust HTS sampler acquisition settings as shown in Table 2 (*see* **Note 16**).
3. After setting up acquisition and plate templates and adjusting HTS settings, save experiment as a template for use in future experiments.

Table 2
HTS acquisition settings

Flow rate	3 μL (up to 10,000 events/s)
Sample volume	24 μL (minimum)
Mix volume	1/2 of total volume in wells
Wash speed	200 μL/s
Wash volume	400 μL
Number of washes	4

3.4.2 Optimization of PMT Voltage Settings

1. Determine optimal PMT voltage settings for the instrument, sample, and reagents being used. If CS&T beads are used to QC the instrument, start with CS&T baseline voltages or lymphocyte/cell-specific target values if available (*see* **Notes 17** and **18**) and the accompanying calculated robust standard deviation (rSD) values for each color to be detected.
2. Using control cells (stained with DAPI only), set gates to exclude non-viable cells, doublets, and debris. Adjust PMT voltages using gated cells (i.e., non-viable cells, doublets and debris excluded) until the robust standard deviation (rSD) of the unstained cells roughly meets the rSD target value and is within the rSD lower and rSD upper limits. If there is more than one cell type in the sample, gate on the cells that are expected to have the lowest levels of autofluorescence for this step. If using co-stains, proceed to **step 4**, otherwise proceed to **step 5**.
3. Multicolor samples: Run a fully stained sample (gated for viability and doublets) at the PMT voltages determined above. Ensure the positives are on scale in the linear range of the detector and not greater than 100,000–120,000 MFI. If they are at or above 200,000, lower the voltage until positives are at 100,000–120,000 MFI. Use these PMT voltages for subsequent steps.
4. Run single-stained compensation beads at the PMT voltages determined in the previous step to ensure that staining is greater than or equal to the staining levels of cells. Decrease PMT voltage, if needed, to ensure that no events are off-scale. If staining of beads is too low, do not raise PMT voltages. In this case, use more antibody or a different antibody.

3.4.3 Sample Acquisition and Data Analysis

1. If BD FACSDiva acquisition software is used, employ the automatic compensation function. Acquire the single-stained compensation controls, calculate and save the resulting compensation values, and apply to all samples (*see* **Note 19**).
2. Set FSC threshold to exclude debris. It is typically best to record all events, and exclude unwanted cells in subsequent analysis.
3. Acquire all unstained control cells, single/full-stains, FMOs, or other control cells in tubes.
4. Attach high throughput sampler apparatus to flow cytometer. Acquire samples from plates using recommended or optimized HTS settings (*see* Table 2 for recommended settings and **Note 20** for the number of events to collect).
5. Analyze data in FACSDiva or third-party analysis software. Use FMO controls and/or unstained wells acquired from plates to set gates for analyzing screen markers (*see* **Note 21**). Use the batch analysis feature for large screens and visually inspect individual plots to ensure the quality of each data point and that the gates are set as desired. Export relevant parameters/statistics (e.g., percent-positive cells, mean fluorescence-intensities) to tables if additional bioinformatics analysis is desired.

4 Notes

1. PBS may be used instead of HBSS if desired. If necessary, 2% fetal bovine serum (FBS) may be used instead of BSA to promote viability, however BSA is preferred as it helps to prevent cell aggregation. Can be prepared in advance and stored at 4 °C for up to 4 weeks. For fixable viability staining, FC buffer without BSA will need to be prepared as well.
2. Monoclonal antibodies are preferred over polyclonal whenever possible, but polyclonal antibodies can be used if necessary. Antibodies directly conjugated to fluorophores are strongly preferred, due to ease of use, increased specificity, and flexibility in reagent choice. When creating a screening panel of antibodies, in general try to have them all conjugated with the same fluorochome, or with as few fluorochromes as possible. We prefer antibodies labeled with PE, FITC/Alexa488 and APC/Alexa647, as this provides the most options. Consider any additional global co-stains that will be used, including expression vector markers such as GFP.
3. Fixation after staining can sometimes increase background fluorescence or decrease fluorescence intensity slightly [12], thus it is preferable to run fresh, unfixed samples. However,

in cases of biohazard concern or time constraints, cells may be fixed by suspending in 1% paraformaldehyde in PBS. Viability stains and staining procedures must be adjusted accordingly. When working with paraformaldehyde, use appropriate personal protective equipment and discard waste in accordance with local regulations.

4. If the screen will be run on an ongoing basis, master plates containing undiluted antibody should be prepared. If multiple screens are to be run, then intermediary plates should be prepared. If preparing 200 μL or less in intermediary plates, deep-well plates do not need to be used.
5. 70 μm mesh is suitable for most cells; when running relatively small cells, such as lymphocytes, a 40 μm filter should be used.
6. When making intermediary plates for multiple screens, it is advisable to make a slight excess; for example, if planning 5 screens, make enough for 6.
7. We recommend a minimum of 50,000 viable cells per antibody, which is a sufficient number in most cases. Some situations may require larger numbers, for example, if a rare subset of cells is to be analyzed.
8. Fixable viability dyes are commercially available. Cells to be fixed should be first stained with a fixable amine-reactive dye, such as LIVE/DEAD Fixable stains. Amine-reactive stains should be used without FBS or BSA. Be sure to select a viability dye that does not conflict with fluorochrome conjugates in the screening panel or on any global co-staining antibodies you plan to use.
9. Blocking with purified IgG helps to prevent non-specific Fc receptor-mediated binding. This is especially important in the case of dim markers, rare markers and low-affinity antibodies. The species of IgG must match the host species in which the staining antibodies were produced. If multiple species of antibodies are present in the screen then all species must be blocked. Alternatively, a commercially available blocking reagent such as BD Fc Block (BD Biosciences) can be used.
10. If no global co-staining is planned, then only a single control tube of unstained cells is needed. If global co-staining is planned, then we recommend the use of FMO controls for each fluorochrome to be included in the panel [13].
11. The choice of co-staining antibodies will be user-determined. Ideally these antibodies will have been titrated by the user to determine optimal concentrations, and fluorochrome conjugates for co-staining antibodies must not overlap with those present in the antibody panel.

12. As it is impractical to titrate a large number of antibodies (368 in our screen), and for some antibodies an appropriate cell type for titration is not available, we use a 1:50 final dilution as our standard concentration for all un-titrated antibodies, which works well for the majority of antibodies tested. However, if a smaller panel of antibodies is to be used and/or specific antibodies have been titrated, these can be used at different dilutions if required. Add them to the intermediary plates at twice the desired final concentration, or leave these wells empty and simply add the antibody directly to the cells on the working plate at the dilution required.
13. Compensation beads: It is important to include beads single-stained for all colors to be included in the screen, even if it is a single-color experiment. This allows PMT voltages to be evaluated and compensation values to be calculated even in the absence of a known positive marker, or when markers are dim or rare. This is especially important for tandem dyes, which should always be lot-matched. IgG specificity of the beads must match the host species of at least 1 antibody for every color used (mouse, rat, rat/hamster, or rabbit). Ensure the staining level of the beads is greater than or equal to the brightest staining levels of cells. In general, aim for a mean fluorescence intensity (MFI) in the 5th decade, but not off scale. This should be tested in advance of the experiment. If cells to be analyzed are comparatively large relative to lymphocytes, larger diameter beads should be used, such as BD CompBeads Plus (BD Biosciences). Compensation beads should be prepared fresh each day.
14. Viability staining: It is highly recommended to use a viability stain to allow for the exclusion of dead cells, which will contribute to non-specific binding. For unfixed cells DAPI or PI are preferred due to ease of use and cost. DAPI typically has less interference with common conjugates such as PE and FITC, and can be excited by both violet and UV lasers as required, providing more options. 1 mg/mL stock solutions can be made and stored in the dark at room temperature.
15. If a very large or very small amount of cells are to be run, the final resuspension volume can be adjusted accordingly. Aim for approximately 5000 events/s at your HTS acquisition settings.
16. The wash volumes should not be altered from the values in Table 2. The flow rate can be reduced if more than 5000 events/s are being processed, and the sample volume can be adjusted for custom screen volumes.
17. Optimizing PMT voltages: Optimal voltage settings are important for resolution sensitivity. While adjusting voltages so that unstained cells appear in the first decade may be adequate for

FITC and PE, this method is not optimal for fluorochromes with longer emissions. While it is best to manually determine optimal voltages for the cell type being analyzed, this is not always practical/possible. In this case, CS&T reference values can be used as a good starting point to minimize the contribution of electronic noise. If these values are not available, use CS&T beads and FACSDiva software to determine them.

18. CS&T vs cell-specific settings: Because CS&T target values are determined using beads, it is usually preferable to use values derived from live cells if they are available for the cytometer you are using, as they will more closely match the optical properties of your sample. Lymphocytes are commonly used for this purpose to create lymphocyte mean target values (LMTVs). Whichever strategy is chosen it is best to have a numerical reference point against which to set PMT voltages. Do not rely on visual estimation of negative controls to arbitrarily set PMT voltages unless absolutely necessary. Keep this process consistent.
19. Applying compensation: While compensation can be calculated and applied after data acquisition using FACSDiva or other third party analysis software (e.g., FlowJo, Tree Star, Ashland, OR; Cytoscape, http://cytoscape.org/), it is best applied immediately after calculation. This allows any potential staining problems to be more easily identified, and ensures all samples in the high throughput run will be acquired with identical settings.
20. Number of events to collect: Aim for a minimum of 10,000 events/well at the final level of gating. Be sure to factor in any gates you will have to apply (e.g., to exclude non-viable cells or to analyze specific sub-populations of cells).
21. Examples of gating strategies for non-costained and co-stained samples can be found in Gedye et al. [8] Supplementary Figs. 2 and 4, respectively.

Acknowledgments

We would like to acknowledge the UHN/SickKids Flow Cytometry Facility for their support throughout the development of this platform. We are also grateful for technical support from Ella Hyatt and Julie Yuan, and manuscript review by Nazleen Lobo. This work was funded by the Ontario Institute for Cancer Research, and in part by the Ontario Ministry of Health and Long Term Care. The views expressed do not necessarily reflect those of the OMOHLTC.

References

1. da Cunha JP, Galante PA, de Souza JE, de Souza RF, Carvalho PM, Ohara DT, Moura RP, Oba-Shinja SM, Marie SK, Silva WA Jr, Perez RO, Stransky B, Pieprzyk M, Moore J, Caballero O, Gama-Rodrigues J, Habr-Gama A, Kuo WP, Simpson AJ, Camargo AA, Old LJ, de Souza SJ (2009) Bioinformatics construction of the human cell surfaceome. Proc Natl Acad Sci U S A 106(39):16752–16757. doi:10.1073/pnas.0907939106
2. Chen G, Gharib TG, Huang CC, Taylor JM, Misek DE, Kardia SL, Giordano TJ, Iannettoni MD, Orringer MB, Hanash SM, Beer DG (2002) Discordant protein and mRNA expression in lung adenocarcinomas. Mol Cell Proteomics 1(4):304–313
3. Gygi SP, Rochon Y, Franza BR, Aebersold R (1999) Correlation between protein and mRNA abundance in yeast. Mol Cell Biol 19 (3):1720–1730
4. Schwanhausser B, Busse D, Li N, Dittmar G, Schuchhardt J, Wolf J, Chen W, Selbach M (2011) Global quantification of mammalian gene expression control. Nature 473 (7347):337–342. doi:10.1038/nature10098
5. Wilhelm M, Schlegl J, Hahne H, Moghaddas Gholami A, Lieberenz M, Savitski MM, Ziegler E, Butzmann L, Gessulat S, Marx H, Mathieson T, Lemeer S, Schnatbaum K, Reimer U, Wenschuh H, Mollenhauer M, Slotta-Huspenina J, Boese JH, Bantscheff M, Gerstmair A, Faerber F, Kuster B (2014) Mass-spectrometry-based draft of the human proteome. Nature 509(7502):582–587. doi:10.1038/nature13319
6. Wollscheid B, Bausch-Fluck D, Henderson C, O'Brien R, Bibel M, Schiess R, Aebersold R, Watts JD (2009) Mass-spectrometric identification and relative quantification of N-linked cell surface glycoproteins. Nat Biotechnol 27 (4):378–386. doi:10.1038/nbt.1532
7. Kim Y, Elschenbroich S, Sharma P, Sepiashvili L, Gramolini AO, Kislinger T (2011) Use of colloidal silica-beads for the isolation of cell-surface proteins for mass spectrometry-based proteomics. Methods Mol Biol 748:227–241. doi:10.1007/978-1-61779-139-0_16
8. Gedye CA, Hussain A, Paterson J, Smrke A, Saini H, Sirskyj D, Pereira K, Lobo N, Stewart J, Go C, Ho J, Medrano M, Hyatt E, Yuan J, Lauriault S, Meyer M, Kondratyev M, van den Beucken T, Jewett M, Dirks P, Guidos CJ, Danska J, Wang J, Wouters B, Neel B, Rottapel R, Ailles LE (2014) Cell surface profiling using high-throughput flow cytometry: a platform for biomarker discovery and analysis of cellular heterogeneity. PLoS One 9(8):e105602. doi:10.1371/journal.pone.0105602
9. Dubois NC, Craft AM, Sharma P, Elliott DA, Stanley EG, Elefanty AG, Gramolini A, Keller G (2011) SIRPA is a specific cell-surface marker for isolating cardiomyocytes derived from human pluripotent stem cells. Nat Biotechnol 29(11):1011–1018. doi:10.1038/nbt.2005
10. Van de Laar E, Clifford M, Hasenoeder S, Kim BR, Wang D, Lee S, Paterson J, Vu NM, Waddell TK, Keshavjee S, Tsao MS, Ailles L, Moghal N (2014) Cell surface marker profiling of human tracheal basal cells reveals distinct subpopulations, identifies MST1/MSP as a mitogenic signal, and identifies new biomarkers for lung squamous cell carcinomas. Respir Res 15:160. doi:10.1186/s12931-014-0160-8
11. Wei Q, Tang YJ, Voisin V, Sato S, Hirata M, Whetstone H, Han I, Ailles L, Bader GD, Wunder J, Alman BA (2015) Identification of CD146 as a marker enriched for tumor-propagating capacity reveals targetable pathways in primary human sarcoma. Oncotarget 6(37):40283–40294. doi:10.18632/oncotarget.5375
12. Stewart JC, Villasmil ML, Frampton MW (2007) Changes in fluorescence intensity of selected leukocyte surface markers following fixation. Cytometry A 71(6):379–385. doi:10.1002/cyto.a.20392
13. Tung JW, Heydari K, Tirouvanziam R, Sahaf B, Parks DR, Herzenberg LA, Herzenberg LA (2007) Modern flow cytometry: a practical approach. Clin Lab Med 27(3):453–468., v. doi:10.1016/j.cll.2007.05.001

Chapter 8

Multiparameter Conventional Flow Cytometry

Katherine M. McKinnon

Abstract

Multicolor flow cytometry is a useful technique when examining mixed populations of cells, such as blood and tissue cells in human and animal samples. The ability to use multiple fluorescent markers simultaneously allows for the identification of multiple cell types, as well as functional markers that further characterize each sample. The introduction of instruments capable of measuring 12-plus colors and new reagents has made this type of flow cytometry both popular and problematic. Adapting a typical staining panel from 4 to 6 color tubes to more than 12 colors is not simply a matter of "plug and play", but must be approached in a systematic manner to achieve a successful multi-parameter staining panel. This chapter will examine the considerations and methods needed to successfully perform multicolor flow cytometry.

Key words Multicolor flow cytometry, Staining, Flow cytometry, Multi-parameter, Immunology

1 Introduction

One of the hallmarks of flow cytometric analysis is its ability to simultaneously and rapidly measure multiple parameters on mixed populations of cells. This technique has become indispensable in numerous fields of study including immunology, virology, cancer biology, and infectious disease monitoring. In the early years of flow cytometry, staining panels were limited to 3–4 colors requiring multiple tubes of cells for each experimental sample. This proved to be problematic when dealing with small samples sizes such as tissue biopsies, pediatric samples or samples from small animal models because there were insufficient cells available for analysis. For example, when many cell populations are defined by multiple markers, such as T_{reg} cells, which require a minimum of 4 markers (CD3, CD4, CD25, and FoxP3) for identification before any other marker such as memory or activation can be considered, utilization of 3–4 colors is only partially helpful. In these early analysis panels, not only were large numbers of cells required, but also large amounts of antibody since each staining tube had to include identifying markers for each cell population under consideration. Even

Teresa S. Hawley and Robert G. Hawley (eds.), *Flow Cytometry Protocols*, Methods in Molecular Biology, vol. 1678, DOI 10.1007/978-1-4939-7346-0_8,

with the introduction of staining reagents and instruments capable of six colors, this requirement for large numbers of cells and reagents persisted. It was not until the introduction of instruments and reagents capable of analyzing more than 12 that the need for large numbers of cells and amounts of antibody has eased. These larger color staining panels also had the advantage of allowing for more detailed analysis of each cell population and sub population.

New flow cytometers can detect more fluorochromes on each sample by using tandem dyes, multiple laser configurations, digital electronics, and software generated compensation matrices. There can be up to eight fluorochromes detected off a single laser and the separation between fluorochomes is narrower than on older 4–6 color instruments. In addition, Quantum Dots (Qdots) and tandem dyes can also be excited by multiple lasers making compensation more complicated. Designing and implementing a staining panel with these new challenges requires a more systematic approach that considers the instrument configuration (lasers, detectors), reagents (availability, clone selection, fluorochrome brightness), spectral overlap (amount of compensation needed) and appropriate controls (Fluorescence Minus One, experimental).

Instrument configurations on digital flow cytometers manufactured by BD Biosciences (San Jose, CA) can be obtained using FACSDiva CS&T software. The instrument configuration is available under the "*Cytometer—View Configurations*" tabs. Proper maintenance and quality control should be standard procedures for all flow cytometers. Quality control protocols for multicolor flow cytometry have been published elsewhere [1, 2] and should be followed on a regular basis along with daily quality control such as using FACSDiva CS&T software and beads. An example of instrument configurations and recommended fluorochromes for a BD LSRII and BD FACSymphony is shown in Fig. 1.

Reagent selection is a critical part of multicolor panel design. For larger multicolor panels, antigen density and relative fluorochrome brightness must be considered when designing a staining panel. Specifically, low density antigens (IL-4, IL-12, CXCR5, CCR7, etc.) should be placed on bright fluorochromes for maximum resolution. Higher density antigens (CD3, CD4, CD8, CD20, CD45, etc.) can be placed on dim fluorochromes [3]. In general, fluorochrome brightness is dependent on laser wavelength, laser power and detector configuration; Table 1 contains examples of flurochrome brightness [4]. Another consideration when selecting reagents is the spectral overlap of each fluorochrome and the amount of compensation needed. Whenever possible, the fluorochromes in an experimental panel should be spread out on multiple lasers to minimize compensation. For example, the combination of FITC, BV605, PE, APC, and BUV395 is a better choice than using FITC, PE, PE-TxRED, PE-CY5, and PE-Cy7 together. Unfortunately, even with advances in fluorochrome

LSR II Configuration

Laser	Dichroic	BP Filter	Fluorochromes
488 nm	505LP	525/50	FITC, Alexa 488, BB515, CFSE, GFP
488 nm	690LP	710/50	PerCP, PerCP-Cy5.5, PerCP-eFluor710, BB700
532 nm		575/26	PE
532 nm	600LP	610/20	PE-TxRed, ECD, PE-CF594, PE-eFluor610, PI
532 nm	635LP	660/20	PE-Cy5
532 nm	685LP	710/50	PE-Cy5.5 (not with PerCP-Cy5.5)
532 nm	755LP	780/60	PE-Cy7
628 nm		670/30	APC, Alexa 647, eFluor660
628 nm	685LP	730/45	Alexa 700, APC-R700
628 nm	755LP	780/60	APC-Cy7, APC-H7, APC-eFluor780, Alexa 780
405 nm		450/50	Pacific Blue, v450, BV421, eFluor450, Live/Dead Violet Dye
405 nm	505LP	525/50	AmCyan, v500, Live/Dead Aqua Dye, BV510, BV480
405 nm	557LP	560/20	Qdot 565, Live/Dead Yellow, BV570
405 nm	570LP	585/42	Qdot 585
405 nm	600LP	610/20	Qdot 605, BV605, eVolve605
405 nm	635LP	670/30	Qdot 655, BV650, eVolve655
405 nm	690LP	710/50	Qdot 705, BV711
405 nm	750LP	780/60	Qdot 800, BV786

FACSymphony Configuration

Laser	Dichroic	BP Filter	Fluorochromes
488 nm	505LP	515/20	FITC, Alexa 488, BB515, CFSE, GFP
488 nm	595LP	610/20	BB630
488 nm	635LP	660/40	PerCP, BB660
488 nm	690LP	695/40	PerCP, PerCP-Cy5.5, PerCP-eFluor710, BB700
488 nm	750LP	780/60	BB790
532 nm		586/15	PE
532 nm	595LP	610/20	PE-TxRed, ECD, PE-CF594, PE-eFluor610, PI
532 nm	635LP	670/30	PE-Cy5
532 nm	690LP	710/50	PE-Cy5.5 (not with PerCP-Cy5.5)
532 nm	750LP	780/60	PE-Cy7
532 nm	770LP	820/60	BYG790
628 nm		670/30	APC, Alexa 647, eFluor660
628 nm	690LP	730/45	Alexa 700, APC-R700
628 nm	750LP	780/60	APC-Cy7, APC-H7, APC-eFluor780, Alexa 780
405 nm		450/50	Pacific Blue, v450, BV421, eFluor450, Live/Dead Violet Dye
405 nm	505LP	515/20	AmCyan, v500, Live/Dead Aqua Dye, BV510, BV480
405 nm	595LP	610/20	Qdot 605, BV605, eVolve605
405 nm	635LP	670/30	Qdot 655, BV650, eVolve655
405 nm	690LP	710/50	Qdot 705, BV711
405 nm	730LP	750/30	BV750
405 nm	750LP	780/60	Qdot 800, BV786
355 nm		379/28	BUV395
355 nm	410LP	450/50	DAPI, Live/Dead Blue Dye
355 nm	450LP	515/30	BUV496
355 nm	525LP	540/30	BUV563
355 nm	635LP	670/30	BUV661
355 nm	690LP	740/35	BUV737
355 nm	770LP	820/60	BUV805

Fig. 1 Instrument configuration for LSRII (BD Biosciences) and FACSymphony (BD Biosciences) flow cytometers in the NCI Vaccine Branch Flow Cytometry Core Facility. The tables include dichroic and bandpass filters for each detector. Recommended dyes are also given for each detector from multiple manufacturers. When designing a staining panel, one fluorochrome should be chosen for each detector

design, tandem dyes will still have to be used to get to more than 12 colors in any multicolor staining panel. This creates an additional challenge because tandem dyes can be excited by multiple lasers further complicating compensation. None of these challenges are insurmountable, but they need to be considered when designing a multicolor staining panel. Further reagent preparation such as antibody titration will be discussed in Subheading 3.1.

Controls for a multicolor flow cytometry experiment need to consider autofluorescence, background staining of antibodies and spectral overlap of fluorochromes. Autofluorescence can be addressed by examining unstained cells in each fluorescence detector during panel optimization. Isotype controls can be used to check background staining of antibodies and single color staining controls (either cells or beads) should be used to set compensation. Background antibody staining and spectral overlap of fluorochromes can cause issues with the determination of positive and negative signal for each marker. When working with large numbers of fluorescent dyes in each sample several considerations need to be addressed. Compensation can cause different distributions of signal in each channel so that a single set threshold for positivity is not practical. To combat this, fluorescence minus one (FMO) controls should be used whenever possible [5]. Briefly a FMO control is made for each fluorochrome-conjugated antibody by staining with all the other antibodies in the panel except the specific reagent

Table 1
Relative fluorochrome brightness

Laser	Dim	Moderate	Bright
355 nm	BUV805 BUV496	BUV395 BUV563	BUV661 BUV737 BV421
405 nm	Pacific Blue V450 V500 eFluor 450 Pacific Orange AmCyan	BV480 BV510 Qdot 705	BV605 BV650 BV711 BV786 Qdot 605 Qdot 655 Qdot 800 eVolve 605 eVolve 655
488 nm	PerCP	FITC Ax488 PerCP-Cy5.5 PerCP-eFluor 710	BB515 BB700 PE PE-CF594 PE-TxRed ECD PE-Cy5 PE-Cy5.5 PE-Cy7
532 nm			PE PE-CF594 PE-TxRed ECD PE-Cy5 PE-Cy5.5 PE-Cy7
640 nm	APC-Cy7 APC-H7	Ax700 APC-eFluor 780 APC-Fire 750	APC Ax647 APC-R700

being tested. Table 2 gives an example of a 12-color panel with FMO controls. Finally, the use of a viability dye such as one of the fixable amine-binding dyes is strongly recommended since dead cells will pick up antibody and introduce staining artifacts.

2 Materials

2.1 Reagents

1. Test samples: PBMC (fresh or thawed from frozen), tissue samples (processed and ficolled), etc.
2. Dulbecco's Phosphate-Buffered Saline (D-PBS) without Ca^{2+} or Mg^{2+}.

Table 2
Example of FMO Controls for a 12-color Experiment

Fluorochrome	1	2	3	4	5	6	7	8	9	10	11	12
FITC	**FMO FITC**	CD45	CD45	CD45	CD45	CD45	CD45	CD45	CD45	CD45	CD45	CD45
PerCP-Cy5.5	CD4	**FMO PerCPCy5.5**	CD4	CD4	CD4	CD4	CD4	CD4	CD4	CD4	CD4	CD4
Pac blue	CD8	CD8	**FMO PacBlue**	CD8	CD8	CD8	CD8	CD8	CD8	CD8	CD8	CD8
Aqua live/ dead	Aqua	Aqua	Aqua	**FMO Aqua**	Aqua	Aqua	Aqua	Aqua	Aqua	Aqua	Aqua	Aqua
BV 605	CD69	CD69	CD69	CD69	**FMO BV605**	CD69	CD69	CD69	CD69	CD69	CD69	CD69
BV650	CD19	CD19	CD19	CD19	CD19	**FMO BV650**	CD19	CD19	CD19	CD19	CD19	CD19
APC	IFN-g	IFN-g	IFN-g	IFN-g	IFN-g	IFN-g	**FMO APC**	IFN-g	IFN-g	IFN-g	IFN-g	IFN-g
Alexa 700	CD3	CD3	CD3	CD3	CD3	CD3	CD3	**FMO Ax700**	CD3	CD3	CD3	CD3
APC-Cy7	CD27	CD27	CD27	CD27	CD27	CD27	CD27	CD27	**FMO APCCy7**	CD27	CD27	CD27
PE	IL-2	IL-2	IL-2	IL-2	IL-2	IL-2	IL-2	IL-2	IL-2	**FMO PE**	IL-2	IL-2
PE-Cy5	TNF-a	TNF-a	TNF-a	TNF-a	TNF-a	TNF-a	TNF-a	TNF-a	TNF-a	TNF-a	**FMO PECy5**	TNF-a
PE-Cy7	CD28	CD28	CD28	CD28	CD28	CD28	CD28	CD28	CD28	CD28	CD28	**FMO PECy7**

The FMO control for each fluorochrome is indicated in **Bold**. For those tubes, the samples will be stained with every fluorochrome except the fluorochrome indicated in **Bold**

3. Fixable amine-binding viability dye: for example, Live/Dead (ThermoFisher, Waltham, MA), Zombie (Biolegend, San Diego, CA), Fixable Viability (BD Biosciences).
4. Fluorochrome-conjugated monoclonal antibodies.
5. Antibody capture beads for compensation: for example, Comp-Bead Anti-Mouse Ig beads (BD Biosciences), COMPtrol beads (Spherotech, Lake Forest, IL), UltraComp beads (eBioscience, San Diego, CA).
6. ArC Amine Reactive Compensation Beads (ThermoFisher) for compensation of viability dye. Cells can be substituted for this compensation control (*see* **Note 1**).
7. Brilliant Stain Buffer (BD Biosciences) if using Brilliant Violet, Ultraviolet or Blue reagents.
8. FACS Wash Buffer for PBMC: D-PBS, 1% BSA or FBS, penicillin-streptomycin.
9. FACS Tissue Wash Buffer for tissue samples or PBMC: D-PBS, 1% FBS, 15 mM HEPES, 2 mM EDTA, penicillin-streptomycin.
10. Fixation Buffer: 1% Paraformaldehyde or ultrapure (methanol-free) formaldehyde in D-PBS.

2.2 Equipment and Supplies

1. 12 × 75 mm polystyrene tubes and caps.
2. 96-well plates: deep-well plates are recommended, standard U-bottomed plates can be used but require more washes.
3. Adhesive plate lids.
4. Multichannel pipette.
5. 12-channel vacuum manifold and length adjuster for aspiration (V&P Scientific, San Diego, CA).
6. Centrifuge with swinging bucket rotor and tube or plate holders.
7. Flow cytometer with multiple lasers and detectors.
8. (Optional) 96-well plate loader for flow cytometer.

3 Methods

3.1 Titration of Antibodies

All antibodies in the staining panel should be titrated for optimal concentration using the stain index (SI). The SI is measurement of relative brightness for a reagent that considers the difference between positive and negative signals in the fluorescence channel and the relative spread of the negative signal [3, 6].

1. Use each fluorochrome-conjugated antibody in a single color experiment to stain a test sample at multiple concentrations or volumes and analyze the data to generate the SI [6] as shown in Fig. 2.

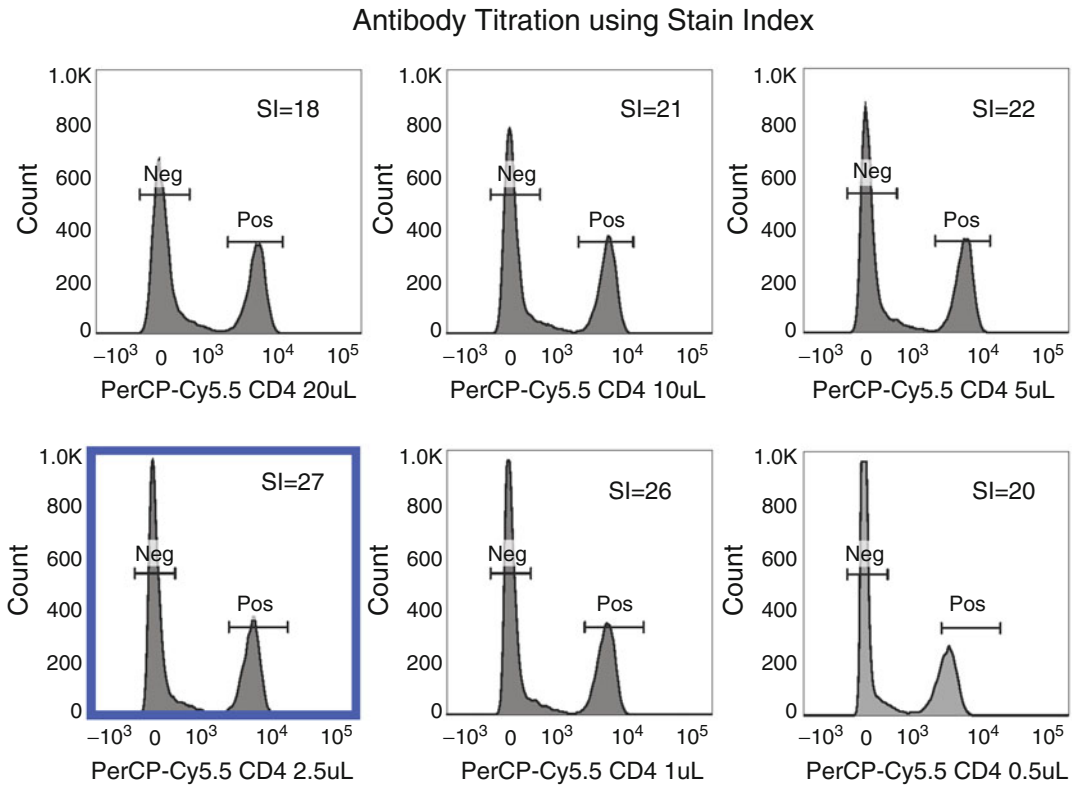

Fig. 2 Example of antibody titration using Stain Index (SI). Non-human primate PBMC were stained with different volumes of CD4 PerCP-Cy5.5 (clone L200, BD Biosciences) and then acquired using a LSRII flow cytometer. Data was analyzed in FlowJo 10.2 software (FlowJo, LLC, Ashland, OR) and the stain index was calculated using the formula SI = D/W

SI = D/W.
D = Difference in Medians between the positive and negative peaks.
W = Width of negative signal calculated as 2× robust Standard Deviation (rSD)

2. Once the optimal concentration for each individual antibody has been determined, stain a test sample with the complete panel of antibodies to see if any adjustments need to be made. For example, antibody concentrations sometimes need to be adjusted to reduce compensation because of spectral overlap in other fluorescence channels (PE-Cy5/APC, PerCP-Cy5.5/BV711, PE-CF594/BV605, etc.).

3.2 FMO Controls

1. Create control samples for each fluorescent channel by staining a representative sample with the complete panel of antibodies minus the specific antibody being tested (*see* Table 2). Ideally, the same type of cells or tissue samples should be used for these controls. However, if cell numbers are low, then an alternate

sample such as PBMC can be substituted, or the FMO controls for well established markers such as lineage markers (CD3, CD19 etc.) can be eliminated.

2. Set up the flow cytometer with appropriate instrument settings and run compensation controls as described in Subheading 3.5.
3. Run the FMO controls and determine background and positivity threshold for each antibody.
4. Optimally this should be a part of every experiment, but low cell numbers may prohibit this control from being performed at every time point. However, this is a critical part of staining panel optimization.

3.3 Tube Staining Procedure

1. Prepare samples by counting cells, washing cells out of media, and resuspending cells at 1×10^7 cells/mL in D-PBS.
2. Put 100 μL of cells into each labeled 12 × 75 mm tube.
3. Add a working concentration of amine-binding fixable viability dye to each tube and incubate for 15 min at room temperature. Buffers containing protein or sodium azide should be avoided during staining with amine-binding fixable viability dyes. Live/Dead Aqua (ThermoFisher #L34966) will be used as an example:
   (a) Add 50 μL of DMSO to vial to dissolve dye.
   (b) Add 50 μL of D-PBS to vial to create working concentration.
   (c) Use 1 μL of working concentration to stain each sample.
4. Resuspend cells in 2 mL of D-PBS and centrifuge at 300 × *g* for 5 min. Decant supernatant and resuspend in 50 μL D-PBS.
5. Prepare a cocktail or master mix of antibodies by calculating how many samples will be stained and adding extra antibodies for 2 additional samples. For example, if 10 samples will be stained, add an amount of each antibody to the master mix that is enough for 12 samples.
6. Add the master mix of antibodies to each sample tube and incubate for 30 min at 4 °C in the dark. The final staining volume is dependent on the number of antibodies and the volume of each antibody (i.e., 12 antibodies/5 μL per antibody will give an antibody cocktail of 60 μL per sample). If using Brilliant Violet, Ultraviolet or Blue reagents, also add 50–100 μL of Brilliant Stain Buffer to the tube in addition to the antibody cocktail.
7. Add 3 mL of FACS Wash Buffer or FACS Tissue Wash Buffer and centrifuge at 300 × *g* for 5 min.
8. Decant supernatant and resuspend in 300–400 μL of Fixation Buffer.

9. Stain single color compensation tubes using either cell controls or antibody capture beads according to manufacturer's instructions.
10. Stain FMO controls if there are sufficient cells.
11. Acquire samples on flow cytometer within 24 h.

3.4 96-Well Plate Staining Procedure

1. Perform **steps 1–6** as in Subheading 3.3 but increase cell concentration to 2×10^7 cells/mL so that 50 μL of cells can be added to each well instead of 100 μL.
2. For 96-well deep-well plates, add 500 μL of FACS Wash Buffer or FACS Tissue Wash Buffer; for standard 96-well U-bottomed plates, add 100 μL.
3. Centrifuge at 300 × *g* for 5 min.
4. Aspirate the supernatant off with vacuum manifold and repeat **steps 2–3** (*see* **Note 2**). For standard 96-well U-bottomed plates, increase the wash volume to 200 μL and repeat the wash step one additional time for a total of three washes.
5. Aspirate the supernatant off with vacuum manifold and resuspend cells in 200 μL of Fixation Buffer.
6. FMO and compensation controls can be stained in the plate as well.
7. Acquire samples on flow cytometer within 24 h. If using the HTS 96-well plate loader (BD Biosciences), transfer samples to standard 96-well U-bottomed plate before acquisition.

3.5 Instrument Setup and Compensation (See Note 3)

1. Confirm that the instrument is working properly by performing daily quality control. For example, use FACSDiva CS&T software and beads.
2. To reduce data file size and optimize instrument performance, delete any detector that is not being used in this panel. In addition, the threshold should also be increased to reduce the amount of debris included in the final data file.
3. Create compensation control samples in the experimental document.
4. In general, compensation values are related to PMT voltage settings. To keep compensation values low, PMT detector settings within a single laser should be kept within 150–200 V of each other. CS&T generated instrument settings are not optimal for flow cytometric analysis of more than 12 colors and should not be used. If there are no available application settings for the staining panel, set each detector at 500 V as a starting point and then adjust accordingly.
5. Stained compensation controls should be used to optimize instrument settings. Use an acquisition template that displays

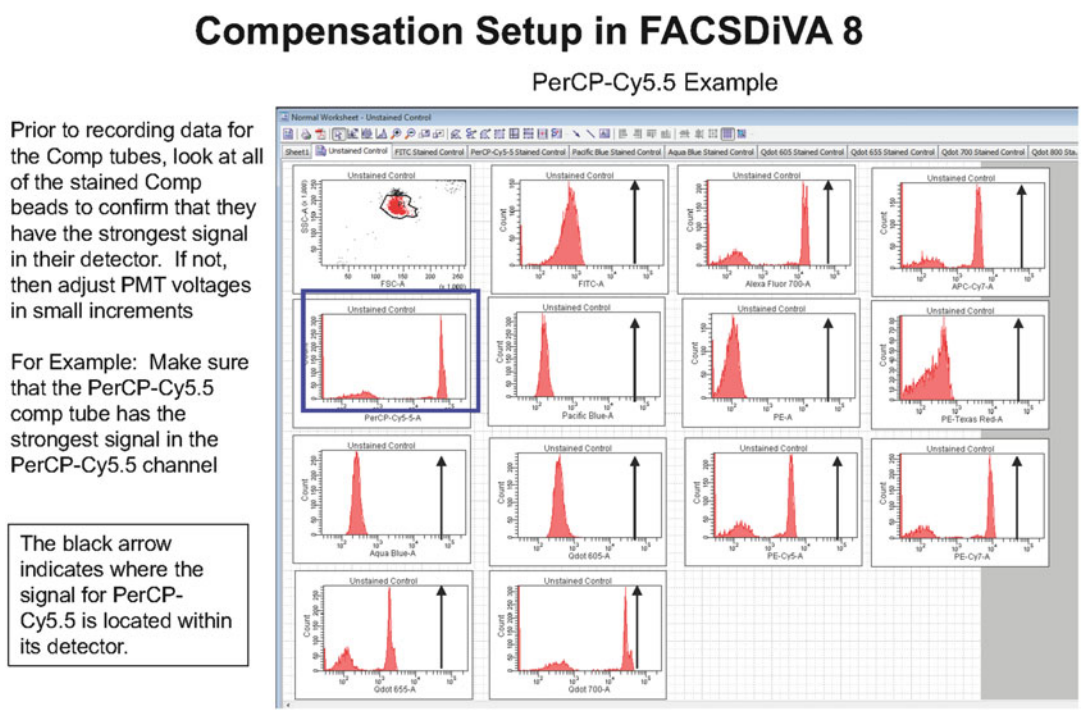

Fig. 3 Example of compensation setup using FACSDiva 8 software. COMPTrol beads were stained with PerCP-Cy5.5 and then examined on a LSRII flow cytometer for spill-over into other fluorescent channels. Since the fluorescence signal was strongest in the PerCP-Cy5.5 channel, the detector settings were considered correct

all the fluorescent channels (the template for "*Unstained Control*" in FACSDiva works well). Run each single color compensation control, making sure that the signal for each fluorochrome is highest in its detector with lower signals in other detectors. If there is an overlapping signal in a different detector, then adjust PMT voltage settings until the conflict is resolved. For example, PerCP-Cy5.5 should have its highest signal in that detector and lower signals in the PE-Cy5, Qdot 700 and AlexaFluor 700 detectors (*see* Fig. 3).

6. Acquire the compensation controls and then calculate compensation using the acquisition software. The software will indicate if there are compensation problems that can be addressed before sample acquisition. Apply compensation to the samples or acquire the samples uncompensated for later compensation using analysis software.
7. Create and label sample files in the experimental document.
8. Acquire samples and collect large numbers of events. Optimally a stopping gate should be placed on the population of interest so that the data file will contain enough events of that population to give an accurate analysis.

14-color Staining Panel - LSRII

Laser	Dichroic	BP Filter	Antibodies and Fluorochromes
488 nm	505LP	525/50	CD14 FITC
488 nm	690LP	710/50	CD4 PerCP-Cy5.5
532 nm		575/26	CD25 PE
532 nm	600LP	610/20	PD-1 PE-CF594
532 nm	635LP	660/20	CD7 PE-Cy5
532 nm	685LP	710/50	
532 nm	755LP	780/60	CD45RA PE-Cy7
628 nm		670/30	CD45RO APC
628 nm	685LP	730/45	CD3 Alexa 700
628 nm	755LP	780/60	CD45 APC-Cy7
405 nm		450/50	CD16 BV421
405 nm	505LP	525/50	Live/Dead Aqua Dye
405 nm	557LP	560/20	
405 nm	570LP	585/42	
405 nm	600LP	610/20	CD19 BV605
405 nm	635LP	670/30	CD8 BV650
405 nm	690LP	710/50	
405 nm	750LP	780/60	Anti Mouse CD45 BV786

23-color Staining Panel - FACSymphony

Laser	Dichroic	BP Filter	Antibody and Fluorochrome
488 nm	505LP	515/20	CXCR5 FITC
488 nm	595LP	610/20	
488 nm	635LP	660/40	
488 nm	690LP	695/40	TGF-B PerCP-Cy5.5
488 nm	750LP	780/60	
532 nm		586/15	Granzyme B PE
532 nm	595LP	610/20	FoxP3 PE-CF594
532 nm	635LP	670/30	CD45RA PE-Cy5
532 nm	690LP	710/50	
532 nm	750LP	780/60	TNF-a PE-Cy7
532 nm	770LP	820/60	
628 nm		670/30	Perforin Alexa 647
628 nm	690LP	730/45	IL-17 APC-R700
628 nm	750LP	780/60	CD4 APC-H7
405 nm		450/50	IL-6 BV421
405 nm	505LP	515/20	CD45RO BV480
405 nm	595LP	610/20	IL-2 BV605
405 nm	635LP	670/30	IL-10 BV650
405 nm	690LP	710/50	IL-4 BV711
405 nm	730LP	750/30	IFN-g BV750
405 nm	750LP	780/60	CD127 BV786
355 nm		379/28	CD8 BUV395
355 nm	410LP	450/50	Live/Dead Blue Dye
355 nm	450LP	515/30	CD16 BUV496
355 nm	525LP	540/30	CD25 BUV563
355 nm	635LP	670/30	CD3 BUV661
355 nm	690LP	740/35	CD56 BUV737
355 nm	770LP	820/60	CD45 BUV805

Fig. 4 Sample staining panels for LSRII and FACSymphony

3.6 Sample Staining Panels

Sample staining panels for 14 colors on a LSRII and 23 colors on a FACSymphony are shown in Fig. 4**.** The 14-color panel has been used to phenotype blood and tissues from humanized BLT mice infected with HTLV-1 on a LSRII flow cytometer. The 23-color panel is suitable for a deep profile of T cells and NK cells, including memory, activation, T_{reg} cells, T_H1 cells, T_H2 cells, T_{FH} cells, T_{H17} cells, CTL responses, and NK responses. It includes intracellular markers and cytokines. The same panel setup and instrument setup discussed in this chapter are appropriate for intracellular staining, but the staining method described in the "Multiparameter Intracellular Cytokine Staining" chapter in this edition should be used for intracellular staining.

4 Notes

1. The ArC beads do not always stain well. Cells are a more consistent control. Briefly, cells are microwaved for a few seconds to induce cell death and then stained with the viability dye.
2. Set up the aspirating manifold using a length adjuster so that it leaves a little space at the bottom of the well and does not disturb the pellet following centrifugation. This reduces cell

loss when staining in 96-well plates. Using an aspiration manifold is preferable to decanting following centrifugation when staining in 96-well plates.

3. The instrument setup in this procedure is based on using a LSRII or FACSSymphony flow cytometer. Other manufacturers make instruments capable of analyzing multiparameter flow cytometry samples. For those instruments, follow the normal quality control procedures. However, the PMT voltage set up should be universal and compensation can be effectively calculated using analysis software such as FlowJo.

References

1. Perfetto SP, Ambrozak D, Nguyen R, Chattopadhyay P, Roederer M (2006) Quality assurance for polychromatic flow cytometry. Nat Protoc 1(3):1522–1530. doi:10.1038/nprot.2006.250
2. Perfetto SP, Ambrozak D, Nguyen R, Chattopadhyay PK, Roederer M (2012) Quality assurance for polychromatic flow cytometry using a suite of calibration beads. Nat Protoc 7 (12):2067–2079. doi:10.1038/nprot.2012.126
3. Maecker HT, Frey T, Nomura LE, Trotter J (2004) Selecting fluorochrome conjugates for maximum sensitivity. Cytometry A 62 (2):169–173. doi:10.1002/cyto.a.20092
4. Fluorochrome Brightness Chart. https://www.bdbiosciences.com/documents/Fluorochrome-Chart-Relative-Brightness.pdf
5. Roederer M (2002) Compensation in flow cytometry. Curr Protoc Cytom Chapter 1:Unit 1 14. doi:10.1002/0471142956.cy0114s22
6. Maecker H, Trotter J (2008) Selecting reagents for multicolor flow cytometry with BD LSR II and BD FACSCanto systems. Nat Methods 5: an6–an7

Chapter 9

Multiparameter Intracellular Cytokine Staining

Patricia Lovelace and Holden T. Maecker

Abstract

Intracellular cytokine staining is a popular method for visualizing cellular responses, most often T-cell responses to antigenic or mitogenic stimulation. It can be coupled with staining for other functional markers, such as upregulation of CD107 or CD154, as well as phenotypic markers that define specific cellular subsets, e.g., effector and memory T-cell compartments, NK cells, or monocytes. Recent advances in multicolor flow cytometry instrumentation and software have allowed the routine combination of 12 or more markers, creating some technical and analytical challenges along the way, and exposing a need for standardization in the field. Here, we will review best practices for antibody panel design and procedural variables for multicolor intracellular cytokine staining, and present an optimized protocol with variations designed for use with specific markers and sample types.

Key words Antigen-specific, Intracellular staining, Multicolor, Polychromatic, Fixation, Permeabilization, AIDS vaccine research, T cells

1 Introduction

With the use of secretion inhibitors such as monensin or brefeldin A, secreted cytokines and other proteins can be retained intracellularly. These proteins thus become available for antibody staining, upon fixation, and permeabilization of the cells [1, 2]. In general, short-term stimulation of cells with mitogen or antigen is required to induce cellular activation and production of cytokines. One common application of this technique is the enumeration and phenotyping of antigen-specific T cells in PBMC [3] or whole blood [4]. This requires stimulation with protein antigens or, commonly, pools of overlapping peptides spanning a protein sequence of interest. The latter, when designed with sufficient length and overlap between peptides, can efficiently stimulate both CD4 and CD8 T-cell responses [5].

A common protocol for antigen-specific stimulation of T cells for intracellular cytokine staining (ICS) is as follows. Whole blood or PBMC are incubated with antigen or peptide mixtures for 6–16 h. Brefeldin A and/or monensin is added at the time of

Teresa S. Hawley and Robert G. Hawley (eds.), *Flow Cytometry Protocols*, Methods in Molecular Biology, vol. 1678, DOI 10.1007/978-1-4939-7346-0_9,

stimulation (for peptides) or after 2 h (for proteins, to allow for intracellular antigen processing, which is compromised by the secretion inhibitor). At the end of the stimulation period, cells can be held at 4–18 °C until ready to process. They are then treated with EDTA to detach adherent cells, fixed (usually with formaldehyde), permeabilized (usually with a detergent), and stained for intracellular determinants. In some cases, surface marker staining is done in conjunction with intracellular staining (this works well for CD3, CD4, and CD8). However, many other cell-surface markers are better stained prior to fixation, because the epitopes recognized by staining antibodies are sensitive to fixation and/or permeabilization.

Intracellular staining for multiple cytokines is now often combined with staining for other functional and phenotypic markers as well. This has been made possible by the availability of flow cytometers with digital signal processing and detectors for 18 or more colors. Mass cytometers (CyTOF) capable of 40+ parameters and using heavy metal ion tags have also been introduced [6]; they are covered elsewhere in this edition. Along with this instrumentation, software for automated calculation of compensation between colors is now routinely used, often in combination with single-stained capture beads that make construction of compensation controls easier and more precise (since the actual experimental antibodies can be used for compensation, an important consideration for some tandem dye conjugates). Finally, software and fluorescent beads to automate instrument setup and track performance over time are now available, making longitudinal standardization of experiments, at least for a single instrument, much easier. Standardization across instruments, especially given the degree of instrument customization seen in the field, can still be difficult, however.

Despite the advances in tools for multicolor flow cytometry, designing optimal multicolor panels still requires some attention. The optical spectrum is limited to such an extent that addition of new fluorescent reagents tends to create more spillover into existing detectors. In some cases, this can severely compromise the ability to use those detectors for measurements requiring high-resolution sensitivity. Recently, a new family of probes (Brilliant Violet, UV, and Blue) was developed in efforts to increase the number of parameters that could be simultaneously measured and to offer brighter probes to replace older, dimmer probes. These polymer-based fluorescent molecules rival phycoerythrin (PE) and allophycocyanin (APC) in useful brightness and sensitivity, and extend the range of emission on the violet and ultraviolet lasers. Introducing one or more of these Brilliant probes to the color panel expands the options for multicolor panels.

General discussions of rules for antibody panel design, along with suggestions for specific fluorochrome combinations and

Table 1
Fluorochrome brightness

	Dim: use for markers with very good separation of positive and negative populations	Medium: use for markers with moderate separation between positive and negative populations	Bright: use for markers with poor separation between positive and negative populations
UV laser	BUV805	BUV395 BUV496 BUV661 BUV737	
Violet laser	V450 V500 Pacific Orange	BV510 BV605 BV786	BV421 BV650 BV711
Blue laser	PerCP	AlexaFluor488 FITC PerCP-Cy5.5	BB515 PE PE-CF594 PE-Cy5 PE-Cy7
Red laser	APC-Cy7 APC-H7	AlexaFluor700	APC AlexaFluor647 APC-R700

panels, have been published [7, 8]. These rules are briefly summarized here.

1. Use the dimmest fluorochromes for brightly staining antibodies (CD45, CD4, CD8, CD3, etc.), while reserving the brightest fluorochromes for dimly-staining antibodies (*see* Table 1).
2. Avoid spillover from a bright cell population into a detector requiring high-resolution sensitivity (*see* Fig. 1). In some cases, two fluorochromes with high spillover between them can be used for markers that identify distinct, nonoverlapping cell populations, thereby negating spillover concerns.
3. Avoid potential artifacts of tandem dye degradation, either by avoiding tandem dyes that are particularly susceptible to breakdown (e.g., APC-Cy7, PE-Cy7), or by choosing reagent combinations such that small amounts of tandem breakdown will not compromise readouts in the parent dye channels (APC or PE). *See* Maecker et al. [7] for further discussion and examples of this issue.

There are also practical considerations to panel design, such as what antibody conjugates are commercially available. In general, it is best to use direct fluorochrome conjugates for multicolor work and for intracellular staining, since nonspecific binding can be a significant concern in these situations.

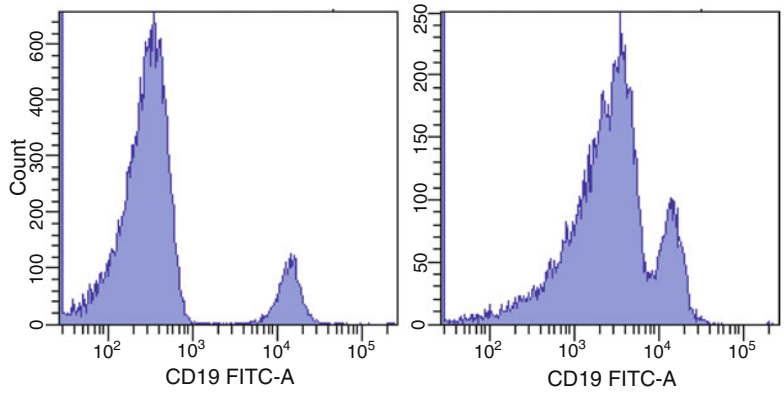

Fig. 1 Effect of a bright signal in AmCyan on resolution sensitivity in FITC. *Left panel*: staining with CD19 FITC alone. *Right panel*: combined staining of CD45 AmCyan and CD19 FITC. Note the spread of the CD19-negative peak, causing loss of resolution sensitivity. This is only a problem when both markers are present on the same cell population (e.g., use of CD3 AmCyan and CD19 FITC would not pose a problem). Similar issues arise whenever there is significant spillover from a bright population in one detector to another detector where high-resolution sensitivity is required

Even direct antibody conjugates can be optimized by titration for a particular application. Optimal titers should be picked on the basis of maximal signal:noise, which is often obtained below the titer recommended by the manufacturer.

While panels will constantly be refined to include new markers of interest, a degree of standardization is helpful, to avoid extensive re-optimization of new panels and provide for some degree of longitudinal comparisons. In Table 2, we provide some suggested panels developed in our laboratory.

Finally, optimal detection of certain marker combinations requires modification of stimulation and processing steps (for example, CD107 or CD154). These variables are summarized in Table 3.

2 Materials

2.1 Reagents

1. Sources of test specimens: heparinized whole blood, freshly isolated PBMC, or cryopreserved PBMC.
2. Isolation of test specimens: Ficoll gradient centrifugation; alternatively, BD Vacutainer Cell Preparation Tubes (BD Diagnostics, Franklin Lakes, NJ) can be used.
3. cRPMI-10: RPMI-1640 medium, 20 mM HEPES, 10% fetal bovine serum, antibiotic/antimycotic solution. When used to thaw cryopreserved PBMC, add benzonase to a final concentration of 25 U/mL, and use this medium for the first wash, then resuspend in cRPMI-10 without benzonase.

Table 2
Some suggested multicolor antibody panels

	8-color T cells 3 memory markers + 2 functions[a]	10-color T cells 1 memory marker + 5 functions[b]	10-color T cells 3 memory markers + 3 functions[c]	13-color T cells 2 memory markers + 7 functions[d]
FITC or AlexaFluor 488	Anti-IFNγ	CD27	Anti-IFNγ	CD107a
PE	Anti-IL-2	CD154	Anti-IL-2	Anti-IL-2
PE-Texas Red or PE-AlexaFluor 610		CD107	Anti-TNFα	CD3
PerCP-Cy5.5	CD28	CD4	CD28	IL-17A
PE-Cy5				CD154
PE-Cy7	CD45RA	Anti-IFNγ	CD45RA	Anti-TNFα
APC or AlexaFluor 647	CD27	Anti-IL-2	CD27	IL-22
AlexaFluor 700		Anti-TNFα	CD3	CD8
APC-H7 or APC-eFluor 780	CD8	CD8	CD8	CD4
Pacific Blue or V450	CD3	CD3	CD4	Anti-IFNγ
AmCyan, Pacific Orange or V500	CD4	CD14	CD14	CD14+CD19+ AViD viability dye
BV605				CCR7
BV785				CD45RO

[a]Used in ref. 9
[b]Modified from panel used for International Flow Cytometry School (IFCS) 2006, Florence, Italy
[c]Used for Multicolor ICS Users Group standardization studies (see also http://maeckerlab.typepad.com for additional panel suggestions and details)
[d]From ref. 10

4. Stimulation antigens: peptide mixes [5] or whole proteins. To prepare lyophilized peptide stock aliquots, resuspend peptides or peptide mixes in DMSO at a concentration of 500 μg/mL/peptide or greater. Store resuspended peptides in aliquots at −80 °C. Alternatively, BD Lyoplates (BD Biosciences, San Jose, CA) that are preconfigured plates containing lyophilized stimulation reagents, costimulatory antibodies, and secretion inhibitor(s) can be used [11].
5. Positive control for stimulation: Staphylococcal enterotoxin B (SEB), 50 μg/mL in sterile PBS.

Table 3
Procedural variables for different functional markers

Variable	IL-2, IL-4, IL-5, IL-13, IFNγ, MIP-1β, TNFα	CD107, CD154	IL-10, TGFβ
Stimulation conditions	6–12 h	5–6 h in the presence of staining antibodies for these markers	12–24 h (serum-free medium for TGFβ[a])
Secretion inhibitor	Brefeldin A	Monensin[b]	Monensin
Fixation/permeabilization system	FACS Lysing Solution, FACS Permeabilizing Solution 2[c]	FACS Lysing Solution, FACS Permeabilizing Solution 2[c]	Cytofix, Cytoperm[d]

[a]Serum-free medium (e.g., AIM V from Invitrogen, Carlsbad, CA) produces much stronger TGFβ responses, presumably because serum contains free TGFβ that blocks staining for this marker
[b]CD107 and CD154 are taken up by endocytic vesicles and degraded. Monensin blocks this degradation by preventing acidification of these vesicles. When doing combined assays with cytokines, a monensin plus brefeldin A combination is recommended (*see* **Note 5**)
[c]BD Biosciences, San Jose, CA. Note that the Cytofix/Cytoperm system (BD Biosciences, San Diego, CA) is also used successfully for these markers by many investigators
[d]BD Biosciences, San Diego, CA

6. (Recommended) Costimulatory antibodies to CD28 and CD49d: 0.1 mg/mL of each in sterile PBS; alternatively, BD FastImmune (BD Biosciences) can be used.
7. Secretion block stock solutions: 5 mg/mL brefeldin A in DMSO; or brefeldin A plus monensin, 2.5 mg/mL of each in 50% DMSO plus 50% methanol.
8. 20 mM EDTA in PBS, pH 7.4; alternatively, BD FastImmune can be used.
9. (Optional) Viability dye: Amine reactive dye for staining non-viable cells.
10. Erythrocyte lysis and cell fixation reagent (e.g., BD FACS Lysing Solution from BD Biosciences).
11. Cell permeabilizing reagent (e.g., BD FACS Permeabilizing Solution 2 from BD Biosciences).
12. Fluorescent-labeled antibodies (*see* Table 2 for recommendations); alternatively, BD Lyoplates can be used [11].
13. Wash buffer: 0.5% bovine serum albumin plus 0.1% NaN_3 in PBS.
14. (Recommended) Anti-immunoglobulin-coated capture beads: anti-mouse Ig, anti-rat Ig, or anti-rat/hamster Ig beads for creating single-color compensation controls.
15. (Optional) Fixative for the reduction of biohazard potential or storage of samples for >24 h prior to acquisition: 1%

paraformaldehyde in PBS; alternatively, BD Stabilizing Fixative (BD Biosciences) can be used.

16. (Optional) CS&T beads and FACSDiva software for data acquisition (BD Biosciences).

2.2 Equipment

1. For whole blood assays, 96-well conical bottom deep-well polypropylene plates and lids. For fresh or frozen PBMC, 96-well conical- or round-bottom polypropylene plates with lids (*see* **Note 1**).
2. 12-channel vacuum manifold with 35 mm prongs for deep-well plates and 7 mm prongs for regular plates (V&P Scientific, San Diego, CA).
3. Plate holders for table-top centrifuge.
4. Polychromatic flow cytometer.
5. (Optional) 96-well plate loader for flow cytometer.

3 Methods

3.1 Cell Preparation

1. For fresh PBMC (*see* **Note 2**): Resuspend at 5×10^6 to 1×10^7 viable cells/mL in warm (37 °C) cRPMI-10 (*see* **Note 3**).
2. For cryopreserved PBMC: Thaw briefly in a 37 °C water bath, then slowly dilute up to 10 mL with warm (37 °C) cRPMI-10 with benzonase, and centrifuge for approximately 7 min at 250 × *g*. Resuspend in a small volume of warm cRPMI-10 (no benzonase), perform a viable cell count, and dilute to a concentration of about 1.5×10^7 viable cells/mL for resting overnight. Incubate at 37 °C for 6–18 h prior to stimulation in a conical centrifuge tube, tilted (*see* **Note 4**). Resuspend and recount cells after the rest. Using this new count, prepare the final suspension at 5×10^6 to 1×10^7 viable cells/mL in warm (37 °C) cRPMI-10.
3. For whole blood assays: Collect whole blood in sodium heparin and store at room temperature for not more than 8 h prior to use.

3.2 Cell Activation

3.2.1 Using Liquid Stimulation Reagents

Add 200 μL of cell suspension per well to an appropriate conical- or round-bottom 96-well plate (deep well for whole blood, standard well for PBMC).

1. Prepare the secretion block reagents.
   (a) For assays not involving CD107 or CD154: Thaw an aliquot of 5 mg/mL brefeldin A stock (*see* **Note 5**). Dilute 1:10 in sterile PBS to make a 50× working stock.
   (b) For assays measuring CD107 and/or CD154: Thaw an aliquot of 2.5 mg/mL brefeldin A plus 2.5 mg/mL monensin stock (*see* **Note 5**). Dilute 1:10 in sterile PBS to make a 50× working stock.

2. Thaw and dilute peptide stock aliquots (*see* **Note 6**) in sterile PBS, if necessary, to achieve a 50× working stock that is between 50 and 100 μg/mL/peptide (when diluted 1:50, this will yield a final concentration of 1–2 μg/mL/peptide).
3. For each stimulation condition, prepare a "master mix" of the 50× working stocks and costimulatory antibodies as follows (always prepare a slight excess of each master mix):
   (a) 4 μL/well peptides, SEB (positive control), or PBS (negative control).
   (b) 4 μL/well brefeldin A or brefeldin A plus monensin.
   (c) 4 μL/well CD28 plus CD49d Ab stock (*see* **Note 7**).
4. Pipet 12 μL of the appropriate master mix into each well containing cells. Mix by gently pipetting.
5. For assays involving CD107 and/or CD154, also add the recommended titer of the antibody conjugate(s) to each well. Minimize exposure to light, particularly for tandem dye conjugates (*see* **Note 8**).
6. Incubate covered plate for 6–12 h at 37 °C (*see* **Notes 9** and **10**).
7. Proceed to Subheading 3.3.

3.2.2 Using BD Lyoplates

1. Add 200 μL of cell suspension directly to the appropriate wells in the stimulation lyoplate, let sit for a few minutes, then pipet up and down thoroughly to mix.
2. Incubate covered plate for 6–12 h at 37 °C (*see* **Notes 9** and **10**).
3. Proceed to Subheading 3.3.

3.3 Viability Dye and Cell-Surface Staining

1. To halt activation and detach adherent cells, add 20 μL per well of 20 mM EDTA in PBS and mix by pipetting.
2. Incubate 15 min at room temperature, then mix again by vigorous pipetting to fully resuspend adhered cells.
3. For PBMC, centrifuge plate at 250 × *g* for 5 min. Aspirate the supernatant with the appropriate vacuum manifold for the plate (*see* **Note 11**). For whole blood, skip to **step 5**.
4. For assays using amine-reactive dye for staining nonviable cells: Resuspend the amine dye at optimum concentration in PBS (usually around 2.5 μg/mL, but this should be determined for individual lots of dye). Resuspend each well with 100 μL of this solution, incubate for 20 min at room temperature, then add 100 μL of wash buffer, and wash as in **step 3** above. Amine dyes can be used with whole blood, but higher concentrations will be required because the blood is not washed into PBS prior to dye staining. The staining intensity may be reduced.

5. Incubate with antibodies:
   (a) For assays using liquid reagents and cell-surface markers other than CD3, CD4, and CD8: For PBMC, first resuspend each well in 100 µL of wash buffer, then add optimal titers of all Abs to cell-surface markers (*see* **Note 12**). For whole blood, add Abs directly to the EDTA-treated whole blood. Incubate 30–60 min at room temperature in the dark. For PBMC, add 100 µL of wash buffer, wash as in **step 3** above, and proceed to Subheading 3.4.1. For whole blood, proceed directly to Subheading 3.4.2.
   (b) For assays using preconfigured lyophilized staining reagents and cell-surface staining Abs: Resuspend the appropriate wells of the surface Ab plate with 50 µL of wash buffer. Let it sit for a few minutes, then pipet up and down thoroughly to mix. Transfer the solution to appropriate wells of the cell plate, incubate for 30–60 min at room temperature in the dark. For PBMC, add 100 µL of wash buffer, wash as in **step 3** above, and proceed to Subheading 3.4.1. For whole blood, proceed directly to Subheading 3.4.2.

3.4 Fixation and Permeabilization

3.4.1 PBMC

1. Resuspend cell pellets with 100 µL of 1× BD FACS Lysing Solution per well. Incubate at room temperature for 10 min in the FACS Lysing Solution (*see* **Notes 13** and **14**).
2. Add 100 µL of wash buffer to each well, then centrifuge plate at 500 × *g* for 5 min (*see* **Note 15**). Aspirate the supernatant with the appropriate vacuum manifold for the plate.
3. Resuspend cell pellets with 200 µL of 1× BD FACS Permeabilizing Solution 2 per well. Incubate at room temperature for 10 min (*see* **Note 14**).
4. Centrifuge the plate at 500 × *g* for 5 min (*see* **Note 15**). Aspirate the supernatant with appropriate vacuum manifold for the plate.
5. Add 200 µL of wash buffer to each well, and wash as in **step 4** above.
6. Add 200 µL of wash buffer to each well, and wash a second time as in **step 4** above.
7. Proceed to Subheading 3.5.

3.4.2 Whole Blood

1. Add 2 mL of room temperature 1× BD FACS Lysing Solution per well, pipetting up and down to mix. Incubate at room temperature for 10 min in FACS Lysing Solution (*see* **Notes 13** and **14**).
2. Centrifuge the plate at 500 × *g*. Aspirate the supernatant with the appropriate vacuum manifold for the plate.

3. Resuspend cell pellets in 1 mL of 1× BD FACS Permeabilizing Solution 2 per well. Incubate at room temperature for 10 min (*see* **Note 14**).
4. Centrifuge the plate at 500 × *g* for 5 min (*see* **Note 15**). Aspirate the supernatant with appropriate vacuum manifold for the plate.
5. Add 1.5 mL of wash buffer to each well, and wash as in **step 4** above.
6. Proceed to Subheading 3.5.

3.5 Intracellular Staining

1. Incubate with antibodies.
   (a) For assays using liquid reagents: Resuspend pellet in 100 μL of wash buffer and add optimal titers of all Abs to intracellular markers and surface markers not already stained. Incubate in the dark at room temperature for 60 min, mixing by pipetting or gentle agitation every 15–20 min.
   (b) For assays using preconfigured lyophilized intracellular staining reagents: Resuspend the appropriate wells of the intracellular antibody plate with 50 μL of wash buffer. Let it sit for a few minutes, then pipette up and down thoroughly to mix. Transfer the solution to the appropriate wells of the cell plate, and incubate at room temperature in the dark for 60 min, mixing by pipetting or gentle agitation every 15–20 min.
2. Add 200 μL of wash buffer (for standard well plates) or 1.5 mL of wash buffer (for deep-well plates) to each well, centrifuge at 500 × *g* for 5 min, and aspirate with an appropriate vacuum manifold.
3. Repeat the wash step once more as in **step 2** above.
4. Resuspend pellets with 150 μL of wash buffer. Store at 4 °C in the dark until ready for data acquisition, which should be performed within 24 h. (Optional) Resuspend pellets with 150 μL of 1% paraformaldehyde in PBS or BD Stabilizing Fixative (*see* **Note 16**).

3.6 Data Acquisition and Analysis

1. First determine optimal PMT settings for the instrument and reagent panel in question. If using CS&T beads and software, start with CS&T baseline voltages, then:
   (a) Run single-stained compensation controls (*see* **Note 17**) and decrease PMT voltage gain, if needed, to ensure that no events are in the highest fluorescence channel. Increase PMT voltage gain, if needed, to ensure that positive peaks are at least twofold brighter in their primary detector compared to other detectors.

(b) Run a fully stained positive control sample and decrease PMT voltage gain, if needed, to ensure that no events are in the highest fluorescence channel. If changes are made, repeat **steps** (**a**) and (**b**) until no more changes are required. Save the resulting settings as an Application Setting in FACSDiva software.

2. Acquire the single-stained compensation controls and use the software's automated algorithm to calculate compensation (*see* **Note 18**).
3. Create a template for acquisition that displays the relevant parameters in the test samples in the form of dot plots. This template need not be the same as that used for analysis, i.e., it does not need to specify all gates or regions of interest. In fact, a simplified acquisition template will allow faster processing of data. However, the template should show any gates used to define the saved population of cells or the stopping criteria (e.g., $CD3^+$ cells).
4. Set an appropriate threshold, usually on FSC or $CD45^+$ events, to eliminate debris and unwanted events. Set the stopping and storage criteria to obtain sufficient events for analysis. It is usually safest to store all events (rather than a gated subset) to allow for re-gating and exploration of other subsets. However, sometimes a threshold or gate on $CD3^+$ cells may be employed in order to reduce file sizes (*see* **Note 19**).
5. Record data from samples.
6. Analyze data using the acquisition software or compatible third-party software. Be sure to define all regions of interest and report the desired statistics on these (*see* **Note 20** and Fig. 1). Where possible, use a batch analysis function to analyze all samples from a given experiment or study and export the statistical data to a spreadsheet (*see* **Note 21**).
7. For large studies, it is helpful to create a database to accept the statistical output files from batch analysis. This database can then be queried to create data tables from subsets of the data, allowing rapid graphing, statistical analysis, background subtraction, conversion to absolute counts, etc.

4 Notes

1. Plates versus tubes: Cells can also be stimulated in 15 mL conical polypropylene tubes, with staining in 12 × 75 mm polystyrene tubes. However, plates are preferred for ease of handling multiple samples, and results for human PBMC are equivalent to those in tubes [12].

2. Fresh PBMC: If PBMC are not to be cryopreserved, they should ideally be prepared on the day of blood draw, then either stimulated the same day, or rested at 37 °C in cRPMI-10 overnight and stimulated the following day. Overnight resting at 37 °C increases the staining intensity of cytokines, but the effect is more pronounced with cryopreserved samples. Overnight shipping of whole blood or PBMC at ambient temperatures can cause a variable decrease in cell function and should be avoided if possible, though shipping PBMC is preferable to shipping whole blood.
3. Higher cell concentrations (1×10^7/mL, 2×10^6/well) should be used when possible, especially when response levels are low and/or there are many cell subsets to enumerate.
4. Cryopreserved PBMC: If cells cannot be stimulated within 24 h of blood draw, they should be cryopreserved by a validated protocol [13]. Upon thawing, recoveries of >60% and viabilities of >80% should be obtained to minimize loss of functional responses. The method of thawing is equally as important as that of cryopreservation [13]. Thawed cells should be rested in cRPMI-10 for 6–18 h at 37 °C to maximize cytokine staining intensity [12]. Some cell loss may occur during this period, so rest at a higher concentration than what will ultimately be used. Recount and resuspend at the desired final concentration after resting.
5. Brefeldin A versus monensin: Secretion of most cytokines of interest (IFNγ, IL-2, etc.) is best inhibited by brefeldin A at 10 μg/mL cells. However, CD107 and CD154 are transiently expressed on the cell surface. Therefore, staining Abs to CD107 and/or CD154 are added to the stimulation culture to bind the antigen(s) as soon as they are expressed. Monensin increases the intensity of staining under these conditions by preventing the acidification and degradation of lysosomal vesicles that contain the recycled CD107 and CD154. Thus, for combined cytokine and CD107 or CD154 detection, 5 μg/mL each of brefeldin A and monensin is recommended.
6. Peptide mixes: Peptide mixes can be prepared and lyophilized as premixed pools of up to several hundred peptides [5]. These can then be resuspended in DMSO at high concentration per peptide, avoiding DMSO toxicity. The total concentration of DMSO in the assay should be kept at <0.5%.
7. Costimulatory antibodies: Antibodies to CD28 and CD49d can increase the cytokine response to protein antigens, peptides, and SEB by amplifying the signal for low-affinity T cells [14]. In occasional donors, they increase cytokine production in the absence of antigen (certain cytokines, like TNFα are more affected).

8. Adding staining Abs during stimulation: As described in **Note 5**, staining Abs to CD107 and CD154 are best added during stimulation, to capture the transiently expressed antigen. Fluorochrome-conjugated Abs are sensitive to light exposure, so they should be handled in low light and, once added, the samples should be incubated in the dark. Certain tandem dyes such as APC-Cy7 and PE-Cy7 are particularly sensitive to light and temperature [7] and are not optimal choices for use in stimulation cultures.
9. Stimulation time: A minimum of 5–6 h allows adequate detection of most proinflammatory cytokines like IFNγ, TNFα, and IL-2 [15]. Increasing the time of incubation (in the presence of brefeldin A) increases cytokine staining intensity, but is not recommended for CD107 or CD154. For whole proteins requiring intracellular processing, a pre-incubation of 2 h prior to adding brefeldin A and/or monensin is recommended [15]. CD8 responses to whole protein antigens can sometimes be detected, and are increased with longer incubation in antigen alone, but not in all donors [16].
10. Automating incubation times: A programmable heat block, incubator, or water bath can be used to time activation, cooling the samples to 4–18 °C at the end of a specified period at 37 °C, and holding them for later processing.
11. A fixed-length vacuum manifold helps achieve consistent washing without undue cell loss in microtiter plates. Because of the small wash volume, a sufficient number of washes and efficient removal of supernatant are essential.
12. CD3, CD4, and CD8 can be stained either before or after fixation and permeabilization. Down-modulation of these antigens occurs to a variable degree depending upon the stimulus. Cells that have down-modulated these antigens can be better detected by intracellular staining (post-fixation and permeabilization) [5], although the overall staining intensity is usually decreased. Most other cell-surface antigens are optimally stained before fixation.
13. Freezing of activated samples: Samples can be frozen at –80 °C directly in FACS Lysing Solution [15, 17]. This allows for samples to be sent to another laboratory for processing, or for longitudinal samples to be accumulated for batch processing.
14. Fixation and permeabilization steps: Solutions for these steps should be stored and used at 22–25 °C. FACS Lysing Solution simultaneously lyses erythrocytes and fixes leukocytes. While erythrocyte lysis is not required for PBMC samples, fixation is still helpful to prevent cell loss prior to permeabilization.

15. Centrifugation speed: All centrifugation post-fixation should be done at higher *g* force (500 × *g*) due to increased cell buoyancy.
16. Use of paraformaldehyde is only helpful when samples are stored for more than 24 h prior to acquisition, or to ensure neutralization of potentially biohazardous samples. In addition to subtle effects on cell scatter and fluorescence, storage in paraformaldehyde can cause degradation of tandem dyes such as APC-Cy7 and PE-Cy7. An alternative fixative, BD Stabilizing Fixative, is available that protects these tandems from degradation, but it is not compatible with AmCyan staining.
17. Compensation controls: Where possible, anti-immunoglobulin-coated capture beads such as BD CompBeads (BD Biosciences) or equivalent are preferred as compensation controls, because they provide a bright and homogeneous population of events stained with the antibody conjugate of interest. Ideally, the same lot of antibody should be used for compensation as is used in the experiment. In practice, however, this is only important for certain tandem conjugates, such as APC-Cy7 and PE-Cy7. The compensation controls should ideally be treated identically to the experimental samples in terms of fixation, etc., although this too is only important for the above tandem dyes.
18. When to apply compensation: While compensation can be calculated and changed at any time by software packages such as FlowJo (Tree Star, Ashland, OR) or FACSDiva, it is helpful to perform compensation before sample acquisition, so that any setup problems can be more readily detected.
19. Number of events to collect: Because multiparameter ICS assays tend to divide responding populations of cells into ever-smaller subsets, it is important to process and collect enough cells per sample to allow statistically significant differences between samples to be detected. The number of events required will depend upon the anticipated levels of responses and background, as well as the number of subsets of responding cells being identified. Statistical tools for sample size calculation can be found at http://maeckerlab.typepad.com
20. Gating of down-modulated cells: Be sure that gates set on CD3, CD4, and CD8 parameters include dim-positive cells, since down-modulation of these markers occurs with activation. When using dynamic gating (*see* **Note 21**), set the region size to the maximum value possible without causing inclusion of neighboring populations. Some donors have a significant population of $CD4^{+}CD8^{dim}$ T cells. This population contains a disproportionate number of cells specific for chronic antigens

such as CMV and HIV, and should be included in the $CD4^+$ T-cell gate to avoid under-reporting of responses.

21. Batch analysis: Dynamic gating tools such "Snap-To" gates in FACS Diva can be used to accommodate staining differences between samples for populations such as $CD3^+$, $CD4^+$, and $CD8^+$ cells (*see* Fig. 1). This in turn allows use of a single analysis template and batch analysis across multiple samples in an experiment or study. However, dynamic gates are not always useful for rare populations, and their specifications (size and movement) need to be adjusted for the data set being analyzed. Batch analysis and dynamic gating thus do not replace the need for visual inspection of all data.

Acknowledgments

Details of this protocol were optimized by Laurel Nomura and Maria Suni (BD Biosciences).

References

1. Jung T, Schauer U, Heusser C, Neumann C, Rieger C (1993) Detection of intracellular cytokines by flow cytometry. J Immunol Methods 159:197–207
2. Prussin C, Metcalfe DD (1995) Detection of intracytoplasmic cytokine using flow cytometry and directly conjugated anti-cytokine antibodies. J Immunol Methods 188:117–128
3. Waldrop SL, Pitcher CJ, Peterson DM, Maino VC, Picker LJ (1997) Determination of antigen-specific memory/effector CD4+ T cell frequencies by flow cytometry: evidence for a novel, antigen-specific homeostatic mechanism in HIV-associated immunodeficiency. J Clin Invest 99:1739–1750
4. Suni MA, Picker LJ, Maino VC (1998) Detection of antigen-specific T cell cytokine expression in whole blood by flow cytometry. J Immunol Methods 212:89–98
5. Maecker HT, Dunn HS, Suni MA, Khatamzas E, Pitcher CJ, Bunde T, Persaud N, Trigona W, Fu TM, Sinclair E, Bredt BM, McCune JM, Maino VC, Kern F, Picker LJ (2001) Use of overlapping peptide mixtures as antigens for cytokine flow cytometry. J Immunol Methods 255:27–40
6. Zivanovic N, Jacobs A, Bodenmiller B (2014) A practical guide to multiplexed mass cytometry. Curr Top Microbiol Immunol 377:95–109
7. Maecker HT, Frey T, Nomura LE, Trotter J (2004) Selecting fluorochrome conjugates for maximum sensitivity. Cytometry A 62:169–173
8. Maecker HT (2009) Multiparameter flow cytometry monitoring of T cell responses. Methods Mol Biol 485:375–391
9. Nomura LE, Emu B, Hoh R, Haaland P, Deeks SG, Martin JN, McCune JM, Dixon DF, Maecker HT (2006) IL-2 production correlates with effector cell differentiation in HIV-specific CD8+ T cells. AIDS Res Ther 3:18
10. Graves AJ, Padilla MG, Hokey DA (2014) OMIP-022: Comprehensive assessment of antigen-specific human T-cell functionality and memory. Cytometry A 85:576–579
11. Maecker HT, Rinfret A, D'Souza P, Darden J, Roig E, Landry C, Hayes P, Birungi J, Anzala O, Garcia M, Harari A, Frank I, Baydo R, Baker M, Holbrook J, Ottinger J, Lamoreaux L, Epling CL, Sinclair E, Suni MA, Punt K, Calarota S, El-Bahi S, Alter G, Maila H, Kuta E, Cox J, Gray C, Altfeld M, Nougarede NM, Boyer J, Tussey L, Tobery T, Bredt B, Roederer M, Koup R, Maino VC, Weinhold K, Pantaleo G, Gilmour J, Horton H, Sekaly RP (2005) Standardization of cytokine flow cytometry assays. BMC Immunol 6:13
12. Suni MA, Dunn HS, Orr PL, deLaat R, Sinclair E, Ghanekar SA, Bredt BM, Dunne JF, Maino VC, Maecker HT (2003) Performance of plate-based cytokine flow cytometry with automated data analysis. BMC Immunol 4:9

13. Disis ML, dela Rosa C, Goodell V, Kuan LY, Chang JC, Kuus-Reichel K, Clay TM, Kim Lyerly H, Bhatia S, Ghanekar SA, Maino VC, Maecker HT (2006) Maximizing the retention of antigen specific lymphocyte function after cryopreservation. J Immunol Methods 308:13–18
14. Waldrop SL, Davis KA, Maino VC, Picker LJ (1998) Normal human CD4+ memory T cells display broad heterogeneity in their activation threshold for cytokine synthesis. J Immunol 161:5284–5295
15. Nomura LE, Walker JM, Maecker HT (2000) Optimization of whole blood antigen-specific cytokine assays for CD4(+) T cells. Cytometry 40:60–68
16. Maecker HT, Ghanekar SA, Suni MA, He XS, Picker LJ, Maino VC (2001) Factors affecting the efficiency of CD8+ T cell cross-priming with exogenous antigens. J Immunol 166:7268–7275
17. Nomura LE, deHaro ED, Martin LN, Maecker HT (2003) Optimal preparation of rhesus macaque blood for cytokine flow cytometric analysis. Cytometry A 53:28–38

Chapter 10

Multiparametric Analysis of Apoptosis by Flow Cytometry

William G. Telford

Abstract

Flow cytometry is the most widely used method for detecting and quantifying apoptosis in mammalian cells. The multiparametric nature of flow cytometry allows several apoptotic characteristics to be combined in a single sample, making it a powerful tool for analyzing the complex progression of apoptotic death. This chapter provides guidelines for combining single-apoptosis assays such as fluorogenic caspase substrates, annexin V binding, DNA dye exclusion, and covalent viability probes into informative multiparametric assays. This multiparametric approach to analyzing apoptosis provides much more information than single-parameter assays that provide only a percentage apoptotic result, given that multiple early, intermediate, and late apoptotic stages can be observed and quantified simultaneously. While much more informative than single-color assays, these multicolor methods can still be analyzed on relatively simple flow cytometers, making them accessible to many laboratories.

Key words Apoptosis, Flow cytometry, Caspase, Fluorogenic caspase substrate, Annexin V, 7-Aminoactinomycin D, Propidium iodide, Pacific Blue, Hoechst dye, Covalent viability probe

1 Introduction

Apoptosis is a critical regulatory process in all tissues, and has been particularly well characterized in the immune system and in tumor cells. Assays based on flow cytometry have been available for over 25 years, and are now by far the most common method for detecting and quantifying apoptosis. They possess many advantages over earlier assays relying on microscopy or cell lysate analysis. They are rapid and quantitative, but most importantly, they analyze cell death in individual cells rather than in bulk populations [1]. The multiparametric nature of flow cytometry also allows the detection of multiple cell death characteristics in a single assay. For example, apoptosis assays that utilize DNA dyes as plasma membrane permeability indicators (such as propidium iodide) can be combined with assays that assess different cellular responses associated with cell death, including mitochondrial membrane potential and annexin V binding to "flipped" phosphatidylserine (PS) [2–5]. Combining multiple measurements for cell death into a single assay has a

Teresa S. Hawley and Robert G. Hawley (eds.), *Flow Cytometry Protocols*, Methods in Molecular Biology, vol. 1678, DOI 10.1007/978-1-4939-7346-0_10,

number of significant advantages. It provides multiple confirmations of apoptotic activity (important in a process that has proven highly variable in character). It also provides a much more comprehensive and multidimensional picture of the entire cell death process, rather than a simple analysis of live versus dead cells. Intrinsic in this second advantage is the ability to combine morphological assays (such as membrane integrity) with assays for biochemical events, such as caspase activation.

Recognition of the critical role of caspases in the death process as both signaling agents and effectors of cell death morphology has led to the development of assays that can measure these important enzymes in situ. Caspase activation represents one of the earliest detectable markers of apoptosis [6]. In most cases, caspase activation precedes degradation in cell permeability, DNA fragmentation, cytoskeletal collapse, and PS "flipping"; caspases are both signal transduction molecules and mediators of these downstream manifestations of cell death. Combining fluorogenic assays of caspase activation with fluorescence-based assays for later characteristics of cell death (such as PS "flipping" and loss of membrane integrity) can provide a very information-rich view of cell death. It is particularly useful in distinguishing the "early" stages of cell death from later events, allowing better analysis of biochemical events during apoptosis cells prior to the complete collapse of the cell structure [7–11].

Several fluorogenic assays for caspase activity have been described, including the OncoImmunin PhiPhiLux system, the FLICA substrates, and the CellEvent Green or NucView 488 substrates [12–17]. All of these assays involve loading of a cell-permeable fluorogenic caspase substrate into cells following treatment with apoptotic stimuli; all "read out" as an increase in fluorescence in the presence of caspase activity. In general, caspase activity is one of the earliest detectable events in apoptosis, and precedes the later morphological damage usually relied on for cell death assessment.

In this chapter, we describe the combination of the PhiPhiLux, FLICA or CellEvent Green, or NucView 488 substrates caspase substrate system with two simultaneous assays for later stages of cell death, annexin V binding to "flipped" PS residues, and cell membrane integrity using DNA binding dyes or a covalent viability probe [17]. All of the above caspase substrates have characteristics that make them useful for integration with other "live" cell apoptosis assays; they are cell-permeable, and possess varying degrees of caspase specificity. PhiPhiLux and CellEvent Green/NucView 488 are relatively non-fluorescent in the intact state, and become fluorescent upon caspase cleavage. All three substrates are based on fluorescent probes with spectral characteristics similar to commonly used probes like fluorescein and rhodamine; this makes them easy to combine with other fluorescent probes [15–17]. The ability to

observe and measure multiple apoptotic phenotypes in a single assay gives a powerful picture of the overall apoptotic process. These assays are applicable to both suspension cells by traditional flow cytometry, and adherent cells using laser scanning cytometry [17]. These assays can take particular advantage of newer flow cytometers with multiple lasers, but are also accessible to older or simpler cytometers with a single 488 nm laser source. Some of these assays require that the cell samples remain "live" and unfixed, requiring prompt analysis. However, others can be fixed with paraformaldehyde following the labeling procedure, allowing analysis at a later time.

2 Materials

The reagents required for multiparametric analysis of apoptosis are described below. To assemble an assay, choose one of the fluorogenic caspase assays, an annexin V conjugate, and either a DNA-binding dye or a covalent viability probe. Caspase assays can be used with DNA-binding dyes or covalent viability probes with no annexin if desired. For cells requiring fixation, FLICA and a covalent viability probe should be used.

2.1 Fluorogenic Caspase Assays

1. PhiPhiLux fluorogenic caspase substrates (OncoImmunin, Inc., Gaithersburg, MD) are a series of fluorogenic enzyme substrates that fluoresce upon cleavage of an incorporated consensus domain. The fluorogenic caspase 3/7 substrate (PhiPhiLux G1D2) consists of an 18-amino acid peptide corresponding to the recognition/cleavage sequence from PARP containing the sequence ZVAD, a target for both caspases 3 and 7 [18]. The substrate is homodoubly labeled with one of several fluorophores (in this case, a fluorescein-like molecule) on the opposite sides of the molecule; in this conformation, the fluorochrome molecules are in close physical proximity, and the fluorescence of the resulting complex is largely quenched [16, 19]. After the substrate enters a cell by passive diffusion and is cleaved by caspase 3 or 7, the unquenched fluorescent fragments become somewhat less cell permeable and will remain in the cell for several hours. However, they will eventually diffuse out of the cell [16, 19], requiring flow cytometric analysis soon after labeling.
   (a) The PhiPhiLux nomenclature indicates both its substrate specificity and the conjugated fluorochrome. The first letter refers to the substrate specificity: G refers to caspase 3/7, E to caspase 1, L to caspase 8, J to caspase 6, etc. The first number refers to the conjugated fluorochrome: 1 is a fluorescein-like fluorochrome, 2 is a rhodamine-like molecule, and 6 to the sulforhodamine-like molecule.

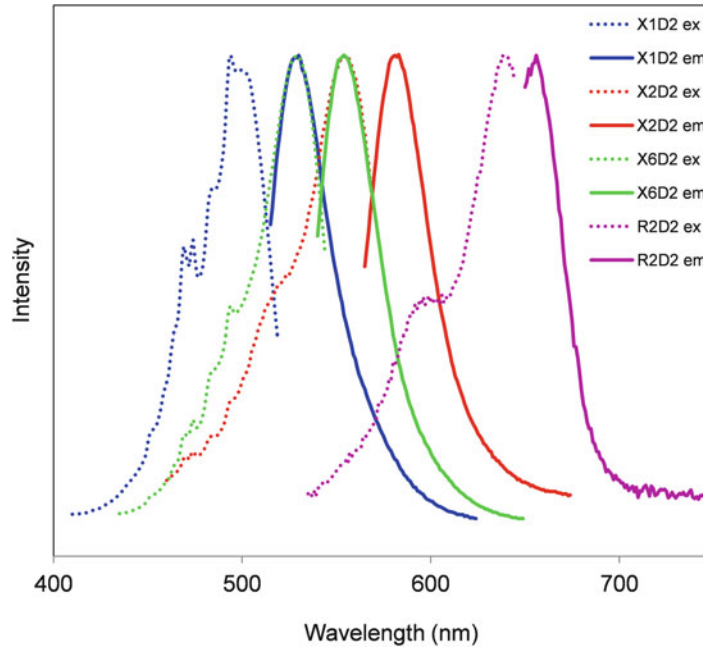

Fig. 1 Spectral characteristics of fluorogenic caspase substrates. Excitation (*dotted lines*) and emission (*solid lines*) spectra for four caspase substrate conjugates: X1D2 (fluorescein-like, used in most of the data presented in this chapter), X2D2 (rhodamine-like), X6D2 (sulforhodamine-like), and R2D2 (Cy5-like)

So G1D2 is specific for caspase 3 with the fluorescein-like probe, and E2D2 is specific for caspase 1 with the rhodamine-like probe. R2D2 is a special case and refers to the Cy5-like molecule, with the caspase indicated beforehand (3-R2D2 for caspase 3, 8-R2D2 for caspase 8). Excitation and emission spectra for all the fluorochrome conjugates (generically referred to as X1D2, X2D2, etc.) are shown in Fig. 1. Special instructions for working with non-fluorescein-based PhiPhiLux reagents are discussed in **Note 1**.

(b) PhiPhiLux G1D2 spectrally resembles fluorescein and can be excited with the standard 488 nm argon-ion or solid-state laser found on most flow cytometers. PhiPhiLux G1D2 is spectrally compatible with many conjugates of annexin V, DNA-binding dyes, and covalent viability probes, as described in Subheading 2.5. All methods and data in this chapter employing the PhiPhiLux reagents used the fluorescein-like PhiPhiLux G1D2 specific for caspase 3/7 unless otherwise indicated.

(c) The PhiPhiLux reagents are roughly 40-fold dimmer in the uncleaved state than following caspase activation.

When camptothecin-treated EL-4 lymphoma cells were labeled with PhiPhiLux G1D2 and analyzed by flow cytometry, the apoptotic cells possess 1–3-orders of magnitude higher fluorescence than the viable cells. Note that even truly viable cells with no apoptotic activity labeled with a caspase substrate will have somewhat higher background fluorescence levels than completely unlabeled cells. Primary cell cultures may show somewhat lower levels of caspase activation than cell lines, with subsequent lower levels of substrate fluorescence; however, background fluorescence may be lower with these cells as well (*see* **Note 2**).

(d) The PhiPhiLux reagents are also available with other fluorescent tags, including rhodamine- and sulforhodamine-like fluorochromes, and a proprietary Cy5-like fluorochrome that can be excited with a red laser. Although traditionally used for microscopy, the rhodamine and sulforhodamine substrates can be readily excited using green or yellow lasers, now common on flow cytometers (*see* **Note 1**). Unless otherwise indicated, all methods and data in this chapter employing PhiPhiLux labeling use the fluorescein-like PhiPhiLux G1D2 specific for caspase 3/7.

(e) The PhiPhiLux reagents are commercially provided at concentrations of 5–10 μM in sealed aliquots and can be stored at 4 °C prior to opening; once the ampule is opened, any remaining substrate should be stored at −20 °C. Avoid repeated freezing and thawing. Shelf life at 4 °C is approximately 3–6 months, over 1 year at −20 °C.

(f) The PhiPhiLux reagents do not covalently bind to caspase molecules, and are therefore not considered caspase inhibitors; theoretically, one caspase enzyme molecule can cleave more than one PhiPhiLux molecule. PhiPhiLux therefore is not immobilized inside the cell. The separated fragments will gradually diffuse out of the cell. For this reason, permeabilization using detergents and fixation using paraformaldehyde is not recommended with PhiPhiLux. This is in contrast to FLICA (described in **item 2**), which covalently crosslinks to caspase sites and is therefore immobilized in the cell. Detergent treatment and fixation are compatible with FLICA.

2. The FLICA reagents (*F*luorochrome *L*inked *I*nhibitors of *C*aspase *A*ctivity) are the second major group of fluorogenic caspase substrates. The FLICA substrates are composed of a caspase consensus cleave domain, flanked by a fluoromethylketone (FMK) protein reactive group, and a fluorochrome, most

commonly fluorescein. They are cell permeable, and are incubated with cells for 30 min to 1 h at 37 °C to load. If a FLICA molecule comes in contact with a caspase via the recognition domain, the FMK group covalently binds to the caspase, and the FLICA molecule is immobilized inside the cell; the caspase enzyme similarly becomes inactivated. Unlike PhiPhiLux, FLICA reagents are always fluorescent. They need to be thoroughly washed out of the cells after labeling to ensure that caspase-negative cells are sufficiently dim to be distinguished from caspase-positives. Caspase-negative cells may be brighter than unlabeled cells due to residual unbound FLICA reagent. Unbound FLICA is removed by multiple centrifugal washings, and the cells are then labeled with additional apoptosis reagents and analyzed. As with PhiPhiLux, caspase-positive cells will be brightly labeled compared to negative cells. FLICA covalently binds to the site of activity via its FMK group. It is therefore immobilized in cells, and is compatible with both subsequent detergent treatment and paraformaldehyde fixation. This is in contrast to PhiPhiLux and CellEvent green/NucView 488 (described in **item 3**) which are incompatible with fixation.

(a) The term FLICA is the commercial name for substrates originally developed by Immunochemistry Technologies LLC (Bloomington, MN) and has come to be used generically. Most FLICA reagents are labeled with fluorescein. FLICA substrates sold by Immunochemistry Technologies LLC are designated as FAM-FLICA, referring to the fluorescein conjugation, followed by the caspase name.

(b) Fluorescein-conjugated FLICA reagents sold by Thermo Fisher Life Technologies (Carlsbad, CA) are termed Vybrant FAM, followed by the caspase designation (i.e., caspase 3/7).

(c) Sulforhodamine-conjugated FLICA reagents are also available from Immunochemistry Technologies LLC and are designated as SR-FLICA, or by the commercial name Magic Red. Like the PhiPhiLux reagents, these are more commonly used for microscopy than flow cytometry, relying on the green or yellow mercury arc lamp lines for excitation. However, the widespread usage of green and yellow lasers on flow cytometers makes this variant useful for flow cytometry as well. A red fluorochrome variant of FLICA, designated FLICA 660, is also available from Immunochemistry Technologies LLC. This reagent is excited with a red laser, usually a HeNe 633 nm or red laser diode ~640 nm (*see* **Note 1**).

(d) FLICA reagents are available with specificities to multiple caspases. Immunochemistry Technologies LLC

manufactures FLICA reagents specific for caspases 1, 2, 3, 6, 7, 8, 9, 10, and 13, as well as a pan or poly caspase version. Thermo Fisher Life Technologies provides fluorescein-conjugated FLICA against caspases 3 and 7 (ZVAD) and a poly caspase version (DEVD). In this chapter, all methods and data show the fluorescein-based caspase 3/7 FLICA reagent unless otherwise noted. The FLICA reagent from both the suppliers is provided as a lyophilized preparation packaged under desiccation. Immediately prior to the assay, solubilize the reagent in dry DMSO, typically at 150× concentration. Use this solution immediately or store it at −20 °C in small aliquots over desiccant for up to 6 months, but avoid freeze/thaw cycles. Dilute the 150× solution in aqueous buffer at a 1:5 ratio to a final 30× concentration. Use this solution within 4 h of preparation and discard any unused reagent. FLICA reagents will rapidly hydrolyze in the aqueous solution, and should not be stored. Add the aqueous FLICA reagent to samples at a final 1× concentration.

(e) Aminomethylcoumarin (AMC) and other coumarin-based FLICA reagents are available from several suppliers as probes for microplate-based caspase assays. These reagents are generally not recommended for intact cell use; they are not very bright, not very cell permeable, and emit in a region of the spectrum with high autofluorescence.

3. CellEvent Green (Thermo Fisher Life Technologies) and NucView 488 (Biotium, Hayward, CA) constitute a third group of fluorogenic caspase substrates. These reagents consist of a DNA-binding molecule that is relatively non-fluorescent in the unbound state, but becomes fluorescent upon binding to DNA. The DNA-binding site is inhibited by a structure containing caspase recognition domain peptide. Like PhiPhiLux and FLICA, these reagents can be loaded into cells by passive diffusion. Upon cleave by a caspase molecule, the DNA-binding site is unmasked. The reagent can then diffuse into the nucleus, where it binds to DNA. Caspase-positive cells therefore appear as brightly labeled compared to caspase-negative cells. Currently, these reagents are available only with a fluorescein-like fluorochrome, with excitation at 488 nm and detection in the fluorescein range. They both function by the same mechanism. They are generally available as pre-prepared solutions that can be diluted directly into samples, usually at a final concentration of 1:1000. Some titration may be necessary for some cell types and concentrations. Both are currently available only for the detection of caspases 3 and 7. Thermo Fisher Life Technologies also manufactures a variant termed

ReadyProbes that is recommended for slide-based samples and imaging. Like PhiPhiLux, CellEvent Green and NucView 488 do not bind covalently to any cellular components, and should not be fixed with paraformaldehyde.

2.2 Annexin V

Annexin V binds to apoptotic cells with "flipped" PS residues on their extracellular membrane leaflet, and is a useful and common assay for apoptosis. Annexin V is available conjugated to many fluorochromes, including fluorescein, Alexa Fluor 488, phycoerythrin (PE), PE-Cy5, allophycocyanin (APC), Cy5, and Alexa Fluor 647, to name a few. It is therefore easy to integrate annexin V labeling into a multicolor protocol. Damaged or necrotic cells with a high degree of membrane permeability can also bind annexin V to their intracellular membrane leaflet, despite their uncertain apoptotic nature (*see* **Note 3**); therefore, a DNA-binding dye as a cell permeability indicator should always be incorporated into annexin V-binding assays. In some cell types, annexin V-binding precedes permeability to a DNA dye, allowing the identification of "earlier" apoptotic cells that are annexin V positive and DNA dye negative. Cells that are both annexin V and DNA-binding dye positive may therefore be either advanced apoptotic or necrotic. Annexin V labeling requires buffers with calcium and magnesium cations.

2.3 DNA-Binding Dyes

There are literally dozens of DNA-binding dyes available with potential utility for detecting apoptotic cells. DNA-binding dyes bind stoichiometrically to DNA by a variety of mechanisms, including intercalation and major/minor groove interactions. At high concentrations, many DNA-binding dyes can be used to analyze cell cycle in permeabilized cells; at lower concentrations, they can be added to "live" unfixed cells to assess viability, with the nonviable cells binding the dye and the viable cells excluding it. DNA-binding dyes are one of the oldest viability assays; dyes like propidium iodide are often added during fluorescent immunophenotyping to exclude dead cells from the analysis. Combined with fluorogenic caspase substrates and annexin V, they make excellent labels for identifying late stage apoptotic and necrotic cells. Many DNA-binding dyes are useful for flow cytometry and apoptosis detection. Some are listed here. Keep in mind that all of the DNA-binding dyes described here have somewhat differing cell permeability characteristics. This will affect the ultimate data analysis (*see* **Note 4**).

1. Propidium iodide (PI): An inexpensive and widely available intercalating DNA-binding dye. PI excites at 488 nm and emits in the 570–630 nm range. Dissolve in deionized water at 1 mg/mL and store in the dark at 4 °C for up to 3 months. Use at a final concentration of 1–2 μg/mL.

2. 7-Aminoactinomycin D (7-AAD): An intercalating/groove-binding DNA-binding dye that also excites at 488 nm but emits in the far red, with an emission peak at approximately 670 nm. 7-AAD is a good alternative to PI where a longer wavelength probe is desired. 7-AAD is also somewhat more cell permeable than PI. Dissolve in 95% EtOH at 1 mg/mL and store at −20 °C. 7-AAD is also water-soluble but is not as stable in aqueous solution; such stocks should not be frozen and thawed repeatedly. EtOH solubilized stock solutions are good for 6 months. Use at a final concentration of 5 μg/mL. Diluted stocks should be used within 24 h. A variant of 7-AAD, SYTOX AADvanced™, is available from Thermo Fisher Life Technologies. This version is prepared with its peptide side chains removed, increasing solubility.
3. Violet-excited DNA-binding dyes: The proliferation of cytometers with multiple lasers has greatly expanded the fluorochromes available for apoptotic analysis. Violet (~405 nm) and red (~640 nm) lasers are now commonly available on flow cytometers. Several red- or violet-excited DNA-binding dyes can substitute for PI or 7-AAD to increase total fluorochrome capability or reduce fluorescence compensation requirements. Hoechst 33258 (several suppliers) is a widely available minor groove DNA-binding dye that is well excited by ultraviolet or violet lasers; it has cell permeability characteristics similar to PI. Prepare Hoechst 33258 as a 1 mg/mL stock in distilled water and store at 4 °C for up to 3 months. Use at a final concentration of 1–5 μg/mL. The DNA dye DAPI (several suppliers) has similar spectral and cell permeability characteristics, and can also be used as a viability dye. Preparation is similar to Hoechst 33258. SYTOX Blue (Thermo Fisher Life Technologies) is another violet-excited DNA dye that can also be used to distinguish dead cells; it is provided as a stock solution at 10 μM and should be diluted at 1:1000 for use. Hoechst 33342 (not to be confused with Hoechst 33258) and DyeCycle Violet (Thermo Fisher Life Technologies) are much more cell permeable than Hoechst 33258 or DAPI; they are not usually used as membrane integrity probes, but can be used to visualize apoptotic chromatin by microscopy.
4. Red-excited DNA-binding dyes: TO-PRO-3 (Thermo Fisher Life Technologies) is a red-excited DNA dye and is relatively cell-impermeant. It can be used as a membrane integrity dye with red laser equipped cytometers. It is provided as a stock solution and should be diluted at 1:1000 for use. DRAQ7 (Biostatus Ltd. Leicester, UK) is also excited by the red laser and can be used similarly. It is provided as stock solutions at 0.3 and 1 mM and can be used at 0.3–1 μM final concentration. SYTOX Red (Thermo Fisher Life Technologies) is another

useful red-excited DNA dye, usually used at 1 μM final concentration.

5. Cell-permeable DNA dyes: DNA dyes with high cell permeability, including Hoechst 33342, the DyeCycle DNA dyes (Thermo Fisher Life Technologies), and DRAQ5 (Biostatus Ltd), are not recommended for measurement of cell permeability by flow cytometry. Both live and dead cells will take up large amounts of these dyes, making it difficult to distinguish viable from apoptotic cells. However, they can be useful for imaging applications, where the change in chromatin structure can be visualized.

2.4 Covalent Viability Probes

These viability probes are a good alternative to DNA-binding dyes for the assessment of membrane integrity, particularly where fixation is required. They are composed of a fluorochrome coupled to protein reactive group, usually a succinimidyl ester. When added to suspension cells, they bind at higher levels to apoptotic cells and lower levels to viable cells, producing a distribution similar to that seen with DNA-binding dyes. Unlike DNA dyes, however, the binding is covalent; the cells can be subsequently fixed with paraformaldehyde and the labeling preserved. The fluorochromes used in covalent viability probes are also the usual low molecular weight fluorochromes used for cell labeling. Their spectral properties are more similar to dyes like fluorescein and less likely to be spectrally incompatible in multicolor labeling. On the other hand, dyes like PI have extremely broad emission spectra and can occupy a lot of space in a multicolor protocol. The fluorochromes used for covalent viability dyes often show less spectral overlap. Covalent viability probes are available from several manufacturers.

1. Thermo Fisher Life Technologies makes the Live/Dead dyes in a variety of colors. The dye name (Live/Dead followed by a color) corresponds to the approximate emission wavelength of the dye. Of particular interest are the UV-, violet- and red-excited variants, which can be easily integrated into multicolor apoptosis assays. Live/Dead Fixable Blue is UV-excited and detected through a blue DAPI filter. Live/Dead Fixable Violet, Aqua and Yellow are violet-excited, and emit in the blue, green, and yellow range. Live/Dead Fixable Long Red and Near IR are red-excited, and emit in the long red and near infrared range.
2. BioLegend (San Diego, CA) manufacturers the Zombie viability probes. They are essentially the same in function as the Live/Dead probes. The color name associated with the dye may correspond to either the excitation or emission wavelength. Zombie UV is UV-excited and detected through a

blue DAPI filter. Zombie Violet, Aqua, and Yellow are violet-excited, and emit in the blue, green, and yellow range.

3. BD Biosciences (San Jose, CA) manufactures the BD Horizon Fixable Viability Stains (FVS), also in a variety of colors. They are labeled according to their emission; so Fixable Viability Stain 450 is violet-excited and emits ~450 nm. Again, the violet- and red-excited variants are of particular interest for flow cytometry.
4. eBiosciences/Affymetrix (San Diego, CA) provides the Fixable Viability Dyes, again in many colors. They are designated by eFluor™ followed by a number roughly corresponding to their emission. So eFluor 450 is violet-excited and emits at ~450 nm.

Note that the dye name may reflect either excitation or emission characteristics. Check Table 1 or the most recent manufacturer's literature.

2.5 Combinations of Fluorochromes

The multiparametric assays described in this chapter combine fluorescent labels for three characteristics of cell apoptosis, namely caspase activation, PS "flipping," and cell permeability. There is considerable flexibility of fluorochrome selection for the investigator depending on the flow cytometric instrumentation available. Three possible combinations are described below, one for analysis on instruments equipped with a single 488 nm laser, a second for instruments equipped with dual 488 nm/red diode or red HeNe lasers, and a third for instruments equipped with blue, red, and violet lasers. While this three-component assay is possible on single-laser instruments, spectral overlap between dyes and required compensation will be minimal on multi-laser cytometers. As with all multicolor flow cytometry experiments, single-color controls to allow calculation of compensation should be prepared and included in the experiment.

2.5.1 Single 488 nm Laser Instruments

These instruments are limited to a single laser, and tend to have only three or four fluorescent detectors. Examples of these include: older flow cytometers from BD Biosciences including the BD FACScan, BD FACSort, or BD FACSCalibur (with no red laser); older flow cytometers from Beckman Coulter (Indianapolis, IN) such as the Coulter Epics XL, or newer cytometers from Beckman Coulter such as the CytoFLEX with the 488 nm only option. At least three fluorescence detectors are needed. The following combination should be used when analysis is limited to this instrument type:

1. PhiPhiLux G1D2, FLICA, CellEvent Green, or NucView 488: Detect this fluorochrome in the fluorescein or FITC detector on most commercial instruments.
2. PE-conjugated annexin V: Detect this fluorochome in the PE detector on most instruments. Apply fluorescence

Table 1
Covalent viability probes: names, excitation/emission wavelengths, recommended lasers, and sources

Covalent viability probe	Excitation max (λ) (nm)	Laser line	Emission max (λ) (nm)
Live/Dead Fixable Blue[a]	350	355 nm, 375 nm, 405 nm	450
Live/Dead Fixable Violet[a]	416	405 nm	451
Live/Dead Fixable Aqua[a]	367	355 nm, 375 nm, 405 nm	526
Live/Dead Fixable Yellow[a]	400	405 nm	575
Live/Dead Fixable Green[a]	495	488 nm	520
Live/Dead Fixable Red[a]	595	532 nm, 552 nm, 561 nm, 594 nm	615
Live/Dead Fixable Far Red[a]	650	633 nm, 640 nm	665
Live/Dead Fixable Near IR[a]	750	633 nm, 640 nm	775
Zombie UV[b]	365	355 nm, 375 nm, 405 nm	452
Zombie Violet[b]	376, 400	355 nm, 375 nm, 405 nm	420
Zombie Aqua[b]	380	355 nm, 375 nm, 405 nm	510
Zombie Yellow[b]	395	405 nm	572
Zombie Green[b]	487	488 nm	515
Zombie Red[b]	600	532 nm, 552 nm, 561 nm, 594 nm	624
Zombie NIR[b]	718	633 nm, 640 nm	745
BD Horizon Fixable Viability Stain 450[c]	406	405 nm	450
BD Horizon Fixable Viability Stain 510[c]	408	405 nm	512
BD Horizon Fixable Viability Stain 520[c]	498	488 nm	521
BD Horizon Fixable Viability Stain 570[c]	547	532 nm, 552 nm, 561 nm	573
BD Horizon Fixable Viability Stain 620[c]	523	532 nm, 552 nm, 561 nm	617
BD Horizon Fixable Viability Stain 660[c]	649	633 nm, 640 nm	660
BD Horizon Fixable Viability Stain 700[c]	657	633 nm, 640 nm	700
BD Horizon Fixable Viability Stain 780[c]	759	633 nm, 640 nm	780
Fixable Viability Dye eFluor 455UV[d]	350	355 nm, 375 nm	455
Fixable Viability Dye eFluor 450[d]	405	405 nm	450
Fixable Viability Dye eFluor 506[d]	405	405 nm	506
Fixable Viability Dye eFluor 520[d]	488	488 nm	522
Fixable Viability Dye 3Fluor 660[d]	633	633 nm, 640 nm	660
Fixable Viability Dye eFluor 780[d]	633	633 nm, 640 nm	780

[a]Thermo Fisher Life Technologies (all names are trademarked)
[b]BioLegend (all names are trademarked)
[c]BD Biosciences (all names are trademarked)
[d]eBiosciences/Affymetric (all names are trademarked)

compensation to separate the PE signal from the caspase substrate and 7-AAD.

3. 7-AAD: Detect this far-red emitting DNA-binding dye in the far red (or PE-Cy5) detector on most commercial instruments. Unfortunately, there is not a good 488 nm excited long red covalent viability probe to substitute for 7-AAD. Covalent viability probes labeled as red are not suitable here as they are typically excited using a red laser.

2.5.2 Dual 488 nm/Red Laser-Equipped Instruments

Many benchtop flow cytometers are equipped with more than one laser, most commonly a red source (most likely a 635 nm red diode or a 633 nm red HeNe laser). The BD FACSort and BD FACSCalibur usually fall into this category, as do some older and minimally equipped BD LSRIIs (BD Biosciences) and BD FACSArias (BD Biosciences). The BD Accuri C6 (BD Biosciences), FC500 (Beckman Coulter), and Handyem HPC-150 cytometer (du Parc Technologique, Quebec, Canada) are dual laser instruments equipped with blue and red lasers. A red laser allows several red-excited fluorochromes to be incorporated into flow cytometry assays, including APC, Cy5, and Alexa Fluor 647. The DNA dyes TO-PRO-3 and SYTOX Red can also be incorporated if a red laser is available. The following combination is suggested for dual laser instrumentation:

1. PhiPhiLux G1D2, FLICA, CellEvent Green, or NucView 488: Detect this fluorochrome in the fluorescein detector on most commercial instruments.
2. APC-conjugated annexin V: Excite this fluorochome with either a red diode or HeNe laser, and detect in the far red range. Little fluorescence compensation is required to separate its signal from PhiPhiLux G1D2 or the DNA-binding dyes described below, making post-acquisition analysis easier. Annexin V conjugates with Cy5 and Alexa Fluor 647 (which are spectrally similar to APC) can be analyzed in the same way.
3. PI or 7-AAD DNA-binding dyes can be incorporated into a cell death assay with a fluorogenic caspase substrate and APC-annexin V. Detect both in the far red detector, usually with a mid-600 nm bandpass (BP) or longpass (LP) filter on most flow cytometers.
4. If a red-excited DNA dye (like TO-PRO-3 or SYTOX Red) or a far red covalent viability probe (like Live/Dead Near IR) is used with the red laser, move annexin V to another detector (such as the PE detector).

2.5.3 Triple 488 nm/Red Laser/Violet Laser-Equipped Instruments

Many modern cytometers are equipped with more than two lasers; violet laser diodes (~405 nm) are typically included as a third excitation source. Instruments include the BD LSR II, BD LSR

Fortessa (BD Biosciences), Gallios (Beckman Coulter), Navios (Beckman Coulter), CytoFLEX (Beckman Coulter), Stratedigm S1400 (Stratedigm, Inc., Campbell, CA), Partec CyFlow (Partec GmbH, Münster, Germany), MACSQuant (Miltenyi Biotec, San Diego, CA), Guava easyCyte (EMD Millipore, Billerica, MA), and NovoCyte (ACEA Biosciences, San Diego, CA). Violet-excited annexin V conjugates and DNA-binding dyes can be easily incorporated into apoptotic assay combinations. Violet-excited probes do not significantly overlap into other fluorescence channels, making them very useful for multicolor assays. Examples are listed below:

1. PhiPhiLux, FLICA, CellEvent Green, or NucView 488: Detect this caspase substrate in the fluorescein detector. Combine it with:
   (a) TO-PRO-3 or SYTOX Red: Either a 488 nm or red-excited DNA-binding dye can be used. PI or 7-AAD could be used here as well, but red-excited DNA dyes will require less compensation.
   (b) Pacific Blue-annexin V: Pacific Blue is a relatively bright violet-excited fluorochrome, and is available in an annexin V conjugate. Pacific Blue does not overlap significantly into other fluorescent channels, and other fluorochromes do not overlap significantly into it, making it very applicable for multiparametric assays.
2. Another possible combination still uses the fluorescein detector for the caspase substrate, but uses:
   (a) DAPI, Hoechst 33258, or SYTOX Blue: These DNA-binding dyes use the violet laser for excitation. SYTOX Blue is somewhat more cell permeable than Hoechst 33258 and DAPI, which are roughly equivalent to PI.
   (b) APC-annexin V: A red laser can be used to excite APC-annexin V. This combination uses three lasers to excite three fluorochromes; as a result, virtually no spectral overlap occurs, and almost no fluorescence compensation is required.
3. Red- or violet-excited covalent viability probes can readily substitute for the DNA dyes mentioned above. Live/Dead Violet, Aqua, and Yellow are all violet-excited and emit in the blue, green, and yellow range. Live/Dead Long Red and Near IR are red-excited and emit in the red and far red region.

2.6 Buffers and Equipment

1. Wash buffer: Dulbecco's PBS (containing calcium and magnesium) supplemented with 2% fetal bovine serum. This is used for cell washing after caspase substrate loading and prior to DNA dye addition, and contains FBS to help maintain cell health during the labeling procedure and reduce apoptosis

during the assay itself. The inclusion of divalent cations is critical for annexin V binding. Buffers from kits can be substituted as long as calcium and magnesium are present.

2. Complete medium: RPMI supplemented with 10% FBS.
3. Dulbecco's PBS (containing calcium and magnesium).
4. Fixative: 2% paraformaldehyde in PBS.
5. Flow cytometer equipped with one, two, or three lasers (*see* Subheading 2.5 for instrument setup with regard to different combinations of fluorochromes).

3 Methods

In this section, we design a labeling system based on the available flow cytometric instrumentation. A typical labeling protocol will consist of: (a) a fluorogenic caspase substrate (Subheading 3.2), (b) an annexin V conjugate (Subheading 3.3), and (c) either a DNA-binding dye (Subheading 3.4) or a covalent viability dye (Subheading 3.5). Labeling will be done in this order. Any spectrally compatible combination of the following probes can be used for cell samples that do not require fixation. For cell samples requiring fixation with paraformaldehyde, FLICA should be combined with a covalent viability dye, but no annexin V labeling (Subheading 3.6).

3.1 Preparation of Cells

EL-4 cells treated with transcriptional or translational inhibitors such as cycloheximide or actinomycin D, or topoisomerase inhibitors like camptothecin or topotecan were used in the all illustrated data. EL4 cells can be treated with cycloheximide at 50 μg/mL or actinomycin D at 5 μg/mL for 6–8 h to induce apoptosis. Camptothecin induces apoptosis in EL4 cells at 2–5 μM over a longer incubation period of 12–16 h. EL4 cells are easily grown and hardy, and can make a useful positive control for more general use (*see* **Note 2**).

1. Harvest cell lines grown in suspension or cultured primary cells. Count the cells prior to centrifugation using a hemocytometer or other counting devices. Transfer cells to 12 × 75 mm cell culture tubes, and centrifuge at 400 × *g* for 5 min.
2. Decant supernatant. Maximum removal of the supernatant is critical; the volume of remaining supernatant should be as low as possible to cause minimal dilution of the caspase substrate. Although cells can be washed prior to labeling, performing the assay in the remaining complete medium supernatant will reduce the amount of incidental cell death occurring during the assay. For cells obtained from clinical or other in vivo sources, centrifuge and resuspend in either an enriched buffer

like the wash buffer or complete medium prior to use, then centrifuge and decant as described above. Caspase substrate loading can be done in a complete medium.

3. Each sample should contain 0.5–1 $\times$ 10^6 cells; increasing this number will saturate the detection reagents and reduce caspase and annexin V labeling efficiency. Adherent cells pose special challenges for apoptotic analysis due to the physical trauma and membrane damage that occur with cell dissociation; analysis in the adherent state by laser scanning cytometry is much preferable to flow cytometry under these circumstances (*see* **Note 3**).

3.2 Fluorogenic Caspase Substrate Labeling

Instructions are given below for the three main types of fluorogenic caspase substrate. CellEvent Green and NucView 488 instructions are the same. Choose one of the fluorogenic caspase probes below. Since annexin V incubation in Subheading 3.3 will be done with the caspase substrates still present, the total caspase substrate incubation time will be the intervals given below plus 15 min in annexin V. For PhiPhiLux labeling, the fluorescein-like PhiPhiLux G1D2 specific for caspase 3/7 is used as an example. For FLICA labeling, the fluorescein caspase 3/7 variant is used as an example.

3.2.1 PhiPhiPhiLux G1D2 Caspase 3/7 Substrate

1. Following the wash step in Subheading 3.1, ensure that as much supernatant is removed from the sample tube, to maximize final substrate volume. Tap each tube to resuspend the cell pellet in the remaining supernatant. The supernatant in each tube will be approximately 50 μL in volume (but not to exceed 100 μL).
2. Add 50 μL of the PhiPhiLux reagent (from 10 μM stock) to each tube and shake gently. The PhiPhiLux reagent should be diluted as little as possible for maximum detection, hence the need for minimal sample supernatant. PhiPhiLux reagent solutions are typically prepared at 10 μM; this will give a final concentration between 3 and 5 μM (in approximately 100–150 μL of total volume).
3. Incubate the tubes for 30–45 min at 37 °C, in a water bath or an incubator. An incubator may be preferred if CO_2 conditions are desired. For both optimal labeling and reasons of economy, the PhiPhiLux reagent can be titered and tested for use between 0.5 and 5 μM. However, this should be done with caution (*see* **Note 5**).
4. Proceed to Subheading 3.3 for annexin V labeling.

3.2.2 FLICA

1. Prior to beginning the assay, reconstitute and dilute the FLICA substrate according to the manufacturer's instructions.

Generally, this consists of reconstituting the FLICA substrate in DMSO to a 150× stock and diluting at 1:5 in wash buffer to a 30× stock. As a reminder, the DMS reconstituted stock can be frozen in aliquots and stored. The 30× stock should be used promptly, and any excess discarded.

2. Following the wash step in Subheading 3.1, ensure that as much supernatant is removed from the sample tube, to maximize final substrate volume. Tap each tube to resuspend the cell pellet in the remaining supernatant. The supernatant in each tube will be approximately 50 μL in volume (but not to exceed 100 μL).
3. Add 300 μL of wash buffer to each tube.
4. Add 10 μL of the FLICA substrate to each tube.
5. Incubate the tubes for 30–45 min at 37 °C, in a water bath or an incubator. An incubator may be preferred if CO_2 conditions are desired.
6. Proceed to Subheading 3.3 for annexin V labeling.

3.2.3 CellEvent Green or NucView 488

1. Both CellEvent Green and NucView are provided as pre-prepared stocks. Warm them to room temperature prior to use.
2. Following the wash step in Subheading 3.1, ensure that as much supernatant is removed as possible from the sample tube in order to maximize final substrate volume. Tap each tube to resuspend the cell pellet in the remaining supernatant. The supernatant in the tubes will be approximately 50 μL in volume (but not to exceed 100 μL).
3. Add 1 mL of wash buffer to each tube.
4. Add 1 μL of either CellEvent Green or NucView 488 to each tube. This amount can be titered up for some cell types.
5. Incubate the tubes for 15–30 min at 37 °C, in a water bath or an incubator. An incubator may be preferred if CO_2 conditions are desired.
6. Proceed to Subheading 3.3 for annexin V labeling.

3.3 Annexin V Labeling

Cells are then labeled with fluorochrome-conjugated annexin V. Since centrifuge washings are minimized in this method to reduce assay-associated cell death, the cells are not washed following caspase substrate loading but are labeled immediately with fluorochrome-conjugated annexin V. The annexin V incubation period will therefore be part of the caspase substrate incubation period as well. Since most cell culture media and serum supplements contain calcium and magnesium, it is assumed that cation concentrations are sufficient to allow annexin V binding to "flipped" PS residues. However, this should be verified; even brief removal of divalent cations will cause immediate dissociation of the annexin V reagent. Subsequent cell washing is therefore done in the

recommended wash buffer containing calcium and magnesium supplemented with FBS (*see* **Note 6**). The following steps will work with all of the above caspase substrate labeling methods.

1. After caspase substrate incubation, remove sample tubes from the incubator or water bath and add the appropriate fluorochrome conjugate of annexin V. Annexin V is generally available in suspension at concentrations ranging from 0.1 to 1 mg/mL. Cell labeling should be carried out at approximately 0.5–5 μg annexin V per sample. Therefore, add 5 μL of a 0.1 mg/mL annexin V solution to PhiPhiLux and FLICA labeled samples (150–300 μL sample volume). For CellEvent Green or NucView 488 labeled samples, add 10 μL of a 0.1 mg/mL annexin V solution (1 mL sample volume). Some titration in advance of the actual experiment might be necessary.
2. Return sample tubes to the water bath or the incubator and incubate for an additional 15 min.
3. Add 3 mL of wash buffer to each tube, centrifuge at 400 × *g* for 5 min and decant.
4. Following the decant step, proceed to Subheading 3.4 for DNA-binding dye labeling or Subheading 3.5 for covalent viability probe labeling. PhiPhiLux, CellEvent Green, and NucView 488 labelings can then proceed directly to the DNA-binding dye or covalent viability probe labeling step. For FLICA labeling, add an additional 3 mL per decanted tube, and centrifuge again at 400 × *g* for 5 min. This additional wash step is critical for FLICA samples, which require removal of unreacted substrate.

3.4 DNA-Binding Dye Labeling

Depending on the instrumentation available, cells can be subsequently labeled with a DNA-binding dye for the assessment of cell permeability in the later stages of apoptosis [6]. Remember that 7-AAD can be used with single-laser instruments. PE-annexin V and PI can be used together on a single-laser instrument, but they are spectrally similar, and compensation of fluorescence may be an issue. 7-AAD is therefore preferable when using PhiPhiLux and PE-annexin V. PI is more readily used with dual-laser instruments (blue-green and red), since annexin V can be detected using the APC detector. TO-PRO-3 and SYTOX Red require a red laser, whereas Hoechst 33258, DAPI, and SYTOX Blue require a violet laser. APC-, Alexa Fluor 647-, and Cy5-conjugated annexin V require a red laser, whereas Pacific Blue-conjugated annexin V requires a violet laser (*see* **Note 4**).

1. Prepare a solution of DNA-binding dye in a complete medium. PI is typically used at 2 μg/mL, 7-AAD at 5 μg/mL, and Hoechst 33258 or DAPI at 2 μg/mL. SYTOX Red and

SYTOX Blue are usually supplied at stock solutions of 5 mM, and should be added at 5 μM (1:1000).

2. Add 0.5 mL of the DNA-binding solution to each decanted sample tube. Maintain samples at room temperature and *analyze within 60 min* (*see* **Note 7**).

3.5 Covalent Viability Probe Labeling

Covalent viability probes make useful indicators for cell permeability and can substitute for the DNA-binding dyes described in Subheading 3.4.

1. As described in Subheading 2.4, covalent viability probes are typically provided as lyophilized stocks. Add the required amount of DMSO to each vial to reconstitute the reagent. Any reagent left at the end of the assay should be discarded or immediately aliquoted and stored at −20 °C for future use.
2. Following the wash and decant step after annexin V labeling (Subheading 3.3), add 3 mL of PBS (containing calcium/magnesium but no protein) to each sample tube. Centrifuge at 400 × *g* for 5 min and decant. This wash buffer step must be protein-free to prevent inactivation of the covalent viability probe.
3. Resuspend the cells in 1 mL of PBS (containing calcium/magnesium but no protein).
4. Add the covalent viability probe. For most manufacturers, this is a 1:1000 dilution of the DMSO stock.
5. Incubate at room temperature for 30 min.
6. Add 3 mL of wash buffer (containing calcium/magnesium and FBS), centrifuge and decant.
7. Resuspend in wash buffer and analyze within 60 min.

3.6 Fixable Assays Using FLICA and Covalent Viability Probes

All of the above assays utilize annexin V, and are therefore not suitable for paraformaldehyde fixation. In addition, the PhiPhiLux, CellEvent Green, and NucView 488 substrates do not covalently crosslink inside cells, and also do not work well with fixation. If a fixable caspase assay is desirable, FLICA can be combined with a covalent viability probe but without annexin V. This pair can be fixed with paraformaldehyde following labeling.

1. Prior to beginning the assay, reconstitute and dilute the FLICA substrate according to the manufacturer's instructions. Generally, this consists of reconstituting the FLICA substrate in DMSO to a 150× stock and diluting at 1:5 in wash buffer to a 30× stock (Subheading 2.1, **item 2**). As a reminder, the DMSO reconstituted stock can be frozen in aliquots and stored. The 30× stock should be used promptly, and any excess discarded.

2. Following the wash step in Subheading 3.1, ensure that as much supernatant is removed from the sample tube, to maximize final substrate volume. Tap each tube to resuspend the cell pellet in the remaining supernatant. The supernatant in the tubes will be approximately 50 μL in volume (but not to exceed 100 μL).
3. Add 300 μL of wash buffer to each sample.
4. Add 10 μL of the FLICA substrate.
5. Incubate the tubes for 30–45 min at 37 °C, in a water bath or an incubator. An incubator may be preferred if CO_2 conditions are desired.
6. Add 3 mL of wash buffer to each tube, centrifuge at 400 × *g* for 5 min and decant.
7. Add 3 mL of PBS, centrifuge at 400 × *g* for 5 min and decant.
8. Resuspend cells in 1 mL of PBS.
9. Add the covalent viability probe. For most manufacturers, this is a 1:1000 dilution of the DMSO stock.
10. Incubate at room temperature for 30 min.
11. Add 3 mL of wash buffer, centrifuge and decant.
12. Add fixative. Cells can be stored at 4 °C following fixation until analysis.

3.7 Flow Cytometric Analysis

Unfixed cells should be analyzed as quickly as possible to maximize fluorescent reagent signal and minimize post-assay apoptotic death. The instrument should be set up and ready for sample acquisition immediately upon completion of the assay. PhiPhiLux in particular should be analyzed promptly, as the cleaved substrate will slowly diffuse out of cells. Samples should be kept at room temperature until analysis; storage at 4 °C may reduce dye dissociation, but can itself induce unwanted apoptosis. Single-color controls for the calculation of compensation are highly recommended. Fluorescent detector assignments and analysis issues are described here.

1. PhiPhiLux, FLICA, CellEvent Green, and NucView 488: These fluorescein-like caspase substrates are detected through the fluorescein detector on most flow cytometers (often with the designation "FITC" or "FL1") using a 530/30 nm or similar narrow BP filter. The spectral properties of all described caspase substrates are similar to fluorescein, requiring some spectral compensation when used simultaneously with PE or PI (and to a lesser extent with 7-AAD).
2. PE-conjugated annexin: Like most PE-conjugated reagents, this reagent is detected through the PE detector on most flow cytometers (often with the designation "PE" or "FL2") using a 575/26 nm or similar BP filter. PE requires some

spectral compensation when used with PhiPhiLux G1D2 and 7-AAD.

3. APC-conjugated annexin: APC is excited with a red laser source and detected through the APC detector on many flow cytometers (sometimes with an "FL4" designation) using a 660/20 nm or similar BP filter. An advantage of APC in multicolor assays is its minimal need for color compensation; there is no significant spectral overlap between caspase substrates, PI or 7-AAD. Cy5 or Alexa Fluor 647 conjugates are spectrally similar to APC, and can be analyzed in the same way.
4. Pacific Blue-conjugated annexin V: Pacific Blue is analyzed using a violet laser; most instruments so equipped have at least two detectors aligned to this laser source. A 450/50 nm or similar filter is typically used to detect this fluorescent probe. Cascade Blue, Alexa Fluor 405 and Brilliant Violet 421 are spectrally similar to Pacific Blue, and are analyzed in the same way.
5. PI: This DNA-binding dye is very bright even at low concentrations, and has a broad emission range, requiring compensation when used with any of the fluorogenic caspase substrates. It can be detected in either the PE (575/26 nm filter) or far red detection channel (typically a red 660–690 nm BP or LP filter). The second choice is preferable to reduce spillover into the fluorescein detector. PE and PI can be analyzed together on older single-laser instruments using the traditional PE detector ("FL2" detector, 575/26 nm) for PE detection, and the longer PE-Cy5 detector ("FL3" detector, 675/20 nm BP or 650 nm LP filter) for PI. However, the close proximity of their spectra makes this analysis difficult. Substitution of PI with 7-AAD is preferable. PI is highly charged, and will contaminate instrument tubing, causing unwanted "shedding" of the dye into later samples. After PI use, the instrument should be thoroughly cleaned with 10% bleach or other detergents to remove the dye.
6. 7-AAD: This DNA-binding dye is not as bright as PI and emits in the far red, allowing its detection in the far red channel on most single-laser flow cytometers (PE-Cy5 or "FL3" detector, 675/20 nm BP or 650 nm LP filter). Some compensation will be required when used with the fluorogenic caspase substrates and PE. SYTOX AADvanced is a 7-AAD variant and can be substituted for 7-AAD (*see* Subheading 2.3, **item 2**).
7. Hoechst 33258, DAPI, and SYTOX Blue: Hoechst 33258 is very bright, and can be excited using either an UV or violet laser source. It is detected through a 450/50 nm or similar filter. It will have minimal spectral overlap into other fluorochromes. Do not confuse Hoechst 33258 with 33342; Hoechst 33342 is far more cell permeable, and is less useful as a discriminator of

membrane permeability loss. DAPI is also usable as a permeability dye, and has spectral properties similar to Hoechst 33258. SYTOX Blue is also violet-excited and emits in the blue range. Like PI, they are highly charged and will adhere tightly to instrument tubing; the instrument should be cleaned thoroughly with 10% bleach or other detergents after use.

8. TO-PRO-3, SYTOX Red, and DRAQ5: These DNA-binding dyes are both excited with a red laser source, usually a red laser diode (~640 nm) or less likely a red HeNe laser (633 nm). They emit in the long red range from 650 to 670 nm, and can be measured using filters and detectors set up for APC.
9. Covalent viability probes: These probes are excited and detected at a variety of wavelengths. *See* Table 1 for excitation conditions. The color name of the probe may correspond to either the excitation or emission wavelength depending on the manufacturer. For example, Live/Dead Near IR (Thermo Fisher Life Technologies) emits in the near infrared, with excitation in the red; however, Zombie UV (BioLegend) excites with a UV laser, but emits in the blue. It should therefore not be assumed that the dye name refers to one or the other. Consult Table 1 and the manufacturer's latest information. Covalent viability probes are available that excite with virtually all laser sources available on flow cytometers including ultraviolet, violet, blue-green, green, yellow, and red. They also emit over the entire visible spectrum, and can be selected to integrate with many fluorochrome combinations. As a rule, the violet and red excited variants are the most useful when designing multiparametric assays for flow cytometry. For example, Live/Dead Aqua and Yellow, or Zombie Aqua and Yellow are violet excited probes that emit in the blue and yellow range, and combine well with fluorescein-based caspase substrates and APC or Alexa Fluor 647 annexin V. Similarly, Live/Dead Near IR and Zombie NIR are red-excited probes that emit in the near infrared range, and combine well with FITC and Pacific Blue annexin V. Many compatible combinations are possible.

3.8 Data Acquisition and Analysis

Good gating is critical for meaningful analysis of apoptosis, and a logical gating strategy should be used to identify the various components of the apoptotic process. Typical gating schemes are illustrated.

3.8.1 Scatter Gating

Many cell lines and some primary cells show a dramatic alteration in forward and side scatter measurements late in the onset of apoptosis. Forward and side scatters are approximate indicators of cell size and optical density, respectively, and reflect both the cell volume loss and intracellular breakdown occurring during apoptotic death. This is clear in Fig. 2, where EL4 cells treated with camptothecin

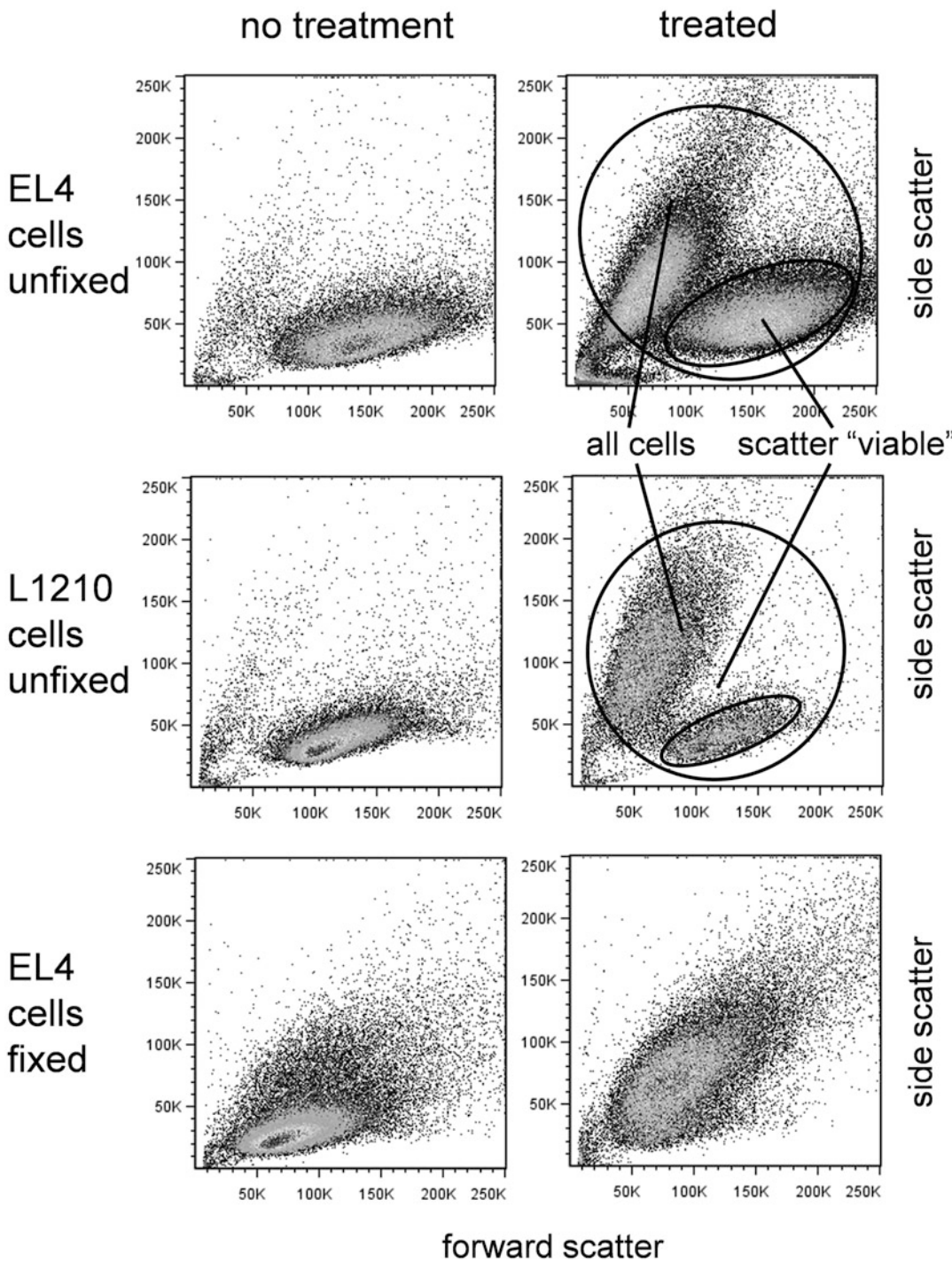

Fig. 2 Scatter properties of viable and apoptotic cells. Forward versus side scatter dotplots of unfixed EL4 cells (*top row*), unfixed L1210 cells (*middle row*), and fixed EL4 cells (*bottom row*). (*Left column*) Untreated cells received no apoptotic agent. (*Right column*) Treated EL4 cells received camptothecin at 5 μM for 16 h, treated L1210 cells received anti-Fas antibodies (clone Jo2) at 1:1000 final concentration for 12 h

show a "scatter viable" cell population with higher forward scatter, and an apoptotic population with reduced forward scatter and increased side scatter. It therefore seems logical to draw a gate around BOTH the scatter viable population AND the apoptotic population, and look at caspase activation, annexin V binding and DNA dye uptake in this total population.

However, the apoptotic population based on scatter is usually at very advanced stage of apoptotic death; the cells are already positive for all markers. The advanced physical perturbation of the cells in this group can also produce positive but highly variable labeling results, interfering with the identification of earlier apoptotic stages. Both viable and apoptotic scatter populations should indeed be gated as the first step in an analysis strategy. However, it is also useful to gate only on the scatter viable cells, and examine early apoptotic markers such as caspase activation only within this group of cells. In many cases, these so-called scatter viable cells are not completely viable; the earliest onset of caspase activation and even annexin V binding can often be observed. This dual approach allows an overall picture of both early and late apoptotic stages, as well as examination of the earliest apoptotic cells. It is therefore recommended that both gating approaches be applied to get a clear picture of the apoptotic process. Examples of gating for both all cells and the scatter viable population are shown in Fig. 2, and in all of the assays.

3.8.2 Annexin V-Binding and DNA-Binding Dye Exclusion

Once the cells are gated for scatter, they should be plotted for annexin V versus DNA dye or covalent viability probe labeling. These events usually occur after caspase activation and are considered "later" markers of apoptosis. Therefore, subpopulations negative or positive for annexin V and DNA dye-binding can be gated for discrimination of "early" and "late" apoptotic cells, and can be subsequently examined for caspase activation. An example of annexin V versus DNA dye labeling for camptothecin-treated EL4 cells is shown in Fig. 3. Scatter viable cells that are both annexin V and DNA dye negative are present, but may show the initiation of caspase activation; this population should be gated. Some cell types may also show either annexin V or DNA dye permeability arising first; these single positive populations can also be gated. Later apoptotic double-positives should be gated as well. These multiple populations can then be displayed for caspase activation.

DNA dyes are not completely interchangeable with regard to exclusion by apoptotic cells (*see* **Note 4**). For example, 7-AAD is somewhat more cell permeable than PI and will label an earlier subset of apoptotic cells. This will affect the overall analysis. For example, if 7-AAD-positive cells are excluded from the analysis (in an attempt to quantify very early apoptotic events), this dye's greater cell permeability will result in a lower apparent number of

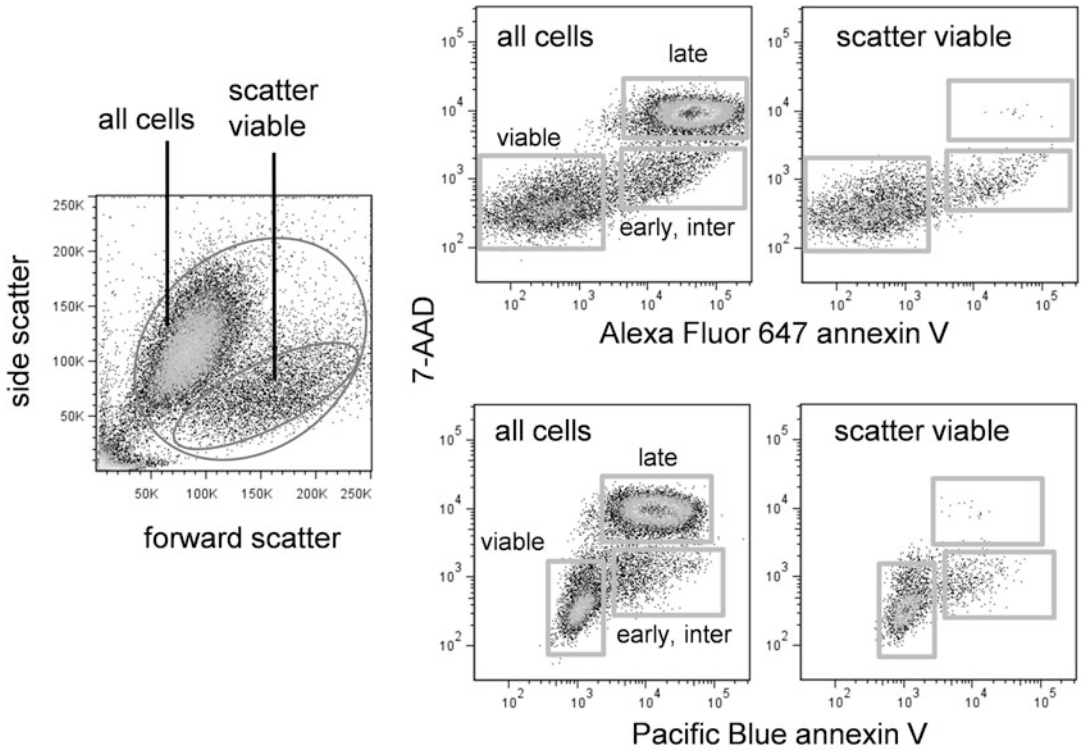

Fig. 3 Annexin V and DNA dye labeling in apoptotic cells. EL4 cells were treated with camptothecin at 5 μM for 16 h. *Left dotplot* shows forward versus side scatter of treated cells. *Top right row* shows Alexa Fluor 647 annexin V versus 7-AAD labeling for all cells (*left plot*) or scatter viable cells only (*right plot*). *Bottom right row* shows Pacific Blue annexin V versus 7-AAD labeling for all cells (*left plot*) or scatter viable cells only (*right plot*)

caspase-positive cells that are DNA dye-negative than if PI were used instead. These differences should be kept in mind when analyzing these early apoptotic subsets.

3.8.3 Annexin V-Binding and Covalent Viability Probes

While functioning by a very different mechanism than DNA-binding dyes, the overall appearance of covalent viability probes will be similar to DNA-binding dyes. Analysis should be similar, identifying and gating on the negatives, single positives (if any) and double positives. The fluorescence distribution of several covalent viability probes is shown in Fig. 4. These probes are usually bright, and viable and apoptotic cells can be easily distinguished.

3.8.4 Fluorogenic Caspase Substrates

After initial annexin V/viability gating, the cells can be observed for caspase activation. Note that even truly viable cells with no apoptotic activity labeled with a caspase substrate will have somewhat higher background fluorescence levels than completely unlabeled cells. All of the caspase substrates bind to viable cells to some degree. Care should be taken to identify both the viable and apoptotic fraction without using an unlabeled control as a cutoff. This background fluorescence is shown in Fig. 5.

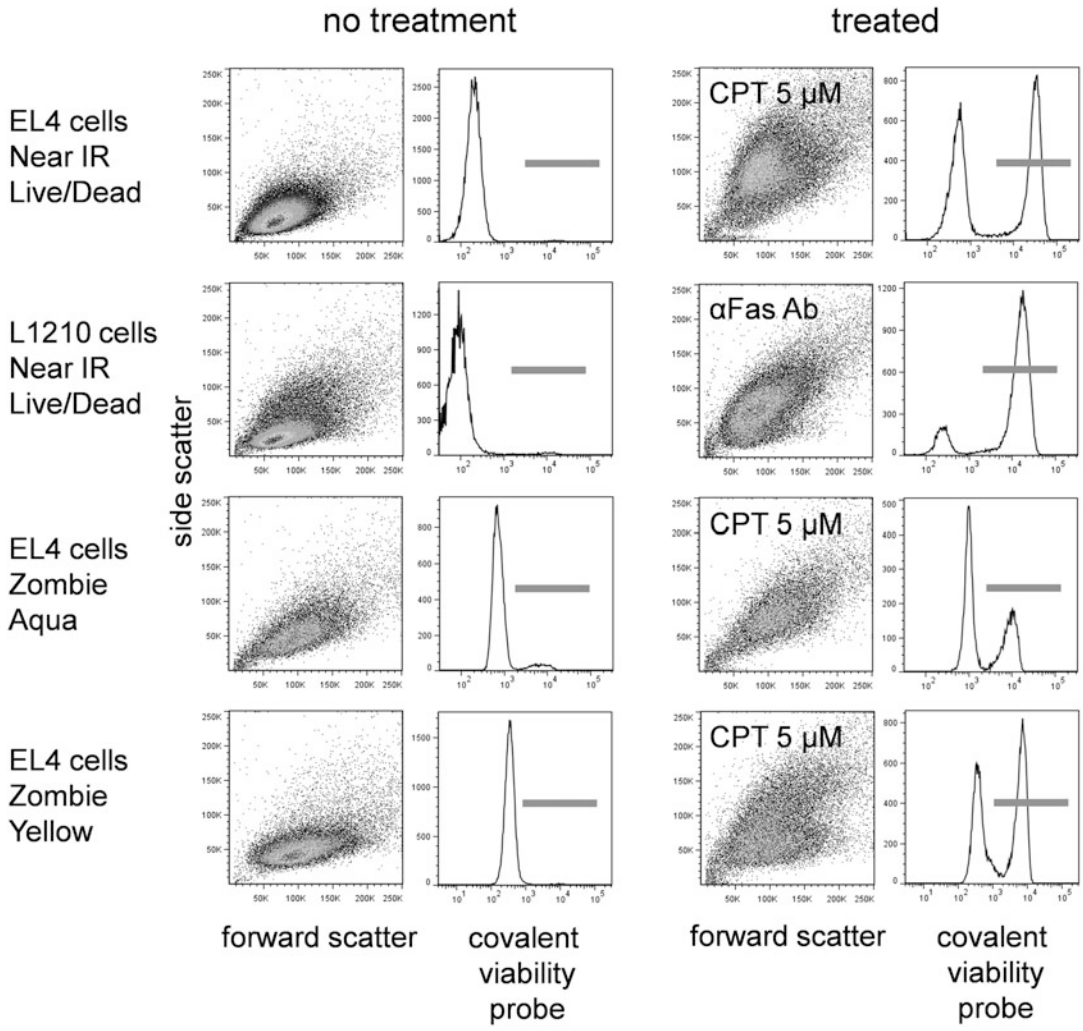

Fig. 4 Covalent viability probe labeling. EL4 cells treated with camptothecin at 5 μM for 16 h or L1210 cells treated with anti-Fas antibody (clone Jo2) at 1:1000 final concentration for 12 h were labeled with the indicated covalent viability probe. Forward versus side scatter dotplots and viability probe histograms are shown for untreated (*left two columns*) and treated (*right two columns*) cells

Once the caspase-negative population is identified, the caspase-positive cells should be clearly distinguishable. As discussed in Subheading 3.8.1, use both a total cell gate and a scatter viable gate to observe the extent of caspase activation. Caspase positive cells are usually present in the scatter viable only population in the presence of an apoptotic inducer.

3.9 Sample Results for Multiparametric Apoptosis Assays

Below are representative data for several combinations of fluorogenic caspase substrate, annexin V and either a DNA-binding dye or a covalent viability probe. In all of the illustrated results, apoptosis was induced in EL-4 murine thymoma cells by treatment with

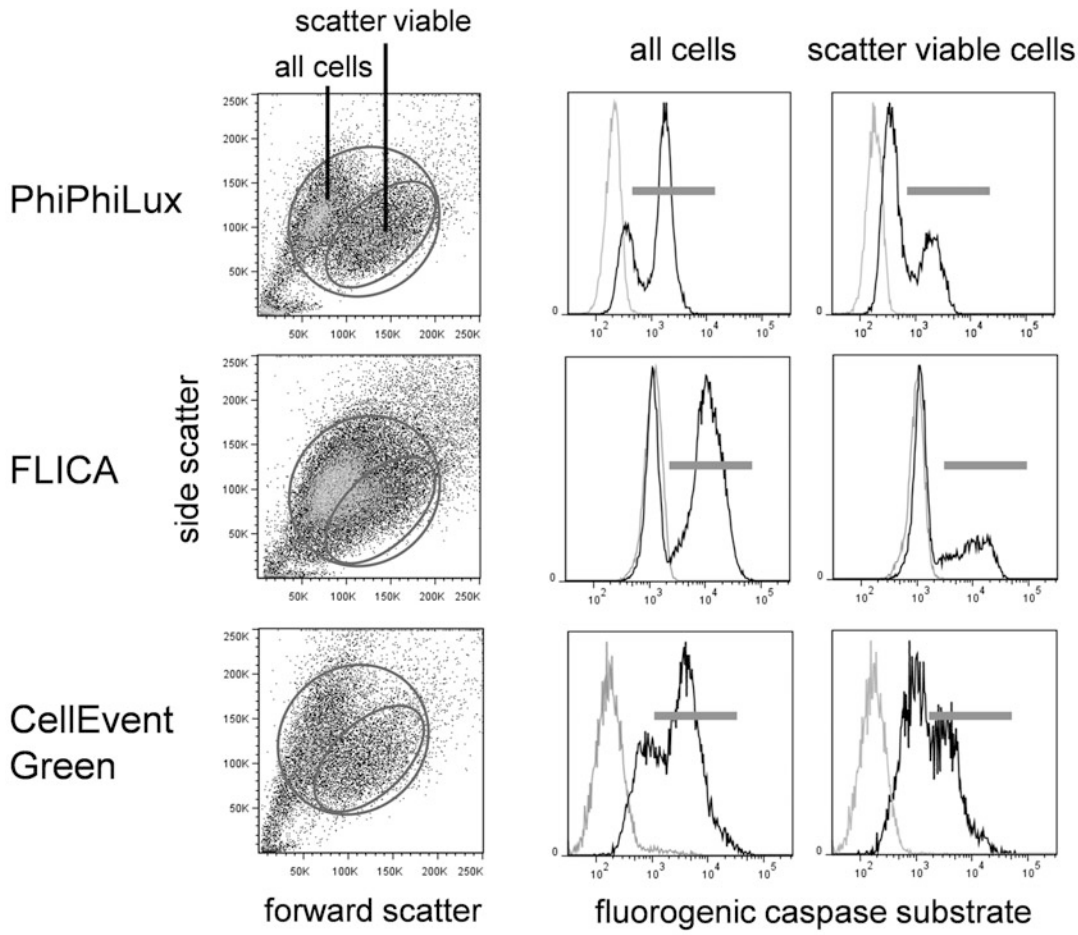

Fig. 5 Fluorogenic caspase substrate fluorescence in viable and apoptotic cells versus cellular autofluorescence. EL4 cells treated with camptothecin at 5 μM for 16 h were labeled with PhiPhiLux G1D2 (*top row*), FLICA (*middle row*), or CellEvent Green (*bottom row*). Forward versus side scatter dot plots (*left column*) with corresponding caspase labeling for all cells (*middle column*) or scatter viable only (*right column*). In the fluorogenic caspase histograms, *black peaks* indicate substrate labeling; *gray peaks* are unlabeled cells

camptothecin at 10 μM for 12 h. The figures both illustrate expected results for the individual components of the multiparametric cell death assay, and demonstrate how the simultaneous analysis of multiple cell death characteristics in a single assay gives a multidimensional picture of the total apoptotic process.

3.9.1 PhiPhiLux, Annexin V, and DNA-Binding Dye

In Fig. 6, EL4 cells treated with camptothecin were labeled with PhiPhiLux, Pacific Blue annexin V, and 7-AAD. As described in Subheading 3.8.1, cells were visualized for forward versus side scatter and gated to include both scatter viable and apoptotic cells, and scatter viable only. Labeling for all three markers can be

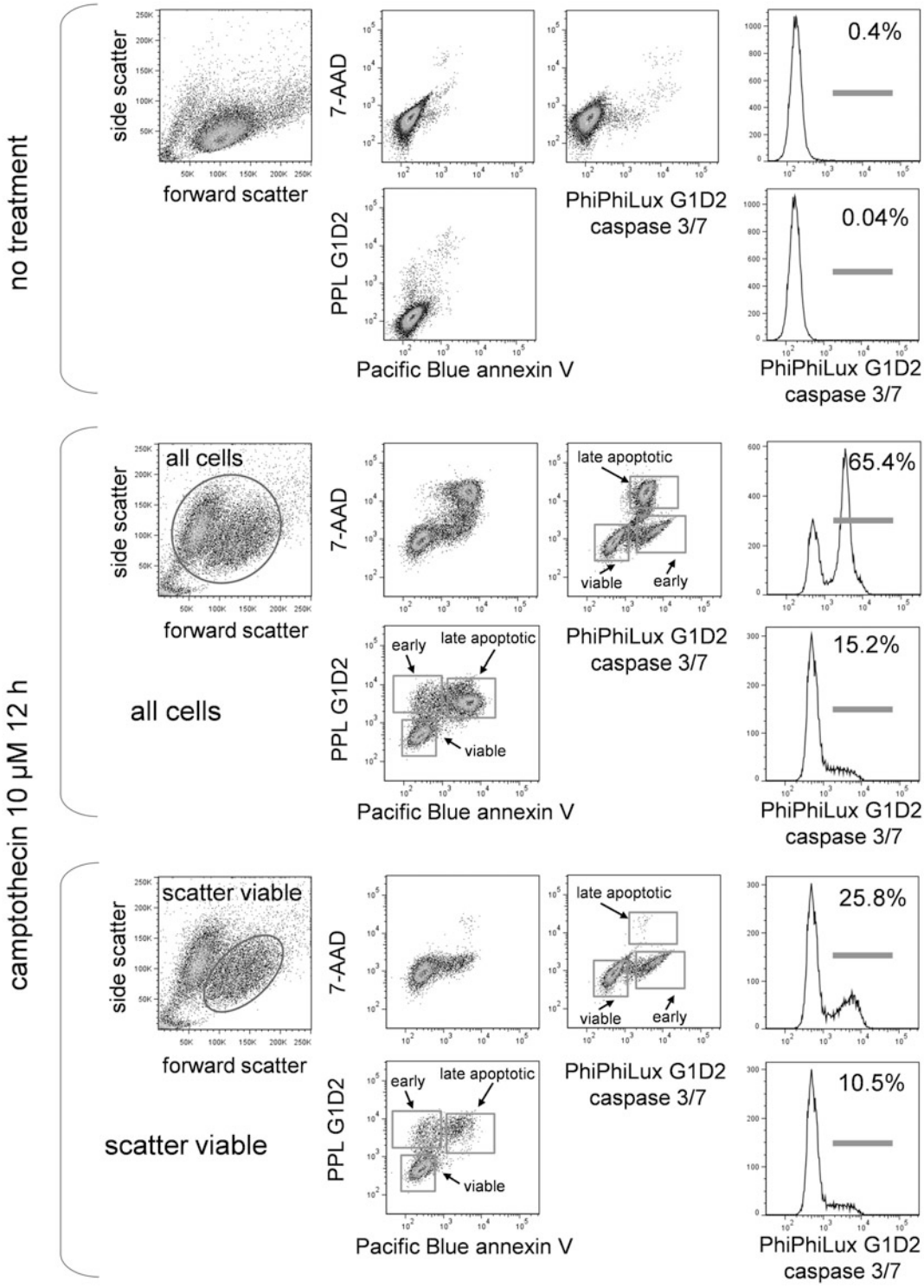

Fig. 6 PhiPhiLux, annexin V, and DNA-binding dye labeling. EL4 cells untreated or treated with camptothecin at 5 µM for 16 h were labeled with PhiPhiLux G1D2, Pacific Blue-conjugated annexin V, and the DNA dye 7-AAD. Scatter dot plots and labeling for all three labels in untreated cells (*upper group*), treated cells gated for all cells (*middle group*), and treated cells gated for scatter viable cells only (*bottom group*) are shown. Stages of cell death are indicated

seen, with PhiPhiLux-positive cells appearing earlier than the other two markers, and in significant numbers in the scatter viable population. Annexin V binding and 7-AAD permeability appear later.

3.9.2 FLICA, Annexin V, and DNA-Binding Dye

In Fig. 7, treated EL4 cells were labeled with FLICA, Pacific Blue annexin V, and 7-AAD. Again, all three markers appear in apoptotic cells, but FLICA labeling precedes the other two and appears in the scatter viable cells as the earliest marker of apoptosis.

3.9.3 CellEvent Green, Annexin V, and DNA-Binding Dye

In Fig. 8, treated EL4 cells were labeled with CellEvent Green, Pacific Blue annexin V, and 7-AAD. The marker distribution and order of appearance is similar to the PhiPhiLux and FLICA labeling in Figs. 6 and 7.

3.9.4 FLICA and Covalent Viability Probe

In Fig. 9, treated EL4 cells were labeled with FLICA followed by the covalent viability probe Live/Dead Near IR, and fixed with paraformaldehyde. Again, caspase activation precedes cell permeability, and multiple stages of apoptosis can be identified. This experiment did not include annexin V labeling; had it been included, the cells could not have been fixed prior to analysis.

3.10 Conclusion

Apoptosis is a highly variable process involving multiple biochemical pathways; therefore, there are no universal morphological or physiological characteristics that are common to apoptosis in all cell types. Cell death in different cell types (even in physiologically or morphologically similar ones) may present very different phenotypes, and may not necessarily be detectable by the same assays. Multiparametric assays for apoptosis are very amenable to the nature of apoptosis, since the investigator is not limited to one characteristic of cell death. Investigators should also be willing to try other apoptotic assays to fully characterize their particular system.

The protocol described in this chapter is readily amenable to the incorporation of antibody immunophenotyping along with the cell death markers, resulting in a very sophisticated "screening out" of dead cells for the measurement of receptor expression in "viable cells." A potentially exciting extension of this method would appear to be the phenotyping of early apoptotic cells, positive for caspase expression but negative for later markers. This method should be approached with care; from a cellular standpoint, caspase activation is probably not an "early" event in cell death, and many alterations in the plasma membrane may have occurred by this timepoint, resulting in aberrant antibody binding to cells as is observed in later cell death. Any cell surface marker expression results obtained by such methodology should therefore be interpreted with caution.

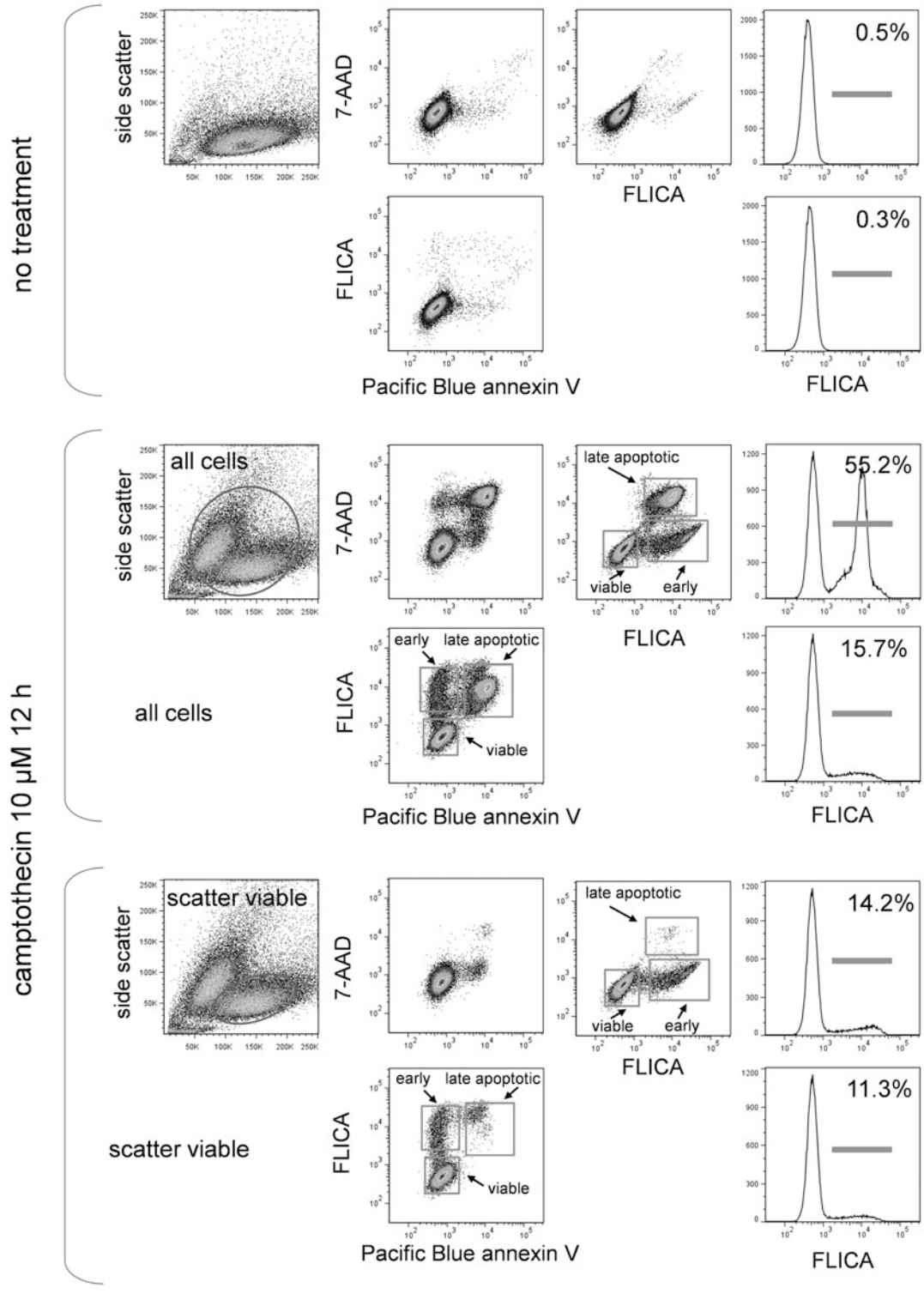

Fig. 7 FLICA, annexin V and DNA-binding dye labeling. EL4 cells untreated or treated with camptothecin at 5 μM for 16 h were labeled with FLICA, Pacific Blue conjugated annexin V and the DNA dye 7-AAD. Scatter dot plots and labeling for all three labels in untreated cells (*upper group*), treated cells gated for all cells (*middle group*), and treated cells gated for scatter viable cells only (*bottom group*) are shown. Stages of cell death are indicated

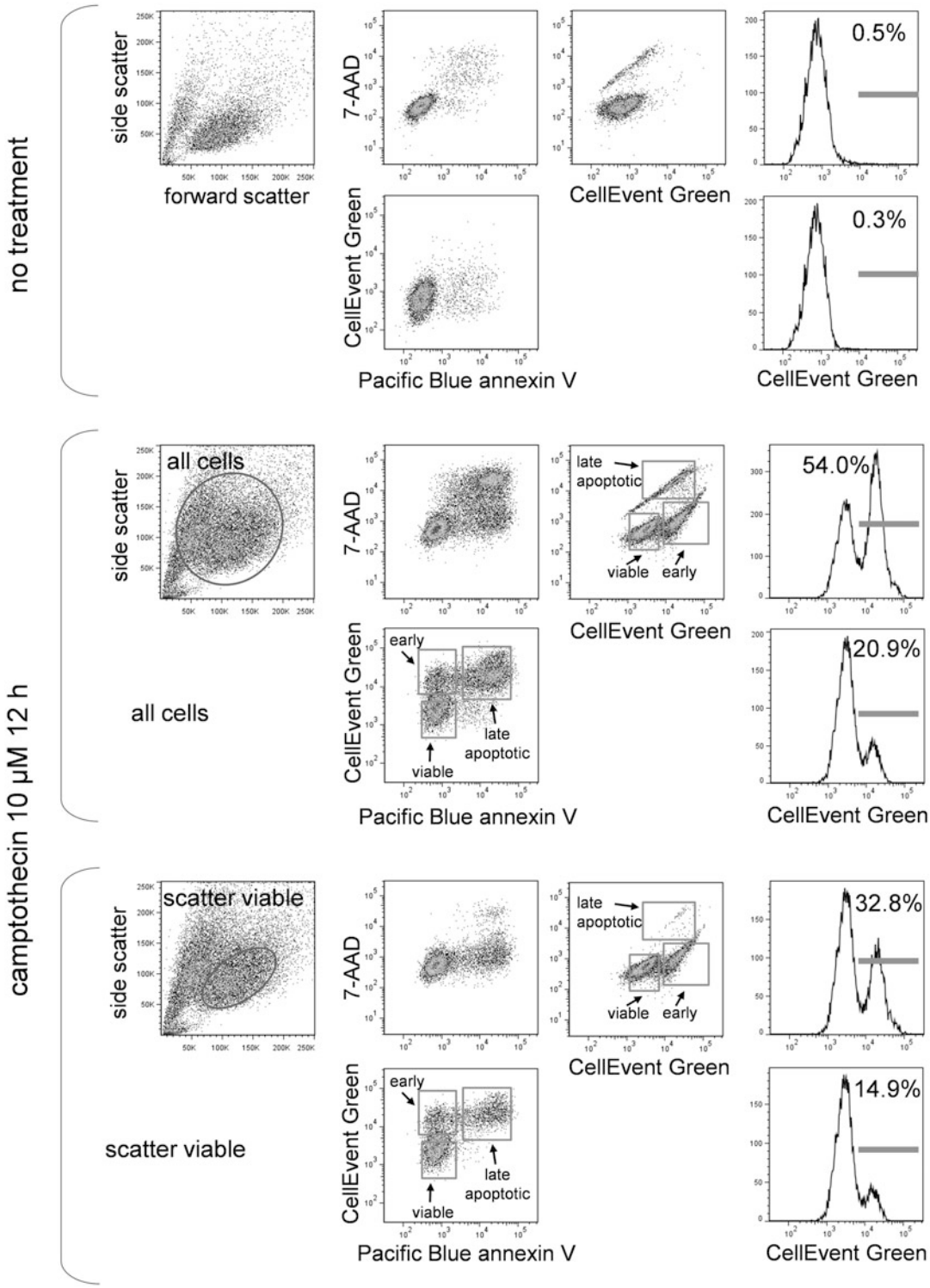

Fig. 8 CellEvent Green, annexin V, and DNA-binding dye labeling. EL4 cells untreated or treated with camptothecin at 5 μM for 16 h were labeled with CellEvent Green, Pacific Blue conjugated annexin V and the DNA dye 7-AAD. Scatter dot plots and labeling for all three labels in untreated cells (*upper group*), treated cells gated for all cells (*middle group*), and treated cells gated for scatter viable cells only (*bottom group*) are shown. Stages of cell death are indicated

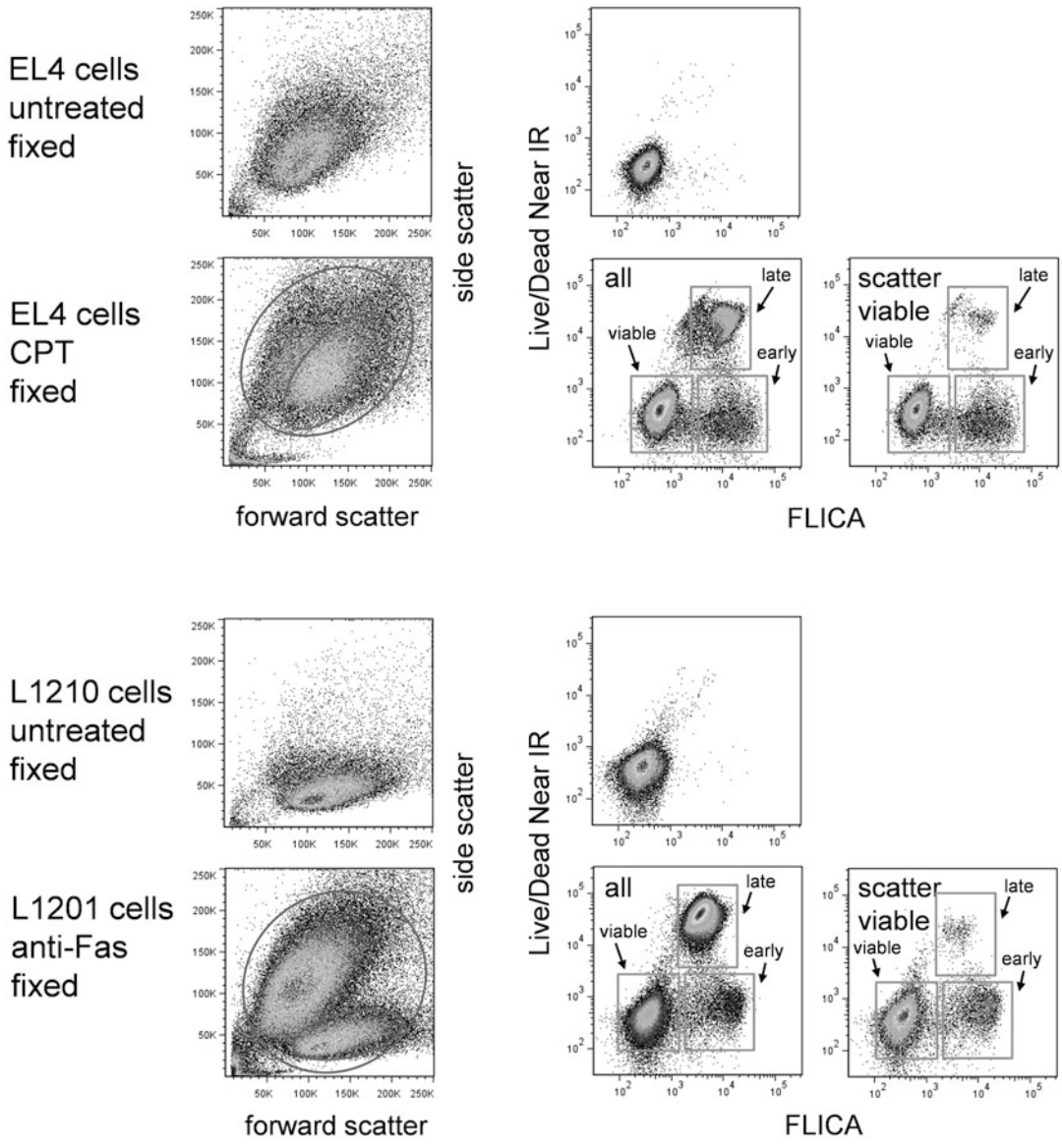

Fig. 9 FLICA and covalent viability dye labeling. EL4 cells untreated or treated with camptothecin at 5 μM for 16 h (*top two rows*) or L1210 cells untreated or treated with anti-Fas antibody (clone Jo2) for 12 h (*bottom two rows*) were labeled with FLICA and the covalent viability dye Live/Dead Near IR (*see* Table 1). Scatter dot plots and labeling for both labels in untreated and treated cells are shown. Stages of cell death are indicated

4 Notes

1. Fluorogenic caspase substrates with alternative fluorophores. Fluorogenic caspase substrates coupled to rhodamine-like, sulforhodamine-like, and Cy5-like fluorophores are also available. The spectra of these probes for the PhiPhiLux substrates

are shown in Fig. 1. None of these probes excites well at 488 nm; the rhodamine and sulforhodamine probes require a green or yellow laser source (532, 552, or 561 nm laser), and the Cy5 probes require red laser excitation. The green- and yellow-excited probes were originally designed for epifluorescence microscopes, which are usually equipped with mercury arc lamp filters that can provide 546 and 577 nm (green and yellow) excitation light. Many flow cytometers are now equipped with lasers in this range, however, making these probes potentially useful for cytometric analysis. Using the rhodamine and sulforhodamine probes limits DNA dye choices; the spectrum of propidium iodide coincides too well with them, and therefore cannot be used simultaneously. 7-AAD and the red-excited DNA binding dyes should also be avoided. The violet-excited DNA binding dyes including DAPI, Hoechst 33258, or SYTOX Blue should be used instead. The violet-excited covalent viability probes should also be used in this situation (Table 1). All of these longer wavelength probes may give better sensitivity than the fluorescein-like versions; cellular autofluorescence is significantly reduced with green to red excitation (compared to 488 nm blue-green), so overall signal-to-background signal is likely to increase.

2. Controls. Good "viable" and apoptotic controls are important for apoptotic analysis of apoptosis, and should be used, particularly when a new cell type or apoptotic stimulus is being investigated. Where possible, an untreated negative control and an independent positive control should be included, the latter being induced by an agent other than that under study (such as a cytotoxic drug). The EL4 cells used in this study are a good example of a control system that is easy to maintain and is reliable. Topoisomerase inhibitors including camptothecin and topotecan, transcriptional inhibitors including cycloheximide and translational inhibitors including actinomycin D and puromycin are all good inducers, and can induce in other cell lines as well. Samples with both the absence and presence of the caspase reagents are also important to include as controls, since the substrate does possess some low but detectable intrinsic fluorescence in the uncleaved state that can be erroneously interpreted as apoptosis without the appropriate control samples. However, unlabeled cells should not be used as a strict guide for gating on caspase labeled cells; they only allow determination of the increase in background from PhiPhiLux labeling. This background can be seen in Fig. 2.
3. Multiparametric analysis of apoptosis in adherent cells. Flow cytometric analysis of apoptosis in adherent cell lines poses special challenges, since the removal of cells from their growth

substrate may itself induce apoptosis. In addition, cell removal methods (such as trypsinization) can trigger false apoptotic indicators, such as aberrant annexin V binding in the absence of true cell death. By far the best solution to this problem is to utilize a slide-based laser scanning cytometer (LSC) for the analysis of apoptosis in these cell types; this specialized flow cytometer can perform cytometric analysis of cells on a flat surface, allowing minimal disruption during cell preparation [20]. Several apoptosis assays utilizing caspase substrates using laser scanning cytometry have been described [17, 21, 22].

4. DNA-binding dyes. All DNA-binding dyes do not have identical cell permeability characteristics. Some DNA dyes will gradually cross the plasma membranes of even viable cells, while others are better excluded. These differences can affect the results obtained from the assay. For example, 7-AAD is somewhat more cell permeable than PI, and may give a slightly greater percentage of apoptotic cells when compared directly to PI. Similarly, SYTOX Blue is slightly more cell permeable than Hoechst 33258, and will also identify an earlier set of apoptotic cells. This difference should be kept in mind while designing cell death assays, and may dictate the use of 7-AAD when this property is desired. Highly permeable DNA binding dyes such as Hoechst 33342, the DyeCycle dye series (Thermo Fisher Life Technologies), and DRAQ5 (Biostatus Ltd.) will enter cells and label their chromatin regardless of their viability state. This may limit their usefulness as apoptotic reagents for flow cytometry. They have however been used to identify morphological changes in chromatin during apoptosis by microscopy and laser scanning cytometry.
5. Caspase substrate specificity and background. While the PhiPhiLux substrates seem reasonably specific for their target caspases, no synthetic substrate is exclusively specific for any particular enzyme. This should be kept in mind for any assay involving specific proteolytic activity. In general, a considerable excess of substrate will encourage low levels of nonspecific cleavage, increasing the non-caspase background of the assay. Titration of the substrate to the lowest concentration able to distinguish activity may be necessary when the specificity of the assay is in doubt.
6. Annexin V critical parameters. Calcium and magnesium are critical for annexin V binding; even brief removal of divalent cations after the binding reaction will result in rapid dissociation from PS residues. The cells must therefore remain in a calcium/magnesium buffer at all stages up to analysis, including all wash buffers.

7. Incubation periods and sample storage. All incubation periods and conditions are critical parameters for this assay, as is prompt analysis of samples following the labeling procedure. Insufficient incubation time for the PhiPhiLux substrates will result in poor labeling; prolonged incubation periods will increase the level of nonspecific substrate binding and cleavage, resulting in high background fluorescence and decreased signal-to-noise ratios. In addition, prolonged storage of cells following the removal of the surrounding PhiPhiLux substrate will eventually result in leakage of the cleaved substrate from the cell, despite its reduced cell permeability in the cleaved state. Overly long annexin V incubation periods will also increase the amount of nonspecific binding to cells, making discrimination of "viable" and apoptotic cells more difficult. Although PI (and to a lesser extent 7-AAD) are relatively impermeant to viable cells, prolonged incubation will cause uptake even in healthy cells. If laboratory conditions do not allow prompt analysis of sample, the FLICA assay with covalent viability probe labeling should be considered. Other cell death assays involving fixed cells such as TUNEL assays or immunolabeling of active caspases not described here should also be considered alternatives.

Acknowledgments

The author wishes to acknowledge Veena Kapoor and Nga Hawk of the National Cancer Institute for excellent technical assistance, and Dr. Zbigniew Darzynkiewicz of the New York Medical College for helpful discussion. Jolene Bradford and Gayle Buller at Thermo Fisher Life Technologies (formerly Molecular Probes) provided valuable technical information regarding fluorescent probes. Beverly Packard and Akira Komoriya also provided information regarding the PhiPhiLux probes, technical assistance and useful discussion. This work was supported by intramural research fund provided by the Center for Cancer Research, National Cancer Institute.

References

1. Telford WG, King LE, Fraker PJ (1994) Rapid quantitation of apoptosis in pure and heterogeneous cell populations using flow cytometry. J Immunol Methods 172(1):1–16
2. Darzynkiewicz Z, Juan G, Li X, Gorczyca W, Murakami T, Traganos F (1997) Cytometry in cell necrobiology: analysis of apoptosis and accidental cell death (necrosis). Cytometry 27 (1):1–20
3. Del Bino G, Darzynkiewicz Z, Degraef C, Mosselmans R, Fokan D, Galand P (1999) Comparison of methods based on annexin-V binding, DNA content or TUNEL for evaluating cell death in HL-60 and adherent MCF-7 cells. Cell Prolif 32(1):25–37
4. Vermes I, Haanen C, Reutelingsperger C (2000) Flow cytometry of apoptotic cell death. J Immunol Methods 243 (1–2):167–190

5. Pozarowski P, Grabarek J, Darzynkiewicz Z (2003) Flow cytometry of apoptosis. Curr Protoc Cytom Chapter 7:Unit 7 19. doi:10.1002/0471142956.cy0719s25
6. Henkart PA (1996) ICE family proteases: mediators of all apoptotic cell death? Immunity 4 (3):195–201
7. Ormerod MG, Sun XM, Snowden RT, Davies R, Fearnhead H, Cohen GM (1993) Increased membrane permeability of apoptotic thymocytes: a flow cytometric study. Cytometry 14 (6):595–602. doi:10.1002/cyto.990140603
8. Castedo M, Hirsch T, Susin SA, Zamzami N, Marchetti P, Macho A, Kroemer G (1996) Sequential acquisition of mitochondrial and plasma membrane alterations during early lymphocyte apoptosis. J Immunol 157 (2):512–521
9. Green DR, Reed JC (1998) Mitochondria and apoptosis. Science 281(5381):1309–1312
10. Overbeeke R, Steffens-Nakken H, Vermes I, Reutelingsperger C, Haanen C (1998) Early features of apoptosis detected by four different flow cytometry assays. Apoptosis 3 (2):115–121
11. Earnshaw WC, Martins LM, Kaufmann SH (1999) Mammalian caspases: structure, activation, substrates, and functions during apoptosis. Annu Rev Biochem 68:383–424. doi:10.1146/annurev.biochem.68.1.383
12. Koester SK, Bolton WE (2001) Cytometry of caspases. Methods Cell Biol 63:487–504
13. Gorman AM, Hirt UA, Zhivotovsky B, Orrenius S, Ceccatelli S (1999) Application of a fluorometric assay to detect caspase activity in thymus tissue undergoing apoptosis in vivo. J Immunol Methods 226(1–2):43–48
14. Belloc F, Belaud-Rotureau MA, Lavignolle V, Bascans E, Braz-Pereira E, Durrieu F, Lacombe F (2000) Flow cytometry detection of caspase 3 activation in preapoptotic leukemic cells. Cytometry 40(2):151–160
15. Bedner E, Smolewski P, Amstad P, Darzynkiewicz Z (2000) Activation of caspases measured in situ by binding of fluorochrome-labeled inhibitors of caspases (FLICA): correlation with DNA fragmentation. Exp Cell Res 259 (1):308–313. doi:10.1006/excr.2000.4955
16. Komoriya A, Packard BZ, Brown MJ, Wu ML, Henkart PA (2000) Assessment of caspase activities in intact apoptotic thymocytes using cell-permeable fluorogenic caspase substrates. J Exp Med 191(11):1819–1828
17. Telford WG, Komoriya A, Packard BZ (2002) Detection of localized caspase activity in early apoptotic cells by laser scanning cytometry. Cytometry 47(2):81–88
18. Lazebnik YA, Kaufmann SH, Desnoyers S, Poirier GG, Earnshaw WC (1994) Cleavage of poly(ADP-ribose) polymerase by a proteinase with properties like ICE. Nature 371 (6495):346–347. doi:10.1038/371346a0
19. Packard BZ, Toptygin DD, Komoriya A, Brand L (1996) Profluorescent protease substrates: intramolecular dimers described by the exciton model. Proc Natl Acad Sci U S A 93 (21):11640–11645
20. Kamentsky LA, Burger DE, Gershman RJ, Kamentsky LD, Luther E (1997) Slide-based laser scanning cytometry. Acta Cytol 41 (1):123–143
21. Packard BZ, Komoriya A, Brotz TM, Henkart PA (2001) Caspase 8 activity in membrane blebs after anti-Fas ligation. J Immunol 167 (9):5061–5066
22. Smolewski P, Bedner E, Du L, Hsieh TC, Wu JM, Phelps DJ, Darzynkiewicz Z (2001) Detection of caspases activation by fluorochrome-labeled inhibitors: multiparameter analysis by laser scanning cytometry. Cytometry 44(1):73–82

Chapter 11

Multiparameter Cell Cycle Analysis

James W. Jacobberger, R. Michael Sramkoski, Tammy Stefan, and Philip G. Woost

Abstract

Cell cycle cytometry and analysis are essential tools for studying cells of model organisms and natural populations (e.g., bone marrow). Methods have not changed much for many years. The simplest and most common protocol is DNA content analysis, which is extensively published and reviewed. The next most common protocol, 5-bromo-2-deoxyuridine S phase labeling detected by specific antibodies, is also well published and reviewed. More recently, S phase labeling using 5′-ethynyl-2′-deoxyuridine incorporation and a chemical reaction to label substituted DNA has been established as a basic, reliable protocol. Multiple antibody labeling to detect epitopes on cell cycle regulated proteins, which is what this chapter is about, is the most complex of these cytometric cell cycle assays, requiring knowledge of the chemistry of fixation, the biochemistry of antibody-antigen reactions, and spectral compensation. However, because this knowledge is relatively well presented methodologically in many papers and reviews, this chapter will present a minimal *Methods* section for one mammalian cell type and an extended *Notes* section, focusing on aspects that are problematic or not well described in the literature. Most of the presented work involves how to segment the data to produce a complete, progressive, and compartmentalized cell cycle analysis from early G1 to late mitosis (telophase). A more recent development, using fluorescent proteins fused with proteins or peptides that are degraded by ubiquitination during specific periods of the cell cycle, termed "Fucci" (fluorescent, ubiquitination-based cell cycle indicators) provide an analysis similar in concept to multiple antibody labeling, except in this case cells can be analyzed while living and transgenic organisms can be created to perform cell cycle analysis ex or in vivo (Sakaue-Sawano et al., Cell 132:487–498, 2007). This technology will not be discussed.

Key words Cell division cycle, Cell proliferation, Mitosis, Mitotic states, Cell states, Antibodies, Monoclonal antibodies, Intracellular antigens, Fixation, Immunochemical staining, Immunofluorescence

1 Introduction

This chapter is narrow in focus, providing methods we have used with human cell lines, dispersed tissue, blood, and bone marrow; however, the methods should apply to most animal cells. The large fraction of multiparametric human cell cycle studies justifies this focus (Table 1). In discussion and references, we did not actively exclude rodent studies but found no compelling reason to cite

Teresa S. Hawley and Robert G. Hawley (eds.), *Flow Cytometry Protocols*, Methods in Molecular Biology, vol. 1678, DOI 10.1007/978-1-4939-7346-0_11,

Table 1
Publications[a]

Cell cycle	309,199	
Cell cycle AND Cytometry[b] AND…	24,217	7.832%
Eukaryote AND…	23,623	97.547%
Animal	22,008	90.878%
Plant	189	0.780%
Fungi	353	1.458%
Bacteria[c]	132	0.545%
Archaea	10	0.041%
Cell cycle AND Cytometry [All Fields] AND Eukaryote AND Animal AND…	22,008	90.878%
Human	13,980	57.728%
Mouse	2586	10.678%
Rat	1227	5.067%
Hamster	302	1.247%
Cell cycle AND Cytometry [All Fields] AND Eukaryote AND Insect AND…	71	0.293%
Drosophila	41	0.169%
Cell cycle AND Cytometry [All Fields] AND Eukaryote AND Worm AND…	13	0.054%
Caenorhabditis elegans	1	0.004%
Cell cycle AND Cytometry [All Fields] AND Eukaryote AND Fungi AND…	363	1.499%
Yeast	348	1.437%
Cell cycle AND Cytometry AND Multiparameter[b] AND…	340	1.404%
Human	**259**	1.070%
Mouse	26	0.109%
Rat	7	0.029%
Hamster	0	
Drosophila	0	
Caenorhabditis elegans	0	
Yeast	3	0.012%

[a]Data were collected by searching PubMed using the listed terms. Multiple or hyphenated words, e.g., "cell cycle" or "multi-parametric" were searched using quotes. In the list, "AND…" denotes that the current row was searched without additional terms and the current row was combined by Boolean "AND" to create the search for the following row. Percentages were calculated with the logical value for denominator, e.g., "Cell cycle" AND Cytometry AND Eukaryote yields 23,623 papers, which is 97.6% of 24,217. All terms were MeSH terms except Cytometry and Multiparameter (see below), which were [All Fields]. Each search was complemented with NOT terms that excluded non-synonomous terms, e.g., … AND animal NOT plant NOT Bacteria… etc

[b]Cytometry = (Cytometry OR Microfluorimetry OR Cytophotometry). Multiparameter = (Multiparameter OR Multi-parametric OR Multicolor OR Polychromatic OR "Multi-parameter" OR "Multi-parametric" OR "Multi-color" OR "Poly-chromatic")

[c]Prokaryote retrieved 0 articles

them. An exception might be cell proliferation history measurements (e.g., CFSE labeling), but this area does not fall under our narrow definition of multiparametric cell cycle analysis (*see* Subheading 1.1). Equally, most work with non-mammalian model organisms (flies, worms, yeast) is not multiparametric and almost exclusively amount to DNA content measurements (sometimes coupled with another probe like GFP). As previously noted [1] a developing yeast niche is imaging flow cytometry [2–4], which is multiparametric cell cycle analysis, but the calculated parameters are morphological, obtained from relatively simple measurement parameters, and not within the scope of this chapter.

1.1 Definition

Here, we define multiparametric cell cycle analysis as measurements and computation aimed at defining or identifying cell cycle compartments, phases, or states and/or quantitative cell cycle phase/state-related expression of biomolecules. This is independent of the means by which a biomolecule is labeled or detected, but methodologically, we present only the combination of DNA-binding dyes and antibodies labeled with fluorescent small molecules or proteins. Technically, a multiparametric analysis wherein a marker is used to define or isolate a cell type and an additional, single parameter aimed at identifying phases or phase-related expression is not multiparametric analysis (e.g., cytokeratin and DNA content). However, in our evaluation of the literature, a large number of publications that we counted as multiparametric cell cycle papers were exactly just that. The idea that we are adhering to here is that within our narrow definition, the intent of multiple parameters is to impart more information about the cell cycle, whereas in assays of cell type (e.g., differentiation markers) and a single-cell cycle parameter, the cell cycle information is one dimensional. Also, we have not purposefully or comprehensively included studies that mainly use cell size, light scatter, and morphology or imaging topological features as parameters in the multiparametric cell cycle analysis class. The reasoning here is almost the same. Cell size and light scatter measurements are most often utilitarian—used to clean the data (e.g., eliminate debris, subtract background). They have rarely been used to impart cell cycle information—most likely because in mammalian cells, the measurements are too broadly distributed and overlapping to be of much use. Imaging feature analysis should be included, because the cell cycle-related translocation of biomolecules is a common and important feature of cell cycle regulation. However, imaging cytometry of the cell cycle is a very understudied area, and most publications do not demonstrate the kind of added information that we are requiring for inclusion.

1.2 History

For a brief and personal history of cytometry and the cell cycle *see* ref. 5. Even more briefly, we recapitulate. The transition from autoradiography (*see* **Note 1**) to DNA content measurements by flow cytometry was a transition from laborious, time-consuming

(days/weeks) effort between experiment and data to measurements, data, and analysis within minutes. Multiparametric work began with microfluorimetry of DNA and RNA in cells stained with acridine orange (AO), developed by Darzynkiewicz and colleagues, that produced a set of protocols that segment the cell cycle into seven compartments (G_0, G_{0T}, G_1A, G_1B, S, G_2, and M). The discovery of AO and Hoechst dye fluorescence quenching by DNA with halogenated pyrimidines and later the ability to detect the halogenated epitopes with monoclonal antibodies rendered cell kinetics (measuring phase transition times) through easily implemented, robust, relatively low-labor procedures yielding precise data. These assays were necessarily bivariate with anti-BrdU or anti-IdU coupled with DNA content. More generally, Jacobberger et al. [6] and Clevenger et al. [7] introduced high-quality intracellular antigen detection by flow cytometry, dependent on monoclonal antibodies, and coupled with DNA content, which led to multiparametric cell cycle analyses of the type presented here (*see* **Note 2**). Using similar approaches, the Darzynkiewicz group eventually defined 8-cell cycle compartments or states (*see* **Note 3**) based on multiple bivariate analyses of various cyclin (*see* **Note 4**) expression patterns. Using the staining scheme we present here, which uses five parameters, at least 13 states can be defined in a single assay with an unprecedented ability to measure the frequency of cells within states that exist for minutes (e.g., late mitosis) or hours (e.g., G1, S). The supporting references for unreferenced statements in this paragraph can be found in [5].

1.3 Rationale

When we started this work, it was driven by an interest in complex cytometric data and a desire to explore the information that could be derived from the complex patterns of clustered events (*see* **Note 5**). The cell cycle was a good system with which to address this interest because even though a proliferating cell population contains cells with different histories, the gene expression programs within those histories are repeated with approximately the same dynamics, and thus from a data point of view, data visualizations for each historical cycle can be represented by a single unified, generic pattern (e.g., *see* Fig. 1 and [10]). Compared to a system where changes occur in successive periods, analytical complexity is simplified for the cell cycle. We worked on this problem from 1993 through 2012. The journey has been rewarding in that we now have the backbone of an extensible system (presented here) that "solves" these complex patterns in terms of correlated simple single-parameter expression profiles over one cell cycle period [11, 12]. This opens up multiparameter cell cycle analysis to a number of parameters limited only by the available antibodies (and cell numbers) using multiple samples and mathematically correlating the results through cell cycle time.

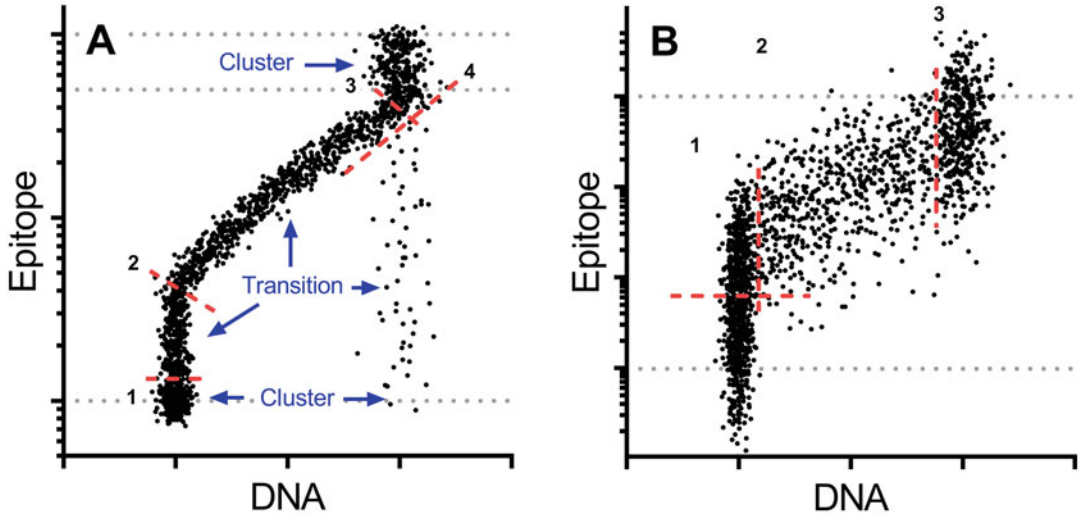

Fig. 1 Bivariate cell cycle expression patterns and terms. (**a**) Pattern for an epitope that is not expressed in early G1 then expressed exponentially through the cell cycle at a constant rate until M, then degraded in M back to background levels. *Red lines* have been placed where the pattern can be segmented meaningfully: (*1*) the boundary between non-expression and the beginning of expression in G1, (*2*) the G_1/S boundary, (*3*) the S/G2 boundary, and (*4*) the first detectable cells in which the epitope decreases through degradation. This hypothetical pattern can be observed when cyclin B1 is measured [8]. The *gray dotted gridlines* are at 1 (background), 50, 100. Degradation begins at 100. (**b**) Expression pattern for a "housekeeping" epitope—expressed from a "steady state" level of 50 at the beginning of G1 to 100 just before cell division. *Red lines* are drawn at (*1*) an objective "early" G1 (e.g., G1A for rRNA [9]) where expression is less than that expressed in late G1/early S, and at (*2*) G1/S and (*3*) S/G2. These patterns were generated by creating an expression profile with 2000 successive calculated (synthetic) time points that were then replaced by a value drawn from a normal Gaussian distribution with mean equal to the profile value and a standard deviation calculated from a coefficient of variation of 10%. Microsoft Excel and GraphPad Prism 7.0 were used. The terms "Cluster" and "Transitions" point to regions where data accumulate (Clusters), which reflect periods wherein at least one of the parameters is expressed at equilibrium levels (synthesis and degradation are balanced), or where data reflect periods of net synthesis or degradation in one or both parameters (Transitions)

1.3.1 The Relationship Between Parameters and Information (I)

Our effort was entirely exploratory with a single idea—that more parameters equate to more information. Of course, this is true in a trivial sense (*see* **Note 6**) because correlating any measurement with the DNA content of an asynchronously cycling cell population delivers the cell cycle-related expression of that parameter in some detail and with precision. In a nontrivial sense, if a parameter is functionally cell cycle related—i.e., if it plays a role in organizing and regulating the rates of transition through various phases or states within the cell cycle, then (when co-measured with another functional variable) there should be a limited set of complex multivariate patterns to which that "parameter vs. parameter" pattern belongs, and that pattern should produce information about the cell cycle of the cell population under study. This nontrivial information is a property of data clusters ("stable" states) and "transition" regions between clusters (Fig. 1a). Relatively uninformative

cell cycle-independent epitopes (*see* **Note 7**), e.g., "housekeeping class" epitopes, should belong to a more restricted pattern set, increasing approximately from ~1× to ~2× as a function of one cell cycle period (Fig. 1b). It is not hard to imagine that the expression of two "housekeeping" epitopes will be highly correlated and uninformative. On the other hand, two parameters that have regulating or organizing functions (i.e., cell cycle-related epitopes (CCRE)) will most likely demonstrate phase/state-specific changes in expression and create a complex pattern when plotted versus each other, or more simply versus DNA content, which is a marker for an organizing activity. Plotting an unknown epitope versus DNA content can identify CCREs. In 1989, Jacobberger presented a sketch of hypothetical bivariate expression patterns (epitope vs. DNA) based on limited experience, limited literature, and imagination [13]. Eleven patterns were drawn with nine considered informative. A "housekeeping" pattern and "negative control" (autofluorescence + nonspecific probe binding) were considered uninformative. In that chapter, real data were shown that were similar to three of the hypothetical patterns. Since then, we have observed or noted from the literature bivariate patterns that essentially recapitulate the ideas behind all of those hypothetical CCRE patterns. Figure 2 is an updated version of this work. This figure, based on synthesized hypothetical data for a cell population with a 22 h cell cycle time and expression, ranges from 50 to 100 or 0.1 to 100 arbitrary units and backgrounds of 10 to 20 units. Each bivariate plot shows DNA-phase specific expression for a set where the expressed parameter of newly divided cells is at half the level at the cytokinetic stage (top two rows) or phase-specific expression from and "off" state to "on" and back to "off" (bottom two rows). Eight of these 13 patterns have been observed. This figure shows that bivariate plots of parameters vs. DNA are informative for CCREs. It also suggests strongly that more parameters will provide more substantive information. For example, the (top, left) pattern represents data synthesized from an expression profile for a parameter synthesized to a high level in G1 and then maintained at that level to the end of the cycle. However, it can only be labeled "G1" because we know the profile. A parameter that begins the cycle high, then degrades to half that level, then resynthesizes back to the high level—all in G1, would look the same. This uncertainty can be resolved by adding one or more parameters. As an example, Fig. 3 shows a plot of G1* vs. G1. Two definitive clusters are identified (ovals) and two transition regions that can only represent an increase and then a decrease in expression (this statement is predicated on having access to the G1 and G1* vs. DNA plots of Fig. 2). This chapter will make this point again, explicitly, on mitotic states with real data (*see* Subheading 3.5 on Analysis). Thus, this section demonstrates that a bivariate analysis

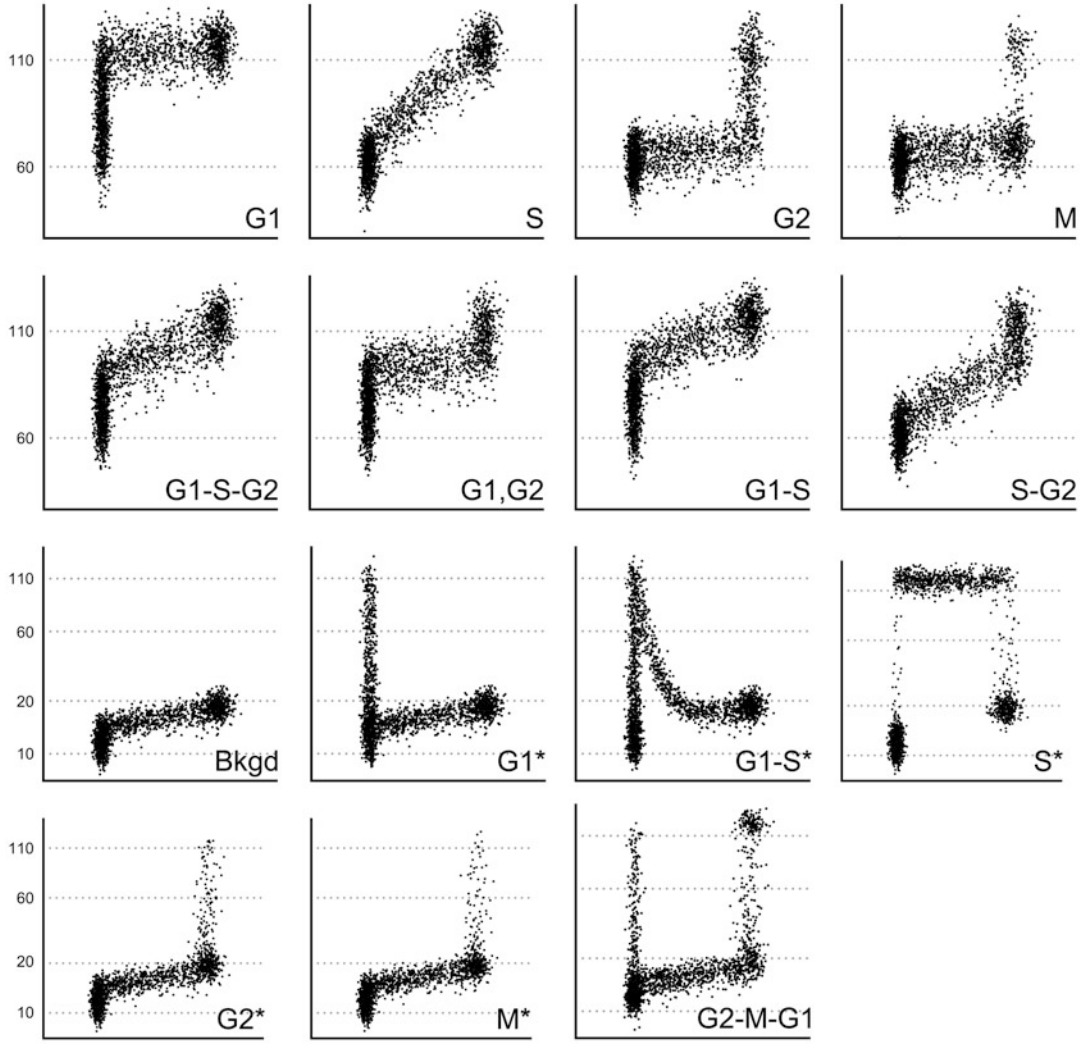

Fig. 2 Cell cycle expression pattern variations. Different patterns were generated from synthetic expression profiles as in Fig. 1 to represent potential patterns of cell cycle-related expression. All data sets have background proportional to cell size (10 → 20 from G1 → M) as shown in the *third row*, *first plot* (Bkgd). The *first row* represents epitopes that are phase specific (labeled) for synthesis but constantly expressed such that at division the epitope levels are divided into two. The *second row* reflects complex phase specificity. The *third* and *fourth rows* show plots that mimic epitopes that are synthesized and then degraded within a single phase (G1*, S*, G2*, M*) or synthesized in one phase and degraded in another (G1–S*, G2–M–G1)

equates to more information than a univariate analysis. When one of the parameters is DNA content, the least information imparted is a quick guess at the phase specificity of expression and expression rates through those phases (G0/G1, S, G2 + M). Of course, the quest is that the pattern imparts more information than that. For example, the expression could be "unscheduled," which could

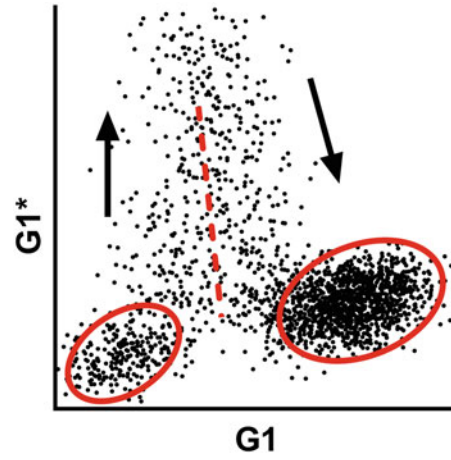

Fig. 3 Bivariate analysis to resolve single-phase synthesis and degradation. The simulated data from Fig. 2 for G1 and G1* were plotted to illustrate partial resolution of the complete expression (synthesis and degradation) in G1*. This approach is exemplified with real data for PHH3 and cyclin B1 to resolve the phosphorylation and dephosphorylation of PHH3 (Fig. 9b)

point to an abnormally regulated process in pre-cancer or cancerous cells (*see* **Note 8**) [14, 15].

Cell states: Multiparametric patterns of CCREs form linked clustered data that can be defined as cell cycle states and the cycle can be modeled as a series of these "finite" states. Figure 4 shows this idea, and it has been conceptually elucidated for mitosis by Pines and Roeder [21], which is essentially that a progression of mitotic states can be defined by the periodic activity of dominant regulatory enzymes. In our approach, cell states are defined by periods of correlated and uncorrelated dynamic expression. Although this view of the cell cycle is appealing (at least to us), in practice it has little use other than as a framework to give us a "short-hand" language with which to discuss various cells states. For example, prophase can be described as having two distinct states based on the expression of phospho-S10-histone H3 and cyclin A2 [1, 16]. This language could play a distinct role in, e.g., a sophisticated platform for measuring the action of drugs on the cell cycle by evaluating the cell frequencies within specific states as functions of time and dose.

The relationship between parameter number and cell states: We have started to ask the question whether the amount of information correlates with parameter number by counting cell states (unpublished), and so far we have not observed a simple relationship. For example, with the parameters DNA (peak signal), DNA (integrated signal), light scatter, cyclin A2, cyclin B1, and phospho-histone H3, we can define at least 15 distinct and easily measured cell compartments (Fig. 4). Hypothetically, adding a single additional

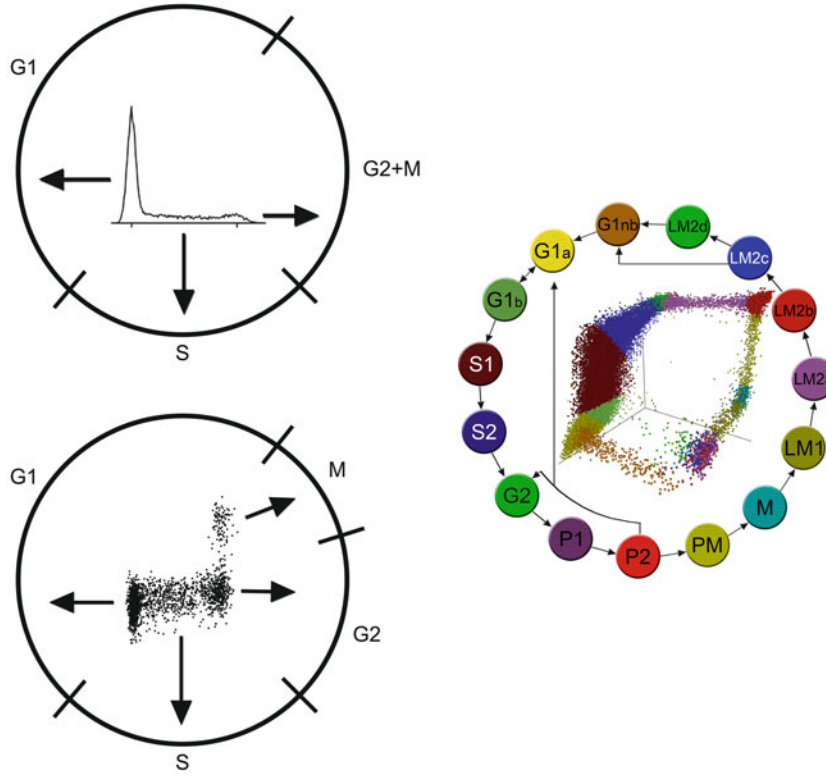

Fig. 4 Relationship of cytometric data to a compartment or state model of the cell cycle. *Upper left*: DNA content data for asynchronous, exponentially growing cultures constitute a bi-modal histogram with three regions, a G1 peak, a G2 + M peak, and between the two, an S phase component that can be thought of as composed of a series of Gaussian distributions equivalent to the G1 and G2 peaks, with successive means and constant CV. The regions correspond to the three phases of the cell cycle, originally defined by DNA labeling and autoradiography. *Lower left*: DNA content vs. a mitotic marker resolve G2 + M into G2 and M. PHH3 labels all mitotic cells, from the earliest states of chromosome condensation in early prophase to telophase and cytokinetic cells [16, 17]; therefore, there is ~100% correlation between this marker and morphologically defined mitosis. Bivariate analysis commonly uses a mitotic region to separate M from interphase and DNA content analysis to estimate G1, S, and G2 fractions. A more correct analysis would be to apply the same principles used in DNA content analysis to single-parameter PHH3 histograms gated on G2 + M cells, or even better—two parameter bivariate multiple Gaussian fitting to deconvolve the two-parameter histogram. A third option, and likely the best option would be to employ probability state modeling [18]. *Right*: Compartment analysis, using regions and Boolean logic as explained in this chapter, invokes a "Finite State"-like model and analysis rather than the classical phase model and analysis. In this analysis, the color-coded cell states are occupied by some frequency of cells, proportional to the time spent in the state, and rate constants that define the rates of transition from state to state [19]. There are at least two points places for uncertainty—the transition from G1a to G1b and the transition from G2 to P2 [20]. Cells have options to move in both directions, which complicates analysis and interpretation

parameter, Ki67, would add only one additional state, early in the cycle (G0), and adding PCNA would be expected to increase that by only one more (*see* **Note 9**). Nevertheless, once we have defined an unambiguous path from the start to the end of the cell cycle

(demarcated by cell division), we can analyze any additional parameter as a cell cycle expression profile [11, 12], unless it is expressed or has significant changes in expression within 1 of our 15 backbone compartments (Fig. 4).

1.3.2 The Relationship Between Parameter Number and Information (II)

Thus, at a minimum, one additional parameter equals one unit of additional information. It seems clear, given that the cell cycle is organized and regulated by thousands of genes, regulatory RNAs, protein/molecule interactions, and protein modifications, that the number of cell states and thus, the amount of additional information past the expression profile of each parameter will be limited—i.e., a good bit of the measurable units will be redundant from a correlated-data point-of-view. Beyond that, the most basic (or perhaps easiest to define) units of useful information constitute a normal/abnormal call. After that, we get into non-quantitative or hard-to-quantify territory. Nevertheless, we hope that we have made the point that the original poorly thought out idea that more parameters equal more information is a sound idea. Whether more parameters equal more useful information is still a valid question (*see* Subheading 1.4), although we hope that the examples in Figs. 2, 3, and 4 and the text of this chapter convince the reader to lean toward "yes."

1.4 Current State of Multiparameter Cell Cycle Analysis

We have looked for evidence that this approach—measuring several parameters within a cell cycle context to generate complex, highly informative cell cycle information, is currently and routinely applied in any area of cell-based science, and we are empty handed. We could have missed rare, high-quality papers, but whether we have or not, it seems clear that "multiparameter cell cycle analysis" does not currently have the research momentum that we believed/believe it could and should have.

To support the above statement, we present Table 1, which shows cell cycle/cytometry-related publication data from a series of PubMed searches. Our purpose was to evaluate the impact of "multiparameter cell cycle analysis." About 8% of "cell cycle [MeSH]" papers were classified by "cell cycle [MeSH]" AND "cytometry." This is a reasonable impact for cytometry. Of these publications, 69% concern human or mouse cells. A search on (cell cycle [MeSH] & cytometry & animal & **human** & multiparameter) accounts for almost all "multiparameter," cytometry, cell cycle papers. However, 234 papers are an under-representation. For example, for the work from our lab, 4 papers are returned by the search, whereas 18 papers qualify as multiparametric cell cycle studies. An examination of 144 papers from this search, covering the dates 1997 to the present, demonstrates that most are bivariate analyses and many included in this list are of the type that detect cell type and then perform univariate cell cycle analysis. Further, 43 papers (**17**%) are from the Darzynkiewicz group, and most of the

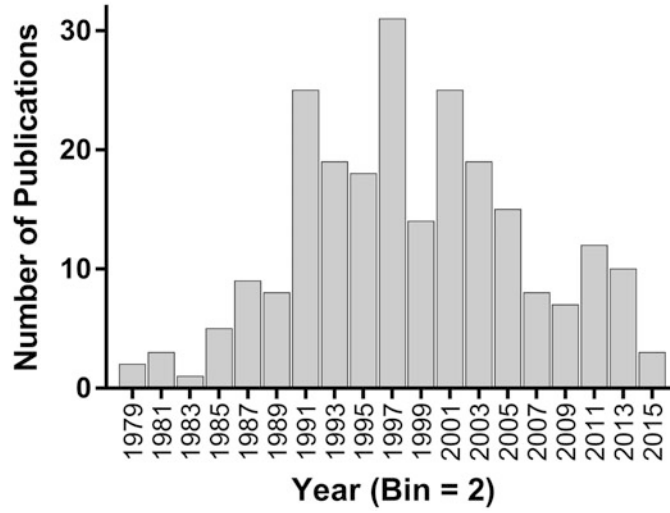

Fig. 5 Publication rates. "Multiparameter Cell Cycle Analysis" papers as defined in the text and in Table 1 were plotted as a histogram, identifying a peak of scientific interest centered on 1997–1998

technologically appealing papers present the technology rather than new biological information. Therefore, within some limits, Table 1 (and an examination of the papers that are detected) illustrates that "multiparameter cell cycle analysis" is a niche area, included in a very small fraction of cell cycle studies, mostly about human cells. Figure 5 puts the niche idea within a historical context and suggests that interest in this niche area peaked some time ago. This state-of-affair exists, ironically, when the tools to develop these assays have never been more extensive and powerful. The tools are instruments, probes, and analytical approaches. Instruments with unprecedented multiparameter capability are commercially available; monoclonal antibodies of high specificity to a large number of protein or function-identifying epitopes are widely available; using fluorescent proteins tags of multiple colors is commonplace; and finally, cytometric analysis and access to software packages continues to grow. On the plus side, this search was performed in Feb 2016 and updated in Mar 2017. There was a 12% increase in the number of papers satisfying the search "Cell Cycle AND Cytometry AND Multiparameter" (Row 20, Table 1).

1.5 Future of Multiparameter Cell Cycle Analysis

The areas where cytometry-based multiparametric cell cycle analysis should prove useful are: (1) evaluation of pre-cancer/cancer versus non-cancer cells, (2) healthy versus non-healthy systems, e.g., the immune system or hematopoiesis, (3) mathematical modeling of the cell cycle, (4) drug development, and (5) pharmacodynamic monitoring of patients in clinical trials and medical practice.

1.6 Common Research Objectives for "Cell Cycle Analysis"

There are five major reasons for cell cycle analysis by cytometry. These are to quantify: (1) the fraction of proliferating cells, (2) the histories of proliferating cells, (3) cell cycle phase or state fractions, (4) phase/state transit times, and (5) the cell cycle-related expression of parameters. In the same order, examples of each modality are: (1) stimulated lymphocyte assays [22, 23] and proliferation antigen detection [24, 25], (2) dye dilution analysis [26], (3) S phase fraction analysis of tumors and hematopoietic malignancies [27, 28] and DNA/cyclin/mitotic marker studies [1, 17, 25, 29–32], (4) cell kinetic studies [33–35], and (5) SV40 large T antigen, p53, cyclin, and modified histone expression studies [11, 12, 36–38]. The latter category reaches its full potential in work from us and collaborators in which parameter expression drives cell cycle models [39, 40].

1.7 Methodology

1.7.1 DNA Content Coupled with Antibodies

Simple cell cycle analysis consists of DNA content measurements. By itself, this is insufficient for measuring the fraction of proliferating cells or complete phase fraction analysis. Quiescent or G_0 cells have the same DNA content as G_1 cells, and, when assaying cell populations that contain non-proliferating and proliferating cells, the best that can be achieved by DNA content measurements is to obtain a proliferation *index* by quantifying the S phase or S + G2 + M phase fractions. A better assay is to label cells by continuous incubation with halogenated pyrimidines over some time period beyond the expected length of the G1 phase (thus, all cycling cells will be labeled), and then detect the labeled cells with antibodies to substituted DNA in cells that are co-stained for DNA content. This does not solve problems within the 4C (C, the genome complement) fraction that can be composed of G_2, M, and endoreduplicating or binucleate G_1 cells from a subpopulation cycling from 4C → 8C. These fractions can be resolved by the methods presented in this chapter, which are also antigen plus DNA content measurements.

1.7.2 Limitations of Antibodies

The limitations of single-parameter DNA content measurements were overcome over a 20-year period from 1985 through 2005. During this time, the value of monoclonal antibodies as specific, quantitative probes for epitope expression in fixed cells and tissues became clear. And with these probes, the entire cell cycle could be quantitatively evaluated and additional new cell states were defined.

Epitope availability: The entire approach rests on one caveat that is difficult to validate—that is, that the probe detects an unbiased fraction of the epitope. Antibody assays are always performed as a function of something else. If the fraction of epitope that is available for reaction with the antibody is changing as a function of "something else," then the assay is subject to misinterpretation, unless that changing availability can be evaluated or measured. In lieu of direct validation, the caveat is supported by the large body of

work that leads to the same answers whether the assay is done in tissue, whole cells, fractionated cells, or cell lysates. The level of possible "masking" (a description of unavailable epitope) follows the order tissue > whole cells > lysates; therefore, the agreement between, e.g., histology, cytometry, and western blots is a relatively powerful validation. We have done several correlative studies between cytometry and western blotting [37, 38, 41].

Antibody specificity and affinity: After the caveat of uniform epitope availability, the next weakness of the approach is the variability in antibody specificity and affinity. Before cytometric or microscopic assays can be relied on, the antibodies involved need to be validated. There are many published examples wherein this was not done. For a critical analysis of one group of widely used antibodies to the p53 protein, *see* Bonsing et al. [42].

Antibody validation: Methods for validating an antibody are not standard and not established. As we have stated previously [1], many commercial antibody catalog sites still do not present validating data or the validating data is of incomplete or poor quality. For the companies that do, the data are rarely if ever quantitative (*see* **Note 10**), and therefore, almost always visual, always anecdotal, and never rigorous (means and standard deviations), and not universally applied—i.e., they sell some with and some without evidence of validation. Perhaps a common method of screening monoclonal antibodies is by ELISA using the purified antigen. This may be fine for producing antibodies that work for immunoblotting electrophoretic gels that get around cross reactions via peptide fractionation, but for cell-based assays in which specific and nonspecific reactions are either integrated (as in flow cytometry) or only crudely differentiable (i.e., by low-resolution localization), it is not sufficient for validation. In cytometric assays, the quality of a reaction is defined by the antigen-antibody avidity versus nonspecific binding and cross-reactive binding to other cell constituents. It is avidity that matters because the increased probability that one or the other antigen combining site will be bound significantly reduces the effective antibody off rate, even though most of the antibody is bound monovalently at any one time. Because each sample type comes with its own set of unique potential background issues, especially for heterogeneous samples like blood and bone marrow, antibodies should be validated and staining should be optimized with these samples. Obviously, this level of assay-specific validation and optimization would be difficult and costly for commercial enterprises; therefore, it is left to the investigator to validate antibodies when using them in previously untested circumstances.

Our approach to validation is the following. First, we preferentially choose antibodies from companies that we trust and that provide some evidence for specificity. Generally, at a minimum,

that means a western blot of whole cell lysates using positive and negative cells with the full molecular weight range displayed. If the epitope is localized in the cell, and/or modulated by drug treatment, evidence of correct localization and/or modulation will lead us to choose one antibody over another. Second, after choosing an antibody, we perform both immuno-blot and flow cytometric titers with negative and positive cell samples. If a negative cell source is unavailable, we default to a negative control with an isotype control and/or secondary antibody (*see* **Note 11**). We design titrations with sufficient data to generate a curve so that we can evaluate signal to noise (e.g., *see* ref. 43, 44). Third, we try to obtain a biological test—siRNA knockdown, gene transfer, virus infection, cytokine stimulation, drug treatment, etc. Fourth, we either perform fluorescence microscopy or laser scanning cytometry [45] to make some check on localization. The working concentrations are defined by the cytometric titration. If our endpoint analysis is laser scanning cytometry, then we re-titer by twofold dilutions around the concentration determined by flow cytometry. This is because we work with higher staining volumes, and volume matters to the signal-to-noise ratio [46].

1.7.3 Fixation

Two general fixation classes: Unlike cell surface immunophenotyping, most (if not all) of the interesting epitopes for cell cycle analysis are inside the cell. This means cells have to be stabilized (fixed)—proteases, nucleases, transporters, channels, and other active molecules need to be inactivated, and the cell needs to be made permeable to large molecules. This has been reviewed extensively [13, 47–55]. Briefly, there are two basic modalities. The first uses denaturation and begins with formaldehyde fixation sufficient to stabilize cells, which is followed by alcoholic dehydration. For epitopes that are sensitive to formaldehyde, the formaldehyde step can be omitted because the dehydration process denatures and inactivates all the activities we worry about. The second modality is non-denaturing, using formaldehyde followed by nonionic or zwitterionic detergent, or saponins. In this case, the formaldehyde is not dispensable because it also serves to cross-link molecules, creating a matrix through which large molecules diffuse slowly—thus, allowing staining and measurement of even soluble epitopes. Nothing used in this latter process efficiently denatures large molecules, and therefore, this is an approximately native state system. In both processes, some molecules are extracted—either completely or partially, and some are displaced (e.g., *see* ref. 7). If the target epitope is involved in tight binding to other molecules, denaturation may be required to "unmask" the epitope (e.g., phospho-Y694-Stat5 requires alcohol fixation [43, 56, 57]). If enough formaldehyde is used for a long enough time, it is possible to make penetration of antibodies difficult, and it is possible to promote "masking" relative

to cells fixed with less formaldehyde. In all of this, there are many variables that can be adjusted. For example, different salts can be used to differentially extract molecules during the fixation step (e.g., *see* ref. 58). Another example is to permeabilize with detergent first and then fix with formaldehyde and alcohol [25]. This removes loosely bound proteins and other molecules. Use of the latter protocol gives a pattern of staining of PCNA versus DNA that identifies S phase better than DNA staining alone. Two studies using this approach are the exploration of new cell cycle states defined by correlated analysis of Ki-67 and PCNA [59] and correlated analysis of Mcm-6 and PCNA [60].

Recent advances in fixation: In recent years, there have been two notable advances in the development of fixation and permeabilization methods. The first is described in a paper by Chow et al. [61] that identifies an alcoholic denaturing procedure that will work on whole blood or bone marrow, leaving light scatter patterns and surface staining intact enough to identify subpopulations by standard immunophenotyping procedures. The second has a similar goal and is described in a patent awarded to Keith Shults and uses heat as the denaturant [62, 63]. A third effort, while not fixation/permeabilization development per se, is valuable. Krutzik and Nolan did a careful analysis of several fixation/permeabilization variants and arrived at formaldehyde followed by methanol as the overall best general approach to phospho-epitopes [64].

1.7.4 Recent Analytical Advances

There is a group of recent papers that deconvolve the complex clustered patterns that one encounters in multiparametric cell cycle analyses [11, 12, 65]. These papers present methods to derive a set of single-parameter "expression over cell cycle time" profiles from multiparametric cell cycle data that completely describe the complex multi-variate histogram patterns that represent all views of the data. Thus, the complex data patterns, arising from the correlated nature of cytometric single-cell data, are completely solved by these approaches. There are two features of this work that are critically important. The first is that the expression profiles are exactly equivalent to the outputs of cell cycle mathematical models based on systems of ordinary differential equations, and therefore presents an almost ideal platform to guide modeling [40]. And second, by deconvolving a set of multiparametric analyses, performed on aliquots of the same cell population, the expression relationship over the cell cycle between two epitopes that have not been measured together can be determined. This means that an open ended study of a very large number (only limited by the number of available cells, the number of available antibodies, dollars, manpower, and time) can be performed, potentially enabling development of highly complex mathematical models.

1.8 List of Key Publications

Table 2 lists a set of papers that anyone new to multiparametric cell cycle analysis should read. There are many, many papers and these were chosen by one of us (jwj) because they cover the major relevant areas. We tried to list only original research papers, but some areas are too broad and cannot be covered with a single research paper, and therefore reviews are listed. However, these are reviews with liberal presentations of data to present ideas or methods. We did not try to cite the first papers to report on a specific subject. Rather, these represent well-written, clearly presented work on the subject. Two of the subjects need some explanation. The first is paraffin-embedded tissue. This is a large area with a large number of papers, most of which are single-parameter DNA analyses. The single listed paper presented an advance that substituted collagenase for pepsin, was carefully done, used two parameters (although the cell cycle analysis was single parameter), and is a good introduction to the subject. The second area is "Drugs." This is also a very large and complex area and many more papers could have been listed. The paper by Kurose et al. [82] presents some signaling data, reflecting DNA repair pathway activities, coupled with DNA content as a basic means of examining drugs that affect the cell cycle by inducing DNA damage, invoking checkpoints, and leading to outcomes that include apoptosis and survival. It is rather easy to think of more complexity from an analytical point of view, but is rather hard to implement. This paper is a good introduction to this complex, and in our opinion underworked, area. This list is a good start, and following the research groups in the list and the papers they cite would constitute a thorough education in multiparametric cell cycle analysis.

2 Materials

In the following sections, a single complete protocol (including antibodies) will be presented to completely resolve the major cell cycle phases, compartments, and states. Analytical steps both during and after data acquisition are also included. A major alternative is to use detergent permeabilization before or after fixation with formaldehyde. These alternatives are available in the referenced literature. This chapter focuses on cell cycle phase/compartment/state-analysis, which is the difficult part to master.

2.1 Cell Culture

1. MOLT-4 cells (ACC 362 from DSMZ, Braunschweig, Germany; or CRL-1582 from ATCC, Manassas, VA) is an easily grown human T-cell leukemia line with a single-stem line, low 4C → 8C subpopulation (*see* **Note 12**), and published records of cyclins E, A2, and B1 expression consistent with wild-type, healthy-cell cyclin regulation [14, 15]. Cells are grown in suspension. K562 cells (ACC 10, DSMZ; CCL-243, ATCC) are a human Chronic Myelogenous Leukemia (CML) cell line

Table 2
Selected key publications

Area	First author	Year	Key title words	Reference
RNA	Darzynkiewicz	1980	New cell cycle compartments	[66]
	Traganos	1982	Unbalanced cell growth	[67]
Fixation and antibodies	Bruno	1992	Effect of ionic strength	[58]
	Mann	1987	Ribonucleotide reductase with DNA content	[68]
	Landberg	1991	Proliferating cell nuclear antigen	[69]
Periodic expression	Darzynkiewicz	1996	Cytometry of cyclin proteins	[70]
	Gong	1995	Growth imbalance and cyclins in synchronized cell cycle	[15]
	Juan	1998	Histone H3 phosphorylation	[71]
History	Poot	1989	Continuous bromodeoxyuridine labeling in cell kinetics	[72]
	Filby	2011	Imaging flow method for cell division history	[10]
Kinetics	Pinto	2006	Bystander responses radiolabelled and unlabeled cells	[73]
	Terry	1992	Continuous labeling with bromodeoxyuridine	[74]
	Terry	1991	Potential doubling times	[75]
	Huang	2013	Kinetics of G2 and M transitions regulated by B cyclins	[32]
Differential extraction	Landberg	1990	Proliferating cell nuclear antigen and Ki67	[59]
	Landberg	1992	Washless staining	[76]
	Frisa	2010	Chromatin bound Mcm6 and PCNA	[60]
Expression profiling	Jacobberger	2008	Mitotic cells	[17]
	Darzynkiewicz	2015	Initiation and termination of S phase	[77]
	Tomasoni	2003	Timing the changes of cyclin E	[78]
	Jacobberger	2012	Dynamic epitope expression	[12]
	Avva	2012	Conversion to relative, “same scale”	[11]
	Kafri	2013	Dynamics extracted from fixed cells	[19]
Analysis and modeling	Yanagisawa	1985	Simulation of bivariate DNA/ bromodeoxyuridine	[79]
	Li	2014	Early versus late S-phase sections: multiscale modeling	[80]
	Weis	2014	A data driven, mathematical model	[40]
Paraffin-embedded tissues	Glogovac	1996	Cancer cells extracted from paraffin-embedded tissue	[81]
Drugs	Kurose	2006	Effects of hydroxyurea and aphidocolin	[82]

that also has a single-stem line with a low level of 4C → 8C cells. The main difference between the two lines relevant to this chapter is that MOLT-4 cells have a longer relative G2 time and therefore a G2 phase that can be distinguished by increasing expression of cyclins A2 and B1.

2. RPMI-1640 medium supplemented with antibiotics and 10% fetal bovine serum (FBS) (*see* **Note 13**).

2.2 Biochemicals and Reagents

1. 16% Formaldehyde, methanol-free, Ultra Pure (Polysciences, Inc., Warrington, PA) (*see* **Note 14**).
2. Methanol (MeOH), spectrophotometric grade, >99%.
3. Phosphate-buffered saline (PBS): 150 mM NaCl, 10 mM phosphate, Na counter ion, pH 7.4. Prepare solution in deionized water and pass through 0.2 μm filter.
4. PBS-BSA: 2% (wt/vol) bovine serum albumin—Fraction V in PBS.
5. Antibodies reactive with: phospho-S10-histone H3-A488 (A488 = Alexa Fluor 488; #9708; Cell Signaling Technology, Waverly, MA; *see* **Note 15**), cyclin A2-PE (PE = Phycoerythrin; Beckman Coulter, Brea, CA; *see* **Note 16**); cyclin B1-A647 (clone GNS1, #554176; A647 = Alexa Fluor 647; BD Biosciences, San Jose, CA; *see* **Note 16**).
6. 4′,6-Diamidino-2-phenylindole (DAPI) solution: Prepare 1 mg/mL stock solution in double distilled water. Dilute working solution to 1 μg/mL in PBS.

2.3 Labware

1. Adjustable pipettors and pipet tips (1–20 and 100–1000 μL); glass or disposable pipettes (1, 5, 10, 25 mL).
2. Microfuge tubes: Snap-cap tubes for assays that will be processed within a few days to weeks. If fixed samples are to be stored for weeks to months, then tubes with rubber o-rings and screw-cap tops are required (otherwise, the samples will dry out). Tubes should be polypropylene.
3. Tissue culture dishes, flasks, or multi-well plates: Any size or type provided they hold more than 2 mL of media.

2.4 Instruments

1. Humidified CO_2 incubator.
2. Biosafety hood Class II.
3. Electrical impedance particle counting instrument (Beckman Coulter) or hemocytometer (Hausser Scientific, Horsham, PA). We use a Sceptor™ (Millipore, Billerica, MA).
4. Phase contrast inverted microscope with 10×, 20×, and 40× lenses (Olympus, Nikon, Leica, or Zeiss).

5. Microfuge: Variable speed, swinging bucket rotor, set at a low speed (*see* **Note 17**).
6. Suction device for removing supernatants. We use house vacuum hooked to a side arm flask with pasteur pipette hooked to rubber tubing hooked to a glass tube through a cork in the top of the side arm flask.
7. Flow cytometer with ultraviolet (UV) and/or violet, blue, and red lasers at a minimum, but add a green or yellow laser if you can, it will make the separation of A488 and fluorescein isothiocyanate (FITC) signals from PE very easy. The data presented in Fig. 6 were acquired on a LSR II (BD Biosciences) equipped with UV (355 nm), violet (405 nm), blue (488 nm), and red (633 nm) lasers. The data presented in Figs. 7, 8, 9, 10, 11, 12, 13 and 14 were acquired on an Attune NxT (Thermo Life Sciences/Invitrogen, Carlsbad, CA) equipped with violet (405 nm), blue (488 nm), yellow (561 nm), and red (637 nm) lasers. The filters were set up to detect DAPI, A488, PE, and A647.

3 Methods

3.1 Culture and Cell Preparation

1. In the examples, cells were growing exponentially as a suspension. MOLT-4 cells do not adhere to the dish, but many hematopoietic cells lines do adhere loosely. Gentle pipetting can be used to remove these cells (*see* **Note 18**).
2. To obtain an exponential culture, MOLT-4 or K562 cells should be serially passaged with splits of 1–2 every 2–3 days if cells are approaching their upper density of 1–2 $\times$ 10^6/mL. Cultures should be split before reaching 2 $\times$ 10^6/mL; otherwise, cells will begin to die as the culture becomes dense.
3. Examine with a phase contrast-inverted microscope. Cells should be free floating single cells. To obtain an even cell suspension, repeatedly pipette the culture. Pipet cells into a large test tube (15 or 50 mL) for cell counts (necessary if pooling flasks or dishes for large numbers of cells) and/or volume adjustments (*see* **step 4**).
4. Count the cells. Adjust cell concentration to 2 $\times$ 10^6/mL either by adding media or centrifuge to concentrate and then add media for correct density.
5. Dispense aliquots of 2 $\times$ 10^6 cells to 1.5 mL microfuge tubes. This works for antigens that are not labile during processing. If working with labile epitopes (e.g., some phospho epitopes), then formaldehyde can be added directly to the tissue culture

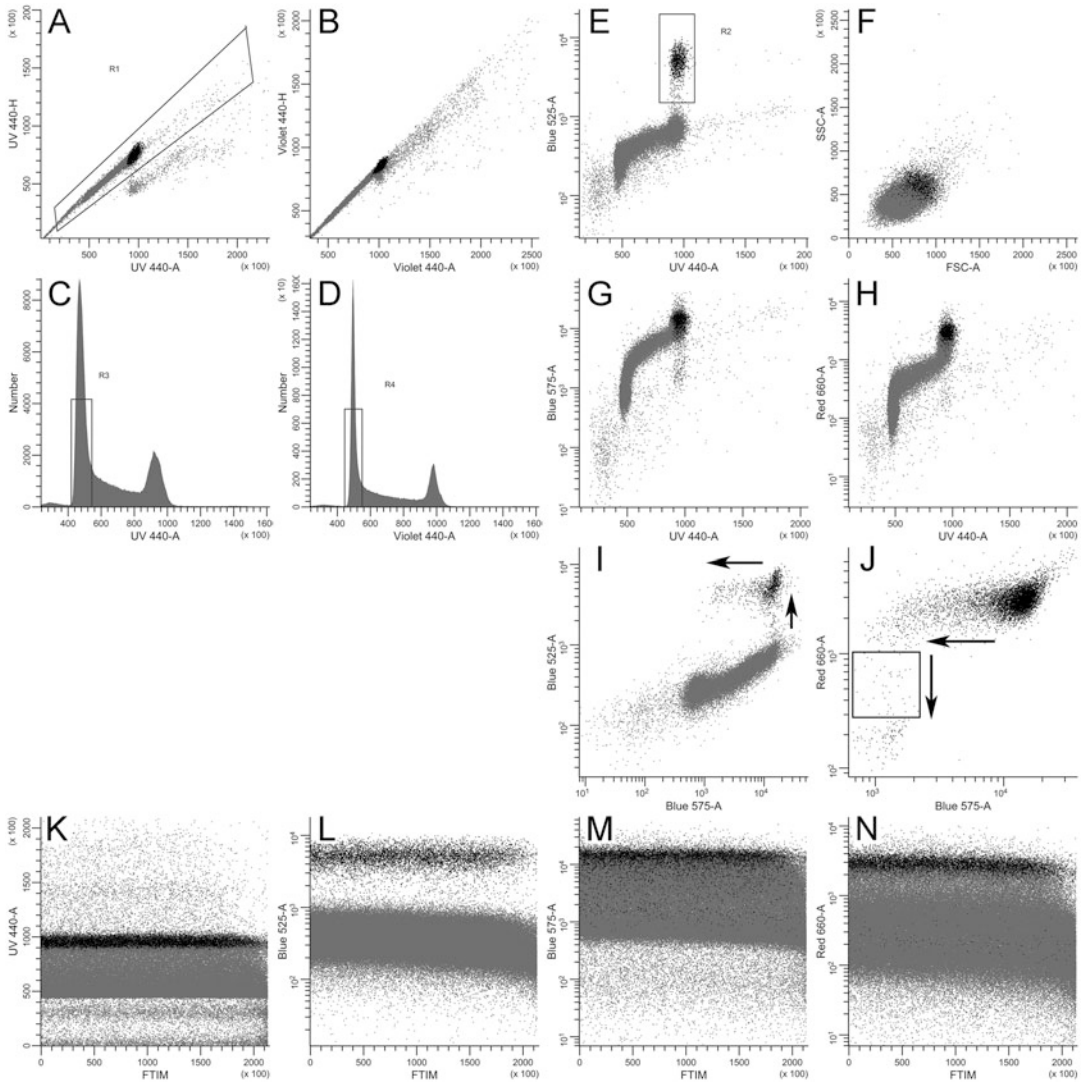

Fig. 6 Data acquisition monitors. MOLT-4 cells stained for DNA (DAPI), PHH3 (A488), cyclin A2 (PE), and cyclin B1 (A647). DAPI was detected with a 440 bandpass (BP) filter, PHH3 with a 525 BP filter, cyclin A2 with a 575 BP filter, and cyclin B1 with a 660 BP filter

vessel or the collection test tube (prior to counting) in a sufficient quantity (generally, 0.125–1%) to inhibit changes in the epitope. After addition of formaldehyde, the protocol is the same as what follows under Subheading 3.2.

3.2 Fixation

1. Move to cold room. All the lab procedures after cells are removed from the incubator and counted are in a cold room at 4 °C. Pipettors, pipet tips, PBS, PBS-BSA reside at 4 °C in the cold room (*see* **Note 19**).

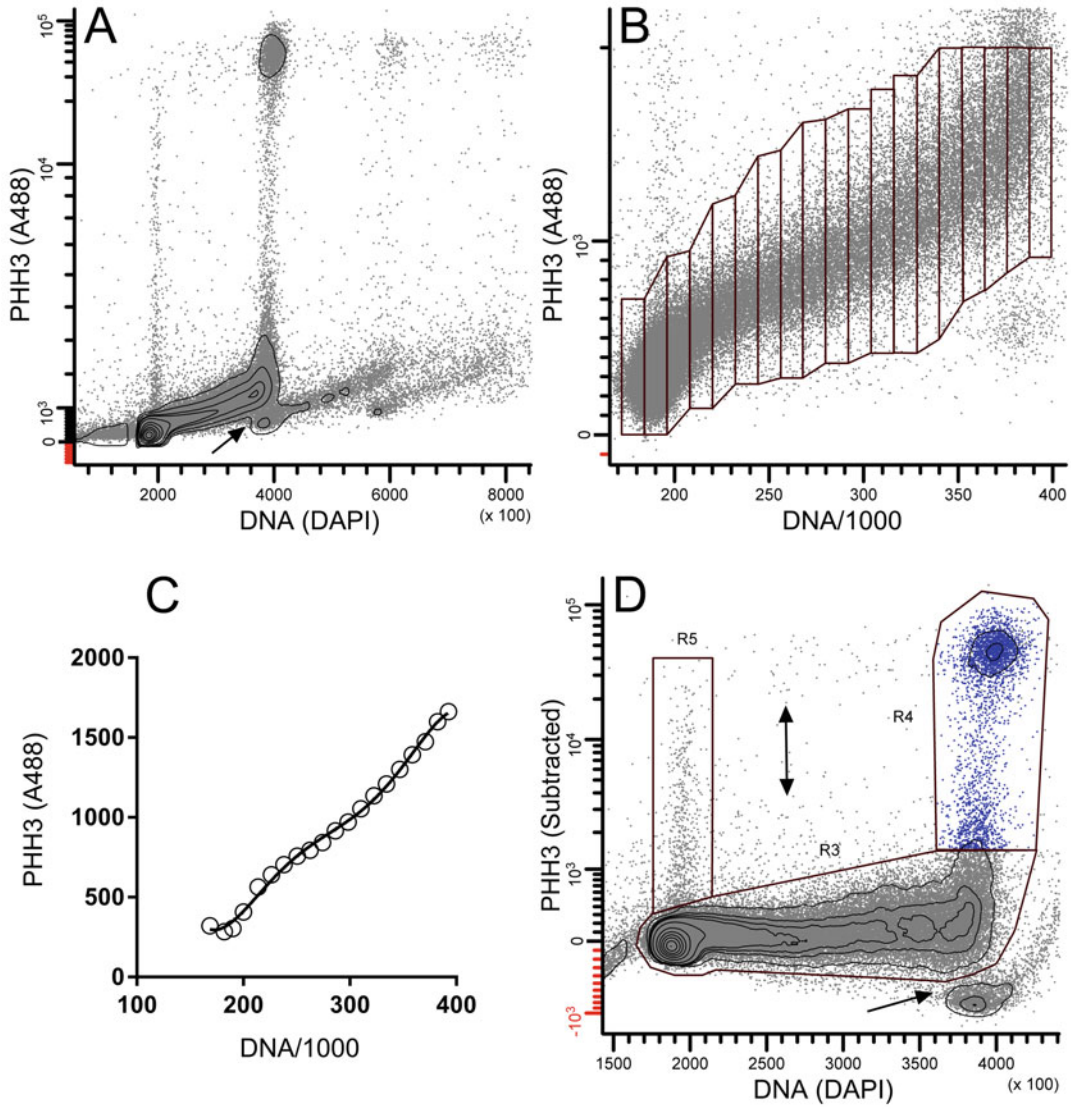

Fig. 7 Analytical step one. Doublet discrimination, orthogonalization, setting mitotic, and G1nb regions. See the text for details. Data for Figs. 7, 8, 9, 10, 11, 12, 13, 14 and 16 are for K562 cells

2. Pellet (centrifuge for 30 s to 1 min) and then wash with 1 mL of PBS. Resuspend in 50 μL of PBS (*see* **Note 20**).
3. Add 450 μL of MeOH (stored at −20 °C). At this point samples can be stored at −20 to −80 °C (*see* **Note 21**).

3.3 Staining

1. Centrifuge cells from fixative and aspirate supernatant. Wash cells twice with 1 mL of PBS and then wash once with 0.5 mL of PBS-BSA. The second, PBS-BSA wash is to begin the blocking process.

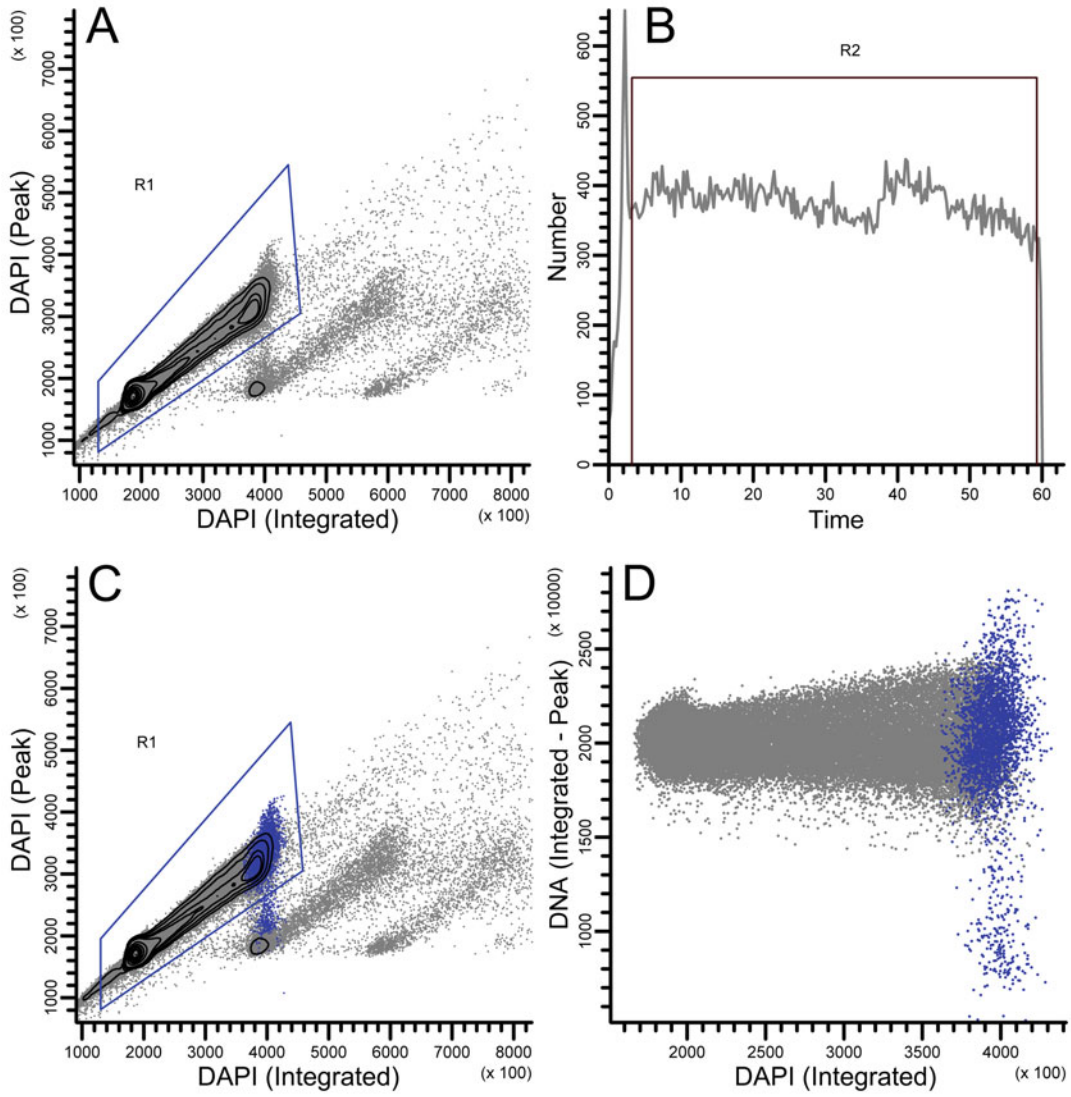

Fig. 8 Analytical step two. Traditional doublet discrimination (**a**), setting a region to restrict analysis to stable events (**b**), visualization of all mitotic events (**c**), orthogonalization of mitotic DNA-peak data (**d**)

2. Resuspend pellet in 50 μL of PBS-BSA containing 0.125 μg anti-cyclin A2-PE, 0.06 μg anti-cyclin B1-A647, and 0.0125 μg anti-phospho-S10-histone H3-A488 (*see* **Note 22**).
3. Incubate at 37 °C for 90 min (*see* **Note 23**).
4. Cool to 4 °C and then wash three times at 15 min per wash (in cold room) with 0.5 mL of PBS-BSA (*see* **Note 24**).
5. Resuspend in 0.5 mL of DAPI solution.

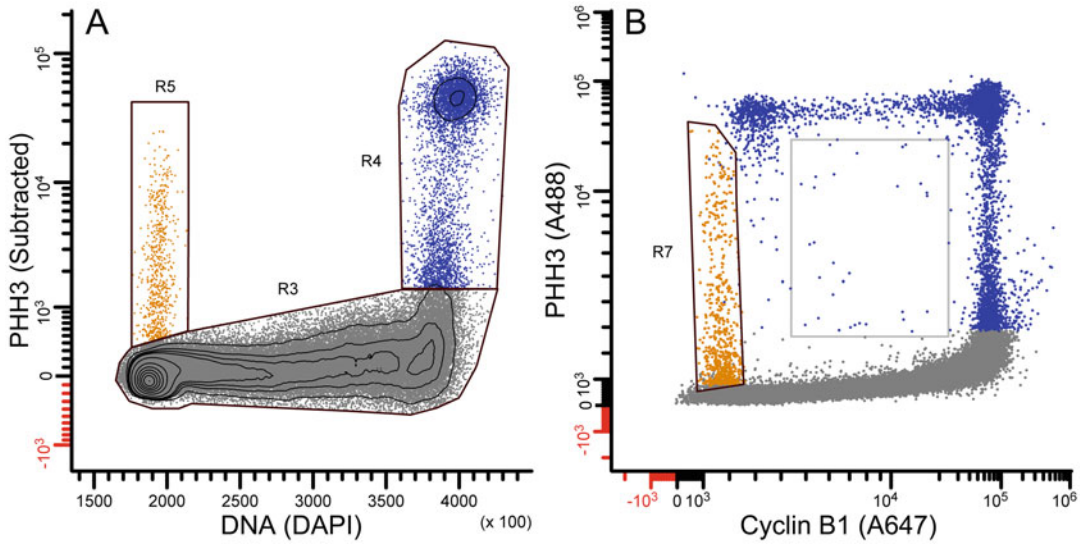

Fig. 9 Analytical step three. Tuning the G1nb gate (R5 AND R7). Note: unclassified events (*gray box*)

3.4 Measurement

1. Use any flow cytometer with violet, blue, green/yellow, and red lasers or alternatively, violet, blue, and red lasers (*see* Subheading 2.4, **item 7**).
2. Figure 6 shows the information that we like to see on the cytometer interface during data acquisition. The key elements are: (1) each parameter is on scale with a minimum of events lost to signals that are below threshold or saturated, (2) signature expression patterns are recognizable, and (3) the parameter modes are stable throughout the run.
   (a) Panels a and b show doublet discriminators based on the integrated (area) and peak (height) signals of DAPI, excited by a UV (panels a, c) and Violet (panels b, d) lasers (*see* **Note 25**). Panels c and d show histograms of DNA content based on the integrated signals. The elements in these panels that we monitor are the distance between 4C singlets and 4C doublets (panels a, b) and the Coefficient of Variation (CV) of the G1 peaks (from R3, R4 in panels c, d). When present, we find it useful to implement both the UV and Violet lasers. The reasoning can be seen in the example presented here. The distance between singlets and doublets is greater in the UV laser data, and therefore, this data set provides the best doublet discriminator. The G1 CV is smaller in the Violet laser data set, and therefore the Violet laser provides the best cell cycle analysis. In other runs on the same instrument performed at different times, we see conjunction of the distance and CV values, and at various times, either the UV or Violet laser will be optimal,

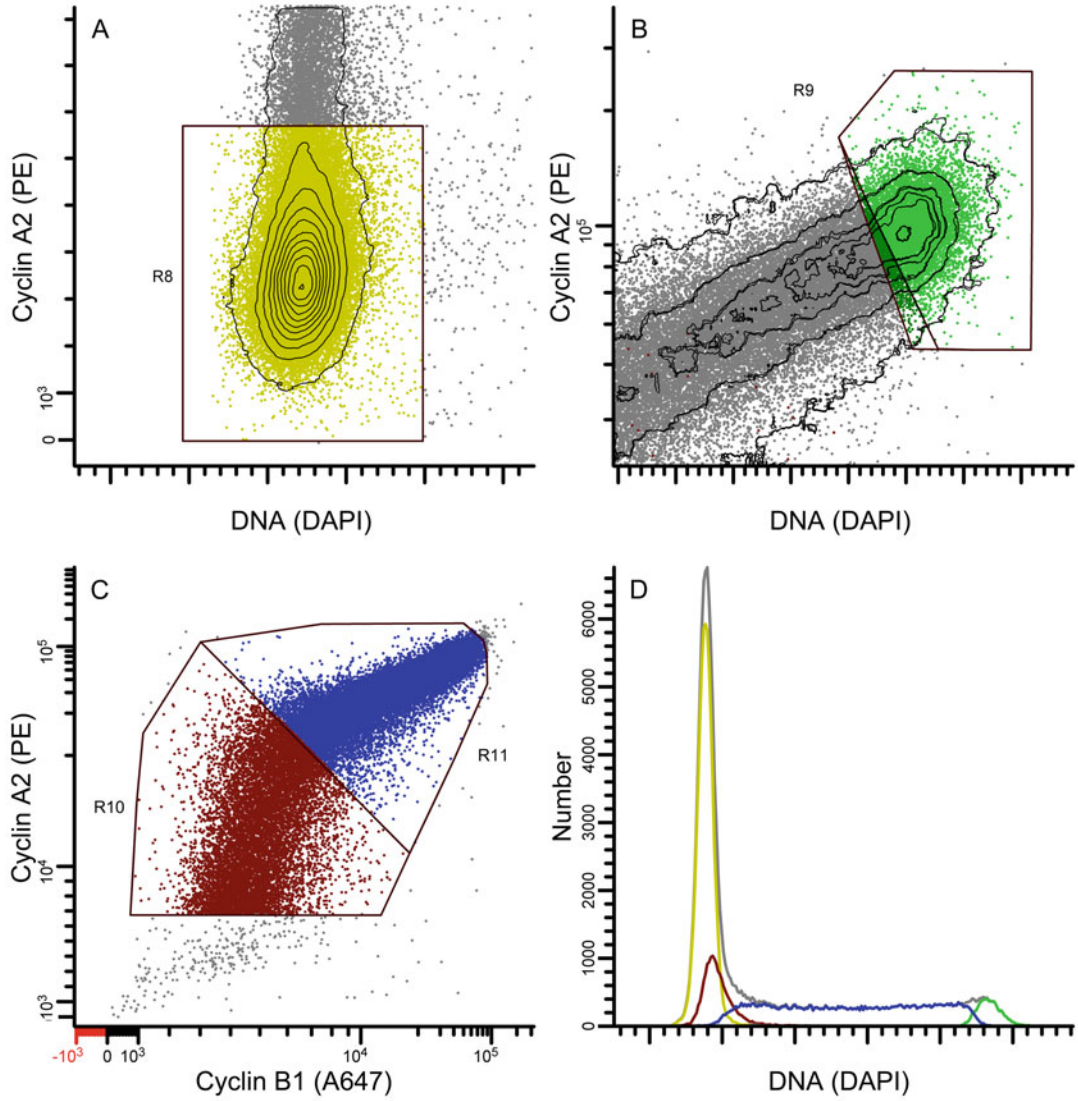

Fig. 10 Analytical step four. Setting regions for G1, G2 (*see* **Note 29**), S1 and S2 (**a**–**c**) and checking the results (**d**). See the text for details

and at other times, there is not enough difference between the two to matter. We do not know why we see this kind of laser-related behavior, but we have observed it often. The regions (R1)—in this case set in panel a, was/is used to gate the remaining panels (b–n). We scale 2C G1 events at 20% of maximum, using the DNA histograms as the guide.

(b) Panels e–j present signature patterns that we monitor. Panel e presents phospho-S10-histone H3 immunofluorescence vs. DNA content. The clearly resolved mitotic cells are color-gated and those colored events are an

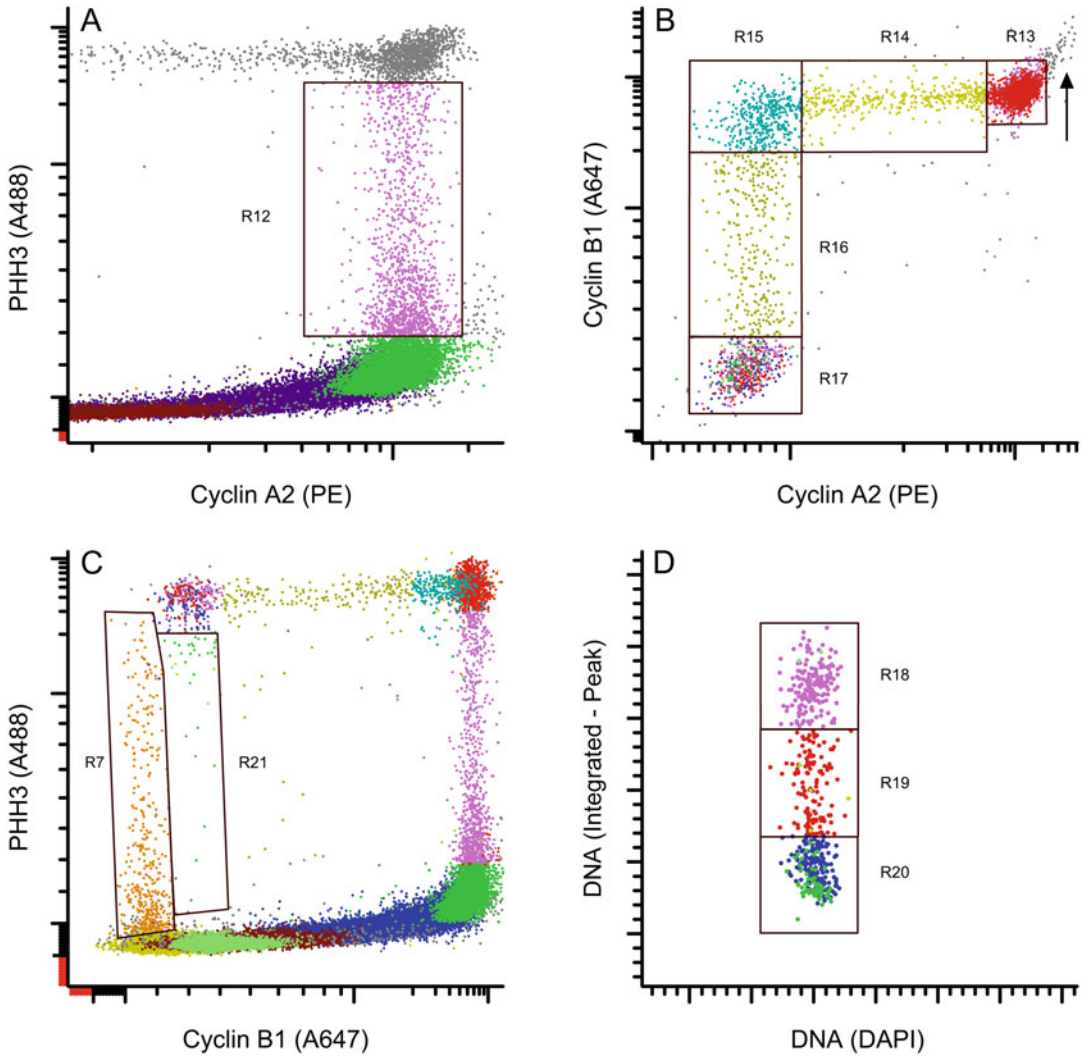

Fig. 11 Analytical step five. Setting the mitotic regions. See the text for details

analytical guide. We expect that they are at the large end of the spectrum of cell sizes, which can be seen in the light scatter (forward vs. right angle, also referred to as FSC vs. SSC) plot (panel f). We expect these events to be both positive and negative for cyclins A2 (panel g) and B1 (panel h). We expect to see rising levels of cyclins A2 and B1 in S phase and G2 (panels g, h) and peak levels of cyclins A2 and B1 in G2 and M (panels g, h, i, j). Finally, we expect to see phospho-S10-histone H3 (PHH3) levels increasing when cyclin A2 levels are peaked and cyclin A2 levels to be decreasing after PHH3 levels are maximal in M phase cells (arrows, panel i), and we expect cyclins A2 and B1 levels to be decreasing in M phase cells at different

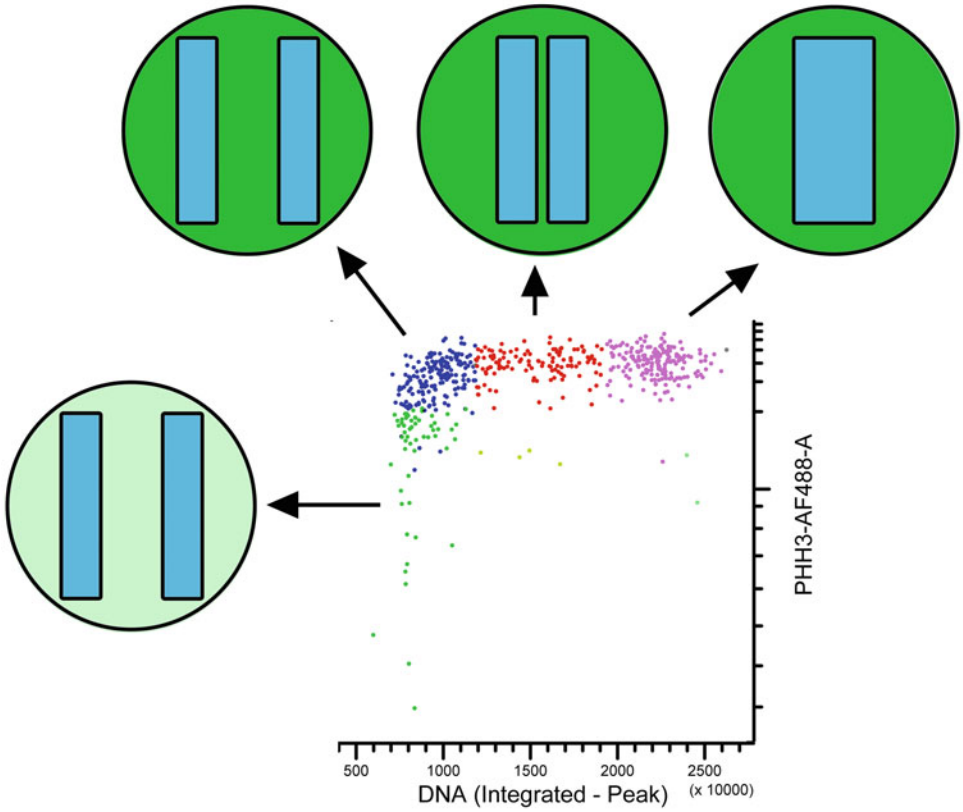

Fig. 12 Parsing LM states. The cell states defined by 4C DNA content, maximum PHH3, and minimum cyclin B1 are separated into three regions, LM2a, LM2b, LM2c, by the DNA content pulse height parameter. LM2a = intact single nuclear region. LM2b = separating chromosome clusters. LM2c = fully separated nuclei. Cells that are actively dephosphorylating PHH3 (*green dots*, LM2d) follow the LM2c state. Cells may divide at either LM2c or LM2d, and perhaps at any level of PHH3 in LM2d. These kinetic arguments are based on some experimentation (BrdU incorporation and label tracking over time and measurement by flow cytometry and LSC analysis) but this area needs further investigation

times, creating a distinct mitotic pattern (arrows, panel j). The plot in panels i is also a check on the compensation between A488 and PE.

(c) We plot each integrated fluorescence parameter versus time to determine the stability of the run. In Fig. 6, we use FTIM, a "calculated" parameter in WinList (Verity Software House, Topsham, ME), which is just the position of each event in the list mode file. This is a fast and easy display of the data over the entire span of the *X* axis, and a surrogate for time under most normal circumstances. It is a common practice to load a sample on a flow cytometer, initiate sample flow and monitor output without collecting data until the sample flow rate stabilizes, then initiate data acquisition. We do that too, but it

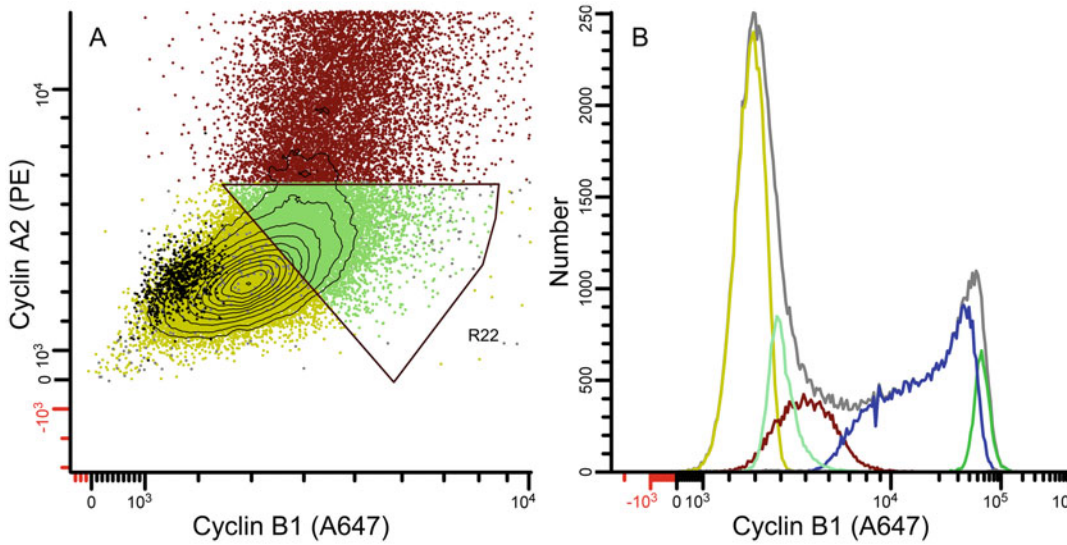

Fig. 13 Analytical step six. This step did not have to be saved for last and could have been done after step three (Fig. 9). (**a**) Setting the region to bisect the cyclin A2 vs. cyclin B1 bivariate G1 data at a right angle to the direction of the data and at the G1–S phase boundary, previously defined at step four. (**b**) Checking the results. G1b is intermediate in cyclin B1 levels, between G1a and S1. Cyclin B1 peaks in G2, as shown (*green Gaussian peak* at *right*). G1nb events are *colored black* here for clarity (**a**), and are two infrequent to be seen in **b**

is important to collect time as a parameter to evaluate the quality of the run. For whatever reason, the signals often decrease over time. This is particularly evident during long runs and for dim signals. If it appears severe, we re-run, given enough sample. In the example here, DNA content (panel k) appears stable while the immunofluorescence parameters (panels l, m, and o) do not. The level of decrease is not severe and this is dealt with during analysis (*see* Subheading 3.5, **step 3**).

3. How many events to acquire? A rational approach (acquiring 10,000 events because everyone else does is not rational) is to set regions around populations of interest and collect at least 400 events, if possible. The standard deviation for counting an event in a region is the square root of the count. Twenty divided by 400 is 0.05, which is a CV of 5% for counting-specific events with precision. In biology, a CV of 5% is a good measurement. It is not always this simple. If the data are spread out such that CV of the data distribution within the sample is high, then more events may be necessary to observe the distribution. In our examples here, the critical region of interest is generally the mitotic cell gate (panel e); however, if we want shape and resolution to panel j, then 400 total events are not enough. When only 400 mitotic events are collected in this example, only three events fall into the region designated

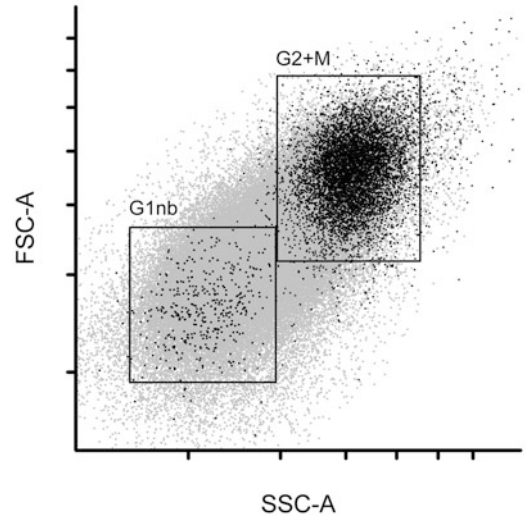

Fig. 14 Checking light scatters. Since we have the smallest, G1nb (new born) cells and the largest, M cells classified by color, we can check the usefulness of light scatter. The figure shows that the distribution of all other cells (*gray*) spans the dataspace of G1nb at the low end and G2 + M at the high end for both forward and right angle light scatters, which means they can be used interchangeably for this cell population as surrogate measures of cell size, although in our experience, SSC is better (see the text)

by the box in panel j (which represents late mitotic cells after metaphase). If we collect all that we can, then 108 events are captured in the late mitotic region. Therefore, this sample was limited by the sample (we collected the entire sample). It is still sufficient, but does not meet our desired metric.

4. Perform analysis offline.

3.5 Analysis

1. Figures 7, 8, 9, 10, 11, 12, 13, and 14 illustrate one of many analyses that can be performed. There are three main information units that can be obtained. The first is the percentages of cells in compartments, phases, or states. The second is the intensity of expression of the epitopes in any state, and the third is the entire cell cycle-related expression profile of those epitopes. To obtain expression profiles, one needs to be able to trace cell cycle progression from compartment to compartment in a forward progression from cell birth to division in an unambiguous manner. It is slightly more complex than that and fully explained in two publications [11, 12]. Here, we will go through the process of creating sequential compartments from the beginning to the end.
2. Figure 7 illustrates nonlinear subtraction of one parameter from another to obtain an improved ability to draw a first set of regions. There are two gates set before this, but presenting

the logic in a slightly reverse order will make sense. Figure 7a is an ungated HyperLog plot of PHH3 vs. DNA. PHH3 is a mitotic marker and these cells are well resolved from G2 cells, although the transition between them is a continuum. The plot provides excellent doublet discrimination when the cytometer is well tuned (singlets through quadruplets can be detected). The stemline G2 cells and 4C or 2C doublet cells are separated (arrow). Figure 7b is a zoomed plot of the interphase illustrating the nonlinear increase in PHH3 from G1 through G2. A region array was generated over the data and the medians calculated for both parameters. Figure 7c is the plot of the median values and a curve calculated from a 5th order polynomial fit to the data by nonlinear regression (GraphPad Prism 7.00.14). Figure 7d shows a HyperLog plot of PHH3 minus the median PHH3 value calculated from the fitted equation. This plot provides better doublet/4C separation (arrow) than the untransformed plot (7a), which can be observed from the contour lines (set at 98% of the data), and additionally, the separation of the regions is easier to draw on ~orthogonal data (*see* **Note 26**). The regions are: R3 = interphase cells without doublets; R4 = mitotic cells, and R5 = freshly divided G1 cells with residual levels of PHH3. Cells in this latter state (G1nb) are actively dephosphorylating histone H3 at S10 (*see* **Note 27**). From this point on, all cells of the 2C → 4C cell cycle can be addressed using Boolean logic as (R3 OR R4 OR R5). The events in the R4 gate have been "color-evented" blue. There are a small number of unexplained events (double arrow, Fig. 7d). Two ideas are that these are apoptotic cells arising from states with high levels of PHH3 (mitotic cells) or cells with aberrant histone H3 phosphorylation or dephosphorylation.

3. Figure 8a re-illustrates, the typical doublet discriminator based on the integrated and peak height DNA content data. The region R1 was set on the singlet 2C → 4C cells, and this region was used to gate the data file and produce a plot of cell number vs. time (Fig. 8b). This can be used as demonstrated in Fig. 6 to evaluate anomalies in the run. For this data set, the plots of parameters vs. time (Fig. 6k–n) supported a stable run throughout, but suggested a surge at the beginning, which was removed from the analysis by gating on region R2. Thus, the all-inclusive cell gate becomes R2 AND (R3 OR R4 OR R5). Figure 8c shows the same plot as Fig. 8a, but the R4 (mitotic) events are highlight by color. A significant number of events fall outside the singlet gate. These are cytokinetic (CK) cells [83], and this is the reason for preferring a doublet discrimination on PHH3 vs. DNA when the data resolution will permit (*see* **Note 28**). We used parameter subtraction again

in Fig. 8d to subtract the DNA peak from the integrated signal, which orthogonalizes the data. The purpose was to provide eventual orthogonal region setting ability for the mitotic cells.

4. In Fig. 9, we define the G1nb population. The properties of these cells are small size, 2C DNA content, elevated but less than mitotic levels of PHH3, and no expression of cyclins A2 or B1. We have set a primary region in Fig. 7 (R5) that captures DNA content and PHH3. In Fig. 9a, PHH3 vs. DNA is shown again, gated on R2 AND (R3 OR R4 OR R5). Figure 9b plots PHH3 vs. cyclin B1. Here, there is an advantage that the autofluorescence plus nonspecific immunofluorescence of late mitotic is higher (~2×) than early G1 cells (both are negative for cyclin B1 expression). This provides an offset, based on cell size, between mitotic and cytokinetic cells and newly divided cells. A second, reinforcing region (R7) was then set to fully define G1nb cells. The uncertain, arbitrary bottom boundaries can be trimmed after color-eventing (R5 AND R7). If R5 is set too deep into the negative main body of the G1 cells, then color evented cyclin B1-positive cells will appear on the plot of PHH3 vs. cyclin B1. Cyclin B1 begins expression in late G1 [40, 84]. Once again, there are unexplained events (gray square in Fig. 9b). The events to the left of the gray square that are not within the R7 region could be cells that have not divided but are in the process of histone H3 dephosphorylation at S10, and thus are hypothetically explained.

5. G1 cells excluding G1nb are defined by 2C DNA content and absence of cyclin A2 expression (Fig. 10a). As mentioned earlier, the boundaries of these gates on the continuum side are arbitrary. There is a region within which cells that are either positive or negative but indistinguishable, and it is within this region that the boundaries are set. We use contours as guides to help us achieve some level of objectivity, but overall setting these regions is a learned art, relying on experience and intuition. The G2 region (R9) is set the same way on the other end of the same plot (Fig. 10b). This plot has been gated on R2 AND R3. The boundaries of S phase were set as shown in Fig. 10c on a plot of Cyclin A2 vs. Cyclin B1, gated on R2 AND R3 AND NOT (R8 OR R9). Because there is a sharp transition (a period of time in which cyclin B1 is expressed at a low rate and cyclin A2 is expressed at high rate vs. a period of time in which both are expressed at high rates), S phase was partitioned into two parts, S1 and S2 (R10, R11). Again, this is an arbitrary decision, but based on objective changes in the biochemistry underlying the data pattern. These choices are checked by plotting the individual cell cycle phases/states/compartments, color coded by their DNA content values (Fig. 10d). The progression of G1 → S1 → S2 → G2 as a

function of DNA and the Gaussian nature of the phase/state DNA contents is supportive (*see* **Note 29**).

6. Figure 11 shows the definition of mitotic states. First, a plot of PHH3 vs. cyclin A2 was used to define P1, early prophase cells (R12) in which the cyclin levels are maximum and the levels of PHH3 are rising. The next mitotic populations were set in sequence using a plot of cyclin B1 vs. cyclin A2 gated on R2 AND R4 with the regions R13, R14, R15, R16, R17 containing the states/compartments P1 + P2 (R13), PM (R14), M (R15), LM1 (R16), LM2a + LM2b + LM2c + LM2d (R17). LM2a, 2b, and 2c cells are definitively defined by R18–R20. P2 cells are defined by (R4 AND R13 AND NOT R12), and LM2a cells are defined by (R4 AND R17 AND NOT (R19 OR R20). Conceptually, a cell transits this data space along a unidirectional path R12 → (R13 AND NOT R12) → R14 → R15 → R16 → (R17 AND R18) → (R17 AND R19) → (R17 AND R20) → (R20 AND R21) → R7, that is—P1 → P2 → PM → M → LM1 → LM2a → LM2b → LM2c → LM2d → G1nb. This sequence correlates with the mitotic stages prophase (P1, P2), prometaphase (PM), metaphase (M, LM1, LM2a), telophase (LM2a, LM2b, LM2c, LM2d), and cytokinesis (LM2c, LM2d). Table 3 simplifies these relationships. In Fig. 11b, the arrow points to cells (gray) leaking through the R2 AND R4 gate which are not actually G2 cells, suggesting that our gating logic is not exact. However, since they are not color evented, they will not be counted in the final analysis. We think these are damaged G2

Table 3
Mitotic population properties

DNA(A)	DNA(H)	CycA2	CyB1	PHH3	Stage	State	Logic	APC/C	AKB	Cdk1	Cdk2
Max	Max	Max	Max	**Inc**	early prophase	P1	R12	Inactive	Active	Active	Active
Max	Max	Max	Max	**Max**	prophase	P2	R13 ! R12	Inactive	Active	Active	Active
Max	Max	**Dec**	Max	Max	prometaphase	PM	R14	Active	Active	Active	Dec
Max	Max	**Min**	Max	Max	metaphase*	M	R15	Active	Active	Active	Inactive
Max	Max	Min	**Dec**	Max	telophase	LM1	R16	Active	Active	Dec	Inactive
Max	Max	Min	**Min**	Max	telophase	LM2a	R17& R18	Active	Active	Inactive	Inactive
Max	**Mid**	Min	Min	Max	cytokinetic	LM2b	R17& R19	Active	Active	Inactive	Inactive
Max	**Min**	Min	Min	Max	cytokinetic	LM2c	R17& R20!R21	Active	Active	Inactive	Inactive
Max	Min	Min	Min	**Dec**	cytokinetic	LM2d	R17&R20&R21	Active	Inactive	Inactive	Inactive

All gates include AND R2 AND R4. The defining differences in populations are bolded. The activity states of APC/C and AKB are inferred from the direct measure of substrate levels (cyclins A2 and B1, and PHH3, respectively). The activity of Cdk1 and Cdk2 is inferred from the levels of the main cyclin binding partners

The stage and state correlations have been verified by cell sorting and microscopy, inhibitor treatments, and laser scanning cytometry. The correlation is not perfect. For example, in one study, PM = 66% prometaphase and 22% metaphase, and 12% other (prophase and telophase) [16]. The imperfection is a combination of methodology and biology. Because of this uncertainty, these biochemical states should not be equated with the stages of mitosis, but thought of as biochemically defined cell states. For a review/commentary piece on mitotic states and stages, *see* Rieder and Pines [21]

Max maximum, *Min* minimum, *Inc.* increasing, *Dec* decreasing, *Logic* Boolean gating logic (! = NOT)

cells that remain in G2 for an extended period and overexpress cyclins A2 and B1, but this remains to be proven. The LM2a and LM2b states have changed since we published this chapter in the first edition of this book. Previously, LM2a was defined as negative for cyclins A2 and B1 and maximal for PHH3, while LM2b was defined similarly but with positive PHH3 levels less than maximum. LM2b is now defined as single cells with maximum PHH3 and nuclei that are separating. LM2c cells have max PHH3 and clearly separated nuclei (*see* Fig. 12 for pictoral description). LM2d cells are defined by decreasing PHH3 (less than maximum) and separated nuclei. Whether morphological parameters like separated nuclei are consonant parameters remains a subject for investigation (*see* **Note 30**).

7. There is one additional compartment left to include. An interphase (R3) plot of cyclins A2 and B1, zoomed to highlight G1, was used to define late G1 cells in which cyclin B1 is beginning expression but cyclin A2 is not (Fig. 13a). Although this feature would not be obvious in the data set presented here, we know to look for this from previous work [40, 84]. We use the presence of the G1nb population (black dots) and the center of the cyclin A2 negative G1 cells as guides. Although definition of this population needs further study and better markers, it is an important population in that it marks the shutdown of the Anaphase Promoting Complex/Cyclosome (APC/C), which helps to keep early G1 cells in an anti-mitotic state. We checked the logic in a single-parameter histogram (Fig. 13b) with color-coded plots of the now G1a (yellow), G1b (light green), S1 (red), S2 (blue), and G2 (dark green). The progression for G1 is G1nb → G1a → G1b. The logic is G1nb = R5 AND R7; G1a = (R3 AND R8) AND NOT ((R5 AND R7) OR R22).
8. As a final check on the quality of the analysis, Fig. 14 is a plot of Forward and Right Angle light scatter (FSC and SSC), both of which are a function of size for cells with homogenous granularity. The G1nb cells, which have just recently divided at the time of fixation, are the population with the smallest cell size and G2 + M phase cells are the largest. The plot shows that these two populations are at the opposite ends of the light scatter plot, which supports that the cells are correctly identified. For these data, the ratios of G2 + M:G1 are 1.7 for FSC and 1.9 for SSC, justifying our preference for side scatter as a measure of size for homogenous populations on most flow cytometers.
9. In the previous writing of this chapter [1], we employed an additional transform of the cyclin data, illustrated in Fig. 15. In that work, we performed a linear subtraction of the

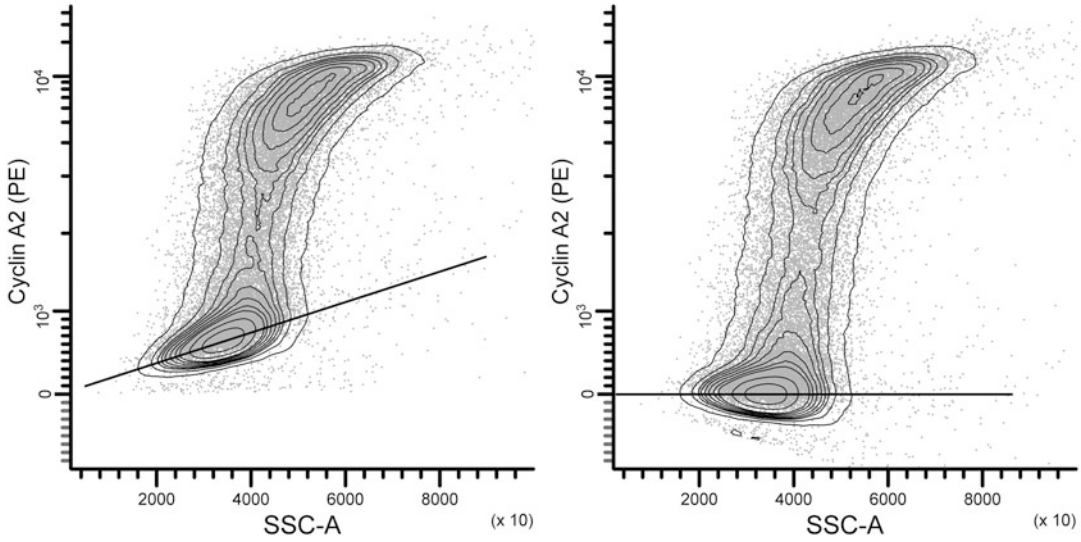

Fig. 15 Subtracting background. The subtraction of a function from a data set as illustrated in Figs. 1 and 2 can be used to subtract background fluorescence (or size-related expression). This is illustrated here for interphase MOLT-4 cells. Cyclin A2 is not expressed in G1. Thus, a linear function, immunofluorescence = slope × light scatter + intercept (**a**), can be subtracted from the immunofluorescence for the G1 cluster for cyclin A2 vs. right angle light scatter (**b**). This has the effect of setting the mean, median, and mode of the G1 cluster close to zero on a HyperLog or Biexponential plot. This increases the resolution for specific immunofluorescence for the largest cells and permits convenient reading of expression from the *Y* axis. In this example, cyclin A2 is expressed about 10,000-fold from the beginning of S to the end of G2

background fluorescence from populations that are biologically negative. This subtraction does two things. First, it increases the resolving power by increasing the distance between the most positive and negative large cells. Second, the expression levels can conveniently be read from the axis with negative expression defined as zero units. Thus, in the figure, cyclin A2 is expressed from 1 to ~10,000 units over the course of interphase. Since, we could illustrate this analytic feature with our previous MOLT-4 analysis, we did not burden the current K562 analysis with that additional transform.

10. It is useful to plot all of the cell cycle compartments defined by the analysis illustrated in Figs. 7, 8, 9, 10, 11, 12, 13, and 14 in one 3D color-evented plot (Fig. 16). This figure visually shows the data path for a cell conceptually moving from G1nb to LM2c or LM2d prior to cell division. Figure 17a is a similar image, originally presented in the first edition of this chapter [1], and presents a snapshot of the analysis for the data shown in Fig. 6. The quantitative results for Fig. 17a are shown in Fig. 17b and listed in Table 4. The accuracy is remarkable considering that the frequencies span nearly three orders of magnitude. The reason for this may be that the use of many constraints (6 parameters (DNA content-integral, DNA

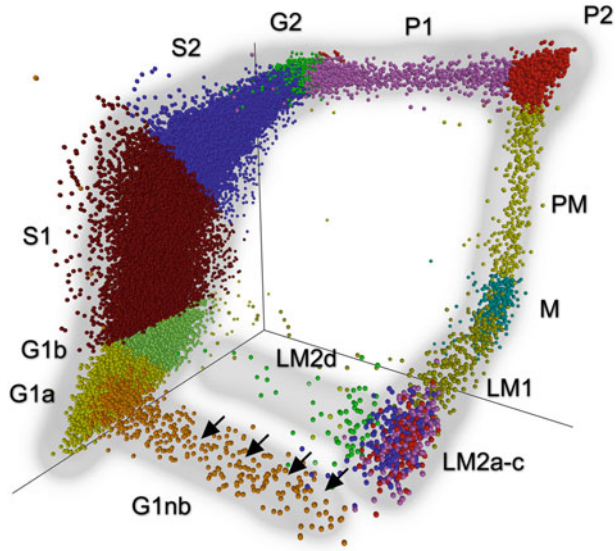

Fig. 16 The enchilada. A three-dimensional plot for cyclin A2 (*Z* axis), cyclin B1 (*Y* axis), and PHH3 (*X* axis), color coded to display assignment of clusters and transitions (cell states) for the K562 cells shown in Figs. 7, 8, 9, 10, 11, 12, 13, 14.

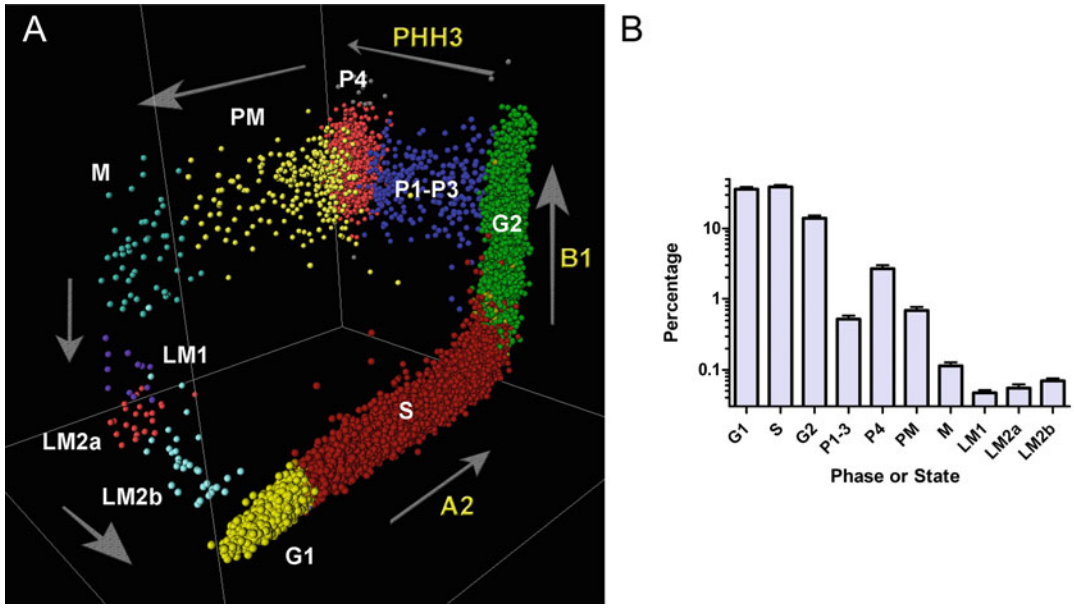

Fig. 17 MOLT4 data. This is a composite of two figures from the previous version of this chapter. The data are for MOLT-4 cells (Figs. 6 and 14). Changes to the nomenclature are: P1–P3 is now P1 and P4 is now P2. The reason for this is to simplify. LM2a is now divided into LM2a and LM2b with LM2c replacing the former LM2b. These latter changes were necessary because of the increased information using DNA peak height to quantify the fractions of late mitotic cells (LM) that have a single or double nucleus. In the analysis shown in Fig. 16, G1 has been divided now into three states: G1nb, G1a, and G1b. This was possible because of the increased clarity imparted by increased cell numbers and better resolution between background immunofluorescence of small and large cells. (**a**) 3D plot. (**b**) Quantification of each cell state/compartment demonstrating excellent statistics (*see* Table 4 for values)

Table 4
Statistics

Phase	Mean (%)	Std Dev (%)	CV (%)
G1	36	5.1	14
S	39	4.8	12
G2	14	2.3	16
P1–3	0.53	0.11	21
P4	3	0.56	21
PM	0.68	0.15	22
M	0.11	0.023	20
LM1	0.05	0.007	15
LM2a	0.05	0.012	22
LM2b	0.07	0.011	16

content-pulse height, SSC, cyclin A2, cyclin B1, PHH3), 21 regions, and 29 Gates) restricts the data space such that any events fulfilling the criteria are highly significant.

Aside from a difference in cell lines and technicians, the main differences between the data sets (MOLT-4, K562) are: (1) data acquisition on a new, highly tuned instrument (as opposed to an instrument that passes specifications but is used in daily operations within a core facility), and (2) the addition of a yellow-green laser without need for any compensation. We do not know (have not made a serious study) that either of these factors produces better quality data, but it seems likely. The main differences are noted as stability of the runs and resolution of doublets, telophase/CK cells, and the LM and G1nb states. The size of the laser beams used in the two respective instruments may have some effect on the resolving power.

11. Although we are not showing it here, the frequency of cells for each region (state) can be plotted on an X axis, and the corresponding levels of each marker within each state plotted on the Y axis to obtain the continuous expression of the marker as a function of time in the cell cycle. The frequency data needs to be corrected for the aging of the population [85], but even without the correction, this calculated expression profile is likely to be more accurate than that which can be achieved in the more standard, non-quantitative practice of synchronizing cells, releasing them, then measuring total expression levels as a function of time by western blot. The methods for performing this "expression profile extraction" have been published [11, 12].

4 Notes

1. Photographic film exposed to ^{3}H–thymidine labeled cells led to the modern cell cycle model with four phases—Gap1 (G_1), S (synthesis), Gap2 (G_2), and M.
2. At the time, the two sources of immunological probes were anti-sera and relatively new monoclonal antibodies. *See* Jacobberger et al. [6] for data relevant to the problems with anti-sera. The problems were: unknown levels of immunoglobulin in pre-immune serum, unknown, low fractions of specific antibody in immune serum, and high nonspecific binding to cells fixed and permeabilized with organic solvents.
3. Compartments, phases, stages, and states are used interchangeably in the literature. We will generally follow that pattern and use them interchangeably; however, multiparametric cell cycle analysis has a need to more precisely define the compartments defined in our parameter-based models. We will leave that problem for another time, but we will employ a not-too-strict hierarchy in terminology. "Compartment" is the most general term, used for any well-defined and measurable class of cells within a dynamic system. "Phase" will be used for the most commonly accepted terms to define the ordered periods within the mammalian cell cycle (interphase, G1, S, G2, and M). "Stage" will be restricted to morphologically defined mitotic classes (prophase, prometaphase, metaphase, telophase), and "state" will refer cell classes that are based on dominant enzyme/molecular complex activities. For example, in this chapter, we will define two states in S phase, imaginatively termed S1 and S2 based on the rates of accumulation of cyclin A2 relative to cyclin B1. We will also use some terms that in our view have no broader classification: e.g., G0, mitosis, and cytokinetic cells—the first defined by an absence of a cell cycle program and the second defined by a process. However, the "phases" M and CK are synonomous with mitosis and cytokinesis.
4. Cyclin = class of cell cycle regulating genes/proteins with cyclins D1, D2, D3, E1, E2, A1, A2, B1, B2, and B3 being the most studied mammalian cyclins.
5. That is, we did not have a hypothesis, but we did have an idea—not very original or profound, but it was based on the successful work of Darzynkiewicz and colleagues with acridine orange and our success using monoclonal antibodies reactive with intracellular antigens. The drive was to understand the measurement system through exploration rather than deep thinking and hypothesis creation—a kind of bottom-up approach

rather than top-down, and the idea was the notion that more (parameters) is better.

6. That is, measuring the G1, S, G2 + M distribution of any parameter produces expression information about that parameter and therefore at least one "unit" of information.
7. From this point, we will use "epitopes" to refer to anything measured as a function of DNA content because our most common mode of parameter detection is by antibody.
8. Unscheduled expression of cyclins has been described [14] and is defined as patterns of expression wherein the cyclin is expressed higher than it would be in normal cells relative to the next most earliest expression state. For example, high expression of cyclin B1 in G_1 would be "unscheduled." Villiard et al. went to great lengths to show that cyclin B1 was expressed in G_1 cells of human T-cell lymphoma lines but either not expressed or expressed at a lower level in normal human T cells [84]. These levels were small but significant. We have measured cyclin B1 in G_1 in all cells that we have examined with GNS1-A647. We have not observed what we would consider large variation in cyclin A2 and B1 expression patterns in human solid tumor cell lines, hTert-immortalized human cell lines, K562, MOLT-4, and normal human T cells. However, we have not tested the cell lines displaying unscheduled expression presented by Gong et al. [14] for cyclin B1. The features of the MOLT-4 patterns shown here describe the cyclin A2 pattern relatively universally in our experience. For cyclin B1, we see essentially two patterns, one with higher G_1 expression coupled with larger variance in the early S phase cells in one pattern relative to the other. The first pattern is typified by K562 cells and normal T cells, and the second pattern is typified by MOLT-4 cells. For some examples of the magnitude of expression differences for cyclin B1 for interphase, *see* Frisa and Jacobberger [38]. For both of these proteins, there is variation in expression to be sure, but these features: (1) cyclin B1 expression starting before cyclin A2, (2) ~linear synthesis of cyclin A2 and nonlinear synthesis of cyclin B1, and (3) degradation of cyclin B1 after cyclin A2, seems to be universal in our experience. In view of our experience, the unscheduled expression of cyclin B1 appears to be largely confined to the differing overall levels of expression and different levels of expression in G_1 (and perhaps differing fractions of cells expressing at the higher levels) rather than different patterns of expression. We have not explored unscheduled expression under conditions of growth imbalance, which has been studied by Gong et al. [15] for MOLT-4 cells. In this case, each of the cyclins D3, E, A, and B1 displayed unscheduled expression as defined above in cultures synchronized with mimosine or double thymidine block.

The abnormalities in cyclin A expression were especially striking after mimosine treatment.

9. This is based on an expected offset for the onset of synthesis of both proteins. In this example, we have ignored possible additional mitotic states based on possible differential degradation of the two proteins.
10. Single positive and negative cytometry histograms may represent quantitative data, but they do not constitute a quantitative analysis.
11. With the advent of gene editing (e.g., Crispr/Cas9), settling for this faulty approach may soon be a thing of the past. It will be increasingly standard practice to create negative cell line controls from parental positive cell lines for validation. These same controls can serve as assay staining standards after the assay is completely developed. For many proteins/epitopes, such cells are currently commercially available for a reasonable cost (www.horizondiscovery.com).
12. The total 4C → 8C cycling population for the culture represented by the data set used in Fig. 6 was 0.7%, and the contaminating fraction of 4C G1 and early S phase cells was ~2% of the stem line G2 + M fraction.
13. For MOLT-4 cells, DSMZ suggests 20% fetal bovine serum. These cells are derived from a leukemia and are not very sensitive to serum concentration and grow well in 10% FBS.
14. First, no one fixes cells with paraformaldehyde, which is an insoluble polymer of formaldehyde. For detailed discussions, search the Purdue University Cytometry Laboratories (PUCL) web site (http://www.cyto.purdue.edu/) on paraformaldehyde. Second, this product comes sealed in glass under nitrogen. Third, the reason to use this high-quality product is that it is supplied at a known concentration (formaldehyde produced from hydrolyzed paraformaldehyde produces a product with an unknown concentration); also, the "ultrapurity" helps to ensure that the least "autofluorescence" is induced in fixed cells.
15. We have used most of the phospho-S10-histone H3 antibodies (pH 3) from Cell Signaling Technology (CST). The unconjugated rabbit polyclonal (#9701) works very well and provides flexibility for secondary reagents. The same is true for the conjugated versions (#9704, #9708). The mouse monoclonal (clone 6G3) works well but does not appear to be available in a conjugated form (previously, it was). The rabbit polyclonal was available in a biotinylated form, which was very useful when other rabbit antibodies were being used in the assay. The rabbit monoclonal is currently available in biotinylated form (#3642). When using the A488 version with anti-cyclin A2-PE, the

spectral overlap of A488 to PE is problematic if a blue laser is used to excite PE. Despite compensation, this seriously degrades the cyclin A2 signal by increasing variance after compensation. It is useful to minimize this by titering the conjugated form of PHH3 to a minimum acceptable signal and substituting unconjugated antibody to keep the concentration at optimum.

16. We previously obtained the cyclin A2-PE antibody as a gift from Vince Shankey at Beckman Coulter, but now purchase it from the same company. An equivalent cyclin A antibody is available from BD Biosciences (clone BF683). We have compared the two antibodies in unconjugated form and they perform equally well. We obtained the GNS1 clone in a bulk form and conjugated it ourselves using the Alexa Fluor conjugating kits or the active dye from Thermo Life Sciences/Invitrogen (Carlsbad, CA).
17. We prefer a Fisher Scientific Micro-centrifuge (Model 59A). Ours finally stopped working after 26 years old. As far as we can tell, this model is no longer made. Some are available from used equipment suppliers and eBay.com. Beckman Coulter sells a 22R microfuge and an S241.5 swinging bucket rotor that look like they will work. Any microfuge or larger format table-top centrifuge can be used. The value of the 59A is that it can be set to spin at very low speed in increments of minutes, or manually turned on and off to spin for seconds. The combination of low speed and swing out rotor is that the cells are pelleted gently and are easily resuspended. This helps for cell recovery and reducing clumping, which is an advantage when working with alcohol-fixed cells.
18. Adherent cells can be trypsinized and pipetted to a single-cell suspension without affecting the cell cycle-related distribution of the cyclins. We have performed PAGE and western blotting on cells before and after trypsinization and observed no reason to be concerned about effects of trypsinization (unpublished).
19. The value of a cold room is that MeOH fixed cells stick to plastic surfaces and cold inhibits this. Working in the cold room is ideal (except for human comfort). If one is not available, this can be done working at room temperature or on ice with room temperature equipment.
20. This is for one to two million cells. We generally scale up if we go higher—e.g., ten million cells are resuspended in 250 μL of PBS and fixed (next step) with 2.25 mL of MeOH. We have not investigated what the scaling factor actually is.
21. Fixed cells in MeOH can be stored for years. However, there is loss of reactivity over time. We believe that loss of epitope reactivity and loss of masking come to equilibrium at about

one half the available epitope. For some antigens we have checked, the patterns of expression are the same (e.g., *see* ref. 29). This is further evidence that the epitopes are exposed in an unbiased manner. They can be stored for days to weeks without concern. Storing at −80 °C will retard epitope loss.

22. Cell Signaling Technology does not print the antibody concentration or amount in most data sheets for their products. We phone to get the information. The way we optimize is to determine the antibody to target ratio—the target in this case being the amount of antigen in a positive cell line, averaged over two million cells and the antibody defined in micrograms. The goal is to react the cells and the antibody in the smallest feasible volume (highest concentration). This produces optimal staining in terms of signal-to-noise ratio [46]. When manufacturers sell us antibodies at dilute concentrations, they enforce reaction volumes that are not optimal.
23. A longer staining time (90 min) produces a better result (higher signal-to-noise ratio). For routine purposes, 30 min is sufficient to achieve good results. Nonspecific antibody diffuses into MeOH fixed cells to equilibrium in 5 min. Specific antibody achieves approximate equilibrium staining (reaches an asymptotic cusp) in 15 min [13, 52]. Staining can also be done at 4 °C or room temperature. The reason we stain at 37 °C is that antibodies develop in vivo at body temperature (39 °C for mice and rabbits).
24. Three washes are better than two, but two are sufficient for routine purposes.
25. See the chapter by Peter Rabinovitch or books by Alice Givan or Howard Shapiro for descriptions of how doublet discrimination works [86–88]. Essentially, identify the G1 cells, then set a quadrilateral gate with sufficient width to enclose the G1 cells, widening it out as a function of intensity to ~2× the width of the G1 population at 4C and ~4× at 8C, etc.
26. It is not necessary to orthogonalize the PHH3 vs. DNA data, especially with complex equations. Most investigators would be satisfied with a linear subtraction. However, this transform did improve the analysis and made it easier to set gates, and the data were more orthogonal than a linear subtraction.
27. For the kinetic argument for these properties, *see* ref. 17.
28. If doublets cannot be discriminated on PHH3 vs. DNA, then the following logic works: (R1 & R2) OR R4. This works because mitotic cells are rare and doublet mitotic cells are even rarer. This logic was used in analyses of the data presented in Figs. 6 and 17.

29. The figure shows two G2 gates (Fig. 10b). The first gate set by eye produced a value of 5.9% G2 cells. Modeling the DNA distribution (Fig. 10d) with ModFit LT (Verity Software House) produced a value of 5.3% G2 cells. The region (R9) was then adjusted to the second setting to produce 5.3% within R9. This same logic could not be applied to the G1 phase fraction that is either over-estimated by DNA content modeling or under-estimated by cyclin A2 expression gating. We use cyclin A2 gating because cyclin A2 gating correlates with BrdU incorporation.
30. The separation of nuclei by peak vs. integral analysis is not likely to perfectly correlate with metaphase vs. telophase. The beginning of visual chromosome separation and 2 standard deviations below the high DNA-peak distribution mode may not align. Further, it is clear that some metaphase cells have depleted cyclin B1 and some telophase cells have residual cyclin B1, so there is not a perfect correlation at the biological level between the biomarkers and the mitotic stage. Integrating mitotic states based on biochemistry and stages based on morphology into a unified analysis would be an important advance in this area.

Acknowledgments

This work was supported by grants from NCI, R01CA73413 to JWJ and P30CA43703 to Stan Gerson, which supports the Cytometry and Imaging Microscopy Core facility in which the cytometry is performed. Additional thanks go to Vince Shankey (retired), Chuck Goolsby (retired), David Hedley (Ontario Cancer Institute), Stan Shackney (deceased), and Elena Holden (Compucyte) for advice and comments on this work for many years; Sue Chow (Ontario Cancer Institute) on fixation and staining, and Bruce Bagwell, Ben Hunsberger, and Chris Bray (Verity Software House) for many innovations in WinList and ModFit that enable or facilitate the analytical part of the work.

References

1. Jacobberger JW, Sramkoski RM, Stefan T (2011) Multiparameter cell cycle analysis. Methods Mol Biol 699:229–249. doi:10.1007/978-1-61737-950-5_11
2. Patterson JO, Swaffer M, Filby A (2015) An imaging flow cytometry-based approach to analyse the fission yeast cell cycle in fixed cells. Methods 82:74–84. doi:10.1016/j.ymeth.2015.04.026
3. Calvert ME, Lannigan JA, Pemberton LF (2008) Optimization of yeast cell cycle analysis and morphological characterization by multispectral imaging flow cytometry. Cytometry A 73(9):825–833. doi:10.1002/cyto.a.20609
4. Blasi T, Hennig H, Summers HD, Theis FJ, Cerveira J, Patterson JO, Davies D, Filby A, Carpenter AE, Rees P (2016) Label-free cell cycle analysis for high-throughput imaging flow cytometry. Nat Commun 7:10256. doi:10.1038/ncomms10256

5. Darzynkiewicz Z, Crissman H, Jacobberger JW (2004) Cytometry of the cell cycle: cycling through history. Cytometry A 58(1):21–32
6. Jacobberger JW, Fogleman D, Lehman JM (1986) Analysis of intracellular antigens by flow cytometry. Cytometry 7(4):356–364
7. Clevenger CV, Bauer KD, Epstein AL (1985) A method for simultaneous nuclear immunofluorescence and DNA content quantitation using monoclonal antibodies and flow cytometry. Cytometry 6(3):208–214
8. Sherwood SW, Rush DF, Kung AL, Schimke RT (1994) Cyclin B1 expression in HeLa S3 cells studied by flow cytometry. Exp Cell Res 211(2):275–281. doi:10.1006/excr.1994.1087
9. Darzynkiewicz Z, Traganos F (1990) Multiparameter flow cytometry in studies of the cell cycle. In: Melamed MR, Lindmo T, Mendelsohn ML (eds) Flow cytometry and sorting, 2nd edn. Wiley-Liss, Inc., New York, p 824
10. Filby A, Perucha E, Summers H, Rees P, Chana P, Heck S, Lord GM, Davies D (2011) An imaging flow cytometric method for measuring cell division history and molecular symmetry during mitosis. Cytometry A 79(7):496–506. doi:10.1002/cyto.a.21091
11. Avva J, Weis MC, Sramkoski RM, Sreenath SN, Jacobberger JW (2012) Dynamic expression profiles from static cytometry data: component fitting and conversion to relative, "same scale" values. PLoS One 7(7):e38275. doi:10.1371/journal.pone.0038275
12. Jacobberger JW, Avva J, Sreenath SN, Weis MC, Stefan T (2012) Dynamic epitope expression from static cytometry data: principles and reproducibility. PLoS One 7(2):e30870. doi:10.1371/journal.pone.0030870
13. Jacobberger JW (1989) Cell cycle expression of nuclear proteins. In: Yen A (ed) Flow cytometry: advanced research and applications, vol 1. CRC Press, Boca Raton, pp 305–326
14. Gong J, Ardelt B, Traganos F, Darzynkiewicz Z (1994) Unscheduled expression of cyclin B1 and cyclin E in several leukemic and solid tumor cell lines. Cancer Res 54 (16):4285–4288
15. Gong J, Traganos F, Darzynkiewicz Z (1995) Growth imbalance and altered expression of cyclins B1, a, E, and D3 in MOLT-4 cells synchronized in the cell cycle by inhibitors of DNA replication. Cell Growth Differ 6 (11):1485–1493
16. Stefan T, Jacobberger JW (2011) Laser scanning cytometry of mitosis: state and stage analysis. Methods Cell Biol 102:341–372. doi:10.1016/B978-0-12-374912-3.00014-6
17. Jacobberger JW, Frisa PS, Sramkoski RM, Stefan T, Shults KE, Soni DV (2008) A new biomarker for mitotic cells. Cytometry A 73 (1):5–15
18. Bagwell CB, Hunsberger BC, Herbert DJ, Munson ME, Hill BL, Bray CM, Preffer FI (2015) Probability state modeling theory. Cytometry A 87(7):646–660. doi:10.1002/cyto.a.22687
19. Kafri R, Levy J, Ginzberg MB, Oh S, Lahav G, Kirschner MW (2013) Dynamics extracted from fixed cells reveal feedback linking cell growth to cell cycle. Nature 494 (7438):480–483. doi:10.1038/nature11897
20. Potapova TA, Sivakumar S, Flynn JN, Li R, Gorbsky GJ (2011) Mitotic progression becomes irreversible in prometaphase and collapses when Wee1 and Cdc25 are inhibited. Mol Biol Cell 22(8):1191–1206. doi:10.1091/mbc.E10-07-0599
21. Pines J, Rieder CL (2001) Re-staging mitosis: a contemporary view of mitotic progression. Nat Cell Biol 3(1):E3–E6. doi:10.1038/35050676
22. Crissman HA, Tobey RA (1974) Cell-cycle analysis in 20 minutes. Science 184 (143):1297–1298
23. Fattorossi A, Battaglia A, Ferlini C (2001) Lymphocyte activation associated antigens. In: Darzynkiewicz Z, Crissman HA, Robinson JP (eds) Cytometry, Methods in cell biology, vol 63, 3rd Part A edn. Academic, San Diego, p 614
24. Endl E, Hollmann C, Gerdes J (2001) Antibodies against the Ki-67 protein: assessment of the growth fraction and tools for cell cycle analysis. In: Darzynkiewicz Z, Crissman HA, Robinson JP (eds) Cytometry, Methods in cell biology, vol 63, 3rd, Part A edn. Academic, San Diego, p 614
25. Larsen JK, Landberg G, Roos G (2001) Detection of proliferating cell nuclear antigen. In: Darzynkiewicz Z, Crissman HA, Robinson JP (eds) Cytometry, Methods in cell biology, vol 63, 3rd, Part A edn. Academic, San Diego, p 614
26. Lyons AB, Hasbold J, Hodgkin PD (2001) Flow cytometric analysis of cell division history using dilution of carboxyfluoroscein diacetate succinimidyl ester, a stably integrated fluorescent probe. In: Darzynkiewicz Z, Crissman HA, Robinson JP (eds) Cytometry, Methods in cell biology, vol 63, 3rd, Part A edn. Academic, San Diego, p 614
27. Braylan RC, Duque RE, Hedley DW, Friedlander ML, Shankey TV, Bauer KD, Visscher DW, Crissman JD, Taylor SG, Shapiro DN, Look

TA, Beckmann E, Mazenet R, Weinberg DS (1993) Section C. Applications in Clinical Oncology. In: Bauer KD, Duque RE, Shankey TV (eds) Clinical Flow Cytometry. 1st edn. Williams & Wilkins, Baltimore, pp 203–372

28. Hedley DW, Shankey TV, Wheeless LL (1993) DNA cytometry consensus conference. Cytometry 14(5):471
29. Sramkoski RM, Wormsley SW, Bolton WE, Crumpler DC, Jacobberger JW (1999) Simultaneous detection of cyclin B1, p105, and DNA content provides complete cell cycle phase fraction analysis of cells that endoreduplicate. Cytometry 35(3):274–283
30. Soni DV, Sramkoski RM, Lam M, Stefan T, Jacobberger JW (2008) Cyclin B1 is rate limiting but not essential for mitotic entry and progression in mammalian somatic cells. Cell Cycle 7(9):1285–1300. 5711 [pii]
31. Juan G, Li X, Darzynkiewicz Z (1997) Correlation between DNA replication and expression of cyclins a and B1 in individual MOLT-4 cells. Cancer Res 57(5):803–807
32. Huang Y, Sramkoski RM, Jacobberger JW (2013) The kinetics of G2 and M transitions regulated by B cyclins. PLoS One 8(12): e80861. doi:10.1371/journal.pone.0080861
33. Zhang D, Jacobberger JW (1996) TGF-beta 1 perturbation of the fibroblast cell cycle during exponential growth: switching between negative and positive regulation. Cell Prolif 29 (6):289–307
34. Sladek TL, Jacobberger JW (1992) Simian virus 40 large T-antigen expression decreases the G1 and increases the G2 + M cell cycle phase durations in exponentially growing cells. J Virol 66(2):1059–1065
35. DiSalvo CV, Zhang D, Jacobberger JW (1995) Regulation of NIH-3T3 cell G1 phase transit by serum during exponential growth. Cell Prolif 28(9):511–524
36. Jacobberger JW, Sramkoski RM, Wormsley SB, Bolton WE (1999) Estimation of kinetic cell-cycle-related gene expression in G1 and G2 phases from immunofluorescence flow cytometry data. Cytometry 35(3):284–289
37. Frisa PS, Lanford RE, Jacobberger JW (2000) Molecular quantification of cell cycle-related gene expression at the protein level. Cytometry 39(1):79–89
38. Frisa PS, Jacobberger JW (2009) Cell cycle-related cyclin B1 quantification. PLoS One 4 (9):e7064
39. Singhania R, Sramkoski RM, Jacobberger JW, Tyson JJ (2011) A hybrid model of mammalian cell cycle regulation. PLoS Comput Biol 7(2): e1001077. doi:10.1371/journal.pcbi.1001077
40. Weis MC, Avva J, Jacobberger JW, Sreenath SN (2014) A data-driven, mathematical model of mammalian cell cycle regulation. PLoS One 9 (5):e97130. doi:10.1371/journal.pone.0097130
41. Frisa PS, Jacobberger JW (2002) Cell density related gene expression: SV40 large T antigen levels in immortalized astrocyte lines. BMC Cell Biol 3:10
42. Bonsing BA, Corver WE, Gorsira MC, van Vliet M, Oud PS, Cornelisse CJ, Fleuren GJ (1997) Specificity of seven monoclonal antibodies against p53 evaluated with western blotting, immunohistochemistry, confocal laser scanning microscopy, and flow cytometry. Cytometry 28(1):11–24
43. Jacobberger JW, Sramkoski RM, Frisa PS, Ye PP, Gottlieb MA, Hedley DW, Shankey TV, Smith BL, Paniagua M, Goolsby CL (2003) Immunoreactivity of Stat5 phosphorylated on tyrosine as a cell-based measure of Bcr/Abl kinase activity. Cytometry A 54(2):75–88
44. Jacobberger JW, Sramkoski RM, Zhang D, Zumstein LA, Doerksen LD, Merritt JA, Wright SA, Shults KE (1999) Bivariate analysis of the p53 pathway to evaluate ad-p53 gene therapy efficacy. Cytometry 38(5):201–213
45. Kamentsky LA, Kamentsky LD (1991) Microscope-based multiparameter laser scanning cytometer yielding data comparable to flow cytometry data. Cytometry 12 (5):381–387
46. Srivastava P, Sladek TL, Goodman MN, Jacobberger JW (1992) Streptavidin-based quantitative staining of intracellular antigens for flow cytometric analysis. Cytometry 13 (7):711–721. doi:10.1002/cyto.990130707
47. Bauer KD, Jacobberger JW (1994) Analysis of intracellular proteins. Methods Cell Biol 41:351–376
48. Camplejohn RS (1994) The measurement of intracellular antigens and DNA by multiparametric flow cytometry. J Microsc 176(Pt 1):1–7
49. Clevenger CV, Shankey TV (1993) Cytochemistry II: immunofluorescence measurement of intracellular antigens. In: Bauer KD, Duque RE, Shankey TV (eds) Clinical flow cytometry, 1st edn. Williams & Wilkins, Baltimore, pp 157–175
50. Jacobberger JW (1991) Intracellular antigen staining: quantitative immunofluorescence. Methods 2:207–218
51. Jacobberger JW (2000) Flow cytometric analysis of intracellular protein epitopes. In: Stewart

CA, Nicholson JKA (eds) Immunophenotyping. Cytometric cellular analysis. Wiley-Liss, Inc., New York, pp 361–405

52. Jacobberger JW (2001) Stoichiometry of immunocytochemical staining reactions. Methods Cell Biol 63:271–298
53. Jacobberger JW, Hedley DW (2001) Intracellular measures of signalling pathways. In: McCarthy DA, Macey MG (eds) Cytometric analysis of cell phenotype and function. Cambridge University Press, Cambridge
54. Koester SK, Bolton WE (2000) Intracellular markers. J Immunol Methods 243 (1–2):99–106
55. Koester SK, Bolton WE (2001) Strategies for cell permeabilization and fixation in detecting surface and intracellular antigens. Methods Cell Biol 63:253–268
56. Woost PG, Solchaga LA, Meyerson HJ, Shankey TV, Goolsby CL, Jacobberger JW (2011) High-resolution kinetics of cytokine signaling in human CD34/CD117-positive cells in unfractionated bone marrow. Blood 117(15): e131–e141. doi:10.1182/blood-2010-10-316224
57. Marvin J, Swaminathan S, Kraker G, Chadburn A, Jacobberger J, Goolsby C (2011) Normal bone marrow signal-transduction profiles: a requisite for enhanced detection of signaling dysregulations in AML. Blood 117(15): e120–e130. doi:10.1182/blood-2010-10-316026
58. Bruno S, Gorczyca W, Darzynkiewicz Z (1992) Effect of ionic strength in immunocytochemical detection of the proliferation associated nuclear antigens p120, PCNA, and the protein reacting with Ki-67 antibody. Cytometry 13 (5):496–501
59. Landberg G, Tan EM, Roos G (1990) Flow cytometric multiparameter analysis of proliferating cell nuclear antigen/cyclin and Ki-67 antigen: a new view of the cell cycle. Exp Cell Res 187(1):111–118
60. Frisa PS, Jacobberger JW (2010) Cytometry of chromatin bound Mcm6 and PCNA identifies two states in G1 that are separated functionally by the G1 restriction point. BMC Cell Biol 11:26. doi:10.1186/1471-2121-11-26
61. Chow S, Hedley D, Grom P, Magari R, Jacobberger JW, Shankey TV (2005) Whole blood fixation and permeabilization protocol with red blood cell lysis for flow cytometry of intracellular phosphorylated epitopes in leukocyte subpopulations. Cytometry A 67(1):4–17
62. Shults KE, Flye LA (2008) Cell fixation and use in phospho-proteome screening. United States Patent
63. Shults KE, Flye LA, Green L, Daly T, Manro JR, Lahn M (2009) Patient-derived actute myeloid leukemia (AML) bone marrow cells display distinct intracellular kinase phosphorylation patterns. J Cancer Manage Res 2009 (1):1–11
64. Krutzik PO, Nolan GP (2003) Intracellular phospho-protein staining techniques for flow cytometry: monitoring single cell signaling events. Cytometry A 55(2):61–70
65. Avva J, Weis MC, Soebiyanto RP, Jacobberger JW, Sreenath SN (2011) CytoSys: a tool for extracting cell-cycle-related expression dynamics from static data. Methods Mol Biol 717:171–193. doi:10.1007/978-1-61779-024-9_10
66. Darzynkiewicz Z, Traganos F, Melamed MR (1980) New cell cycle compartments identified by multiparameter flow cytometry. Cytometry 1(2):98–108. doi:10.1002/cyto.990010203
67. Traganos F, Darzynkiewicz Z, Melamed MR (1982) The ratio of RNA to total nucleic acid content as a quantitative measure of unbalanced cell growth. Cytometry 2(4):212–218. doi:10.1002/cyto.990020403
68. Mann GJ, Dyne M, Musgrove EA (1987) Immunofluorescent quantification of ribonucleotide reductase M1 subunit and correlation with DNA content by flow cytometry. Cytometry 8(5):509–517. doi:10.1002/cyto.990080512
69. Landberg G, Roos G (1991) Antibodies to proliferating cell nuclear antigen as S-phase probes in flow cytometric cell cycle analysis. Cancer Res 51(17):4570–4574
70. Darzynkiewicz Z, Gong J, Juan G, Ardelt B, Traganos F (1996) Cytometry of cyclin proteins. Cytometry 25(1):1–13
71. Juan G, Traganos F, James WM, Ray JM, Roberge M, Sauve DM, Anderson H, Darzynkiewicz Z (1998) Histone H3 phosphorylation and expression of cyclins a and B1 measured in individual cells during their progression through G2 and mitosis. Cytometry 32 (2):71–77
72. Poot M, Schmitt H, Seyschab H, Koehler J, Chen U, Kaempf U, Kubbies M, Schindler D, Rabinovitch PS, Hoehn H (1989) Continuous bromodeoxyuridine labeling and bivariate ethidium bromide/Hoechst flow cytometry in cell kinetics. Cytometry 10(2):222–226. doi:10.1002/cyto.990100215
73. Pinto M, Azzam EI, Howell RW (2006) Bystander responses in three-dimensional cultures containing radiolabelled and unlabelled human cells. Radiat Prot Dosim 122 (1–4):252–255. doi:10.1093/rpd/ncl460

74. White RA, Terry NH (1992) A quantitative method for evaluating bivariate flow cytometric data obtained using monoclonal antibodies to bromodeoxyuridine. Cytometry 13 (5):490–495. doi:10.1002/cyto.990130507
75. Terry NH, White RA, Meistrich ML, Calkins DP (1991) Evaluation of flow cytometric methods for determining population potential doubling times using cultured cells. Cytometry 12(3):234–241. doi:10.1002/cyto.990120305
76. Landberg G, Roos G (1992) Flow cytometric analysis of proliferation associated nuclear antigens using washless staining of unfixed cells. Cytometry 13(3):230–240. doi:10.1002/cyto.990130304
77. Darzynkiewicz Z, Zhao H, Zhang S, Lee MY, Lee EY, Zhang Z (2015) Initiation and termination of DNA replication during S phase in relation to cyclins D1, E and a, p21WAF1, Cdt1 and the p12 subunit of DNA polymerase delta revealed in individual cells by cytometry. Oncotarget 6(14):11735–11750. doi:10.18632/oncotarget.4149
78. Tomasoni D, Lupi M, Brikci FB, Ubezio P (2003) Timing the changes of cyclin E cell content in G1 in exponentially growing cells. Exp Cell Res 288(1):158–167
79. Yanagisawa M, Dolbeare F, Todoroki T, Gray JW (1985) Cell cycle analysis using numerical simulation of bivariate DNA/bromodeoxyuridine distributions. Cytometry 6(6):550–562. doi:10.1002/cyto.990060609
80. Li B, Zhao H, Rybak P, Dobrucki JW, Darzynkiewicz Z, Kimmel M (2014) Different rates of DNA replication at early versus late S-phase sections: multiscale modeling of stochastic events related to DNA content/EdU (5-ethynyl-2'deoxyuridine) incorporation distributions. Cytometry A 85(9):785–797. doi:10.1002/cyto.a.22484
81. Glogovac JK, Porter PL, Banker DE, Rabinovitch PS (1996) Cytokeratin labeling of breast cancer cells extracted from paraffin-embedded tissue for bivariate flow cytometric analysis. Cytometry 24(3):260–267. doi:10.1002/(SICI)1097-0320(19960701)24:3<260::AID-CYTO9>3.0.CO;2-L
82. Kurose A, Tanaka T, Huang X, Halicka HD, Traganos F, Dai W, Darzynkiewicz Z (2005) Assessment of ATM phosphorylation on Ser-1981 induced by DNA topoisomerase I and II inhibitors in relation to Ser-139-histone H2AX phosphorylation, cell cycle phase, and apoptosis. Cytometry A 68(1):1–9. doi:10.1002/cyto.a.20186
83. Gerashchenko BI, Hino M, Hosoya H (2000) Enrichment for late-telophase cell populations using flow cytometry. Cytometry 41 (2):148–149
84. Viallard JF, Lacombe F, Dupouy M, Ferry H, Belloc F, Reiffers J (2000) Different expression profiles of human cyclin B1 in normal PHA-stimulated T lymphocytes and leukemic T cells. Cytometry 39(2):117–125
85. Bagwell CB (1993) Theoretical aspects of flow cytometry data analysis. In: Bauer KD, Duque RE, Shankey TV (eds) Clinical flow cytometry, 1st edn. Williams & Wilkins, Baltimore, pp 41–61
86. Givan AG (2001) Flow cytometry first principles, 2nd edn. Wiley-Liss, Inc., New York
87. Rabinovitch PS (1993) Practical considerations for DNA content and cell cycle analysis. In: Bauer KD, Duque RE, Shankey TV (eds) Clinical flow cytometry, 1st edn. Williams & Wilkins, Baltimore, pp 117–142
88. Shapiro HM (2003) Practical flow cytometry, 4th edn. Wiley, Hoboken

Chapter 12

Monitoring Cell Proliferation by Dye Dilution: Considerations for Probe Selection

Joseph D. Tario Jr., Alexis N. Conway, Katharine A. Muirhead, and Paul K. Wallace

Abstract

In the third edition of this series, we described protocols for labeling cell populations with tracking dyes, and addressed issues to be considered when combining two different tracking dyes with other phenotypic and viability probes for the assessment of cytotoxic effector activity and regulatory T cell functions. We summarized key characteristics of and differences between general protein and membrane labeling dyes, discussed determination of optimal staining concentrations, and provided detailed labeling protocols for both dye types. Examples of the advantages of two-color cell tracking were provided in the form of protocols for: (a) independent enumeration of viable effector and target cells in a direct cytotoxicity assay; and (b) an in vitro suppression assay for simultaneous proliferation monitoring of effector and regulatory T cells.

The number of commercially available fluorescent cell tracking dyes has expanded significantly since the last edition, with new suppliers and/or new spectral properties being added at least annually. In this fourth edition, we describe evaluations to be performed by the supplier and/or user when characterizing a new cell tracking dye and by the user when selecting one for use in multicolor proliferation monitoring. These include methods for:

(a) Assessment of the dye's spectral profile on the laboratory's flow cytometer(s) to optimize compatibility with other employed fluorochromes and minimize compensation problems;

(b) Evaluating the effect of labeling on cell growth rate;

(c) Testing the fidelity with which dye dilution reports cell division;

(d) Determining the maximum number of generations to be included when using dye dilution profiles to estimate fold population expansion or frequency of responder cells; and

(e) Verifying that relevant cell functions (e.g., effector activity) remain unaltered by tracking dye labeling.

Key words Cell division, Cell tracking, CellTrace™ dyes, CellVue® dyes, Cytotoxicity, Dye dilution proliferation assay, Flow cytometry, PKH dyes

Teresa S. Hawley and Robert G. Hawley (eds.), *Flow Cytometry Protocols*, Methods in Molecular Biology, vol. 1678, DOI 10.1007/978-1-4939-7346-0_12,

1 Introduction

The number of fluorescent dyes commercially available for cell tracking, and the subset useful for proliferation monitoring (reviewed in [1]), continues to expand rapidly, with new suppliers and/or new spectral properties continually being added [2–4]. Although diverse in their chemistries and fluorescence characteristics, these reagents can be grouped into two main classes based on their mechanism of cell labeling. Dyes of one class, here referred to as "protein dyes," react with proteins to form a covalent bond. Dyes of the other class, here referred to as "membrane dyes," stably intercalate into the lipid bilayer of cell membranes via strong hydrophobic associations. The term "proliferation dye" will be used here to refer to dyes of either class that: (a) exhibit sufficiently good chemical and metabolic stability to partition approximately equally between daughter cells at mitosis; and (b) are sufficiently non-perturbing, even at high initial labeling intensities, to allow multiple rounds of cell division to be followed based on dye dilution.

Due to their stability of cell association, cell tracking dyes of both classes are often used for in vivo studies of cell trafficking and recruitment in contexts such as transplantation [5, 6], infection [7, 8], stem cell identification [9, 10], and cancer immunotherapy [11]. Both dye types have also proven valuable for a wide range of in vitro studies including antigen presentation [12–14], mechanism and specificity of cytotoxic effector killing [15–17] (Subheading 3.6), and regulatory T cell activity [18, 19]. Infectious agents [20, 21], subcellular components (e.g., plasma membrane) [22, 23] can also be tracked, as can the fate and bioactivity of cell-derived vesicles [24–26]. Combining fluorescent cell tracking dyes with stably expressed genetic markers has become increasingly common as the spectral choices available for probe types have increased. This strategy has been used to monitor extent and/or symmetry of cell division [27–29], something not possible with genetic markers alone, and also to detect active cycling in T cells responding to antigen, both before tracking dye dilution was evident and after daughter cells could no longer be distinguished from unlabeled cells [8].

Monitoring the proliferative status of stem/progenitor and immune cells is among the most common applications of both classes of cell tracking dyes [1, 2, 18, 19, 27, 30, 31], due to the significant limitations associated with alternative methods. Using dye dilution to assess extent of cell division avoids safety and regulatory issues associated with tritiated thymidine incorporation, which is ill-suited for single cell analysis of mixed populations, detects only cells actively synthesizing DNA during the pulse, and does not allow isolation of daughter cells for follow-on analyses (e.g., immunophenotyping, gene expression, proteomics, or

functional assays). Non-radioactive DNA precursors (bromodeoxyuridine, BrdU; ethynyldeoxyuridine, EdU) are compatible with single cell detection by flow cytometry using a variety of fluorochromes but also detect only cells actively synthesizing DNA during the pulse, and because detection requires fixation and permeabilization, viable daughter cells cannot be isolated for functional studies. Although BrdU and EdU also dilute out as cells proliferate, toxicity associated with high levels of incorporation [32] means that they typically cannot be used to monitor more than one or two rounds of cell division before labeled cells can no longer be distinguished from unlabeled ones.

The spectral capabilities of flow and imaging cytometers and the range of choices available for cell tracking dyes have both expanded dramatically since the third edition of this chapter, increasing our ability to design multiplex, high parameter studies to decipher complex biological systems [5, 8, 14, 22, 25]. This makes it even more essential to know the advantages—and limitations—of given tracking dye(s) in order to select probe(s) well-matched to the needs of a given application, particularly as new dyes become available. Key considerations for obtaining bright, homogeneous labeling with tracking dyes differ considerably from those for labeling with antibodies, and also for protein dyes vs. membrane dyes [2, 19, 33, 34]. Subheadings 3.1 and 3.2 describe the protocols used to label cultured U937 cells and human peripheral blood mononuclear cells (PBMC) for the work presented here. Assessment of spectral compatibility with available instrumentation configuration(s) and other fluorochromes has become even more critical as choices have expanded. This is discussed in Subheading 3.3, using data collected for three protein dyes (CellTrace™ Violet, CellTrace™ CFSE, and CellTrace™ Far Red) and three membrane dyes (PKH67, PKH26, and CellVue® Claret) on two different flow cytometers to illustrate the impact of laser configuration, laser power, and optical filter choices on stain index for each dye, and as a consequence, the degree of spectral overlap/compensation required in other spectral windows.

Before a new cell tracking dye is used for proliferation monitoring, it is important to verify that the rate of dilution is linearly correlated with the rate of cell growth in a system where unstained cells are also present and where growth can be independently measured. Subheading 3.4 illustrates two methods for doing this using continuously dividing cultured tumor cell lines. In systems where both responders and non-responders are present, mathematical modeling [1, 34, 35] is often used to quantify: (a) extent of population expansion in response to a stimulus (typically reported as “Proliferation Index” or “Expansion Index”); and/or (b) proportion of the initial population able to proliferate in response to that stimulus (typically reported as “Precursor Frequency” or “Percent Divided”). In such cases, it is also important to know the

maximum number of daughter generations that can be followed before highly divided dye-positive cells begin to overlap with unstained cells. This is illustrated in Subheading 3.5 for lymphocyte cultures proliferating in response to stimulation with anti-CD3 and anti-CD28 antibodies. Finally, it is essential for each laboratory to verify for their particular cell type that the final labeling conditions chosen do not alter the proliferative behavior or functional potency of labeled cells relative to unlabeled controls (Subheadings 3.5 and 3.6, respectively).

2 Materials

2.1 Cell Isolation and Cell Culture

1. Complete Medium (CM): RPMI 1640 supplemented with 10% heat inactivated fetal bovine serum (FBS), 25 mM HEPES, 0.1 mM non-essential amino acids, 1 mM sodium pyruvate, 2 mM fresh glutamine, 50 μg/mL gentamicin sulfate, and 5×10^{-5} M β-mercaptoethanol.
2. 10% Formaldehyde, methanol free, ultra-pure. Dilute to 2% in PBS (pH 7.4) and store refrigerated.
3. Hanks' Balanced Salt Solution (HBSS) without phenol red, magnesium, or calcium. Store at room temperature until opened, then at 4–8 °C.
4. Histopaque®-1077. Store at 4–8 °C and use at room temperature.
5. IL-2 (Aldesleukin Proleukin for injection, NDC 53905-991-01; Novartis, New York, NY). Dilute stock (2.2×10^6 IU/mL) in sterile HBSS to 1×10^5 IU/mL, aliquot, and store at −80 °C. Do not refreeze after thawing; store at 4–8 °C and discard thawed product after 7 days.
6. Phosphate Buffered Saline (PBS): Prepare 10× stock containing 1.37 M NaCl, 27 mM KCl, 100 mM Na_2HPO_4, and 18 mM KH_2PO_4. Adjust to pH 7.4 with HCl if necessary. Sterilize by 0.2 μm filtration and store at room temperature. Prepare 1× working solution by dilution of one part with nine parts tissue culture grade water.
7. Human peripheral blood mononuclear cells (hPBMC). Isolate hPBMC from heparinized peripheral blood or from TRIMA filters [19] using the laboratory's standard density gradient fractionation protocol, with the addition of a final low-speed wash ($300 \times g$) to minimize platelet contamination (*see* **Note 1**).
8. K562 Cell Line (*see* **Note 2**). Kind gift of Dr. Myron S. Czuczman, Roswell Park Cancer Institute, Buffalo, New York; also available for purchase (American Type Culture Collection, Manassas, VA).

9. U937 Cell Line (*see* **Note 2**). Generously provided by Paul Guyre, Lebanon, NH; also available for purchase (American Type Culture Collection).
10. 24-well polystyrene plates are useful for plating quadruplicate samples for kinetic studies.
11. 96-well U-bottom polypropylene stripwell plate consisting of 1.1 mL polypropylene tubes in strips of 8, racked in plates and sterile.

2.2 Antibodies

1. 1.0 mg/mL anti-CD3 (clone OKT3) and 1.0 mg/mL anti-CD28 (clone 28.2). Azide free, unconjugated preparations (eBioscience, San Diego, CA).
2. CD45 allophycocyanin (APC, clone 2D1) and CD45 Brilliant Violet 510 (BV510, clone HI30) (BD Biosciences, San Jose, CA).

2.3 Flow Cytometry Reagents

1. FCM Buffer: 1× PBS (pH 7.2) supplemented with 1% bovine serum albumin (BSA), 0.1% sodium azide, and 40 μg/mL tetrasodium ethylenediaminetetraacetic acid.
2. 4′,6-diamidino-2-phenylindole (DAPI). Reconstitute powdered solid to 5 mg/mL in deionized water and store at 4–8 °C. Prepare a working stock by diluting to 5 μg/mL in deionized water. Add 5 μL of working stock to each 100 μL of cells (0.25 μg/mL final) and let stand on ice for 30 min prior to data acquisition.
3. 7-Aminoactinomycin D (7-AAD). Reconstitute powdered solid to 1 mg/mL in PBS and store at −20 °C. Prepare a working stock by diluting thawed 1 mg/mL stock to 100 μg/mL in PBS and store at 4–8 °C. Add 4 μL of working stock to each 100 μL of cells (4 μg/mL final) and let stand on ice for 30 min prior to data acquisition.
4. Rainbow 6-Peak Calibration Particles for Instrument setup (Spherotech, Lake Forest, IL). Use for establishing reference intensities in employed fluorescence detectors as described in Subheading 3.4.1.
5. AccuCount Particles for cell counting (Spherotech). Use for single platform cell enumeration as described in Subheading 3.4.1.
6. PKH26 Reference Microbeads (Sigma-Aldrich, St. Louis, MO). Use for single platform cell enumeration as described in Subheading 3.4.1.

2.4 Cell Tracking Dyes

1. CellTrace™ Violet (CTV), CellTrace™ CFSE (CFSE), and CellTrace™ Far Red (CTFR) (ThermoFisher Scientific, Waltham, MA); CytoTrack™ Yellow (CYY) (Bio-Rad, Hercules, CA). CFSE is also available from other suppliers. Reconstitute

lyophilized aliquots for cell labeling according to the manufacturer's recommended concentrations: 5 mM for CTV, 5 mM for CFSE (*see* **Note 3**), 1 mM for CTFR, and 500× for CYY. Labeling chemistries are similar for all four dyes: non-fluorescent precursor compounds freely diffuse across the plasma membrane into the cytoplasm, where their acetate substituents are cleaved by non-specific esterases. This results in trapping of the charged fluorescent product and random protein labeling via covalent bond formation between free amino substituents and the dye's succinimidyl esters.

2. PKH67, PKH26, and CellVue® Claret (CVC) fluorescent cell linker kits (Sigma-Aldrich). Kits contain 1 mM dye solutions in ethanol and cell labeling diluent for general cell membrane labeling (Diluent C). CVC is also available from another supplier (Molecular Targeting Technologies, Inc., West Chester, PA). Store tightly capped at room temperature to avoid evaporation of ethanol and associated increases in dye concentration. If any dye solids are visible, sonicate dye stocks to redissolve before use and verify that dye absorbance remains within the range specified on the Certificate of Analysis available for each kit. These dyes are incorporated into membranes based on hydrophobic forces that drive partitioning from the aqueous phase in which the dyes are highly insoluble, into cell membranes where they are stably retained due to strong non-covalent interactions between their long alkyl tails and those of membrane lipids.

2.5 Flow Cytometers and Data Analysis Software

For routine data acquisition, any flow cytometer capable of acquiring forward and side scatter, DAPI, BV421, BV510, FITC, PE, and APC would be appropriate. Data in this chapter were collected using five different flow cytometers. For all figures showing flow cytometric data, axis labels follow the convention of ref. 36.

1. LSR II (BD Biosciences). Fitted with 355 nm (100 mW), 405 nm (25 mW), 488 nm (20 mW), 561 nm (50 mW), and 640 nm (40 mW) lasers. From the 488 nm laser, FSC and SSC were measured using 488/10 nm bandpass (BP) filters. From the 355 nm laser, DAPI fluorescence was measured using a 450/50 nm BP filter. From the 405 nm laser, CTV fluorescence was measured using a 450/50 nm BP filter, and CD45-BV510 was measured using a 525/50 nm BP filter. From the 488 nm laser, CFSE and PKH67 fluorescence were measured using a 530/30 nm BP filter, and 7-AAD fluorescence was measured using a 695/40 nm BP filter. From the 561 nm laser, PKH26 fluorescence was measured using a 582/15 nm BP filter. From the 640 nm laser, CTFR, CVC, and CD45-APC fluorescence were measured using a 660/20 nm BP filter.

2. LSR Fortessa (BD Biosciences). Fitted with 355 nm (60 mW), 405 nm (50 mW), 488 nm (50 mW), and 640 nm (40 mW) lasers. From the 488 nm laser, FSC and SSC were measured using 488/10 nm BP filters. From the 355 nm laser, DAPI fluorescence was measured using a 450/50 nm BP filter. From the 405 nm laser, CTV fluorescence was measured using a 450/50 nm BP filter, and CD45 BV510 fluorescence was measured using a 525/50 nm BP filter. From the 488 nm laser, CFSE and PKH67 fluorescence were measured using a 530/30 nm BP filter and PKH26 fluorescence was measured using a 575/26 nm BP filter. From the 640 nm laser, CTFR and CVC fluorescence were measured using a 670/14 nm BP filter.
3. MACSQuant Analyzer 10 (Miltenyi Biotec, San Diego, CA). Fitted with 405 nm (40 mW), 488 nm (30 mW), and 635 nm (21.5 mW) lasers. From the 488 nm laser, FSC and SSC were measured using 488/10 nm BP filters. From the 405 nm laser, CTV fluorescence was measured using a 450/50 nm BP filter. From the 488 nm laser, CFSE and PKH67 fluorescence were measured using a 525/50 nm BP filter, and PKH26 and CYY fluorescence were measured using a 585/40 nm BP filter. From the 640 nm laser, CTFR and CVC fluorescence were measured using a 655–730 nm spectral window.
4. MACSQuant VYB (Miltenyi Biotec). Fitted with 405 nm (40 mW), 488 nm (50 mW), and 561 nm (100 mW) lasers. From the 561 nm laser, FSC and SSC were measured using 561/10 nm BP filters. From the 405 nm laser, CTV fluorescence was measured using a 450/50 nm BP filter. From the 488 nm laser, CFSE and PKH67 fluorescence were measured using a 525/50 nm BP filter. From the 561 nm laser, PKH26 was measured using a 585/15 nm BP filter, and CTFR and CVC fluorescence were measured using a 661/20 nm BP filter.
5. NovoCyte 3000 (ACEA Biosciences, San Diego, CA). Fitted with 405 nm (50 mW), 488 nm (60 mW), and 640 nm (40 mW) lasers. From the 488 nm laser, FSC and SSC were measured using 488/10 nm BP filters. From the 405 nm laser, CTV fluorescence was measured using a 445/45 nm BP filter. From the 488 nm laser, CFSE and PKH67 fluorescence were measured using a 530/30 nm BP filter, and PKH26 fluorescence was measured using a 572/28 nm BP filter. From the 640 nm laser, CTFR and CVC fluorescence were measured using a 675/30 nm BP filter.
6. FACS DiVa™ 8.0.1 (BD Biosciences).
7. FCS Express 6.0 (De Novo Software, Glendale, CA).
8. FlowJo™ v10.2 (FlowJo, LLC, Ashland, OR).
9. WinList™ v8.0 (current version is v9.0) and ModFit LT™ v4.0 (Verity Software House, Topsham, ME).

3 Methods

Virtually any eukaryotic cell can be stained with either class of tracking dye after a single-cell suspension has been obtained (*see* **Notes 4** and **5**). The labeling conditions described below have been successfully used to stain human peripheral blood mononuclear cells (hPBMCs) and cultured cells used for the proliferation and cytotoxicity assays discussed here, but are likely to require modification for other cell types, assay systems, or dye combinations (*see* **Notes 6** and **7**). Although CTV, CFSE, and CTFR are used herein to represent a typical protein labeling dyes; and PKH67, PKH26, and CellVue® Claret to represent typical membrane labeling dyes, many other tracking dyes are available and the principles described here also apply to optimization of staining conditions and flow cytometer choice for use of those dyes.

3.1 Cell Line and hPBMC Labeling with Protein Dyes (CTV, CFSE, CTFR, or CYY)

The method for CellTrace labeling described here is a simplification of the protocol described by Quah and Parish [33]. The method for CYY labeling is the manufacturer's recommended protocol, as adapted for the labeling of cultured U937 cells.

1. Prepare a stock solution in anhydrous dimethyl sulfoxide (DMSO) by adding the recommended volume to the provided pre-weighed single use vial, vortexing, and visually inspecting the vial to ensure complete dissolution. The manufacturer's recommended stock concentrations are: 5 mM for CTV, 5 mM for CFSE (*see* **Note 3**), 1 mM for CTFR, and 500× for CYY.
2. Wash cells to be labeled twice in serum-free PBS (or HBSS). After resuspension of the cell pellet from the first wash, remove an aliquot for cell counting (*see* **Note 8**). After a final wash, resuspend cells in serum-free buffer (*see* **Note 9**) at a final concentration of 1×10^7 cells/mL (range for hPBMC: $0.5–50 \times 10^6$ cells/mL), using a tube that will hold at least six times the volume of the cell suspension. For CYY labeling, pellet cells and carefully aspirate supernatant.
3. Immediately prior to cell labeling, prepare working solutions of CellTrace dyes (50 μM for CTV and CFSE; 10 μM for CTFR) by making a 100-fold dilution of the DMSO stock solution from **step 1** in PBS (*see* **Note 10**). Prepare a 2× working solution of CYY by making a 250-fold dilution of the DMSO stock solution from **step 1** in PBS.
4. For a final staining concentration of 1 μM CellTrace dye, add appropriate amount of working dye solution per milliliter of cell suspension: 20 μL/mL of cells for CFSE or CTV; 100 μL/mL of cells for CTFR (e.g., to stain 2 mL of hPBMC at a final concentration of 1×10^7 cells/mL and 1 μM CTV, add 40 μL

of working dye solution; *see* **Notes 7**, **11**, and **12**). For a final staining concentration of 2× CYY, resuspend cell pellet from **step 2** in 100 µL of working dye solution per 10^6 cells (e.g., to stain 5 × 10^6 U937 at a final concentration of 10^7 cells/mL and 2× CYY, resuspend cell pellet from **step 2** in 500 µL of 2× working solution prepared in **step 3**).

5. Immediately triturate or vortex tube briefly to disperse Protein Dye throughout cell suspension. Incubate at ambient temperature (~21 °C) for 5–15 min, with occasional mixing either manually or on a rotator, protected from light (*see* **Notes 13** and **14**).
6. Stop the reaction by adding a 5× volume of CM or a 1× volume of FBS and mixing well (*see* **Note 15**). Centrifuge at 400 × *g* for 5 min at ~21 °C and discard the supernatant.
7. Wash the cells twice with 5–10 volumes of CM. After resuspension of the cell pellet from the first wash, remove an aliquot for cell counting. After the final wash, adjust cell concentration to the desired cell density for functional testing during the final resuspension in CM.
8. Assess recovery, viability, and fluorescence intensity profile of labeled cells immediately post-staining to determine whether to proceed with assay setup (ref. 19; *see* **Note 16**).
9. At 24 h post-labeling, verify that labeled cells are well enough resolved from unstained cells for purposes of the assay to be performed and that Protein Dye fluorescence can be adequately compensated in spectral windows to be used for measurement of other probes (Subheading 3.3; *see* **Note 17**). If samples are to be fixed and analyzed in batch mode, verify that loss of intensity due to fixation does not compromise the ability to distinguish the desired number of daughter generations (*see* **Note 18**).
10. Verify that labeled cells are functionally equivalent to unlabeled cells (Subheading 3.6; *see* **Note 19**).

3.2 Cell Line and hPBMC Labeling with Membrane Dyes (PKH26, PKH67, or CVC)

The method described here is illustrated in detail in ref. 34.

1. Wash cells to be labeled twice in serum-free PBS or HBSS (*see* **Note 9**), using a conical polypropylene tube (*see* **Note 20**) sufficient to hold at least six times the final staining volume in **step 5**. After resuspension of the cell pellet from the first wash, remove an aliquot for cell counting (*see* **Note 8**) and determine the volume needed to prepare a 2× working cell suspension (**step 4** below) at a concentration of 1 × 10^8 cells/mL for hPBMCs (range = 2–100 × 10^6 cells/mL), or 2 × 10^7 cells/mL for U937 cells. For example, to stain a total of 5 × 10^7 hPBMCs at a final concentration of 5 × 10^7 cells/mL, the volume of 2× cell suspension would be 0.5 mL.

2. Following the second wash in **step 1**, aspirate the supernatant, taking care to minimize the amount of buffer remaining (no more than 15–25 μL) while avoiding aspiration of cells from the pellet (*see* **Note 21**). Flick the tip of conical tube once or twice with a finger to disperse the cell pellet in the small amount of fluid remaining, but avoid significant aeration since this reduces cell viability.
3. Prepare 2× working dye solution of PKH67, PKH26, or CVC. To a second conical polypropylene tube (*see* **Note 20**), add the same volume of Diluent C staining vehicle (provided with each membrane dye kit) calculated in **step 1** for the preparation of the 2× cell suspension. Add the appropriate amount of 1 mM ethanolic dye stock to the Diluent C (e.g., for a 2× working dye solution to give a final dye concentration of 5 μM after admixture with 2× cells in **step 5**, add 5 μL of dye stock to 0.5 mL of Diluent C). Gently vortex tube to ensure complete dispersion of dye in diluent, avoiding loss of fluid to cap or as droplets on walls. Proceed with **steps 4** and **5** as rapidly as possible (*see* **Notes 22** and **23**).
4. Prepare a 2× cell suspension by adding the volume of Diluent C calculated in **step 1** to the partially resuspended cell pellet from **step 2**. Triturate 3–4 times to ensure complete dispersion of the pellet and proceed immediately to **step 5**. Avoid excessive mixing, which reduces cell viability.
5. Rapidly admix the 2× cell suspension prepared in **step 4** into the 2× working dye solution prepared in **step 3**, triturating 3–4 times immediately upon completion of addition in order to achieve as nearly instantaneous exposure of all cells to the same amount of dye as is possible (*see* **Notes 24** and **25**).
6. After 3 min, stop the labeling by adding a 5× volume of CM (containing 10% FBS) or a 1× volume of FBS or other cell-compatible protein and mixing well (i.e., if 1 mL of cells was combined with 1 mL of dye, then add 10 mL of CM or 2 mL of FBS; *see* **Note 26**). Centrifuge at 400 × *g* for 5 min at ~21 °C and discard the supernatant.
7. Wash the cells twice with 5–10 volumes of CM, transferring to a clean conical polypropylene tube after the first wash for maximum efficiency (*see* **Note 27**) and removing an aliquot for cell counting. After the final wash, count and resuspend the cells in CM at the final desired cell density for functional testing.
8. Assess recovery, viability, and fluorescence intensity profile of labeled cells immediately post-staining to determine whether to proceed with assay setup (*see* **Note 16**).
9. Verify that labeled but non-proliferating cells (e.g., unstimulated control) are well enough resolved from unstained cells for

purposes of the assay to be performed and that membrane dye fluorescence can be adequately compensated in adjacent spectral windows used for measurement of other probes (Subheading 3.3; *see* **Note 28**).

10. Verify that labeled cells are functionally equivalent to unlabeled cells (Subheading 3.6; *see* **Note 19**).

3.3 Spectral Characterization

Cell tracking dyes are commonly combined with each other, with fluorescent antibodies, and/or with genetic markers to enable: (a) in vitro or in vivo tracking of phenotypically defined subsets within heterogeneous populations (e.g., [5, 22]); or (b) identification and characterization of cell populations that do or do not proliferate in response to a given stimulus (e.g., [8, 18, 37]). The multiplicity of spectral detection options available on most digital flow cytometers means that when selecting fluorochrome combinations for such studies it is important to evaluate the impact of candidate cell tracking dye(s) on the ability to simultaneously detect other common fluorochromes. This must be done in the context of each cytometer's optical configuration, taking into account relative signal intensities expected from the different probes. Due to the extremely bright staining typically obtained with all cell tracking dyes, spectral overlap into channels excited by the same laser and signal arising from cross-laser excitation must both be taken into account. Where cells of interest are in limited supply, this can conveniently be done using cultured cells as described below.

1. Harvest logarithmically growing U937 cells and label with tracking dye(s) of interest as described in Subheading 3.1 or 3.2.
2. Configure the flow cytometer to acquire data from all fluorescence detection channels and adjust FSC and SSC detector voltages to ensure that cells of interest are resolved from electronic noise/small debris and large aggregates.
3. Use unlabeled cells to establish voltage settings that place their measured fluorescence distribution fully on-scale within the first decade (preferably >95% of events with intensity $\geq$0). Using the same instrument settings, confirm that each labeled cell population is fully on-scale in the primary detection channel for the tracking dye being evaluated (*see* **Note 29**).
4. Use data analysis software to generate single-parameter histograms for each detection channel as shown in Figs. 1 and 2. Histograms should be serially gated on: bivariate plots of Time vs. SSC-A to eliminate any events associated with unstable flow rate; FSC-A vs. FSC-H to eliminate doublet events (*see* **Note 30**); and FSC-A vs. SSC-A to discriminate cellular events from small debris.

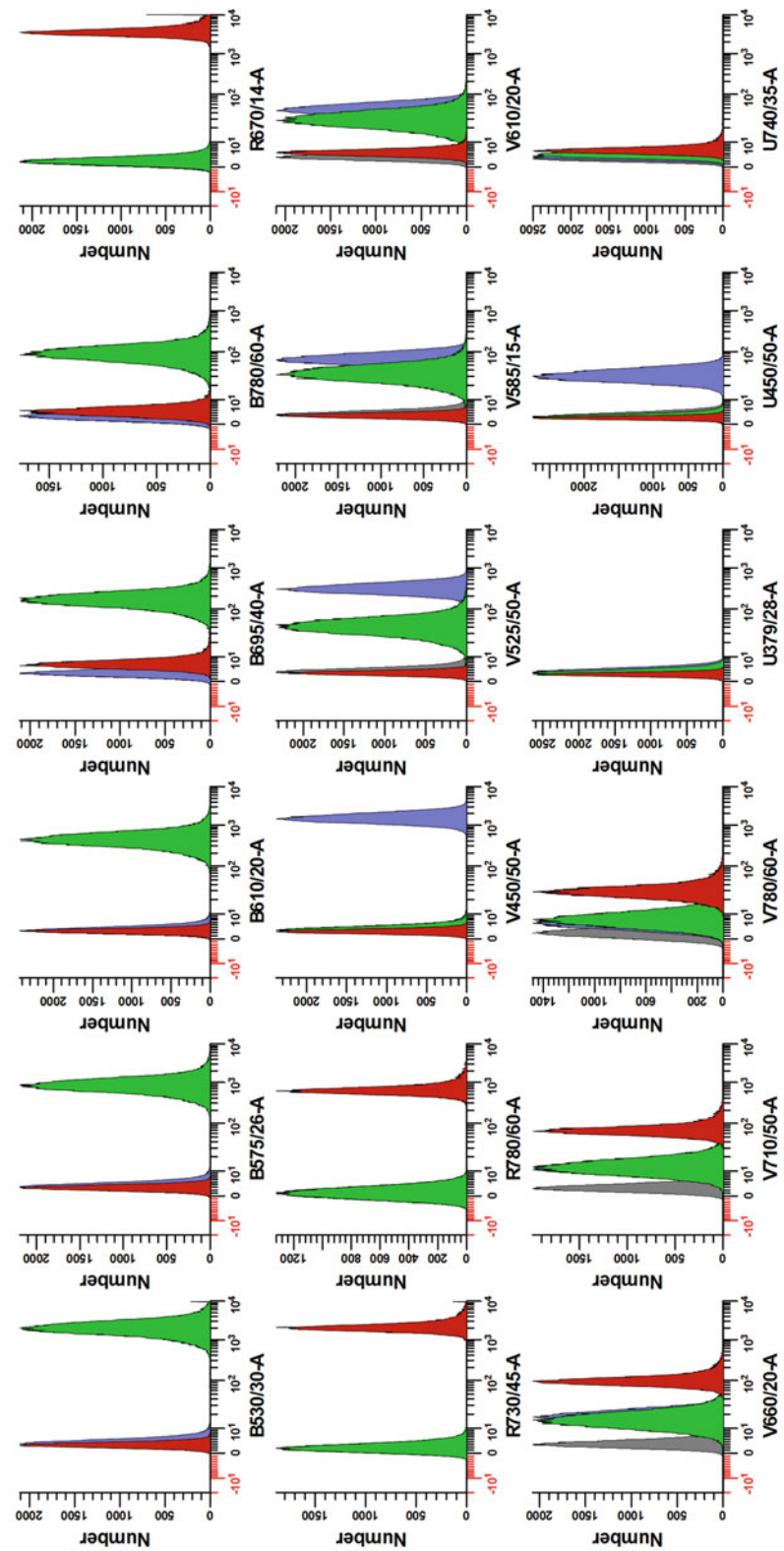

Fig. 1 Spectral profiles of selected protein dyes on BD LSR Fortessa cytometer. U937 cells were labeled as described in Subheading 3.1 at final concentrations of 1×10^7 cells/mL and either 10 μM CFSE, 10 μM CTV, or 1.25 μM CTFR (*see* **Note 31**). All samples were analyzed 24 h post-labeling so that CFSE could be run at voltage settings that placed unlabeled U937 cells in the first decade for each fluorescence detector, as would typically be done for a dye dilution study. When evaluating compatibility of a given tracking dye with other fluors, both spectral overlap and cross-laser excitation characteristics of dye-labeled cells must be considered (*see* **Note 32**). Compensation settings required under these conditions are shown in Table 1a and compensation settings for the same samples run on a BD LSRII are shown in Table 1b (*see* **Note 33**)

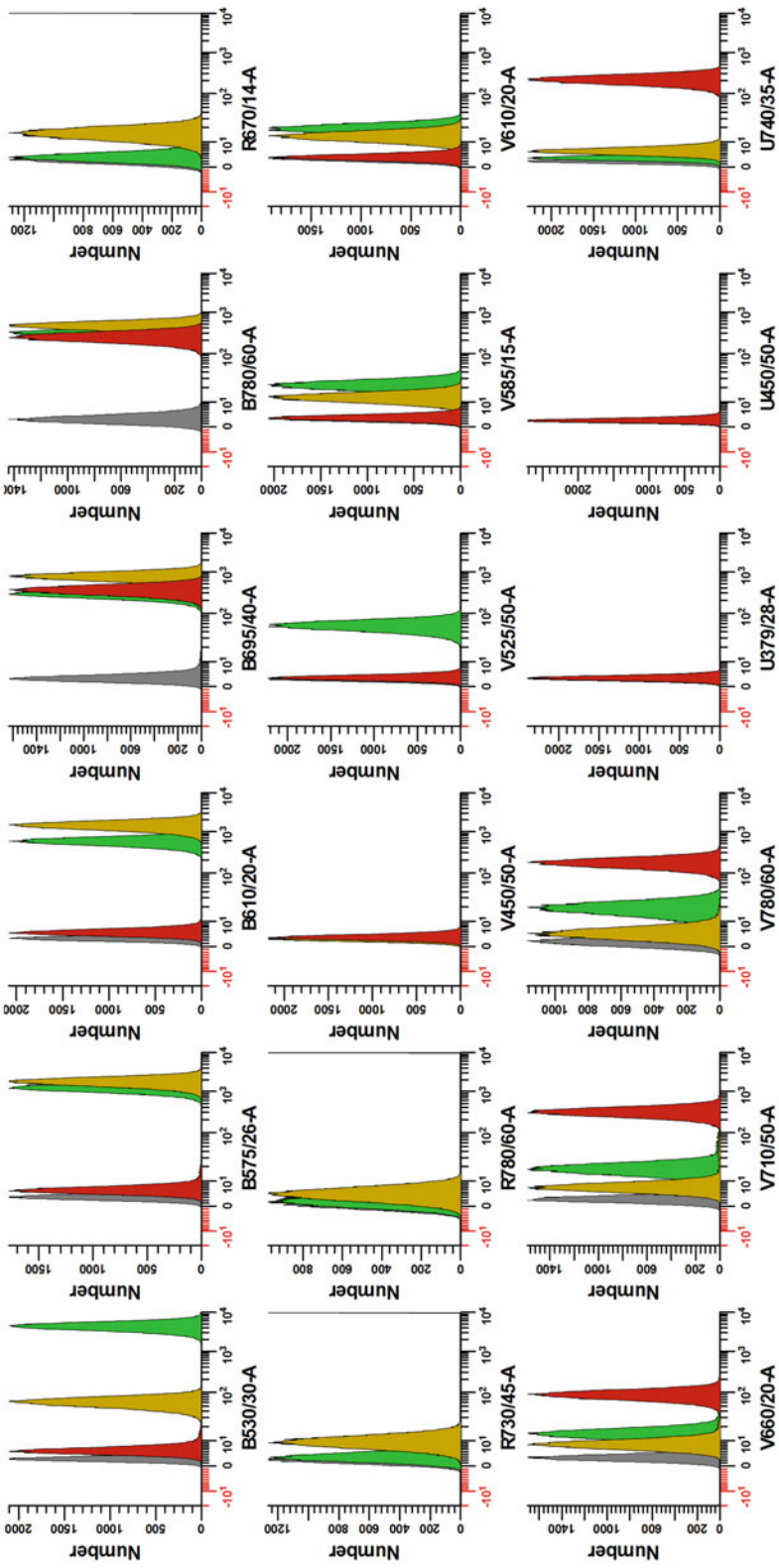

Fig. 2 Spectral profiles of selected membrane dyes on BD LSR Fortessa cytometer. U937 cells were labeled as described in Subheading 3.2 at final concentrations of 1×10^7 cells/mL and either 10 μM PKH67, 10 μM PKH26, or 10 μM CVC. Since membrane dyes exhibit minimal division-independent dye losses, all samples were analyzed immediately post-labeling at voltage settings that placed unlabeled U937 cells in the first decade for each fluorescence detector. Again, both spectral overlap and cross-laser excitation characteristics of dye-labeled cells must be evaluated for compatibility with other fluors (*see* **Note 32**). Compensation settings required for PKH67 and PKH26 under these conditions are shown in Table 1a and compensation settings for the same samples run on a BD LSRII are shown in Table 1b (*see* **Note 33**). Spectral overlap data for CVC, which was off-scale high in all detectors associated with the 640 nm laser, are shown in Table 2 (*see* **Note 34**)

Table 1a
LSR Fortessa: % compensation required as a function of dye and concentration

Laser	Detector	CTV 10 μM	CFSE 10 μM	PKH67 10 μM	PKH26 10 μM	CTFR 5 μM	CTFR 2.5 μM	CTFR 1.25 μM
	B530/30	0.2	Primary	Primary	3.3	0.0	0.0	0.0
	B575/26	0.1	41.9	28.4	Primary	0.0	0.0	0.0
	B610/20	0.1	21.4	12.9	81.4	0.0	0.0	0.0
	B695/40	0.1	7.8	5.2	42.1	0.5	0.2	0.2
	B780/60	0.1	4.3	5.1	24.2	0.3	0.1	0.1
	R670/14	0.1	0.0	0.0	0.8	Primary	Primary	Primary
	R730/45	0.1	0.0	0.0	0.5	206.9	62.7	59.8
	R780/60	0.0	0.0	0.0	0.2	82.8	19.9	18.4
	V450/50	Primary	0.0	0.0	0.1	0.0	0.0	0.0
	V525/50	19.8	1.9	1.3	0.1	0.0	0.0	0.0
	V585/15	4.4	1.5	0.5	0.6	0.0	0.0	0.0
	V610/20	3.0	1.3	0.4	0.7	0.3	0.1	0.1
	V660/20	1.1	0.6	0.3	0.4	12.9	3.2	2.9
	V710/50	0.7	0.5	0.3	0.3	9.1	2.2	2.0
	V780/60	0.3	0.3	0.3	0.2	3.7	1.0	0.8
	U379/28	0.2	0.0	0.0	0.1	0.0	0.0	0.0
	U450/50	2.0	0.0	0.0	0.1	0.0	0.0	0.0
	U740/35	0.2	0.1	0.0	0.2	0.5	0.2	0.2

5. Generate color-coded instrument- and dye-specific table(s) of quantitative compensation values. Access the spectral cross-over/compensation matrix data for each dye from the analyses performed in **step 4**, copy-and-paste it into spreadsheet software such as Microsoft Excel, and apply "Conditional Formatting" to the data cells (Tables 1a, 1b).
6. When fluorescence intensity distributions are partially or fully off-scale in the primary channel when the unlabeled distribution is placed in the first decade (e.g., CTFR and CVC at 10 μM), accurate values for % overlap or compensation cannot be determined (*see* **Note 31**). In such cases, raw intensity data can be used to determine which detectors will be most affected by overlap from a given dye, including detectors affected by cross-laser excitation (Table 2; *see* **Notes 32–34**). It does not matter which measure of central tendency is used (e.g., median, mean, geometric mean, etc.), provided that all fluorescence measurements employ the same metric.
7. Assess the effect of cytometer optical configuration on Stain Index. For any given dye, compensation and cross-laser excitation issues in non-primary channels must be balanced against the ability to detect the desired number of cell generations in the primary channel. Figure 3 illustrates the use of Stain Index

Table 1b
LSRII: % compensation required as a function of dye and concentration

Laser	Detector	CTV 10 μM	CFSE 10 μM	PKH67 10 μM	CTFR 5 μM	CTFR 2.5 μM	CTFR 1.25 μM
	B530/30	1.1	Primary	Primary	0.0	0.1	0.1
	B695/40	0.5	5.6	4.4	0.3	0.2	0.3
	R660/20	0.7	0.0	0.0	Primary	Primary	Primary
	R730/45	0.5	0.0	0.0	142.6	166.8	102.4
	R780/60	0.3	0.0	0.0	44.1	41.8	41.4
	V450/50	Primary	0.0	0.0	0.0	0.0	0.0
	V525/50	97.1	1.8	1.2	0.0	0.0	0.1
	V610/20	19.3	1.2	0.4	0.3	0.3	0.3
	V660/20	9.1	0.7	0.3	10.7	10.1	10.0
	V710/50	4.1	0.4	0.2	5.2	4.9	4.8
	V780/60	2.4	0.3	0.3	2.7	2.5	2.5
	U450/50	12.0	0.0	0.0	0.0	0.0	0.0
	U530/30	6.3	0.3	0.0	0.0	0.0	0.0
	Y582/15	0.8	0.1	0.0	0.0	0.0	0.1
	Y610/20	0.7	0.1	0.0	1.1	1.0	1.1
	Y670/30	0.4	0.0	0.0	0.9	0.8	0.8
	Y710/50	0.4	0.0	0.0	8.6	7.9	7.8
	Y780/60	0.5	0.0	0.0	5.2	4.7	4.7

0-10%	10-20%	20-40%	40-60%	>60%	Primary

to compare the extent to which cells stained with PKH26, CTFR, or CVC can be resolved from unstained cells on four different cytometers (*see* **Notes 35** and **36**).

3.4 Evaluating Effects on Cell Growth and Linearity of Dye Dilution

Cultured cell lines are also useful for testing whether there is a linear correlation between the rate of cell growth and the rate of dye dilution for a particular cell tracking dye. Such systems allow direct measurement of growth by cell counting, whereas indirect measures such as tritiated thymidine uptake must be used to estimate the extent of proliferation in more complex systems (e.g., hPBMC; *see* Table S1 of ref. 1). Before evaluating the linearity of dilution, however, it is necessary to verify that the staining conditions used do not alter cell growth rate compared with that of unlabeled cells. Subheadings 3.4.1 and 3.4.2 describe methods for testing dye effects on growth rate using (a) parallel cultures of stained and unstained cells or (b) co-cultures of stained and unstained cells, respectively. Subheading 3.4.3 illustrates how the resulting data can be used to evaluate the linearity of dye dilution.

Table 2
Geometric mean intensities in non-primary channels

Fortessa

Laser	Detector	CTFR 10 μM	CVC 10 μM
	B530/30	4	6
	B575/26	4	6
	B610/20	4	5
	B695/40	46	350
	B780/60	27	237
	R670/14	Primary	Primary
	R730/45	9990	9979
	R780/60	6938	9977
	V450/50	3	3
	V525/50	4	3
	V585/15	4	3
	V610/20	24	4
	V660/20	1069	91
	V710/50	748	312
	V780/60	303	172
	U379/28	3	3
	U450/50	3	2
	U740/35	46	207

LSRII

Laser	Detector	CTFR 10 μM	CVC 10 μM	PKH26 10 μM
	B530/30	4	4	71
	B695/40	31	212	527
	R660/20	9870	Primary	8
	R730/45	9994	9980	10
	R780/60	5839	2409	4
	V450/50	1	0	0
	V525/50	3	3	3
	V610/20	32	3	14
	V660/20	1445	81	10
	V710/50	704	213	7
	V780/60	358	148	5
	U450/50	2	3	3
	U530/30	2	3	3
	Y582/15	4	10	4353
	Y610/20	138	22	Primary
	Y670/30	114	228	136
	Y710/50	1144	5147	1403
	Y780/60	681	4235	945

1st decade	2nd decade	3rd decade	4th decade	Off-scale hi

3.4.1 Relative Growth Rate of Stained vs. Unstained Cultures Using Counting Beads (Non-volumetric Cytometer)

Beads from different vendors may be employed (e.g., as indicated in Subheading 2.3, **items 5** and **6**), so long as their fluorescence can be distinguished from that of labeled cells in at least one detection channel. Although it is not necessary to know the absolute concentration of beads/mL, a sufficient number of beads should be present in the initial culture to allow a statistically meaningful number (>100) to be counted when high-density cultures are harvested and analyzed by flow cytometry at later time points.

1. Harvest logarithmically growing U937 cells and label with tracking dye of interest as described in Subheading 3.1 or 3.2, leaving an aliquot of harvested cells unlabeled to serve as a dye-naïve control. Adjust labeled and unlabeled cell suspensions to 2.5×10^5 cells/mL in CM.
2. Prepare counting beads for addition to cell cultures by removal of azide and detergents. From the stock solution of fluorescent counting beads, remove an aliquot sufficient to give a

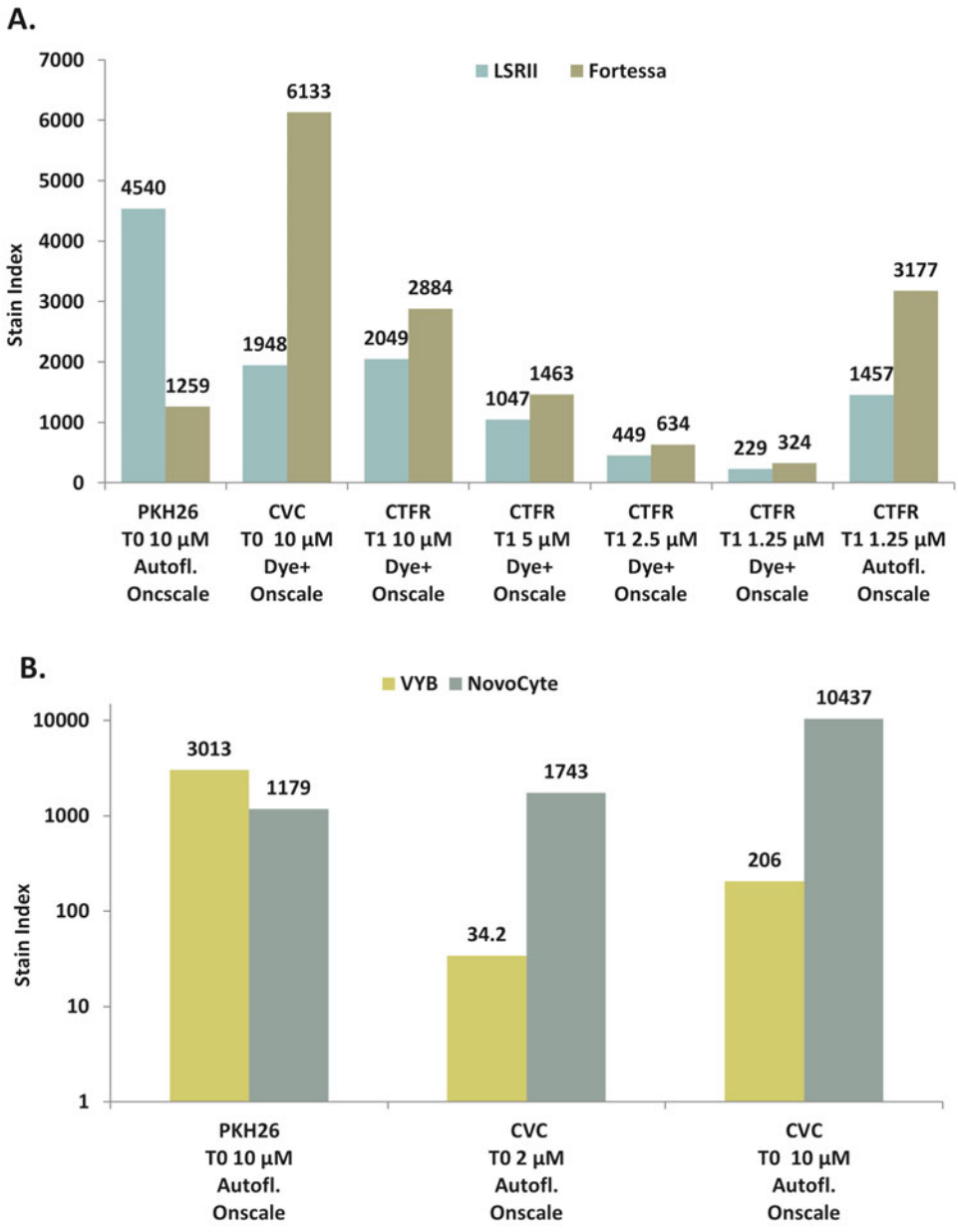

Fig. 3 Effect of cytometer configuration and dye negative population placement on stain indices for selected tracking dyes (*see* **Note 35**). U937 cells were labeled as described in Subheading 3.1 (1.25–10 µM CTFR) or Subheading 3.2 (10 µM PKH26, 2–10 µM CVC) at a final concentration of 1×10^7 cells/mL and analyzed on the indicated cytometers at the time point when a dye dilution analysis would be started (T0 = immediately post-labeling for PKH26 and CVC; T1 ~24 h post-labeling for CTFR). Wherever possible, detector voltages were set to place an unstained control sample fully on-scale in the first decade and stained cells were analyzed under the same conditions ("Autofl. On-scale"). For samples where dye-positive cells were partly or completely off-scale when unstained cells were fully on-scale in the first decade, detector voltage was reduced to place dye positive cells on-scale and unstained cells were visualized using a bi-exponential scale ("Dye+ On-scale"). Stain Index was calculated using Formula 1 of **Note 35**. (Panel **a**) As expected, the Stain

concentration of 2.5–10 $\times$ 10^4 beads/mL after admixing with the cell suspension to be used for culture initiation (for example, if a bead concentration of 10 $\times$ 10^4/mL is desired after admixing with 50 mL of cell suspension, aliquot a volume of bead stock containing at least 5 $\times$ 10^6 beads). Centrifuge the bead suspension at 400 $\times$ *g* for 5 min at ~21 °C, discard the supernatant, and wash twice with 10 mL CM, discarding the supernatant after each centrifugation. After the last wash, resuspend beads in 1 mL of CM.

3. To the cell suspension from **step 1**, add washed beads from **step 2** at the volume needed to give a final bead concentration of 2.5–10 $\times$ 10^4 beads/mL but do not exceed 1% of the volume of cell suspension (for example, if 5 $\times$ 10^6 beads were washed and resuspended in 1 mL CM, adding 200 μL of bead suspension to 40 mL of cell suspension gives a final bead concentration of 2.5 $\times$ 10^4 beads/mL).
4. Mix cell and bead suspensions to homogeneity and separately plate 1 mL of each of suspension into replicate wells of a 24-well flat bottom polystyrene plate for each time point in the kinetic study (e.g., to evaluate 6 time points in quadruplicate, plate 24 wells). Incubate labeled and unlabeled cell cultures in a humidified 37 °C incubator with 5% CO_2 for 7 days.
5. Harvest replicate samples of plated cell cultures for each time point into 12 $\times$ 75 mm round bottom tubes by triturating each well to homogeneity using a P1000 pipette fitted with a clean, sterile tip, and place tubes on ice. For the T0 samples, this should be performed immediately after plating the suspensions from **step 4**, in order to ascertain the starting cell-to-bead ratio.
6. After collecting the samples for Day 3 and Day 5, triturate all remaining wells in the plate as in **step 5**. Remove and discard 500 μL of mixed cell/bead suspension from each well, and replenish with 500 μL of pre-warmed, CO_2-equilibrated CM

Fig. 3 (continued) Index for PKH26 was higher using the 50 mW 561 nm laser on the LSR II (excitation efficiency @ 561 nm ~65% of maximum) than using the 50 mW 488 nm laser on the Fortessa (excitation efficiency @ 488 nm ~20% of maximum). Also as expected, the Stain Index for CTFR decreased on both instruments as dye concentration used for labeling was decreased from 10 to 1.25 μM. Note however, that Stain Index values obtained for cells labeled with 1.25 μM CTFR were substantially higher on both cytometers when detector voltages were set to place unstained cells fully on-scale (AutoFl. On-scale) than when voltages were reduced to place cells stained with 10 μM fully on-scale (Dye+ On-scale) (*see* **Note 36**). (Panel **b**) U937 cells labeled with PKH26 or CVC and an unstained control were analyzed on the indicated instruments during the Bowdoin 2016 Annual Course in Flow Cytometry. Again, the Stain Index for PKH26 was higher when this dye was excited using the 561 nm laser on the MACSQuant VYB than when the 488 nm laser on the NovoCyte was used, whereas CVC was more efficiently excited by the 640 nm laser on the NovoCyte than the 561 nm laser on the VYB

in order to maintain the cultures in log phase growth. After addition of CM, collect a post-dilution sample to verify that cell-to-bead ratio has not changed (i.e., no more than 5% difference from pre-dilution ratio).

7. Add an appropriate viability dye (50 μL of a 5 μg/mL DAPI solution or 40 μL of a 100 μg/mL 7-AAD solution) to each milliliter of harvested cells and incubate on ice for 30 min prior to data acquisition. Do not wash or further manipulate harvested cell suspensions, in order to avoid selective losses of either cells or beads.
8. Acquire harvested samples using a flow cytometer, collecting forward and side scatter characteristics (pulse area, height, and width) as well as all relevant fluorescence detection channels (pulse area). Ensure that the acquisition threshold is configured to allow fluorescent beads and cells to be collected using the same instrument settings. Using the gating strategy summarized in Fig. 4a, set a "Stopping Gate" on R4 and strive to collect 2500 fluorescent beads.
9. Establish the appropriate detector voltage for each dye's primary detection channel, placing unlabeled controls fully on-scale in the first decade and confirm that labeled cells are fully on-scale. If >5% of labeled cells are off-scale high, reduce voltage as needed to bring them on-scale and re-acquire unlabeled controls.
10. After voltages have been satisfactorily configured for each dye's detector, acquire fluorescent Rainbow 6-Peak Calibration Particles and record mean intensity values from all peaks that are well resolved and fully on-scale in a given detector. To ensure consistent fluorescence intensities and enable direct comparison of data that is collected on separate days, use the recorded intensities as target values when re-establishing detector voltages on subsequent days of the experiment.
11. Using appropriate software and the gating strategy illustrated in Fig. 4a, quantify the number of beads acquired during sample analysis. Use serially gated bivariate plots of: Time vs. SSC-A to include only events associated with stable flow rate (R1); FSC-A vs. FSC-H to eliminate doublet events (R2); and FSC-A vs. SSC-A to discriminate bead events (R3) from cellular events. Gating on "R1&R2&R3," create a bivariate plot for any two detectors where beads are expected to be brighter than cells (e.g., Y710/50-A and V780/60-A) and establish a "beads-only" region (R4). Use the combined "R1&R2&R3&R4" gate to generate a bivariate beads-only plot of Time vs. FSC-A and establish a rectangular region (R5) to exclude doublet bead events and provide a singlet bead count.

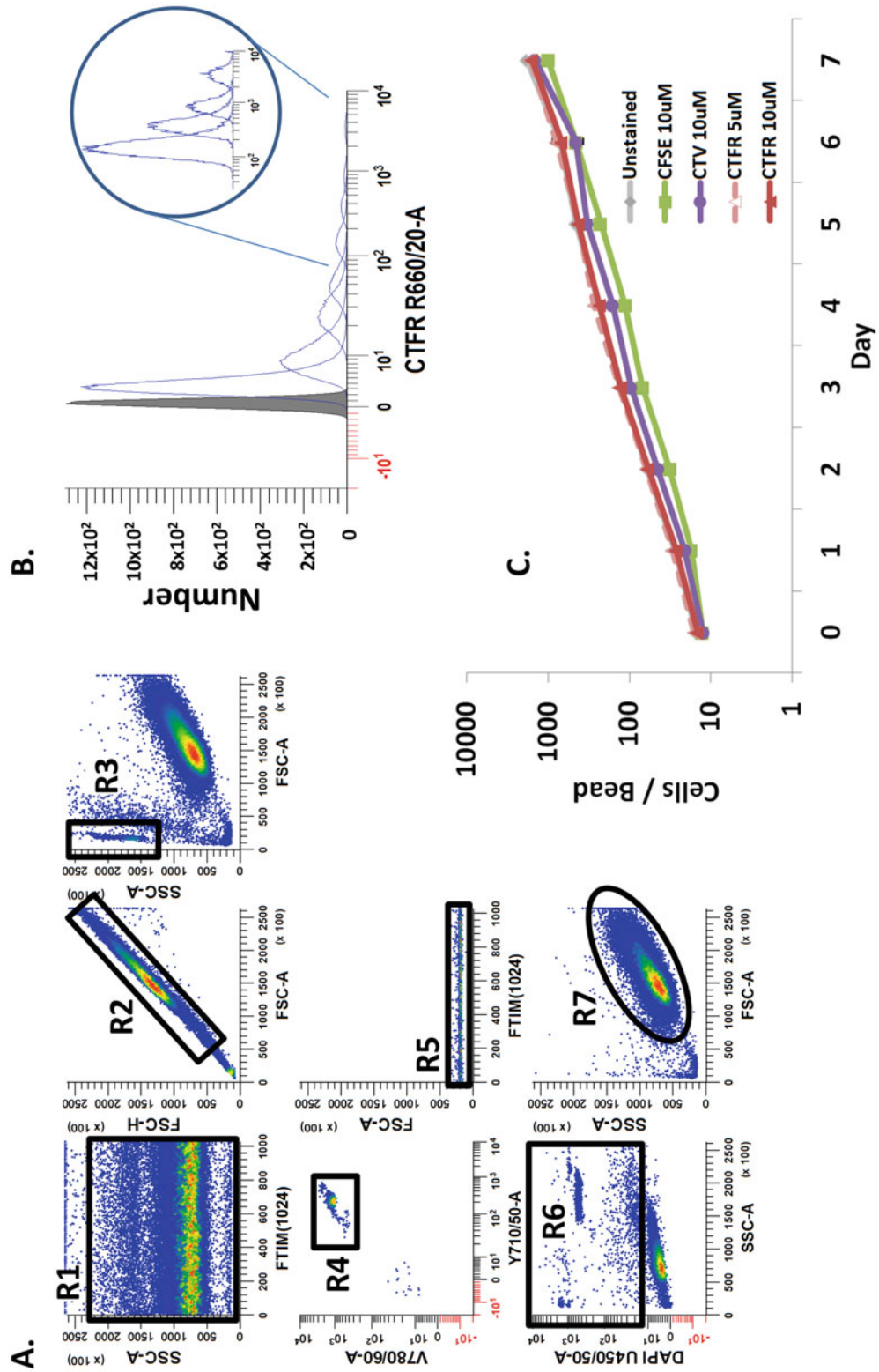
A.
B.
C.
R1
R2
R3
R4
R5
R6
R7
SSC-A
FSC-A
FSC-H
FTIM(1024)
V780/60-A
Y710/50-A
DAPI U450/50-A
CTFR R660/20-A
Number
Cells / Bead
Day
Unstained
CFSE 10uM
CTV 10uM
CTFR 5uM
CTFR 10uM

12. Separately, quantify the number of viable singlet cells acquired during sample analysis (Fig. 4a). Use an "R1&R2" gated plot of SSC-A vs. DAPI U450/50-A (or 7-AAD B695/40-A for CTV) to identify dead cells and beads (R6), and "NOT R6&R1&R2" gated plot of FSC-A vs. SSC-A to distinguish small debris from live U937 cells (R7) and a "NOT R6&R1&R2&R7" gated histogram of dye fluorescence (e.g., CTFR R660/20-A) to provide a singlet cell count and monitor dye dilution over time (Fig. 4b).
13. Calculate cell-to-bead ratio (Cells/Bead) for each acquired sample by dividing the number of events in the "NOT R6&R1&R2&R7" gate (cells) by the number of events in the "R1&R2&R3&R4&R5" gate (beads). For the unstained control and each dye labeled population, plot Cells/Bead vs. Time (Fig. 4c), and use the slope of log(Cells/Bead) vs. time to calculate population doubling times.
14. It is important to note that this method can only be employed in cell systems where phagocytes (e.g., monocytes, macrophages, or dendritic cells) are not present, as they can internalize the counting beads as illustrated in Fig. 5, and render it impossible to obtain accurate "Cell/Bead" ratios. Since the counting beads are fluorescent, it is relatively simple to determine by microscopy or ImageStream cytometry (EMD Millipore, Billerica, MA) whether cells are internalizing beads.

3.4.2 Relative and Absolute Growth Rate Determination in Co-cultures (Volumetric Cytometer)

Cytometers with volumetric cell counting capability allow growth rate to be monitored in absolute units (cells/mL) as well as relative units (% labeled cells in co-cultures) without the addition of counting beads.

1. Harvest logarithmically growing U937 cells and label with tracking dye of interest as described in Subheading 3.1 or 3.2.

Fig. 4 Relative growth rate determination using counting beads (Subheading 3.4.1). U937 cells were labeled as in Subheading 3.1 at the concentrations of CTV, CFSE, or CTFR indicated in Panel **c** and a final concentration of 1×10^7 cells/mL. After addition of 3×10^4 beads/mL to each sample, parallel cultures of labeled and unlabeled cells were cultured for 7 days, with addition of fresh CM on Days 3 and 5 to maintain logarithmic growth. On each day, quadruplicate wells for each test article were separately triturated to homogeneity, harvested, stained with DAPI (CFSE, CTFR) or 7-AAD (CTV) for viability assessment, and acquired on the LSRII cytometer. (Panel **a**) Data files were analyzed using the gating strategy described in Subheading 3.4.1, **steps 11** and **13**, with a Stopping Gate (R4) set to 2500 beads. (Panel **b**) Histogram overlays for viable U937 cells ('NOT R6&R1&R2&R7') present in unstained (filled distribution) and Day 0–Day 7 CTFR-labeled cultures, normalized to the volume of sample associated with a bead count of 250. Inset: Days 0–3 on an expanded scale. (Panel **c**) Cell/Bead ratio increased over time at similar rates in all samples, indicating that growth rate was not altered by labeling with any of the three dyes at the concentrations tested. Calculated doubling times ranged from a low of 24.8 h (unstained cells) to 26.3 h (CFSE stained cells)

2. For co-cultures, add 1×10^5 stained cells and 1×10^5 unstained cells to a sufficient amount of CM to give a final volume of 10 mL and place in a 25 cm^2 culture flask. For parallel cultures, add 2×10^5 stained cells in a sufficient amount of CM to yield a final volume of 10 mL. To a control flask, add 2×10^5 unstained cells in a sufficient amount of CM to yield a final volume of 10 mL. Incubate in a humidified 37 °C incubator with 5% CO_2 for 5–7 days.
3. Immediately after cells are placed in culture flasks, and at approximately 24 h intervals thereafter, mix well by triturating and withdraw a 1.0 mL aliquot for flow cytometric analysis. On

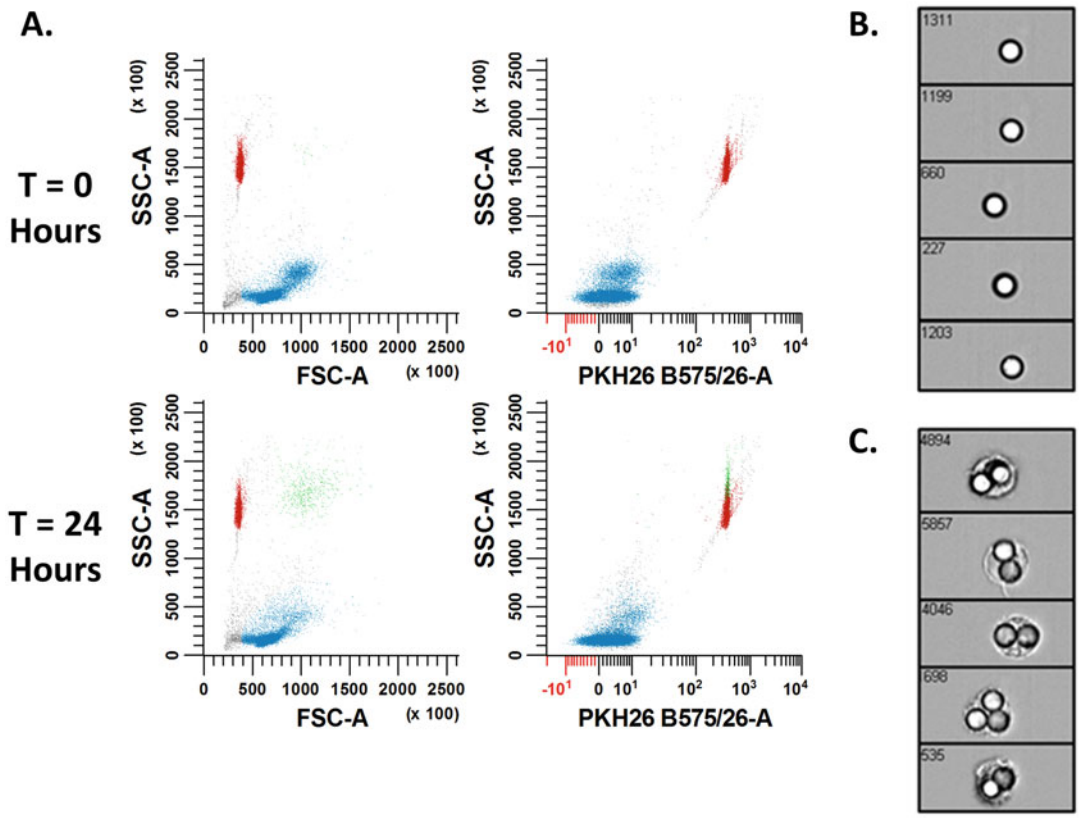

Fig. 5 The presence of phagocytes invalidates use of counting beads for relative growth rate determination. When PKH26 counting beads (*red* events) are added to unstimulated cultures of unstained hPBMC (Panel **a**, $T = 0$ h), they are readily distinguished from mononuclear cells (*blue* events). After 24 h in culture (Panel **a**, $T = 24$ h), hPBMCs with the highest FSC-A (presumed to be monocytes) increase in side scatter and become PKH26 positive (*green* events). Analysis of the $T = 24$ sample on an ImageStream$^{®X}$ Mark II imaging flow cytometer (EMD Millipore) confirmed that the red, $FSC^{low}SSC^{high}PKH26^{high}$ events were singlet PKH26 beads (Panel **b**) while the *green*, $FSC^{high}SSC^{high}PKH26^{high}$ events were phagocytes that had engulfed multiple PKH26 beads (Panel **c**). Phagocyte ingestion of beads caused lymphocyte to bead ratio (ratio of $FSC^{low}SSC^{low}PKH26^{-low}$ blue events to $FSC^{low}SSC^{low}PKH26^{high}$ *red* + *green* events) to increase from 1.53 at $T = 0$ to 2.25 at $T = 24$ although there was no cell growth during this period

Day 3 after trituration, remove the entire volume of cell suspension and dispense 2.5 mL back into culture flask, reserving 1.0 mL for pre-dilution analysis. Add 7.5 mL fresh pre-warmed, CO_2-equilibrated CM to maintain logarithmic cell growth, mix well by triturating, and withdraw a second 1.0 mL (post-dilution) sample.

4. Use the laboratory's standard reference material(s) to ensure that the flow cytometer is giving reproducible intensity values in all detectors to be used (as described in Subheading 3.4.1). Configure the flow cytometer to acquire data from all fluorescence detection channels and adjust FSC and SSC detector voltages to ensure that cells of interest are resolved from electronic noise/small debris and large aggregates.
5. Use unlabeled cells to establish voltage settings that place their measured fluorescence distribution fully on-scale within the first decade in the primary detection channel for each tracking dye being evaluated. Using the same instrument settings, confirm that the labeled cell populations are fully on-scale. If more than 5% of the labeled cells fall off-scale high, decrease detector voltage to bring the labeled cells fully on-scale, re-acquire the unlabeled cells at the new setting.
6. Use appropriate software to generate a single-parameter histogram for each tracking dye in its primary detection channel. At a minimum, histograms should be serially gated on: bivariate plots of Time vs. SSC-A to eliminate any events associated with unstable flow rate; FSC-A vs. SSC-A to discriminate cellular events from small debris and large aggregates; and additional viability and/or doublet gates as needed.
7. For data analysis, restrict the evaluated population to viable U937 on a bivariate plot of FSC-A vs. SSC-A, circumscribe the viable cell population with an elliptical region (P1), and establish analysis regions for labeled and unlabeled populations on the P1-gated fluorescence intensity histograms (Fig. 6a).
8. Using the gated histograms, record the following for each time point at which labeled and unlabeled cell populations remain non-overlapping (*see* **Notes 37** and **38**): (a) labeled cells/mL; (b) unlabeled cells/mL; (c) dilution factor from **step 3** [pre-dilution cell count divided by post-dilution cell count], if appropriate; and (d) % labeled cells.
9. Using Microsoft Excel or similar software, compare growth rates for labeled vs. unlabeled cells by plotting % labeled cells vs. Time (Fig. 6b) and cells/mL vs. Time (Fig. 6c) to identify concentration(s) that do not impair cell growth.

3.4.3 Assessing Linearity of Dye Dilution

Once labeling conditions that do not perturb cell growth rate have been established, absolute cell counts obtained from parallel cultures or co-cultures (as described in Subheadings 3.4.1 and 3.4.2)

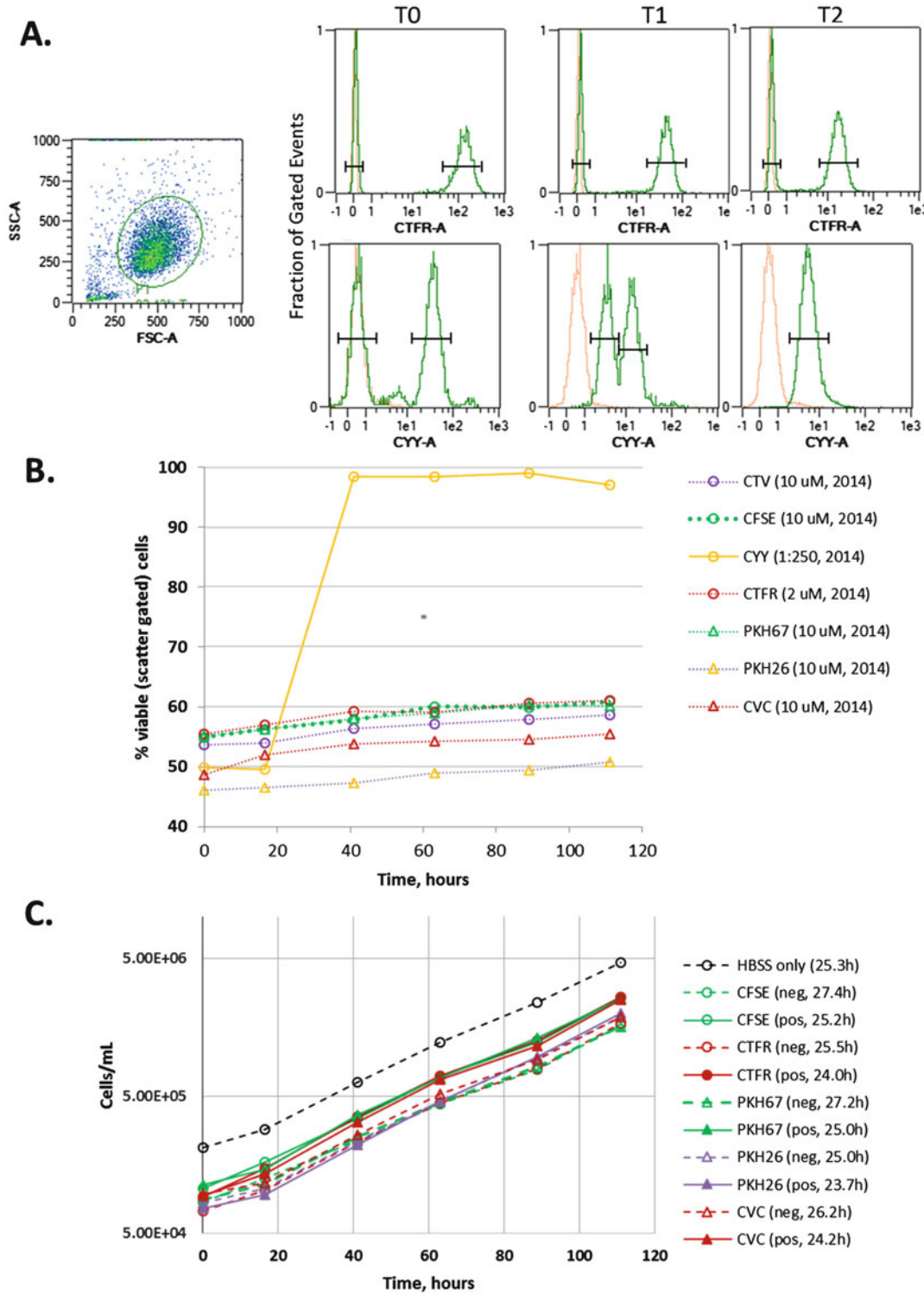
A.
SSC-A
FSC-A
T0
T1
T2
Fraction of Gated Events
CTFR-A
CYY-A
B.
% viable (scatter gated) cells
Time, hours
CTV (10 uM, 2014)
CFSE (10 uM, 2014)
CYY (1:250, 2014)
CTFR (2 uM, 2014)
PKH67 (10 uM, 2014)
PKH26 (10 uM, 2014)
CVC (10 uM, 2014)
C.
Cells/mL
Time, hours
HBSS only (25.3h)
CFSE (neg, 27.4h)
CFSE (pos, 25.2h)
CTFR (neg, 25.5h)
CTFR (pos, 24.0h)
PKH67 (neg, 27.2h)
PKH67 (pos, 25.0h)
PKH26 (neg, 25.0h)
PKH26 (pos, 23.7h)
CVC (neg, 26.2h)
CVC (pos, 24.2h)

can be used to evaluate the correlation between cell growth rate and dye dilution rate.

1. For each dye and time point (T) after culture initiation (T0), calculate:
   (a) Fold Growth = count (*T*)/count (T0)
   (b) Fold Dye Dilution = median fluorescence intensity (T0)/median fluorescence intensity (*T*)
2. Use Microsoft Excel or similar software to plot Fold Growth vs. Fold Dye Dilution for each dye of interest (Fig. 7; *see* **Note 39**). A perfect twofold decrease in dye intensity at each cell division would give a linear correlation with slope = 1.0.

3.5 Further Considerations for Cell Proliferation Monitoring

Although cultured cell systems are useful for establishing spectral compatibility with other fluorescent probes (Subheading 3.3; Figs. 1 and 2) and linearity of dye dilution for a given cell tracking dye (Subheading 3.4; Fig. 7), additional considerations arise when the biology of interest includes both responders and non-responders (e.g., immune cell populations responding differentially to a specific stimulus). In such cases, mathematical modeling is used to quantify the frequency of cells within the starting population that go on to respond to the stimulus and/or overall expansion within the responding subpopulation. Because no currently

Fig. 6 Relative and absolute growth rate determination using volumetric counting. U937 cells were separately stained with each of the indicated tracking dyes as in Subheadings 3.1 and 3.2 (final concentrations: 1×10^7 cells/mL and 10 μM dye) and placed in 1:1 co-culture with unstained cells as in Subheading 3.4.2. An unstained control at the same total density was cultured in parallel. Aliquots withdrawn at each time point were acquired on a MACSQuant 10 Analyzer during the Bowdoin 2014 Annual Course in Flow Cytometry. Fluorescence histograms for each dye, gated on light scatter (P1, Panel **a**) to eliminate debris and aggregates, were used to determine absolute counts (cells/mL) and % stained cells at each time point. *Green* histograms denote co-cultures; *pink* histograms denote the unstained control. (Panel **a**) Baseline separation between stained and unstained populations was maintained through Day 5 for CTFR co-cultures (*upper histograms*) and those for all other dyes except CYY (*lower histograms*). For CYY, two approximately equal populations were still distinguishable in the Day 1 co-culture (*lower middle histogram*) but the "unstained" population was ~7-fold brighter than the unstained control and was beginning to merge with the stained population, which had decreased 2.7-fold in intensity from Day 0 to Day 1. By Day 2, only a single population was evident in co-culture (*lower right histogram*). CYY was the only dye for which unstained cells exhibited such a rapid and extensive right shift, suggesting that the cause was dye-specific and not due to trogocytosis or other cell-type specific transfer mechanisms (*see* **Note 38**). (Panel **b**) Stable values for % dye positive cells over time indicated that cells labeled with CTV, CFSE, PKH67, PKH26, CTFR, or CVC were growing at rates similar to unstained cells in co-cultures. In contrast, % CYY stained cells increased dramatically from Day 1 to Day 2 due to loss of resolution between stained and "unstained" cells (*see* Panel **a**). (Panel **c**) Plots of absolute cell counts vs. time (Day 3 value = average of pre- and post-dilution counts) confirmed that both stained ("pos") and unstained ("neg") populations grew logarithmically during the 5 day co-culture period, with doubling times (indicated in *parentheses*) similar to those of the unstained control culture (*see* plot legend)

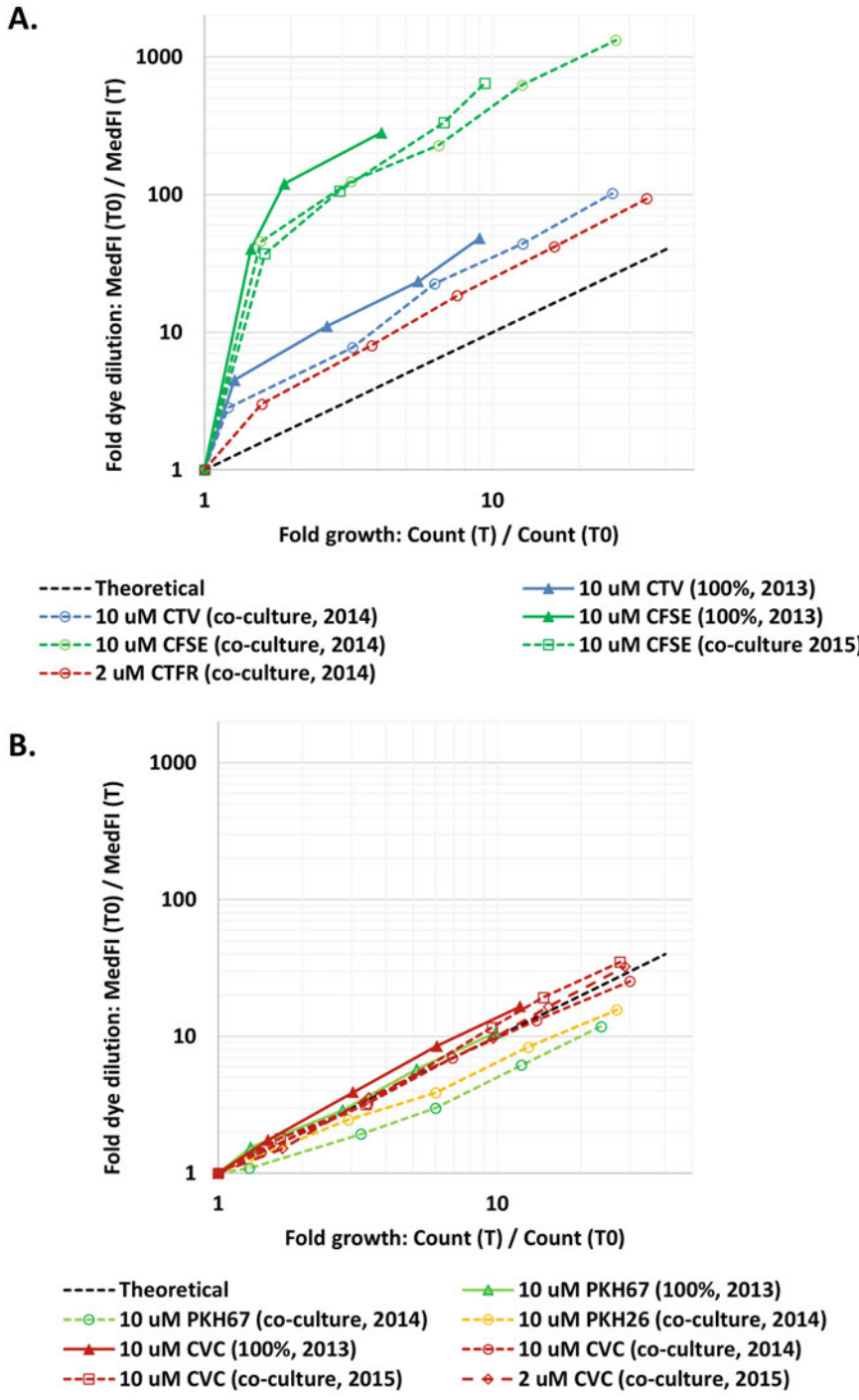

Fig. 7 Correlation between growth rate and dye dilution rate (Subheading 3.4.3; *see* **Note 39**). U937 cells labeled as described in Fig. 6 and unstained controls were placed in separate parallel cultures (Subheading 3.4.2; 2013 data) or in 1:1 co-cultures (Subheading 3.4.2; 2014 and 2015 data) for 4–5 days. Aliquots withdrawn at each time point were acquired on three different MACSQuant 10 Analyzers during the

available tracking dyes of either type give baseline resolution between daughter generations, selection of an appropriate proliferation dye requires knowing the number of daughter generations that can be reliably discriminated from undivided non-responders using a given dye. This is determined by several factors: (a) the highest tolerated labeling concentration, which will dictate the initial cell labeling intensity; (b) extent of division-independent dye loss for a given dye (Fig. 7a); and (c) effect of stimulation on the autofluorescence of dye-naïve cells. In addition, in situations where a distinguishable non-responder peak is not present, it is important to know whether the location of stained but unstimulated controls from the same time point can be used as a surrogate to establish the expected location of non-responders in the stimulated sample. Assessment of these considerations is illustrated here using hPBMC stimulated with anti-CD3 and anti-CD28 to generate a polyclonal T cell response.

1. Generate a preparation of hPBMCs from peripheral blood using the laboratory's standard density gradient fractionation protocol, with the addition of a final low-speed wash ($300 \times g$) to minimize platelet contamination (*see* **Note 1**).
2. Enumerate harvested cells using the laboratory's preferred methodology.
3. Label hPBMCs with desired tracking dye (Subheadings 3.1. and 3.2). Reserve a sufficient number of unlabeled hPBMCs to employ as autofluorescence assay controls; generally, an equal number of dye-labeled and unlabeled cells are required.
4. Adjust unlabeled and dye-labeled cells to 2×10^5 cells/mL in CM and divide both labeled and unlabeled hPBMC into two equal volumes. To half of each cell suspension add azide-free anti-CD3 (clone OKT3) to a final concentration of 1 μg/mL plus anti-CD28 (clone 28.2) to a final concentration of 0.5 μg/mL (stimulated culture). Leave the other half unstimulated.
5. Separately dispense 0.5 mL (1×10^5 total cells) of each test article into quadruplicate wells of a 96-well U-bottom polypropylene stripwell plate for each time point to be evaluated, and

Fig. 7 (continued) 2013–2015 Annual Courses in Flow Cytometry and analyzed as described in Fig. 6. (Panel **a**) All protein dyes tested exhibited much greater dye dilution between T0 and T1 (~20 h) than could be attributed to cell growth alone, reflecting the early, division-independent intensity loss characteristic of this dye class. CTV and CTFR showed less division-independent dye loss than CFSE, as indicated by their lesser T0–T1 dilution despite similar growth rates for all three dyes (1.3–1.6-fold increase in cell counts). During the remainder of the culture period dye dilution was linear for all three dyes and more closely reflected cell growth rate, with slopes slightly greater than theoretical (range: 1.4–1.8). (Panel **b**) All membrane dyes tested exhibited relatively linear dilution from throughout the entire culture period, with slopes similar to or slightly less than theoretical (range: 0.6–1.2)

incubate in a humidified 37 °C incubator with 5% CO_2 for 96 h (*see* **Note 40**). For example, to evaluate 5 time points in quadruplicate, establish 20 stimulated wells and 20 unstimulated wells for each dye-positive hPBMC test article; in parallel, establish 20 stimulated wells and 20 unstimulated wells for unlabeled (dye-negative) control cells.

6. At each time point, remove the appropriate dye-positive and dye-negative stripwell tubes from the plate that corresponds to the indicated time point, and return the remainder to the humidified 37 °C incubator with 5% CO_2. Separate individual tubes from each selected strip, lightly vortex to resuspend cells and then transfer the stripwell tubes to the bottom of individually labeled 12 × 75 mm tubes, without washing or manipulating the samples.
7. Add an appropriate viability dye (25 μL of a 5 μg/mL DAPI solution or 20 μL of a 100 μg/mL 7-AAD solution) to each tube containing 0.5 mL of cultured cells and let stand on ice for 30 min prior to data acquisition.
8. Acquire data on the flow cytometer as described in Subheading 3.4.1, **steps 9** and **10**.
9. Use appropriate software (e.g., WinList, FCS Express, or FlowJo) and the gating strategy shown in Fig. 8a to analyze acquired data. Use serially gated bivariate plots of: Time vs. SSC-A to include only events associated with stable flow rate (R1); FSC-A vs. FSC-H to select single cells (R2) and eliminate doublets; SSC-A vs. DAPI-A (or 7-AAD-A) to exclude dead cells (R3); FSC-A vs. SSC-A to define cellular events (R4); and the relevant fluorescence parameter(s) vs. SSC-A to generate fluorescence histograms for unlabeled or tracking dye labeled lymphocytes (*see* **Note 41**).
10. For every experimental condition assayed, generate overlay histograms of unlabeled and dye-labeled fluorescence distributions from each time point and stimulation condition, as illustrated in Fig. 8b, c. Identify the intensity at which highly divided cells can no longer be distinguished from the background fluorescence associated with unstained but stimulated cells. This will determine the maximum number of daughter generations that can accurately be modeled when estimating the fraction of the original population responding to a given stimulus and/or the extent of population expansion during the response (*see* **Note 37**).
11. Use appropriate peak modeling software (e.g., ModFit LT, FCS Express, or FlowJo) to analyze the viable, singlet, lymphocyte dye dilution histograms acquired at each time point from unstimulated (Fig. 8b) and stimulated (Fig. 8c) cultures and obtain the best fit to each according to the principles described

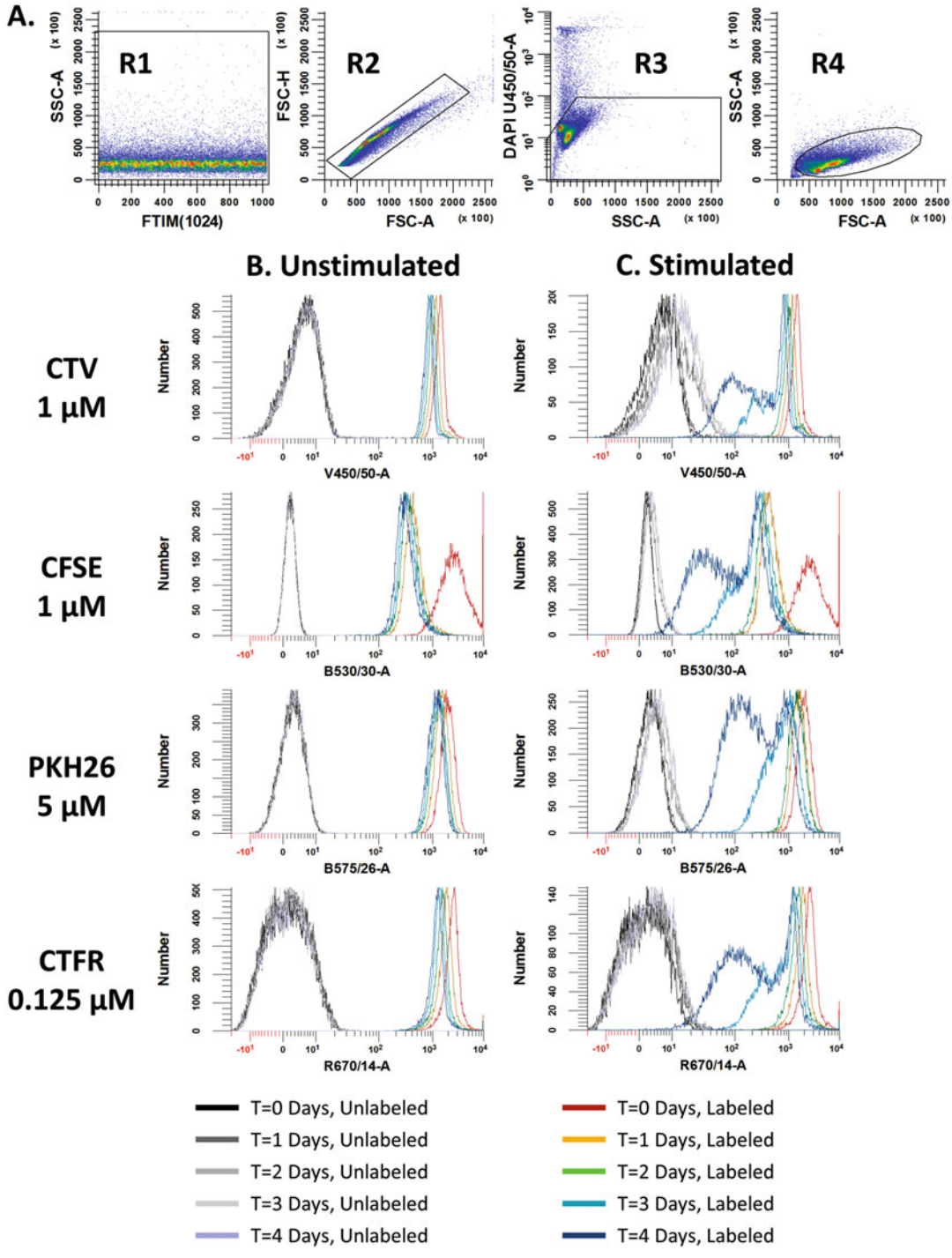

Fig. 8 Effect of dye choice on division-independent dye dilution and ability to resolve highly divided cells from unlabeled cells (Subheading 3.5). hPBMC were separately stained with the indicated tracking dyes as described in Subheadings 3.1 and 3.2 (final cell concentration: 1×10^7 cells/mL for CTV, CFSE, and CTFR; 5×10^7 cells/mL for PKH26; final dye concentrations as shown) and cultured in quadruplicate without (Panel

in ref. 34 (*see* **Note 37**). For each unstimulated control sample, record the median intensity of the highest intensity (parental) peak reported by the model (MFI, Parental). For each stimulated sample, record the median intensity of the highest intensity (non-responder) peak reported by the model (MFI, Non-Responders). To determine whether dye dilution occurs at the same rate in non-proliferating cells under stimulated vs. unstimulated conditions, plot MFI, Non-responders vs. MFI, Parental as shown in Fig. 9. For such a plot, a slope of 1.0 indicates that there are no metabolic or other differences causing a systematic difference in the rate of dye dilution in stimulated vs. unstimulated cultures.

3.6 Evaluating the Effect of Tracking Dye Labeling on other Cellular Functions

In addition to proliferation monitoring, cell tracking dyes can be used for measuring cytotoxic effector cell activity by flow cytometry. This method does not require radioactivity and has the advantage of being able to measure killing at the single cell level even when targets and effectors cannot be distinguished on the basis of light scatter. The protocol described here uses killing of a cultured cell line (K562) by lymphokine-activated killer (LAK) cells as a model system, but the principles and general procedures are applicable to virtually any effector–target combination.

3.6.1 Generation of Stained LAK Effector Cells

1. Prepare hPBMCs from peripheral blood using the laboratory's standard density gradient fractionation protocol, with the addition of a final low-speed wash ($300 \times g$) to minimize platelet contamination (*see* **Note 1**). Enumerate harvested cells using the laboratory's preferred methodology and adjust cells to 1×10^7 hPBMC/mL in HBSS.

Fig. 8 (continued) b) or with (Panel **c**) anti-CD3 + anti-CD28 stimulation. Data were acquired on an LSR Fortessa flow cytometer; one representative result is shown for each test condition. (Panel **a**) Data files were collected using the gating strategy shown, with a Stopping Gate of 50,000 events in R4. Representative data and gating regions are shown for one of four replicate 96 h cultures. (Panel **b**) Overlays show Day 0–4 histograms for viable singlet lymphocytes from unstimulated cultures. Since lymphocytes do not proliferate under these conditions, T0–T1 intensity decreases represent division-independent dye loss. As was seen for U937 cells (Fig. 7a), CTV and CTFR showed much less division-independent dye loss than CFSE. (Panel **c**) Overlays show Day 0–4 histograms for viable singlet lymphocytes ('R1&R2&R3&R4' gate) in anti-CD3 + anti-CD28 stimulated cultures. As previously observed ([33]), stimulated but unstained lymphocytes exhibit measurably increasing autofluorescence over time, particularly in the V450/50 channel. As a result, even though CTV exhibits less division-independent early dye loss than CFSE, the ability to resolve unstained cells from stained but highly divided cells on Days 3 and 4 post-stimulation is actually slightly worse for cells labeled with 1 μM CTV than for those labeled with 1 μM CFSE. In situations where it is important to maximize resolution of unstained vs. highly divided cells but CTV concentration cannot be further increased without impacting cell function (*see* Subheading 3.6), use of a longer emitting tracking dye (e.g., PKH26, CTFR, CVC) may prove helpful

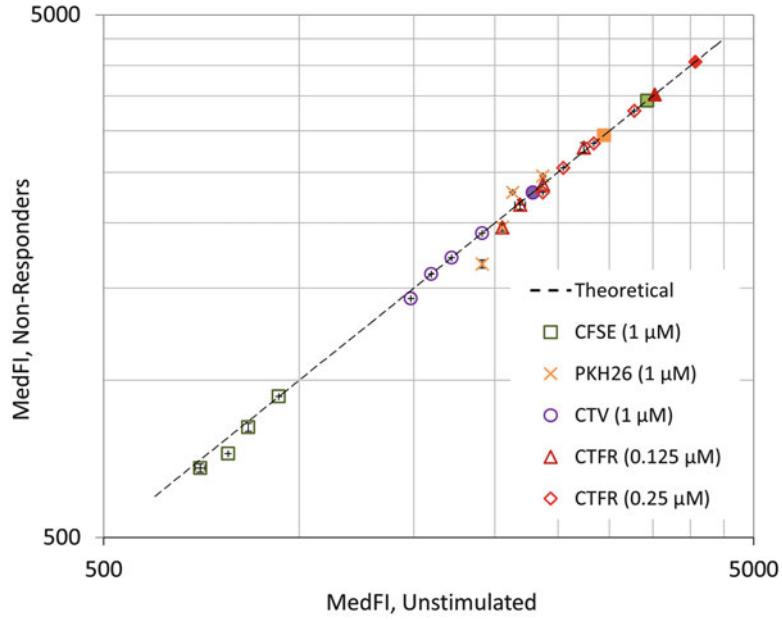

Fig. 9 Effect of stimulation on rate of dye dilution in non-proliferating lymphocytes (Subheading 3.5). ModFit LT v4.0 was used to fit the quadruplicate histograms acquired each day for unstimulated (Fig. 8a) and stimulated (Fig. 8b) hPBMC cultures as previously described ([34]). The mean value for median fluorescence intensity (medFI) reported by the best fit model for unstimulated quadruplicates was plotted against mean value for medFI reported by the best fit model for non-proliferating cells ("non-responders") in the stimulated quadruplicates. Error bars (± 1 standard deviation) are shown but in many cases are smaller than the plotted symbols. The T0 value for each dye is shown as a filled symbol with remaining time points shown as unfilled symbols. Despite the much greater initial intensity drop for CFSE, all four dyes studied gave slopes close to theoretical (range 1.0–1.1). This indicates that if there is not a distinct peak corresponding to the non-responders, the unstimulated control can provide a good estimate of its position in the stimulated histogram

2. Label hPBMC with desired tracking dye according to the procedures described in Subheadings 3.1 and 3.2 (*see* **Note 42**).
3. Assess recovery, viability, and fluorescence intensity profile of labeled cells immediately post-staining to determine whether to proceed with assay setup (*see* **Note 43**).
4. Resuspend labeled hPBMC in CM at 3×10^6 cells/mL (typically 5–10 mL total volume) and incubate upright in a T25 flask with 1000 IU/mL of IL-2 at 37 °C for 4 days to generate LAK effector cells. Establish a parallel flask of unstained hPBMC for use as assay and instrument setup controls (Subheadings 3.6.3 and 3.6.4).
5. On Day 4, harvest LAK effector cells, triturating to disperse any cell clusters into a single cell suspension. Wash once with 50 mL CM, count and resuspend at 1×10^7 cells/mL in CM.

3.6.2 Labeling K562 Target Cells

1. On Day 4 of the LAK induction period, harvest logarithmically growing K562 targets (*see* **Note 44**). Wash cells twice with 50 mL HBSS, count and adjust to 1×10^7 cells/mL in HBSS.
2. Label K562 cells with desired cell tracking dye according to the procedures described in Subheadings 3.1 and 3.2.
3. Assess recovery, viability, and fluorescence intensity profile of labeled cells immediately post-staining to determine whether to proceed with assay setup (*see* **Note 43**).
4. Wash tracking dye-labeled K562 targets twice in 15 mL CM. Count and adjust to 1×10^5 cells/mL in CM.

3.6.3 Cytotoxicity Assay

1. In a 96-well round bottom polypropylene plate, make triplicate serial 1:2 dilutions of the LAK effectors as follows: Pipet 200 μL of the stained LAK cell suspension into the first well, and 100 μL of CM into each of seven adjacent wells. Serially transfer 100 μL of LAK cells from the first well to the second, then from the second to the third, etc., ending with a transfer of 100 μL from well 7 to well 8 and removal of 100 μL of cell suspension from well 8.
2. Add 100 μL of stained K562 targets to each well, creating effector to target ratios of 100:1, 50:1, 25:1, 12.5:1, 6.2, 3.1, 1.6, and 0.8:1 (total volume per well: 200 μL).
3. Add 100 μL of targets and 100 μL of effectors to the target-only and effector-only wells respectively, followed by 100 μL of CM (*see* Table 3 for recommended assay and staining/instrument setup controls). Incubate the plate at 37 °C for 4 h (*see* **Note 45**).
4. After the incubation period has elapsed, label test wells directly in the 96-well plate on ice for 30 min with a saturating amount of anti-CD45 antibody (*see* **Note 46**).
5. Transfer the contents of each well into individually labeled 12 × 75 mm round bottom tubes compatible with the laboratory's flow cytometer. Wash each well with 200 μL of cold FCM buffer and transfer wash fluid to the appropriate tube.
6. Wash each sample once with 3 mL of cold FCM buffer and resuspend the resultant cell pellets in the residual volume remaining (~50 μL). Add 150 μL of FCM buffer to each tube to yield a final volume of ~200 μL.
7. Add 8 μL of 7-AAD (100 μg/mL stock) for CTV-labeled LAK cells; or 10 μL of DAPI (5 μg/mL stock) for CTFR-labeled or unlabeled LAK cells. Let stand for 30 min on ice so 7-AAD or DAPI can equilibrate before initiating acquisition of flow cytometric data (*see* **Note 47**).

3.6.4 Flow Cytometric Acquisition and Analysis

1. Establish appropriate voltage settings using autofluorescence and single color controls from Table 3 (*see* **Notes 43** and **48**).

Table 3
Recommended assay and staining/instrument setup controls for dual cell tracking cytotoxicity assay (Subheading 3.6)

	Cells	Label	Treatment	Comments
Assay Controls[a]	LAK effectors only	CTV, CVC, or CTFR	Incubate with assay samples	*Negative control*: Used to calculate spontaneous LAK cell death
	K562 targets only	PKH67 or CFSE	Incubate with assay samples	*Negative control*: Used to calculate spontaneous K562 cell death
	K562 (heat killed) + LAK effectors	PKH67 or CFSE CTV, CVC, or CTFR	Incubate with assay samples	*Positive control*: only appropriate for assessment by 7-AAD or DAPI exclusion, not bead enumeration
	LAK cells	None	Same *E*:*T* ratios as test samples	*Staining control*: Used to verify that tracking dye labeled cells kill equivalently to unlabeled cells[b]
Instrument Controls[c]	K562 cells	None	None	Select voltage for LAK-channel[d]
	K562 cells	PKH67 or CFSE	None	Select voltage for K562 channel; set color compensation for all other channels; set negative region in LAK channel
	K562 cells	CD45-PacBlue or CD45-BV510	None	Set CD45 threshold or gate to include both targets and effectors (K562 MFI < LAK MFI)
	LAK cells	None[e]	None	Select voltage for $K562^{neg}$ channel[f]
	LAK cells	CTV, CVC, or CTFR	None	Select voltage for LAK channel; set color compensation in all other channels; set negative region in K562 channel
	LAK cells	CD45-PacBlue or CD45-BV510	None	Color compensation
	LAK cells	7-AAD or DAPI	Heat killed[g]	Color compensation

[a]Negative and positive Assay Controls are included in the experimental plate with test samples, or set up in parallel with the experimental plate, to verify that the expected biological outcomes can be recognized using the chosen instrument conditions

[b]Needed only to establish optimized staining conditions for tracking dye when assay is first being implemented in the laboratory; not required on a routine basis

[c]Instrument Controls are used to establish instrument voltages and compensation settings

[d]Use of unstained LAK to select high voltage for the CTV or the "far red" (CVC or CTFR) detectors would place unstained K562 cells midscale due to their much greater autofluorescence. Therefore, unstained K562 cells were used instead to maximize dynamic range

[e]For unstained LAK cell controls, it will be necessary to set up a separate culture of unstained hPBMC with IL-2 at the same time as the PKH67 or CFSE stained hPBMCs

[f]Use of unstained K562 to select high voltage for the "green" (PKH67 or CFSE) detector would place unstained LAK cells off-scale low due to their much lower autofluorescence. Therefore unstained LAK cells were used instead to maximize dynamic range

[g]To heat kill, incubate at 56 °C for 30 min. K562 cells could also be used but light scatter properties after heat killing differ substantially from those seen after LAK killing

2. Using the single color controls from Table 3, adjust compensation settings according to your laboratory and/or instrument manufacturer's standard procedures.
3. Acquire data on the flow cytometer and analyze data using the gating strategy described in Fig. 5 of ref. 19 and summarized in **steps 4–9** below (*see* **Notes 46** and **49**).
4. Evaluate all acquired events on a bivariate plot of SSC-A vs. CD45-A, using a rectangular region (R1) to restrict the subsequent analysis to CD45+ cellular events (and bead events, if added; *see* **Note 49**).
5. Gate R1 inclusive events to a bivariate plot of FSC-A vs. SSC-A, and use an irregular region (R2) to exclude any contaminating debris, but include all live and dead target and effector cells. If present, bead events should be separately circumscribed by a rectangular region (R3).
6. A reciprocal gating strategy is applied to assess target and effector cell numbers and viability. This strategy is used because substantial differences in autofluorescence exist between targets and effectors (*see* Table 3) which render it difficult to establish instrument settings that provide complete resolution between K562 targets labeled with Tracking Dye 1 ($TD1^{pos}$) and LAK cells that are $TD1^{neg}$. Much better resolution is possible by using a second tracking dye to identify LAK cells ($TD2^{pos}$). Events satisfying the Boolean definition of R1&R2 ($CD45^{pos}$ cells) are gated to a bivariate plot of TD2 fluorescence vs. Viability Dye fluorescence (*see* **Note 47**). Use a rectangular region (R4) to identify all target cells ($TD2^{neg}$). Then construct a gated (R1&R2&R4) bivariate plot of TD1 fluorescence vs. Viability Dye fluorescence to enumerate live (R5) vs. dead (R6) $TD1^{pos}$ target cells.
7. Use a similar reciprocal strategy to quantify live vs. dead effector cells. First, gate $CD45^{pos}$ cells (R1&R2) separately to a bivariate plot of TD1 fluorescence vs. Viability Dye fluorescence and use a rectangular region (R7) to identify $TD1^{neg}$ effector cells. Then construct a gated (R1&R2&R7) bivariate plot of TD2 fluorescence vs. Viability Dye fluorescence to enumerate live (R8) vs. dead (R9) effector cells.
8. If counting beads are employed in the assay, enumerate them first on a gated (R3) bivariate plot of any two fluorescence parameters that yield good separation between broad-spectrum fluorescent beads and any cellular events that may have contaminated R3. Discriminate the counting beads from cellular events with a rectangular region (R10).
9. Construct a gated (R3&R10) bivariate plot of TIME vs. FSC-A, and employ a rectangular region (R11) to circumscribe all singlet beads in chronological continuity.

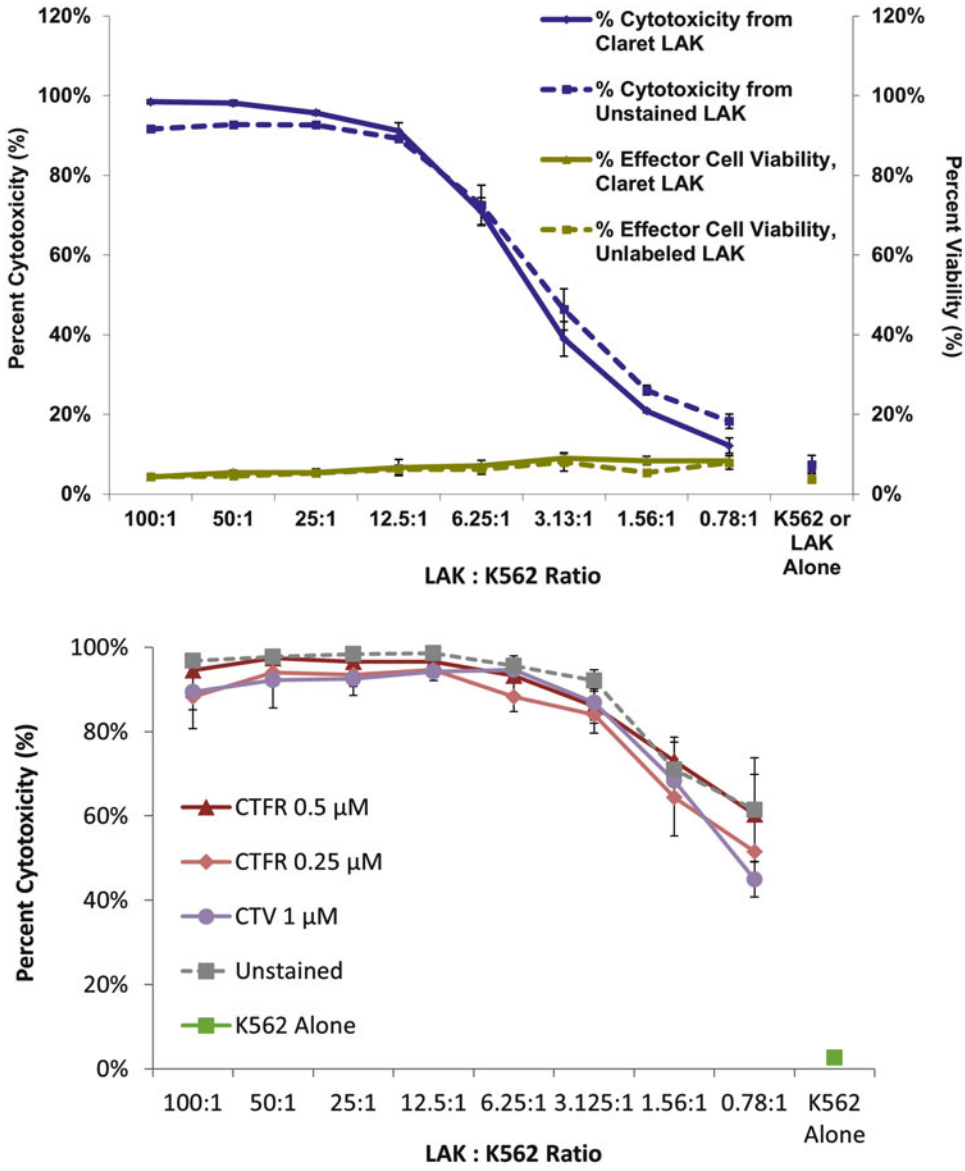

Fig. 10 LAK cell mediated killing of K562 targets is unaffected by staining. LAK cells were independently labeled with CTV, CVC, or CTFR as described in Subheadings 3.1 and 3.2 and incubated with K562 cells labeled with PKH67 or CFSE at the indicated effector-to-target (*E*:*T*) ratios for 4 h at 37 °C. Test samples and controls (Table 3) were analyzed using the gating strategy described in Fig. 5 of ref. 19 and **steps 4–7** of Subheading 3.6.4. LAK cells used in Panels **a** and **b** were derived from the same donor several years apart. (Panel **a**: reproduced from ref. 19, with permission) LAK-induced cytotoxicity of PKH67-labeled K562 cells was assessed for each condition as percent of target cells that took up 7-AAD. As an internal control, percentage of dead LAK effectors (*green lines*) was assessed at each *E*:*T* ratio and verified to be acceptably low and relatively constant. To determine whether CVC staining affected LAK cytolytic potential, parallel studies were performed using CVC stained (*solid lines*) or unstained (*dashes*) LAK effectors. The data indicate that LAK cells kill K562 cells in a concentration-dependent manner, and that labeling with CVC did not affect their function. Representative data are shown from one of two replicate experiments analyzed on an LSRII cytometer; data points represent the mean ± 1 standard deviation of triplicate samples. Final staining concentrations used:

10. Calculate % cytotoxicity using the formula below (*see* Fig. 10 and **Note 49**).

$$\%\text{Cytotoxicity} = \frac{(\text{TD1}^+ \text{ Viability Dye}^+ \text{events})}{\text{Total number of TD1}^+ \text{events}}$$

Similarly, % viable LAK effector cells is calculated as:

$$\%\ \text{Viable Effectors} = \frac{(\text{TD2}^+ \text{ Viability Dye}^- \text{ events})}{(\text{Total number of TD2}^+ \text{ events})}$$

11. An alternative method uses a calculation comparable to the approach used in a standard ^{51}Cr release assay, using region R11 to enumerate singlet beads and region R5 to enumerate live K562 targets (*see* **Note 49** and ref. 19 for details). The number of non-viable effectors in the assay can be calculated similarly; using regions R11 and R9 (*see* **Note 50**). This may be helpful in troubleshooting if target cell killing is lower than expected and/or in longer-term assays in which some effector cell death is expected.

4 Notes

1. Platelets present in variable amounts act as "hidden" sources of added protein or membrane that can affect labeling efficiency even when hPBMC and dye concentrations are carefully reproduced. The addition of a final low-speed wash step (5 min at 300 × *g*) minimizes platelet contamination of hPBMC and improves the consistency of staining with both protein and membrane labeling dyes.
2. Maintain cell cultures in the logarithmic growth phase in CM using a fully humidified 37 °C incubator with 5% CO_2.

Fig. 10 (continued) LAK effector cells—5 × 10^7 cells/mL, 5 μM CellVue® Claret; K562 targets—1 × 10^7 cells/mL, 10 μM PKH67. CD45+ effectors and targets were identified by staining with anti-CD45 Pac Blue (*see* **Note 46**). (Panel **b**) LAK-mediated killing of CFSE-labeled K562 cells was assessed as a function of protein dye (CTV or CTFR) and staining concentration used (CTFR). For each condition, target cell viability was determined based on percent of target cells that took up DAPI. The data indicate that LAK cells kill K562 cells in a concentration-dependent manner, and that at the staining concentrations used neither CTV nor CTFR affected LAK cytolytic function. Final staining concentrations used: LAK effectors—1 × 10^7 cells/mL, dye concentrations as indicated on plot; K562 targets—1 × 10^7 cells/mL, 10 μM CFSE. CD45+ effectors and targets were identified by staining with anti-CD45 APC (when CTV was used to label LAKs) or anti-CD45 BV510 (for CTFR-labeled or unlabeled LAKs; *see* **Note 46**). Representative data are shown from one of two replicate experiments analyzed on an LSRII flow cytometer; data points represent the mean ± 1 standard deviation of triplicate samples

3. Commercially available single use vials of CellTrace™ dyes offer the convenience of pre-weighed amounts of dye for dissolution in small volumes (18 μL) of DMSO but cost significantly more per milligram than bulk dye. CFSE is available as a bulk powder reagent, and if purchased, it should be accurately weighed out and made up as a 5 mM stock solution (MW 557.47 g/mol) in freshly opened anhydrous DMSO. Aliquots of 5 mM CFSE dye stock in DMSO can be stored in a dessicator at −20 °C for several months. Repeated freezing and thawing of a given aliquot should be avoided since DMSO takes up moisture from the air, which reduces labeling efficiency, due to hydrolysis of both the diacetate ester moieties required for entry into cells and the succinimidyl ester moieties required for covalent reaction with amino groups under physiologic conditions. If the entire contents of a bulk dye vial are dissolved in a calculated volume of DMSO, final dye concentration should be confirmed spectrophotometrically (e.g., by absorption at 490 nm) and adjusted as needed for consistency, since exact weights contained may vary sufficiently from vial to vial to require re-titration of new vs. old dye stocks in order to avoid toxicity.
4. Lymphocytes and monocytes are typically isolated from anticoagulated blood using standard Ficoll Hypaque density centrifugation techniques, but cryopreserved PBMCs, adherent cell lines (harvested using trypsinization), and non-adherent lines are also suitable for staining. Cells may be labeled while adherent by flooding the culture dish or flask with dye solution. However, this typically gives considerably more heterogeneous intensity distributions, especially for membrane dyes [38], and makes their interpretation in dye dilution proliferation assays more complex. Labeling of single cell suspensions is therefore generally preferred.
5. Labeled cells are typically placed back into culture for in vitro assays or injected into animal models for in vivo functional studies. Standard sterile technique should therefore be followed throughout the labeling protocols described in Subheadings 3.1 and 3.2.
6. The amount of dye required for bright but non-toxic staining will in general increase as total number and/or size of cells to be stained increases. However, exact concentrations resulting in over-labeling and loss of function will vary depending on cell type and class of tracking dye used (e.g., Table S1 in ref. 1). Therefore, appropriateness of final cell concentration *and* final tracking dye concentration used for labeling should always be verified by comparing viability and functionality of labeled vs. unlabeled cells. Similarly, both cell *and* dye concentrations used for labeling should be reported in any publication.

7. The total number of cells to be stained will depend on the number of replicates and controls required by the experimental protocol. Staining intensities are most easily reproduced when staining is done in volumes ranging from 0.5 to 2.0 mL. Once an approximate cell concentration has been established based on these factors, a preliminary dye titration experiment is recommended to determine or verify the optimal concentration of tracking dye [19, 39, 40].
8. Obtaining reproducible starting intensities from study-to-study requires accurately reproducing both dye and cell concentrations. Cell counting using a Coulter Counter or other automated cell counter is recommended rather than manual counting using a hemocytometer, since results of replicate hemocytometer counts often vary by as much as 15–20%.
9. Exogenous protein reduces labeling efficiency for both protein and membrane dyes and is therefore normally removed by washing the cells with a protein-free buffer such as PBS or HBSS prior to staining. However, when labeling must be done at relatively low cell concentrations due to limited numbers of cells or other experimental concerns, the addition of exogenous protein may aid in protecting against over-labeling and resultant loss of cell viability or functionality [15]. If the addition of exogenous protein must be avoided due to other experimental considerations, the working dye stock prepared in Subheading 3.1, **step 3** may be further diluted in buffer prior to initiation of cell labeling in Subheading 3.1, **step 4**. The time between initial dilution and initiation of cell labeling should be minimized since hydrolysis begins immediately upon dilution of the DMSO stock into the aqueous solution and proceeds very rapidly. Alternatively, resuspension in a serum-free culture medium will also reduce labeling efficiency and potential for over-labeling, due to the presence of free amino acids that compete for reaction with the protein dye.
10. If bulk CFSE powder has been previously dissolved in DMSO and frozen, ensure that the aliquot to be used is completely thawed prior to preparation of the working stock, but minimize the length of time that the DMSO stock is exposed to ambient conditions to limit uptake of moisture. The CFSE working stock solution should be clear and colorless. If there is any sign of yellowing it should not be used, since this indicates conversion to the charged fluorescent hydrolysis product carboxyfluorescein, which will not enter cells.
11. These concentrations were chosen such that following a 24 h stabilization period, the fluorescence intensity of non-dividing lymphocytes should fall in the uppermost two decades of the

intensity scale when unstained cells are placed in the first decade (*see* also **Notes 18** and **36**).

12. For an hPBMC concentration of 1×10^7/mL, final concentrations of up to 1.0 μM for CFSE, CTV, or CTFR are recommended to avoid over-labeling. These dyes label proteins at random sites and unintended modification of critical residues can interfere with signal transduction pathways, proliferation, and other cell functions even when cell viability remains acceptable (*see* Table S1 in ref. 1). More extensive labeling increases the likelihood of altered cell function(s) and the extent of labeling is a function of dye concentration, cell concentration, labeling time, and labeling conditions (temperature, mixing, etc.). Final cell and dye concentrations given here should therefore be taken only as a starting point and verified in each user's experimental system.
13. Because uptake into cells and reaction with free amino groups occurs rapidly, it is important to disperse the dye solution quickly and evenly throughout the cell suspension immediately after addition.
14. Once formed by hydrolysis, the fluorescent forms of CTV, CFSE, and CTFR are sensitive to photobleaching. Therefore, covering with aluminum foil or placing in a darkened location is recommended to protect tubes or wells containing labeled cells from exposure to high-intensity light or prolonged exposure to room light.
15. The inclusion of protein in the stop solution is essential, since it reacts with and inactivates unbound dye. Free amino acids in culture medium further aid in the inactivation. Alternatively, PBS or HBSS containing 1–2% serum albumin may be used as a stop solution.
16. For starting cell numbers of 10^7 or more, recoveries of at least 85% and viabilities of at least 90% should be obtained for freshly drawn hPBMC (e.g., Fig. 1a and Table 3 in ref. 41). However, recoveries typically decrease at lower cell numbers and may also be lower for preparations in which the cells are older or have been subjected to other stresses (e.g., pheresis, elutriation, or cryopreservation and thawing). Staining intensity and CV will vary for different cell types, but a bright, symmetrical fluorescence intensity profile coupled with poor recovery and/or viability usually indicates substantial over-labeling and the need to increase cell concentration, decrease dye concentration; or both. Conversely, heterogeneous and/or dim staining (<2 log separation from unstained control) coupled with good recovery and viability suggests under-labeling and the need to decrease cell concentration, increase dye concentration; or both.

17. All protein dyes available to date exhibit varying degrees of dye dilution in non-proliferating cells (e.g., unstimulated lymphocytes), with rapid proliferation-independent intensity loss during the first 24 h post-labeling followed by a slower intensity loss thereafter ([2, 42] and Fig. 8). Unfixed CFSE stained samples taken immediately post-labeling are NOT appropriate compensation controls because they are so much brighter than samples taken at subsequent time points that they typically cannot be run on the same intensity scale when unstained cells are placed within the first decade (*see* Fig. 2 of ref. 19). For proliferation assays based on CFSE dye dilution, it is therefore critical to select a staining concentration that gives adequate separation from unstained cells at 24 h without unacceptable fluorescence overlap into spectral detection channels used to measure other reagents (Figs. 1 and 2; Tables 1a, 1b and 2).
18. Fixation of protein labeled cells in EtOH [43] or methanol-free formaldehyde [19] leads to further loss of cell-associated dye (30–50% decrease in fluorescence intensity for CFSE [19]; 5–25% for CTV; 10–20% for CTFR), most likely due to loss of small but stably labeled peptides or proteins as cell membranes become permeable. Fortunately, the decrease in intensity between fresh and fixed cells does not appear to affect the shape of dye dilution profiles, which can still be used to deduce cell proliferation history so long as the decreased fluorescence of fixed cells does not compromise the ability to resolve the desired number of generations from unstained cells. Because the extent of intensity loss upon fixation varies, all samples or time points from a given experiment should be treated identically.
19. For dye dilution proliferation assays using hPBMC (or PBMC from other species), it may be necessary to use an independent method such as ^{3}H-thymidine incorporation (*see* Table S1 in ref. 1) to verify that cell function is unaltered by labeling with tracking dye at the chosen concentration.
20. Like most membrane intercalating dyes, PKH26, PKH67, and CellVue Claret contain both aromatic chromophores and lipophilic alkyl tails that readily adsorb to the walls of polystyrene tubes or plates. This can substantially reduce labeling efficiency, particularly when working at dye concentrations of 2 μM or less. Use of polypropylene tubes is recommended to minimize adsorptive dye loss and maximize reproducibility of labeling. Use of conical rather than round bottom tubes is highly recommended, since this facilitates more complete removal of salt-containing media or buffers prior to cell labeling (*see* **Note 21**).

21. Although the membrane dyes are modestly soluble in polar organic solvents such as ethanol, their long alkyl chains tend to self-associate in aqueous solutions. The presence of salts increases this tendency and reduces the efficiency of general membrane labeling, although phagocytic cells can become differentially labeled by taking up dye aggregates. In our experience, the best method for maximizing fluid removal while minimizing cell loss is to use a sterile disposable 200 μL pipette tip fitted at the end of a vacuum aspirator. This reduces the aperture size, provides a more controlled aspiration rate, and makes it easier to accurately position the point of suction relative to the cell pellet. Other commonly used techniques for supernatant removal can substantially reduce both quality of staining and cell recovery when labeling with membrane dyes. Tube inversion and blotting typically leaves ~100 μL of supernatant, leading to significant salt remaining in Subheading 3.2, **step 2** and reduced labeling efficiency in Subheading 3.2, **step 5**. Further aspiration to reduce the amount of fluid risks loss of cells at the top of the pellet that have been loosened as fluid drained back down the side of the tube.
22. The PKH and CellVue® dyes label via rapid partitioning from the aqueous phase into cell membranes. Final staining intensity is a function of both dye concentration and cell/membrane concentration present in the staining step. Dye concentrations required for bright but non-perturbing staining therefore vary with cell type/size as well as cell concentration (e.g., Table 1 of ref. 19), making it important to accurately reproduce—and publish—both dye and cell concentrations in order to obtain reproducible results.
23. Diluent C is an aqueous, isotonic, iso-osmotic, salt-free staining vehicle that contains neither organic solvents nor physiologic salts. Although it is designed to maximize dye solubility and minimize cell toxicity for short periods (up to 30 min), the longer cells and dye are exposed to Diluent C the more likely that: (a) staining efficiency will decrease due to dye aggregation; and (b) decreased cell viability or function may result from lack of physiologic salts. Subheading 3.2, **steps 2–5** should therefore be completed in as short a period as possible, preferably <5 min. When multiple samples are to be labeled, it is recommended that processing through the first wash of Subheading 3.2, **step 7** be completed for each sample before the next sample is stained. Remaining steps may then be carried out in parallel for all samples.
24. Hydrophobic partitioning of PKH and CellVue dyes into cell membranes occurs very rapidly, being essentially complete within <1 min after admixing 2× cells with 2× dye. To obtain bright, homogeneous staining it is important to use a mixing

technique in which all cells are exposed to the same concentration of dye at the same time. As illustrated in ref. 34, this is much more easily achieved by admixing similar volumes of dye and cells than by trying to disperse a small volume of ethanolic dye into a much larger volume of cell suspension.

25. In theory, results should be the same whether 2× cells are admixed with 2× dye or vice versa and this is true for experienced users. Our experience when teaching new users has been that that they more reliably obtain bright homogeneous staining by adding 2× cells to 2× dye. This minimizes the chance that a drop of cells on the wall of the tube may remain unstained if it is above the level of admixed solution or stain at lower intensity if there is a delay between addition and mixing of 2× dye with 2× cells.
26. Some literature protocols suggest use of CM, which contains 10% FBS, as the stop reagent. However, our experience has been that use of neat FBS results in more efficient removal of unbound dye (due to its higher protein concentration) and reduced likelihood of forming dye aggregates large enough to sediment with cells during subsequent wash steps (due to its lower ionic strength). If CM is used, a larger volume (5× rather than 1×) is recommended to ensure sufficient protein to adsorb all unbound dye.
27. Even when polypropylene tubes are used (*see* **Note 20**), some dye adsorption to tube walls may occur. Therefore, washing efficiency is improved if cells are transferred to a fresh polypropylene tube after aspiration of stop solution and resuspension of the cell pellet for the first wash in Subheading 3.2, **step 6**. This is particularly important if CM is used as the stop reagent (*see* **Note 26**), since carryover of dye particles may result in inadvertent labeling of other cell types present in the culture.
28. In contrast to protein dyes, the fluorescence intensity of PKH26, PKH67, or CellVue Claret-labeled cells does not decrease significantly in the absence of cell proliferation and their intensity is stable to fixation with neutral methanol-free formaldehyde. A small aliquot of cells fixed at T0 may therefore be used as a compensation control to evaluate overlap of membrane dye signal into spectral regions used to detect other reagents. For an example of typical controls to set up for a lymphocyte proliferation assay, *see* Table 2 in ref. 41. As with protein dyes, inability to achieve adequate color compensation indicates the need to reduce dye concentration, increase cell concentration, or both during the staining step.
29. For a new cell type or the first use of a tracking dye new to the laboratory, it may be necessary to adjust the final staining

conditions to give fluorescence intensities that fall in the uppermost two decades of the intensity scale.

30. FSC-A vs. FSC-H were used for doublet discrimination on the BD LSR Fortessa and LSRII data shown in Figs. 1 and 2, and Tables 1a, 1b and 2. Other cytometers may require a different combination of pulse shape parameters for optimal doublet discrimination.
31. In the study shown, the initial goal was to compare the extent of spectral overlap for U937 cells stained with equimolar concentrations of five established proliferation dyes (CTV, CFSE, PKH26, and CVC) with the then-new CTFR on two different cytometers. Equimolar labeling conditions for CFSE, CTV, and CTFR (10^7 cells/mL, 10 μM dye) gave CTFR intensities that were off-scale high in all detectors associated with 640 nm excitation on both cytometers.
32. In theory, it is desirable to use the highest non-perturbing concentration of tracking dye in order to maximize the number of daughter generations that can still be distinguished from unstained cells. In practice, the resulting color overlap (Tables 1a, 1b) can lead to compensation problems in adjacent spectral window(s). The extent of spectral overlap will depend on both the tracking dye and the optical configuration of the cytometer. For example, on the Fortessa:
    (a) CTV spectral overlap is seen in the detectors associated with the 405 nm laser but is only substantial in the V525/50-A channel, and cross-laser excitation is noted only in the 355 nm excited, U450/50-A channel (Fig. 1);
    (b) CFSE (Fig. 1) and PKH67 (Fig. 2) give substantial spectral overlap in all channels associated with the 488 nm laser, with modest cross-laser excitation in all 405 nm-excited channels except V450/50-A;
    (c) CTFR (Fig. 1) and CVC (Fig. 2) give high levels of spectral overlap in all 640 nm-excited channels. For both dyes, modest cross-laser excitation is noted in 405 nm-excited channels that are restricted by bandpass filters near their emission range (660–780 nm). For CVC, cross-laser excitation is also noted in the 355 nm-excited U740/35-A channel;
    (d) For PKH26 (Fig. 2), substantial spectral overlap is seen for all channels associated with the 488 nm laser, with negligible cross-laser excitation measured in any other channels.
33. Stained samples were analyzed at ~24 h post labeling for protein dyes (Fig. 1) or immediately post-labeling for membrane dyes (Fig. 2) and percent overlap in each non-primary channel was calculated using WinList v8.0. Comparing measurements

from the two cytometers, it is apparent that spectral overlap and compensation issues (Tables 1a, 1b) were more problematic for CTV on the LSRII than on the Fortessa, and for both CFSE and PKH67 on the Fortessa than on the LSRII. On the Fortessa, for example, >40% compensation is required for CFSE in the PE channel (B575/26) and ~30% for PKH67. On the LSRII, where the PE channel is Y582/15, no significant compensation is required for either of the green proliferation dyes. Although the 10 μM PKH26 sample was fully on-scale in its primary channel (B575/26) on the Fortessa, where it is suboptimally excited by the 488 nm laser, it was completely off-scale high on the LSRII, where it is much more optimally excited by the 561 nm laser.

Percent compensation cannot be calculated where the peaks are completely off-scale high in their primary channel, as was seen for 10 μM CTFR and 10 μM CVC stained cells on both instruments. A preliminary titration indicated that the CTFR peak was not fully on-scale until staining concentration was reduced from 10 to 1.25 μM. WinList v8.0 was able to obtain a % overlap value for all three CTFR samples where the median intensity was on-scale, but compensation values for the 2.5 μM and 5 μM samples are overestimated because intensity in the primary channel is underestimated due to the peak being increasingly off-scale.

34. In Table 2, autofluorescence was set to be fully on-scale in the first decade in all channels except the primary channel (where the voltage was adjusted to place the stained cells fully on-scale in the last decade). Values shown are geometric mean fluorescence intensities, not % compensation. Comparing the two cytometers in this fashion indicates that:
    (a) While it would be possible to use CTFR or CVC with PE-Cy7 on the Fortessa, where it would be detected in B780/60, compensation is likely to be difficult-to-impossible on the LSRII where PE-Cy7 is detected in Y780/60;
    (b) Significant yellow cross-laser excitation is observed with both CVC and CTFR;
    (c) Less violet cross-laser excitation is observed with CVC than with CTFR.
35. Figure 3 uses median fluorescence intensity and robust standard deviation (rSD; a metric available in WinList 9.0, FCS Express v5, or in FACSDiVa 6.0 from BD Biosciences) to calculate a non-parametric Stain Index according to Formula 1 below. For normally distributed data, the SD and the rSD are considered to be equivalent measurements [44].

Formula 1:

$$\text{Stain Index} = \frac{\text{Median Fluorescence Intensity}_{\text{Labeled Cells}} - \text{Median Fluorescence Intensity}_{\text{Unlabeled Cells}}}{\text{rSD}_{\text{Unlabeled Cells}}}$$

An alternative non-parametric Stain Index can also be calculated in FlowJo using the 5th, 50th, and 95th percentiles [45].

Formula 2:

$$\text{Stain Index}_{\text{non-parametric}} = \frac{3.29 \times \left(\text{50th percentile}_{\text{positive}} - \text{50th percentile}_{\text{negative}}\right)}{\text{95th percentile}_{\text{negative}} - \text{5th percentile}_{\text{negative}}}$$

36. When detector voltage is decreased to bring tracking dye positive cells on-scale, the relative decrease in median intensity and rSD for unstained cells is disproportionately smaller than the decrease for dye positive cells. This results in an artificially low value when Stain Index is calculated using Formula 1 of **Note 35** because the change in the denominator is smaller than that in the numerator.
37. Once labeled and unlabeled cell populations begin to overlap, dye dilution no longer remains proportional to extent of cell division because highly divided cells cannot be distinguished from autofluorescence. Any proliferation modeling done in this overlap region will be invalid since the underlying assumption of linear dye dilution is violated.
38. In addition to indicating whether stained and unstained cells are growing at comparable rates (Fig. 6b), comparison of unstained cell intensities in co-cultures with those of a completely unstained control (Fig. 6a) allows detection of "dye transfer", something that is not possible using parallel cultures of stained and unstained cells (Fig. 4b). When such an increase is seen (e.g., [3]), it is important to determine whether it is dye-related (e.g., transfer of free dye between labeled and unlabeled cells) or cell-related (e.g., cytoplasmic transfer via membrane "podia" or tunneling nanotubes [46, 47]), transfer of labeled membrane via trogocytosis [48–50], or uptake of extracellular vesicles carrying labeled proteins or membrane [24]. Although U937s and other tumor cell lines are known to undergo self-trogocytosis [48], the rapid and unusually large intensity increase seen for seen for CYY compared with CTV and other dyes studied suggested that the "dye transfer" shown in Fig. 6b was dye-specific. The authors' experience (to be published elsewhere) has been that trogocytosis-related shifts in intensity for the unstained population are typically smaller than that seen for

CYY and tend to be reflected as right skew in the intensity profile.

39. For the U937 cultures shown in Fig. 7, dye dilution reflects the sum of proliferation-dependent and proliferation-independent processes. All protein dyes available to date exhibit some dye dilution in non-proliferating cells (e.g., unstimulated lymphocytes), with varying rates of rapid intensity loss during the first 24 h post-labeling followed by similar rates of slower intensity loss thereafter ([2, 42]; Fig. 7a). In contrast, membrane dyes typically exhibit more consistent dye dilution rates beginning immediately post-labeling (Fig. 7b). Surprisingly, while over staining with membrane dyes may not reduce viability or functionality, it can sometimes result in increased T1 fluorescence intensity compared with T0 intensity (*see* Fig. 1 in ref. 1 and Fig. 1 in ref. 41). The most likely explanation is stacking and self-quenching of dye in the plasma membrane at T0 that is relieved as dye redistributes into intracellular membranes via normal membrane trafficking mechanisms [38]. Dye dilution appears to proceed linearly with cell division once stacking/quenching is relieved, presumably because the total number of molecules per cell does not change, and membrane dyes are typically pH insensitive in physiologic ranges. For assay systems where proliferation monitoring is to be initiated immediately (e.g., continuously growing cell lines or transfectants), cell and/or dye concentration(s) in the staining step should be chosen to ensure that dye dilution proceeds linearly from T0. Over-labeling may also result in stacking/quenching for protein dyes but a similar increase in intensity from T0 to T24 has not been reported, presumably because such an increase would be more than offset by the characteristic division-independent intensity loss seen for these dyes during the same period.
40. If many wells in the 96-well plate remain empty, it is recommended that wells surrounding test and control cells for the assay be filled with CM to minimize evaporation in the assay wells.
41. On Days 0 and 1, Region R4 of Fig. 8 is restricted to include only lymphocytes (low FSC and low SSC) and exclude monocytes (moderate FSC and moderate SSC). On Day 2 post-stimulation, no monocytes are evident in the scatter plot and lymphocytes remain within the restricted R4 region. On Days 3 and 4 post-stimulation, as lymphocyte proliferation becomes evident, region R4 is expanded as illustrated in Fig. 8 to ensure that blasting cells are included in the dye dilution analysis.
42. Regardless of which class of tracking dyes is used, labeling prior to LAK induction with IL-2 is preferable to post-

induction labeling. This is particularly true if CFSE or other protein dyes are used, since staining immediately before assay initiation runs the risk that early dye efflux could result in unintended transfer of label to target cells [51].

43. Cell and dye concentrations given in Fig. 10 were selected to yield staining intensities that: (a) were on-scale in the upper two decades of the fluorescence intensity scale when unstained cells were placed in the first decade; and (b) could readily be compensated in adjacent spectral channels. Slight peak asymmetry is of somewhat less concern when labeling targets or effectors for a cytotoxicity assay as opposed to a proliferation assay, but it is important to ensure that 100% of a given cell type is labeled with the chosen tracking dye so that they can clearly be distinguished from cells that are unlabeled (e.g., co-stimulatory cells) or those that are labeled with a different tracking dye.
44. Use of target cells obtained from high-density cultures should be avoided, due to the presence of significant numbers of apoptotic and/or dead cells. Such cells will readily stain with tracking dyes but will give highly variable staining with 7-AAD, DAPI, or other dyes used to determine viability by dye exclusion, making it much more difficult to establish the intensity limit above which a target cell is to be considered non-viable.
45. For longer term assays, it may be desirable to set up the plate with a border of CM-filled wells around the periphery in order to minimize evaporation-associated variability in cell and cytokine concentrations in the assay wells.
46. CD45 was used as a gating parameter because both LAK and K562 are CD45+ (although K562 are dimmer than LAK). A low SSC threshold (*see* **Note 49**) was used to reduce debris but required substantial care to insure that all events corresponding to both dead and live targets and effectors were included above the threshold. An alternative strategy would be to set a CD45 threshold that included all cellular events (live and dead), avoiding the necessity for a side scatter threshold.
47. For flow cytometers with a UV laser, DAPI is a suitable viability dye for use with all of the cell tracking dyes used in Fig. 10. For flow cytometers without a UV laser, 7-AAD is a suitable viability dye for use with CTV.
48. Choice of optimized labeling conditions for tracking dye(s) should have already established that stained cells will be on-scale, without events accumulating in the highest channel, when compensation is set to 0% and voltages are adjusted to place unstained control cells in the first decade but sufficiently above the left axis such that events do not accumulate in the lowest channel. In addition, it is critical to recognize that cells

labeled with tracking dyes can be extremely bright, requiring substantially decreased detector voltage settings compared with those used for detection of immunofluorescence. If the tracking dye signal in a secondary channel (set to a higher detector voltage) is greater than its intensity in the primary channel, it will be impossible to properly compensate for tracking dye overlap in the secondary channel [51]. In this case, reduced staining with reduced concentrations of tracking dye (s) may be required.

49. In this assay, it is possible to assess cell killing using two different metrics: (a) as % of targets able to exclude a viability probe (DAPI); and (b) using counting beads to enumerate the number of viable target cells that remained when effectors were present vs. when they were absent (*see* Fig. 5 in ref. 19 for details). In the event that fluorescent counting beads are employed, it is important to note that these beads can have very low forward scatter characteristics. Accordingly, it will not be possible to reliably set an acquisition threshold on this parameter while ensuring that all bead events are collected. In this case, side scatter can be used as the thresholding parameter. Alternatively, if the use of anti-CD45 labeling is incorporated into the assay, it is likely that broad-spectrum enumeration beads will also fluoresce in the CD45 detection channel. If so, thresholding can be established based on the fluorescence intensity measurement for this parameter, provided that it allows for the inclusion of all leukocytes and bead events.
50. The number of non-viable effectors present in the assay can be calculated similarly, using a Tracking Dye vs. 7-AAD histogram as gated in Fig. 5 of ref. 19, plot 6 (gated on 'NOT R6&R1&R2&R5') and then dividing the number of dead effectors (Tracking Dye and 7-AAD dual positive; R11) by the total number of effectors (Tracking Dye positive; R10+R11).

Acknowledgements

The authors have had the opportunity to work with many wonderful people on the development of these techniques over the years. In particular, they would like to acknowledge the technical support and intellectual contributions of Bruce Bagwell (Verity Software House), Kylie M. Price (The Malaghan Institute of Medical Research), Rebecca McHugh (Miltenyi Biotec), Garret Guenther (ACEA Biosciences), Jolene Bradford (ThermoFisher Scientific), Karen Kwarta (Sigma-Aldrich), and Amy Noble (Millipore Sigma). They would also like to thank the Classes of 2013–2016 from the Bowdoin and Albuquerque Annual Courses in Flow Cytometry (Research Methods and Applications) and the vendors

that supplied the many different tracking dyes evaluated during these courses.
Flow cytometry was performed at Roswell Park Cancer Institute's Department of Flow and Image Cytometry Laboratory, which was established in part by equipment grants from the NIH Shared Instrument Program, and receives support from the Core Grant (5 P30 CA016056-29) from the National Cancer Institute to the Roswell Park Cancer Institute.

References

1. Wallace PK, Tario JD Jr, Fisher JL, Wallace SS, Ernstoff MS, Muirhead KA (2008) Tracking antigen-driven responses by flow cytometry: monitoring proliferation by dye dilution. Cytometry A 73(11):1019–1034. doi:10.1002/cyto.a.20619
2. Quah BJ, Parish CR (2012) New and improved methods for measuring lymphocyte proliferation in vitro and in vivo using CFSE-like fluorescent dyes. J Immunol Methods 379(1-2):1–14. doi:10.1016/j.jim.2012.02.012
3. Filby A, Begum J, Jalal M, Day W (2015) Appraising the suitability of succinimidyl and lipophilic fluorescent dyes to track proliferation in non-quiescent cells by dye dilution. Methods 82:29–37. doi:10.1016/j.ymeth.2015.02.016
4. Zhou W, Kang HC, Grady M, Chambers KM, Dubbels B, Melquist P, Gee KR (2016) CellTrace™ Far Red & CellTracker™ Deep Red—long term live cell tracking for flow cytometry and fluorescence microscopy. J Biol Methods 3(1):e38. doi:10.14440/jbm.2016.113
5. Chen P, Aguilar OA, Rahim MM, Allan DS, Fine JH, Kirkham CL, Ma J, Tanaka M, Tu MM, Wight A, Kartsogiannis V, Gillespie MT, Makrigiannis AP, Carlyle JR (2015) Genetic investigation of MHC-independent missing-self recognition by mouse NK cells using an in vivo bone marrow transplantation model. J Immunol 194(6):2909–2918. doi:10.4049/jimmunol.1401523
6. Chauhan SK, Saban DR, Dohlman TH, Dana R (2014) CCL-21 conditioned regulatory T cells induce allotolerance through enhanced homing to lymphoid tissue. J Immunol 192(2):817–823. doi:10.4049/jimmunol.1203469
7. Bosschaerts T, Guilliams M, Stijlemans B, Morias Y, Engel D, Tacke F, Herin M, De Baetselier P, Beschin A (2010) Tip-DC development during parasitic infection is regulated by IL-10 and requires CCL2/CCR2, IFN-gamma and MyD88 signaling. PLoS Pathog 6(8):e1001045. doi:10.1371/journal.ppat.1001045
8. Kinjyo I, Qin J, Tan SY, Wellard CJ, Mrass P, Ritchie W, Doi A, Cavanagh LL, Tomura M, Sakaue-Sawano A, Kanagawa O, Miyawaki A, Hodgkin PD, Weninger W (2015) Real-time tracking of cell cycle progression during CD8+ effector and memory T-cell differentiation. Nat Commun 6:6301. doi:10.1038/ncomms7301
9. Takizawa H, Regoes RR, Boddupalli CS, Bonhoeffer S, Manz MG (2011) Dynamic variation in cycling of hematopoietic stem cells in steady state and inflammation. J Exp Med 208(2):273–284. doi:10.1084/jem.20101643
10. Goldenberg-Cohen N, Iskovich S, Askenasy N (2015) Bone marrow homing enriches stem cells responsible for neogenesis of insulin-producing cells, while radiation decreases homing efficiency. Stem Cells Dev 24(19):2297–2306. doi:10.1089/scd.2014.0524
11. Kozlowska AK, Kaur K, Topchyan P, Jewett A (2016) Adoptive transfer of osteoclast-expanded natural killer cells for immunotherapy targeting cancer stem-like cells in humanized mice. Cancer Immunol Immunother 65(7):835–845. doi:10.1007/s00262-016-1822-9
12. Schneiders FL, Prodohl J, Ruben JM, O'Toole T, Scheper RJ, Bonneville M, Scotet E, Verheul HM, de Gruijl TD, van der Vliet HJ (2014) CD1d-restricted antigen presentation by Vgamma9Vdelta2-T cells requires trogocytosis. Cancer Immunol Res 2(8):732–740. doi:10.1158/2326-6066.CIR-13-0167
13. Bonaccorsi I, Morandi B, Antsiferova O, Costa G, Oliveri D, Conte R, Pezzino G, Vermiglio G, Anastasi GP, Navarra G, Munz C, Di Carlo E, Mingari MC, Ferlazzo G (2014) Membrane transfer from tumor cells overcomes deficient phagocytic ability of plasmacytoid dendritic cells for the acquisition and presentation of tumor antigens. J Immunol 192(2):824–832. doi:10.4049/jimmunol.1301039
14. van der Zouwen B, Kruisselbrink AB, Frederik Falkenburg JH, Jedema I (2014) Collateral damage of nonhematopoietic tissue by hematopoiesis-specific T cells results in graft-versus-host disease during an ongoing profound graft-versus-leukemia reaction. Biol

Blood Marrow Transplant 20(6):760–769. doi:10.1016/j.bbmt.2014.03.002

15. Quah BJ, Wijesundara DK, Ranasinghe C, Parish CR (2012) Fluorescent target array killing assay: a multiplex cytotoxic T-cell assay to measure detailed T-cell antigen specificity and avidity in vivo. Cytometry A 81(8):679–690. doi:10.1002/cyto.a.22084
16. Kramski M, Schorcht A, Johnston AP, Lichtfuss GF, Jegaskanda S, De Rose R, Stratov I, Kelleher AD, French MA, Center RJ, Jaworowski A, Kent SJ (2012) Role of monocytes in mediating HIV-specific antibody-dependent cellular cytotoxicity. J Immunol Methods 384 (1-2):51–61. doi:10.1016/j.jim.2012.07.006
17. Hausler SF, Del Barrio IM, Diessner J, Stein RG, Strohschein J, Honig A, Dietl J, Wischhusen J (2014) Anti-CD39 and anti-CD73 antibodies A1 and 7G2 improve targeted therapy in ovarian cancer by blocking adenosine-dependent immune evasion. Am J Transl Res 6(2):129–139
18. Veerappan A, VanWagner LB, Mathew JM, Huang X, Miller J, Lapin B, Levitsky J (2016) Low incidence of acute rejection in hepatitis B virus positive liver transplant recipients and the impact of hepatitis B immunoglobulin. Hum Immunol 77(4):367–374. doi:10.1016/j.humimm.2016.02.009
19. Tario JD Jr, Muirhead KA, Pan D, Munson ME, Wallace PK (2011) Tracking immune cell proliferation and cytotoxic potential using flow cytometry. Methods Mol Biol 699:119–164. doi:10.1007/978-1-61737-950-5_7
20. Jin JO, Zhang W, Du JY, Yu Q (2014) BDCA1-positive dendritic cells (DCs) represent a unique human myeloid DC subset that induces innate and adaptive immune responses to Staphylococcus aureus Infection. Infect Immun 82(11):4466–4476. doi:10.1128/IAI.01851-14
21. Balogh A, Pap M, Marko L, Koloszar I, Csatary LK, Szeberenyi J (2011) A simple fluorescent labeling technique to study virus adsorption in Newcastle disease virus infected cells. Enzyme Microb Technol 49(3):255–259. doi:10.1016/j.enzmictec.2011.06.005
22. Katajisto P, Dohla J, Chaffer CL, Pentinmikko N, Marjanovic N, Iqbal S, Zoncu R, Chen W, Weinberg RA, Sabatini DM (2015) Stem cells. Asymmetric apportioning of aged mitochondria between daughter cells is required for stemness. Science 348(6232):340–343. doi:10.1126/science.1260384
23. Levaot N, Ottolenghi A, Mann M, Guterman-Ram G, Kam Z, Geiger B (2015) Osteoclast fusion is initiated by a small subset of RANKL-stimulated monocyte progenitors, which can fuse to RANKL-unstimulated progenitors. Bone 79:21–28. doi:10.1016/j.bone.2015.05.021
24. Pegtel DM, Cosmopoulos K, Thorley-Lawson DA, van Eijndhoven MA, Hopmans ES, Lindenberg JL, de Gruijl TD, Wurdinger T, Middeldorp JM (2010) Functional delivery of viral miRNAs via exosomes. Proc Natl Acad Sci U S A 107(14):6328–6333. doi:10.1073/pnas.0914843107
25. Zomer A, Maynard C, Verweij FJ, Kamermans A, Schafer R, Beerling E, Schiffelers RM, de Wit E, Berenguer J, Ellenbroek SI, Wurdinger T, Pegtel DM, van Rheenen J (2015) In Vivo imaging reveals extracellular vesicle-mediated phenocopying of metastatic behavior. Cell 161(5):1046–1057. doi:10.1016/j.cell.2015.04.042
26. Pasalic L, Williams R, Siupa A, Campbell H, Henderson MJ, Chen VM (2016) Enumeration of extracellular vesicles by a new improved flow cytometric method is comparable to fluorescence mode nanoparticle tracking analysis. Nanomedicine 12(4):977–986. doi:10.1016/j.nano.2015.12.370
27. Pece S, Tosoni D, Confalonieri S, Mazzarol G, Vecchi M, Ronzoni S, Bernard L, Viale G, Pelicci PG, Di Fiore PP (2010) Biological and molecular heterogeneity of breast cancers correlates with their cancer stem cell content. Cell 140 (1):62–73. doi:10.1016/j.cell.2009.12.007
28. Ghiabi P, Jiang J, Pasquier J, Maleki M, Abu-Kaoud N, Rafii S, Rafii A (2014) Endothelial cells provide a notch-dependent pro-tumoral niche for enhancing breast cancer survival, stemness and pro-metastatic properties. PLoS One 9(11):e112424. doi:10.1371/journal.pone.0112424
29. Verbist KC, Guy CS, Milasta S, Liedmann S, Kaminski MM, Wang R, Green DR (2016) Metabolic maintenance of cell asymmetry following division in activated T lymphocytes. Nature 532(7599):389–393. doi:10.1038/nature17442
30. Demmers MW, Korevaar SS, Betjes MG, Weimar W, Rowshani AT, Baan CC (2014) Limited efficacy of immunosuppressive drugs on CD8+ T cell-mediated and natural killer cell-mediated lysis of human renal tubular epithelial cells. Transplantation 97(11):1110–1118. doi:10.1097/TP.0000000000000108
31. Lawson MA, McDonald MM, Kovacic N, Hua Khoo W, Terry RL, Down J, Kaplan W, Paton-Hough J, Fellows C, Pettitt JA, Neil Dear T, Van Valckenborgh E, Baldock PA, Rogers MJ, Eaton CL, Vanderkerken K, Pettit AR, Quinn JM, Zannettino AC, Phan TG, Croucher PI (2015) Osteoclasts control reactivation of

dormant myeloma cells by remodelling the endosteal niche. Nat Commun 6:8983. doi:10.1038/ncomms9983

32. Zhao H, Halicka HD, Li J, Biela E, Berniak K, Dobrucki J, Darzynkiewicz Z (2013) DNA damage signaling, impairment of cell cycle progression, and apoptosis triggered by 5-ethynyl-2′-deoxyuridine incorporated into DNA. Cytometry A 83(11):979–988. doi:10.1002/cyto.a.22396
33. Quah BJ, Parish CR (2010) The use of carboxyfluorescein diacetate succinimidyl ester (CFSE) to monitor lymphocyte proliferation. J Vis Exp 44. doi:10.3791/2259
34. Tario JD Jr, Humphrey K, Bantly AD, Muirhead KA, Moore JS, Wallace PK (2012) Optimized staining and proliferation modeling methods for cell division monitoring using cell tracking dyes. J Vis Exp 70:e4287. doi:10.3791/4287
35. Roederer M (2011) Interpretation of cellular proliferation data: avoid the panglossian. Cytometry A 79(2):95–101. doi:10.1002/cyto.a.21010
36. Roederer M (2015) A proposal for unified flow cytometer parameter naming. Cytometry A 87(8):689–691. doi:10.1002/cyto.a.22670
37. Amson R, Pece S, Lespagnol A, Vyas R, Mazzarol G, Tosoni D, Colaluca I, Viale G, Rodrigues-Ferreira S, Wynendaele J, Chaloin O, Hoebeke J, Marine J-C, Di Fiore PP, Telerman A (2012) Reciprocal repression between P53 and TCTP. Nat Med 18(1):91–99. http://www.nature.com/nm/journal/v18/n1/abs/nm.2546.html#supplementary-information
38. Rousselle C, Barbier M, Comte VV, Alcouffe C, Clement-Lacroix J, Chancel G, Ronot X (2001) Innocuousness and intracellular distribution of PKH67: a fluorescent probe for cell proliferation assessment. In Vitro Cell Dev Biol Anim 37(10):646–655
39. Horan PK, Melnicoff MJ, Jensen BD, Slezak SE (1990) Fluorescent cell labeling for in vivo and in vitro cell tracking. Methods Cell Biol 33:469–490
40. Wallace PK, Palmer LD, Perry-Lalley D, Bolton ES, Alexander RB, Horan PK, Yang JC, Muirhead KA (1993) Mechanisms of adoptive immunotherapy: improved methods for in vivo tracking of tumor-infiltrating lymphocytes and lymphokine-activated killer cells. Cancer Res 53(10 Suppl):2358–2367
41. Bantly AD, Gray BD, Breslin E, Weinstein EG, Muirhead KA, Ohlsson-Wilhelm BM, Moore JS (2007) CellVue Claret, a new far-red dye, facilitates polychromatic assessment of immune cell proliferation. Immunol Invest 36(5-6):581–605. doi:10.1080/08820130701712461
42. Ko KH, Odell R, Nordon RE (2007) Analysis of cell differentiation by division tracking cytometry. Cytometry A 71(10):773–782. doi:10.1002/cyto.a.20437
43. Matera G, Lupi M, Ubezio P (2004) Heterogeneous cell response to topotecan in a CFSE-based proliferation test. Cytometry A 62(2):118–128. doi:10.1002/cyto.a.20097
44. Biosciences B (2012). https://www.bdbiosciences.com/documents/Robust_Statistics_in_BDFACSDiva.pdf. Accessed on 2 April 2017
45. Stain Index Calculations using Flow Cytometry Software. https://www.sickkids.ca/research/FCF/documents/tools/StainIndexusingFlowSoftware.pdf. Accessed on 2 April 2017
46. Oh DJ, Martinez AR, Lee GM, Francis K, Palsson BO (2000) Intercellular adhesion can be visualized using fluorescently labeled fibrosarcoma HT1080 cells cocultured with hematopoietic cell lines or CD34(+) enriched human mobilized peripheral blood cells. Cytometry 40(2):119–125
47. Lou E, Fujisawa S, Morozov A, Barlas A, Romin Y, Dogan Y, Gholami S, Moreira AL, Manova-Todorova K, Moore MA (2012) Tunneling nanotubes provide a unique conduit for intercellular transfer of cellular contents in human malignant pleural mesothelioma. PLoS One 7(3):e33093. doi:10.1371/journal.pone.0033093
48. LeMaoult J, Caumartin J, Daouya M, Switala M, Rebmann V, Arnulf B, Carosella ED (2015) Trogocytic intercellular membrane exchanges among hematological tumors. J Hematol Oncol 8:24. doi:10.1186/s13045-015-0114-8
49. Decaup E, Mirshahi P, Rafii A, Mirshahi M, Fournié J, Poupot M (2011) Oncologic trogocytosis protects tumour stromal cells from γδ cell cytotoxicity. J Life Sci 5:986–995
50. Li KJ, Wu CH, Shen CY, Kuo YM, Yu CL, Hsieh SC (2016) Membrane transfer from mononuclear cells to polymorphonuclear neutrophils transduces cell survival and activation signals in the recipient cells via anti-extrinsic apoptotic and MAP kinase signaling pathways. PLoS One 11(6):e0156262. doi:10.1371/journal.pone.0156262
51. Tario JD Jr, Gray BD, Wallace SS, Muirhead KA, Ohlsson-Wilhelm BM, Wallace PK (2007) Novel lipophilic tracking dyes for monitoring cell proliferation. Immunol Invest 36(5-6):861–885. doi:10.1080/08820130701712933

Chapter 13

Immunophenotypic Identification of Early Myeloerythroid Development

Cornelis J.H. Pronk and David Bryder

Abstract

Myeloerythroid-restricted precursor cells, derived from multipotent hematopoietic stem cells, give rise to mature cells of the granulocyte, monocyte, erythroid, and/or thrombocytic lineages. High-resolution profiling of the developmental stages, from hematopoietic stem cells to mature progeny, is important to be able to study and understand the underlying mechanisms that guide various cell fate decisions. Also, this approach opens for greater insights into pathogenic events such as leukemia, diseases that are most often characterized by halted differentiation at defined immature precursor levels. In this chapter, we provide protocols and discuss approaches concerning the analysis and purification of immature myeloerythroid lineages by multiparameter flow cytometry. A wealth of literature has demonstrated the feasibility of similar approaches also for the human system. However, in this chapter, we focus on the identification of bone marrow cells derived from C57BL/6 mice, in which flow cytometry-based immunophenotypic applications have been most widely developed. This should allow also for its application in genetically modified models on this background. For maximal reproducibility, all protocols described have been established using reagents from commercial vendors to be analyzed on a flow cytometer with factory standard configuration.

Key words Flow cytometry, Hematopoiesis, Myelopoiesis, Erythropoiesis myeloerythropoesis, Immunophenotype, Cell isolation, Differentiation

1 Introduction

Most effector cells have a limited lifespan. Therefore, appropriate control of homeostasis in the blood system requires the constant production of new blood cell elements. This production is the result of multiple differentiation events, where all different types of mature effector cells are derived from bone marrow-residing hematopoietic stem cells (HSCs). HSCs can at the single cell level both self-renew and differentiate into all separate hematopoietic lineages, thereby allowing for lifelong hematopoiesis [1].

The immediate progeny of HSCs are multipotent progenitor cells that retain full lineage potential but have lost extensive self-renewal ability. Such multipotent progenitors, in turn, give rise to a set of oligopotent progenitors with more restricted developmental

Teresa S. Hawley and Robert G. Hawley (eds.), *Flow Cytometry Protocols*, Methods in Molecular Biology, vol. 1678, DOI 10.1007/978-1-4939-7346-0_13,

potential. Upon further differentiation, these progenitors mature into lineage-restricted progeny, from which all the mature blood cells eventually arise (Fig. 1a). As many of these subsets constitute only a minor fraction of all cells found in a measurement of a bulk population of non-enriched bone marrow cells, it is obvious that measurement of the bulk population in most cases is not sufficient to deduce information about a defined cellular stage or developmental pathway. The subset of interest would simply "drown" in the noise contributed by other cell types. Therefore, to detail hematopoietic lineage development, it is necessary to purify cells not only with appropriate lineage affiliation but ultimately also at defined developmental stages.

Many years advances in flow cytometry nowadays routinely allow for the simultaneous assessment of multiple proteins on cells [2]. Thereby, it is possible to resolve complex combinatorial expression patterns that associate with functionally distinct cellular properties. The multiparametric analysis is here key, since no single protein has to date been identified that alone can be used to phenotypically define HSCs and/or their downstream immature progeny [3, 4]. Rather, a panel of markers has to be evaluated simultaneously.

Using 5-parameter flow cytometry, the prospective identification of oligopotent common lymphoid progenitors (CLPs) [5] and common myeloid progenitors (CMPs) [6] proposed that the first step in hematopoietic lineage restriction is the mutual exclusion of myeloerythroid from lymphoid potential. However, this fundamental concept has been challenged in multiple studies. Some reports have detected myeloid output from CLPs [7–10] and a CLP-independent pathway was described that can give rise to lymphoid cells [11]. Also, loss of megakaryocyte/erythroid (Meg/E) potential prior to lymphoid and granulocytic/monocytic divergence [12–14] has been described and, in fact, some divergence towards a Meg/E fate has been suggested to occur already at the HSC level [15–17]. Following observations that have questioned the strict bifurcation of lymphoid versus myeloerythroid development and the existence of a CMP at single cell level, we screened the myeloid progenitor compartment for additional cell surface markers that could potentially reveal such heterogeneity. This effort led to the identification of three markers: CD150, CD105, and CD41 that in combination with several previously described markers can be used to define a hierarchy of myeloid progenitors at high resolution (Fig. 1b) [18, 19]. This isolation scheme has been taken advantage of in many publications since its presentation in 2007. More recently, the cellular properties of these cell types were further consolidated using single-cell RNA sequencing [20].

This chapter provides protocols for flow cytometric detection and purification of immature myeloerythroid progenitor subsets

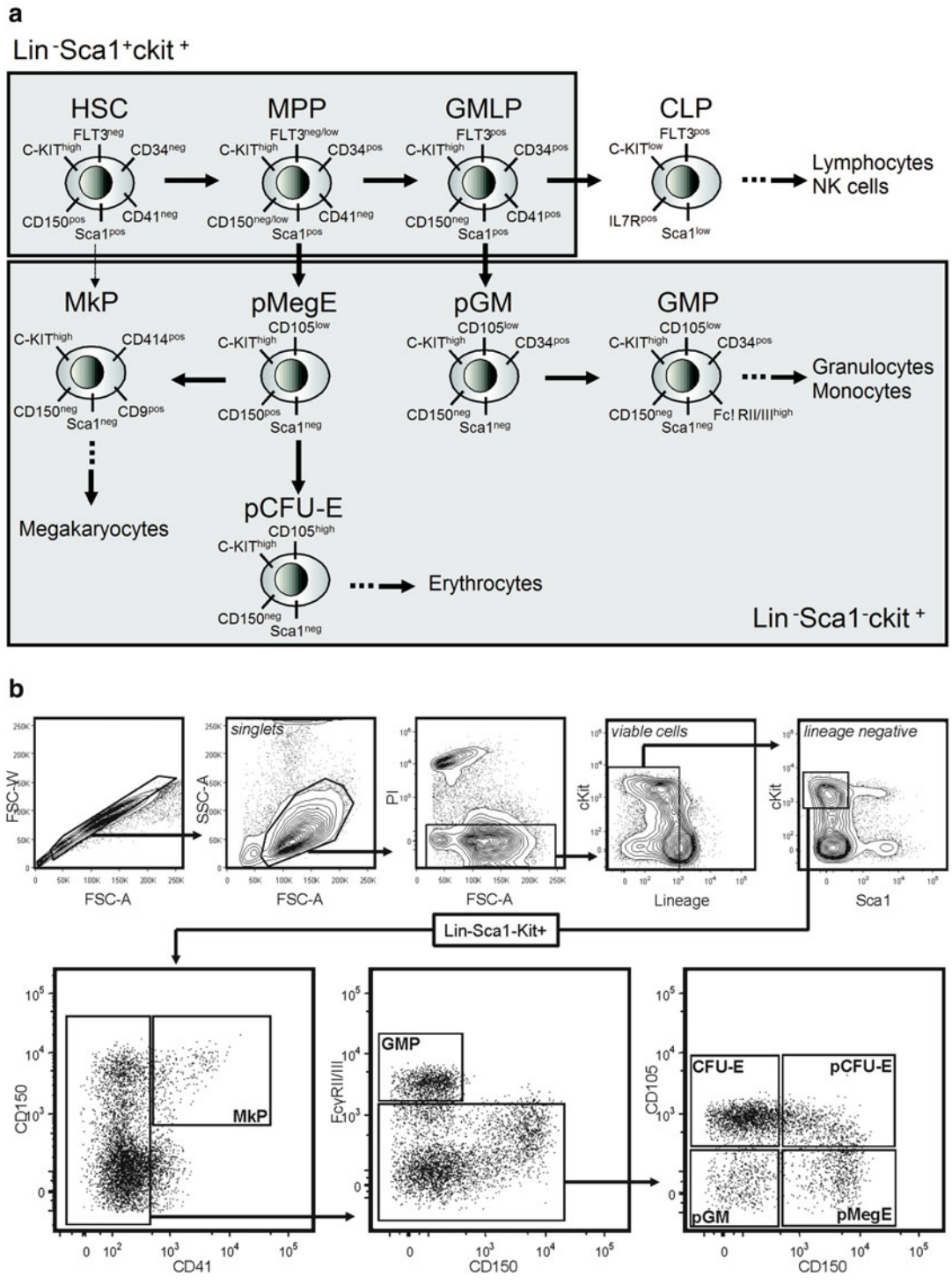

Fig. 1 Schematic and flow cytometry-based overview of early hematopoiesis. (**a**) Schematic overview of the first developmental stages in the differentiation from the multipotent HSC towards progeny possessing oligo- and unilineage potentials. For each cell type, a selection of cell surface protein expression capable of flow cytometry-based detection is depicted. Note that differentiation towards a T cell fate via thymic precursors is

from mouse bone marrow, including early bipotent progenitors for the erythroid/megakaryocyte lineages (pMegE), early monopotent erythroid (pCFU-E and CFU-E) and megakaryocyte progenitors (MkP) as well as primitive granulocyte/macrophage progenitors (pGM and GMP). We provide detailed protocols for cell isolation and cell surface staining and describe approaches that can be used to appropriately manage instrument settings, data acquisition, and data analysis.

2 Materials

All reagents mentioned in this section should be stored in dark, at 4 °C, unless otherwise indicated.

2.1 Isolation and Preparation of Mouse Bone Marrow Cells

1. C57BL/6 mice. All procedures involving experimental animal work must have approval from the local ethics committees and performed according to national legislation.
2. 70% Ethanol.
3. Sterile or ethanol-cleaned surgical instruments: Fine scissors, bone-cutting scissors, two forceps, scalpel.
4. Mortar and pestle.
5. Sterile pipettes.
6. Sterile polypropylene tubes.
7. 70 μm Falcon cup-type filters.
8. Erythrocyte lysing solution: Prepare a 10× stock by dissolving 16.58 g NH_4Cl, 2 g $KHCO_3$, and 0.744 g EDTA to a volume of 200 mL H_2O. Adjust pH to 7.4. Dilute stock to a 1× working solution with distilled H_2O immediately prior to use.
9. Staining and cell preparation buffer: Phosphate buffered saline (PBS), 2% (v/v) fetal bovine serum, 2 mM EDTA.
10. Vacuum suction device.
11. Cell counting device: Bürker counting chamber or automatic cell counter.
12. Refrigerated centrifuge.

Fig. 1 (continued) not depicted in this figure. (**b**) Flow cytometry-based strategy for high-resolution polychromatic fractionation of murine myeloerythroid precursors according to the protocol described herein. *HSC* hematopoietic stem cell, *MPP* multipotent progenitor, *GMLP* granulocyte–monocyte–lymphoid primed MPP, *CLP* common lymphoid progenitor, *pGM* pre-granulocyte/macrophage, *GMP* granulocyte/monocyte progenitor, *pMegE* pre-megakaryocyte/erythrocyte, *pCFU-E* pre-colony forming unit—erythrocytes, *MkP* megakaryocyte progenitor

2.2 Pre-enrichment of Mouse Bone Marrow Cells

All reagents described herein are used at predetermined optimal concentrations.

1. Materials described under Subheading 2.1.
2. Degassed staining and cell preparation buffer (*see* **Note 1**).
3. Sterile or clean pipette tips.
4. Sterile or clean Eppendorf tubes.
5. Biotin-conjugated "anti-lineage" antibodies: Ter119 (clone TER119), CD4 (clone GK1.5), CD8 (clone 53-6.7), B220 (clone RA3-6B2), Gr-1 (clone RB6-8C5), Mac-1 (clone M1/70).
6. Anti-biotin MicroBeads, autoMACS cell separator including all necessary buffers, or MACS MS/LS cell separation columns with the corresponding MACS separator magnet (Miltenyi Biotec, Bergisch Gladbach, Germany).

2.3 Cell Surface Staining of Mouse Bone Marrow Cells

All reagents described herein are used at predetermined optimal concentrations.

1. Materials described under Subheadings 2.1 and 2.2.
2. Quantum Dot (Qdot) 605-conjugated Streptavidin (Invitrogen/Thermo Fisher Scientific, Carlsbad, CA) or Brilliant Violet (BV) 605-conjugated Streptavidin (BioLegend, San Diego, CA).
3. Fluorochrome-labeled anti-mouse antibodies against indicated cell surface markers (*see* **Note 2**) as depicted in Table 1: Sca1 (clone E13-161.7), CD41 (clone MWReg30), FcγRII/III (clone 2.4G2), CD105 (clone MJ7/18), CD150 (clone TC15-12F12.2), cKit (or CD117, clone 2B8).
4. Viability dye: A non-cell membrane permeable DNA-binding dye, such as 1 mg/mL Propidium Iodide (PI) solution in water (*see* **Note 3**).

2.4 Compensation Procedures

1. Materials described in Subheadings 2.1–2.3.
2. Flow cytometer with lasers and filter setup concordant with the excitation and emission spectra of the used fluorochromes. The protocols in this chapter are based on acquisition on a FACSAria (BD Biosciences, San Jose, CA) flow cytometer equipped with three lasers (375-nm Violet laser, 488-nm blue laser, 635-nm red laser), with three detectors for the Violet, six detectors for the Blue, and three detectors for the Red laser.
3. Antibody capture beads (e.g., BD™ CompBeads; anti-rat/hamster or anti-mouse Ig, κ) and/or splenocytes, used to generate single fluorochrome-labeled samples (SS).

Table 1
Staining protocol

	Pacific blue	BV605	FITC	PE	Cy7PE	PETXR	APC	APC-eFluor780
Unstained[a]								
SS[b]	+							
SS[b]		+						
SS[b]			+					
SS[b]				+				
SS[b]					+			
SS[b]						–[c]		
SS[b]							+[d]	
SS[b]								+
FMO FITC[e]	Sca1	Lineage[f]	–	FcγRII/III	CD105	PI	CD105	cKit
FMO Cy7PE[e]	Sca1	Lineage[f]	CD41	FcγRII/III	–	PI	CD105	cKit
FMO APC[e]	Sca1	Lineage[f]	CD41	FcγRII/III	CD105	PI	–	cKit
Sample	Sca1	Lineage[f]	CD41	FcγRII/III	CD105	PI	CD105	cKit

Experimental staining protocol, including single-stained (SS) controls for instrument setup, as well as fluorescent minus one (FMO) controls for gate setting/analysis purposes
[a]Unstained cells (or negative capture beads) are used to set detector PMTs
[b]SS = single-stained controls, using capture beads or, for instance, splenocytes for automated compensation
[c]PI (Propidium iodide) is detected in most channels of the blue laser and thereby the choice of detector for dead cell exclusion is relatively flexible. No SS sample is required for detecting PI; however, this parameter should be included in the compensation matrix in order to compensate for spectral leakage from other channels into the viability channel
[d]The CD150 antibody does not bind to the capture beads that we are referring to here. Therefore, use another APC-conjugated antibody, preferably from the same provider
[e]FMO = fluorescence minus one. Usage and preparation are outlined in the text
[f]Lineage = cocktail with mature blood cell lineage markers. In this protocol, we use biotinylated anti-Ter119, B220, CD4, CD8, Gr1, and CD11b antibodies that are subsequently visualized with a secondary Streptavidin-BV605 reagent

2.5 Acquisition, Gating Strategies, and Sorting of Target Cells

1. Materials described in Subheadings 2.1–2.4.
2. Fluorescence-activated cell sorter (FACS) with a cell-sorting device, including a single-cell depositor to perform clone sorting.
3. Appropriate fluorescence minus one (FMO) controls (*see* Table 1 and **Note 4**).

2.6 Analysis and Presentation of Data

1. Flow cytometry analysis software (*see* **Note 5**).

3 Methods

3.1 Isolation and Preparation of Mouse Bone Marrow Cells

In this Subheading, we describe the dissection of mouse bones and subsequent recovery of bone marrow cells.

1. Euthanize mice according to a locally approved procedure.
2. Disinfect the skin of the mouse with 70% ethanol using a spray bottle. Prepare 1 mL cold buffer per mouse to collect the bones.
3. Using clean instruments, make a transverse cut in the abdominal area and draw the skin laterally to open the abdominal cavage.
4. Inspect liver and spleen for possible signs of disease, abdominal carcinomas, or organomegaly. Signs of disease should be a very rare event in young wild-type mice.
5. Cut off both feet. Hold the knee joint with one forceps, the proximal part of the tibia with the other forceps, and bend the latter anterior to break off the tibia. Clear the tibia from tissues (muscles, tendons, etc.) using a scalpel and put bones in cold buffer.
6. Grab distal femur with one pair of forceps and the knee joint with the other, and bend the latter anterior to break off the knee joint. Cut the tibia loose as proximal as possible, clear from other tissues using a scalpel, and transfer to cold buffer.
7. To isolate the iliac crest (*see* **Note 6**), hold with a pair of forceps the site (bone fragment) from which the tibia was cut, cut about 1 cm upwards medially from the forceps, and pull out the crista. Remove other tissues and transfer to cold buffer.
8. After isolation of all bone fragments, transfer to a mortar, and gently crush the bones. Flush crushed bones with isolation buffer and pipette up and down with cold buffer followed by filtering the suspension (70-μm cup filter) into an appropriately sized collection tube (*see* **Note 7**).
9. Centrifuge the cell suspension at 400 × *g* for 10 min and resuspend cell pellet in 1× lysis buffer if red blood cell lysis is performed (*see* **Note 8**) 200 μL/mouse. Incubate for 1 min at room temperature. Add isolation buffer (1 mL per mouse) and filter to rid clumps of cell debris. Centrifuge again at 400 × *g* for 10 min and resuspend in an appropriate volume of isolation/staining buffer.

This relatively fast method should yield a recovery of bone marrow cells in the range of 1–1.5 × 10^8 cells per mouse (= one mouse BM equivalent).

3.2 Pre-enrichment of Mouse Bone Marrow Cells

In this Subheading, we describe the enrichment for the target populations using the negative selection of cells expressing mature "lineage markers," the so-called lineage depletion (*see* **Note 9**). These

lineage-depleted cells are the cells of interest, since cells within the more immature bone marrow compartments lack expression of these markers [21, 22]. For several reasons, we find pre-enrichment of the sample advantageous when cells are subjected to sorting (*see* **Note 10**) [3]. Enrichment for lineage-negative cells is performed using either an autoMACS according to instructions from supplier or MACS separation columns and separator magnets as described below. For quantitative analysis of population frequencies in the unfractionated bone marrow, the sample or an aliquot of the sample is not enriched (*see* **Note 11**) and bone marrow cells are directly targeted for cell surface staining (Subheading 3.3).

1. Centrifuge cell suspension (at 400 × *g* for 10 min; these same speed and time are used throughout) and resuspend one mouse BM equivalent in 200 μL buffer, containing anti-lineage antibodies at predetermined concentrations.
2. Incubate on ice for 15 min, wash with 1 mL buffer per mouse equivalent, and centrifuge.
3. Resuspend in 100 μL buffer per mouse equivalent. Vortex anti-biotin Microbeads stock, add 10 μL of Microbeads stock per mouse equivalent, then mix and incubate on ice for 20 min. Vortex once or twice during incubation.
4. Wash with 1 mL buffer per mouse equivalent, centrifuge, and resuspend in 250–500 μL buffer per mouse equivalent (although a minimum of 1 mL).
5. Place the column on the magnet (for one mouse: use MS columns; for two or more mice: use LS columns) and rinse columns (for MS columns: twice with 1 mL buffer; for LS columns: twice with 3 mL buffer). Alternatively, use an auto-MACS system according to manufacturer's instructions.
6. Place a 70-μm Falcon cup-type filter on top of the column and apply cells to the column. Apply three times washing volume (1 mL for MS and 3 mL for LS columns) to the filter/column and collect the lineage-depleted fraction.
7. If lineage-positive cells are needed (for instance, to evaluate enrichment efficiency), take column from the magnet, add 1 volume of washing volume and flush out the lineage-positive enriched fraction (*see* **Note 12**).

3.3 Cell Surface Staining of Mouse Bone Marrow Cells

Prior to the actual staining of cells, antibody cocktails (containing antibodies at predetermined concentrations in staining buffer) are prepared for those staining steps in which cells are stained with two or more antibodies simultaneously. This includes both antibody cocktails for the actual samples, as well as for the FMO (*see* **Note 4**) controls (*see* **Note 13**). The staining volumes indicated herein can be adjusted depending on cell numbers.

1. Following enrichment by lineage depletion, aliquot a small fraction of the enriched cells to separate Eppendorf tubes for FMO controls. Centrifuge cells and resuspend all FMOs (50 μL per FMO) and sample(s) (50 μL per mouse equivalent) in staining buffer (*see* **Note 14**).
2. Add an equal volume of antibody cocktail at double the optimal concentrations to reach a final optimal concentration of antibodies.
3. Incubate for 30 min on ice in the dark.
4. Wash and resuspend at a cell density of 10^8 cells/mL of buffer containing PI at a 1:1000 diluted concentration.
5. Store dark on ice until acquisition on the flow cytometer.

3.4 Compensation Procedures

As compensation in multi-color stainings becomes increasingly complicated for each additional parameter, we use automatic software compensation. Ideally, compensation is performed using identical material (cells) and antibodies as in the actual experiment. However, many of the cell surface proteins in the described stainings are expressed on very infrequent population and/or at dim levels, complicating compensation procedures. Capture beads provide a good alternative and are therefore recommended in these protocols (*see* **Note 15**).

1. Prepare single-stained compensation controls by aliquoting 100 μL buffer into an Eppendorf tube for each of the fluorochromes used herein and add 25 μL (or a small droplet) of CompBeads to each tube (vortex bead stock first). No compensation control is generated for PI.
2. Add 1 μL of primary antibody to each tube and mix. In the case of markers that are detected with secondary reagents (i.e., biotinylated lineage antibodies), stain capture beads first with the primary antibody (for instance, B220-biotin), then wash and add the secondary reagents. In the case where primary fluorochrome antibodies are not recognized by capture beads (i.e., the wrong isotype of species of primary antibody), use an appropriate fluorochrome-conjugated primary antibody recognized by the capture beads (*see* **Note 15**).
3. Vortex and incubate for 10 min on ice in the dark. Resuspend each compensation control in 400 μL buffer and put aside dark on ice.
4. Aliquot 500 μL to an Eppendorf tube and add two drops of negative control CompBeads.
5. Take the unstained cells to the flow cytometer to set PMT values for all detectors, including the channel dedicated to the PI signal.

6. Acquire all single-stained compensation controls (including the negative control beads) and calculate compensation values across all included detectors according to software instructions.

3.5 Acquisition, Gating Strategies, and Sorting of Target Cells

We recommend to always filter samples directly prior to acquisition to minimize the risk of clogs.

3.5.1 Acquisition

1. Filter an aliquot of the lineage-enriched cell fraction and run on the flow cytometer to set appropriate gains for forward and side scatter.
2. Filter samples and run all FMO controls, followed by the actual sample(s).
3. When sorting, acquire a sufficient amount of events to set sorting gates.
4. For frequency determination, acquire sufficient amounts of events to obtain statistically sound data with sufficient power (*see* **Notes 10** and **11**).

In our experiments, we use the BD FACSAria with a 70-μm nozzle and run the flow cytometer at high (70 psi) pressure. We follow the manufacturer's recommendations on drop-drive frequency at this pressure (typically 88–90 kHz).

3.5.2 Gate Setting Strategies

In this Subheading, we provide a strategy on how to set gates that define the different immature myeloerythroid cellular subsets. We will base this discussion on the plots as depicted in Fig. 1b (*see* **Note 16**). Please note that most parameters are presented using a biexponential or "logicle" display [23] that uses alternative scaling of the lower end of the axis. This allows for presentation also of negative values and avoids events from "sticking to the axes," thereby maximizing visualization of data [3].

1. Figure 1b, upper plots, most left: Displaying FSC-area against FSC-height allows for the exclusion of most cellular doublets.
2. Figure 1b, upper plots, second from the left: PI-positive cells (i.e., dead cells) are excluded.
3. Figure 1b, upper plots, middle: Plotting FSC-area versus SSC-area excludes smaller or larger particles such as unwanted cells and debris.
4. Figure 1b, upper plots, second from the right: Lineage-negative cells are defined by plotting cKit versus lineage. Most cKit high cells are lineage negative/low. This gate could be difficult to define on an enriched sample (as in Fig. 1b) and is easier set in an unenriched sample, such as in Fig. 3b, right plot.
5. Figure 1b, upper plots, most right: This gate is set based on other "reference cells" within the same plot. Sca-1 negativity is based on absent Sca-1 expression in the majority of cKit

medium-expressing cells. The high cKit expression is compared to cKit expression in $cKit^{+}Lin^{-}Sca1^{+}$ (KLS) cells. A more generous gate for Sca-1 expression will include cells that are more immature and a more generous gate for cKit expression will primarily include more immature erythroid-restricted progenitors.

6. Figure 1b, lower plots, left: We see two alternatives to set these gates. When performing these stainings for the first time, we strongly recommend including FMOs for gate setting controls. The gates in this plot are set based on a FMO-APC and FMO-FITC as presented in Fig. 2a, left panels. However, preparation of FMOs for each parameter could be time-consuming and/or difficult. In addition, FMOs are of little use to separate cells that express medium versus high levels of a certain antigen (as could be the case for CD105 in some of the myeloerythroid staining protocols [19]). Therefore, we frequently use internal reference populations (IRPs) and find these of great value [3]. IRPs are cell populations within the tested sample that can serve as positive or negative references, as illustrated in Fig. 2b. A requirement for the use of IRPs is pre-existing knowledge of cell surface expression of the marker of interest within these IRPs, obtained through, for instance, the use of FMO in earlier experiments and/or based on information from the literature.
7. Figure 1b, lower plots, middle: FcγRII/III high versus negative/low expressing cells are defined by FcγRII/III expression in the CD150-positive cells in this plot.
8. Figure 1b, lower plots, right: The gates in these plots are defined by FMOs for Cy7PE and APC as illustrated in Fig. 2a, or can alternatively be set based in an IRP as presented in Fig. 2b.

3.5.3 Single-Cell and Bulk Sorting of Target Cells

1. Set up the flow cytometer as described above. Take the samples (including FMOs) and run enough events (about 20,000–30,000 of lineage-depleted cells) to allow for proper gate setting as described in Subheading 3.5.2 (*see* **Note 16**).
2. Optimize the FACS sorter for cell sorting (set drop delay, position side stream, etc.) according to manufacturer's protocol. As the cellular subset in these protocols is relatively infrequent, it is important to sort in the highest purity mode.
3. Adjust the speed of sample acquisition dependent on the purity of the sample. Too high speed increases the electronic abort rate, while viability can be affected if sorting procedure takes too long. For bulk sorting, we typically run at a higher speed (about 4000–6000 events/s) than for single-cell sorting

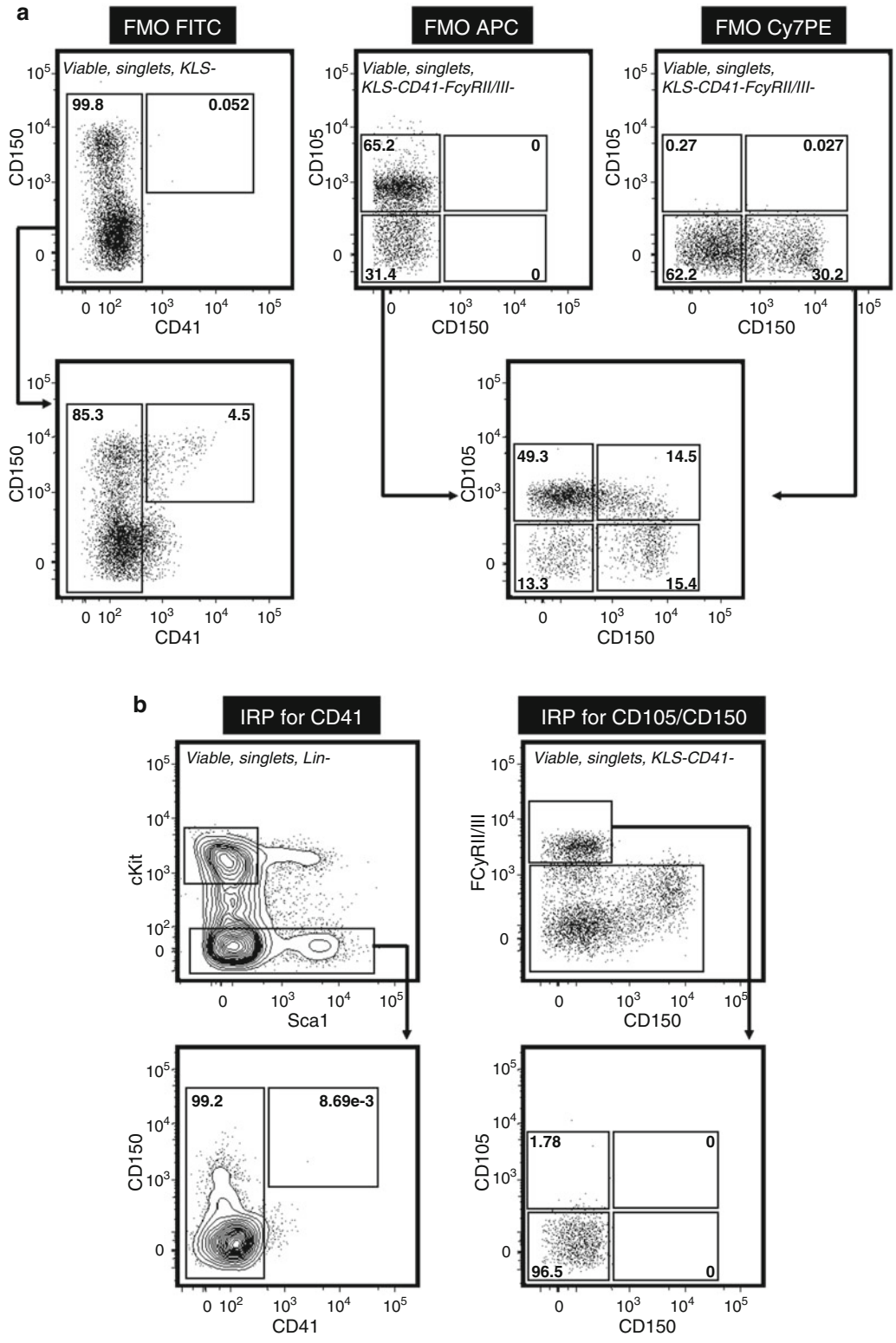

Fig. 2 Gate setting controls. (**a**) These samples were stained simultaneously with the sample in Fig. 1b, with the exclusion of the indicated fluorochromes, allowing for FMO (fluorescence minus one) analysis as illustrated. (**b**) Within the sample in Fig. 1b, previously defined internal reference populations (IRPs) were used to define negative versus positive expression levels of CD41 (*left panels*) or CD105 and CD150 (*right panels*) within the KLS- and KLS-CD41-FcγRII/III-populations, respectively

(about 1000 events/s). These sort rates are on the low end and can be enhanced, and ultimately depends on parameters such as the sheath pressure and droplet rates. As a general guide, do not exceed a cellular sort rate above the drop-drive frequency/4 (for instance, using a drop-drive frequency of 90 kHz, a theoretical maximum would be 22,500 cells/s).

4. Decide prior to cell sorting the number of desired target cells and sort the exact number desired cells directly in the appropriate media used in downstream applications (cell culture media, lysis buffer, etc.) (*see* **Note 17**).
5. When performing co-cultures with, for instance, stromal cells or transplantation with bone marrow support cells, sort the target cells in the medium that already contains the other cell type.
6. When sorting cells directly into plates (Terasaki, 96- and 48-well plates or other formats for culturing cells, as well as 96-well plates or "PCR-strips" for subsequent molecular analysis), we sort our cells directly into plates containing appropriate media/buffer (*see* **Notes 18** and **19**).
7. When sorting into tubes, vortex the collection tube directly prior to sorting (to try to avoid sorted cells to stick to the sides) and vortex directly after to mix cells in the media. We recommend using high-retention tubes to avoid cells adhering to the tube wall (*see* **Note 20**).

3.6 Analysis and Presentation of Data

Some principles for the analysis of these data were already discussed in Subheading 3.5.2. We see some additional considerations that should be taken into account.

1. For frequency determination of cellular subsets in total bone marrow cells, calculate frequencies as the percentage of the total, live cells (i.e., Fig. 1b, gate in middle plot, upper row) as presented in Fig. 3, right plot.
2. In plots with many events, use contour plots. However, in cases of very low numbers of events these plots may become misleading; then use dot plots instead.
3. Of the different commercial analysis software we have tested to date, we find Mac-based FlowJo analysis software to be a good compromise in terms of options, stability, and speed. This latter point may become an issue in those cases when multiple, very large data files are to be analyzed.

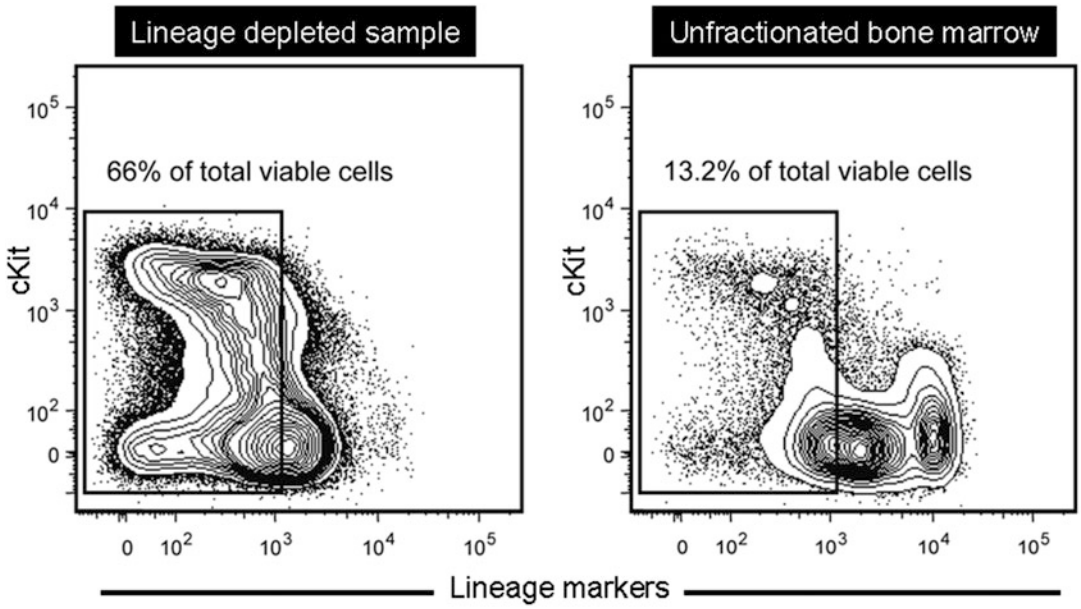

Fig. 3 Advantage of pre-enrichment for analysis and sorting purposes. Parallel to the staining of the enriched sample in Fig. 1b, an aliquot of unenriched (unfractionated) bone marrow cells was stained according to similar procedures and an equal amount of events (300,000) was acquired on the flow cytometer. Pre-enrichment of a sorting sample results in higher frequencies of lineage-negative live cells (*left plot*), compared to an unenriched sample (*right plot*), highlighting its major advantage during cell sorting as discussed in **Note 10**

4 Notes

1. Manufacturer's protocol recommends using degassed buffer to obtain optimal MACS-based selections and recovery. However, we have found that using media prepared at least 24 h prior to experimentation, combined with a filter placed on top of the column when loading the cell suspension, also yields acceptable selection and recovery.
2. Antibodies used herein are commercially available at one or several suppliers; we obtain most antibodies from BD Biosciences (San Jose, CA), eBioscience (San Diego, CA), or BioLegend (San Diego, CA).
3. We tend to prefer PI over other "viability dyes" because of its brightness, relatively long shelf life, and easy handling (i.e., no need to prepare intermediate stock solutions).
4. FMO controls are used as biological or "gate setting" controls and are important when defining a negative versus positive gate for cells expressing dim levels of a certain cell surface marker (i.e., no clear separation between a negative and positive population).

5. Analysis can be performed using the acquisition software of the cytometer, although we prefer more specialized flow cytometry analysis software such as FlowJo for Macintosh (TreeStar Inc, Ashland, OR).
6. The recovery in one mouse from two femurs and two tibiae is around $0.8–1.2 \times 10^8$ unfractionated bone marrow cells (variability is dependent on the size of mice and typically therefore of mouse age and gender). By isolating cells also from the two hip bones, although technically somewhat more demanding, this yield can be increased with another $0.2–0.4 \times 10^8$ cells.
7. It is our experience that crushing rather than flushing bones using a syringe renders a higher yield of cells. Other investigators have in addition claimed that certain cellular subsets do not release effectively using flushing [24].
8. We usually perform lysis of red blood cells when the cells are only subjected to analysis. When staining cells for sorting and subsequent functional enumerations, we usually do not lyse the sample as we suspect a negative impact of the lysing procedure on the viability of certain cell subsets.
9. As an alternative to depletion of lineage-negative cells, enrichment for cKit (CD117)-expressing cells can be used. However, we have noted that cKit enrichment negatively influences the fluorescent signal for cKit on the flow cytometer. Presumably, this is because the fluorochrome-conjugated 2B8 clone used to visualize cKit expression is the same antibody coated on cKit magnetic beads, hence partially blocking efficient staining. This makes careful titration of cKit beads necessary (the recommended amount of beads from the supplier does not allow appropriate visualization of cKit with 2B8). Also, we previously performed lineage depletion using the Dynal bead system (Invitrogen/Thermo Fisher Scientific) that uses selection for sheep anti-rat magnetic Dynabeads binding to purified anti-lineage antibodies, but find this method inferior in terms of enrichment efficiency, handling speed, and cost.

   In this protocol, we do not use any purified antibodies that typically are visualized by fluorochrome-conjugated goat anti-rat antibodies. However, if one chooses to include a purified antibody, then both the primary and secondary stains are performed prior to enrichment as the anti-lineage antibodies used herein were generated in the rat.
10. Pre-enrichment of the sample, as opposed to staining *and sorting* from unfractionated bone marrow cells, is advantageous for several reasons. *First*, cell surface staining on a pre-enriched sample that contains higher frequencies of the target cells will give both better signals and less unspecific staining as well as less noise. *Second*, when sorting for these infrequent

cellular subsets, pre-enrichment of the sample increases the frequencies of the cells of interest (Fig. 3), giving a superior purity, yield, and recovery of the cells of interest when compared to sorting from a non-enriched sample, in addition to dramatically reducing sorting time.

11. Sometimes, it is desirable to obtain information on frequencies of these subsets as a percentage of the total, live bone marrow cells and a pre-enriched sample fails to provide this information. In such case, an unenriched and enriched sample is prepared, stained, and acquired for each individual mouse.
12. Here, we recommend to recover the lineage-positive fraction and include an aliquot in the staining protocol in order to evaluate enrichment efficiency (i.e., no or hardly any lineage-negative cells should be present in this sample), especially when inexperienced with the methodology. In addition, a small aliquot of lineage-enriched cells is useful to later set FSC/SSC-gains on the flow cytometer when setting up the instrument (*see* Subheading 3.5.1, **step 1**).
13. In this protocol, there is no real need for the preparation of a separate antibody cocktail for each of the FMO, as well as the sample(s). Instead, make a "base-cocktail" that contains 2× concentrations FcγRII/III, Sca1, cKit, and Streptavidin-(BV605). Take 3 × 100 μl from this cocktail for each of the FMOs and add the two appropriate (lacking) antibodies for each of the FMOs at 2× concentration. Thereafter, complete the "base-cocktail" by adding CD41, CD105, and CD150 at 2× concentration (NB: now the volume is altered and requires adjustment of the antibody volume added to obtain correct concentrations).
14. "Traditional Fc-blocking" to prevent unspecific binding cannot be used herein, as FcγRII/III is one of the targeted parameters in this protocol. This issue can however be circumvented by incubating the enriched cells in FcγRII/III-PE, prior to Fc-block and subsequent staining with the additional antibodies. However, note that we typically do not perform Fc-blocking. The staining volume can be decreased when pooling cells from multiple mice. Lineage-depleted cells from up to 10 mice are stained in approximately 500–600 μL antibody cocktail, and cells from up to 15 mice can be stained in approximately 1 mL antibody cocktail. These volumes are of course dependent on the efficiency of the pre-enrichment.
15. Be aware of the availability of different types of capture beads, each possessing affinities for different classes of antibodies. The capture beads used herein bind to most antibodies used in protocols established for mouse cells (because historically most anti-mouse antibodies are of rat species). However, in

some specific cases, no antibody binding occurs to these beads, as is the case for the anti-CD150 antibodies (a mouse IgG2a lambda isotype). In those cases, to prepare the single-stained compensation control use instead another antibody conjugated with a similar fluorochrome, preferably from the same supplier. An alternative is the use of splenocytes, instead of capture beads, to prepare compensation controls. In such cases, it needs however to be established that the antigen of interest is expressed on splenocytes, and preferably at relatively high levels. Washing and centrifugation procedures for capture beads and splenocytes are identical to those for bone marrow cells.

16. Gate setting purely for analysis purposes allows for the gates to be immediately adjacent to one another, in order to not exclude any events from the analysis. However, when sorting, we use more restrictive gate setting as compared to the gate settings shown in Fig. 1b in order to enhance the purity of the sorted cells.
17. We prefer not to wash cells following sorting, as this will inevitably mean loss of cells. However, one exception might be in the case of sorting large numbers of cells into a relatively small volume since the sheath buffer we use (commercial from BD Biosciences) contains a low amount of detergent. In those cases, one could consider to wash and count the cells afterward, alternatively to setup and run the FACS machine with PBS instead.
18. Performing cell culture experiments, and especially more long-term culturing, always involves a risk of contamination during incubation. We prepare and stain our cells non-sterile on the laboratory bench and use non-sterile but relatively fresh staining buffers and non-sterile but clean plastics. However, target plates and target media are always (prepared) sterile. Opening a cell culture plate by the FACS sorter increases the risk of obtaining contaminating particles in the culture medium and should therefore be kept to a minimum. In addition to running a long-clean cycle with ethanol of the FACS sorter, we always clean all surfaces on and around the FACS sorter with 70% ethanol, use gloves, and try to minimize traffic around the machine. Taking these precautions, we find contamination not to be a problem.
19. In a similar manner as in the previous note, samples and sort plates are managed with care when performing sorting for subsequent molecular analysis, especially when performing RNA isolation of the target cells. Always use gloves, spray surfaces with *RNA-away* (or similar solutions), and directly

transfer the plate (or tube) to dry ice for fast and timely freezing after completed sorting.

20. As in the previous note, when sorting for subsequent molecular analysis such as RNA extraction, adhere to a similar handling of the sample and sorted tube.

Acknowledgements

This work was supported by grants from the Swedish Cancer Foundation, the Swedish Medical Research Council, the Swedish Pediatric Childhood Cancer Foundation, and ERC consolidator grant 615068.

References

1. Bryder D, Rossi DJ, Weissman IL (2006) Hematopoietic stem cells: the paradigmatic tissue-specific stem cell. Am J Pathol 169 (2):338–346
2. Perfetto SP, Chattopadhyay PK, Roederer M (2004) Seventeen-colour flow cytometry: unravelling the immune system. Nat Rev Immunol 4(8):648–655
3. Rundberg Nilsson A, Bryder D, Pronk CJ (2013) Frequency determination of rare populations by flow cytometry: a hematopoietic stem cell perspective. Cytometry A 83 (8):721–727. doi:10.1002/cyto.a.22324
4. Mayle A, Luo M, Jeong M, Goodell MA (2013) Flow cytometry analysis of murine hematopoietic stem cells. Cytometry A 83 (1):27–37. doi:10.1002/cyto.a.22093
5. Kondo M, Weissman IL, Akashi K (1997) Identification of clonogenic common lymphoid progenitors in mouse bone marrow. Cell 91(5):661–672
6. Akashi K, Traver D, Miyamoto T, Weissman IL (2000) A clonogenic common myeloid progenitor that gives rise to all myeloid lineages. Nature 404(6774):193–197
7. Allman D, Sambandam A, Kim S, Miller JP, Pagan A, Well D, Meraz A, Bhandoola A (2003) Thymopoiesis independent of common lymphoid progenitors. Nat Immunol 4 (2):168–174
8. Balciunaite G, Ceredig R, Massa S, Rolink AG (2005) A B220+ CD117+ CD19- hematopoietic progenitor with potent lymphoid and myeloid developmental potential. Eur J Immunol 35(7):2019–2030
9. Rumfelt LL, Zhou Y, Rowley BM, Shinton SA, Hardy RR (2006) Lineage specification and plasticity in CD19- early B cell precursors. J Exp Med 203(3):675–687
10. Mansson R, Zandi S, Anderson K, Martensson IL, Jacobsen SE, Bryder D, Sigvardsson M (2008) B-lineage commitment prior to surface expression of B220 and CD19 on hematopoietic progenitor cells. Blood 112(4):1048–1055
11. Ghaedi M, Steer CA, Martinez-Gonzalez I, Halim TY, Abraham N, Takei F (2016) Common-lymphoid-progenitor-independent pathways of innate and T lymphocyte development. Cell Rep 15(3):471–480. doi:10.1016/j.celrep.2016.03.039
12. Adolfsson J, Mansson R, Buza-Vidas N, Hultquist A, Liuba K, Jensen CT, Bryder D, Yang L, Borge OJ, Thoren LA, Anderson K, Sitnicka E, Sasaki Y, Sigvardsson M, Jacobsen SE (2005) Identification of Flt3+ lympho-myeloid stem cells lacking erythro-megakaryocytic potential a revised road map for adult blood lineage commitment. Cell 121(2):295–306
13. Lai AY, Kondo M (2006) Asymmetrical lymphoid and myeloid lineage commitment in multipotent hematopoietic progenitors. J Exp Med 203(8):1867–1873
14. Yoshida T, Ng SY, Zuniga-Pflucker JC, Georgopoulos K (2006) Early hematopoietic lineage restrictions directed by Ikaros. Nat Immunol 7(4):382–391
15. Nestorowa S, Hamey FK, Pijuan Sala B, Diamanti E, Shepherd M, Laurenti E, Wilson NK, Kent DG, Gottgens B (2016) A single-cell resolution map of mouse hematopoietic stem and progenitor cell differentiation. Blood 128(8): e20–e31. doi:10.1182/blood-2016-05-716480
16. Sanjuan-Pla A, Macaulay IC, Jensen CT, Woll PS, Luis TC, Mead A, Moore S, Carella C,

Matsuoka S, Jones TB, Chowdhury O, Stenson L, Lutteropp M, Green JC, Facchini R, Boukarabila H, Grover A, Gambardella A, Thongjuea S, Carrelha J, Tarrant P, Atkinson D, Clark SA, Nerlov C, Jacobsen SE (2013) Platelet-biased stem cells reside at the apex of the haematopoietic stem-cell hierarchy. Nature 502 (7470):232–236. doi:10.1038/nature12495

17. Grover A, Sanjuan-Pla A, Thongjuea S, Carrelha J, Giustacchini A, Gambardella A, Macaulay I, Mancini E, Luis TC, Mead A, Jacobsen SE, Nerlov C (2016) Single-cell RNA sequencing reveals molecular and functional platelet bias of aged haematopoietic stem cells. Nat Commun 7:11075. doi:10.1038/ncomms11075
18. Pronk CJ, Attema J, Rossi DJ, Sigvardsson M, Bryder D (2008) Deciphering developmental stages of adult myelopoiesis. Cell Cycle 7 (6):706–713
19. Pronk CJ, Rossi DJ, Mansson R, Attema JL, Norddahl GL, Chan CK, Sigvardsson M, Weissman IL, Bryder D (2007) Elucidation of the phenotypic, functional, and molecular topography of a myeloerythroid progenitor cell hierarchy. Cell Stem Cell 1(4):428–442
20. Drissen R, Buza-Vidas N, Woll P, Thongjuea S, Gambardella A, Giustacchini A, Mancini E, Zriwil A, Lutteropp M, Grover A, Mead A, Sitnicka E, Jacobsen SE, Nerlov C (2016) Distinct myeloid progenitor-differentiation pathways identified through single-cell RNA sequencing. Nat Immunol 17(6):666–676. doi:10.1038/ni.3412
21. Spangrude GJ, Heimfeld S, Weissman IL (1988) Purification and characterization of mouse hematopoietic stem cells. Science 241 (4861):58–62
22. Uchida N, Aguila HL, Fleming WH, Jerabek L, Weissman IL (1994) Rapid and sustained hematopoietic recovery in lethally irradiated mice transplanted with purified Thy-1.1lo Lin-Sca-1+ hematopoietic stem cells. Blood 83(12):3758–3779
23. Parks DR, Roederer M, Moore WA (2006) A new "Logicle" display method avoids deceptive effects of logarithmic scaling for low signals and compensated data. Cytometry A 69 (6):541–551
24. Haylock DN, Williams B, Johnston HM, Liu MC, Rutherford KE, Whitty GA, Simmons PJ, Bertoncello I, Nilsson SK (2007) Hemopoietic stem cells with higher hemopoietic potential reside at the bone marrow endosteum. Stem Cells 25(4):1062–1069. doi:10.1634/stemcells.2006-0528

Chapter 14

Flow Cytometry Assays in Primary Immunodeficiency Diseases

Maurice R.G. O'Gorman

Abstract

Inborn errors of immunity are the cause of the primary immunodeficiency diseases, an extremely diverse group of genetic defects that are inherited in Mendelian fashion and result in the impairment of development and/or function of key components of the immune system. Since the last publication of this chapter in 2011, there have been approximately 100 new primary immunodeficiency diseases officially classified by the "Expert Committee for Primary Immunodeficiency" who met in 2015 and the numbers will continue to rise with the continued evolution and widespread adoption of genomic technologies. The ultimate diagnostic modality involves the identification of a mutation in a gene whose product is known to be involved in immunity. DNA sequencing is however still a rather time-consuming technology. Flow cytometry applications have evolved that are rapid, specific, and relatively inexpensive to screen for abnormalities associated with primary immunodeficiency diseases. The numerous flow cytometry procedures that have been developed to detect abnormalities in peripheral blood cells of primary immunodeficiency patients can barely be covered in an entire book, let alone one chapter. Instead of attempting to cover each disease with a specific assay or test, we will review four procedures each covering one of the three following broad forms of immune abnormalities observed in primary immunodeficiency, i.e., immune subset abnormalities, immune marker abnormalities, and immune function abnormalities.

Key words Lymphocyte subsets, Primary immunodeficiency disease, Flow cytometry, Oxidative burst, X-linked hyper IgM syndrome (XHIM) CD40 ligand, Routine immunophenotyping, Autoimmune lymphoproliferative syndrome (ALPS)

1 Introduction

The increased availability and widespread adoption of genomic technologies combined with an increased understanding of the complexities involved in effecting and regulating a normal immune response have resulted in the molecular elucidation of an ever increasing number of primary immunodeficiency diseases (PIDs) [1]. At the first WHO-sponsored meeting of experts involved in the treatment and investigation of primary immunodeficiency diseases in 1970 [2], 16 primary immunodeficiency diseases were identified and classified [3]. An update from the International Union of

Teresa S. Hawley and Robert G. Hawley (eds.), *Flow Cytometry Protocols*, Methods in Molecular Biology, vol. 1678, DOI 10.1007/978-1-4939-7346-0_14,

Immunological Societies primary immunodeficiency diseases classification committee was presented in 2007 [4]. Following the latest biennial meeting in London, UK in the spring of 2015, approximately 280 PIDs were classified, characterized, and published [1]. All of the PIDs are grouped into nine different tables (previously eight, with the newest group being Table IX—"Phenocopies of PID" [1]) (*see* Table 1 for a summary of the nine categories).

Many of the classified PIDs have an abnormality (subset, marker, or function) that could ultimately be detected by a flow cytometry-based application (although it must be acknowledged that not all abnormalities would be "specific" for a particular condition). A description of each of the immune abnormalities with an accompanying flow cytometry procedure may one day be accomplished but is well beyond the scope and space available for this chapter. Instead, in the next few paragraphs, I will provide four examples of flow cytometry procedures used to screen and/or detect the immune abnormality associated with their respective primary immunodeficiency disease.

It is practical to simplify all immune abnormalities amenable to flow cytometric evaluation to only three broad categories: (a) relative subset abnormalities, i.e., mutations in genes that affect the maturation and/or differentiation of specific cell subset(s), e.g., mutations in the Bruton tyrosine kinase gene, *BTK*, that affect the maturation and differentiation of B cells; (b) specific marker abnormalities, i.e., mutations in genes that affect only the expression of a specific marker on the surface or within the cell, e.g., CD40 ligand expression on activated CD4-positive T cells; or (c) functional abnormalities, i.e., mutations in genes that affect a specific immune function, e.g., mutations in genes coding for components of the NADPH oxidase that prevent the elaboration of an oxidative burst and the killing of phagocytosed microbes.

Leukocyte subset abnormalities defined by the measurement of the relative and absolute number of specific subsets represent the most common application of clinical flow cytometry. Specific cell surface, intracellular, and/or intra-nuclear marker abnormalities are also routinely detected by flow cytometry. Lastly, there are several physiologic cell functions whose activity can be assessed with the appropriate reagents and a flow cytometer. In this chapter, we will describe flow cytometry applications that have been adopted for use in a clinical setting to screen for primary immunodeficiency in each of the general categories (i.e., subset abnormalities, marker abnormalities, functional abnormalities). A more comprehensive flow cytometry-based treatise of the individual primary immunodeficiency diseases can be found in ref. [5].

1.1 Primary Immunodeficiency Diseases

Each discovery of a new primary immunodeficiency can be thought of as an "experiment of nature," a term coined originally by Robert A. Good in the mid-1950s [6] in reference to the fact that each case of a new primary immunodeficiency disease has taught us

Table 1
At the latest meeting of the "International Union of Immunological Societies Experts Committee for Primary Immunodeficiency" held in London, UK in 2015, a consensus regarding the classification of newly characterized disorders was published as Tables I–IX. The categories of each of the Tables with a salient example of a disease(s) are listed below [1, 8]

Group	Disease example in each Group
Table I. Combined T and B cell immunodeficiencies	Severe combined immunodeficiency (SCID) and CD40 ligand deficiency
Table II. Predominantly antibody deficiencies	Btk deficiency (X-linked agammaglobulinemia) and Common variable immunodeficiency disorders
Table III. Other well-defined immunodeficiency syndromes	Wiskott–Aldrich syndrome and DiGeorge anomaly
Table IV. Diseases of immune dysregulation	Autoimmune lymphoproliferative syndrome (ALPS) and Familial hemophagocytic lymphohistiocytosis
Table V. Congenital defects of phagocyte number function or both	Congenital neutropenia and Chronic granulomatous disease
Table VI. Defects in innate immunity	IL-1 receptor-associated kinase 4 (IRAK4) deficiency and MyD88 deficiency
Table VII. Autoinflammatory disorders	Periodic fever syndromes and Blau syndrome
Table VIII. Complement deficiencies	Hereditary angioedema (C1 inhibitor deficiency) and Paroxysmal nocturnal hemoglobinuria
Table IX. Phenocopies of PID	Somatic mutations in TNFRSF6 mimicking ALPS and Autoantibodies to interferon gamma mimicking interferon gamma receptor deficiency

something about the normal functioning of the inordinately complex immune system. From a clinical perspective, it is common to think of patients with a primary immunodeficiency to suffer from an increased susceptibility to both the frequency and severity of infections with opportunistic and pathogenic organisms. However, we now know that the scope and breadth of the clinical presentations classified as primary immunodeficiency disease includes more than an increased susceptibility to infections. Autoimmunity, autoinflammatory disorders, allergy, atypical hemolytic uremic syndrome, and paroxysmal nocturnal hematuria are examples of immune abnormalities and disorders now classified as primary immunodeficiency states. Increased susceptibility to infection does however remain the most common clinical presentation in primary immunodeficiency, and any patient with a history of an excessive number of infections, unusual infections, or difficult-to-treat infections warrants an evaluation for a primary immunodeficiency disease. A large international effort (the Primary Immunodeficiency Resource Center, www.info4pi.org) spearheaded by the Jeffrey Modell Foundation is aimed at increasing the awareness of

primary immunodeficiency in the general public and amongst medical professionals. Any individual with two or more of the ten warning signs below (as posted in international airports around the world) should speak with a physician about the possible presence of a primary immunodeficiency disease: (1) four or more new ear infections within 1 year; (2) two or more serious sinus infections within 1 year; (3) 2 or more months on antibiotics with little effect; (4) two or more pneumonias within 1 year; (5) failure of an infant to gain weight or grow normally; (6) recurrent, deep skin or organ abscesses; (7) persistent thrush in mouth or fungal infection on skin; (8) need for intravenous antibiotics to clear infections; (9) two or more deep-seated infections including septicemia; and (10) a family history of primary immunodeficiency.

1.2 Initial Evaluation

A patient suspected of a primary immunodeficiency should have a thorough clinical and family history as well as a physical exam. Depending on the clinical presentation and history, initial laboratory tests should include a CBC with a differential followed by testing of more specific immune parameters including quantitative serum immunoglobulin levels, complement levels, specific antibody determinations, and a flow cytometric assessment of the major leukocyte subsets. The most appropriate and encompassing screening assessment of the major leukocyte subsets is performed by what we refer to as "routine immunophenotyping" (described in more detail in Subheading 3.1). Based on these initial laboratory results and in the context of the history, physical and other laboratory tests, more specific flow cytometry procedures (i.e., specific subset, marker, or functional abnormalities) may be assessed. Finally, once a presumptive diagnosis is made, it is highly recommended that the underlying molecular etiology be ascertained by sequencing the DNA of the appropriate gene(s) in order to confirm the diagnosis and to allow for appropriate counseling and treatment.

Below are presented four flow cytometry procedures, one that is routine (immunophenotyping) and three that are performed in more specialized laboratories experienced in the diagnostic assessment of primary immunodeficiency disease. Routine immunophenotyping is now available in most hospital laboratories internationally and is probably the most valuable laboratory test for the general assessment of the cellular components of the immune system. Many of the primary immunodeficiencies result in abnormalities in the relative and absolute representation of specific lymphocyte subsets, some of these abnormalities being more specific than others. Examples of a few specific abnormalities that are associated with specific immunodeficiency diseases are presented in Fig. 1.

A more specialized flow cytometry procedure is presented which comprises a panel of monoclonal antibodies designed specifically to measure T cells that do not express CD4 or CD8 (referred to as double-negative T cells) but express the alpha/beta form of

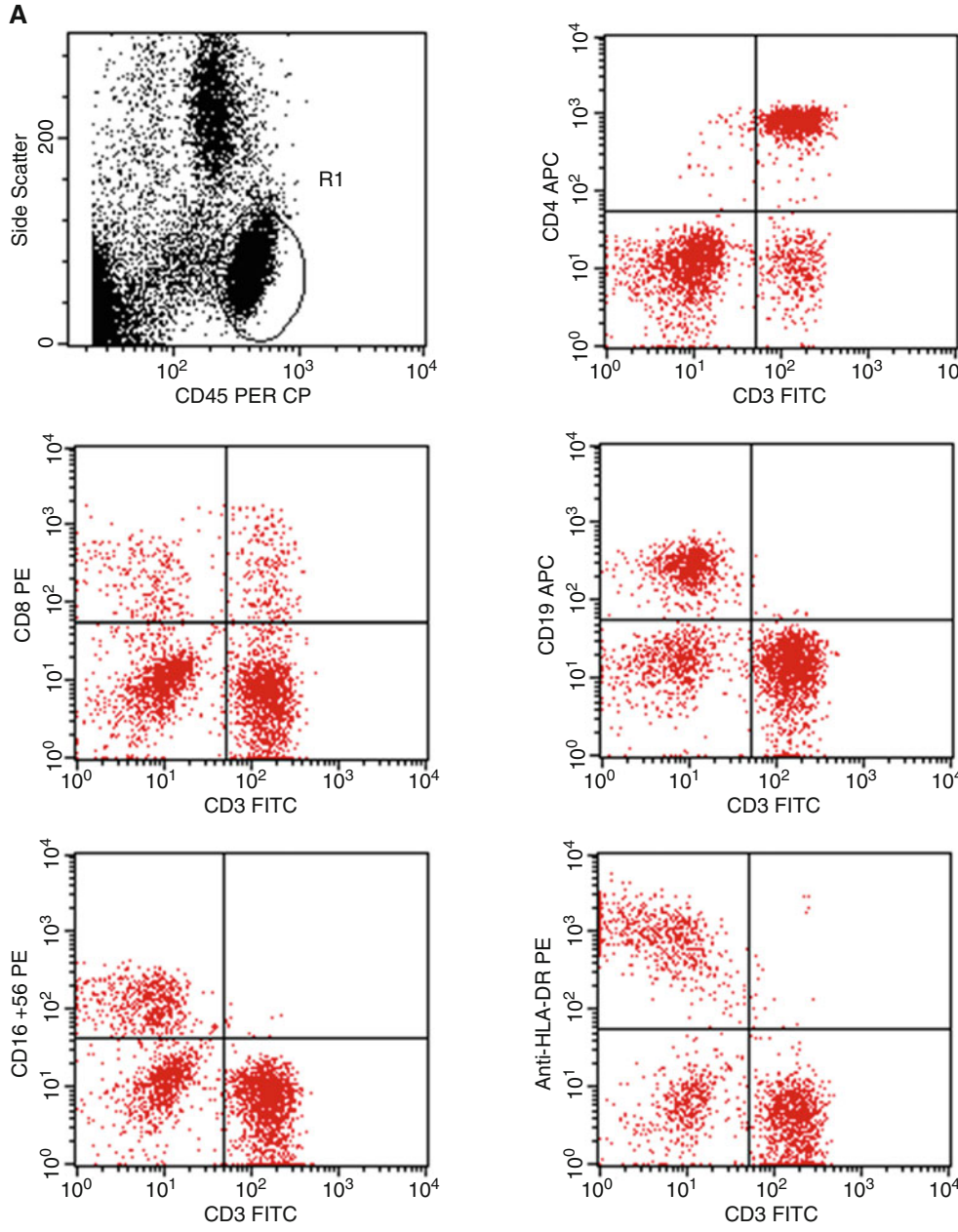

Fig. 1 (**a**) Routine immunophenotyping results on a patient with a ZAP70 mutation. (**b**) CD3+CD8 bright population in a normal healthy control (*left panel*) vs. the patient with the ZAP70 mutation (*right panel*). Note the absence of the bright CD8+ T cells within the *circle* on the *right panel*. (**c**) Results of routine immunophenotyping on a patient with MHC Class II deficiency. Note the absence of the CD3-HLA-DR+ population (B cells) in the patient (**b**) vs. the healthy control (**a**)

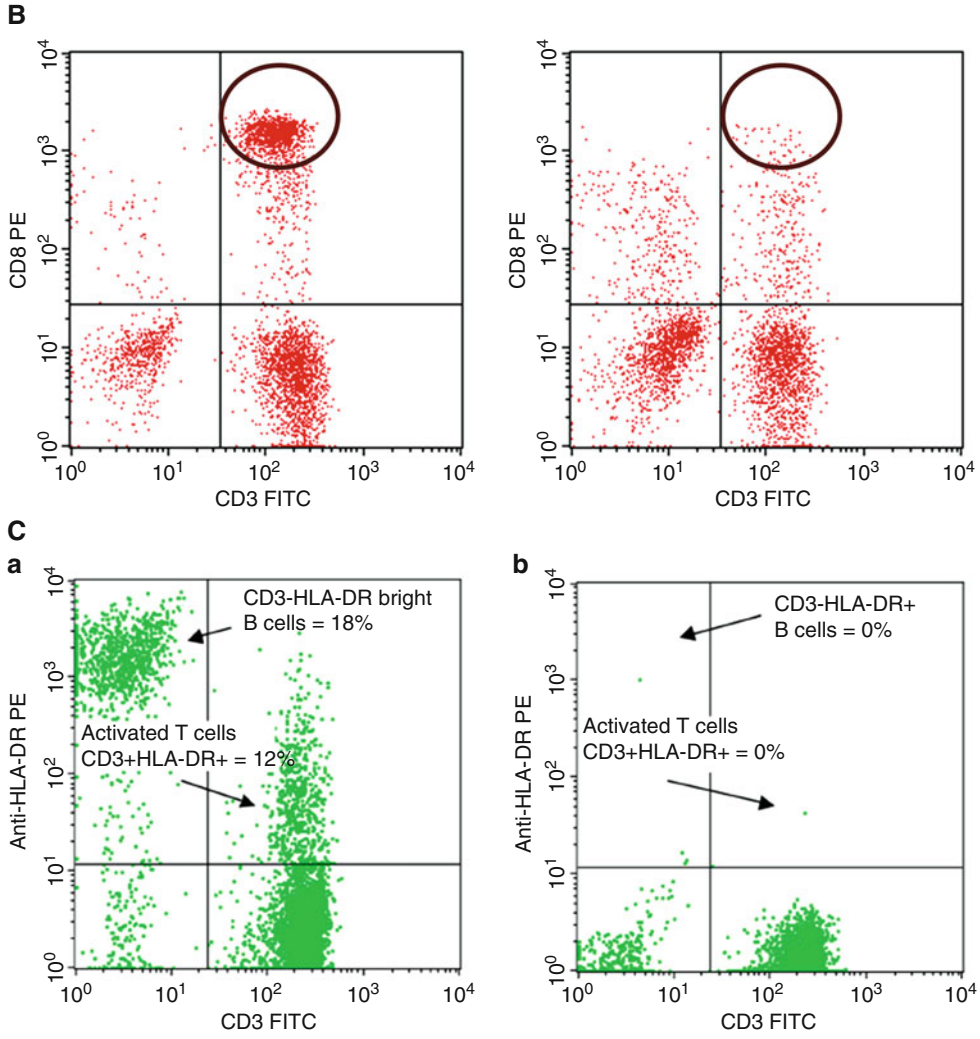

Fig. 1 (continued)

the T cell receptor. Increases in the relative proportion of this subset occur in a PID referred to as "autoimmune lymphoproliferative syndrome" (ALPS) and is one of the required components in the diagnostic criteria for ALPS.

A function-based flow cytometry procedure designed to measure the level of reactive oxygen species produced during an oxidative burst provides an assessment of the functional abnormality associated with the primary immunodeficiency, chronic granulomatous disease.

Lastly, a flow cytometry procedure that combines a functional abnormality with a specific marker abnormality is described for the measurement of CD40 ligand levels expressed on T helper cells following in vitro activation. Abnormalities in the gene encoding the CD40 ligand result in the X-linked hyper IgM syndrome, also known as CD40 ligand deficiency.

2 Materials

2.1 Routine Immunophenotyping Panel for the Screening Diagnosis of Primary Immunodeficiency Disease

1. 1× FACS Lysing solution (BD Biosciences, San Jose, CA): Dilute 10× stock solution 1:10 with deionized H_2O. Store at room temperature. The solution is stable for 3 months.
2. BD MultiTest reagents (BD Biosciences): MultiTest-6 color TBNK (CD3-FITC/CD16+56-PE/CD45-PerCP-Cy5.5/CD4-PE-Cy7/CD19-APC/CD8-APC-Cy7).
3. CD3-FITC/HLA-DR-PE and CD45-PerCP single reagents (BD Biosciences). Each antibody reagent, sufficient for 50 tests, is provided in 1 mL of buffered saline with gelatin and 0.1% sodium azide. When stored at 2–8 °C, antibody reagents are stable until the expiration date on the label. Antibody reagents should not be frozen or exposed to direct light during storage or during incubation with cells.
4. Single-use BD Trucount tubes, containing a freeze-dried pellet of fluorescent beads (BD Biosciences).
5. Two levels of cellular controls: Streck CD-Chex and Low CD4 CD-Chex (Streck, Omaha, NE).
6. Isoton II Sheath fluid (Beckman Coulter Life Sciences, Indianapolis, IN).
7. Flow cytometer: FACSCanto II equipped with FACSCanto and FACSDiva software (BD Biosciences).
8. 12 × 75 mm polystyrene round bottom tubes.
9. Micropipettes (10 and 20 μL) and pipette tips.
10. Electronic reverse pipettor (BD Biosciences).
11. Vortex mixer.
12. Centrifuge.

2.2 Measurement of CD3+CD4-CD8-TCR Alpha/Beta+ T Cells for the Diagnosis of Autoimmune Lymphoproliferative Syndrome

1. 1× FACS Lysing solution (*see* Subheading 2.1, **item 1**).
2. Ca^{2+} and Mg^{2+} free Phosphate Buffered Saline (PBS) or Dulbecco's Phosphate Buffered Saline (DPBS). Store at room Temperature. Unopened PBS is stable until Expiration Date; when opened, it expires in 30 days.
3. 1% paraformaldehyde (PFA) fixative solution: Prepare 1% PFA from 16% PFA using normal saline. Store at 2–8 °C. It is stable for 3 months from preparation date. Caution: vapor harmful, carcinogenic.
4. Monoclonal antibodies: CD4-PE, CD8-PE, α/β TCR-FITC, γ/δ TCR-FITC (all from BD Biosciences), CD3-APC (Beckman Coulter Life Sciences).
5. Clinical flow cytometer capable of detecting 4–10 colors (e.g., BD FACSCalibur equipped with CellQuest software; BD Biosciences).

6. 12 × 75 mm polystyrene round bottom tubes.
7. Pipettes (5, 10, 20, and 100 μL) and pipette tips.
8. Vortex mixer.
9. Centrifuge.

2.3 Oxidative Burst Assay for the Screening Diagnosis of Chronic Granulomatous Disease

1. Dihydrorhodamine 123 (DHR 123) (Invitrogen/Thermo Fisher Scientific, Fullerton, CA) stock solution: Add 2 mL of dimethyl formamide (DMF) (Sigma-Aldrich, St. Louis, MO) to a 10-mg vial of DHR 123. Make sure that the plastics used are not dissolved by DMF. Make 100-μL aliquots of the stock solution (5 mg/mL) and store at −70 °C for 1 year.
2. Phorbol 12-myristate 13-acetate (PMA) (Sigma-Aldrich) stock solution: Add 1 mL of dimethyl sulfoxide (DMSO) to a 5-mg vial of PMA and mix. Add 4 mL of DMSO for a stock concentration of 1 mg/mL. Make 100-μL aliquots and store at −70 °C. At this temperature, PMA is stable for 6 months.
3. Erythrocyte lysing stock solution: 10× concentration of ammonium chloride (NH_4Cl) lysing solution (Pharmingen/BD Biosciences, San Diego, CA).
4. PBS (*see* Subheading 2.2, **item 2**).
5. Washing solution: 2.5 g sodium azide, 10 mL fetal calf serum, 1000 mL PBS. Filter and sterilize. Store at 4 °C. Washing solution is stable for 6 months when stored at 4 °C.
6. 1% PFA fixative solution (*see* Subheading 2.2, **item 3**).
7. Flow cytometer (*see* Subheading 2.2, **item 5**).
8. 12 × 75 mm polystyrene round bottom tubes.
9. Micropipettes and pipette tips; transfer pipettes.
10. Vortex mixer.
11. Centrifuge.
12. Shaking water bath at 37 °C.

2.4 In Vitro Induced CD40 Ligand (CD154) Upregulation for the Screening Diagnosis of X-Linked Hyper IgM Syndrome (CD40 ligand Deficiency)

2.4.1 Detection of CD154 Upregulation Using a Monoclonal Antibody Specific for CD154

1. PMA (*see* Subheading 2.3, **item 2**).
2. Calcium Ionophore (Sigma-Aldrich) stock solution: Add 1 mL of DMSO to a 1-mg vial of calcium ionophore for a stock concentration of 1 mg/mL. Make 100-μL aliquots and store at −70 °C.
3. Monoclonal antibodies: CD40L-PE, MsIgG1-PE, CD8-FITC, CD3-FITC, CD69-PE, CD3-PerCP (all from BD Biosciences).
4. RPMI culture medium: RPMI-1640, 2 mM L-Glutamine, 100 units/mL penicillin, 100 μg/mL streptomycin.
5. 1× FACS Lysing solution (*see* Subheading 2.1, **item 1**).

6. PBS (*see* Subheading 2.2, **item 2**).
7. Flow cytometry wash solution: PBS, 1% FCS, 0.1% sodium azide.
8. 1% PFA (*see* Subheading 2.2, **item 3**).
9. Flow cytometer (*see* Subheading 2.2, **item 5**).
10. 12 × 75 mm polystyrene round bottom tubes.
11. Pipettes and pipette tips.
12. Centrifuge.
13. 37 °C CO_2 incubator.

2.4.2 Detection of CD154 Upregulation Using a CD40-Receptor-Human IgG Chimeric Recombinant Protein

1. PMA (*see* Subheading 2.3, **item 2**).
2. Calcium Ionophore (*see* Subheading 2.4.1, **item 2**).
3. Monoclonal antibodies: CD8-FITC, CD3-FITC, CD69-PE, CD3-PerCP (all from BD Biosciences).
4. Recombinant Human CD40/Fc Chimera (R&D Systems, Minneapolis, MN).
5. Goat $F(ab')_2$ anti-human IgG-PE (Southern Biotech, Birmingham, AL).
6. RPMI culture medium (*see* Subheading 2.4.1, **item 4**).
7. 1× FACS Lysing solution (*see* Subheading 2.1, **item 1**).
8. PBS (*see* Subheading 2.2, **item 2**).
9. Flow cytometry wash solution (*see* Subheading 2.4.1, **item 7**).
10. 1% PFA (*see* Subheading 2.2, **item 3**).
11. Flow cytometer (*see* Subheading 2.2, **item 5**).
12. 12 × 75 mm polystyrene round bottom tubes.
13. Pipettes and pipette tips.
14. Centrifuge.
15. 37 °C CO_2 incubator.

3 Methods

3.1 Routine Immunophenotyping Panel for the Screening Diagnosis of primary Immunodeficiency Disease

3.1.1 Sample Preparation

1. Label an appropriate number of Trucount tubes for each patient and control. Before use, verify that the Trucount bead pellet is intact and within the metal retainer at the bottom of the tube. If not, discard the tube and replace it with another.
2. Add 20 μL of the 6-color MultiTest antibody reagent to the first tube (Tube #1) and 10 μL each of the CD3-FITC/HLA-DR-PE Simultest and CD45 PerCP (or CD45-PerCP-Cy5.5 can be substituted) antibodies into the second tube (Tube #2).
3. Add 50 μL of well-mixed EDTA whole blood to each patient tube and each level of Streck whole blood to each control tube

(we recommend running one set of controls per day) using the BD electronic reverse pipette (*see* **Note 1**).

4. Incubate the samples at room temperature in the dark for 15 min.
5. Add 450 μL of 1× FACS Lysing solution to each tube and vortex immediately.
6. Incubate the samples at room temperature in the dark for 15 min.
7. Samples should be stored at 2–8 °C and acquired on the FACSCanto within 1 h of lysing using the FACSCanto software for Tube #1 (*see* Subheading 3.1.3) and FACSDiva software for Tube #2 (*see* Subheading 3.1.4) (*see* **Note 2**).
8. Use FACSCanto software to check the bead lot numbers. Choose "*Tools>Lot IDs.*" Choose "*Absolute Count Beads*" and enter or verify the lot number and bead information on the bead-tubes foil pouch is correct. DO NOT mix lot numbers.

3.1.2 FACSCanto Setup

The FACSCanto cytometer must be calibrated before each use and optimized assay settings must be implemented prior to sample collection. It is highly recommended that manufacturer's instructions be followed. In our laboratory, 7-Color Setup Beads are run before acquisition to automatically set the voltages and compensation for the parameters used in acquiring the 6-color monoclonal antibody combination. These settings are maintained and used for the acquisition of the second tube using the FACSDiva software. List mode data files acquired using both FACSCanto (Tube #1 = 6-color combination) and FACSDiva software (Tube #2 = 3-color combination) are then analyzed in each of the respective software programs. For the first tube (6-color panel), the lymphocyte gate (CD45 vs. right angle light scatter) is reviewed and optimized (to include the entire cluster of lymphocytes), and the FACSCanto software automatically calculates the proportions and absolute numbers of the major lymphocyte subsets, i.e., T, B, NK, T helper, and T cytotoxic lymphocyte subset percentages and absolute counts. In summary, we recommend that the manufacturer's instructions for the FACSCanto setup, acquisition, and analysis of the 6-color panel first tube be followed. Our second tube (CD45, CD3, HLA-DR) is a custom combination and is not currently amenable to automated acquisition and analysis of the FACSCanto. FACSDiva software is used for both the acquisition and analysis (i.e., measurement) of the CD3+ HLADR+ lymphocytes. In the final assessment of the routine immunophenotyping panel for each patient, the CD3 lymphocyte percentage and absolute count in each tube are compared to each other and valuable quality control parameters (*see* Subheading 3.1.5).

3.1.3 FACSCanto Acquisition and Analysis of the 6-color Tube

1. Acquire the 6-color TBNK tubes from both patients and cellular controls using an automated FACSCanto software. Verify the accuracy of the "expert gating." All leukocyte populations should be clearly defined, i.e., lymphocytes, monocytes, and granulocytes. The lymphocyte population is gated using low right angle light scatter (also known as side scatter) and bright CD45 fluorescence (*see* Fig. 2). Lymphocyte subsets are displayed as distinct populations (*see* **Note 3**). Adjust gates by holding down the left mouse button and dragging them to the appropriate location.
2. When all gates are adjusted, print the screen.
3. After printing, go to the next specimen by clicking the ▶ icon.
4. Repeat **steps 1–3** for all specimens in the run.
5. Close FACSCanto software and login to FACSDiva software.

3.1.4 FACSDiva Acquisition and Analysis of the 3-color Tube

1. Link the instrument settings to the 7-Color Setup Beads run prior to acquisition using the "Lyse No Wash settings." Collect 2500 lymphocyte events. Create an acquisition template to include three dot plots (*see* Fig. 3). On the first dot plot, display all events in a dot plot of right angle light scatter vs. CD45-PerCP, with one analysis gate for the total lymphocyte subset and another for the beads (use this dot plot to calculate the total number of bead events acquired). On the second dot plot, display all events in a dot plot of right angle light scatter vs. CD3 and draw an analysis gate around the CD3+ T cell cluster (use this dot plot for the total number of T cell events). Draw a third dot plot which will display only those events which fall into the lymphocyte gate. The CD3 vs. HLA-DR plot will be used to calculate the percentage of lymphocytes that are both CD3+ and HLA-DR+. Save this setup as your experiment template for future use.
2. During the analysis, adjust the lymphocyte gate on the dot plot of right angle light scatter (Y axis) vs. CD45-PerCP (X-axis). Ensure clean separation between debris (low CD45 and low right angle light scatter) and monocytes (similar CD45 intensity but higher right angle light scatter) by adjusting the lymphocyte gate as required. Set the second gate to encompass the entire bead population (*see* the upper left plot in Fig. 2).
3. In the third graph, adjust the quadrants so that the activated T cells (CD3+HLA-DR+) are in the upper right quadrant (*see* **Note 4**).
4. Record the following statistics from the analysis: total number of bead events (first dot plot), total number of CD3+ lymphocyte events (second dot plot), as well as percentage of CD3+ T lymphocytes (third dot plot: upper right plus lower right quadrants) and CD3+HLA-DR+ cells (third dot plot: upper right quadrant only) (*see* **Note 5**).

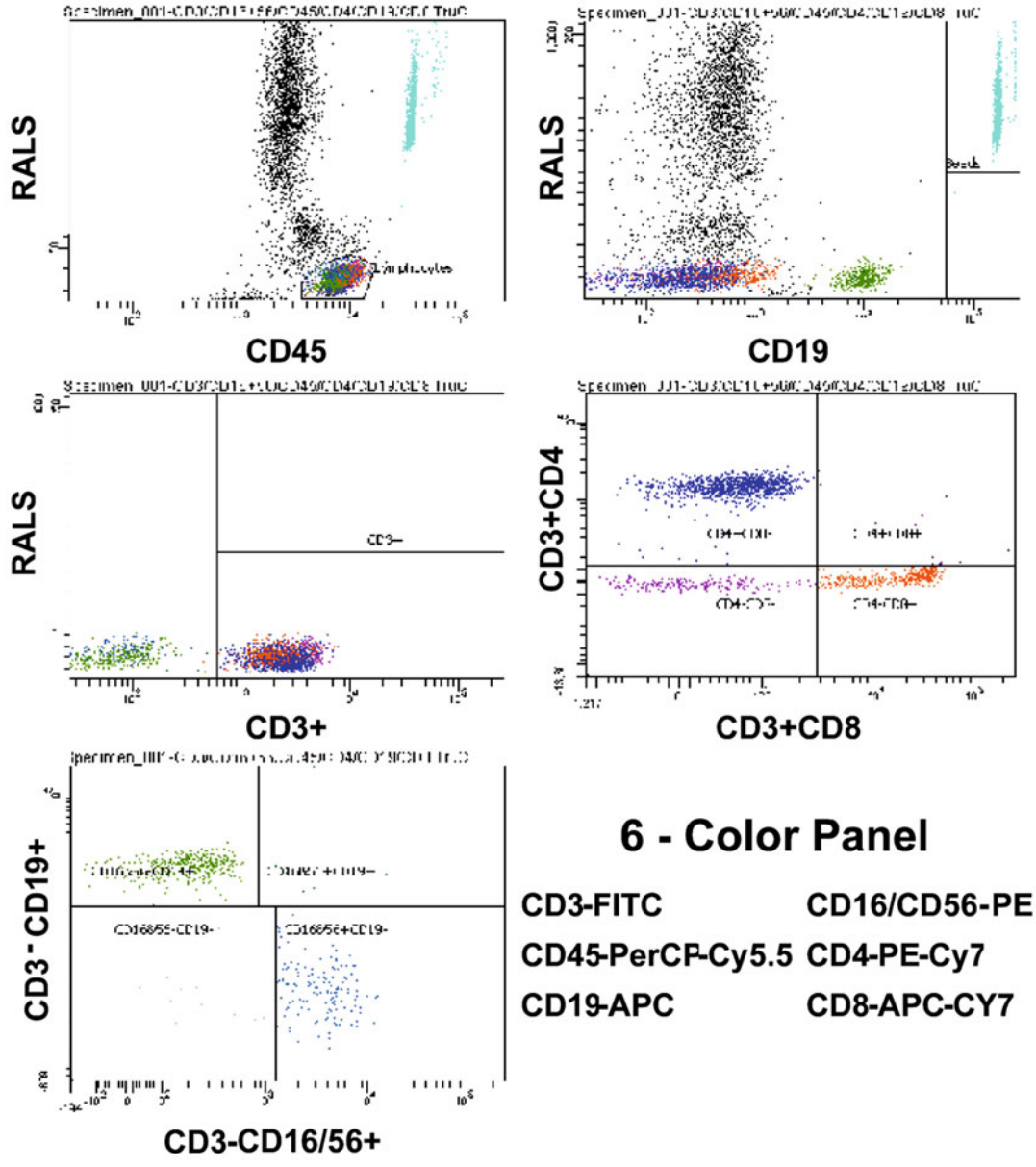

Fig. 2 Representative dot plots and gating strategy of 6-color routine immunophenotyping performed on a FACSCanto II flow cytometer using an automated FACSCanto software

5. Calculate absolute CD3+ T cell counts (*see* **Note 6**) and record the percentage of CD3+ events and the percentage of CD3 +HLA-DR+ events.

3.1.5 Quality Control

1. Cellular Controls. The percentages and absolute counts of each of the subsets measured on both the low and the regular cellular control samples must fall within the limits established

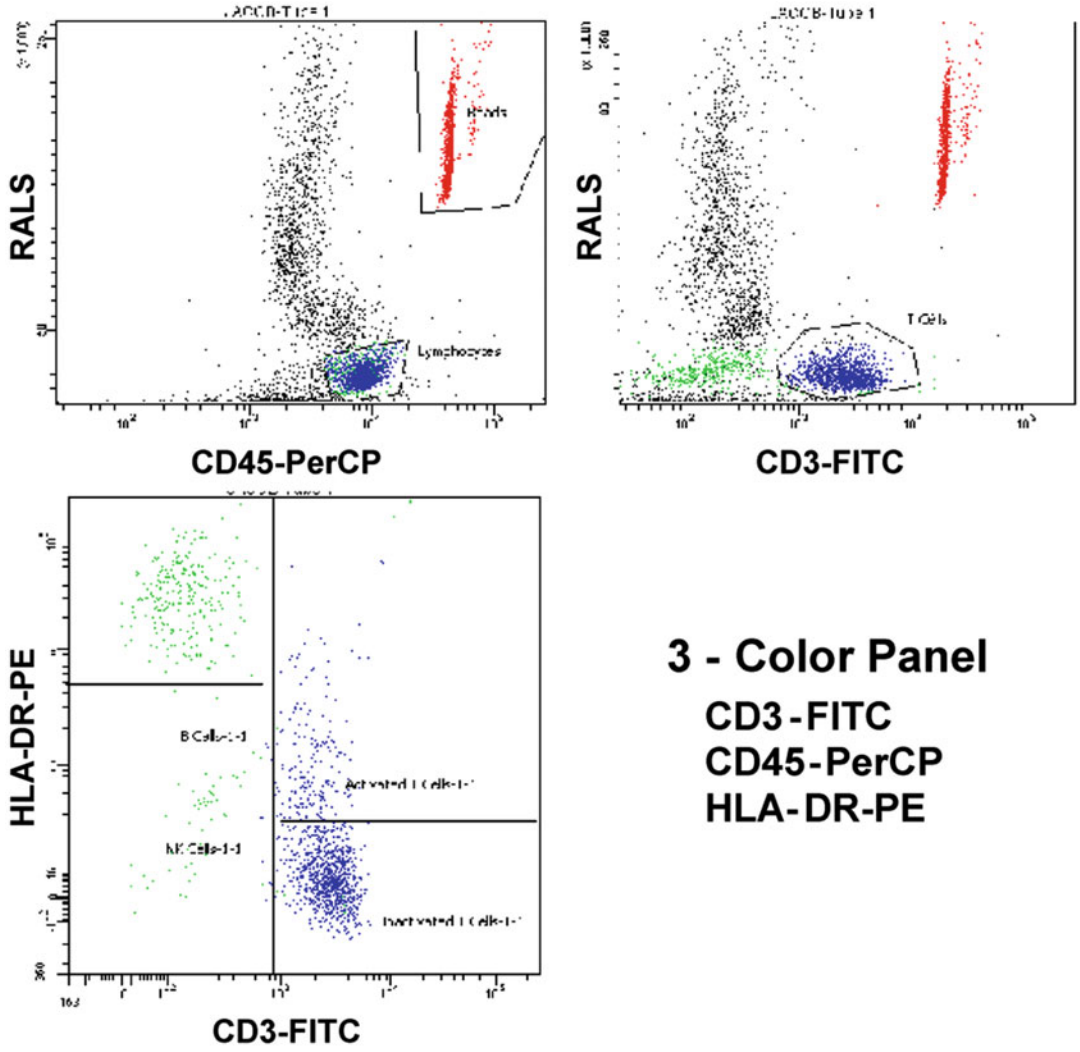

Fig. 3 Flow cytometry evaluation of the co-expression of CD3 and HLA-DR on lymphocytes. The level of HLA-DR of lymphocytes is a measure of the level of in vivo immune activation, whereas the absence of HLA-DR expression on lymphocytes has been associated with a primary immunodeficiency

in-house (highly recommended) or printed on the package insert. If there are gross differences between the results obtained on the cellular controls and the defined ranges for each lymphocyte, subsets do not report patient results until/unless the cause of the problem is identified. Significant abnormalities observed with the cellular control material usually signify a problem. This must be addressed before the results of patient samples can be properly interpreted.

2. Internal Quality Control on Patient Samples:
   (a) The CD3 percentages of Tube 1 (6-color TBNK) and Tube 2 (CD3/HLA-DR) must differ by <5%.
   (b) The absolute count difference between Tube 1 and Tube 2 must be <15%.

(c) The lymphosum must be 100 ± 5.

(d) The sum of the CD4 and CD8 subsets must be within 10% of the mean of the CD3 population. If the CD3 mean is 10% or greater, the gamma/delta panel must be run (unless the patient has been tested previously). Acquire and analyze in FACSDiva. CD3+gamma/delta+ >15% is one explanation of why the T cell subsets do not add up to the CD3 total.

(e) If any of the other criteria above are not within the specified limits, the following actions should be taken:
- All values are reviewed for clerical or transcription errors.
- FCS files are re-analyzed.
- If these actions do not correct the criteria into acceptable ranges whether or not the cellular control results are in range, the assay is repeated.

3.2 Measurement of CD3+CD4-CD8-TCR Alpha/Beta+ T Cells for the Diagnosis of Autoimmune Lymphoproliferative Syndrome

3.2.1 Sample Preparation

1. Label three 12 × 75 mm tubes for both the control and the patients.
2. Add 100 μL of well-mixed EDTA whole blood to each patient and control tube.
3. Add the appropriate FITC-, PE-, and APC-conjugated antibodies to each tube. Vortex to mix. See Below.

TUBE	FITC (20 μL)	PE (20 μL)		APC (10 μL)
1	IgG1	CD4	CD8	CD3
2	α/β TCR	CD4	CD8	CD3
3	γ/δ TCR	CD4	CD8	CD3

4. Incubate the samples for 20 min at room temperature in the dark.
5. Add 2 mL of 1× FACS lysing solution to each tube and vortex.
6. Incubate the samples at room temperature in the dark for 10 min.
7. Centrifuge the sample tubes at 400 × *g* for 5 min at room temperature.
8. For each tube, aspirate the supernatant and vortex the tube.
9. Add 2 mL of PBS to each tube and vortex.
10. Centrifuge at 400 × *g* for 5 min.
11. For each tube, aspirate the supernatant and vortex the tube.
12. Add 0.5 mL of 1% PFA to each tube and vortex gently.

3.2.2 Acquisition and Analysis Using CellQuest Software

1. Acquisition is performed manually in CellQuest. Use the ALPS Panel as the acquisition panel.
2. Instrument settings:
   (a) Find the cytometer tab in the toolbar and click on it.
   (b) Choose instrument settings from the drop-down list. A new window will open up showing the current instrument settings. To select the correct settings, click on "open." A file folder will open up to allow for the correct instrument settings file to be chosen. The instrument settings are all saved in Data → instrsettings → instrument settings → Lyse Wash settings.
   (c) The chosen instrument settings will now display in the window. To accept them click on "Set." The window should read "*Displaying: Current Status*" when the settings have successfully been set.
   (d) Click done.
3. Back to the template, in the Browser window update all the information needed.
   (a) Directory: click on change next to the Directory. Select the folder to be DATA → BD Files → F-MMDDYY. If there is no current folder with the correct date, create a new folder and use this naming convention to rename it.
   (b) Change the Sample ID to patient's name and MRN.
4. Acquire at least 20,000 T cell (CD3+) events. After acquiring for approximately 4 min, the fluid level of the tubes must be carefully monitored so that tube is not run dry. After 5 min, the acquisition should be paused and saved.
5. Perform analysis and calculations as illustrated in Fig. 4. Briefly, the first region (R4) is made on a dot plot of all events with CD3 on the abscissa and side scatter on the ordinate axis. The contents of this gate are then displayed on a dot plot of forward angle light scatter on the *X*-axis and right angle light scatter on the Υ-axis and a second region (R5) is drawn to exclude debris and doublets. The contents of these two regions (R4 and R5 = Total Clean T cells) represent the total T cells and the denominator in calculating the percentage of T cells that are CD4-CD8- and express the alpha/beta form of the T cell receptor. R4 and R5 are combined and displayed on two additional dot plots: one with CD4 and CD8 on the *X*-axis, and alpha/beta T cell receptor on the Υ-axis; the other with CD4 and CD8 on the *X*-axis, and gamma/delta T cell receptor on the Υ-axis. The upper left quadrant of each plot represents alpha/beta+CD4-CD8- T cells and gamma/delta+CD4-CD8- T cells, respectively. An alternative gating strategy can be used as follows: Display the contents of clean T cells on a

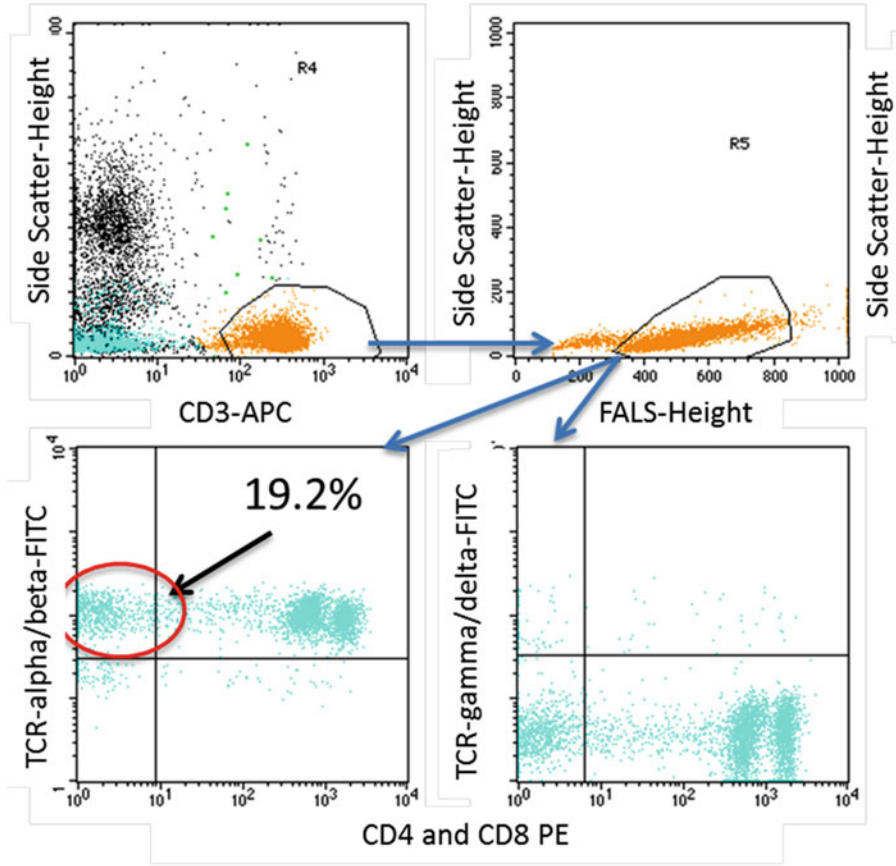

Fig. 4 Representative dot plots and gating strategy illustrating a very high proportion (19.2%) of T cells (CD3+) that are CD4- and CD8- (double-negative T cells) and expressing the alpha/beta form of the T cell receptor (19.2% of T cells). This result is consistent with a diagnosis of ALPS. Note that unlike normal healthy controls where the majority of the double-negative T cells express the gamma/delta form of the T cell receptor, very few double-negative T cells in this patient express the gamma/delta form of the T cell receptor (see *dot plot* in the *lower right corner*)

third dot plot with CD3 on the *X*-axis and CD4 and CD8 on the *Y*-axis, and draw a third region around the cells that are CD3+ but CD4- and CD8-. The contents of all three regions (double-negative clean T cells) are then displayed on a histogram of either alpha/beta T cell receptor or gamma/delta T cell receptor for the measurement of the number of events that are positive for either T cell receptor.

6. Calculate the percentage of alpha/beta-positive double-negative T cells by dividing the
# of alpha/beta+CD4-CD8- T cells by the # of Total Clean T cells.

3.3 Oxidative Burst Assay for the Screening Diagnosis of Chronic Granulomatous Disease

3.3.1 Sample Preparation

1. Prepare working dilution of DHR 123 (45 μg/mL). Add 30 μL of DHR 123 stock solution (5 mg/mL) to 3.33 mL of PBS and vortex. DHR 123 is extremely light sensitive. Keep stock and working dilutions of DHR 123 in the dark at all times.
2. Prepare working dilution of PMA (10 μg/mL). Add 10 μL of PMA stock (1 mg/mL) to 1 mL of PBS and vortex. PMA is extremely light sensitive. Keep stock and working dilutions of PMA in the dark at all times.
3. Prepare 1× NH_4CL lysing solution by adding 2.0 mL of 10× NH_4CL lysing solution and 18.0 mL of distilled, deionized water to a clean beaker or flask.
4. Label three tubes for each patient and control to be assayed. Tube #1: No dye/unstimulated; Tube #2: Plus dye/unstimulated; Tube #3: Plus dye/stimulated. Add 900 μL of PBS and 100 μL of well-mixed whole blood to each tube.
5. Add 25 μL of the DHR 123 solution to Tubes #2 and 3 (final concentration = 1.125 μg/mL). Incubate for 15 min at 37 °C in the shaking water bath.
6. Add 10 μL of PMA to Tube #3 (final concentration = 100 ng/mL). Incubate all three tubes for 15 min at 37 °C in a shaking water bath. After this incubation period, centrifuge the tubes at 400 × *g* and remove supernatant with a transfer pipette.
7. Lyse the pellet by adding 2.5 mL of the NH_4CL lysing solution and incubate for 15 min in the dark at room temperature. It is imperative to vortex both at the beginning and at the end of the lysing procedure. If many RBCs remain after the first lysis, repeat the lysing procedure.
8. Wash twice with 2 mL of washing solution.
9. Vortex, add 0.5 mL of 1% PFA, and vortex again.
10. Specimen is ready to be acquired on the flow cytometer (*see* **Note 7**).

3.3.2 Acquisition and Analysis Using CellQuest Software

1. Standard instrument quality control must be followed prior to acquisition.
2. Open the CellQuest software and load appropriately established instrument "settings." Create an acquisition template of forward vs. right angle light scatter and gate on the granulocyte cluster. While in the "Setup," adjust forward and right angle light scatter parameters of Tube #1 such that the lymphocyte, monocyte, and granulocyte clusters are clearly discernable.
3. Set an electronic analysis gate around the granulocyte cluster and adjust the fluorescence (FL1 detector fitted with a 530/30

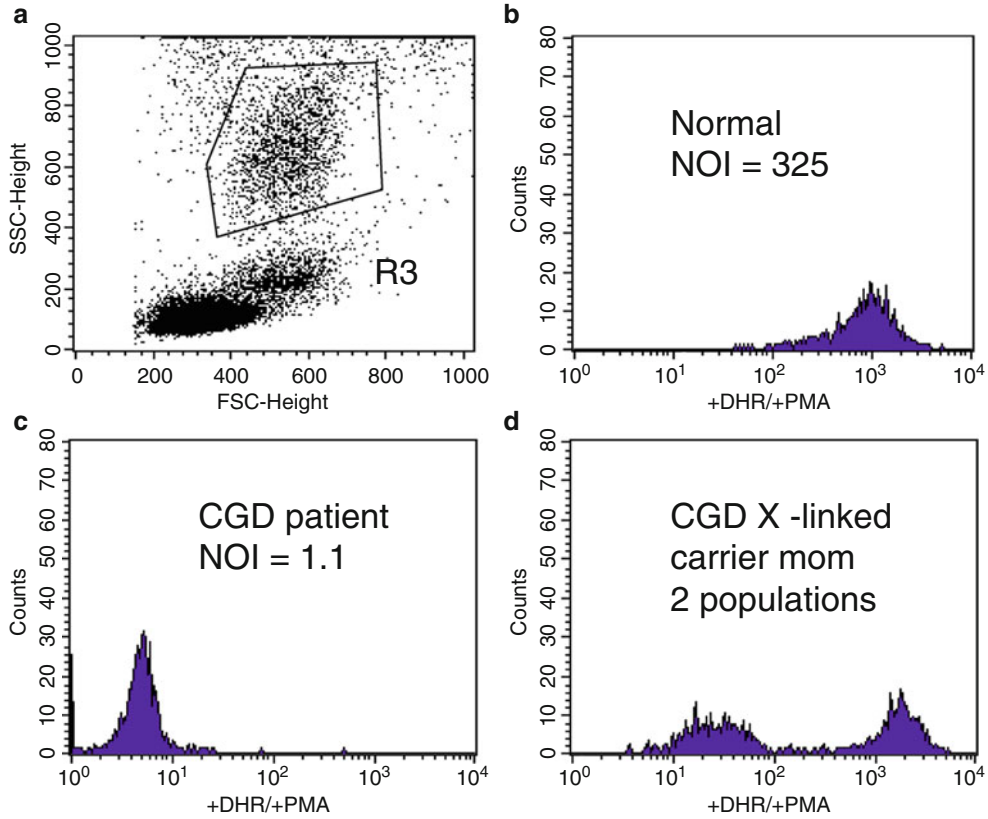

Fig. 5 Flow cytometric assay used as screening diagnostic assay for Chronic Granulomatous Disease

bandpass filter) to be in the first decade on a 4-decade log scale (<channel 10) (*see* **Note 8**).

4. Deselect "setup" option and acquire 10,000 events for each of the three tubes after entering the appropriate patient and tube identifying information.
5. Create an analysis document with forward vs. right angle light scatter and set an analysis gate around the granulocyte cluster. Create a single-parameter histogram to display the FL1 fluorescence of the events in the granulocyte analysis gate and measure the median fluorescence in each of the tubes (*see* Fig. 5).
6. Calculate the normal oxidative index (NOI) by dividing the mean fluorescence of Tube #3 by the mean fluorescence obtained in Tube #2 (*see* **Note 9**).

3.4 CD40 Ligand (CD154) Upregulation Induced In Vitro for the Screening Diagnosis of X-Linked Hyper IgM Syndrome (CD40 Ligand Deficiency)

3.4.1 Detection of CD154 Upregulation Using a Monoclonal Antibody Specific for CD154

1. Prepare working dilution of PMA (final concentration in **step 5** = 15 ng/mL):
   (a) Add 3 μL of 1 mg/mL stock to 5 mL of culture medium.
   (b) Add 1 mL of (a) to 1 mL of culture medium and mix.
   (c) Add 1 mL of (b) to 1 mL of culture medium for final dilution.
2. Prepare working dilution of Calcium Ionophore (final concentration in **step 5** = 400 ng/mL):
   (a) Add 18 μL of 1 mg/mL stock to 3 mL of culture medium and mix.
   (b) Add 1 mL of (a) to 0.5 mL of culture medium for final dilution.
3. For each sample tested, label two tubes: one for the "unstimulated" control and one for the "stimulated" test sample.
4. To the "unstimulated" tube add 800 μL of culture medium and 200 μL of well-mixed whole blood.
5. To the "stimulated" tube add 600 μL of culture medium, 200 μL of whole blood, 100 μL of PMA working dilution, and 100 μL of Calcium Ionophore working dilution.
6. Vortex tubes gently, cap loosely or put parafilm loosely over the tops, and place in a dark CO_2 (5%) incubator at 37 °C for 4 h.
7. After incubation, vortex gently. Add 2 mL of PBS and spin at 700 × *g* for 5 min.
8. Aspirate supernatant completely. Resuspend pellet in PBS such that the final volume is 300 μL (3 samples of 100 μL each will be stained from each tube).
9. Samples are to be stained with the following monoclonal antibody panel (100 μL of sample and 10 μL of each antibody):
   (a) Tube #1: CD8-FITC/MsIgG1-PE/CD3-PerCP.
   (b) Tube #2: CD8-FITC/CD40L-PE/CD3-PerCP.
   (c) Tube #3: CD3-FITC/CD69-PE.
10. Label three tubes containing the mAb combinations above for the unstimulated cells and three for the stimulated cells.
11. Add 100 μL of cell suspension to each tube, vortex, and incubate at room temperature for 20 min.
12. At the end of the incubation period, add 2 mL of 1× FACS Lysing solution to each tube, vortex, and incubate for 10 min at room temperature. Vortex extensively for 5 min.
13. Spin tubes at 700 × *g* for 5 min. Decant and wash two times with flow cytometry wash solution (i.e., add 1 mL of wash, vortex, spin, decant, and repeat).
14. Add 0.5 mL of 1% PFA to each tube and vortex.

15. Acquire and analyze 10,000 events on the FACSCalibur flow cytometer using CellQuest software (*see* **Note 10**).

3.4.2 Detection of CD154 Upregulation Using a Chimeric CD40-Receptor-Human IgG Recombinant Protein

1. Prepare working dilution of PMA (final concentration in **step 5** = 15 ng/mL):
   (a) Add 3 μL of 1 mg/mL stock to 5 mL of culture medium.
   (b) Add 1 mL of (a) to 1 mL of culture medium and mix.
   (c) Add 1 mL of (b) to 1 mL of culture medium for final dilution.
2. Prepare working dilution of Calcium Ionophore (final concentration in **step 5** = 400 ng/mL):
   (a) Add 18 μL of 1 mg/mL stock to 3 mL of culture medium and mix.
   (b) Add 1 mL of (a) to 0.5 mL of culture medium for final dilution.
3. For each sample tested, label two tubes: one for the "unstimulated" control and one for the "stimulated" test sample.
4. To the "unstimulated" tube add 800 μL of culture medium and 200 μL of well-mixed whole blood.
5. To the "stimulated" tube add 600 μL of culture medium, 200 μL of whole blood, 100 μL of PMA working dilution, and 100 μL of Calcium Ionophore working dilution.
6. Vortex tubes gently, cap loosely or put parafilm loosely over the tops, and place in a CO_2 incubator at 37 °C for 4 h.
7. After incubation, vortex gently. Add 2 mL of PBS and spin at 700 × *g* for 5 min.
8. Aspirate supernatant completely. Resuspend pellet in PBS such that the final volume is 300 μL.
9. Samples are to be stained with the following monoclonal antibody panel:
   (a) Tube #1: CD8-FITC/Human IgG-PE/CD3-PerCP.
   (b) Tube #2: CD8-FITC/Human CD40/Fc Chimera—Anti-Human IgG-PE/CD3-PerCP.
   (c) Tube #3: CD3-FITC/CD69-PE.
10. Label three tubes containing the mAb combinations above for the unstimulated cells and three for the stimulated cells. The staining process is a three-step process with complete washing steps after the addition and incubation of each antibody or antibody combination.
11. Add 20 μL of the Recombinant Human CD40/Fc Chimera antibody to Tube #2 for both the stimulated and unstimulated cells. (Tubes #1 and #3 are not stained with any antibody in this step, but undergo the same incubation and washing steps.)

12. Add 100 μL of cell suspension to each tube, vortex, and incubate at room temperature in the dark for 20 min.
13. Add 1 mL of flow cytometry wash solution. Vortex and centrifuge at 700 × *g* for 5 min.
14. Pipet and dispose of supernatant using a transfer pipet.
15. Repeat wash procedure (i.e., add 1 mL of wash solution, vortex, centrifuge, and pipet and dispose of supernatant).
16. Add 10 μL of Anti-Human IgG-PE to Tubes #1 and #2. Incubate at room temperature in the dark for 20 min.
17. Add 1 mL of flow wash solution. Vortex and centrifuge at 700 × *g* for 5 min.
18. Pipet and dispose of supernatant using a transfer pipet.
19. Repeat wash procedure (i.e., add 1 mL of wash solution, vortex, centrifuge, and pipet and dispose of supernatant).
20. Add 10 μL of CD8-FITC and CD3-PerCP to Tubes #1 and #2 for both the stimulated and unstimulated tubes. Add 10 μL of CD3-FITC and CD69-PE to Tube #3 for both the stimulated and unstimulated tubes.
21. At the end of the incubation period, add 2 mL of 1× FACS Lysing solution to each tube, vortex, and incubate for 10 min at room temperature. Vortex extensively for 5 min.
22. Spin tubes at 700 × *g* for 5 min. Decant and wash two times with flow cytometry wash solution (i.e., add 1 mL of wash solution, vortex, spin, decant, and repeat).
23. Add 0.5 mL of 1% PFA to each tube and vortex.
24. Acquire and analyze 2500 CD3+CD8- events on the FACSCalibur flow cytometer using CellQuest software.

3.4.3 Flow Cytometric Analysis

The lymphocyte activation protocol used in both procedures results in the downregulation of the CD4 molecule on T cells. The antigen of interest, CD40L, is preferentially expressed on CD4+ T cells. Since it is not possible to gate on the CD4+ T cells, a negative gating strategy is employed. In both procedures (*see* Subheadings 3.4.1 and 3.4.2), cells in Tube #1 are labeled with CD8-FITC/IgG-PE and CD3-PerCP. A gate is drawn around the cells which express CD3 but do not express CD8, the majority of which are CD4+ T cells. Therefore, an initial gate is drawn around the lymphocytes, then using Boolean logic draw a second gate around the population of cells which express CD3 but do not express the CD8 molecule. Alternatively, if it is not possible to draw a gate around the lymphocyte cluster based on light scatter parameters only, the first gate can be drawn around the CD3-positive cells on a dot plot of right angle light scatter vs. CD3, and then follow the same steps as above (*see* Fig. 6).

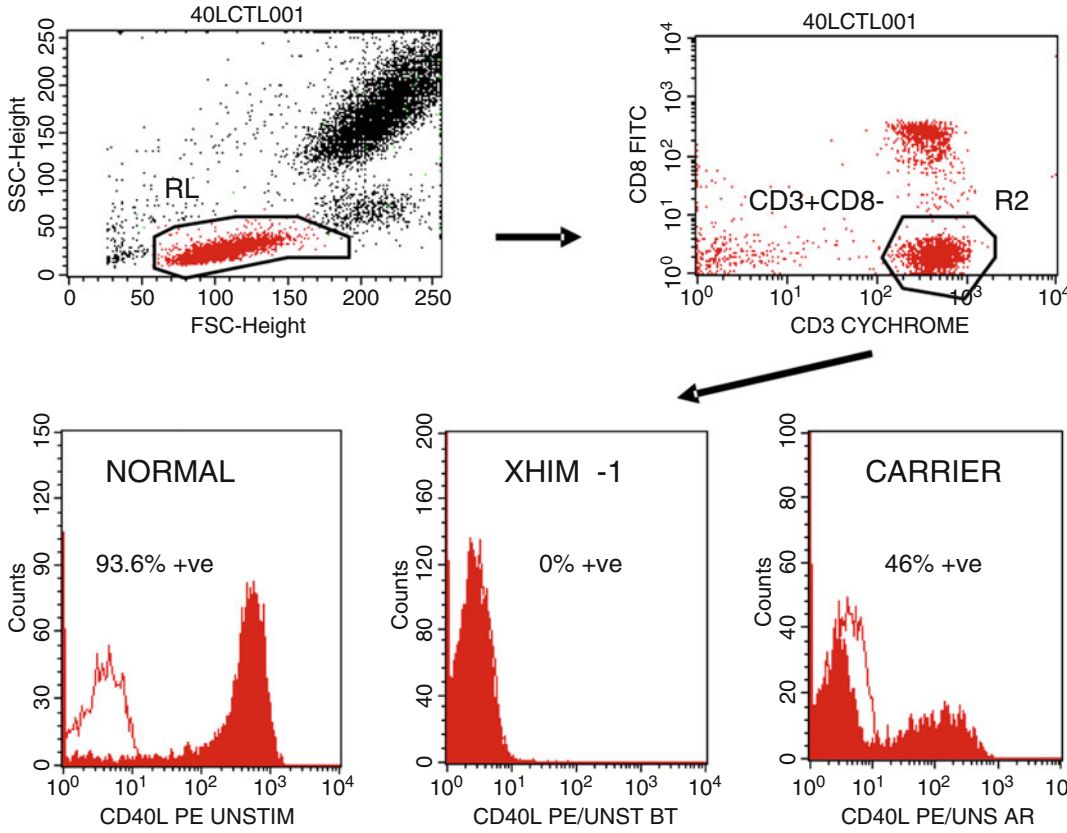

Fig. 6 CD40 ligand (CD154) upregulation induced in vitro for the screening diagnosis of X-linked Hyper IgM Syndrome (CD40 ligand Deficiency)

1. Using Tube #1, set the positive/negative discriminator such that <2% of the cells are positive, i.e., >98% of the cells are negative.
2. The level of CD40L is then determined on the cells in Tube #2 as the percentage of CD3+CD8- cells that express either of the following:
   (a) CD40L fluorescence greater than the isotype control, in the procedure using a monoclonal antibody specific for CD154 (*see* Subheading 3.4.1).
   (b) Human CD40/Fc Chimera—Anti-Human IgG PE fluorescence greater than the isotype control, in the procedure using a chimeric CD40-receptor-human IgG recombinant protein (*see* Subheading 3.4.2).
3. Tube #3 contains a panel of mAb which is used as the in vitro stimulation control. This control consists of measuring the level of CD69 expressed on resting cells vs. the expression after 4 h using the same stimulation protocol. Lymphocytes are gated based on light scatter properties and then again based on the positive expression of CD3. The level of CD69 on both resting and activated CD3+ lymphocytes is then determined.

3.4.4 Quality Control and Normal Reference Range

A normal healthy control is always run in parallel with the patient's specimen. Failure of the control to fall within the established ranges for Human CD40/Fc Chimera expression and CD69 expression necessitates a test repeat. The level of expression of CD69 must be >85% and the level of Human CD40/Fc Chimera expression must be >80% (*see* **Note 11**).

4 Notes

1. Accuracy of the blood volume is critical. The pipet tip should be wiped on the top of the inside of the primary specimen container to remove any residual blood located on the outside of the pipet tip (i.e., ensure it does not go into the staining tubes). Deliver the blood volume into the Trucount tube just above the metal retainer. If a droplet of blood has been delivered from the pipet but is still clinging to the pipet tip, lightly touch the droplet to the side of the Trucount tube, this last drop must be in the tube. BD antibodies are titrated for 2×10^7 cells/mL so the amount of whole blood used may need to be adjusted for specimens that are leukopenic or leukocytotic. In this case, absolute counts should be derived from CBC and differential results.
2. Proper mixing is important to obtain accurate absolute counts so each specimen should be well mixed prior to acquisition.
3. Patients that do not show distinct populations may have "run-up," which requires a pre-wash and re-staining.
4. The CD3+ T cells expressing HLA-DR is a continuum from negative to positive. As such we have run several samples stained for CD3 and CD45 without HLA-DR in order to determine where to set the cutoff between positive and negative HLA-DR expression on the CD3+ T cells.
5. Lymphocytes that are CD3- but strong HLADR+ represent the B lymphocyte population. The latter population is used as an additional quality control parameter (as B cell percentages between the 2 tubes must differ by <5%) and the absolute counts must be within 15%.
6. The absolute T cell count (Absolute number of T cells/μL) is calculated by the following formula:

   # of CD3+ events/# bead events × # of beads/tube/test volume.

   Both the percentage of T cells as well as the absolute number of T cells must be in agreement between the two different tubes in the panel. These quality control parameters are measured in each assay, and if the agreement fails, the analysis is repeated. If the reanalysis fails the QC parameters (i.e. greater than or equal

to 5% difference in the percentage of CD3 between tubes 1 and 3 and/or >15% difference in CD3 absolute T cell counts between tubes 1 and 2), the sample must be re-stained and the assay repeated.

7. Samples must be acquired immediately after the addition of PFA. NOTE: PFA fixation leads to the slow leakage of the oxidized (fluorescent) dye from the granulocytes leading to a significant reduction in fluorescence measured and the geometric mean in Tube #3. The latter can lead to incorrect calculation of the normal oxidative index and an inaccurate result.
8. Tube 1 has no dye and has not been stimulated. This is a true-negative tube in terms of fluorescence generated specifically from the DH123 dye (excited at 488 nm with peak emission approx. 529 nm) and is used to evaluate the fluorescence generated in tubes #2 and #3.
9. This assay is used to measure the ability of granulocytes to elaborate an oxidative burst as a screening test for chronic granulomatous disease (CGD). The normal range, measured as the NOI, is >30. It is known that the light scatter of the granulocytes from CGD patients is not affected by the genetic mutations. Therefore, the light scatter pattern of the granulocytes from patients and the light scatter pattern of the granulocytes from carriers that express the X chromosome with the CGD mutation do not differ from healthy controls. Light scatter patterns generated from older samples may generate variable granulocyte light scatter patterns. In such cases, it is recommended that the fluorescence generated from Tube #3 be used ungated. The cluster of granulocytes generating a positive fluorescence result (brightest signal) can then be identified by backgating.
10. Samples can be kept overnight in the dark at 4 °C.
11. The CD40 ligand is encoded by a gene located on the X chromosome. As with other X-linked disorders, maternal carriers of the mutated genes have some cells that express the normal gene, whereas other cells will express the X chromosomes that carry the mutated gene. In such carriers, the expression of the CD40 ligand (or the CD40 chimera) will show a bimodal distribution with the normal cells expressing normal levels, while those cells expressing the X chromosome that carry the mutation will express abnormal levels of the CD40 ligand. It must also be noted that mutations have been detected that result in abnormal CD40 ligand signaling but that result in apparently normal CD40 ligand levels when measured by flow cytometry [7]. In such cases, it is recommended that the patient's DNA be sequenced for CD40 ligand gene mutations.

References

1. Picard C, Al-Herz W, Bousfiha A, Casanova JL, Chatila T, Conley ME, Cunningham-Rundles C, Etzioni A, Holland SM, Klein C, Nonoyama S, Ochs HD, Oksenhendler E, Puck JM, Sullivan KE, Tang ML, Franco JL, Gaspar HB (2015) Primary immunodeficiency diseases: an update on the classification from the International Union of Immunological Societies Expert Committee for primary immunodeficiency 2015. J Clin Immunol 35(8):696–726. doi:10.1007/s10875-015-0201-1
2. Fudenberg HH, Good RA, Hitzig W, Kunkel HG, Roitt IM, Rosen FS, Rowe DS, Seligmann M, Soothill JR (1970) Classification of the primary immune deficiencies: WHO recommendation. N Engl J Med 283(12):656–657. doi:10.1056/NEJM197009172831211
3. Fudenberg H, Good RA, Goodman HC, Hitzig W, Kunkel HG, Roitt IM, Rosen FS, Rowe DS, Seligmann M, Soothill JR (1971) Primary immunodeficiencies. Report of a World Health Organization Committee. Pediatrics 47 (5):927–946
4. Geha RS, Notarangelo LD, Casanova JL, Chapel H, Conley ME, Fischer A, Hammarstrom L, Nonoyama S, Ochs HD, Puck JM, Roifman C, Seger R, Wedgwood J, International Union of Immunological Societies Primary Immunodeficiency Diseases Classification C (2007) Primary immunodeficiency diseases: an update from the International Union of Immunological Societies Primary Immunodeficiency Diseases Classification Committee. J Allergy Clin Immunol 120 (4):776–794
5. O'Gorman MRG (2008) Role of flow cytometry in the diagnosis and monitoring of primary immunodeficiency disease. In: O'Gorman MRG (ed) Handbook of human immunology, 2nd edn. CRC Press, Boca Raton, FL, pp 267–311
6. Good RA, Zak SJ (1956) Disturbances in gamma globulin synthesis as experiments of nature. Pediatrics 18(1):109–149
7. Seyama K, Nonoyama S, Gangsaas I, Hollenbaugh D, Pabst HF, Aruffo A, Ochs HD (1998) Mutations of the CD40 ligand gene and its effect on CD40 ligand expression in patients with X-linked hyper IgM syndrome. Blood 92(7):2421–2434
8. International Union of Immunological Societies Expert Committee on Primary I, Notarangelo LD, Fischer A, Geha RS, Casanova JL, Chapel H, Conley ME, Cunningham-Rundles C, Etzioni A, Hammartrom L, Nonoyama S, Ochs HD, Puck J, Roifman C, Seger R, Wedgwood J (2009) Primary immunodeficiencies: 2009 update. J Allergy Clin Immunol 124 (6):1161–1178. doi:10.1016/j.jaci.2009.10.013

Chapter 15

Real-Time Deformability Cytometry: Label-Free Functional Characterization of Cells

Maik Herbig, Martin Kräter, Katarzyna Plak, Paul Müller, Jochen Guck, and Oliver Otto

Abstract

Real-time deformability cytometry (RT-DC) is a microfluidic technique that allows to capture and evaluate morphology and rheology of up to 1000 cells/s in a constricted channel. The cells are deformed without mechanical contact by hydrodynamic forces and are quantified in real-time without the need of additional handling or staining procedures. Segmented pictures of the cells are stored and can be used for further analysis. RT-DC is sensitive to alterations of the cytoskeleton, which allows, e.g., to show differences in cell cycle phases, identify different subpopulations in whole blood and to study mechanical stiffening of cells entering a dormant state. The abundance of the obtainable parameters and the interpretation as mechanical readout is an analytical challenge that needs standardization. Here, we will provide guidelines for measuring and post-processing of RT-DC data.

Key words Label-free cytometry, Microfluidics, Image analysis, Automated segmentation, Morphometry, Rheology, Cell mechanics, Cytoskeleton, Linear mixed models

1 Introduction

Flow cytometry is a widely used technique in biological sciences, which dates back to the 1970s. Fluorescent markers are used for labeling cell structures of interest to make them detectable using an excitation laser and a photomultiplier tube. Most importantly, many fluorescent markers can be measured simultaneously for thousands of single cells per second, which allows studying cellular behavior and expression patterns. During the last decades, the technique has been broadly applied, especially in the field of cell biology and multiple marker strategies were developed to decipher, for example, heterogeneous cell populations such as whole blood [1]. Before applying the technique, fluorescent markers need to be introduced into the cells, which can be expensive, time-consuming procedure, and might cause unexpected reactions and alterations of cells. To circumvent these complications, cell physical and

Teresa S. Hawley and Robert G. Hawley (eds.), *Flow Cytometry Protocols*, Methods in Molecular Biology, vol. 1678, DOI 10.1007/978-1-4939-7346-0_15,

morphological features fell into spotlight as label-free markers to elucidate functional properties. The scatter signals, e.g., could be used to reveal information about the cell size and the refractive index [2]. More advanced morphological and rheological parameters allow characterizing biomechanical features of single cells or whole tissues but are not accessible using fluorescence-based cytometers. Cell elasticity can represent the migrative and microcirculative capacity of cancerous cells [3–5] and lead to the effective detection of metastatic cells [6, 7]. Dividing and differentiating stem and progenitor cells can be distinguished from mature cells as shown by follow-up studies on human myeloid precursor cells and mesenchymal stem cells developing toward certain differentiation lineages [8, 9]. Additionally, mechanical properties can detect pathological alterations, e.g., of monocytes during inflammation [10] or of red blood cells under plasmodium infection [11]. These features are accessible without cell labeling using techniques such as micropipette aspiration, optical tweezers, optical stretcher, or atomic force microscopes.

However, the mentioned methods have a very limited throughput of less than 1 cell/s, which is not comparable to commercial flow cytometers with a throughput of more than 50,000 cells/s. A low throughput leads to extended measurement times, limits the possibility to track time-dependent processes and increases bias when measuring rare cell events in heterogeneous populations. To overcome these issues, different laboratories have developed methods leveraging microfluidics, a technology that aims at controlling small volumes of fluids in engineered channel geometries of micrometer size [12]. Some microfluidic-based methods allowing for high-throughput measurement of cell compliance are described in the following:

(a) Micro-constriction arrays [10, 13, 14]: Cells are passing through constrictions that are smaller than their nucleus. Direct contact with the constriction wall hinders the cells and the transit time is measured by image analysis to estimate elasticity and viscosity. The throughput is ≈3 cells/s and the time scale at which forces are applied depends on the mechanical properties of the cells. The effect of drugs interfering with the cytoskeleton and the nucleus on the deformability of cells has been measured, for example, for a suspended myelogenous leukemia cell line (K562) and a breast carcinoma cell line (MDA-MB-231).

(b) Microchannel resonator [15]: The microchannel resonator is a variant of the method above, with the constriction located on an oscillating cantilever. The change of the resonance frequency is analyzed and allows to obtain very precisely the buoyant mass of cells, the time they need to enter and the time to pass through the constriction. These quantities are

used to conclude about differences in deformability and friction of cancer cell lines with different metastatic potential (H1975, HCC827, TMet, TnonMet, and TMet-Nkx2-1, L1210). Additionally, the effect of drugs interfering with the cytoskeleton on the deformability has been shown. The timescale at which the force is applied varies between 5 and 1000 ms, depending on the mechanical and frictional properties of the cells. This results in a throughput between 1 and 200 cells/s.

(c) Hydropipetting [16]: A contact-free stretching of cells is achieved by perpendicular flows, accelerating the cells abruptly, while a high-speed camera records the aspect ratio, which serves as a measure of deformability. Experiments have been carried out using Jurkat, HeLa, and MCF7 cell lines treated with drugs, affecting the cytoskeleton and an effect on deformability has been observed. The throughput of the method is up to 65,000 cells/s.

(d) Deformability cytometry [17]: Deformability cytometry is also a contact-free stretching method. It uses forces originating from an extensional flow, which leads to non-laminar flow conditions in this region, which are hard to describe theoretically. The abrupt deceleration when the opposing flows meet results in high strain rates that deform the cells in less than 30 μs. A mechanical readout is obtained by measuring the aspect ratio. The throughput is up to 2000 cells/s.

Micro-constriction arrays and microchannel resonators can be used not only to study deformability, but also the interaction of cells with the constriction surface. A caveat of micro-constrictions is that the range of transit times spans almost four orders of magnitudes. One possible reason for this could be the different alignment of the cells when entering the channel. Hydropipetting and deformability cytometry align the cells using inertial focusing and allow measuring cells of different sizes. A drawback is that both methods require extremely high frame rates, producing an enormous amount of data which cannot be directly streamed to a computer, but needs to be stored on the camera during the experiment. Therefore, the measurement time is limited to some seconds, depending on the memory of the camera. The result of a measurement is available after offline analysis of the captured data, which takes 15–20 min.

Real-time deformability cytometry (RT-DC) tries to overcome these limits by using a constriction channel with a diameter moderately larger than the size of the probed cells (*see* Fig. 1a). Hydrodynamic forces originating from the parabolic flow profile in the channel (*see* Fig. 1b) can deform the cells. The micrometer-sized channel geometry and the viscosity of the measurement buffer

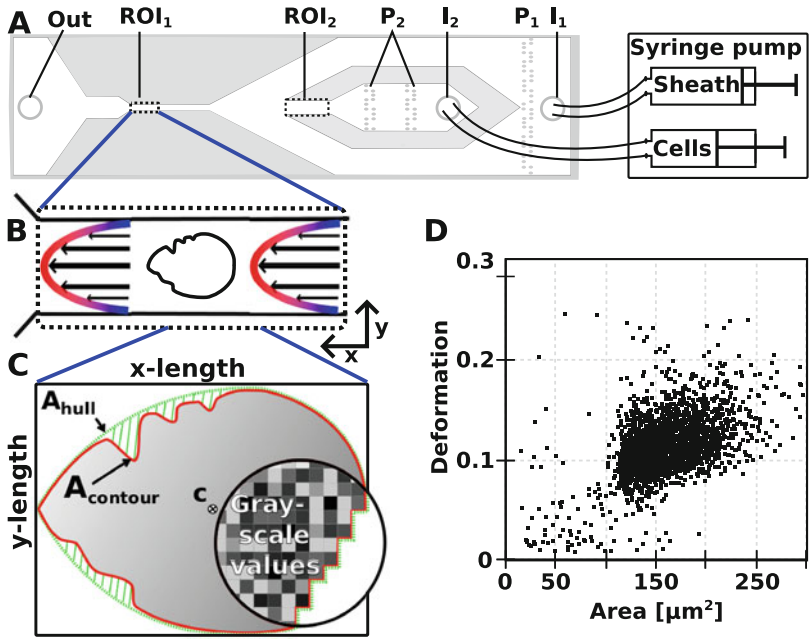

Fig. 1 Chip layout, flow profile, measured parameters, and typical scatterplot. (**a**) Sketch of the microfluidic structure. Sheath and cell suspension fluid, controlled by two syringe pumps, are inserted at inlet I_1 and I_2, respectively and are filtered by rows of pillars P_1 and P_2. The cell stream is focused by a narrowing of 100 µm width (ROI_2), before it meets the sheath flow, which focuses the stream to the middle of the constriction. At the end of the constriction is the first region of interest ROI_1, where cells can be captured in the deformed state. The initial state, before forces are applied can be recorded in ROI_2. (**b**) Forces, inducing the deformation originate from the parabolic flow profile in the channel. (**c**) Sketch of a cell showing the measured quantities during an RT-DC experiment. A bounding box defines the extent in *x* and *y* directions. The contour of the tracked cell and the corresponding convex hull define areas ($A_{contour}$ and A_{hull}). The position of the cell is given by the centroid (**c**), determined from the contour. Additionally, a bright-field image is recorded and the gray-scale values inside the contour are used to calculate parameters that quantify visual properties like brightness. (**d**) Typical scatterplot obtained from a HL60 measurement, showing the deformation parameter on the ordinate and the cross-sectional area of single cells on the abscissa

result in a laminar flow profile (Reynolds number is ≈0.1 [18]) and sufficient shear forces (≈1 µN [19]) to deform eukaryotic cells at flow rates below 1 µL/s. Depending on the flow rate and cell concentration, several hundreds to thousands of cells/s are passing through the channel and are captured by a high-speed camera, operating at 2000 frames/s. Again, such high measurement rates can lead to large amounts of data and the extraction of morphological and rheological parameters can be a computationally expensive task. RT-DC performs the analysis in real-time for up to 1000 cells/s. For image analysis, the contour of the cell is obtained after background subtraction and thresholding, using a border following algorithm [20]. While the cells are being flushed through the region of interest, several morphological and rheological parameters are recorded and the image and contour of every measured

cell is stored in an efficient way (≈20 MB/1000 cells). In principle, this real-time analysis allows sorting cells based on extracted parameters in a downstream sorting device.

This chapter summarizes details about necessary soft- and hardware for RT-DC, shows which parameters can be extracted during or after an experiment, discusses how to analyze the obtained data, and most importantly, shows possible complications that can occur in any of these steps.

2 Materials

2.1 Chip Layout

The central unit of RT-DC is the microfluidic chip. Figure 1a shows a scheme of the chip layout. Sheath fluid and cell suspension fluid are provided from the rightmost and the middle inlet, respectively ("I_1" and "I_2" in Fig. 1a). Pillar structures ("P_1" and "P_2" in Fig. 1a) near both inlets are used to remove large objects and decrease the possibility of clogging of the system. After the pillar region, the path for the cell flow is narrowed to a 100 μm wide section called "reservoir" ("ROI_2" in Fig. 1a) before it meets the paths carrying the sheath flow. This design allows to hydrodynamically focus the cell flow toward the constriction, which has a length of 300 μm. The region of interest to record cells in a deformed state is located at the end of this constriction ("ROI_1" in Fig. 1a). The outlet is at the leftmost opening of the chip ("Out" in Fig. 1a).

2.2 Chip Fabrication

1. Silicon wafer master preparation:
   (a) The layout is printed on a photo mask, which is then transferred to a silicon wafer using photolithography.
   (b) The 4–in. silicon wafer is first spin-coated with a photoresist (AZ 15nXT, MicroChemicals GmbH, Germany) at 2000 rpm for 4 s with an acceleration of 5000 rpm/s.
   (c) The layer is baked at 110 °C for 5 min, before exposure to UV light (690 mJ/cm^2) through a chromium mask (JD Photo-Tools, UK) using a mask aligner (EVG 620).
   (d) Afterward, the exposed substrate is baked at 120 °C for 2 min, immersed in AZ 400K development solution (MicroChemicals GmbH, Germany) for 3 min to remove the resist that was not irradiated by light, and then dried with nitrogen.
   (e) The height of the obtained structures is measured by step-height analysis with a profilometer, equipped with a 2 μm tip.
   (f) A drop of 1H,1H,2H,2H-Perfluorodecyltrichlorosilane (ABCR, Germany) is released on a microscope slide and placed in a desiccator with the master. The desiccator is

placed under vacuum causing the silanizing agent to evaporate and to form a monolayer on the surface of the master that prevents polymer adhesion. The master can be reused several times.

2. Chip production:
   (a) A mixture of polydimethylsiloxane (PDMS, SYLGARD®, Dow Corning, USA) and curing agent (10:1 w/w) is prepared, degassed, poured over the master, and cured for 60 min at 65 °C to get the solution polymerized. Then the PDMS chip can be removed from the master.
   (b) PDMS is a transparent material that allows visualizing the channels using a microscope. In order to connect the microfluidic chip to the tubing, a biopsy puncher is used (Biopsy Punch with Plunger, size 1.5 mm, pfm medical AG, Germany) to create holes (in the regions "I_1", "I_2," and "Out" in Fig. 1a) of suitable size.
   (c) Finally, a cover glass (thickness 2, Hecht, Germany) is covalently bound to the PMDS layer using plasma activation (50 W, 30 s, Plasma Cleaner Atto, Diener Electronic, Germany) to seal the structures (*see* **Note 1**).

2.3 Setup

1. The microfluidic chip is mounted on the stage of an inverted microscope (Axiovert 200M, Zeiss, Germany) and a 40x objective with NA = 0.75 (Neofluar®, Zeiss, Germany) provides the necessary magnification.
2. Bright-field images are captured by a high-speed camera (EoSens CL MC1362, Mikrotron, Germany), which is mounted to one port of the microscope. The camera has a CMOS sensor with 1280 × 1024 pixels each of which has a size of 14 μm. Image transfer to a standard PC is achieved using a full camera-link frame grabber card (NI-1433, National Instruments, Germany). The light source is an LED (CBT-120, Luminus Devices, USA), which is triggered by the camera. To minimize motion blurring, the LED shutter time is reduced to a 2 μs light pulse for each image (*see* **Note 2**).
3. A syringe pump with two modules (NemeSyS, Cetoni, Germany) is used to provide very accurate flow rates for two syringes simultaneously, delivered to the microfluidic chip by PEEK tubings (Postnova Analytics, Germany).
4. Real-time image analysis is achieved by leveraging the OpenCV computer vision library [21]. OpenCV runs very efficiently in a C/Labview environment and performs background subtraction, thresholding, smoothing, and a border finding algorithm on multiple CPU cores in real-time for up to 1000 cells/s.

Table 1
Recommended minimum and maximum cell sizes (Diameter: *d*; Area: *A*) for different channel widths

Channel width [μm]	d_{min} [μm]	d_{max} [μm]	A_{min} [μm²]	A_{max} [μm²]
10	3	9	7	64
20	6	18	28	254
30	9	27	64	573
40	12	36	113	1018

Table 2
Flow rates for a 20 μm wide channel constriction

Region	Flow rate in channel [μL/s]	Sample flow rate [μL/s]	Sheath flow rate [μL/s]
Channel	0.04	0.01	0.03
Channel	0.08	0.02	0.06
Channel	0.12	0.03	0.09
Reservoir	0.12	0.03	0.09

5. The acquisition software can be programmed individually or the commercial software ShapeIn (Zellmechanik Dresden, Germany) can be used to perform RT-DC experiments. ShapeIn also allows to manage measurements, to regulate the syringe pumps and to control the camera.

2.4 Channel Constriction Width (ROI_1)

1. Depending on the size of the measured cells, different cross-sections of the central channel have to be used. The cell diameter (d) should cover 30–90% of the channel width (l) to reach a detectable deformation. Table 1 shows recommended ranges for d and area for certain channel widths.
2. To reach similar shear forces for a different channel width (l), the flow rates have to be chosen accordingly and can be calculated using the equation: $Q' = Q\left(\frac{l'}{l}\right)^3$ [22]. Sensible flow rates Q for $l = 20$ μm can be obtained from Table 2. Choosing the sheath flow rate three times as large as the cell flow rate has proven to provide reliable focusing.

2.5 Measurement Buffer (MB)

For RT-DC experiments, it is of advantage to suspend cells in a particular measurement buffer (MB) with elevated density and viscosity to reduce sedimentation and allow for long time measurements (*see* **Note 3**). Additionally, an increased viscosity leads to higher shear stress in the channel, which causes deformation of

Table 3
Viscosity of the measurement buffer at different flow rates and channel widths at 24 °C

10 μm channel		20 μm channel		30 μm channel	
Q [μL/s]	η' [mPas]	Q [μL/s]	η' [mPas]	Q [μL/s]	η' [mPas]
0.016	5.8	0.04	5.7	0.16	5.4
0.032	4.6	0.08	4.5	0.24	4.7
0.048	4.1	0.12	4.0	0.32	4.3

cells even at low flow rates. MB can be produced using an appropriate medium for the considered cells (e.g., phosphate buffered saline (PBS)) and 0.5% (w/v) methyl cellulose (4000 cPs, Alfa Aesar, Germany). The final buffer should have a zero shear viscosity of 15 mPas at 24 °C, a controlled osmolarity (e.g., 310–330 mOsm/kg) and a controlled pH (e.g., 7.4). The viscosity η of the MB shows a shear-thinning effect, which can be described by a power law relation: $\eta = K\dot{\gamma}^{n-1}$, with the shear stress $\dot{\gamma}$ and coefficients K and n. Shear-thinning leads to a decrease of η for increasing flow rates Q and has been measured for a PBS-based MB with the above-mentioned physical properties in chips with a channel width l of 20 μm and 30 μm [23]. Additionally, the viscosity depends on the temperature ϑ, which leads to the following formula for viscosity [23] for this particular MB:

$$\eta = 179\tilde{n}\left(7.922\tilde{n}\frac{Q}{l^3}\right)^{-0.323}\tilde{n}\left(\frac{\vartheta}{23.2}\right)^{-0.866}.$$

$([\eta] = mPas, [Q] = m^3/s, [l] = m, [\vartheta] = °C)$

Viscosities for different channel widths and flow rates are given in Table 3. The quantification of viscosity becomes especially important when material parameters, e.g., the elastic modulus, need to be calculated, because the shear stress depends on the viscosity.

The measurement device, measurement software, and consumables such as microfluidic chips and measurement buffer are commercially available (Zellmechanik Dresden, Germany). The open-source analysis software for RT-DC data, "ShapeOut" is written using the programming language "python" and can be downloaded from GitHub [24]. ShapeOut allows to analyze and visualize RT-DC data sets.

2.6 Data Acquisition

Typically, two kinds of measurements are performed consecutively. First, cells are measured in a deformed state in the channel constriction ("ROI_1" in Fig. 1a) and second, the initial shape is retrieved in a region before the constrictions, where cells move slowly and negligible hydrodynamic forces act on them ("ROI_2" in Fig. 1a).

The following parameters can be recorded during the measurement ("online-analysis"):

1. Area: The projected cross-sectional area of the cells is obtained from the number of pixels within the boundary of the cell, defined by the contour (A_{contour} in Fig. 1c, *see* also **Note 4**).
2. x length and y length: A bounding box around the whole cell defines its length in x and y direction (*see* Fig. 1c).
3. Aspect ratio: the ratio of x and y length of a cell.
4. Circularity: (C) is a parameter that relates area (A) to the perimeter (P) of an object using the equation: $C = \frac{2\sqrt{\pi A}}{P}$ and is defined between 0 and 1. For a perfect circle, circularity is one and any deviation from a circle will cause a decrease in circularity. Therefore, circularity can be used as a measure of deformation of cells. To avoid a dramatic increase of the perimeter if the object shows irregularities such as protrusions (as indicated in Fig. 1c), first a convex hull is fitted around the object. Then circularity is determined using the area (A_{hull} in Fig. 1c) and the perimeter of this convex hull, applying the above equation.
5. Deformation: $D = 1 - C$ (*see* **Note 5**).
6. Inertia ratio: The second moment of area can be used to quantify how area is distributed in space [25]. Patches of area far away from the centroid (c in Fig. 1c) have higher contributions. The second moment of area is calculated for the x- and y-direction according to the following equations:
   $I_{xx} = \int\int_A y^2\,dx\,dy$ and $I_{yy} = \int\int_A x^2\,dx\,dy$ and the inertia ratio relates both: $I = \frac{I_{yy}}{I_{xx}}$. The inertia ratio is 1 for a symmetric object and increases for an elongation in the x-direction.
7. Area ratio: The ratio between the area of the convex hull (A_{hull} in Fig. 1c) and the area of the contour (A_{contour} in Fig. 1c) defines the area ratio (R): $R = \frac{A_{\text{hull}}}{A_{\text{contour}}}$, which is closely linked to solidity $S = \frac{1}{R}$. The area ratio is 1 for a smooth and convex object and >1 if the shape has concave parts. Examples of cells with different area ratio values are shown in Fig. 2a.
8. Frame time: Time when a cell was measured.
9. Brightness: Mean of all pixel intensities inside the contour (*see* Fig. 1c).
10. Standard deviation of brightness: Width of the distribution of pixel intensities.
11. X position: Location of the centroid of the cell within the ROI in the flow direction.
12. Y position: Location of the centroid of the cell within the ROI orthogonal to the flow direction.

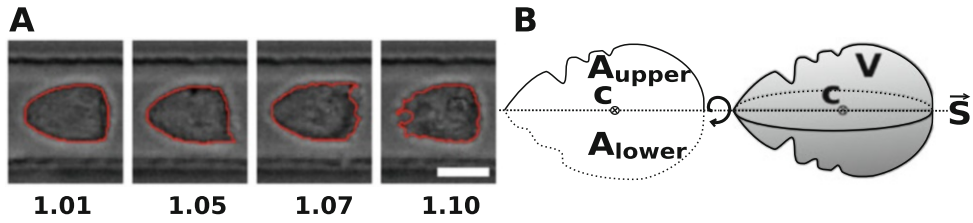

Fig. 2 Area ratio and volume of cells. (**a**) Images and tracked contour (*red*) of chosen HL60 cells of similar size with different area ratio values. Cells with an area ratio below 1.05, usually have a smooth and convex contour, whereas higher area ratio values go along with irregular shapes. Scale bar: 10 μm. (**b**) The centroid (c) of the contour and the flow direction define a symmetry axis $\vec{S}$. This axis divides the cell in an upper and lower part. To obtain volume, both parts are rotated 360° around the $\vec{S}$, individually. The resulting two values for volume are averaged. The quadratic channel geometry and the arising symmetric shear forces justify the assumption of rotational symmetry

Since all contours and images are stored, additional parameters that are computationally more expensive to obtain, can be determined in post-processing analysis steps. Some parameters that are of special interest are listed in the following:

13. Symmetry ratio *y*: The symmetry ratio S_y is the ratio of the area above and below the symmetry axis $\vec{S}$: $S_y = \frac{A_{up}}{A_{low}}$. $\vec{S}$ is defined by the centroid (c in Fig. 1c) and the flow direction. Similarly, the symmetry ratio in *x* direction, S_x is the ratio of the area left and right of a symmetry axis, orthogonal to the flow direction: $S_x = \frac{A_{\text{left}}}{A_{\text{right}}}$.
14. Volume: To calculate the volume of the cell, first the contour is split into an upper and lower part, defined by the symmetry axis $\vec{S}$, as indicated in Fig. 2b. The upper and the lower part are rotated individually around $\vec{S}$, each resulting in a value for volume. Finally, both values are averaged [26]. This estimation is based on the assumption that the cell has rotational symmetry around $\vec{S}$. Green's theorem and the Gaussian divergence theorem are used to express the volume as a line integral and to finally obtain an algorithm that uses the Cartesian coordinates of the contour only.
15. Differential deformation: Differential deformation describes the change of deformation from the initial state, measured in the reservoir ("ROI_2" in Fig. 1a), to the deformed state, measured in the channel ("ROI_1" in Fig. 1a). For technical reasons, it is currently not yet possible to capture the same cell in both regions. Therefore, a bootstrapping algorithm is applied, which employs the whole distributions of deformations of a channel and a reservoir measurement to get a median from both, which are compared. For more details *see* Subheading 3.3.3, **step 2**.
16. Elastic modulus: Elastic modulus (E) describes cell stiffness, based on assumptions of a model. An analytical model [19]

describes cells as fully elastic objects and uses linear elasticity theory and hydrodynamics to describe how shear forces deform these objects. For more details *see* Subheading 3.3.3, **step 3**.

17. Phi: The orientation of an object can be found by rotating the coordinate system until the inertia ratio is maximized. Typically, cells are aligned ($\varphi = 0$) in the channel and randomly distributed in reservoir measurements.

Additional information to quantify shape or gray-scale levels can be retrieved, e.g., by computing Zernike moments, Fourier descriptors, Haralick features, linear binary patterns, or threshold adjacency statistics. Further on deep learning methods can be applied to the data.

Depending on the biological background, one or several of these parameters might be of interest and need to be compared between different samples and a significance level for the effect needs to be computed. We follow an approach using linear mixed models which has the advantage that differences due to biological variation are considered. For conclusions about changes of mechanical properties, certain boundary conditions have to be met. These unique conditions and the linear mixed model are discussed in more detail in Subheading 3.3.4.

3 Methods

3.1 Cell Preparation

Cells have to be resuspended in MB. After centrifugation with appropriate settings (e.g., 5 min at 115 × *g*), the supernatant is removed completely and the cells are gently resuspended in at least 100 μL of MB at a concentration of less than 6 million cells/mL. Incomplete removal of the supernatant will lead to a dilution effect, changing the MB properties and experimental results. This effect is especially dramatic if a small volume of MB is used to resuspend the cells. Very low cell concentrations (<0.5 million cells/mL) can be used as well, but result in long measurement times since the frequency of events is low. If large objects such as cell clumps are present in the sample, it should be filtered using a 40 μm or 70 μm strainer. As RT-DC is made for cells in suspension, adherent cells need to be detached first by using, e.g., trypsin. This process of detachment, in combination with the lack of focal adhesions, potentially changes the state of the cells resulting in time-dependent measurement results which have to be tightly observed.

3.2 Measurement

1. Switch on PC, microscope, LED, camera, and syringe pump.
2. Place a chip with suitable channel width in the dedicated holder on the microscope stage.

3. Fill two 1-mL syringes with MB.
4. Remove any air bubbles from the syringes.
5. Connect each syringe to a 25 cm long PEEK tubing and fill the tubing with MB.
6. Assemble both syringes with attached tubing at both modules of the syringe pump.
7. Start the sheath syringe with +0.1 μL/s (=max. Flow rate for 20 μm chips; can be chosen higher for 30 μm chips and lower for smaller channel geometries).
8. When a droplet emerges at the end of the tubing, insert it into the rightmost inlet of the microfluidic chip ("I_1" in Fig. 1a) which is dedicated to the sheath flow.
9. Plug an outlet tubing into the leftmost opening of the chip ("Out" in Fig. 1a).
10. When a droplet emerges at the middle opening of the chip (I_2 in Fig. 1a), the chip should be air-free.
11. Start the syringe pump dedicated for the sample with +1 μL/s until a drop emerges at the end of the tubing.
12. Insert the tubing into your vial containing the sample suspended in MB.
13. Draw at least 50 μL of the sample into the tubing by using a negative flow rate of −1 μL/s.
14. Start the sample syringe with +0.1 μL/s and plug the corresponding tubing into the middle opening of the chip ("I_2" in Fig. 1a).
15. Start the acquisition software, find the chip structures using the xy-stage and move the field of view to the end of the channel ("ROI_1" in Fig. 1a).
16. When cells are approaching the channel inlet, adjust the focus until there is a thin bright halo around the cells, like shown in Fig. 3 (*see* **Note 4**).

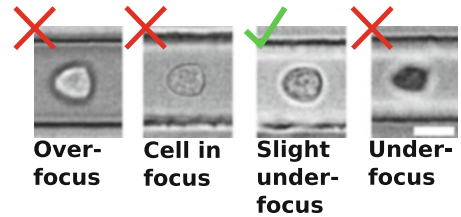

Fig. 3 Focus setting. The tracking algorithm of RT-DC is dependent on a slight under-focus, which results in a slim bright halo around the cell. The cells look darker than the background in this setting. Scale bar: 10 μm

17. Select the channel width and the gating strategy for acquisition appropriately in the acquisition software (for a 20 μm channel a standard setting is a minimum length and height of 3 μm, a maximum length of 80 μm and a maximum height of 20 μm).
18. Create a folder for the measurement.
19. Set a particular flow rate (*see* Table 2) and wait for >1 min to allow the fluid flow to balance in the whole system.
20. Run the first measurement in the channel ("ROI_1" in Fig. 1a) and acquire between hundred to several thousand cells, depending on the application, the presence of subpopulations and the amount of available cells. For homogenous samples, at least 1000 cells should be measured.
21. Repeat the experiment at different flow rates (*see* Table 2) to apply different mechanical stresses and always wait for >1 min in-between measurements.
22. Shift the field of view to the reservoir ("ROI_2" in Fig. 1a) and measure at only one flow rate. This will give you the reference condition of the un-deformed cells.

Typically, the measured events are visualized during the experiment in a scatter plot showing area and deformation. Fig. 1d shows such a scatterplot, obtained from a measurement of a human leukemia cell line (HL60) in a 20 μm wide channel at a flow rate of 0.04 μL/s. Most of the events are located between 150 and 200 μm^2 and have a deformation value of 0.12. There are also clearly some events indicating small objects, which could be debris.

3.3 Analysis

In the following, analysis guidelines are shown that can be performed, e.g., using the freeware ShapeOut.

3.3.1 Quality Check

1. Channel width and focus: Load the data sets into the free analysis software ShapeOut [24] and display them in area vs. deformation scatterplots. Check that large cells are not touching the channel wall by clicking at points in the scatter plot (to preview the image recorded for the given event). The focus of the cells should be such that the cells are darker than the background and have a slim bright halo, as indicated in Fig. 3.
2. Time consistency: Plot frame time on the *x*-axis and deformation on the *y*-axis. The resulting scatterplot should show no trend or interruption at any time-point.
3. Flow rate dependency of deformation: Before studying deformation, or any other parameter quantifying mechanical properties, it has to be verified that the cells are actually deformed due to hydrodynamic forces in the channel by comparing measurements at different flow rates. Higher flow rates should result in higher deformation values and deformation values from channel measurements (Fig. 4a, b) should be larger than

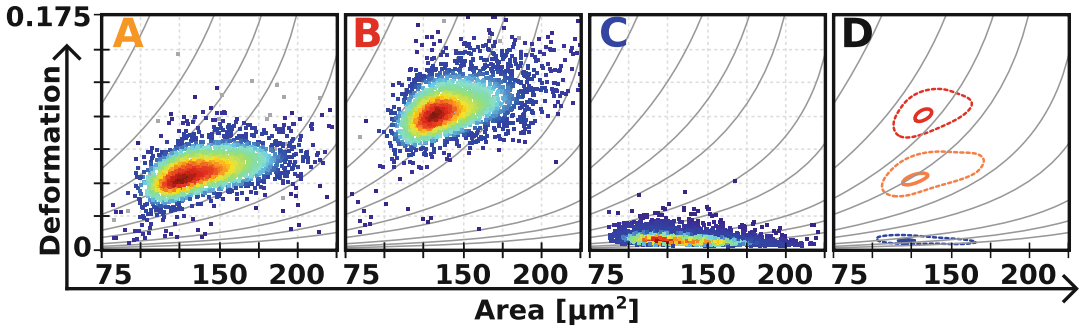

Fig. 4 Scatterplots, isodensity lines, and flow rate dependent deformation: Measurement of HL-60 cells at different flow rates. Cells with area ratio above 1.05 are filtered out. (**a** and **b**) are channel measurements at a flow rate of 0.04 μL/s and 0.12 μL/s, respectively. The higher flow rate results in higher deformation values. The color of the scatter points reflects the density of events. (**c**) A reservoir measurement, which shows very low deformation values. (**d**) A "contour plot" summarizes the distributions of several experiments. This plot shows the 50% and 90% isodensity lines of A, B, and C

deformation values from reservoir measurements (Fig. 4c). A convenient qualitative way to compare experiments and different conditions is to use isodensity lines (Fig. 4d). These lines are calculated from applying a kernel density estimator to the data. The location of highest event density is displayed in red, while events in regions with low density are plotted blue, as shown in Fig. 4a–c. At the transition from green to yellow, the density is approximately 50% of the maximum density, shown by a dashed isodensity line in Fig. 4d. Figure 4d also shows the 90% isodensity lines (solid lines) and summarizes the channel measurements at two different flow rates and a reservoir measurement of a human leukemia cell line (HL60), which clearly shows a flow rate-dependent deformation.

4. Steady-state deformation: The extensive length of the constriction of 300 μm is supposed to provide a steady-state deformation of cells in the measurement region (ROI_1). To test this, a data set needs to be plotted in deformation vs. x-position space. This plot would show a correlation if the deformation did not reach a steady state.

3.3.2 *Filter Settings*

1. Area: Debris, doublets, or big chunks of material should be filtered out by setting a certain range of area or by using a polygon filter around the population of interest. Polygon filters define arbitrary gating lines and are available in ShapeOut.
2. Area Ratio (R): For RT-DC an ideal object is fully convex and has therefore an area ratio close to 1. This allows a quantification of deformation based on a border following algorithm and ultimately extraction of material properties of cells, e.g., the elastic modulus. Since concave parts in the cells (*see* Fig. 1c) are not suited for the algorithm, those shapes have to be excluded

from the analysis using the area ratio. It is not possible to give an area ratio filter setting that is valid for all studies. The following range is a suggestion based on experience:

(a) 1.0–1.03: very strict filter that only allows very convex objects

(b) 1.0–1.05: less strict but will exclude most doublets and irregularly shaped objects

(c) 1.0–1.07: upper threshold for rheological studies (doublets and irregularly shaped objects might pass the filter)

3. *y*-position in the channel: For rheological studies, only cells which are aligned in the middle of the channel should be considered because they have been exposed to symmetric shear forces. This is also a boundary condition of the analytical model [19], which can be used to extract the elastic modulus. A good practice is to set a filter range using the mean of the y positions ($\bar{y}$) and its standard deviation (σ_y): $\bar{y} \pm \sigma_y$.
4. Other filters: Depending on the individual sample, other parameters such as brightness should be checked to remove unwanted subpopulations of cells.

3.3.3 Analyzing Mechanical Readout

1. Deformation and inertia ratio: Elongation of objects can be quantified in various ways, e.g., using the aspect ratio, circularity, or the second moment of area. Deformation is obtained using circularity and shown during the experiment for each measured cell. Therefore, it is one of the first parameters experimenters are in contact with when using RT-DC. The irregularity of objects tends to increase the deformation value. For the analysis of samples with a high area ratio ($R > 1.05$), the inertia ratio should be preferred over deformation since irregularities have less effect on the inertia ratio value. Aspect ratio is often not a good measure of the cell deformation, because the steady-state shape of cells in the channel is bullet-like, with an aspect ratio close to one, even though the cell is clearly deformed.
2. Differential deformation: The initial shape of cells can be measured in the reservoir. If the initial shape of cells deviates from a circle ($D > 0$), the deformation measured in the channel will be a superposition of the initial shape and the deformation induced by the channel. This can be especially problematic if samples with different deformation in the reservoir need to be compared. Differential deformation corrects for the deformation in the reservoir by subtracting it from the deformation measured in the channel. Since it is not yet possible to measure the same cell in both regions, a bootstrapping algorithm is applied, which allows to obtain statistical representations for reservoir and channel measurement. The algorithm is depicted

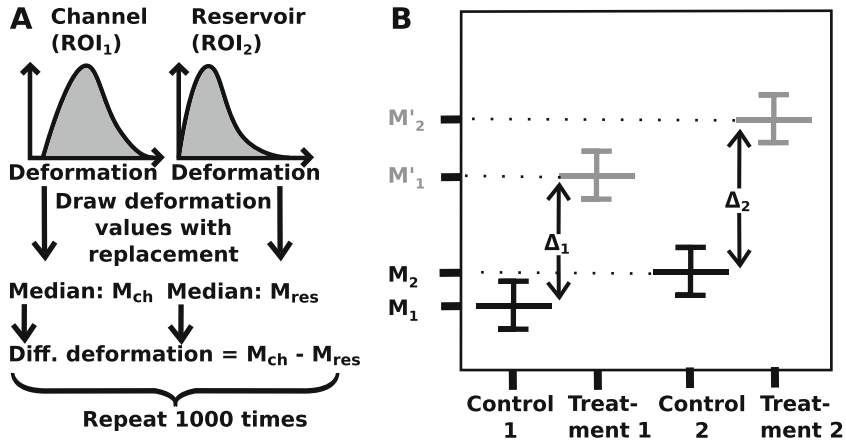

Fig. 5 Differential deformation and linear mixed models. (**a**) Differential deformation: Differential deformation is obtained by drawing *n* deformation values from the reservoir measurement with replacement, where *n* equals to the number of samples (bootstrapping). Next, the median *M* of this sampling distribution is determined. The median is preferred because it is robust for outliers. The same procedure is applied for a corresponding channel measurement and the difference of both medians results in one differential deformation value. By repeating this procedure 1000 times, a distribution of differential deformations is obtained, which can be used for further analysis. (**b**) Linear mixed models: Sketch shows a boxplot of a duplicate measurement of a control and a treatment state. The median-level *M* of the control and also the distance Δ between control and treatment is different for each replicate. These variations are very typical for RT-DC experiments and linear mixed models allow to perform analyses for these degrees of freedom

in Fig. 5a and explained in the following. Let d_{ch} and d_{res} be vectors of length n and m representing deformation values from a channel and reservoir measurement. To obtain a distribution of differential deformations, the following steps need to be conducted:

(a) Draw randomly n values from d_{ch} and m values from d_{res} with replacement to obtain a sampling distribution for the channel and reservoir measurement, respectively.

(b) Calculate the median M_{ch} and M_{res} for the sampling distribution of the channel and reservoir measurement. The median is preferred above the mean because it is more robust for outliers.

(c) Subtract M_{res} from M_{ch} to obtain the first differential deformation value.

(d) Repeating **step a–c** one thousand times results in a distribution of differential deformation values.
This distribution of differential deformations can be used for further statistical analysis.

3. Elastic modulus: Elastic modulus (E) is a parameter for cell stiffness that is independent of cell size. Neither deformation, circularity, differential deformation nor inertia ratio does suffice to parameterize cell stiffness, because all depend on cell

size. A large cell will be exposed to higher shear forces in the channel because it comes closer to the channel wall and deform more compared to a small cell with identical elastic properties. An analytical model has been presented earlier [19], which uses linear elasticity theory and Stokes equation to describe how fully elastic spheres deform under hydrodynamic shear stresses. The model assumes that the object is initially perfectly round and the deformation itself does not change the flow profile around the cell. This is only true for small deformations ($D < 0.02$). The model can be used to calculate the deformations of objects of certain elastic modulus and cell size for different flow rates, viscosities, and channel widths. It also allows determining "isoelasticity lines," which describe the dependence of area and deformation and are shown in Fig. 4 as curved gray lines. By calculating many isoelasticity lines, a lookup table (LUT) can be created, which assigns an elastic modulus to each pair of deformation and area values. It can be used to extract the elastic modulus from measurements of thousands of cells. The LUT is universal, i.e., it can be rescaled to account for changes in viscosity η', flow rate Q, or channel width l' according to the equation $E' = \frac{Q'\eta' l'^3}{Q\eta l'^3} E$ [19]. Using this equation, flow rate-dependent viscosity changes ("shear-thinning") can be addressed (*see* Subheading 2.5). Additionally, the pixel size of the CMOS camera causes an offset deformation. Both shear-thinning and the offset deformation need to be considered when calculating the elastic modulus [23]. Due to the underlying assumptions and boundary conditions, the applicability of the model is limited to deformation values up to 0.02. However, recently a more elaborate numerical model [27] has confirmed the original results of the analytical model and extended it to much greater deformations.

3.3.4 Statistical Test

RT-DC allows measuring hundreds to thousands of cells within seconds. For quantification of the results, it needs to be tested if, e.g., a certain treatment has a significant effect on cells. A conventional *t*-test on such a large number of events will render even very small differences that might arise from biological variation significant. Therefore, it is important to study the reproducibility of the effect of a treatment by considering replicates. A linear mixed model can be designed for such a purpose and allows obtaining significance levels for the effect. For the following explanation of the method, it is assumed that a "control" state and a "treatment" state was measured for biological replicates. Each control measurement can have a different median value (M_1 and M_2 in Fig. 5b), which is expressed by varying intercepts in the linear mixed model. Additionally, the effect of the treatment can be different for each replicate (Δ_1 and Δ_2 in Fig. 5b), which means a differing slope in the linear mixed model. These degrees of freedom can be expressed

by a so-called random intercept and random slope model. The programming language R [28] together with the R-package *lme4* [29] allow designing such a model and to fit it to the data. For the statistical test, a similar model that is only lacking the effect term ("null model") has to be fitted to the experimental data as well. Both models, one including and one missing the effect term are compared using a likelihood ratio test [30] by applying the function "*anova*" from the R package "*stats*." Then Wilks theorem [31] can be used to obtain a *p*-value from the likelihood ratio. This *p*-value indicates the probability that the null hypothesis (both models are identical) is correct. Because the models only differ by the effect term, the *p*-value also indicates the significance of the effect. The source code for the model and the test is available under an open-source license and can be found in the Git-repository of ShapeOut [24]. ShapeOut offers a GUI to access these functions in the "Analysis"-Tab. First, the parameter which should be tested has to be defined. Next, each measurement needs to be assigned to the control or treatment group. The used linear mixed model is a paired test. Therefore, the algorithm needs clarification, which control and treatment measurements remain together by giving them the same repetition number in the corresponding drop-down menu. The output is a .txt file that contains all information from *lme4* and *anova* about the fitted model, the *p*-value and the effect size.

Statistical tests for area, volume, deformation, differential deformation, and elastic modulus are discussed in the following:

1. Statistical tests on area and volume: RT-DC is a very precise technique to study properties of cells that are related to their size. *P*-values can be obtained using linear mixed models. Since the projected area will increase when cells are deformed, comparative studies on area should preferably use measurements from the reservoir. In addition, volume is not dependent on deformation, can be calculated from the projected area, and can thus be used to compare channel measurements.
2. Statistical test on deformation: Deformation is a quantity that describes the shape of cells and can be even used as a mechanical readout if:
   (a) Area ratio is small ($R < 1.07$).
   (b) The area of the compared samples is not significantly different in the reservoir.
   (c) And if the deformation in the reservoir of the compared samples is not significantly different.

   Condition (b) is important, because two samples could have identical elastic properties, but different sizes. Then the cells of the larger sample would be subjected to higher shear forces and deform more in the channel. In

Table 4
Requirements for the usage of certain mechanically relevant parameters to compare samples

	Parameter		
Requirement	**Deformation**	**Differential deformation**	**Elastic modulus**
Area not sign. diff. in reservoir	Necessary	Necessary	Not necessary
Deformation not sign. diff. in reservoir	Necessary	Not necessary	Necessary

such a case the elastic modulus could be used. In case condition (c) is not fulfilled, differential deformation should be used.

3. Statistical test using differential deformation: If samples have significantly different deformations in the reservoir, one must expect that the deformation in the channel is a superposition of the initial shape and the deformation induced by shear stress in the channel. Differential deformation considers both contributions and should be used in a linear mixed model.
4. Statistical test using elastic modulus: If mechanical properties of two samples need to be compared, but a statistical test on the reservoir data shows that cells are different in area but not different in deformation, then the elastic modulus can be used in a linear mixed model for channel measurements to decouple the effects of area and deformation. Please *see* Subheading 3.3.3, **step 3** for more details like boundary conditions for applicability.

   Table 4 gives an overview, which mechanical parameter should preferably be used, dependent on the statistical difference of area and deformation of the reservoir measurements between the compared groups.

3.4 Conclusion

RT-DC is an emergent technique with many possible applications in biological and biomedical studies. Particularly appealing is the possibility to characterize cells and sensitively detect physiological and pathological changes in cell function without any external marker. The guidelines laid out in this book chapter constitute the current best practice and should ensure that results from different studies will stay comparable. For some possible complications that can occur, *see* **Notes 1–8**.

4 Notes

1. Leaking of chips: To make leaking of chips visible, it is important to wipe the chip entirely dry when all tubing is connected and the syringe pumps are running. Liquid, emerging at the

transition between glass and PDMS, is an obvious indicator for a chip that is not well sealed. The flow rates in such a chip cannot be controlled and the chip should be discarded.

2. Motion blurring: To capture moving objects, it is important that the objects do not move too far during illumination. For a flow rate of 0.04 μL/s, cells will move approximately with a speed of 0.16 m/s in a 20 μm channel. Cells at this speed will move 0.32 μm during the exposure time of 2 μs, which equals approximately the length of one pixel (0.34 μm for a 40× magnification). From this follows that cells move three pixels for a flow rate of 0.12 μL/s. Even higher flow rates lead to unacceptable image blurring, because it could elevate the measured deformation artificially.
3. Sedimentation: Due to the high density of the MB, cells sediment very slowly allowing for long measurements. A rule of thumb is that the cell measurement frequency drops to half in 30 min.
4. Real cell size: RT-DC does not allow for measuring accurate cell sizes, because the projected area is dependent on the focus. For RT-DC experiments, a slight under-focus setting is used which allows to obtain a slim bright halo around the cells. This is necessary for the correct tracking of cells. Furthermore, area can be affected by deformation, because the projected area will increase if an object is deformed in the channel. Volume can be used as a workaround for this problem, but the focus dependence will persist.
5. Limitation of deformation values: Since deformation is defined by parameters that are pixel-precise, the deformation itself will show a discrete pattern if the magnification is not sufficient. Additionally, deformation is affected by the pixel size of the CMOS camera, because the projection of a perfectly round object on such a pixel grid will result in a jagged object with a deformation value larger than zero. For a resolution of 0.34 μm/pixel, the lowest measurable deformation value of a cell with an area of 160 μm^2 is 0.0045. This offset deformation increases for small objects and tends to be zero for large objects [23].
6. Clogging during the experiment: Large chunks of cell material can cause clogging of the channel, which can cause a decrease of the measurement frequency. The pillars at the sample and sheath inlet ("P_1" and "P_2" in Fig. 1a) help to reduce the chance of clogging, but monitoring the measurement frequency during the experiment and inspecting the channel inlet between the measurements is recommended. The filters should be checked after each experiment to make sure no obstruction could have caused a flow rate instability. An example measurement with an artifact caused by clogging is shown in a scatterplot with deformation and time on the axes in

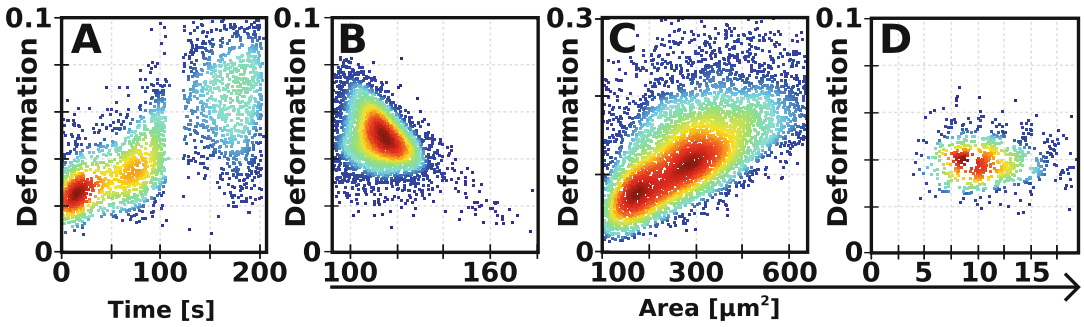

Fig. 6 Problems during a measurement. (**a**) Clogging of the channel can lead to an interrupted deformation signal. Partial clogging can cause increased deformation. (**b**) This particular pattern can occur if an *x*-length filter does not allow objects above a certain length. The negative slope arises because large objects are only tracked if they are not too elongated in *x*-direction. (**c**) If cells are too large for the used channel, they will be squeezed by the channel walls. This leads large cells to deform much more than small cells. (**d**) Very small cells only have a low number of pixels defining their perimeter and area. This can cause a striped pattern in a deformation vs. area scatterplot, because only discrete values are possible

Fig. 6a. Ongoing softening indicates a partial clogging which only allows cells to pass by squeezing through. Most remarkable in Fig. 6a is a period of time where no events exist. This indicates that cells could not pass the channel because of an entirely blocked channel.

7. Too restrictive *x*-length filter: A filter for *x*-length can be applied during the measurement or in the analysis software ShapeOut. If the *x*-length is chosen too small, large cells will only pass the filter if they are not too elongated. This causes a strong negative correlation of deformation and area as shown in Fig. 6b. This issue is especially important during a measurement, because cells that are excluded by the filter are not recorded and will be missing in the resulting data set.
8. Limitation of cell sizes: The size of the cells should be checked in order to choose an appropriate channel width as indicated in Table 1. Large cells exceeding the channel diameter will be squeezed by the walls and a strong correlation between area and deformation will occur (for an example *see* Fig. 6c). The lower limit is defined by the resolution of the camera and the magnification of the objective. Below a certain cell size, area and deformation values will become discrete and a characteristic striped pattern will occur in the data (for an example *see* Fig. 6d). This can be prevented by using an objective with a higher magnification.

Acknowledgments

We thank the BIOTEC/CRTD Microstructure Facility (partly funded by the State of Saxony and the European Fund for Regional Development—EFRE) and Dr. Salvatore Girardo for the

development and production of the master templates. We acknowledge financial support from the Alexander von Humboldt Foundation (Alexander von Humboldt Professorship to J.G.), the Sächsisches Ministerium für Wissenschaft und Kunst (TG70 grant to O.O. and J.G.), the Bundesministerium für Bildung und Forschung (ZIK grant to O.O. under no. 03Z22CN11), and the European Union's Seventh Framework Programme under grant agreement no. 632222 (Proof-Of-Concept Grant FastTouch to J.G.).

Conflict of Interest Statement

O.O. is co-founder and CEO of Zellmechanik Dresden distributing the technology.

References

1. Shapiro HM (2003) Practical flow cytometry. Wiley, Hoboken. doi:10.1002/0471722731
2. Green RE, Sosik HM, Olson RJ, DuRand MD (2003) Flow cytometric determination of size and complex refractive index for marine particles: comparison with independent and bulk estimates. Appl Opt 42:526. doi:10.1364/AO.42.000526
3. Lautenschlager F, Paschke S, Schinkinger S et al (2009) The regulatory role of cell mechanics for migration of differentiating myeloid cells. Proc Natl Acad Sci 106:15696–15701. doi:10.1073/pnas.0811261106
4. Tse JM, Cheng G, Tyrrell JA et al (2012) Mechanical compression drives cancer cells toward invasive phenotype. Proc Natl Acad Sci U S A 109:911–916. doi:10.1073/pnas.1118910109
5. Darling EM, Zauscher S, Block JA, Guilak F (2007) A thin-layer model for viscoelastic, stress-relaxation testing of cells using atomic force microscopy: do cell properties reflect metastatic potential? Biophys J 92:1784–1791. doi:10.1529/biophysj.106.083097
6. Guck J, Schinkinger S, Lincoln B et al (2005) Optical deformability as an inherent cell marker for testing malignant transformation and metastatic competence. Biophys J 88:3689–3698. doi:10.1529/biophysj.104.045476
7. Lekka M, Laidler P, Gil D et al (1999) Elasticity of normal and cancerous human bladder cells studied by scanning force microscopy. Eur Biophys J 28:312–316. doi:10.1007/s002490050213
8. Ekpenyong AE, Whyte G, Chalut K et al (2012) Viscoelastic properties of differentiating blood cells are fate- and function-dependent. PLoS One 7:e45237. doi:10.1371/journal.pone.0045237
9. Darling EM, Topel M, Zauscher S et al (2008) Viscoelastic properties of human mesenchymally-derived stem cells and primary osteoblasts, chondrocytes, and adipocytes. J Biomech 41:454–464. doi:10.1016/j.jbiomech.2007.06.019
10. Lange JR, Steinwachs J, Kolb T et al (2015) Microconstriction arrays for high-throughput quantitative measurements of cell mechanical properties. Biophys J 109:26–34. doi:10.1016/j.bpj.2015.05.029
11. Hosseini SM, Feng JJ (2012) How malaria parasites reduce the deformability of infected red blood cells. Biophys J 103:1–10. doi:10.1016/j.bpj.2012.05.026
12. Tabeling P (2005) Introduction to microfluidics. Oxford University Press, New York
13. Rosenbluth MJ, Lam WA, Fletcher DA (2008) Analyzing cell mechanics in hematologic diseases with microfluidic biophysical flow cytometry. Lab Chip 8:1062–1070. doi:10.1039/b802931h
14. Lange JR, Goldmann WH, Alonso JL (2016) Influence of αvβ3 integrin on the mechanical properties and the morphology of M21 and K562 cells. Biochem Biophys Res Commun 478:1280–1285. doi:10.1016/j.bbrc.2016.08.111
15. Byun S, Son S, Amodei D et al (2013) Characterizing deformability and surface friction of cancer cells. Proc Natl Acad Sci 110:7580–7585. doi:10.1073/pnas.1218806110
16. Dudani JS, Gossett DR, Tse HTK, Di Carlo D (2013) Pinched-flow hydrodynamic stretching

of single-cells. Lab Chip 13:3728. doi:10.1039/c3lc50649e

17. Gossett DR, Tse HTK, Lee SA et al (2012) Hydrodynamic stretching of single cells for large population mechanical phenotyping. Proc Natl Acad Sci 109:7630–7635. doi:10.1073/pnas.1200107109
18. Otto O, Rosendahl P, Mietke A et al (2015) Real-time deformability cytometry: on-the-fly cell mechanical phenotyping. Nat Methods 12:199–202. doi:10.1038/nmeth.3281
19. Mietke A, Otto O, Girardo S et al (2015) Extracting cell stiffness from real-time deformability cytometry: theory and experiment. Biophys J 109:2023–2036. doi:10.1016/j.bpj.2015.09.006
20. Suzuki S, Be K (1985) Topological structural analysis of digitized binary images by border following. Comput Vis Graph Image Process 30:32–46. doi:10.1016/0734-189X(85)90016-7
21. Bradski G (2000) The OpenCV library. Dr Dobbs J Softw Tools 25:120–126
22. Mietke A (2014) Theoretical and experimental analysis of cell deformations by hydrodynamic forces in microfluidic channels. Technische Universität Dresden
23. Herold C (2017) Mapping of deformation to apparent young's modulus in real-time deformability cytometry. arXiv:1704.00572
24. Müller P, et al. (2015) ShapeOut: analysis software for real-time deformability cytometry [Software]. Available at https://github.com/ZELLMECHANIK-DRESDEN/ShapeOut
25. Beer FP, Johnston ER Jr, Mazurek D, Cornwell P (2012) Vector mechanics for engineers: statics and dynamics, 10th edn. McGraw-Hill International, New York
26. Geoff Olynyk (2012) File Exchange - MATLAB Central – Mathworks. http://de.mathworks.com/matlabcentral/fileexchange/36525-volrevolve/content/volRevolve.m. Accessed 1 Jan 2017
27. Mokbel M, Mokbel D, Mietke A et al (2017) Numerical simulation of real-time deformability cytometry to extract cell mechanical properties. ACS Biomater Sci Eng. doi:10.1021/acsbiomaterials.6b00558
28. R Core Team (2015) R: a language and environment for statistical computing. R Foundation for Statistical Computing, Vienna, Austria. https://www.R-project.org/
29. R Core Team (2015) R: a language and environment for statistical computing. R Foundation for Statistical Computing, Vienna, Austria. https://www.R-project.org/
30. Mood AM, Graybill FA, Boes DC (1974) Introduction to the theory of statistics. McGraw-Hill International, New York
31. Wilks SS (1938) The large-sample distribution of the likelihood ratio for testing composite hypotheses. Ann Math Stat 9:60–62. doi:10.1214/aoms/1177732360

Chapter 16

Nuclear Cytometry: Analysis of the Patterns of DNA Synthesis and Transcription Using Flow Cytometry, Confocal Microscopy, and RNA Sequencing

David W. Galbraith, Elwira Sliwinska, and Partha Samadder

Abstract

Eukaryotes are defined by cells that contain a nucleus and other membrane-bound organelles. Cytometric analysis in situ, utilizing imaging, provides a useful understanding of the structure and function of the various subcellular components, particularly when combined with methods that preserve the living state. In terms of information provided by the observation of eukaryotic nuclei, imaging has provided a wealth of information about cellular multiplication. When organisms are present in multicellular form (tissues and organs), this property does not generally confound imaging cytometry. Multicellular eukaryotic species present immediate problems when being considered for analysis using flow cytometry which requires suspensions of single particles. Although some eukaryotic cell types exist as natural single cell suspensions (cf. the erythropoietic system), for other tissues and organs, strategies are required to produce single particle suspensions. This chapter illustrates the application of flow cytometry combined with confocal microscopy to analyze complex organs, focusing on properties of the plant nucleus, and then goes on to describe how suspensions of nuclei can be prepared from tissues and organs, and used for flow cytometric analysis of cellular and transcriptional states. The application of these techniques to animal species is also discussed with the implication that this strategy is universally applicable for the characterization of nuclei within tissues that cannot readily be converted into suspensions of cells.

Key words Eukaryotes, Nuclei, Fluorescent proteins, Genome size, Ploidy, Endoreduplication, Confocal microscopy, Flow cytometry, Transcriptional analyses, RNA amplification

1 Introduction

1.1 Flow Cytometric Analysis of Complex Tissues and Organs: The Mitotic Cycle and Endoreduplication in Plants

Higher plants provide an excellent example of the problems encountered when applying cytometric procedures to the types of complex multicellular structures characteristic of higher eukaryotes. Thus, for flow cytometry, at the very least, means have to be found to convert these structures into suspensions of mono- or polydisperse particles that can pass through the instrument. Although the tissues and organs of plant and animal species can be converted into single cell suspensions following enzymatic

Teresa S. Hawley and Robert G. Hawley (eds.), *Flow Cytometry Protocols*, Methods in Molecular Biology, vol. 1678, DOI 10.1007/978-1-4939-7346-0_16,

digestion, this process is by no means universal, and the act of separating cells can perturb the subsequent measurements. A simple solution involves the analysis of cellular homogenates, a prime early example being the measurement of nuclear DNA contents [1, 2]. For plants, nuclei can be released from any living tissue/organ (leaf, root, hypocotyl, flower, seed, etc.) by chopping using a razor blade and, after staining them with an intercalating (e.g., propidium iodide) or base-specific (e.g., 4′,6-diamidino-2-phenylindole) fluorochrome, a profile of the nuclear DNA contents is readily obtained. Instead of a fluorochrome, transgenic lines expressing a Fluorescent Protein gene product targeted to and accumulated in the plant [3] or animal [4] nucleus can be productively employed, in combination with DNA-specific fluorochromes, to define specific cell types and thereby explore the activity of the cell division cycle in a cell type-specific manner [3–5].

Proliferating eukaryotic cells, in general, pass through four phases in the mitotic cycle: G_1, a first period of cell growth during which a nucleus possesses a 2C DNA content (C – DNA content of a holoploid genome with chromosome number *n*), S, DNA replication phase which results in a doubling of DNA content (from 2C to 4C); G_2, a second period of cell growth, during which a nucleus possesses a 4C DNA content; and M, mitosis, when genetic material is divided into two daughter nuclei (the DNA content being reduced from 4C to 2C). Non-proliferative cells usually enter a quiescent G_0 state from the G_1 phase of the cell cycle. In the case of plants, differentiated, specialized cells, such as those of endosperm, suspensor, hypocotyl or root hair, often undergo endoreduplication, during which the nuclei go through repeated rounds of DNA replication that are not followed by mitosis (endocycles), resulting in endopolyploid cells (4C → 8C → 16C → 32C, etc., even up to 4096C) [6–10]. The occurrence of somatic cells having different nuclear DNA contents arranged in this type of multiplicative series is termed polysomaty, and this phenomenon is encountered in over 90% of angiosperms [11]. For some species (cf. *Arabidopsis thaliana*) polysomaty is encountered within most of the somatic tissues [12]. Since the result of flow cytometric analysis is usually displayed in the form of a histogram of the fluorescence intensity, with easily distinguished peaks corresponding to nuclei with different DNA contents, the method can be conveniently used to study the cell cycle and endoreduplication. Flow cytometry is currently the most popular method for nuclear DNA content analysis because it is easy to use, accurate, inexpensive, and can be employed, with some caveats, for any family, genus, and species including animals [4, 13–15].

This chapter provides detailed information as to the best ways, using flow cytometry to analyze cell cycle and degree of endoreduplication in homogenates of single-nucleus suspensions originated from different plant parts, and to integrate these with

transcriptomics technologies aiming at characterization of gene expression and with localization of the cells of different ploidies in the living seedlings by confocal microscopy. It also provides information concerning the characterization of nuclei from mammalian tissue and organ homogenates. Our laboratories have had considerable experience working with flow cytometers and sorters, including the Partec CCA and CyFlow SL Green, the Beckman-Coulter MoFlo and Cell Lab Quanta SC, the BD Biosciences LSR II, FACSAria, and Accuri C6, the BioRad S3, the ACEA Biosciences NovoCyte, and the Invitrogen Attune NxT. The methods, which are described here only for a subset of these instruments in interests of space, are applicable to all platforms, with only slight instrument-specific modifications.

1.2 Applying Flow Sorting for the Analysis of Nuclei of Different Cell Types and at Different Stages of the Cell Cycle/ Endocycle

The ability of flow cytometers to define minor subpopulations of cells within heterogeneous suspensions according to their optical properties allows subsequent purification of these subpopulations for study using flow sorting. We have previously shown that flow sorting can be applied for the direct isolation of nuclei from tissue and organ homogenates of plants [16], and we have extended this approach to nuclei within homogenates produced from animal tissues and organs [4, 15]. One of the advantages of the method of tissue and organ chopping [1] is that it involves minimal experimental manipulations and does not require that the nuclei be purified by centrifugation. This is important since it avoids the non-specific adhesion of nuclei that can occur during centrifugation. The value of nuclear sorting for characterization of nuclear state has been recently enhanced by the development of molecular methods of RNA manipulation and amplification allowing whole genome transcriptional analyses from single nuclei [15], as noted in the following section.

1.3 RT-PCR, RNA Sequencing, and Transcript Analysis

The nucleus represents the predominant site of transcriptional activity within the cell. The production of transcripts, mRNA processing, and polyadenylation occurs co-transcriptionally within the nucleus. We and others have shown, somewhat unexpectedly, that the composition of polyadenylated transcripts within the nucleus and the whole cell is largely concordant for both animal and plant species [16–21]. Since the process of homogenization, done on ice and involving rapid dilution of the cellular contents, arrests biochemical processes more-or-less instantly, this means that the polyadenylated complement of nuclear RNA can be used to define the transcriptional state of the cell from which it is derived (*see* **Note 1**). The approach of isolating nuclei is also less likely to perturb gene expression than the process of conversion of solid tissues and organs into single cell suspensions through enzymatic digestion of extracellular polymers, since this process requires temperatures much elevated above freezing and significant times of incubation.

Our initial analyses of the transcriptional states reported by isolated nuclei [16, 17] involved sorting of large numbers of nuclei (up to 100,000) and a transcriptional read-out provided by microarrays. With the advent of sequencing for whole-genome transcript profiling (RNAseq), particularly in Next Generation (NextGen) configurations, and with the availability of molecular technologies emphasizing minimal intrinsic amplification bias, we were able to sample transcriptional states across the entire genome of single nuclei [15]. Despite its wide adoption, NextGen sequencing does have its downsides: cost is always a consideration, as is the cycle time required for data production, and the overhead for data management is particularly significant. Single nucleus (and single cell) transcriptional analyses are inherently attractive, since they provide unparalleled insight into the contributions of single cells to populations, and they also permit defining transcriptional states without preconditions or even pre-existing markers (so-called "agnostic" analyses) simply through sequencing of each and every single cell or nucleus within a population. However, this can rapidly get out of hand, and a means to avoid unnecessary sequencing of uninteresting transcriptomes (in many cases, those of a majority of cells within a tissue) becomes essential. This chapter outlines means for agnostic transcriptional analyses based on single nuclei, and provides a cheap and convenient pre-screening of transcriptional states, using qPCR, to avoid unnecessary RNA-seq overhead.

1.4 Localization of Nuclei with Different DNA Content Using Image Analysis

Flow cytometry does not provide information on the spatial location of nuclei of different ploidies, being at different stages of the cell cycle or having different endoreduplicative states within tissues and organs. For this purpose, microscopic techniques have to be employed. Confocal microscopy is particularly important since it allows the creation of 3D images in real time (time-lapse imaging), and therefore the possibility of visualizing sequential events in a living cell. Laser scanning confocal microscopy (LSCM), based on fluorescence, produces images of high resolution by eliminating out-of-focus light; it is noninvasive and enable volume analysis of the sample [22], which makes it suitable for localization of nuclei of different ploidies in intact plant tissue and for observations of dynamics of DNA synthesis during plant growth [10, 23]. For still images, staining nuclei with the same fluorochromes as used in flow cytometry is appropriate, but for recording long time-course movies, using transformed plants with a Fluorescent Protein in the nucleus is more suitable because the protein is constantly synthetized in plant cells and does not bias their physiological processes.

For time-lapse studies, a suitable system for growing plants has to be adopted. Such system has been developed for studying Arabidopsis seed germination and early seedling growth [10, 24], using a chambered cover glass and an inverted confocal microscope.

When the embryo/seed is placed at the base of the chamber (on the cover glass) and covered with a growth medium (e.g., agar or Murashige and Skoog medium [25]), its axis and then root elongates along the cover glass and therefore is perfectly positioned for recording images. With a plain agar as a medium, since it does not provide nutrition for plant growth, observations can be conducted only for a few days, while when MS medium is used plants grow normally for a prolonged time. The latter medium requires maintaining sterile conditions, however. The confocal imaging described here was done using a Leica TCS SPE-II confocal microscope, but the methods should be generally applicable to other instruments with only minor modifications.

The classification of the nucleus to the certain ploidy using fluorescence microscopy is possible because there is a well-documented linear relationship between nuclear size and DNA content [26–28], although it is not absolute. For example, nuclear volume did not appear to be closely correlated with DNA content in the root of *Zea mays* [29]. Nevertheless, measurements of nuclear fluorescence after collecting a stack of optical sections (Z-stack) by confocal microscopy, together with flow cytometric measurement of DNA content, provides a reliable system for studying ploidy distributions across various tissues.

2 Materials

As a general precaution, always employ good laboratory practice in your experiments. Work with standard protective equipment and clothing, and clean the work area with 70% ethanol. All chemicals should be reagent grade.

2.1 Isolation of Nuclei

1. Chopping buffer [1]: 45 mM $MgCl_2$, 30 mM sodium citrate, 20 mM MES, pH 7.0 adjusted with NaOH. Filter sterilize and store as 50 mL aliquots at −20 °C.
2. Propidium iodide (PI) stock solution: 1 mg/mL in deionized water (diH_2O). Store as 1 mL aliquots at −20 °C. Once thawed, the solution is stable at room temperature, but should be protected from light.
3. 4′,6-diamidino-2-phenylindole (DAPI) stock solution: 0.1 mg/mL in diH_2O. Store as 1 mL aliquots at −20 °C until the day of use.
4. DNAase-free ribonuclease (RNAase) A stock solution: 10 mg/mL in diH_2O. Store as 1 mL aliquots at −20 °C until the day of use.
5. Scalpels, double-edged shaving razor blades designed for classic safety shaving razors (from any reputable company),

CellTrics® 20 and 30-μm disposable filters (Sysmex Partec, Görlitz, Germany), Falcon 35-μm nylon mesh cell-strainer cap (BD Biosciences, San Jose, CA), sterile 60 × 15 mm disposable plastic petri dishes.

2.2 Sorting and Analysis of Nuclei

1. Flow cytometer calibration beads.
2. AcGFP/EGFP Flow Cytometer Calibration Beads (TaKaRa Clontech, Mountain View, CA).
3. DEPC-treated water, DNase/RNase-free water.
4. RNA*later*.
5. Power SYBR Green Master Mix (ThermoFisher Scientific, Waltham, MA).
6. REPLI-g WTA Single Cell Kit (Qiagen, Valencia, CA).
7. IDT PrimerQuest tools (www.idtdna.com/primerquest/home/index).
8. 96-well plates.
9. Flow cytometers: analyzer and sorter.
10. PCR thermocycler.

2.3 Germinating Seeds and Growing Seedlings for Observation of DNA Synthesis in Real Time

1. Seeds of transformed Arabidopsis line expressing Fluorescent Proteins in the nucleus.
2. Nunc One-chamber Lab-Tek chambered coverglass (Sigma-Aldrich, St. Louis, MO).
3. Agar 0.8% (w/v).
4. Forceps, petri dishes, filter paper (disks of the size of the petri dish).
5. Confocal microscope.

3 Methods

3.1 Preparation of Nuclei

3.1.1 Isolation from Plant Organs

1. Excise plant organs and tissues using forceps and a scalpel. If necessary (roots in soil, for example), prewash the organs with diH_2O and blot dry. Immediately immerse the excised samples in ice-cold chopping buffer (2 mL per 0.5 g fresh weight tissue) contained in a 60 × 15 mm plastic petri dish. Perform the remaining procedures on ice. Optimal results are obtained with the homogenization being done in a walk-in cold room.
2. Chop the samples using a new double-edged safety shaver razor blade for 2–3 min. Chopping is conveniently done placing the petri dish on a square metal (stainless steel or brass) plate resting on a bed of ice in a large plastic tray.
3. Filter the sample through a CellTrics 30-μm filter to remove large debris.

3.1.2 Isolation from Animal Organs

1. Excise organs from wild-type or transgenic mice following euthanasia. Perform homogenization with a double-edged razor blade in a chopping buffer as described in Subheading 3.1.1, using approximately 100 mg fresh weight of tissue/mL buffer.
2. Pass the homogenate through a Falcon 35-μm cell-strainer cap followed by passages through CellTrics 30- and 20-μm filters to remove debris.

3.1.3 Staining with Fluorochromes

Homogenates are stained with fluorochromes according to the purpose of the experiment and the configuration of the cytometer. In this chapter, we describe the use of PI and DAPI. These two fluorochromes are compatible with the Partec CCA and BD LSRII, but DAPI fluorescence is not readily excited using the standard configuration of the FACSAria (in the absence of a violet laser) and CyFlow SL Green.

1. PI: Add 2.5 μL of RNAase (10 mg/mL) to a labeled tube. Add 0.5 mL filtered homogenate. Incubate on ice for 10 min. If you plan to use the nuclei for transcript profiling, the RNAase step should be omitted (*see* **Note 2**). Add PI to a final concentration of 50 μg/mL. Fresh tissue homogenates can be analyzed immediately, or can be incubated on ice in darkness for any period of time that is convenient for the homogenization, staining, and analysis pipeline. It is important to verify that staining is complete, and that the amount of fluorescence is stable during storage. In general, homogenates prepared from dry tissues (i.e., seeds) require incubation after staining for 20–30 min.
2. DAPI: Add 0.5 mL filtered homogenate to a tube containing sufficient DAPI stock solution to give a final concentration of 2 μg/mL. Measurements can be made immediately. For dry tissues (e.g., chopped seeds), incubate on ice in darkness for 20–30 min.
3. One-step procedure: For high-throughput applications, a one-step procedure can be employed, in which the fluorochrome is added to the chopping buffer, to the concentrations indicated above, prior to homogenization.

3.2 Analysis of the Proportion of Nuclei with Different DNA Contents Using Flow Cytometry

Switch on the flow cytometer and establish that the instrument is operating according to the manufacturer's specifications. The following methods are specific to the Partec CCA, Partec CyFlow Green, and BD LSR II.

3.2.1 Using the Partec CCA

1. Before switching on the cytometer, check waste and sheath fluid bottles and empty or refill them, as required. Start the DPAC program in an external computer (this program has more evaluation options than the inbuilt one). Perform validation of the cytometer using calibration beads (2.5 μm Partec Calibration Beads UV).
2. For cell cycle analysis, set the amplification to linear, and for endoreduplication measurements, use logarithmic amplification. The DAPI fluorescence signals in the Partec CCA are screened using the following optical configuration: KG1 heat protection filter, BG12 and UG1 short-pass filters, GG435 long-pass filter, and a dichroic mirror TK420. Analysis of the homogenate is based on fluorescence signals produced from an HBO lamp producing UV illumination, since this is a one-parameter instrument that does not detect light scatter.
3. Introduce a sample to the sample port; data acquisition will start automatically. Take a few seconds as a pre-run to allow the counting rate to stabilize at about 30–50 nuclei/s. Clear the histogram and acquire data until reaching at least 1000 nuclei in the highest peak. Data acquisition for a single sample will occupy 5–10 min, depending on the number of peaks and the sample concentration.
4. For non-endoreduplicated species/tissues, two peaks, representing 2C (G_1/G_0) and 4C (G_2) nuclei, will typically appear, while additional peaks (8C, 16C, 32C, etc.) will be seen for tissues exhibiting somatic endoreduplication (Figs. 1 and 2). Establish the number of nuclei in each peak automatically or

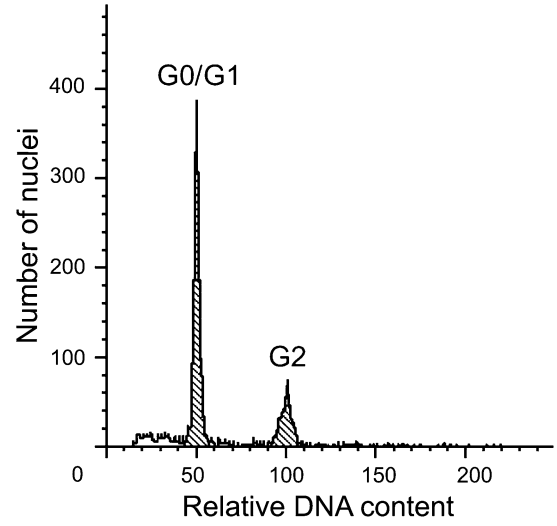

Fig. 1 Flow cytometric analysis of homogenates prepared from the root of onion using the Partec CCA flow cytometer. Uniparametric histogram of DAPI fluorescence, linear amplification

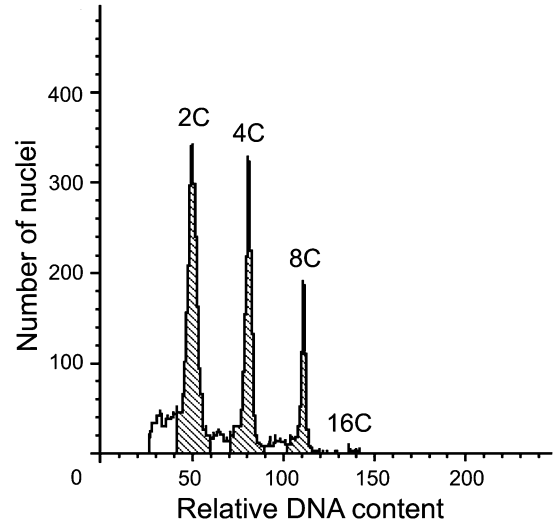

Fig. 2 Flow cytometric analysis of homogenates prepared from the radicle of cucumber seed using the Partec CCA flow cytometer. Uniparametric histogram of DAPI fluorescence, logarithmic amplification

manually by application of the Peak Analysis option in DPAC software and calculate the percentages of the nuclei with different DNA content using Microsoft Excel.

3.2.2 Using the Partec CyFlow SL Green

1. Before or after switching on the cytometer, but before starting analyses, check the waste and sheath fluid bottles, and empty or refill them, as required. When the cytometer is on, start the FloMax software. Perform validation of the cytometer using calibration beads (Partec Calibration Beads green).
2. Set the three-panel template as follows: an univariate histogram of FL2, a bivariate dot-plot SSC versus FL2, and a bivariate dot-plot SSC versus FSC (Fig. 3). The third plot can be useful for detecting additional non-nuclear populations in the presence of staining inhibitors in the plant cell cytosol.
3. For cell cycle analysis, set the FL2 channel for linear amplification and, for endoreduplication measurements, logarithmic amplification. The fluorescence signals in the CyFlow SL Green are screened using long-pass filter RG 590 E and DM 560 A. Analysis of the homogenate is based on light scatter and fluorescence signals produced from a solid-state laser with emission at 532 nm. Data acquisition is triggered on fluorescence (*see* **Note 3**).
4. Perform analysis in the same way as described for the Partec CCA (*see* Subheading 3.2.1). However, with the CyFlow SL

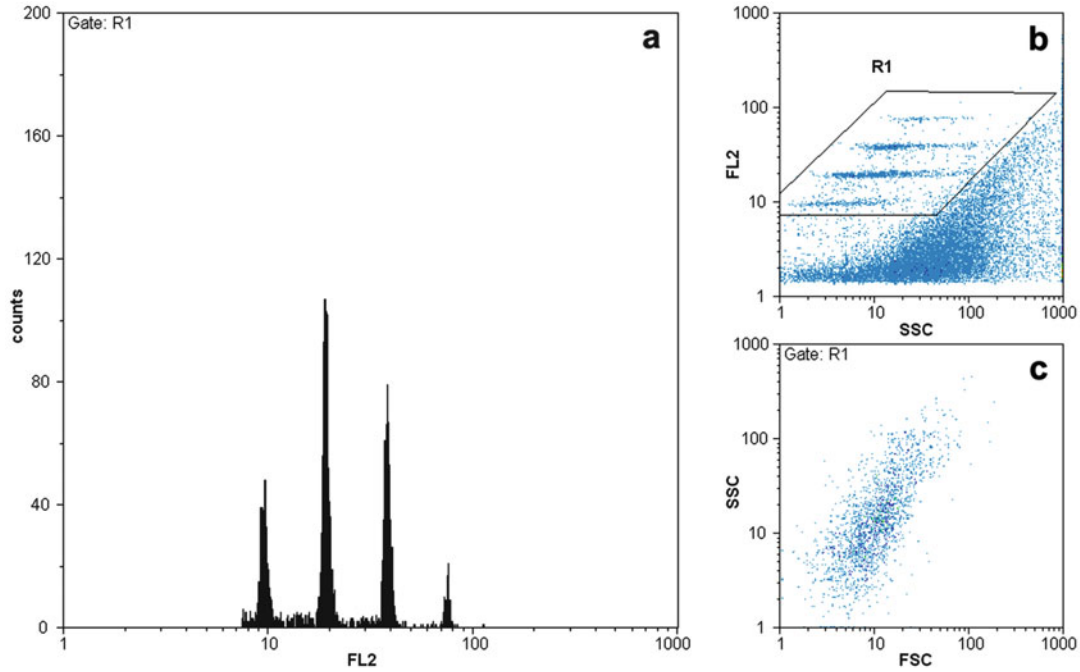

Fig. 3 Flow cytometric analysis of homogenates prepared from the root and hypocotyl of 3-day-old seedling of *Arabidopsis thaliana* using CyFlow SL Green flow cytometer. (**a**) Uniparametric histogram of PI fluorescence (FL2), gated on region R1 of panel (**b**). (**b**) Biparametric dot plot of SSC versus FL2. (**c**) Biparametric dot plot of FSC versus SSC

Green, eliminate by gating any non-specific signals coming from debris, clustered nuclei, etc. Only the gated signals representing nuclei are included in the histogram of fluorescence intensities (Fig. 3). Acquire a polygonal or amorphous gate on a dot-plot SSC versus FL2 and establish the regions of identification for each ploidy category on a uniparametric histogram, using the FloMax software. Calculate the percentages of the nuclei in these ploidy categories using Microsoft Excel.

3.2.3 Using the BD LSR II for Analysis of Nuclei Stained with DNA Fluorochromes or Expressing Fluorescent Proteins

We have previously described how to use this instrument for the analysis of the nuclear DNA contents of plant homogenates stained with PI, and for homogenates prepared from transgenic plants accumulating nuclear GFP [2]. Here we describe comparable methods for the analysis of mammalian tissue homogenates, in this case from transgenic mice expressing nuclear-targeted GFP and non-transgenic controls [4].

1. Power on the instrument and allow it to warm up. Empty the waste tank and refill the sheath tank as required. Launch the BD FACSDiva software and perform validation of the cytometer using calibration beads.

2. Create an acquisition panel that comprises two bivariate dot plots (log PI or log DAPI area versus 90° light scatter, and log PI or log DAPI area versus log GFP area) and one linear histogram (PI or DAPI area). The fluorescence signals in the histogram panel are defined by the following laser excitation parameters and filter combinations: (a) GFP: excitation at 488 nm (20 mW) and detection with a 525/50 bandpass (BP) filter, (b) PI: excitation at 532 nm (150 mW) and detection with a 660/20 nm BP filter, and (c) DAPI: excitation at 355 nm (60 mW) and detection with a 450/50 nm BP filter. Trigger on DAPI or PI fluorescence as appropriate for the specific experiments.
3. Adjust the photomultiplier HV and amplification settings to bring the population of nuclei into the midranges of the dot plots. Apply threshold to the PI or DAPI fluorescence signal and adjust its magnitude to eliminate the debris appearing in these plots without impairing detection of the (more fluorescent) nuclei. Typical settings are: FSC 550 V, SSC 264 V, GFP channel 302 V, DAPI channel 267 V, and PI channel 570 V.
4. Operate the flow cytometer at the "LO" flow rate (12 μL sample/min), representing a data acquisition rate of 200–500 events/s. Collect data to a total count of >2000 nuclei/sample, and analyze using FACSDiva, or export in the form of FCS3.0 files for analysis using other comparable software packages such as NovoExpress (ACEA Biosciences, San Diego) (Fig. 4). Compensation is not necessary in this situation (*see* **Note 4**).
5. Place a polygonal gate around the area containing nuclei found within the biparametric density plots, noting that the nuclei occupy very discrete regions of the biparametric plots (Fig. 4a, e, Regions R1-R4) with debris comprising an amorphous region below, and derive gated uniparametric histograms of GFP and DAPI (or GFP and PI, data not shown; *see* ref. 4). A bi-range gate can then be used to enumerate the proportions of GFP-negative and GFP-positive nuclei for each sample.

3.3 Flow Sorting of Nuclei

We use as an example the sorting of mammalian tissue homogenates from transgenic mice pancreas expressing nuclear-targeted GFP and from non-transgenic B6 mice used as a negative control [4]. The following procedures are specific to the BD Biosciences FACSAria IIu for the detection of PI and GFP fluorescence or DAPI and GFP fluorescence in the nucleus. This method is applicable to other platforms with only slight instrument-specific modifications.

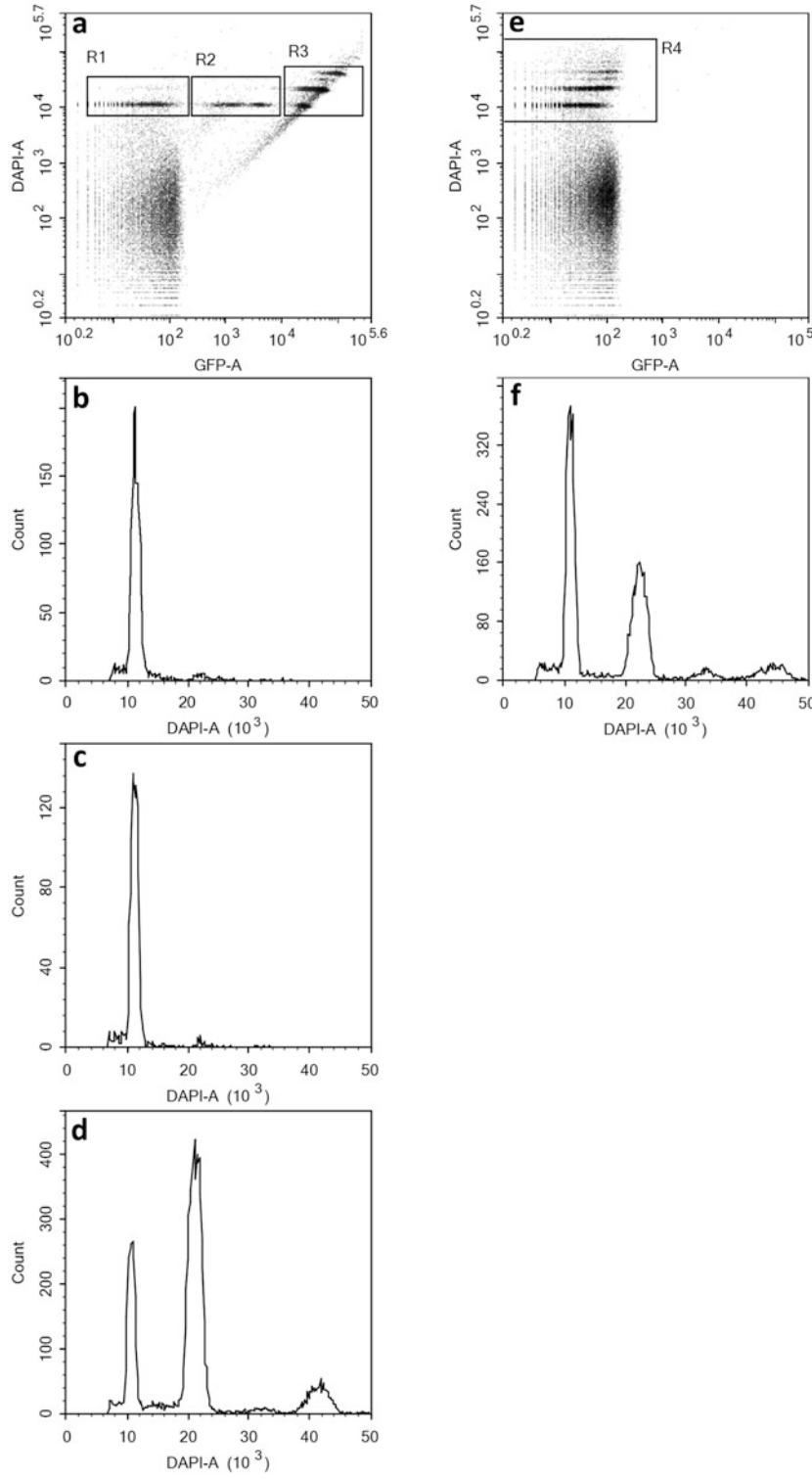

Fig. 4 Flow cytometric analysis of homogenates prepared from a transgenic mouse pancreas expressing a histone-GFP fusion protein. (**a**–**d**) and from a control (non-transgenic) mouse (**e**, **f**) using the LSR II flow cytometer. (**a**, **e**) Biparametric analysis of DAPI fluorescence (pulse area signal) versus GFP (pulse area signal).

1. Power on the instrument and allow it to warm up for at least 30 min before the start of sorting and data collection. Launch the BD FACSDiva software and check the performance of the sorter according to the manufacturer's specifications.
2. Set up the experiment with an acquisition panel comprising two bivariate dot plots (log PI or log DAPI area versus 90° light scatter, and log PI or log DAPI area versus log GFP area), and one linear histogram (PI or DAPI area). AcGFP/EGFP Flow Cytometer Calibration Beads are used to define cytometer settings for sorting of Green Fluorescent nuclei.
3. The fluorescence signals in the histogram panel are defined by the following laser excitation parameters and filter combinations: (a) PI: excitation at 532 nm (13 mW) and detection with a 610/20 nm BP filter, (b) GFP: excitation at 488 nm (13 mW) and detection with a 530/30 BP filter, and (c) DAPI: excitation at 407 nm (10 mW) and detection with a 450/40 nm BP filter. Amplification settings are typically as follows: FCS 269 V, SSC 258 V, GFP channel 313 V, and PI channel 439 V.
4. Employ slow flow rate (e.g., 1927 events/s) for sorting. Trigger on PI or DAPI fluorescence as appropriate for the specific experiments. Use FACSDiva for analysis or export the data as FCS3.0 files for analysis using other software packages.
5. Immediately prior to sorting, clean the instrument with bleach followed by 100% ethanol and DEPC-treated water. Adjust the sorting module to sort one green nucleus into the center of each designated well of a 96-well plate. Verify the exact positioning of the sorted droplet in the center of each well by sorting one AcGFP/EGFP Flow Cytometer Calibration Bead onto an empty 96-well plate tightly covered with parafilm. Adjust the sorting module if the position of the tiny spot is not centered on each well.
6. Dispense 7 μL of RNA*later*® into each well prior to sorting PI- or DAPI-stained nuclei into a 96-well plate. Sort one nucleus per well.

Fig. 4 (continued) The pancreatic nuclei are found in the three regions denoted R1, R2, and R3, in proportions of 11.4, 10.3, and 78.3%. (**b**) Uniparametric analysis (DAPI fluorescence, linear scale) of the nuclei in R1. (**c**) Uniparametric analysis (DAPI fluorescence, linear scale) of the nuclei in R2. (**d**) Uniparametric analysis (DAPI fluorescence, linear scale) of the nuclei in R3. (**f**) Uniparametric analysis (DAPI fluorescence, linear scale) of the nuclei in R4 (from [4])

3.4 Extraction of polyA$^+$ RNA from Flow-Sorted Single Nuclei and Amplification of DS-cDNA

Synthesis of double-stranded cDNA (DS-cDNA) from single nuclei can be performed using the REPLI-g WTA Single Cell Kit, which conveniently accommodates a 96-well plate format for the sorted nuclei. The RNA synthesis kit provides a simple and consistent means to generate DS-cDNA suitable to use for downstream qPCR and NextGen sequencing. This protocol merges information taken from the Qiagen Single Cell Handbook and Tang et al. [30]. The complete protocol takes about 4 h after sorting the single nuclei.

1. Single PI- or DAPI-stained nuclei are sorted from homogenates of organs of non-transgenic B6 mice or of transgenic mice expressing nuclear-targeted GFP into each well of a 96-well plate. Immediately add 4 μL of lysis buffer to each well and mix the plate by vortexing, followed by centrifugation at 218 × *g* for 30 s. Continue incubation at 24 °C for 5 min, followed by heating to 95 °C for 3 min in a PCR thermocycler. Cool the reaction mixture on ice.
2. Add 2 μL of gDNA Wipeout Buffer to each well and mix the plate by vortexing, followed by centrifugation at 218 × *g* for 1 min. Incubate the plate at 42 °C for 10 min in a PCR thermocycler.
3. Prepare the Quantiscript RT mix as follows:

Component	Volume/ reaction (1×)	Total volume for a 96-well plate (100×)[a]
RT/polymerase buffer	4 μL	400 μL
Oligo dT primer	1 μL	100 μL
Quantiscript RT enzyme mix	1 μL	100 μL
Total volume	6 μL	600 μL for a 96-well plate, add 6 μL/well

[a]Scaled up according to the number of reactions

4. Add 6 μL of Quantiscript RT mix to each well. After vortexing and centrifugation at 218 × *g* for 1 min, incubate the plate at 42 °C for 60 min. Stop the reaction by incubating at 95 °C for 3 min, followed by cooling on ice.

5. Prepare the ligation mix as follows:

Component	Volume/reaction (1×)	Total volume for a 96-well plate (100×)[a]
Ligase buffer	8 μL	800 μL
Ligase mix	2 μL	200 μL
Total volume	10 μL	1000 μL for a 96-well plate, add 10 μL/well

[a]Scaled up according to the number of reactions

6. Add 10 μL of freshly prepared ligation mix to the RT reaction from **step 4**, followed by vortexing and centrifugation at 218 × *g* for 1 min.
7. Continue incubation at 24 °C for 30 min. Stop the reaction by incubation at 95 °C for 5 min, followed by cooling on ice.
8. Prepare the REPLI-g SensiPhi amplification mix as follows:

Component	Volume/ reaction (1×)	Total volume for a 96-well plate (100×)[a]
REPLI-g reaction buffer	29 μL	2900 μL
REPLI-g SensiPhi DNA polymerase	1 μL	100 μL
Total volume	30 μL	3000 μL for a 96-well plate, add 30 μL/well

[a]Scaled up according to the number of reactions

9. Add 30 μL of the freshly prepared REPLI-g SensiPhi amplification mix to the ligation reaction, followed by vortexing and centrifugation at 218 × *g* for 30 s. Continue incubation at 30 °C for 2 h. Stop the reaction by incubating at 65 °C for 5 min, followed by cooling on ice. If not to be used immediately, store the amplified cDNA at −20 °C at a minimum concentration of 100 ng/μL.

3.5 Quantitative RT-PCR Analysis and cDNA Sequencing

The amplified cDNA can be directly incorporated into sequencing pipelines following procedures specific for the individual NextGen sequencing platform. NextGen cDNA sequencing, although consistently ramping down in costs over time, nevertheless represents a significant consumption of resources both in terms of machine time, and with respect to the downstream bioinformatics overhead. For these reasons, it is prudent to employ qPCR as a pre-screen for nuclei of interest, based on the steady-state levels of transcripts that are indicative of cell-of-origin, thereby avoiding repetitive sequencing of nuclei that are not of experimental interest. This protocol is illustrated for mouse pancreatic nuclei individually sorted from organ homogenates [4].

1. Design primers for the gene sequences using IDT PrimerQuest tools. In this example, screening was done for expression from the following sequences:

Primer name	Oligo sequence (5′-3′) Forward	Oligo sequence (5′-3′) Reverse	Size (bp)
B2M	CCACTGAGACTGATACATACGC	CTTGATCACATGTCTCGATCCC	91
EGFP	ACGTAAACGGCCACAAGTTC	AAGTCGTGCTGCTTCATGTG	187
Linker-H2B	GGTTATTGTGCTGTCTCATCATTT	CAGACTTCGCTGGCTCTG	106
Amylase	CTGGATTGGACCACCCAATAA	TCCTGATTTGACGCCATCTG	110
Albumin	GCTGCAAGAAACCTAGGAAGA	GGTTCAGGATTGCAGACAGATA	110

β2 microglobulin (B2M) is a housekeeping gene, its protein product being present on all nucleated cells. EGFP allows detection of transcripts encoding a nuclear targeted (histone EGFP) gene fusion. The Linker-H2B primer allows detection of a *Pdx1/Cre*-mediated Floxed-OUT transcript. The cell-specific amylase primer detects nuclei from acinar cells, and the albumin primer provides an organ-specific (liver positive, pancreas negative) control. For more details, *see* Samadder et al. [4].

2. Prepare qRT-PCR amplification mix as follows:

Component	Volume/reaction (1×) (μL)	Total volume for a 96-well plate (15×)[a] (μL)
2× power SYBR mix	10	150
cDNA from single nuclei	5	75
10 μM forward primer	2	30
10 μL reverse primer	2	30
DNase/RNase free H_2O	1	15
Total volume/ reaction	20	

[a]Scaled up according to the number of reactions

3. Dilute the amplified DNA/cDNA (*see* Subheading 3.4, **step 9**) 1:100, and use 5 μL for each 20 μL reaction assay. Perform qRT-PCR using a PCR thermocycler (e.g., ABI 7300 PCR thermocycler).

4. The PCR cycling conditions are as follows:

Stage	# of cycle	Temperature	Time
Stage 1	1	50 °C	2 min
Stage 2	1	95 °C	10 min
Stage 3	40–45	95 °C 60 °C	15 s 1 min
Stage 4 (dissociation stage)	1	95 °C 60 °C 95 °C	15 s 30 s 15 s
Stage 5	1	4 °C	End HOLD

5. Repeat the experiment 3–4 times, using *B2M* gene as a reference. Record the mean Ct values (less than 40) and calculate the standard deviations. Relative specific gene transcript levels are calculated based on the ratio of the PCR product quantity of the gene product over that of the *B2M* control. An example of identification of pancreatic nuclei according to cell type-of-origin is provided in Fig. 5.

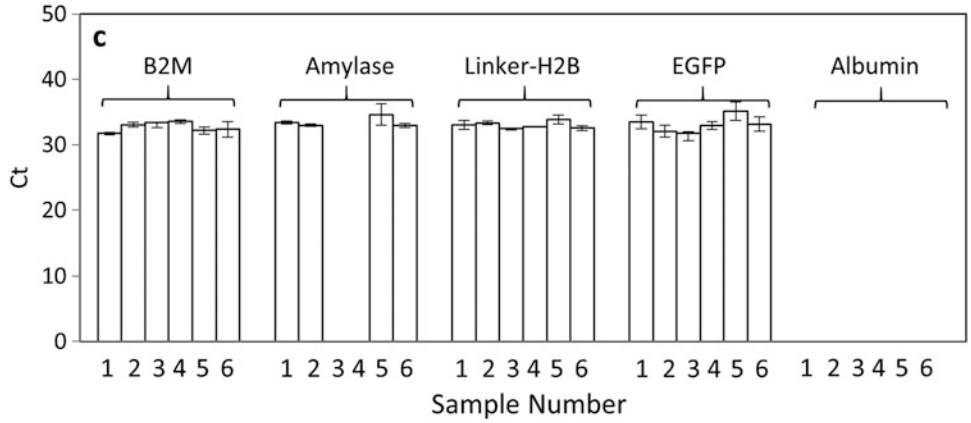

Fig. 5 Analysis of expression within flow-sorted nuclei RT-qPCR was employed for characterization of the presence or absence of transcripts corresponding to known pancreatic markers for the cell of origin, as well as to the housekeeping and transgenes (Linker-H2B and GFP). Six GFP-accumulating nuclei were singly sorted into a 96-well plate and processed for RT-PCR. "B2M" is β2-microglobulin. "Linker" depicts all transcripts from the NT-GFP locus, and "EGFP" depicts NT-GFP transcripts that encode H2B-GFP. Ct values of less than 40 were recorded. Error bars represent technical triplicates from the single nucleus. Albumin is used as an organ-specific negative control (from [4], Fig. 9c)

3.6 4-Dimensional Imaging of the Patterns of DNA Amplification Using Transformed Plants Expressing Fluorescent Protein in the Nucleus

We use as an example a Leica TCS SPE-II confocal microscope equipped with three 10 mW solid state lasers providing excitation wavelengths of 488, 532, and 635 nm, and fully tuneable emission ranges from 430 to 750 nm.

3.6.1 Image Acquisition

1. Imbibe the seeds for 3–6 h at room temperature in a petri dish on filter paper wetted to about 70–80% relative substrate moisture content. This step makes the testa softer and therefore easier to remove for observation of germination. If intact seeds are to be sown, imbibition is recommended to make them stick to the cover glass during covering by agar.
2. For germination observations, isolate the embryos using a dissecting microscope, and for seedling growth observations, use intact seeds. Place them (8–10 per chamber) on the base of Lab-Tek chamber, and cover with agar chilled to about 35–40 °C (just before solidification). Apply a thin layer of agar first and when it solidifies, add another 4 mL agar. This prevents the seeds from moving away from the cover glass.
3. Incubate the chambers for the desired period of time (*see* **Note 5**) at room temperature.
4. Switch on the Leica TCS SPE-II confocal microscope and its computer. Start the LAS AF software and, in the Configuration Panel, activate the laser appropriate for excitation of the Fluorescent Protein present in the transgenic Arabidopsis line you are using (e.g., 488 nm for GFP, and 532 nm for YFP or RFP). In the Acquire Panel, load the setting for this Fluorescent Protein and set the Acquisition Mode for xyzt.
5. Place the Lab-Tek chamber on the stage and find the region of interest under bright field illumination. Switch to fluorescence illumination provided by the mercury lamp system to check the expression of the Fluorescent Protein.
6. Using live acquisition, set the beginning and end positions for Z-stack collection, a Z-step size of about 1 μm and a time interval of 15 min. Collect the images (*see* **Note 6**).

3.6.2 Image Analysis

1. Create movies using the 3D and Process Tools of LAS AF.
2. The files produced by LAS AF can be used directly by Imaris (Bitplane Scientific Software; Fig. 6b) or after transferring them as AVI or MOV files by the Image J (NIH) software. Both the area and the volume measurements can be employed to establish the ploidy of the recorded nuclei.

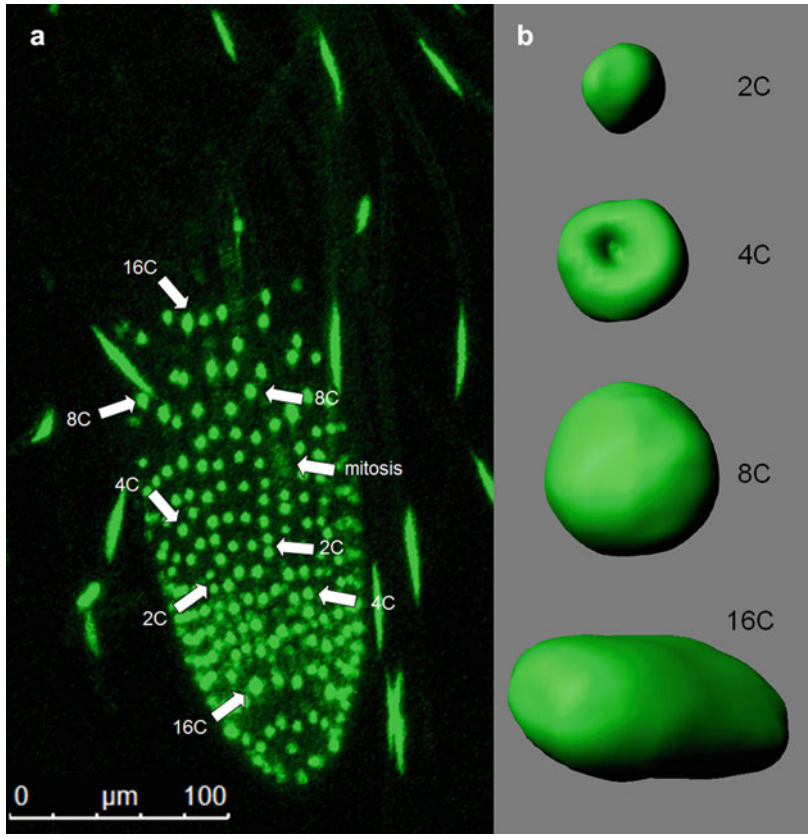

Fig. 6 Confocal imaging of the root cap of the transgenic line NLS-GFP-GUS of an *Arabidopsis thaliana* 3-day-old seedling. (**a**) Identification of nuclei at various stages of endoreduplication. (**b**) Nuclei of different ploidies after volume rendering using the Imaris software

3. For classification of nuclei, measure the size of the 2C and 4C nuclei using dividing cells. The DNA content in the nucleus just before mitosis is 4C and after the division 2C. Flow cytometric analysis provides information on the highest ploidy in the studied tissue. Based on these data, assess the sizes corresponding with particular ploidies and prepare maps of nuclei ploidies at a few time points (Fig. 6a). This allows tracking of DNA synthesis over time.

4 Notes

1. Homogenization issues. The described method of tissue homogenization features extreme simplicity and rapidity. No centrifugation steps are involved, which minimizes non-specific nuclear aggregation. The chopping process, which is done

using an ice-cold chopping buffer, arrests cellular biochemical processes at the point of cell disruption. The slicing open of cells, since it occurs randomly across the tissue or organ, therefore randomly samples the nuclei. Further, since the nuclei are in general much smaller than the cells, they are less likely to be damaged by the chopping.

2. Nuclear fluorochrome considerations. For analysis of the transcriptional state of flow-sorted nuclei, the RNAase treatment employed with PI staining for quantitative nuclear DNA content determinations must be eliminated. This means that the fluorescent signal produced by the nuclei corresponds to a composite measure of DNA and of double-stranded nuclear RNA. Interestingly, the CVs of the major peaks in the uniparametric fluorescence distributions are not seriously degraded by omitting RNAase.
3. Triggering on fluorescence during flow data acquisition. When used for analysis of cell suspensions, data acquisition by flow cytometers is generally triggered by some combination of the forward-angle and 90°–light scatter signals. This is because all cells in the suspension produce scatter signals, with only a minority of these producing fluorescent signals according to the specificity of the fluorescent stains that are used. When used for analysis of cellular homogenates, as we describe, triggering on light scatter has significant problems. Most of the light scattering signals detected by the flow cytometer originate from cellular organelles and subcellular debris in the homogenate, with the nuclei of interest representing a very minor proportion. If triggering is enabled on light scatter, the resultant high rate of triggering overwhelms the data acquisition circuitry. In contrast, triggering on fluorescence eliminates from consideration all non-fluorescent debris, which is simply ignored by the instrument. The flow cytograms of plant and animal homogenates stained with nuclear fluorochromes are broadly similar, although differences will be seen in the background debris associated with the presence of unique organelle classes (e.g., chloroplasts in plant homogenates prepared from photosynthetic organs). The position in flow fluorescence-space of the nuclei is easy to establish for both animal and plant homogenates, since the nuclei produce very discrete signals (CVs of DNA fluorescence that are typically less than 5%), and so provide easily identifiable regions on two-dimensional dot-plots. Typical activities observed in the operation of the cell division cycle, and sometimes the endoreplication cycle, provide further confirmation of the correct identification of the positions of the nuclei.
4. Compensation. Appropriate selection of fluorochromes and excitation and detection wavelengths allows identification of

settings under which compensation is not required. Thus, in Fig. 4 the observation that the nuclear DNA contents (DAPI fluorescence intensities) are the same for GFP-accumulating and non-transgenic control nuclei indicates little to no fluorescence spill-over between the two detection channels.

5. Timing for germination/seedling growth observations. Each seed lot exhibits a unique speed of germination which can vary significantly between lots. Therefore, before starting the experiment on studying germination and/or seedling growth, the timing of the phases: (a) testa rupture, (b) endosperm rupture, (c) radicle protrusion, and (d) collet hairs development should be established. This simplifies preparing a schedule for the experiment.
6. Collection of images. While the seed axis/seedling root elongates, the region of interest is usually moving. Therefore, the stage (after switching off scanning) has to be moved from time to time to track the same nuclei.

Acknowledgments

Development of methods for flow analysis and sorting of mouse organ nuclei was done with support from the National Cancer Institute of the U.S. National Institutes of Health (awards number R21 CA164690, and P30 CA023074) and the Arizona Department of Health (ABRC ABC 13530).

References

1. Galbraith DW, Harkins KR, Maddox JM, Ayres NM, Sharma DP, Firoozabady E (1983) Rapid flow cytometric analysis of the cell cycle in intact plant tissues. Science 220 (4601):1049–1051. doi:10.1126/science.220.4601.1049
2. Galbraith DW, Lambert GM (2012) High-throughput monitoring of plant nuclear DNA contents via flow cytometry. Methods Mol Biol 918:311–325. doi:10.1007/978-1-61779-995-2_16
3. Zhang C, Gong FC, Lambert GM, Galbraith DW (2005) Cell type-specific characterization of nuclear DNA contents within complex tissues and organs. Plant Methods 1(1):7. doi:10.1186/1746-4811-1-7
4. Samadder P, Weng N, Doetschman T, Heimark RL, Galbraith DW (2016) Flow cytometry and single nucleus sorting for Cre-based analysis of changes in transcriptional states. Cytometry A 89(5):430–442. doi:10.1002/cyto.a.22847
5. Galbraith DW, Janda J, Lambert GM (2011) Multiparametric analysis, sorting, and transcriptional profiling of plant protoplasts and nuclei according to cell type. Methods Mol Biol 699:407–429. doi:10.1007/978-1-61737-950-5_20
6. Nagl W (1976) DNA endoreduplication and polyteny understood as evolutionary strategies. Nature 261(5561):614–615
7. Gendreau E, Traas J, Desnos T, Grandjean O, Caboche M, Hofte H (1997) Cellular basis of hypocotyl growth in Arabidopsis thaliana. Plant Physiol 114(1):295–305
8. Dilkes BP, Dante RA, Coelho C, Larkins BA (2002) Genetic analyses of endoreduplication in Zea mays endosperm: evidence of sporophytic and zygotic maternal control. Genetics 160(3):1163–1177
9. Sliwinska E (2009) Nuclear DNA replication and seed quality. Seed Sci Res 19:15–25

10. Sliwinska E, Mathur J, Bewley JD (2012) Synchronously developing collet hairs in Arabidopsis thaliana provide an easily accessible system for studying nuclear movement and endoreduplication. J Exp Bot 63 (11):4165–4178. doi:10.1093/jxb/ers099
11. D'Amato F (1984) Role of polyploidy in reproductive organs and tissues. In: Johri BM (ed) Embryology of angiosperms. Springer, Berlin, pp 519–566
12. Galbraith DW, Harkins KR, Knapp S (1991) Systemic Endopolyploidy in Arabidopsis thaliana. Plant Physiol 96(3):985–989
13. Brown JK, Lambert GM, Ghanim M, Czosnek H, Galbraith DW (2005) Nuclear DNA content of the whitefly Bemisia tabaci (Aleyrodidae: Hemiptera) estimated by flow cytometry. Bull Entomol Res 95(4):309–312
14. Galbraith DW (2009) Simultaneous flow cytometric quantification of plant nuclear DNA contents over the full range of described angiosperm 2C values. Cytometry A 75 (8):692–698. doi:10.1002/cyto.a.20760
15. Grindberg RV, Yee-Greenbaum JL, McConnell MJ, Novotny M, O'Shaughnessy AL, Lambert GM, Arauzo-Bravo MJ, Lee J, Fishman M, Robbins GE, Lin X, Venepally P, Badger JH, Galbraith DW, Gage FH, Lasken RS (2013) RNA-sequencing from single nuclei. Proc Natl Acad Sci U S A 110(49):19802–19807. doi:10.1073/pnas.1319700110
16. Zhang C, Barthelson RA, Lambert GM, Galbraith DW (2008) Global characterization of cell-specific gene expression through fluorescence-activated sorting of nuclei. Plant Physiol 147(1):30–40. doi:10.1104/pp.107.115246
17. Barthelson RA, Lambert GM, Vanier C, Lynch RM, Galbraith DW (2007) Comparison of the contributions of the nuclear and cytoplasmic compartments to global gene expression in human cells. BMC Genomics 8:340. doi:10.1186/1471-2164-8-340
18. Jacob Y, Michaels SD (2008) Peering through the pore: the role of AtTPR in nuclear transport and development. Plant Signal Behav 3 (1):62–64
19. Haenni S, Ji Z, Hoque M, Rust N, Sharpe H, Eberhard R, Browne C, Hengartner MO, Mellor J, Tian B, Furger A (2012) Analysis of C. elegans intestinal gene expression and polyadenylation by fluorescence-activated nuclei sorting and 3′-end-seq. Nucleic Acids Res 40 (13):6304–6318. doi:10.1093/nar/gks282
20. Deal RB, Henikoff S (2010) A simple method for gene expression and chromatin profiling of individual cell types within a tissue. Dev Cell 18 (6):1030–1040. doi:10.1016/j.devcel.2010.05.013
21. Deal RB, Henikoff S (2011) The INTACT method for cell type-specific gene expression and chromatin profiling in Arabidopsis thaliana. Nat Protoc 6(1):56–68. doi:10.1038/nprot.2010.175
22. Paddock SW (1999) An introduction to confocal imaging. Methods Mol Biol 122:1–34
23. Sliwinska E, Mathur J, Bewley JD (2015) On the relationship between endoreduplication and collet hair initiation and tip growth, as determined using six Arabidopsis thaliana root-hair mutants. J Exp Bot 66 (11):3285–3295. doi:10.1093/jxb/erv136
24. Sliwinska E, Bassel GW, Bewley JD (2009) Germination of Arabidopsis thaliana seeds is not completed as a result of elongation of the radicle but of the adjacent transition zone and lower hypocotyl. J Exp Bot 60 (12):3587–3594. doi:10.1093/jxb/erp203
25. Murashige T, Skoog F (1962) A revised medium for rapid growth and bioassays with tobacco tissue cultures. Physiol Plant 15:473–497
26. Silcock DJ, Francis D, Bryant JA, Hughies SG (1990) Changes in nuclear DNA content, cell and nuclear size, and frequency of cell division in the cotyledons of *Brassica napus* L. during embryogenesis. J Exp Bot 41:401–407
27. Sugimoto-Shirasu K, Roberts K (2003) "Big it up": endoreduplication and cell-size control in plants. Curr Opin Plant Biol 6(6):544–553
28. Jovtchev G, Schubert V, Meister A, Barow M, Schubert I (2006) Nuclear DNA content and nuclear and cell volume are positively correlated in angiosperms. Cytogenet Genome Res 114(1):77–82. doi:10.1159/000091932
29. Davidson D, Pertens E, Eastman M (1978) Nuclear and cell sizes in different regions of root meristems of *Zea mays*. Ann Bot 42:1429–1438
30. Tang F, Barbacioru C, Wang Y, Nordman E, Lee C, Xu N, Wang X, Bodeau J, Tuch BB, Siddiqui A, Lao K, Surani MA (2009) mRNA-Seq whole-transcriptome analysis of a single cell. Nat Methods 6(5):377–382. doi:10.1038/nmeth.1315

Chapter 17

Flow Cytometric FRET Analysis of Protein Interactions

László Ujlaky-Nagy, Péter Nagy, János Szöllősi, and György Vereb

Abstract

In the past decades, investigation of protein–protein interactions in situ in living or intact cells has gained expanding importance as structure/function relationships proposed from bulk biochemistry and molecular modeling experiments required confirmation at the cellular level. Förster (fluorescence) resonance energy transfer (FRET)-based methods are excellent tools for determining proximity and supramolecular organization of biomolecules at the cell surface or inside the cell. This could well be the basis for the increasing popularity of FRET. In fact, the number of publications exploiting FRET has exploded since the turn of the millennium. Interestingly, most applications are microscope-based, and only a fraction employs flow cytometry, even though the latter offers great statistical power owed to the potentially huge number of individually measured cells. However, with the increased availability of multi-laser flow cytometers, strategies to obtain absolute FRET efficiencies can now be relatively facilely implemented. In this chapter, we intend to provide generally useable protocols for measuring FRET in flow cytometry. After a concise theoretical introduction, recipes are provided for successful labeling techniques and measurement approaches. The simple, quenching-based population-level measurement, the classic ratiometric, intensity-based technique providing cell-by-cell actual FRET efficiencies, and a more advanced version of the latter, allowing for cell-by-cell autofluorescence correction are described. An Excel macro pre-loaded with spectral data of the most commonly used fluorophores is also provided for easy calculation of average FRET efficiencies. Finally, points of caution are given to help design proper experiments and critically interpret the results.

Key words Förster resonance energy transfer, Fluorescence resonance energy transfer, Flow cytometry, Protein interactions, Molecular proximity, FCET

1 Introduction

Modern biochemistry and molecular biology have served to identify hundreds of pairs of cellular proteins that are in vitro capable of interacting with each other. These protein–protein interactions are crucial in both maintaining the stable "resting" state of cells and in driving activation processes that allow cells to respond to external

Electronic supplementary material: The online version of this chapter (doi:10.1007/978-1-4939-7346-0_17) contains supplementary material, which is available to authorized users. This is also available under the link: http://biophys.med.unideb.hu/FRETcalc.

Teresa S. Hawley and Robert G. Hawley (eds.), *Flow Cytometry Protocols*, Methods in Molecular Biology, vol. 1678, DOI 10.1007/978-1-4939-7346-0_17, © Springer Science+Business Media LLC 2018

stimuli. Hence it becomes more and more important to be able to detect such interactions in situ inside or on the surface of cells. Fluorescence techniques are widely used to quantify molecular parameters of various biochemical and biological processes in vivo because of their inherent sensitivity, specificity, and temporal resolution. The combination of fluorescence spectroscopy with flow cytometry provided a solid basis for rapid and continuous improvements in these technologies. A major asset in studying molecular level interactions was the application of Förster resonance energy transfer (FRET) to cellular systems. Applying fluorescently labeled antibodies, proteins, lipids, or other biomolecules either using organic dyes or fluorescent fusion proteins, the FRET technique can be used to determine inter- and intra-molecular distances of cell surface components in biological membranes, as well as molecular associations inside live or intact cells. Excellent reviews are available on the applicability of FRET to biological systems as well as descriptions and comparison of various approaches. Only a few are quoted here [1–6].

FRET is a special phenomenon in fluorescence spectroscopy during which energy is non-radiatively transferred from an excited *donor* molecule to an *acceptor* molecule (Fig. 1) [7]. For the process to occur, a set of conditions have to be fulfilled:

1. The emission spectrum of the donor has to overlap with the absorption spectrum of the acceptor. The larger the overlap, the higher the rate of FRET is.
2. The emission dipole vector of the donor and the absorption dipole vector of the acceptor need to be close to parallel. The rate of FRET decreases as the angle between the two vectors increases. In biological situations where molecules are free to move (rotate), we generally assume that dynamic averaging takes place, i.e., the donor and the acceptor assume many possible steric positions during the excited state lifetime of the donor, among them those that can yield an effective transfer of energy. There are cases when the aforementioned assumption of dynamic averaging is most likely correct (e.g., antibodies labeled by fluorescent dyes bound to the antibody via flexible linkers), however in some cases it is certainly incorrect (e.g., fluorescent dyes intercalated into DNA). FRET taking place between proteins tagged by GFP (green fluorescent protein) or its derivatives represents an intermediate case in which the assumption of dynamic averaging is a relatively good approximation.
3. The distance between the donor and acceptor should be between 1 and 10 nm.

This latter phenomenon is the basis of the popularity of FRET in biology: The distance over which FRET occurs is small enough

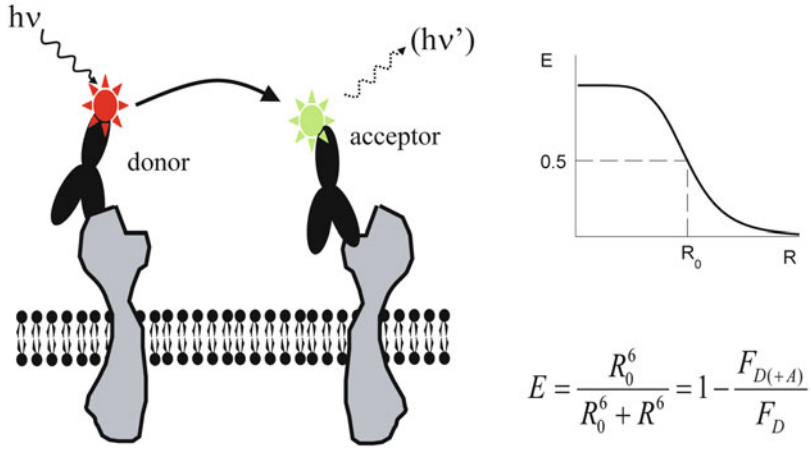

Fig. 1 FRET basics. In FRET, an excited fluorescent molecule, called *donor*, donates energy to an *acceptor* molecule by a dipole-dipole resonance energy transfer mechanism. The acceptor then may emit this energy as a photon, provided it is fluorescent. The usual term for characterizing the efficiency of FRET is E, which is the ratio of excited-state donor molecules relaxing by FRET to the total number of excited donors. A simple way to assess this ratio is to measure donor fluorescence in the absence (F_D) and in the presence ($F_{D(+A)}$) of an acceptor, to obtain $E = 1 - F_{D(+A)}/F_D$. The rate of energy transfer is dependent on the negative sixth power of the distance R between the donor and the acceptor, resulting in a sharply dropping curve when plotting E against R, centered around R_0. R_0 is the distance where $E = 0.5$, that is, where there is a 50% chance that the energy of the excited donor will be transferred to the acceptor. As the separation between the donor and acceptor increases, E decreases, and at $R = 2R_0E$ is already getting negligible

to characterize the proximity of possibly interacting molecules, under special circumstances it even provides quantitative data on exact distances, and, additionally, information on the spatial orientation of molecules or their domains. Hence the very apropos term from Stryer, who equaled FRET to a "spectroscopic ruler" [8]. The usual term for characterizing the efficiency of FRET is E, which is the ratio of excited state donor molecules relaxing by FRET to the total number of excited donors. The rate of the energy transfer process is dependent on the negative sixth power of the distance between the donor and the acceptor, resulting in a sharply dropping curve, practically eliminating FRET above a separation of 10 nm for the usual fluorophores (Fig. 1). Conversely, as the distance reaches values below 1 nm, strong ground-state interactions or transfer by exchange interactions become dominant at the expense of FRET [9].

The occurrence of FRET has profound consequences on the fluorescence properties of both the donor and the acceptor. An additional de-excitation process is introduced in the donor, which decreases the fluorescence lifetime and the quantum efficiency of the donor, rendering it less fluorescent. The decrease in donor fluorescence (often termed *donor quenching*) can be one of the most facilely measured spectroscopic characteristics that indicate

the occurrence of FRET. Additionally, since the acceptor is excited as a result of FRET, those acceptors that are fluorescent will emit photons (proportional to their quantum efficiency) also when FRET occurs. This is called *sensitized emission* and can also be a good measure of FRET.

Flow cytometric FRET (FCET) methods that can be implemented on commercial flow cytometers exploit one or both of these phenomena. The main advantage carried by the flow cytometric approach is the ability to examine large cell populations in a short time, and still providing FRET efficiency values up to single cell resolution. While the flow cytometric approach inherently results in averaging the fluorescence over each cell, it is less prone to errors originating from low signal-to-noise ratios. Overall, the joint use of flow cytometric and microscopic FRET approaches can vastly enhance our understanding of certain biological systems, especially when interactions among more than two molecules need to be considered, and/or the interactions change upon detachment or attachment of the cells [10–12].

In a simplified scenario, population averages from the flow cytometer can be used to estimate an overall FRET efficiency for the whole cell population measured. While in theory there are at least 22 different possible approaches to quantifying FRET [13], some of these have never been tested, and many require a (usually microscope-based) system where cells or their compartments can be revisited once or several times for completing the measurement. Among the eight approaches applicable to flow cytometry, most require extensive modification of the equipment. The majority of these methods are based on the measurement of conventional hetero-FRET in which spectroscopically different donor and acceptor molecules interact with each other. However, there is another modality of FRET, which takes place between identical fluorophores, i.e., when the donor and acceptor fluorophores are of the same kind. The only manifestation of this phenomenon, called homo-FRET, is the decreased fluorescence anisotropy of the fluorophore population. Although instruments capable of recording polarized fluorescence intensities do not abound, the measurement of homo-FRET makes the quantitative analysis of large-scale protein clusters possible, since the fluorescence anisotropy changes inversely with the average number of proteins in a cluster [14, 15]. Measuring anisotropy can also be useful in hetero-FRET systems, as it offers higher sensitivity for assessing conformational changes at the nano-scale, due to the simultaneous detection of changes of proximity and relative orientations of the FRET donor and acceptor [16, 17].

Another type of modification to flow cytometers, which allows for the measurement of fluorescence lifetimes, opens a new window on flow cytometric FRET measurements. Lifetime-based FRET measurements obviate the need to quantitate the acceptor, and

provide absolute FRET efficiencies based on the decrease of donor lifetime in the presence of the acceptor. The utility of lifetime-based FRET measurements has recently been demonstrated for microfluidics-based flow cytometry [18], and a commercially available flow cytometer capable of measuring fluorescence lifetime has been applied to FRET-based high-throughput screening of caspase activity [19].

The approaches discussed in this chapter are based on hetero-FRET; the simple donor quenching-based FCET method, as well as the more complex, but fully quantitative ratiometric, intensity-based FCET have already been extensively and successfully applied to biological systems. Finally, we shall describe a modification of the latter approach that allows a cell-by-cell correction for autofluorescence, and thus can reduce the uncertainty of the quantitative determination of FRET when fluorescence signals are low. The necessary mathematical details will be introduced along with the measurement procedure, so that the importance and utility of the various control samples can be fully appreciated. An Excel spreadsheet is also provided to allow the quick and easy calculation of intensity-based FRET efficiencies from ensemble averages. The methods introduced herein can also be used for quantitating interactions among three different molecular entities labeled with three spectrally distinct appropriate fluorophores (for details please *see* [20]).

2 Materials

2.1 Cellular Systems

1. The easiest targets of FCET measurements are cells growing in suspension such as those of lymphoid origin that can directly be labeled in suspension.
2. Cells that grow attached to substratum need to be trypsinized. Use a trypsin-EDTA solution that is appropriate for the cell line examined. Usually, 0.05% w/v trypsin and 2 mM EDTA work well, but cells that have spent a longer time in the same culture dish or express a massive extracellular matrix may need a more vigorous treatment. In our experience, a 5 min trypsin-EDTA treatment does not decrease cell surface receptor levels by more than 5%.

2.2 Fluorophores

1. The choice of fluorophore must be appropriate for the lasers of the flow cytometer to be used [21], the availability of labeled antibodies, compatible with other fluorophores measured co-temporarily, or the native fluorescence of the sample. Since this latter is usually more prominent in the blue-green emission region, it is advisable to use fluorophores that emit in the red and far-red spectral range [22].

Table 1
The most frequently used fluorophore pairs adequate for FRET measurements

Donor	Acceptor
Fluorescein, Alexa Fluor 488, Atto 488, FlAsH	Rhodamine (TRITC), Alexa Fluor 546, Alexa Fluor 555, Cy3, Atto 550, Alexa Fluor 594, ReAsH, Texas red
Rhodamine, Alexa Fluor 546, Alexa Fluor 555, Cy3, Atto 550, Phycoerythrin	Cy5, Cy5.5, Alexa Fluor 633, Atto 633, Alexa Fluor 647, Atto 647 N, Allophycocyanin
Alexa Fluor 594	Alexa Fluor 700
CFP and variants, such as cerulean	YFP and variants, such as Venus
eGFP	tagRFP, mCherry, and other red FPs (*see* **Note 2**)
YFP	mKATE2, mCherry, mScarlet (*see* **Note 2**)

2. The most straightforward method of labeling is using fluorophore-conjugated antibodies. If possible, direct labeling with conjugated primary antibodies should be the choice. Indirect labeling usually diminishes FRET owed to the greater separation of fluorophores in the sandwich of antibodies, but it might also be possible that FRET will occur between otherwise more distant targets if a large molecular labeling complex is built up [22]. Also, the polyclonal nature of most secondary antibodies can cause unwanted difficulties in interpreting the results.
3. Labeling the proteins of interest with fluorescent proteins is another option. While the molecular biology behind these approaches exceeds the scope of this chapter, the most useful fluorescent protein pairs are also listed in Table 1 (*see* **Notes 1** and **2**).
4. In Subheadings 2.3 and 2.4, we shall describe the use of fluorescently labeled antibodies, however, the FCET protocols described in the chapter are equally applicable to fluorescent fusion proteins, labeled substrates or toxins, and directly labeled proteins that are microinjected into cells.

2.3 Labeling Target Epitopes in the Membrane Using Fluorescent Antibodies

1. PBS (for washing): 137 mM NaCl, 3 mM KCl, 10 mM Na_2HPO_4, 1.8 mM KH_2PO_4, pH 7.4 (*see* **Note 3**).
2. PBS + 0.1% BSA (for labeling).
3. PBS + 1% formaldehyde (for fixation).
4. Fluorescently labeled antibodies, with donor and acceptor dye.

2.4 Labeling Intracellular Targets Using Fluorescent Antibodies

1. PBS (for washing).
2. PBS + 0.1% BSA + 0.1% (v/v) Triton X-100 (for permeabilization and labeling, *see* also **Note 4**).
3. PBS + 1% formaldehyde (for fixation).
4. Fluorescently labeled antibodies, with donor and acceptor dye.

2.5 Evaluation Software

For simple donor-quenching measurements (*see* Subheading 3.3), median or trimmed mean data exported from the flow cytometry program of choice can be used. For the initial evaluation of intensity-based, ratiometric FRET measurements (detailed under Subheading 3.4), one can also use the median and trimmed mean of cell populations. An Excel spreadsheet has been prepared to aid the readers of this chapter in easily calculating FRET efficiencies from such ensemble data. The spreadsheet is pre-loaded with spectral data of the most popular fluorophores and offers the selection of these fluorophores and the applied laser lines from pull-down menus. Then it leads the user through the input of necessary measurement data in logical order, to finally calculate the FRET efficiency. The spreadsheet and its instruction manual can be downloaded from http://biophys.med.unideb.hu/FRETcalc, To obtain FRET efficiencies on a cell-by-cell basis, samples can be analyzed with those flow cytometric data analysis programs that can derive further parameters from list mode data using equations. Alternatively, these calculations can be done in a spreadsheet program after obtaining the parameters needed for correction factors and exporting the list mode data from any flow cytometry program of choice. Finally, there is a custom made program [23] (available at http://biophys.med.unideb.hu/ReFLEX) which can be used to perform the complete analysis, including the calculation of necessary factors and the cell-by-cell distribution of FRET.

3 Methods

3.1 Sample Preparation and Labeling

3.1.1 Sample Preparation

1. Measurement of donor quenching caused by FRET is simple, but cannot be used for cell-by-cell data analysis of FRET efficiency. In the classical approach introduced for the cell-by-cell measurement of FRET [24–26], the donor and acceptor fluorophores are excited separately using the appropriate laser line. In a perfected approach, autofluorescence at the individual cell's level can be taken into correction during calculations, rather than using the autofluorescence histogram means [22]. This improves the dispersion of FRET histograms, but one should always remember that inherent (Poissonian and additive) measurement noise that tends to dominate at low signals (low protein expression levels) cannot be eliminated even with a cell-by-cell autofluorescence correction.

2. In general, the following samples are necessary:
   (a) Sample 1. Unlabeled cells.
   (b) Sample 2. Cells with epitope A labeled with the donor.
   (c) Sample 3. Cells with epitope A labeled with the acceptor.
   (d) Sample 4. Cells with epitope B labeled with the donor.
   (e) Sample 5. Cells with epitope B labeled with the acceptor.
   (f) Sample 6. Cells with epitope A labeled with the donor and epitope B labeled with the acceptor.
   (g) Sample 7. Cells with epitope B labeled with the donor and epitope A labeled with the acceptor.
   One of sample 3 or 5 may be omitted: The α factor (*see* later at Eqs. 4, 25 and 26) can be determined either from samples 2 and 3, or from samples 4 and 5. It is preferable, however, to determine it from both pairs of samples, as major discrepancies between the two can be a sign of the adverse effect of labeling on the binding affinity of one or more of the antibodies, or a low signal-to-noise ratio in one of the samples. If such is the case, accept the α factor derived from the more abundant molecule. The spillage factors (S, *see* Eq. 2 and onwards) can also be determined from both single labeled epitopes, but that with a higher expression is expected to yield the more reliable results (*see* **Note 5**).

   Samples 6 and 7 are complementary in the sense that they provide FRET efficiencies in "the two opposite directions," i.e. from epitope A to B, and from epitope B to A. If one epitope is expressed in great molar excess of the other, labeling that one with the acceptor yields a more efficient FRET, but interpretation can be somewhat intricate. However, if the labels can be swapped, and the measurement repeated, a more complete picture can be obtained (*see* also Subheading 3.6, **step 6**).

3. If a positive control with known molecular interactions is known, it is advisable to have another set of samples labeling these molecules on the same cell type along the principles in **step 2**. Since major histocompatibility complex (MHC) class I molecules, comprising the heavy chain and the light chain (β2 microglobulin) are expressed on many cells, and the two chains of MHC I are in close proximity, antibodies against these proteins with the same fluorophores as those against the proteins of our interest provide a useful positive control. It is best to label the light chain with donor, as not all heavy chains may be complexed with light chains, but there are no free light chains on the cell surface. Alternatively, two different monoclonal antibodies against the same protein, one carrying the

donor and the other acceptor, make a good positive control. If these positive controls do not exhibit FRET, one can most often assume that the antibodies used are in steric competition and mutually exclude each other's binding (see also Subheading 3.6, **step 2**). For such cases, an almost foolproof positive control would be to apply the first, monoclonal antibody with the donor, and then label this antibody with polyclonal secondary antibodies carrying the acceptor dye. The stochastic nature of the binding of secondary antibodies, as well as the somewhat arbitrary distribution of dye molecules on both the primary and the secondary antibodies very likely gives rise to some degree of FRET.

4. Additional information needed for the calculations:
   (a) The dye/protein molar ratio of all antibodies used.
   (b) The molar absorption coefficients of all dyes used at the wavelength of the laser applied.
   (c) The quantum efficiencies of the dyes used may be needed, if any of the fluorescence intensities used to determine the α factor is below 3–5 times the background (see Subheading 3.4, **step 5**).
5. Harvesting cells (for adherent cells only). Adherent cells grown in 75 cm^2 flasks are detached using trypsin-EDTA solution. After rinsing the flask with trypsin-EDTA twice, leave only a thin layer of it over the cells for the optimized short time. Then add 10 mL medium with FCS to stop the trypsin and restitute the calcium concentration, and homogenize the suspension by pipetting. Let cells recover for 20 min in the flask. It has been determined that after gentle trypsinization, most cell surface proteins are either unchanged or totally recovered within 20–30 min (*see* **Note 6**).

3.1.2 Labeling Extracellular Epitopes

1. Wash cells with ice-cold PBS and centrifuge suspension.
2. Repeat washing.
3. Add one million cells per sample tube and store on ice.
4. Label cells with (usually) 5–50 μg/mL final concentration of antibodies (should be above saturating concentration that was determined previously, in order to avoid crosslinking by the bivalent antibody) in 50 μL total volume of PBS–0.1% BSA mixture for 10–30 min on ice (*see* **Note 7**).
5. Wash cells twice with ice-cold PBS and centrifuge suspension.
6. Fix cells with PBS + 1% formaldehyde in 500–1000 μL.
7. Store samples in refrigerator or cold room until measurement. Samples can be stored for up to a week, and may be kept for backup even after the first measurement.

3.1.3 Labeling Intracellular Epitopes

1. Wash cells with ice-cold PBS and centrifuge suspension.
2. Repeat washing.
3. Add one million cells per sample tube and store on ice.
4. Label cells with (usually) 5–50 μg/mL final concentration of antibodies (should be above saturating concentration that was determined previously, in order to avoid crosslinking by the bivalent antibody) in 50 μL total volume of PBS–0.1% BSA–0.1% Triton X-100 for 30–120 min on ice (*see* **Note 4**).
5. Wash cells twice with ice-cold PBS–0.1% BSA–0.1% Triton X-100: fill up the tube with the wash buffer, centrifuge at 600 × *g* for 6 min, remove supernatant, fill up the tube again with the wash buffer, let unbound label diffuse out for ~5 min, and centrifuge again.
6. Fix cells with PBS + 1% formaldehyde in 500–1000 μL.
7. Store samples in refrigerator or cold room until measurement. Samples can be stored for up to a week, and may be kept for backup even after the first measurement.

3.2 Flow Cytometric Measurements

1. Before measurement, resuspend the cells with gentle shaking and if clumps are detected upon examination in the microscope, run the suspension through a fine sieve.
2. Always examine labeled cells dropped on a microscopic slide in the fluorescence microscope to verify proper cellular position (e.g., membrane) of the label.
3. Start with Sample 1 (Background) as a negative control.
4. Set FSC and SSC in linear mode so as to see your population on the scatter plot (SSC/FSC dot plot).
5. Set fluorescence channels in logarithmic mode, if wide-range linear digital acquisition is not available. Use the following fluorescence channels:
   (a) Donor excitation—Donor emission (donor channel, I_1).
   (b) Donor excitation—Acceptor emission (FRET channel, I_2).
   (c) Acceptor excitation—Acceptor emission (acceptor channel, I_3).
   (d) Donor, or independent excitation—independent emission (optional autofluorescence channel, I_4, only for Subheading 3.5) (*see* **Note 8**).

   The choice of excitation wavelengths and emission filters should be driven, in order of preference, by the optimal sensitivity of detection, including minimization of background, followed by the availability of labels that best exploit the lasers and optics at our disposal.

6. Set I_1, I_2, I_3, and I_4 voltages so that mean fluorescence intensities are about 10^1 for the unlabeled Sample 1.
7. Run Samples 2 and 4 (Donor-only) and adjust I_1, I_2, and I_4 voltages so that mean fluorescence intensities are in the acquisition range.
8. Run Samples 3 and 5 (Acceptor-only) and adjust I_2 and I_3 voltages so that mean fluorescence intensities are in the acquisition range.
9. Save instrument settings.
10. Create the following plots:
    (a) FSC/SSC dot plot.
    (b) I_1, I_2, I_3, and I_4 histograms for monitoring intensities.
    (c) I_1/I_2, I_1/I_3, and I_2/I_3 dot plots for monitoring the correlation of signals.
11. Run sample 1 and create Gate 1 on the FSC/SSC dot plot around intact cells.
12. Format plots so that only events in Gate 1 are displayed.
13. Define a statistics window to show the mean fluorescence intensities of all histograms from the gated events.
14. Set the cytometer to acquire 20,000 events.
15. Run all samples.

3.3 Quick Estimation: Donor Quenching FRET in Flow Cytometry

1. Measurement of donor quenching is probably the easiest way to perform a FRET experiment, but simplicity comes at a price. In these kinds of measurements, the *average* fluorescence intensities of two different samples (donor-labeled and double-labeled, i.e., samples 2 and 6 or samples 4 and 7 in Subheading 3.1.1, **step 2**) are compared. Therefore, FRET cannot be calculated on a cell-by-cell basis; instead, a population average is measured. It is assumed that the difference between the donor-only and the double-labeled samples is owed to the presence of the acceptor. Since it is practically impossible to meet this requirement for cells transfected with fluorescent protein variants, FRET measurements based on donor quenching can be done only on antibody-labeled cells.
2. Use the fluorescence from a donor-only labeled sample ($I_{1(2)}$) corrected for the background fluorescence in that channel ($I_{1(1)}$); as well as the fluorescence of the sample double labeled with donor and acceptor ($I_{1(6)}$) also corrected for the background fluorescence.
3. FRET efficiency is calculated as

$$E = 1 - \frac{I_{\text{Donor+Acceptor}} - I_{\text{background}}}{I_{\text{Donor}} - I_{\text{background}}} = 1 - \frac{I_{1(6)} - I_{1(1)}}{I_{1(2)} - I_{1(1)}} \quad (1)$$

Since $I_{1(2)}$ and $I_{1(6)}$ are measured on distinct samples, only the histogram means from the two populations can be considered here. This is one of the main disadvantages of the method and hence it is only suggested as a quick and rough estimate of whether FRET, and thus molecular proximity occurs. However, it is a quite useful approach when signals are low compared to background/autofluorescence (*see* **Note 9**).

3.4 Evaluation of Flow Cytometric FRET Based on Donor and Acceptor Fluorescence (Intensity-Based Ratiometric FCET)

1. Based on Monte-Carlo simulations, Berney and Danuser have suggested that in order to obtain stable FRET measurements, energy transfer is best observed in the FRET channel, i.e., by excitation of the donor and a measurement of the acceptor emission. Methods estimating FRET from the donor signal in the presence and absence of acceptor are less robust [5]. The evaluation scheme presented below relies on measuring donor quenching and sensitized acceptor emission at the same time, and provides an analytical solution to calculate not only the FRET efficiency from them, but also the corrected fluorescence intensities that could be measured if FRET did not take place.
2. In a sample labeled with both the donor and the acceptor, the intensities measured in each channel (I_1 through I_4, see Subheading 3.2, **step 5**) are composed of the contribution of donor, FRET, acceptor and autofluorescence signals to that channel, and the crosstalk signals from all or some of the other channels. In this classical approach, we shall assume that the autofluorescence in each channel does not vary much from cell to cell, and consequently we will reduce our analysis to the donor, FRET, and acceptor channels, taking their respective signals as I_1, I_2, and I_3 after subtracting the average autofluorescence (mean fluorescence of unlabeled cells) from each channel. In analysis terms, this means that $I_{1(1)}$, $I_{2(1)}$, and $I_{3(1)}$ histogram means need to be determined and subtracted as a constant from the respective list mode data for Samples 2–7. *All intensities in the following steps of Subheading 3.4. are assumed to be background corrected!*
3. On the donor-only sample that has the greater signal, determine the spectral correction factors S_1 and S_3 characterizing the spillover of donor fluorescence from the donor channel to the FRET and acceptor channels, respectively, according to the following equations (*see* **Note 10**):

$$S_1 = \frac{I_2}{I_1}, \quad S_3 = \frac{I_3}{I_1} \tag{2}$$

4. On the acceptor-only sample that has the greater signal, determine the spectral correction factors S2 and S4 characterizing the spillover of acceptor fluorescence from the acceptor

channel to the FRET and donor channels, respectively, according to the following equations (*see* **Note 10**):

$$S_2 = \frac{I_2}{I_3}, \quad S_4 = \frac{I_1}{I_3} \tag{3}$$

5. Determine factor α. Use a donor and an acceptor-labeled sample which are labeled by the same antibodies, but conjugated to the two different fluorophores. Calculate the mean background-corrected I_1 fluorescence intensity of the donor-only sample, and the mean background-corrected I_2 fluorescence intensity of the acceptor-labeled sample. Determine α according to the following equation (*see* **Note 11**):

$$\alpha = \frac{I_{2,\mathrm{a}}}{I_{1,\mathrm{d}}} \frac{\varepsilon_{\mathrm{d}} L_{\mathrm{d}} N_{\mathrm{d}}}{\varepsilon_{\mathrm{a}} L_{\mathrm{a}} N_{\mathrm{a}}} \tag{4}$$

where ε_{d} and ε_{a} are the molar absorption coefficients of the donor and the acceptor, respectively, at the donor excitation wavelength (i.e., the excitation wavelength used for I_1 and I_2), L_{d} and L_{a} are the labeling ratios (i.e., number of fluorophores per antibody), and N_{d} and N_{a} are the number of target epitopes of the donor- and acceptor-labeled antibodies, respectively. N_{d} and N_{a} can be omitted from the calculations if the simple method of labeling the same epitope once with donor-, and then with acceptor-conjugated antibody is used, as called for under Subheading 3.1.1, **step 2** (*see* also **Note 5**). The use of robust estimators of central tendency (trimmed mean, median) instead of the mean is preferable if the distribution is wide or there are outlier events significantly distorting the mean. If cells transfected with FP variants are used, a different approach has to be used for the determination of α which is described in detail elsewhere [27].

6. For the double-labeled samples, the I_1, I_2 and I_3 intensities can be expressed according to the following equations:

$$I_1 = I_{\mathrm{D}}(1 - E) + I_{\mathrm{A}} \cdot S_4 + I_{\mathrm{D}} \cdot E \cdot \alpha \cdot \frac{S_4}{S_2} \tag{5}$$

$$I_2 = I_{\mathrm{D}}(1 - E) \cdot S_1 + I_{\mathrm{A}} \cdot S_2 + I_{\mathrm{D}} \cdot E \cdot \alpha \tag{6}$$

$$I_3 = I_{\mathrm{D}}(1 - E) \cdot S_3 + I_{\mathrm{A}} + I_{\mathrm{D}} \cdot E \cdot \alpha \cdot \frac{1}{S_2} \cdot \frac{\varepsilon^{\mathrm{D}}_{\lambda\mathrm{A}} \cdot \varepsilon^{\mathrm{A}}_{\lambda\mathrm{D}}}{\varepsilon^{\mathrm{D}}_{\lambda\mathrm{D}} \cdot \varepsilon^{\mathrm{A}}_{\lambda\mathrm{A}}} \tag{7}$$

where E is the FRET efficiency, I_{D} and I_{A} are the unquenched donor and direct acceptor fluorescence intensities, ε denotes the molar absorption coefficient of the donor (D) or acceptor (A) labeled in the upper index, at the donor (λD) or acceptor (λA) excitation wavelengths.

7. From the above system of equations E can be calculated as follows:

$$E = \frac{S_2(I_2 - I_1S_1 - I_3S_2 + I_1S_2S_3 + I_3S_1S_4 - I_2S_3S_4)}{\alpha\left(\frac{\varepsilon^D_{\lambda A}\cdot\varepsilon^A_{\lambda D}}{\varepsilon^D_{\lambda D}\cdot\varepsilon^A_{\lambda A}} - 1\right)(I_2S_4 - I_1S_2) + S_2(I_2 - I_1S_1 - I_3S_2 + I_1S_2S_3 + I_3S_1S_4 - I_2S_3S_4)} \quad (8)$$

8. In most cases the above equation can be simplified by neglecting some of the constants. For example, S_3, S_4 and the $\frac{\varepsilon^D_{635}\cdot\varepsilon^A_{488}}{\varepsilon^D_{488}\cdot\varepsilon^A_{635}}$ absorption ratio are negligible for the Cy3-Cy5 donor-acceptor pair measured on a FACSCalibur (BD Biosciences, San Jose, CA). In this case the equation can be rewritten in the following form:

$$E = \frac{I_2 - I_1S_1 - I_3S_2}{I_1(\alpha - S_1) + I_2 - I_3S_2} \quad (9)$$

9. During data analysis, it is advised to follow a general scheme. First, one needs to determine the mean background intensities and the autofluorescence correction factors. Then calculate the alpha factor and spectral overspill parameters (S-factors) from the acceptor- and donor-labeled samples. With these parameters in hand, now the energy transfer efficiency can be determined on a cell-by-cell basis.

3.5 FCET with Cell-by-Cell Autofluorescence Correction

If the fluorescence intensity of the samples is comparable to autofluorescence, subtraction of a constant autofluorescence value can result in serious errors in the calculation. In a modified version of the approach described in Subheading 3.4, the fourth fluorescence intensity I_4 is used to correct for the autofluorescence of each cell [22] (*see* also **Note 12**). In addition to analysis steps described under Subheading 3.4, perform the following steps:

1. From the unlabeled Sample 1, determine factors B_1, B_2 and B_3 characterizing the spillover of autofluorescence from the autofluorescence channel to the donor, FRET and acceptor channels, respectively.

$$B_1 = \frac{I_1}{I_4}, \quad B_2 = \frac{I_2}{I_4}, \quad B_3 = \frac{I_3}{I_4} \quad (10)$$

   Note that the intensities used here are not background corrected. However, for calculating all the S factors in subsequent steps, background corrected intensities should be used.

2. For the donor-labeled sample used for calculating S_1 and S_3, also determine factor S_5 characterizing the spectral spillover of

donor fluorescence from the donor channel to the autofluorescence channel:

$$S_5 = \frac{I_4}{I_1} \tag{11}$$

3. For the acceptor-labeled sample used for assessing S_2 and S_4, also determine factor S_6 characterizing the spectral spillover of acceptor fluorescence from the acceptor channel to the autofluorescence channel:

$$S_6 = \frac{I_4}{I_3} \tag{12}$$

4. The fluorescence intensities of the double-labeled samples can be expressed by the following set of equations:

$$I = \mathrm{AF} \cdot B_1 + I_\mathrm{D}(1 - E) + I_\mathrm{A} \cdot S_4 + I_\mathrm{D} \cdot E \cdot \alpha \cdot \frac{S_4}{S_2} \tag{13}$$

$$I_2 = \mathrm{AF} \cdot B_2 + I_\mathrm{D}(1 - E) \cdot S_1 + I_\mathrm{A} \cdot S_2 + I_\mathrm{D} \cdot E \cdot \alpha \tag{14}$$

$$I_3 = AF \cdot B_3 + I_\mathrm{D}(1 - E) \cdot S_3 + I_\mathrm{A} + I_\mathrm{D} \cdot E \cdot \alpha \cdot \frac{1}{S_2} \cdot \frac{\varepsilon_{\lambda\mathrm{A}}^{\mathrm{D}} \cdot \varepsilon_{\lambda\mathrm{D}}^{\mathrm{A}}}{\varepsilon_{\lambda\mathrm{D}}^{\mathrm{D}} \cdot \varepsilon_{\lambda\mathrm{A}}^{\mathrm{A}}} \tag{15}$$

$$I_4 = AF + I_\mathrm{D}(1 - E) \cdot S_5 + I_\mathrm{A} \cdot S_6 + I_\mathrm{D} \cdot E \cdot \alpha \cdot \frac{S_6}{S_2} \tag{16}$$

where AF denotes the autofluorescence intensity of single cells, and I_1 through I_4 are the actual fluorescence values measured, without subtracting the average background.

5. The above set can be converted to a system of linear equations by substituting the variable $I_\mathrm{D} \cdot E$ by X.

$$I = AF \cdot B_1 + I_\mathrm{D} + I_\mathrm{A} \cdot S_4 + X \cdot \left(\alpha \cdot \frac{S_4}{S_2} - 1\right) \tag{17}$$

$$I_2 = AF \cdot B_2 + I_\mathrm{D} \cdot S_1 + I_\mathrm{A} \cdot S_2 + X \cdot (\alpha - S_1) \tag{18}$$

$$I_3 = AF \cdot B_3 + I_\mathrm{D} \cdot S_3 + I_\mathrm{A} + X \cdot \left(\alpha \cdot \frac{1}{S_2} \cdot \frac{\varepsilon_{\lambda\mathrm{A}}^{\mathrm{D}} \cdot \varepsilon_{\lambda\mathrm{D}}^{\mathrm{A}}}{\varepsilon_{\lambda\mathrm{D}}^{\mathrm{D}} \cdot \varepsilon_{\lambda\mathrm{A}}^{\mathrm{A}}} - S_3\right) \tag{19}$$

$$I_4 = AF + I_\mathrm{D} S_5 + I_\mathrm{A} \cdot S_6 + X \cdot \left(\alpha \cdot \frac{S_6}{S_2} - S_5\right) \tag{20}$$

6. The solution of this equation system in general can be expressed as:

$$X = \frac{\begin{vmatrix} 1 & S_5 & S_6 & I_4 \\ B_1 & 1 & S_4 & I_1 \\ B_2 & S_1 & S_2 & I_2 \\ B_3 & S_3 & 1 & I_3 \end{vmatrix}}{\begin{vmatrix} 1 & S_5 & S_6 & \alpha\frac{S_6}{S_2} - S_5 \\ B_1 & 1 & S_4 & \alpha\frac{S_4}{S_2} - 1 \\ B_2 & S_1 & S_2 & \alpha - S_1 \\ B_3 & S_3 & 1 & \alpha \cdot \frac{1}{S_2} \cdot \frac{\varepsilon^D_{\lambda A} \cdot \varepsilon^A_{\lambda D}}{\varepsilon^D_{\lambda D} \cdot \varepsilon^A_{\lambda A}} - S_3 \end{vmatrix}}, I_D = \frac{\begin{vmatrix} 1 & I_4 & S_6 & \alpha\frac{S_6}{S_2} - S_5 \\ B_1 & I_1 & S_4 & \alpha\frac{S_4}{S_2} - 1 \\ B_2 & I_2 & S_2 & \alpha - S_1 \\ B_3 & I_3 & 1 & \alpha \cdot \frac{1}{S_2} \cdot \frac{\varepsilon^D_{\lambda A} \cdot \varepsilon^A_{\lambda D}}{\varepsilon^D_{\lambda D} \cdot \varepsilon^A_{\lambda A}} - S_3 \end{vmatrix}}{\begin{vmatrix} 1 & S_5 & S_6 & \alpha\frac{S_6}{S_2} - S_5 \\ B_1 & 1 & S_4 & \alpha\frac{S_4}{S_2} - 1 \\ B_2 & S_1 & S_2 & \alpha - S_1 \\ B_3 & S_3 & 1 & \alpha \cdot \frac{1}{S_2} \cdot \frac{\varepsilon^D_{\lambda A} \cdot \varepsilon^A_{\lambda D}}{\varepsilon^D_{\lambda D} \cdot \varepsilon^A_{\lambda A}} - S_3 \end{vmatrix}} \tag{21}$$

7. From this, the FRET efficiency E can be calculated according to:

$$E = \frac{X}{I_D} \tag{22}$$

When using the Cy3-Cy5, or the Alexa Fluor 546-Alexa Fluor 647 FRET pairs, and assigning the FL1 channel of a FACSCalibur to measuring the cellular autofluorescence (I_4), the S_3, S_4, S_6 factors and the $\frac{\varepsilon^D_{635} \cdot \varepsilon^A_{488}}{\varepsilon^D_{488} \cdot \varepsilon^A_{635}}$ absorption ratio become negligible and the equation takes a much simpler form that can be used for calculating E as a new cellular parameter in the list mode file (*see* **Note 13**):

$$E = 1 + \frac{\alpha(I_4 B_1 - I_1)}{I_2 - B_2 I_4 + \alpha(I_1 - B_1 I_4) - I_1 S_1 + B_1 I_4 S_1 - I_3 S_2 + B_3 I_4 S_2 + S_5(B_2 I_1 - B_1 I_2 - B_3 I_1 S_2 + B_1 I_3 S_2)} \tag{23}$$

3.6 Interpretation of FCET Data

1. Although FRET can provide very useful information about molecular proximity and associations, it has its own limitations. The most serious drawback of FRET is that it has restricted capacity in determining absolute distances because FRET efficiency depends not only on the actual distance between the donor and acceptor, but also on their relative orientation. It is still quite good at determining relative distances, namely, whether the two labels are getting overall closer or farther upon a certain treatment/condition. Even when measuring relative distances, care must be taken to ensure that the orientation does not change between the two systems to be compared. In such cases, combination of FRET measurements with polarization can be a useful approach to resolve the two distinct effects [16]. Fluorophores attached to proteins via flexible

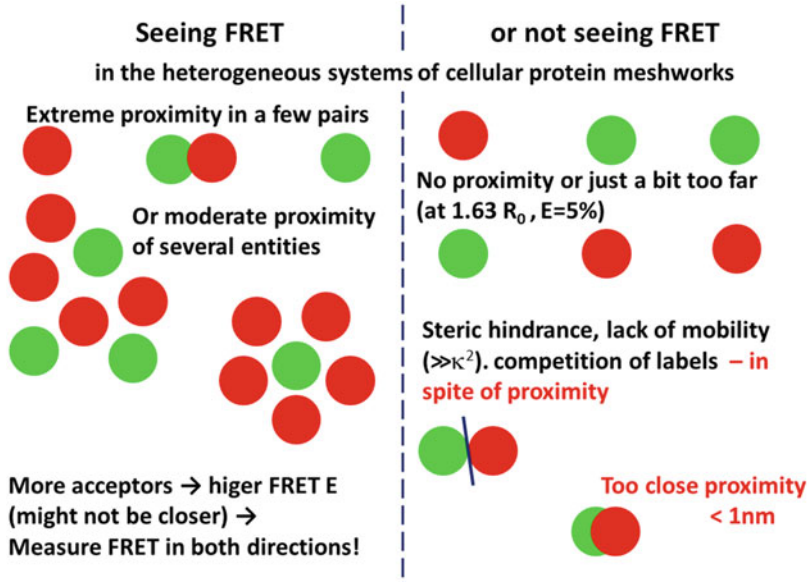

Fig. 2 FRET in the heterogeneous systems of cellular protein meshworks. Interpretation of FRET measurements can be a challenge. When FRET above noise occurs without doubt, it could result from both the extreme proximity in a few molecular pairs, and no contact between the rest, or a moderate proximity of most particles. A high acceptor to donor ratio—both in terms of fluorophores on antibodies or the actual molecular species under investigation, yields higher FRET efficiency without a change in proximity. The former can be exploited for tuning the sensitivity of our FRET measurements, while the latter must be controlled by swapping the donor and the acceptor. However, one thing is certain: if FRET has been measured with certainty, there must be the molecular proximity of some kind. Contrary, if there is no FRET, our only secure conclusion is that there is no FRET. The factors behind need further investigation. There may be proximity, but at the verge of detectability with the system used—at $1.63R_0$, FRET efficiency is only $E = 5\%$. A different labeling strategy (Fab, indirect labeling), a longer linker, or a dye pair with greater R_0 could shed light on this. There could be steric hindrances that preclude efficient FRET, which could also be addressed by altering the labeling strategy. The lack of sufficient mobility of the fluorophores, their fixation in the wrong orientation could also cause the absence of FRET. Longer linkers, gentler or no fixation can bring FRET back. Sometimes proximity could be so extreme that the labels used prevent each other from binding. Such competition alone is a sign of proximity, but diminishes FRET itself. Another, though the rare option is that the labels are so close that direct ground state and exchange interactions take precedence over FRET. Finally, if all these could be excluded, lack of proximity can be hypothesized with greater confidence.

linkers (such as a 6–12 carbon linker in the case of dyes or a few glycines in the case of fluorescent proteins) are relatively free to rotate, which allows for the donor and acceptor to assume several spatial orientations during the excited state lifetime of the donor (called dynamic averaging) [28], which allows for optimal FRET measurements in complex biological systems. Conversely, rigid systems, or changes of donor–acceptor orientation to positions less favoring FRET can lead to underestimation of actual proximity (Fig. 2). Thus, it is advisable to use alternative approaches in order to convincingly prove the reason for observed changes in FRET efficiency. For example,

when fluorescent antibodies are used, if antibodies against different epitopes are available, it is advisable to test them as well.

2. Another problem is that FRET has very sharp distance dependence. Owing to this, it is difficult to measure relatively long distances because the rate of FRET gets very low: if the donor and acceptor are within $1.63 \times R_0$ distance, energy transfer is detectable, if they are farther apart, energy is transferred with very little efficiency. Due to this sharp decrease, the absence of FRET is not a direct proof of the absence molecular proximity between the epitopes investigated. Also, absence of FRET can be caused by steric hindrance even for neighboring molecules or protein domains (Figs. 2 and 3a). Additionally, proximity of the labels within 1 nm usually causes ground-state interactions or transfer by exchange interactions to become dominant at the expense of FRET [9]. On the other hand, presence of FRET to any appreciable extent above the experimental error of measurement is the strong evidence for molecular interactions.
3. Indirect immunofluorescent labeling strategies may be applied to FRET measurements if suitable fluorophore-conjugated mAbs are not available, or as an approach to enhancing the specific fluorescence signal (*see* **Note 14**). In such cases, special attention should be paid to the fact that the size of the antibody complexes used affects the measured FRET efficiency values. Application of a larger antibody complex could cause a decrease in FRET efficiency due to the geometry of the antibody complexes, since when antibody or (Fab) complexes become larger, the actual distance between the donor and acceptor fluorophores can increase (Fig. 3b) [22]. It is also possible, however, that using monoclonal whole antibodies, FRET is observed, but using Fab fragments of the same antibodies voids FRET through steric hindrance (Fig. 3a). Thus, FRET values cannot be compared directly to each other if they are obtained using different labeling strategies. Another related pitfall is the possible overestimation of proximities upon using indirect labeling, since one could conceive a molecular assembly where there is no interaction between the observed entities, as intermolecular distances are considerable, but if they are not exceedingly large, extending the range of interaction with the size of the second antibody, and providing a multiplicity or orientations with polyclonal antibodies could still result in efficient FRET (Fig. 3c).
4. Another possibility for increasing the fluorescence signal is to use phycoerythrin (PE) or allophycocyanin (APC) labeled antibodies, since PE and APC have exceptional brightness. However, the sizes of these molecules are comparable to, or even greater than whole antibodies. Due to steric limitations, the measurable FRET efficiency values can be low, at the border of

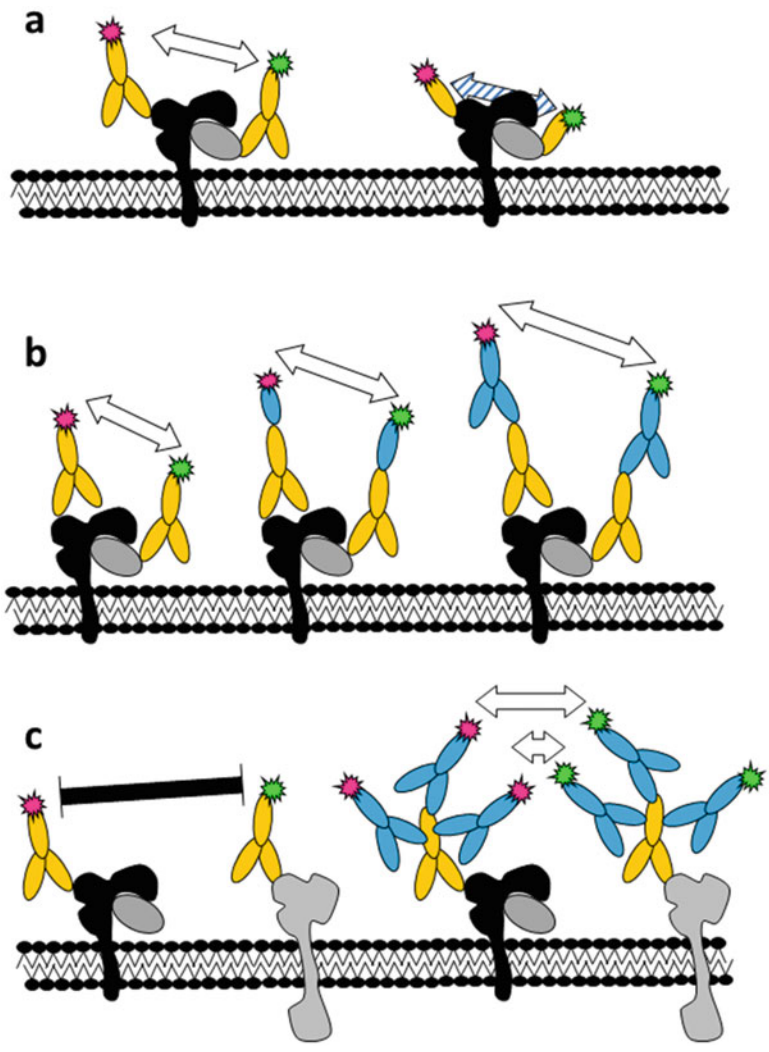

Fig. 3 FRET modified by labeling strategies. (**a**) Applying Fab fragments in place of whole antibodies can reduce flexibility, mobility and compact the system to such an extent that steric hindrance might occur. (**b**) Increasing the size of the labeling molecular complex—e.g. from direct labeling through secondary Fab-s to secondary whole Ab-s—has been shown to increase the estimated distance (reduce FRET efficiency). (**c**) In the event that there is no molecular interaction between two entities, but (for example owed to high surface density) they are not dispersed very far, applying (polyclonal) secondary antibodies could still yield measurable FRET efficiency

detection limit [29]. Nonetheless, even these low FRET efficiency values might have a biological meaning, since the accuracy of measurements is greatly improved owing to the high level of specific signals. Along similar lines of thought, FRET efficiency can be increased through increasing the dye/antibody ratio for the acceptor [30]. Appropriate positive and negative controls can help make the decision whether given

molecules are associated or not on the basis of the measured FRET efficiency values.

5. When studying cells labeled with donor and acceptor conjugated monoclonal antibodies, averaging is performed at different levels. The first averaging follows from the random conjugation of the fluorescent label. An additional averaging is brought about by the actual distribution of separation distances between the epitopes labeled with monoclonal antibodies. The same ensemble FRET efficiency can be obtained with all donor–acceptor pairs separated by about the same distance, and with some pairs at extreme proximity and the rest outside FRET range (Fig. 2). This multiple averaging, an inevitable consequence of the non-uniform stoichiometry, explains why the goals of FRET measurements are so uniquely different in the case of purified molecular systems on the one hand, and in the case of in situ labeled membrane or cytoplasmic molecules on the other hand. In the former case, FRET efficiency values can be converted into absolute distances, while in the latter, relative distances and their changes are investigated.
6. Calculation of distance relationships from energy transfer efficiencies is easy in the case of a single-donor/single-acceptor system if the localization and relative orientation of the fluorophores are known. If the FRET measurements are performed on the cell surface or inside the cell, many molecules might not be labeled at all; many could be single without a FRET pair, while others may be in smaller groups of heterooligomers, creating higher rates of FRET than expected from standalone pairs (Fig. 2). A large number of epitopes labeled with the acceptor increases E by increasing the rate of FRET, rather than actually meaning that the two epitopes investigated are closer to each other. If, in these cases, reversing the labeling still results in large E values, the proximity can be considered verified. However, if reversing the ratio of donor:acceptor to >1 makes FRET disappear, it is possible that we have previously seen random colocalizations owed to the high number of acceptors. One can use model calculations to predict the average distance of donors and acceptors assuming random distribution, and compare the predictions of the calculations to the observed FRET efficiencies [26, 31–34]. Alternatively, examining the dependence of FRET on acceptor density and on the donor–acceptor ratio can help decide whether the proteins form clusters or are randomly distributed [35]. However, the donor/acceptor ratios should be in the range of 0.1–10 [5] if we want to obtain reliable FRET measurements. Outside this range, noise and data irreproducibility propagate unfavorably, rendering accurate FRET efficiency calculations impossible. It

also needs to be noted that even random associations resulting from high expression levels of certain proteins must be regarded as biologically relevant.

4 Notes

1. Owing to the very large number of available fluorophores, it is impossible to present a thorough listing of even the most widely used combinations. Excitation and emission spectra of molecules for donor–acceptor pair selection can be checked at one of the following websites: Becton-Dickinson Fluorescence Spectrum Viewer (*http://www.bdbiosciences.com/us/s/spectrumviewer*) or Thermo Fisher Scientific Fluorescence SpectraViewer (*https://www.thermofisher.com/hu/en/home/life-science/cell-analysis/labeling-chemistry/fluorescence-spectraviewer.html#*). Additionally, most manufacturers of optical filters offer their own spectra viewers, including Chroma (https://www.chroma.com/spectra-viewer), Semrock (https://searchlight.semrock.com/), and Omega (https://www.omegafilters.com/curvomatic/). The number of available GFP variants has exploded in recent years. Papers to aid the selection of the optimal GFP variant have been published by the Tsien Laboratory [36, 37]. A detailed characterization of classical GFP variants for FRET experiments is also available [38]. Further developments have recently been reviewed in [39].
2. Red emitting fluorescent proteins are known to incompletely mature and therefore in tandem chimeric constructs where both donor and acceptor are in the same molecule, one cannot expect a 1:1 ratio for them; in fact, the average ratio will change from cell to cell. Furthermore, owing to the incomplete maturation, exact proximity measurements cannot be performed reliably. A new red fluorescent protein, mScarlet, however, offers improved maturation speed in addition to its record brightness and quantum yield (70%) [40]. An additional, often overlooked caveat regarding measurements with fluorescent proteins is their sensitivity to fixatives, both crosslinking (formaldehyde) and dehydrating/precipitating (ethanol, acetone) types.
3. HEPES buffer (125 mM NaCl, 5 mM KCl, 20 mM HEPES, 1 mM $CaCl_2$, 1.5 mM $MgSO_4$, pH 7.2) can also be used throughout instead of PBS, both for extra- and intracellular labeling.
4. Instead of 0.1% Triton X-100, 0.1% (w/v) saponin can be used. The saponin stock solution (20% w/v in dH_2O) should be stored frozen. Optimizing the signal and minimizing

background for intracellular labeling is a must, but beyond the scope of the present chapter.

5. At least one donor-only and one acceptor-only sample are needed for spillage factors, and, in the simplest case, the same epitope labeled with the same antibody once conjugated with the donor dye, and once with the acceptor dye is needed for calculating the α factor. (If these antibodies are not available, the donor-only and acceptor-only samples can be used for calculating the α factor, provided we determine, in an independent, calibrated experiment the median number of donor and acceptor labeled epitopes.) It is always prudent, however, to prepare all the samples for obtaining independent determinations of both the α factor and the FRET efficiencies.
6. One needs to determine labeling intensity as a function of time after trypsinization for the particular proteins examined.
7. Time of labeling should also be optimized previously. Usually, incubation beyond 10 min does not increase labeling intensity on membrane proteins by more than 10%. Also, saturating concentrations of each antibody must be established.
8. The excitation and emission wavelengths for channel I_4 are to be chosen such that the donor and acceptor fluorophores will not contribute considerably to the fluorescence intensity measured here. The main point is to obtain a fluorescence signature which is measured independent of the donor and acceptor channels (i.e., at least the excitation or the emission wavelength should differ from those of other detection channels), but can be used for calculating the contribution of cellular autofluorescence to these channels. There are alternatives to the arrangement proposed here but this example is the one applicable to most commercial flow cytometers (*see* Subheading 3.5).
9. There is always one additional control to make, and that is to check for competition of the antibody carrying the acceptor with donor labeling. This should be done with the unlabeled antibody against the "acceptor" epitope, and any decrease of donor fluorescence caused by adding the unlabeled antibody should be attributed to competition rather than donor quenching owed to FRET. Needless to say, competition between labeling antibodies is likely also a sign of molecular proximity, albeit not as readily quantitated as FRET.

   In some rare cases, an antibody can increase the binding of another antibody. This enhancement can also lead to misinterpretation of FRET data. For example, if the acceptor-labeled antibody increases the binding of the donor-labeled antibody, the unquenched donor intensity of the donor + acceptor double-labeled sample is larger than that of the donor-only sample, so the FRET calculated by comparing the donor

intensity of the double-labeled sample and the donor-only sample will be underestimated. In some cases, the acceptor fluorescence may spill over to the donor channel, and the assumption that the background (i.e., non-donor) fluorescence intensity of the double-labeled sample is equal to the fluorescence intensity of the unlabeled sample does not hold. In such a case, a sample labeled by the acceptor conjugated antibody and the unlabeled antibody against the donor epitope (to correct for the competition between the two antibodies) is to be used for background subtraction. An equation taking acceptor spillover and competition effects into account can be written in the following form:

$$E = 1 - \frac{I_{\text{Donor+Acceptor}} - I_{\text{Blank\_donor+Acceptor}}}{I_{\text{Donor+Blank\_acceptor}} - I_{\text{background}}} \tag{24}$$

where $I_{\text{Blank\_donor+Acceptor}}$ and $I_{\text{Donor+Blank\_acceptor}}$ denote, respectively, the fluorescence intensities (measured in the donor channel) of the sample tagged with the unlabeled antibody against the donor epitope and the acceptor-conjugated antibody, and that of the sample tagged with the donor-conjugated antibody and the unlabeled antibody against the acceptor epitope.

10. Although the spectroscopic spillover factors S_1 through S_6 are not expected to show any cell-by-cell heterogeneity, their cell-by-cell determination also has certain advantages. Performing mathematical calculations with cells having low fluorescence intensity introduce a large error into the calculations. Omitting these cells from the determination of the S factors greatly increases the reliability of these calculations. Obtaining reliable S factors, however, does not mean that these factors will yield comparably reliable FRET efficiencies for cells that are weakly labeled. The stochastic distribution of emitted photons worsens signal to noise in proportion to the square root of decreased fluorescence. In these cases, a maximum likelihood estimation for the population may serve well, similar to the microscopic approach described in [41, 42].
11. The factor α is necessary to relate the actual fluorescence emission by the sensitized acceptor measured in the acceptor channel to the fluorescence one could measure in the donor channel from the donor if the quanta that are transferred in FRET had been emitted by the donor. This proportionality factor relates to the Q quantum efficiencies of the acceptor (index A) and donor (index D), and the detection efficiencies η in the acceptor and donor channels for photons emitted by the acceptor and the donor, respectively:

$$\alpha = \frac{Q_A \eta_A}{Q_D \eta_D} \tag{25}$$

However, for practical purposes, α is more easily determined by measuring the same number of excited donor and acceptor molecules, respectively, in the donor and acceptor channels, and normalizing them to their molar absorption coefficients (*see* Eq. 4). In Eq. 4 for α, there is a contribution from the sample labeled only with acceptor excited at the donor wavelength. Usually, this fluorescence intensity is rather small, thus giving the main error-source in the calculations.To decrease this error, α should be determined using a protein that is abundant on our cells and recalculated for the actual antibodies used in the experiment. The fluorescence quantum yields of the dyes may depend on the type of antibody they are attached to and even on the labeling ratio L, thereby affecting the value of α. The α factor determined for a given donor–acceptor antibody pair can be used for other antibody pairs labeled with the same dyes provided its value is corrected for the differences in the quantum yields:

$$\alpha_2 = \alpha_1 \frac{Q_{A,2}}{Q_{A,1}} \frac{Q_{D,1}}{Q_{D,2}} \tag{26}$$

where subscript "1" refers to the antibody pair for which α has been determined previously, and subscript "2" refers to the new antibody pair with higher fluorescence intensity. Of course, such a correction requires the determination of quantum yields for both antibody pairs.

12. As already pointed out, autofluorescence values that are high compared to the donor and acceptor intensities can seriously disperse the calculated FRET efficiency distributions. Therefore, it is advisable to decrease the autofluorescence level as much as possible. A straightforward way to achieve this is to use yellow or red fluorescent dyes, since cellular autofluorescence becomes progressively weaker in the red region of the visible spectrum [22].
13. The simplified equation 23 is tested for the particular filter setup listed in Table 2.
14. Optimizing the sensitivity of FRET measurements is a formidable challenge. To make the measurable range of molecular interactions as large as possible, donor–acceptor dye pairs should be chosen with the maximal spectral overlap. However, this will increase the cross talk between detection channels. At the same time, the higher the amount of spectral spillover compared to the FRET signal proper, the lower the reliability of the experiment. Therefore, efforts have to be made to

Table 2
Filter setup in a FacsCalibur for cell-by-cell autofluorescence correction with red-shifted fluorophores

Channel	Excitation (nm)	Emission filter (nm)
I_1	488	585 BP
I_2	488	670 LP
I_3	635	661 BP
I_4	488	530 BP

minimize spectral spillover. A prudent approach at optimizing the choice of fluorophores and filters to reach a balance between these contradictory requirements results in the recognition that the normalized fluorescence of applied dyes is an even more important asset ameliorating the detection of FRET through improved signal to noise ratio, and, collectively, AlexaFluor546 with AlexaFluor647 appears to be a most favorable FCET pair in a typical biological system [21].

In addition, the labeling ratio of the acceptor has a substantial influence on the measured FRET efficiency; decreasing or increasing the acceptor labeling ratio can be utilized to manipulate the FRET response of the acceptor–donor pair and therefore is a tool for optimizing the sensitivity of FRET measurements [30].

Acknowledgements

The authors were supported by the following grants: Hungarian National Research Fund K119690, K120302, Hungarian National Development Agency GINOP-2.3.2-15-2016-00044, GINOP-2.3.3-15-2016-00003.

Electronic Supplementary Materials

Additional data 1Using the Excel FRET calculator (ZIP 567 kb)

References

1. Szollosi J, Damjanovich S, Matyus L (1998) Application of fluorescence resonance energy transfer in the clinical laboratory: routine and research. Cytometry 34(4):159–179

2. Bastiaens PIH, Squire A (1999) Fluorescence lifetime imaging microscopy: spatial resolution of biochemical processes in the cell. Trends Cell Biol 9(2):48–52

3. Clegg RM (2002) FRET tells us about proximities, distances, orientations and dynamic properties. J Biotechnol 82(3):177–179
4. Vereb G, Szollosi J, Matko J, Nagy P, Farkas T, Vigh L, Matyus L, Waldmann TA, Damjanovich S (2003) Dynamic, yet structured: The cell membrane three decades after the Singer-Nicolson model. Proc Natl Acad Sci U S A 100(14):8053–8058
5. Berney C, Danuser G (2003) FRET or No FRET: a quantitative comparison. Biophys J 84(6):3992–4010
6. Shrestha D, Jenei A, Nagy P, Vereb G, Szollosi J (2015) Understanding FRET as a research tool for cellular studies. Int J Mol Sci 16 (4):6718–6756. doi:10.3390/ijms16046718
7. Förster T (1946) Energiewanderung und Fluoreszenz. Naturwissenschaften 6:166–175
8. Stryer L, Haugland RP (1967) Energy transfer: a spectroscopic ruler. Proc Nat Acad Sci USA 58:719–726
9. Dexter DL (1953) A theory of sensitized luminescence in solids. J Chem Phys 21 (5):836–850
10. Fazekas Z, Petras M, Fabian A, Palyi-Krekk Z, Nagy P, Damjanovich S, Vereb G, Szollosi J (2008) Two-sided fluorescence resonance energy transfer for assessing molecular interactions of up to three distinct species in confocal microscopy. Cytometry A 73(3):209–219. doi:10.1002/cyto.a.20489
11. Petras M, Lajtos T, Friedlander E, Klekner A, Pintye E, Feuerstein BG, Szollosi J, Vereb G (2013) Molecular interactions of ErbB1 (EGFR) and integrin-beta1 in astrocytoma frozen sections predict clinical outcome and correlate with Akt-mediated in vitro radioresistance. Neuro-oncology 15 (8):1027–1040. doi:10.1093/neuonc/not046
12. Horvath GL, Langhoff P, Latz E (2016) Toll-like receptor interactions measured by microscopic and flow cytometric FRET. Methods Mol Biol 1390:41–64. doi:10.1007/978-1-4939-3335-8_3
13. Jares-Erijman EA, Jovin TM (2003) FRET imaging. Nat Biotechnol 21(11):1387–1395
14. Szabo A, Horvath G, Szollosi J, Nagy P (2008) Quantitative characterization of the large-scale association of ErbB1 and ErbB2 by flow cytometric homo-FRET measurements. Biophys J 95(4):2086–2096. doi:10.1529/biophysj.108.133371
15. Bene L, Ungvari T, Fedor R, Nagy I, Damjanovich L (2015) Dual-laser homo-FRET on the cell surface. Biochim Biophys Acta 1853 (5):1096–1112. doi:10.1016/j.bbamcr.2015.02.001
16. Ungvari T, Gogolak P, Bagdany M, Damjanovich L, Bene L (2016) Perrin and Forster unified: dual-laser triple-polarization FRET (3polFRET) for interactions at the Forster-distance and beyond. Biochim Biophys Acta 1863(4):703–716. doi:10.1016/j.bbamcr.2016.02.002
17. Bene L, Gogolak P, Ungvari T, Bagdany M, Nagy I, Damjanovich L (2016) Depolarized FRET (depolFRET) on the cell surface: FRET control by photoselection. Biochim Biophys Acta 1863(2):322–334. doi:10.1016/j.bbamcr.2015.12.003
18. Nedbal J, Visitkul V, Ortiz-Zapater E, Weitsman G, Chana P, Matthews DR, Ng T, Ameer-Beg SM (2015) Time-domain microfluidic fluorescence lifetime flow cytometry for high-throughput Forster resonance energy transfer screening. Cytometry A 87(2):104–118. doi:10.1002/cyto.a.22616
19. Suzuki M, Sakata I, Sakai T, Tomioka H, Nishigaki K, Tramier M, Coppey-Moisan M (2015) A high-throughput direct fluorescence resonance energy transfer-based assay for analyzing apoptotic proteases using flow cytometry and fluorescence lifetime measurements. Anal Biochem 491:10–17. doi:10.1016/j.ab.2015.08.022
20. Fabian A, Horvath G, Vamosi G, Vereb G, Szollosi J (2013) TripleFRET measurements in flow cytometry. Cytometry A 83 (4):375–385. doi:10.1002/cyto.a.22267
21. Horvath G, Petras M, Szentesi G, Fabian A, Park JW, Vereb G, Szollosi J (2005) Selecting the right fluorophores and flow cytometer for fluorescence resonance energy transfer measurements. Cytometry A 65(2):148–157. doi:10.1002/cyto.a.20142
22. Sebestyen Z, Nagy P, Horvath G, Vamosi G, Debets R, Gratama JW, Alexander DR, Szollosi J (2002) Long wavelength fluorophores and cell-by-cell correction for autofluorescence significantly improves the accuracy of flow cytometric energy transfer measurements on a dual-laser benchtop flow cytometer. Cytometry 48 (3):124–135
23. Szentesi G, Horvath G, Bori I, Vamosi G, Szollosi J, Gaspar R, Damjanovich S, Jenei A, Matyus L (2004) Computer program for determining fluorescence resonance energy transfer efficiency from flow cytometric data on a cell-by-cell basis. Comput Methods Programs Biomed 75(3):201–211. doi:10.1016/j.cmpb.2004.02.004
24. Szollosi J, Tron L, Damjanovich S, Helliwell SH, Arndt-Jovin D, Jovin TM (1984)

Fluorescence energy transfer measurements on cell surfaces: a critical comparison of steady-state fluorimetric and flow cytometric methods. Cytometry 5(2):210–216

25. Damjanovich S, Tron L, Szollosi J, Zidovetzki R, Vaz WL, Regateiro F, Arndt-Jovin DJ, Jovin TM (1983) Distribution and mobility of murine histocompatibility H-2Kk antigen in the cytoplasmic membrane. Proc Natl Acad Sci U S A 80(19):5985–5989
26. Tron L, Szollosi J, Damjanovich S, Helliwell SH, Arndt-Jovin DJ, Jovin TM (1984) Flow cytometric measurement of fluorescence resonance energy transfer on cell surfaces. Quantitative evaluation of the transfer efficiency on a cell-by-cell basis. Biophys J 45(5):939–946
27. Nagy P, Bene L, Hyun WC, Vereb G, Braun M, Antz C, Paysan J, Damjanovich S, Park JW, Szollosi J (2005) Novel calibration method for flow cytometric fluorescence resonance energy transfer measurements between visible fluorescent proteins. Cytometry A 67 (2):86–96. doi:10.1002/cyto.a.20164
28. Dale RE, Eisinger J, Blumberg WE (1979) The orientational freedom of molecular probes. The orientation factor in intramolecular energy transfer. Biophys J 26(2):161–193. doi:10.1016/S0006-3495(79)85243-1
29. Batard P, Szollosi J, Luescher I, Cerottini JC, MacDonald R, Romero P (2002) Use of phycoerythrin and allophycocyanin for fluorescence resonance energy transfer analyzed by flow cytometry: advantages and limitations. Cytometry 48(2):97–105
30. Fabian AI, Rente T, Szollosi J, Matyus L, Jenei A (2010) Strength in numbers: effects of acceptor abundance on FRET efficiency. Chemphyschem 11(17):3713–3721. doi:10.1002/cphc.201000568
31. Wolber PK, Hudson BS (1979) An analytic solution to the Forster energy transfer problem in two dimensions. Biophys J 28(2):197–210
32. Dewey TG, Hammes GG (1980) Calculation on fluorescence resonance energy transfer on surfaces. Biophys J 32(3):1023–1035
33. Snyder B, Freire E (1982) Fluorescence energy transfer in two dimensions. A numeric solution for random and nonrandom distributions. Biophys J 40(2):137–148
34. Szollosi J, Damjanovich S, Balazs M, Nagy P, Tron L, Fulwyler MJ, Brodsky FM (1989) Physical association between MHC class I and class II molecules detected on the cell surface by flow cytometric energy transfer. J Immunol 143(1):208–213
35. Kenworthy AK, Edidin M (1998) Distribution of a glycosylphosphatidylinositol-anchored protein at the apical surface of MDCK cells examined at a resolution of <100 A using imaging fluorescence resonance energy transfer. J Cell Biol 142(1):69–84
36. Shaner NC, Steinbach PA, Tsien RY (2005) A guide to choosing fluorescent proteins. Nat Methods 2(12):905–909. doi:10.1038/nmeth819
37. Rodriguez EA, Campbell RE, Lin JY, Lin MZ, Miyawaki A, Palmer AE, Shu X, Zhang J, Tsien RY (2017) The growing and glowing toolbox of fluorescent and photoactive proteins. Trends Biochem Sci 42(2):111–129. doi:10.1016/j.tibs.2016.09.010
38. Patterson GH, Piston DW, Barisas BG (2000) Forster distances between green fluorescent protein pairs. Anal Biochem 284(2):438–440. doi:10.1006/abio.2000.4708
39. Bajar BT, Wang ES, Zhang S, Lin MZ, Chu J (2016) A guide to fluorescent protein FRET pairs. Sensors (Basel) 16(9). doi:10.3390/s16091488
40. Bindels DS, Haarbosch L, van Weeren L, Postma M, Wiese KE, Mastop M, Aumonier S, Gotthard G, Royant A, Hink MA, Gadella TW Jr (2017) mScarlet: a bright monomeric red fluorescent protein for cellular imaging. Nat Methods 14(1):53–56. doi:10.1038/nmeth.4074
41. Nagy P, Szabo A, Varadi T, Kovacs T, Batta G, Szollosi J (2014) Maximum likelihood estimation of FRET efficiency and its implications for distortions in pixelwise calculation of FRET in microscopy. Cytometry A 85(11):942–952. doi:10.1002/cyto.a.22518
42. Nagy P, Szabo A, Varadi T, Kovacs T, Batta G, Szollosi J (2016) rFRET: a comprehensive, Matlab-based program for analyzing intensity-based ratiometric microscopic FRET experiments. Cytometry A 89(4):376–384. doi:10.1002/cyto.a.22828

Chapter 18

Overview of Fluorescence Lifetime Measurements in Flow Cytometry

Jessica P. Houston, Zhihua Yang, Jesse Sambrano, Wenyan Li, Kapil Nichani, and Giacomo Vacca

Abstract

The focus of this chapter is time-resolved flow cytometry, which is broadly defined as the ability to measure the timing of fluorescence decay from excited fluorophores that pass through cytometers or high-throughput cell counting and cell sorting instruments. We focus on this subject for two main reasons: first, to discuss the nuances of hardware and software modifications needed for these measurements because currently, there are no widespread time-resolved cytometers nor a one-size-fits-all approach; and second, to summarize the application space for fluorescence lifetime-based cell counting/sorting owing to the recent increase in the number of investigators interested in this approach. Overall, this chapter is structured into three sections: (1) theory of fluorescence decay kinetics, (2) modern time-resolved flow cytometry systems, and (3) cell counting and sorting applications. These commentaries are followed by conclusions and discussion about new directions and opportunities for fluorescence lifetime measurements in flow cytometry.

Key words Time-resolved flow cytometry, Fluorescence lifetime, Frequency-domain, Time-domain, FRET

List of Variables:

$N^*(t)$	Number of molecules in excited state at time t
k	Sum of de-excitation rates
k_{nr}	Sum of radiation-less de-excitation pathways
k_{em}	Rate of fluorescence emission
k_r	Sum of radiative de-excitation pathways
α_i	Pre-exponential factor
$E(t)$	Emission intensity as a function of time (t)
E_0	Maximum emission intensity
m_{em}	Depth of modulation of emission signal

(continued)

Teresa S. Hawley and Robert G. Hawley (eds.), *Flow Cytometry Protocols*, Methods in Molecular Biology, vol. 1678, DOI 10.1007/978-1-4939-7346-0_18,

ϕ	Phase of any modulated signal
M	Total depth of modulation for any modulated signal
ϕ_{em}	Phase of modulated emission signal
ϕ_{ex}	Phase of modulated excitation signal
$\Delta\phi$	Phase shift between excitation and emission modulated signals
ω	Angular modulation frequency
$I(t)$	Intensity of fluorescence
τ	Fluorescence lifetime of the fluorophore
m_{ex}	Depth of modulation of excitation signal
a	Laser beam height and to the velocity of a cell crossing the laser beam at t_0

1 Introduction

The measurement of the fluorescence lifetime with a flow cytometer is an old concept that is experiencing a re-emergence owing to new applications and advancing technologies. In fact, the earliest published and patented versions of time-resolved flow cytometry are circa 1992 [1–4]. Such demonstrations involved laboratory-constructed instruments with large, high-powered lasers and external frequency-domain laser modulation devices (discussed in later sections). Since these early demonstrations, new lasers, data systems, detector, and technologies have emerged, thus advancing how cell counters make time-resolved measurements. Included in this chapter is a discussion of these aspects of time-resolved cytometry as well as an overview of cell and microsphere experiments that utilize the fluorescence lifetime as an analysis or sorting parameter.

The fluorescence lifetime, often mathematically represented by the Greek symbol tau (τ), is the average time an excited fluorophore spends in an energetic state and vibrational level prior to relaxation back to a non-excited ground state. The step-wise photo-physics behind fluorescence excited state phenomena (also reviewed more descriptively later) culminate in photon emission following an exponential decay kinetic process. The timing of fluorescence decay is similar across many organic fluorophores used in life sciences and flow cytometry. Average fluorescence lifetimes range from 1 to 30 ns, and individual fluorophores might experience a shift in their average lifetime by an addition or reduction by hundreds of picoseconds (e.g., 100–1000 ps) [5]. Table 1 includes a list of the many fluorescence lifetime values measured with time-resolved flow cytometry.

Table 1
List of fluorescence lifetimes of fluorophores that have been measured by time-resolved flow cytometry

Fluorophore/fluorescence species	Fluorescence lifetime (nanoseconds), citation	Time-resolved cytometry details
Ethidium bromide (unbound)	24.0 [3]	FD, Ar-Ion 488-nm laser at 30 MHz
DNA-Check 5949™ microspheres	6.9 [6]	FD, Ar-Ion 488-nm laser at 30 MHz
Fluorosbrite 18142 microspheres	3.4 [6]	FD, Ar-Ion 488-nm laser at 30 MHz
Fluorosbrite 10095 microspheres	3.5 [6]	FD, Ar-Ion 488-nm laser at 30 MHz
Immunocheck fluorospheres	7.1 [6]	FD, Ar-Ion 488-nm laser at 30 MHz
Propidium iodide (unbound)	1.3 [7]	FD, Ar-Ion 407-nm laser at 10 MHz
Propidium iodide (bound)	12.0 [7]	FD, Ar-Ion 407-nm laser at 10 MHz
Fluorescein isothiocyanate (FITC)	4.0 [7]	FD, Ar-Ion 488-nm laser at 29 MHz
Phycoerythrin-Texas Red-alpha-Thy-1.2	2.4 [8]	FD, Ar-Ion 488-nm laser at 10 MHz
Phycoerythrin (PE)	1.2 [8]	FD, Ar-Ion 488-nm laser at 10 MHz
Phycoerythrin-Cy5	1.7 [8]	FD, Ar-Ion 488-nm laser at 10 MHz
Ethidium monoazide	7.0 [8]	FD, Ar-Ion 488-nm laser at 10 MHz
7-Aminoactinomycin-D	0.7 [8]	FD, Ar-Ion 488-nm laser at 10 MHz
Phycoerythrin-alpha-Thy-1.2	1.6 [8]	FD, Ar-Ion 488-nm laser at 10 MHz
Yellow-Green™	2.1 [9]	FD, Ar-Ion 488-nm laser at 10 MHz
Syto 9™ green fluorescent stain	4.1 [9]	FD, Ar-Ion 488-nm laser at 10 MHz
Spherotech 8-peak Rainbow™ fluorospheres	3.9 [9]	FD, Ar-Ion 488-nm laser at 10 MHz
Teal fluorescent protein (TFP)	2.9 [10]	FD, 445-nm diode laser at 25 MHz
Dark Citrine (dCit)-TFP	1.9 [10]	FD, 445-nm diode laser at 25 MHz
Ethidium bromide (bound)	19.3 [11]	FD, 488-nm diode laser at 3 MHz
Enhanced green fluorescent protein	4.2 [12]	FD, 488-nm diode laser at 6 MHz

(continued)

Table 1
(continued)

Fluorophore/fluorescence species	Fluorescence lifetime (nanoseconds), citation	Time-resolved cytometry details
Flow-Check™ fluorospheres	7.0 [13]	FD, 488-nm diode laser, square wave with 50% duty cycle at 5 MHz
Fluorescein	4.2 [13]	FD, 488-nm diode laser, square wave with 50% duty cycle at 5 MHz
Alexa Fluor™ 488	4.2 [13]	FD, 488-nm diode laser, square wave with 50% duty cycle at 5 MHz
Acridine orange	4.0 [13]	FD, 488-nm diode laser, square wave with 50% duty cycle at 5 MHz
Green fluorescence protein	2.7 [14]	TD, pulsed 520-nm solid state laser
di-4-ANEPPDHQ	0.2, 1.5 [14]	TD, pulsed 520-nm solid state laser

The method of acquisition is described for each lifetime measured where FD and TD describe frequency-domain and time-domain, respectively. The laser modulation for FD systems is provided and assumed sinusoidal unless otherwise noted. The values are average fluorescence lifetimes measured from a large population of cells or microspheres

A variety of biochemical factors influence fluorescence relaxation times for fluorescent molecules that are on the surface or interior of a cell. Reports show fluorescence lifetimes shorten/lengthen owing to changes in the microenvironment that surround the fluorophore such as the pH, ion concentration, temperature, or oxygen concentration [2, 15]. Additionally, the near-proximity of a fluorophore to a molecular quencher or the occurrence of energy transfer between two fluorophores will cause a shift in the average fluorescence lifetime [14, 16, 17] of one or more fluorophores involved in this process. The shortening or lengthening of the fluorescence lifetimes under different circumstances gives rise to many applications that include but are not limited to drug screening, drug delivery, contrast agent development, differentiation between spectrally overlapping fluorophores, solvent-induced relaxation experiments, collisional quenching between fluorophores, and Förster resonance energy transfer assays [8, 14, 18–20]. With fluorescence lifetime quantification, it is also possible to study basic cellular functions and phenomena such as cellular metabolism, DNA and RNA content, ATP synthesis, mitochondrial function, protein conformational changes, protein–protein interactions, protein mis-localization intracellularly, and cell signaling [10, 12, 18, 20–26]. In this chapter, we will mostly review lifetime shifts of common fluorophores used in flow cytometry, and also provide a review of fluorescence lifetimes for fluorophores that bind to micron-sized silica or polymeric spheres (i.e.,

microspheres), which are mostly used for calibration of fluorescence lifetime hardware.

The advantage of the fluorescence lifetime as a cytometry parameter is that it can be quantitative. The average fluorescence lifetime is independent of a fluorophore's excitation and emission spectrum and thus independent of the number of photons emitted by an excitable molecule as well as the total number of excitable molecules present (i.e., fluorophore concentration). Therefore, being independent of emission intensity, the fluorescence lifetime can be used to distinguish between two or more fluorophores that have similar emission spectra. In other words, the emission contribution of each fluorophore can be accounted for by the measured fluorescence lifetime and not by the sum of the detected light emitted within a wavelength bandwidth (i.e., color range). The fluorescence lifetime is also proportional to a fluorophore's quantum yield and thus a quantitative trait that can help understand the yield as a definitive contributing factor in the fluorescence "brightness" as opposed to the amount of fluorophore present, quantum efficiency, or other instrumentation variables that affect brightness.

In flow cytometry, the fluorescently labeled cell or microsphere moves through an optical excitation source at a constant velocity, limiting the amount of time fluorescence can be measured. The transit time is between 1 and 10 μm; therefore, nanosecond-scale fluorescence lifetimes are only measured hundreds to thousands of times before the cell departs the detector pathway. The rapid laser transit also prevents cells from being repeatedly scanned rendering the detection of lifetime gradients across the cell challenging. Therefore, reports of time-resolved flow cytometry, to-date, include measurements of average fluorescence lifetimes even though a single fluorophore may be exhibiting a range of fluorescence lifetimes within the cell or multiple fluorophores may be present and emitting in a similar spectral range.

The detection of multiple fluorescence lifetimes with a flow cytometer is discussed as an application in later sections, however it is worth noting here that this technique is common within the imaging community. That is, Fluorescence Lifetime Imaging Microscopy (FLIM) systems, which are often time-resolved adaptations of confocal and multi-photon instruments, provide multi-pixel images of fluorescence lifetime gradients across single cells. Additionally, FLIM instruments can obtain multi-exponential decay information indicating the presence of one or more fluorescence lifetime within a cell [27–31]. In contrast to FLIM instruments, time-resolved flow cytometers detect a single fluorescence lifetime; however, cytometers provide high-throughput cell sorting and counting as opposed to FLIM [9, 11, 32, 33]. Another point to be made here is that other fluorescence dynamics measurement fields (e.g., fluorimetry, spectroscopy, optical imaging, and diffuse optical tomography) measure fluorescence lifetimes through

different machinations for in vitro and in vivo use. This chapter does not review the breadth of time-resolved systems in microscopy and spectroscopy. The reader is referred to the publication by Lakowicz 2007 [34] or other publications that review fluorescence dynamics measured with non-high-throughput systems.

2 Fluorescence Lifetime Theory

The excitation of a fluorescent molecule through the absorption of light of a given energy leads to a complex relaxation process whereby excited electrons return to the ground state via a series of de-excitation processes (i.e., radiative vs. non-radiative energy release). Generally, in flow cytometry, the timing of the decay kinetic process is ignored and only the total number of photons that are released during relaxation are tracked. Therefore, cytometric instruments that can measure the rate of fluorescence decay not only integrate the total number of photons released when electrons radiatively relax to the ground state, but also clock this process, which occurs at decaying exponential rate. Much is known about the rate of decay of organic fluorophores owing to a formalized mathematical definition of fluorescence dynamics using a probabilistic viewpoint. Fluorescence decay can be represented with an ordinary differential rate equation (Eq. 1) because fluorescence follows first-order kinetics, where N is the number of excited fluorophores at time t. In this equation, k is the rate constant representing the total of all rates of the de-excitation processes including the rate of fluorescence, internal conversion, intersystem crossing, vibrational energy relaxation, and other energy dissipation processes [5, 35].

$$\frac{dN(t)}{dt} = -kN(t) \tag{1}$$

The sum of n number of rate constants can be represented by Eq. 2, and all are equivalent to either nonradiative (k_{nr}) or radiative processes (k_{r}). In other words, the summation is the total of all kinetic rate constants representing energy dissipation.

$$k = k_1 + k_2 + k_3 + k_4 + \ldots + k_n \ldots = k_{\mathrm{r}} + k_{\mathrm{nr}} \tag{2}$$

Experimentally we observe that relaxation of the electrons from an excited state(s) occurs following first-order kinetics, which is approximated by the solution to Eq. 1, shown here in Eqs. 3 and 4, which represent decay based on: N number of fluorophores decayed, or the fluorescence intensity decay, I, following excitation with an initial intensity, α.

$$N(t) = N(0) \cdot e^{-kt} \tag{3}$$

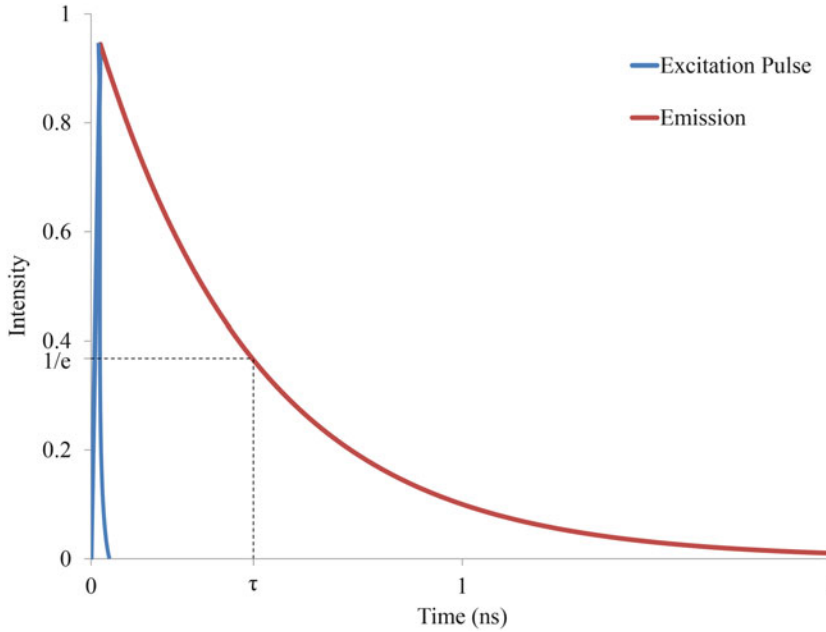

Fig. 1 Graphical representation of time-domain approaches to fluorescence lifetime measurements: a pulsed laser (*blue*) is used to excite the cell and/or fluorescent particle. The intensity of the fluorescence emission by the excited sample (*red*) decreases in an exponential fashion as a function of time. The lifetime is defined when the intensity decreases to 1/e

$$I(t) = \alpha \cdot e^{-t/\tau} \tag{4}$$

Equation 4 follows what is observed experimentally in which light of a high intensity but small pulse width, $I(0)$, or α, is used to excite a fixed amount of fluorophore molecules at an initial time, $t = 0$. The resulting fluorescence emission at time, t, is therefore $I(t)$, and decays exponentially. Figure 1 illustrates this with a graph of the initial pulse of light (i.e., simulation with a delta function) and resulting fluorescence decay.

Equation 4 is in terms of the fluorescence lifetime, τ, which is the time for the emission intensity to reach $1/e$ of the original excitation value, or for the number of relaxed molecules to reach 36.8% of the total number of excited fluorophores.

The fluorescence lifetime full representation is:

$$\tau = \frac{1}{k} = \frac{1}{(k_{\text{em}} + k_{\text{nr}})} \tag{5}$$

where k_{em} is the rate constant for radiative decay through fluorescence emission. During any multi-exponential decay process that might occur (e.g., emission by a mixture of fluorophores with different fluorescence lifetimes), the equation can be restated as a summation of first-order decay kinetic events. The addition accounts for each type of fluorophore, which collectively emit and

contribute to the total signal. Equation 6 provides this summation where α_i is the initial excitation intensity absorbed by each specie, i, and τ_i is the fluorescence lifetime corresponding to that specie.

$$I(t) = \sum_{i=1}^{n} \alpha_i \cdot e^{-t/\tau_i} \tag{6}$$

3 Time-Resolved Flow Cytometry

Two general methods are taken to make flow cytometers able to measure single or multiple fluorescence decay kinetics. Collectively, the methods are considered *time-resolved* and subsequently categorized as either time-domain or frequency-domain approaches.

Frequency-domain measurements are common because the methodology minimizes the hardware and signal processing modifications necessary for fluorescence lifetime transformation. Frequency-domain measurements involve sinusoidal (or square wave) modulation of the laser excitation source at a radio frequency (RF) of 1–100 MHz. When a fluorescently labeled cell is excited with this type of sinusoidal modulation, the intensity of emitted light, which decays as an exponential function of time (*see* Eq. 4), carries the same modulation frequency. However, the amplitude is attenuated and the phase is shifted owing to the fluorescence decay kinetics. Figure 2 illustrates this concept, where a high-frequency modulated excitation signal is plotted with a sinusoidal emission signal, which has the same modulation but a shift in phase and attenuation of the RF amplitude. The fluorescence lifetime is calculated from the information in the modulated signal using (generally) a Fourier transformation of the exponentially decayed function which depends on time. As shown by Eq. 7, the frequency-domain representation of the modulated emission intensity, $E(t)$, can be represented by a harmonic function which depends on angular modulation frequency (ω), phase (ϕ), and modulation amplitude (m_{em}). If the harmonic modulation follows a square wave shape, as opposed to sinusoidal, Eq. 8 is modified to represent a square wave as a summation of multiple odd harmonics (*see* Jenkins et al. for a thorough description [13]).

$$E(t) = E_0[1 + m_{\mathrm{em}} \sin(\omega t - \phi)] \tag{7}$$

Both the amplitude and phase of the emission signal are compared to the amplitude and phase of the excitation signal in order to find the amplitude demodulation and phase shift between these two signals (excitation and emission). This step is important because both values are proportional to the fluorescence lifetime.

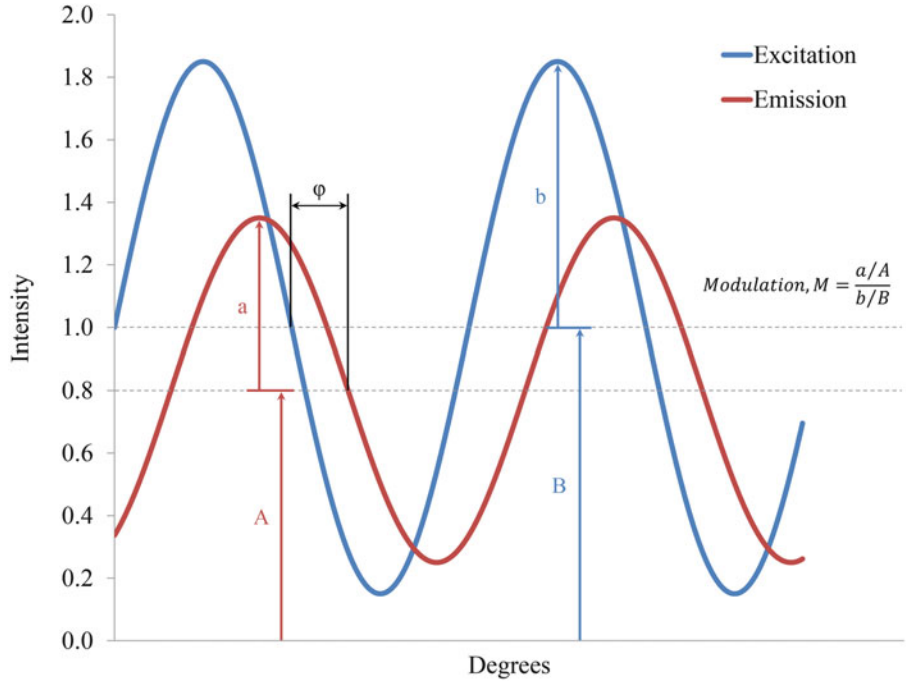

Fig. 2 Graphical representation of the frequency-domain method for the fluorescence lifetime measurement. The measurement is conducted using a radio-frequency modulated excitation signal (*blue*). The subsequent emission is modulated at the same angular frequency but delayed in phase (ϕ) and amplitude demodulated (M). The excited state lifetime can be determined by using phase delay and demodulation

The relationships between the fluorescence lifetime and amplitude demodulation, M, and phase shift, $\Delta\phi$, are provided in Eqs. 8 and 9. The demodulation is calculated by dividing the modulation depth of the emission signal by modulation of excitation. The phase shift, $\Delta\phi$, is found by subtracting the emission phase from the excitation phase, which is measured with the side scatter signal in flow cytometry.

$$M = \frac{1}{\sqrt{1 + (\omega\tau)^2}} \quad \text{or} \quad \tau = \frac{\sqrt{\left(\frac{m_{ex}^2}{m_{cm}^2} - 1\right)}}{\omega} \tag{8}$$

$$\tau = \frac{\tan \Delta\phi}{\omega} \tag{9}$$

The frequency-domain concept in the context of a flow cytometry process is also graphically illustrated in Fig. 3. The continuous wave yet modulated excitation source is focused onto fluorescently labeled moving cells, which are counted as they cross the laser beam and emit amplitude-attenuated and phase-shifted fluorescence. As seen in Fig. 3, the signal that is detected is Gaussian in shape and superimposed with an RF component. The Gaussian shape is a result of simulating a Gaussian mode laser output with

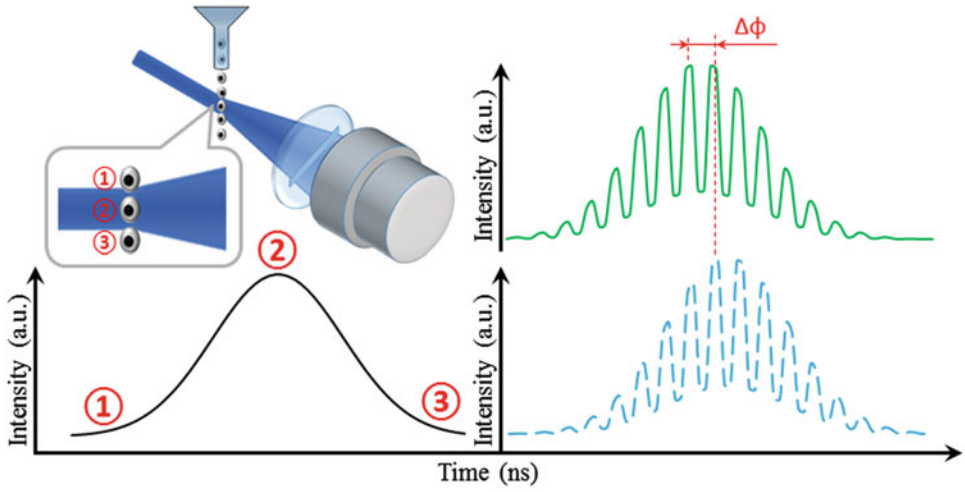

Fig. 3 (*Top left*) Fluorescent particles or cells (*small circular shapes*) pass through a continuous laser beam and the result is an emission or light scatter signal that increases and decreases to resemble a Gaussian shape (*bottom left*). The illustration depicts the signal rise and fall dependent on the particle's position in the laser beam. The particle is partially illuminated at position 1 when entering the laser beam, generated signal achieves highest intensity of the Gaussian profile when particle reaches position 2 and gradually decreases to 0 when particle leaves the laser beam at position 3. (*Right panel*) Representative fluorescence and side-scatter waveforms that result with frequency-domain flow cytometry. The phase shift ($\Delta\Phi$) between the reference (side-scatter channel) and the emission signal is used to compute the average fluorescence lifetime

a spherical particle passing through the perfectly aligned beam at an ideal laminar velocity profile. Equation 7 is a mathematical approximation of the emission collected by a flow cytometer, combining both the sinusoidal component as well as the Gaussian function:

$$E(t) = E_0[1 + m_{\text{em}} \sin(\omega t - \phi_{\text{em}})] \cdot e^{-a^2(t-t_0)^2} \tag{10}$$

The calculation of the fluorescence lifetime in flow cytometry requires digitization of fluorescence emission as well as an excitation reference signal. Therefore, the correlated side scattered light signal (mathematical approximation in Eq. 11) is used as the reference.

$$E(t) = E_0[1 + m_{\text{ex}} \sin(\omega t - \phi_{\text{ex}})] \cdot e^{-a^2(t-t_0)^2} \tag{11}$$

The digitized signals represented by Eqs. 10 and 11 are processed with a discrete Fourier Transform, Goertzel algorithm, non-linear regression, or other favored signal processing step that results in an accurate measure of the phase and amplitude of each correlated waveform for all cells measured. The type of digital signal processing will vary depending on the speed required to calculate the fluorescence lifetime as a real-time parameter for cell counting and/or cell sorting [9, 36].

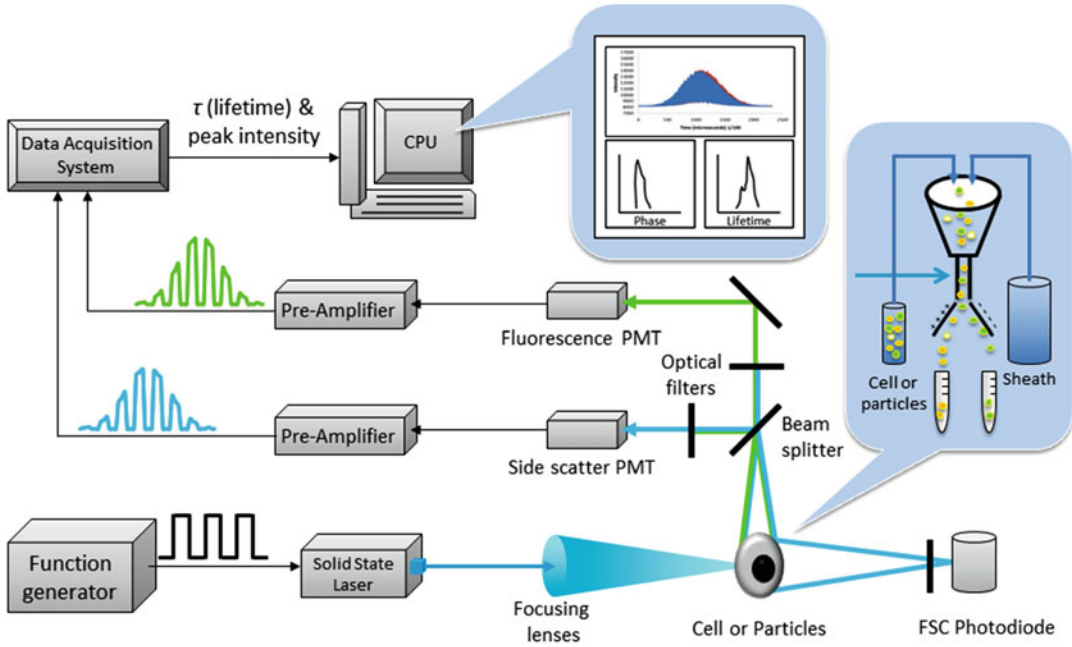

Fig. 4 Schematic that illustrates the basic components of a frequency-domain flow cytometer. The instrument depicted might be a result of a retrofitted commercial flow cytometer or "home-built" system. Cells passing through a square-wave and digitally modulated laser diode emit fluorescence and side scatter, which are detected by photomultiplier tubes (PMTs). The PMT output is routed to high frequency preamplifiers and subsequently digitized directly with a high speed digital data acquisition system. Either real-time or off-line histograms are formed using digital signal processing or calculations off-line with MATLAB, for example

Figure 4 is an illustration schema of frequency-domain flow cytometry. In this schematic, the laser modulation is represented by a square wave function with a fundamental RF frequency. Among a variety of ways to optimize frequency-domain instruments, one important consideration is the photoelectron transit time spread of the photo-multiplier tube detectors. A PMT specified with a minimum spread is optimal for the output response when short pulses, or rapidly modulating light are collected. Additional considerations are the use of solid state laser diodes that can be directly modulated, the need for preamplifier with high frequency capabilities, as well as data acquisition systems with digitization rates compatible with MHz frequencies.

Frequency-domain systems were first introduced as "phase-sensitive flow cytometry" [1, 37–39], taking the form of analog homodyning systems. A thorough review of the operation of these instruments is provided by Houston et al. (2012) [36]. Briefly, phase-sensitive flow cytometry led to a range of instrumentation capabilities and configurations including early versions of digital lifetime acquisition at one modulation frequency (20-MHz), simultaneous modulation of laser excitation at 16-MHz and 45-MHz,

and many demonstrations with labeled cells and microspheres [6, 8, 16, 21, 40–42]. Some examples toward the advancement of frequency-domain flow cytometry include work by Jenkins et al., Sands et al., and Cao et al. [10, 11, 43]. Jenkins and colleagues leveraged square wave RF laser modulation to extract multiple phase shifts from the multiple odd harmonics that result when a square wave is decomposed with Fourier methods. Sands and Cao introduced the use of the phasor plot in flow cytometry. A phasor plot combines the phase shift, ϕ, and demodulation, M, parameters from a frequency-domain fluorescence measurement. Within a phasor plot, points on a graph are at a radial distance from the pole, which is equal to the measured demodulation. The angle between the phasor axis (x-axis) and the radius is called the phasor angle, which is equal to the angle of phase shift (*see* Fig. 5). Presenting data in this fashion provide a visual tool to reveal differences in fluorescence lifetimes as a result of the phase shift and demodulation values. The FLIM and fluorimetry community have been implementing phasor plots for several years [27, 44, 45] because of the ease with which one can visualize distributions of

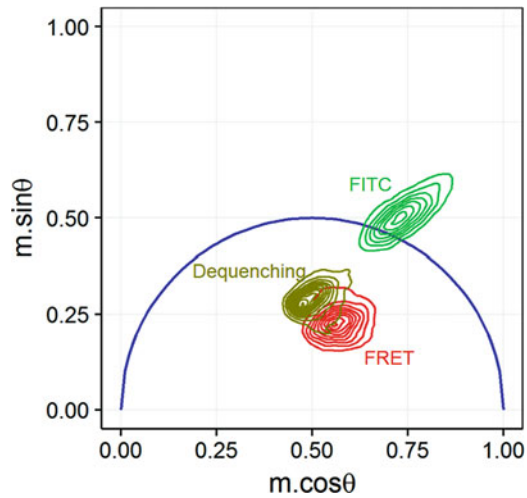

Fig. 5 A MATLAB-generated phasor plot. The graph is an *x* vs *y* polar plot and is a common lifetime visualize tool in FLIM and is now emerging in time-resolved flow cytometry. In this figure, a simulation was performed with frequency-domain modulation of 25 MHz and two independent fluorescence lifetimes (19 and 4-ns). The points located on semicircle are vectors with magnitude and directions which equal the demodulation and phase shift, respectively. The points that fall on the semicircle represent signals from single exponential fluorescence decay kinetics. A line joining two of the simulated single fluorescence lifetime points is added to show where any other vector (phase and modulation component of a fluorescence signal) might be located if the fluorescence lifetime falls in between the single lifetime values which the line connects (i.e., between 4 and 19 ns)

multiple lifetime components taken from an image of a group of cells. The pseudophasor plot was first introduced in flow cytometry for cell sorting [10]. The pseudophasor plot graphs the real and imaginary components of the Fourier output as a 2-D histogram so that sort gates can be based on values that are dependent on fluorescence decay kinetics.

In other frequency-domain cytometry advancements, phase-filtering and microfluidic systems were developed. The phase-filtering approach is an adaptation of phase and modulation measurements; it provides a way to sort cells based on a fluorescence lifetime value under conditions where the entire cell population expresses equal fluorescence output (i.e., color and intensity). The approach is performed with population distributions whereby the entire cell suspension emits at similar emission levels, yet a fraction of the population has a different fluorescence lifetime, perhaps owing to the presence of a particular biochemical or molecular feature present within that smaller percentage of cells. Thus phase-filtering will enable the isolation and sorting of the desired cell fraction by collecting the phase-shifts cell-by-cell and processing the values with frequency-domain mixing hardware and subsequently connecting to a sorting instrument's data acquisition board [11]. In other modern frequency-domain cytometry systems, microfluidic chips were combined with RF laser modulation sources and aligned in a sequential manner in order to alternate bright and dark zones for cells to pass through. In one example, the laser excitation sources were aligned in series for fluorescent protein photobleaching studies and to understand the unique excited state kinetics (i.e., ground state depletion) of protein variants [32, 33, 46].

The second form of time-resolved flow cytometry involves time-domain methods; methods that are not frequency-domain are categorized herein as time-domain. With time-domain approaches, the fluorescence decay is observed over time with single photon counting detectors, then measured and fit using single or multiple exponential decay functions. The measurement is practiced by pulsing the excitation laser source and with precise timing collecting the emission photons after laser pulsation. The decaying emission is collected by gating a detector, which involves activating its photosensitivity simultaneous to laser pulsation and then deactivating the detector after a short time for photons to be counted during fluorescence decay. This method when integrated with flow cytometry hardware requires precise timing and is coupled with off-line analyses to fit exponential decay data and provide a fluorescence lifetime output, which can then be turned into a cytometric parameter and plotted in a histogram format.

Some recent examples of time-domain cytometry systems are described herein. In 2013, Li et al. developed a pseudo-time-resolved system with a "fluorescence lifetime excitation cytometry by kinetic dithering" (FLECKD) instrument. The system takes

hydrodynamically focused cells and rapidly moves a finely focused laser across each cell multiple times before the cell exits the detection region. This essentially "dithers" the laser via an acousto-optic deflector so rapidly that the result is similar to pulsing the laser [47]. The pulse width of the dithered laser is approximately 25-ns FWHM, and the beam is moved approximately 10–20 times across each moving cell. With the FLECKD instrument, Li et al. were able to observe single exponential fluorescence decays for a range of fluorescent microspheres and cells. Figure 6 is a figure adapted from Li et al. to illustrate this concept. Recently, Nebdal et al. modified an automated microscope platform and combined it with a microfluidic chip in order to extract fluorescence decay kinetics of cells passing through the microfluidic channels [14]. A picosecond pulsed laser source excited each sample, and time-correlated single photon counting (TCSPC) was performed with a detector. Off-line analysis using non-linear regression permitted acquisition of fluorescence lifetimes. Similarly, time-domain cytometry examples described in the literature [48–50] include CCD detectors that are gated to collect emission over longer times (i.e., milliseconds). Cytometry systems that collect the timing of phosphorescence have

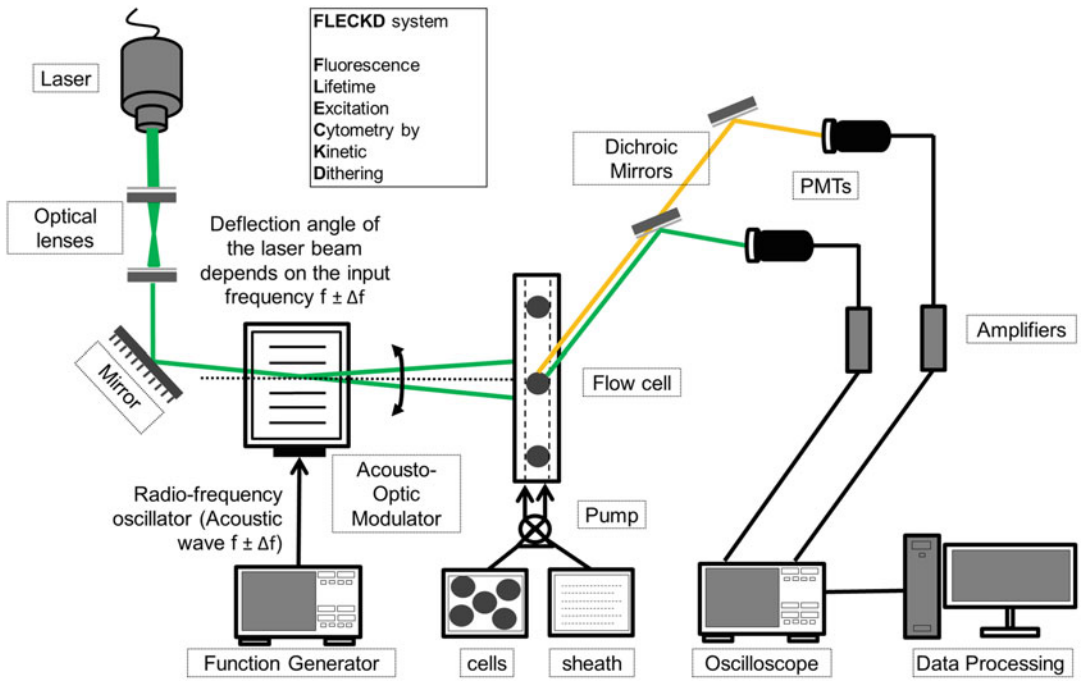

Fig. 6 Schematic of the fluorescence lifetime excitation by kinetic dithering (FLECKD) system. A continuous laser beam is focused onto an acoustic-optic deflector, which dithers the laser beam across the flow cell in a lateral direction multiple times as the event (i.e., cell or microsphere) is moving. This system acquires data with an oscilloscope, however a high data acquisition system is a possible way to collect data in real-time for the cytometric throughput

been developed using CCD camera systems, and are mentioned here because of the high-throughput nature and time-domain approach.

A recent report by Cao and colleagues showed the ability to measure average fluorescence lifetimes [51] with an approach that is neither time-domain nor frequency-domain per se. The premise was to use cytometry to measure the fluorescence lifetime with neither pulsed nor modulated lasers. Demonstrations were validated where cytometry data in the form of standard waveforms were processed for the inherent information they carry, which leads to a calculation of the average fluorescence lifetime cell-by-cell at a nominal cytometric throughput. The fluorescence lifetime was proven to be proportional to the average peak-to-peak pulse delay between correlated fluorescence and scattered light signals. Signal processing steps were tested to see which algorithm best fit the cytometrically collected Gaussian-like waveforms. The promising aspect of this paradigm is that it shows how any existing commercial instrument is inherently capable of detecting average fluorescence lifetime measurements. As described, there are many versions of time-resolved flow cytometers and expectedly many more applications. The section that follows provides a summary of the single cell analyses performed with systems such as those described previously.

4 Applications of Time-Resolved Flow Cytometry

Single cell counting and sorting applications of time-resolved flow cytometry range from measurement of exogenous fluorophores to fluorescent proteins. Each application ranges in purpose and advantage, and provides unique methods for understanding intracellular phenomena. Table 2 provides a comprehensive list of a variety of time-resolved applications where fluorescence lifetimes were reported for a variety of cell or microsphere measurements.

4.1 Exogenous Fluorophores and Microspheres

Early time-resolved flow cytometry experiments (pre-2000s) concentrated on fluorescence lifetime measurements of propidium iodide (PI), ethidium bromide (EB), and fluorescein isothiocyanate (FITC), all of which are organic fluorophores that intercalate into nucleic acids or proteins after cellular fixation. PI, EB, and FITC have average fluorescence lifetimes of 12.0-, 19.3-, and 4.0-ns, respectively [3, 7, 19–21, 23, 40, 53, 54] and which depend on how they are bound to molecules within the cell. For example, phase-sensitive flow cytometry instruments measured the fluorescence lifetime shift of EB, which changes when intercalated into nucleic acids. Phase-sensitive flow cytometers also measured the fluorescence lifetime of PI when it nonspecifically binds to proteins within fixed cells. The fluorescence lifetime of FITC was measured

Table 2
Chronological listing of the various time-resolved flow cytometry instruments and applications described in the literature

Year, citation	Title of time-resolved cytometry instrument development and/or application	Approach
1993 [1]	A flow cytometer for resolving signals from heterogeneous fluorescence emissions and quantifying lifetime in fluorochrome-labeled cells/particles by phase-sensitive detection	Frequency domain
1993 [4]	Resolution of fluorescence signals from cells labeled with fluorochromes having different lifetimes by phase-sensitive flow cytometry	Frequency domain
1993 [2]	Fluorescence lifetime-based sensing of pH, Ca^{2+}, K+ and glucose	Frequency domain
1993 [3]	Phase-resolved fluorescence lifetime measurements for flow cytometry	Frequency domain
1994 [39]	Phase-sensitive detection methods for resolving fluorescence emission signals and directly quantifying lifetime	Frequency domain
1994 [6]	Fluorescence lifetime measurements in a flow cytometer by amplitude demodulation using digital data acquisition techniques	Frequency domain
1995 [40]	Simultaneous dual-frequency phase-sensitive flow cytometric measurements for rapid identification of heterogeneous fluorescence decays in fluorochrome-labeled cells and particles	Frequency domain
1996 [16]	Analysis of fluorescence lifetime and quenching of FITC-conjugated antibodies on cells by phase-sensitive flow cytometry	Frequency domain
1996 [52]	Time-resolved fluorescence-decay measurement and analysis on single cells by flow cytometry	Time domain
1996 [21]	Interactions of intercalating fluorochromes with DNA analyzed by conventional and fluorescence lifetime flow cytometry utilizing deuterium oxide	Frequency domain
1997 [18]	Monitoring uptake of ellipticine and its fluorescence lifetime in relation to the cell cycle phase by flow cytometry	Frequency domain
1997 [20]	Differential effects of deuterium oxide on the fluorescence lifetimes and intensities of dyes with different modes of binding to DNA	Frequency domain
1998 [41]	Flow cytometric fluorescence lifetime analysis of DNA-binding probes	Frequency domain
1998 [53]	Fluorescence lifetime measurement of free and cell/particle-bound fluorophore by phase-sensitive flow cytometry	Frequency domain
1998 [23]	Apoptosis induced with different cycle-perturbing agents produces differential changes in the fluorescence lifetime of DNA-bound ethidium bromide	Frequency domain
1998 [41]	Flow cytometric characterization and classification of multiple dual-color fluorescent microspheres using fluorescence lifetime	Frequency domain
1999 [7]	Fluorescence intensity and lifetime measurement of free and particle-bound fluorophore in a sample stream by phase-sensitive flow cytometry	Frequency domain

(continued)

Table 2 (continued)

Year, citation	Title of time-resolved cytometry instrument development and/or application	Approach
1999 [54]	Enhanced immunofluorescence measurement resolution of surface antigens on highly autofluorescent, glutaraldehyde-fixed cells analyzed by phase-sensitive flow cytometry	Frequency domain
1999 [8]	Discrimination of damaged/dead cells by propidium iodide uptake in immunofluorescently labeled populations analyzed by phase-sensitive flow cytometry	Frequency domain
1999 [24]	Simultaneous analysis of relative DNA and glutathione content in viable cells by phase-resolved flow cytometry	Frequency domain
2000 [8]	Flow cytometric, phase-resolved fluorescence measurement of propidium iodide uptake in macrophages containing phagocytized fluorescent microspheres	Frequency domain
2001 [25]	Time-resolved fluorescence measurements	Frequency domain
2003 [26]	Fluorescence lifetime-based discrimination and quantification of cellular DNA and RNA with phase-sensitive flow cytometry	Frequency domain
2006 [55]	Effect of polystyrene microsphere surface to fluorescence lifetime under two-photon excitation	Time domain
2007 [56]	Practical time-gated luminescence flow cytometry. I: concepts	Time domain and frequency domain
2010 [9]	Digital acquisition of fluorescence lifetime by frequency-domain flow cytometry	Frequency domain
2010 [57]	Resolving multiple fluorescence decays from single cytometric events	Frequency domain
2011 [43]	Flow cytometric separation of spectrally overlapping fluorophores using multifrequency fluorescence lifetime analysis	Frequency domain
2012 [36]	Capture of fluorescence decay times by flow cytometry	Frequency domain
2012 [32]	Microfluidic flow cytometer for quantifying photobleaching of fluorescent proteins in cells	Micro fluidic
2012 [58]	Time-gated orthogonal scanning automated microscopy (OSAM) for high-speed cell detection and analysis	Time domain
2012 [59]	Microfluidic sorting of microtissues	Micro fluidic
2013 [11]	Cytometric sorting based on the fluorescence lifetime of spectrally overlapping signals	Frequency domain
2013 [12]	Subcellular localization-dependent changes in EGFP fluorescence lifetime measured by time-resolved flow cytometry	Frequency domain
2014 [10]	Measuring and sorting cell populations expressing isospectral fluorescent proteins with different fluorescence lifetimes	Frequency domain
2014 [51]	Expanding the potential of standard flow cytometry by extracting fluorescence lifetimes from cytometric pulse shifts	Non time/ frequency domain

(continued)

Table 2
(continued)

Year, citation	Title of time-resolved cytometry instrument development and/or application	Approach
2014 [47]	Fluorescence lifetime excitation cytometry by kinetic dithering	Time domain
2014 [49]	Tunable lifetime multiplexing using luminescent nanocrystals	Time domain
2014 [60]	High-throughput measurement of the long excited-state lifetime of quantum dots in flow cytometry	Frequency domain
2014 [48]	On-the-fly decoding luminescence lifetimes in the microsecond region for lanthanide-encoded suspension arrays	Time domain
2014 [46]	Microfluidic flow cytometer for multiparameter screening of fluorophore photophysics	Frequency domain and micro fluidic
2014 [61]	High-throughput time-correlated single photon counting	Time domain and micro fluidic
2014 [62]	À la fizeau in flow: pulse shape-assisted fluorescence lifetime	Frequency domain
2015 [13]	Toward the measurement of multiple fluorescence lifetimes in flow cytometry: maximizing multi-harmonic content from cells and microspheres	Frequency domain
2015 [14]	Time-domain microfluidic fluorescence lifetime flow cytometry for high-throughput Förster resonance energy transfer screening	Time domain and micro fluidic
2015 [50]	Tuning upconversion luminescence lifetimes of KYb2F7: Ho3+ nanocrystals for optical multiplexing	Time domain
2015 [63]	High-speed multiparameter photophysical analyses of fluorophore libraries	Frequency domain and micro fluidic
2015 [33]	Time and frequency-domain measurement of ground-state recovery times in red fluorescent proteins	Time domain and frequency domain
2015 [64]	A high-throughput direct fluorescence resonance energy transfer-based assay for analyzing apoptotic proteases using flow cytometry and fluorescence lifetime measurements	Frequency domain

when conjugated to antibodies and bound to cell surface receptors [16]. The phase-sensitive flow cytometry measurements of PI, EB, and FITC involved fluorescently labeled mammalian cell cultures (e.g., Chinese hamster ovary, mouse thymus) and in some cases these fluorophores were measured when imbibed into microspheres [21, 25, 40]. A notable example of phase-sensitive cell counting includes the measurement of DNA content in the presence of RNA. The fluorescence lifetime of EB when intercalated into DNA is different and distinct from RNA, and therefore provides an alternative for cell cycle measurements [25, 26].

In general, there have been a wide range of time-resolved flow cytometry studies involving bright, exogenous organic

fluorophores that are bound to fixed or viable cells. The purpose of each lifetime study varies, and they are too numerous to describe herein. Refer to Table 2 for a chronological overview of different applications. Some examples include work discovering the effects of deuterium oxide on the decay kinetics of EB, monitoring DNA and glutathione content with Hoechst 33342 and monobromobimane; discriminating damaged vs. dead cells using PI, detecting bound from un-bound cell surface receptors with FITC, and determining the order of the bi-layer lipid membrane with a lipophilic dye, di-4-ANEPPDHQ [16, 18, 23, 26, 42, 65]. The overall goal of many time-resolved measurements is to show that the fluorescence lifetimes provide a means to discriminate intracellular markers that are otherwise non-detectable with fluorescence intensity-only cytometry.

4.2 Fluorescent Proteins

In addition to the bright and commonly used organic fluorophores, a variety of fluorescent proteins (FPs) have been measured with time-resolved flow cytometry. The expression of fluorescent proteins in single cells contributes to functional cellular information that can be obtained with a flow cytometer such as protein–protein interactions, protein conformation, protein movement, gene expression, and cell signaling, for example. With time-resolved cytometry, the fluorescence lifetime of the expressed proteins adds a quantitative parameter owing to the fact that FPs generally have lower quantum yields, broad emission spectra, weaker fluorescent signals, and are susceptible to photobleaching. For example, time-resolved flow cytometry might discriminate between the dim FP signal and autofluorescence background, which can be an issue in flow cytometry (i.e., complicates compensation).

Fluorescent proteins might also experience quenching or excited state lifetime shifts when exposed to different microenvironments and therefore can indirectly indicate intracellular biochemistry. For example, a time-resolved experiment explored the ability to measure GFP position within a cell by inducing GFP movement from diffuse cytoplasmic expression to collective aggregates during autophagy. GFP was fused to LC3 protein, which localizes within autophagosomes during the autophagy process. The fluorescence lifetime was measured when GFP was diffusely expressed in the cell and when it was collected into the punctate regions. The average fluorescence lifetime shortened by 0.4 ns during autophagy [12]. The benefit of measuring protein movement in the context of autophagy is the potential for high-throughput screening of compounds that might inhibit or affect autophagy using the GFP lifetime as a metric for reporting the stage of autophagy. In other fluorescent protein studies, complex fluorescence dynamics were studied with red fluorescent proteins and measured with frequency-domain flow cytometry [32]. The RFP expressers were evaluated for irreversible and reversible

photobleaching phenomena as well as characterization of [46] photostability and photoactivatable features [33].

Fluorescent protein expression in cells measured with flow cytometers is often coupled with cell sorting. Therefore, if sort gates depend on fluorescence lifetime parameters, cell populations can be separated based on quantitative FRET efficiencies, quantum yields of the proteins, and dim protein expressers. In a recent example, fluorescent protein fusions in *Saccharomyces cerevisiae* were expressed and cells were sorted based on the measured excited state lifetimes [10]. The yeast cell study took average fluorescence lifetimes of teal fluorescent protein (TFP) and TFP when fused to dark-state Citrine fluorescent protein (dCit). Fluorescence lifetime differences existed owing to non-radiative energy transfer within the TFP-dCit construct as compared to TFP alone. Yet, the difference in the TFP vs TFP-dCit emission signal alone was not enough to sort *S. Cerevisiae* cell populations. Whereas the fluorescence lifetime-dependent parameters led to clearly distinct subpopulations when graphically represented by a pseudo-phasor plot. Described in previous sections, a phasor plot is analogous to a 2-D histogram where each event (i.e., dot) is positioned on the quadrant by the measured angle and magnitude, which are functions of fluorescence lifetime. In this example, cell sorts were possible based on fluorescence dynamics of the proteins expressed in cells when the fluorescence intensity was not enough to separate the subpopulations. However, sorting based on the fluorescence lifetime of proteins has another added benefit in that it provides a new approach for screening and isolating protein variants with high quantum yields. In a short report, Yang et al. described how the fluorescence lifetimes of near-infrared fluorescent proteins (iRFPs) expressed in *Escherichia coli* can be used to isolate variants with high quantum yields [66]. During the development of iRFP libraries, it is valuable to have a high-throughput sorting instrument that can separate cells with high quantum yield variants. The quantum yield is proportional to the fluorescence lifetime, thus a sorting parameter that can be used to isolate bright and stable proteins from those that appear bright for other reasons (i.e., quantum efficiency, number of FP molecules present, instrumentation artifacts). Overall fluorescent protein measurements with cytometry can benefit from fluorescence lifetime measurements, particularly in cases that involve energy transfer and protein interactions.

4.3 Förster Resonance Energy Transfer

A number of recent time-resolved applications either with or without fluorescent proteins have involved Förster resonance energy transfer (FRET) bioassays. FRET is a non-radiative energy transfer event between a fluorescent donor and fluorescent acceptor molecule. The fluorescence lifetime is a quantitative metric for FRET

because the donor fluorescence lifetime shortens by several hundred picoseconds when it is quenched by energy transfer with the acceptor molecule [5, 14, 30, 64, 67]. FRET efficiencies are validated by measuring average fluorescence lifetime [17], and therefore make precise measurements of protein-to-protein interactions or protein conformational changes [68–70]. One of the first demonstrations of FRET measured by time-resolved flow cytometry involved a study to screen the expression of caspases that are involved in apoptosis. Suzuki and co-workers labeled cells with fluorescent proteins (e.g., GFP, RFP) and exogenous fluorophore (Alexa dyes) FRET pairs. The FRET pairs, or "*bioprobes*," were linked by peptide sequences that were cleavable by caspase enzymes. Therefore, the bioprobes provided an indirect measure of caspase levels during apoptosis induction [64]. Other time-resolved FRET measurements in flow cytometry include GFP-RFP fusions linked by different lengths of peptide bridges. FRET efficiencies between GFP and RFP were measured using fluorescence lifetime changes, and were expectedly different depending on the length of the oligopeptide linker. In the same study, FRET efficiencies were measured by detecting GFP lifetime shortening when engaged in FRET with Cy3. An epidermal growth factor receptor (EGFR)-bound GFP interacted with an anti-phosphotyrosine antibody-bound Cy3 fluorophore. The study evaluated the activation of epidermal growth factor receptor tyrosine phosphorylation because the Cy3 bound antibody was recruited to the phosphorylated tyrosine site on EGFR and therefore was able to engage in FRET with the GFP [14].

5 Conclusion

As reviewed above, there are a wide variety of time-resolved flow cytometers as well as fluorescence lifetime applications that can be used for cell counting and sorting. Although these techniques are not marketed commercially, they are now enhancing the way flow cytometry can be utilized. It is beneficial as well that detecting fluorescence lifetimes or decay-kinetic dependent values with a flow cytometer does not remove the ability to detect traditional data parameters such as peak intensity, pulse width, and pulse area. Therefore, modulated or pulsed excitation light sources merely add to the parameter space for cytometric data collection and might even be adopted on new spectral cytometry or imaging cytometry systems.

The addition of fluorescence lifetime detection via digital or other data processing methods increases the total amount of information available to researchers. Off-line time-resolved parameters that may be of value to single cell analyses are possible with specialty computer programs that incorporate algorithms which process the

time-resolved signals into meaningful averages (e.g., regression of exponential decay into a lifetime value or Fourier analysis of multi-frequency signals into phase and modulation values). Post-processing requires MATLAB or another software program that can import digitized data and reprocess the numbers into list mode values whereby the fluorescence lifetime is the graphed parameter. In contrast, real-time fluorescence lifetime parameters are processed on-chip with programmable digital data acquisition systems (i.e., combined with FPGAs) using programming languages with simple and rapid algorithms (e.g., discrete Fourier transforms, Goertzel algorithms). The on-line analyses are particularly useful for cell sorting at nominal sort rates.

Future work in fluorescence lifetime measurements with a flow cytometer might involve more complicated approaches such as non-modulated waveform analyses, higher frequency modulation, digital heterodyning, or frequency aliasing, for example. Frequencies higher than the Nyquist frequency can be analyzed by exploiting aliased signals because this approach circumvents the limitations of analyzing frequencies beyond the digitization rate of the data system. It is desirable to inspect higher modulation frequencies because they lead to larger phase perturbations for the short fluorescence lifetime values (i.e., 100–500 ps). With aliasing, frequencies above any inherent Nyquist limit can be available as fold over frequencies, therefore frequencies higher than the Nyquist limit can be accessed. Aliasing is but only one example of how frequency-domain systems can be improved or expanded upon for better resolution of the fluorescence lifetime as a parameter.

In terms of the application space, future work may likely involve ways in which the fluorescence lifetime can be used to discriminate among spectrally overlapping signals, which is a recurring challenge in flow cytometry. Most applications lead back to the fact that the fluorescence lifetime is independent of fluorophore concentration and spectral emission and excitation wavelengths. Also emerging are single cell applications that build on measurements made using FLIM. Many opportunities remain for flow cytometry, which offers high-throughput cell counting or sorting measurements not present with lifetime microscopy. One untapped application is the measurement of autofluorescence lifetime shifts during bound and un-bound states of the metabolite, nicotinamide adenine dinucleotide (NADH). This specie is not only brightly autofluorescent but also has a unique free and protein-bound fluorescence lifetime [71]. Cytometry measurements of NADH can lead to high-throughput metabolic mapping of single cells and therefore add to current knowledge about cellular transformation from glycolytic states to oxidative phosphorylation. With the changing NADH decay kinetics, there is a need to detect when and how much of an intracellular species experiences a shift in its fluorescence lifetime. The quantification of multiple fluorescence lifetimes is

therefore quite valuable and can be applied to other intrinsic or extrinsic fluorophores.

Overall the rise in the number of flow cytometry assays that incorporate time-resolved measurements suggests a growing interest in high-throughput tools that count or sort cells based on the fluorescence lifetime. This chapter summarizes the various ways in which cytometrists have implemented lifetime measurements as well as the modern application space for these systems. A variety of machinations can be taken to transform existing cytometers into time-resolved systems or to build "ground-up" cytometers with this capability. Regardless, new analysis approaches and applications such as phasor plots combined with FRET should evolve in parallel to best leverage this measurement into an approach that provides meaningful biological information.

References

1. Steinkamp JA, Yoshida TM, Martin JC (1993) Flow cytometer for resolving signals from heterogeneous fluorescence emissions and quantifying lifetime in fluorochrome-labeled cells/particles by phase-sensitive detection. Rev Sci Instrum 64(12):3440–3450
2. Lakowicz JR, Szmacinski H (1993) Fluorescence lifetime-based sensing of pH, Ca 2+, K+ and glucose. Sens Actuators B Chem 11 (1):133–143
3. Pinsky BG, Ladasky JJ, Lakowicz JR, Berndt K, Hoffman RA (1993) Phase-resolved fluorescence lifetime measurements for flow cytometry. Cytometry A 14(2):123–135
4. Steinkamp JA, Crissman HA (1993) Resolution of fluorescence signals from cells labeled with fluorochromes having different lifetimes by phase-sensitive flow cytometry. Cytometry A 14(2):210–216
5. Lakowicz JR (2013) Principles of fluorescence spectroscopy. Springer Science & Business Media, New York
6. Deka C, Sklar LA, Steinkamp JA (1994) Fluorescence lifetime measurements in a flow cytometer by amplitude demodulation using digital data acquisition technique. Cytometry A 17(1):94–101
7. Steinkamp JA, Keij JF (1999) Fluorescence intensity and lifetime measurement of free and particle-bound fluorophore in a sample stream by phase-sensitive flow cytometry. Rev Sci Instrum 70(12):4682–4688
8. Steinkamp JA, Lehnert BE, Lehnert NM (1999) Discrimination of damaged/dead cells by propidium iodide uptake in immunofluorescently labeled populations analyzed by phase-sensitive flow cytometry. J Immunol Methods 226(1):59–70
9. Houston JP, Naivar MA, Freyer JP (2010) Digital analysis and sorting of fluorescence lifetime by flow cytometry. Cytometry A 77 (9):861–872
10. Sands B, Jenkins P, Peria WJ, Naivar M, Houston JP, Brent R (2014) Measuring and sorting cell populations expressing isospectral fluorescent proteins with different fluorescence lifetimes. PLoS One 9(10):e109940
11. Cao R, Pankayatselvan V, Houston JP (2013) Cytometric sorting based on the fluorescence lifetime of spectrally overlapping signals. Opt Express 21(12):14816–14831
12. Gohar AV, Cao R, Jenkins P, Li W, Houston JP, Houston KD (2013) Subcellular localization-dependent changes in EGFP fluorescence lifetime measured by time-resolved flow cytometry. Biomed Opt Express 4(8):1390–1400
13. Jenkins P, Naivar MA, Houston JP (2015) Toward the measurement of multiple fluorescence lifetimes in flow cytometry: maximizing multi-harmonic content from cells and microspheres. J Biophotonics 8(11–12):908–917. doi:10.1002/jbio.201400115
14. Nedbal J, Visitkul V, Ortiz-Zapater E, Weitsman G, Chana P, Matthews DR, Ng T, Ameer-Beg SM (2015) Time-domain microfluidic fluorescence lifetime flow cytometry for high-throughput Förster resonance energy transfer screening. Cytometry A 87(2):104–118
15. Okabe K, Inada N, Gota C, Harada Y, Funatsu T, Uchiyama S (2012) Intracellular temperature mapping with a fluorescent polymeric thermometer and fluorescence lifetime imaging microscopy. Nat Commun 3:705

16. Deka C, Lehnert BE, Lehnert NM, Jones GM, Sklar LA, Steinkamp JA (1996) Analysis of fluorescence lifetime and quenching of FITC-conjugated antibodies on cells by phase-sensitive flow cytometry. Cytometry A 25 (3):271–279
17. Gopich IV, Szabo A (2012) Theory of the energy transfer efficiency and fluorescence lifetime distribution in single-molecule FRET. Proc Natl Acad Sci U S A 109(20):7747–7752
18. Sailer BL, Valdez JG, Steinkamp JA, Darzynkiewicz Z, Crissman HA (1997) Monitoring uptake of ellipticine and its fluorescence lifetime in relation to the cell cycle phase by flow cytometry. Exp Cell Res 236(1):259–267
19. Steinkamp JA, Valdez YE, Lehnert BE (2000) Flow cytometric, phase-resolved fluorescence measurement of propidium iodide uptake in macrophages containing phagocytized fluorescent microspheres. Cytometry 39(1):45–55
20. Sailer BL, Nastasi AJ, Valdez JG, Steinkamp JA, Crissman HA (1997) Differential effects of deuterium oxide on the fluorescence lifetimes and intensities of dyes with different modes of binding to DNA. J Histochem Cytochem 45 (2):165–175
21. Sailer BL, Nastasi AJ, Valdez JG, Steinkamp JA, Crissman HA (1996) Interactions of intercalating fluorochromes with DNA analyzed by conventional and fluorescence lifetime flow cytometry utilizing deuterium oxide. Cytometry A 25(2):164–172
22. Sailer BL, Steinkamp JA, Crissman HA (1997) Flow cytometric fluorescence lifetime analysis of DNA-binding probes. Eur J Histochem 42:19–27
23. Sailer BL, Valdez JG, Steinkamp JA, Crissman HA (1998) Apoptosis induced with different cycle-perturbing agents produces differential changes in the fluorescence lifetime of DNA-bound ethidium bromide. Cytometry A 31 (3):208–216
24. Keij JF, Bell-Prince C, Steinkamp JA (1999) Simultaneous analysis of relative DNA and glutathione content in viable cells by phase-resolved flow cytometry. Cytometry A 35 (1):48–54
25. Steinkamp JA (2001) Time-resolved fluorescence measurements. Curr Protc Cytom:1.15. 11–11.15. 16
26. Cui HH, Valdez JG, Steinkamp JA, Crissman HA (2003) Fluorescence lifetime-based discrimination and quantification of cellular DNA and RNA with phase-sensitive flow cytometry. Cytometry A 52(1):46–55. doi:10.1002/cyto.a.10022
27. Digman MA, Caiolfa VR, Zamai M, Gratton E (2008) The phasor approach to fluorescence lifetime imaging analysis. Biophys J 94(2): L14–L16. doi:10.1529/biophysj.107.120154
28. Skala MC, Riching KM, Gendron-Fitzpatrick A, Eickhoff J, Eliceiri KW, White JG, Ramanujam N (2007) In vivo multiphoton microscopy of NADH and FAD redox states, fluorescence lifetimes, and cellular morphology in precancerous epithelia. Proc Natl Acad Sci U S A 104 (49):19494–19499. doi:10.1073/pnas.0708425104
29. Periasamy A, Elangovan M, Elliott E, Brautigan DL (2002) Fluorescence lifetime imaging (FLIM) of green fluorescent fusion proteins in living cells. Methods Mol Biol 183:89–100. doi:10.1385/1-59259-280-5:089
30. Chen Y, Mills JD, Periasamy A (2003) Protein localization in living cells and tissues using FRET and FLIM. Differentiation 71 (9–10):528–541. doi:10.1111/j.1432-0436.2003.07109007.x
31. Sun Y, Periasamy A (2015) Localizing protein-protein interactions in living cells using fluorescence lifetime imaging microscopy. Methods Mol Biol 1251:83–107. doi:10.1007/978-1-4939-2080-8_6
32. Lubbeck JL, Dean KM, Ma H, Palmer AE, Jimenez R (2012) Microfluidic flow cytometer for quantifying photobleaching of fluorescent proteins in cells. Anal Chem 84(9):3929–3937
33. Manna P, Jimenez R (2015) Time and frequency-domain measurement of ground-state recovery times in red fluorescent proteins. J Phys Chem B 119(15):4944–4954
34. Boens N, Qin W, Basarić N, Hofkens J, Ameloot M, Pouget J, Lefèvre J-P, Valeur B, Gratton E, van de Ven M, Silva ND, Engelborghs Y, Willaert K, Sillen A, Rumbles G, Phillips D, AJWG V, van Hoek A, Lakowicz JR, Malak H, Gryczynski I, Szabo AG, Krajcarski DT, Tamai N, Miura A (2007) Fluorescence lifetime standards for time and frequency domain fluorescence spectroscopy. Anal Chem 79 (5):2137–2149. doi:10.1021/ac062160k
35. Becker W (2012) Fluorescence lifetime imaging–techniques and applications. J Microsc 247 (2):119–136
36. Houston JP, Naivar MA, Jenkins P, Freyer JP (2012) Capture of fluorescence decay times by flow cytometry. Curr Protoc Cytom:1.25.1–1.25.21
37. Steinkamp JA, Crissman HA (1993) Resolution of fluorescence signals from cells labeled with fluorochromes having different lifetimes by phase-sensitive flow cytometry. Cytometry 14(2):210–216
38. Pinsky BG, Ladasky JJ, Lakowicz JR, Berndt K, Hoffman RA (1993) Phase-resolved

fluorescence lifetime measurements for flow cytometry. Cytometry 14(2):123–135

39. Steinkamp JA (1994) Phase-sensitive detection methods for resolving fluorescence emission signals and directly quantifying lifetime. Methods Cell Biol 42:627
40. Deka C, Cram LS, Habbersett R, Martin JC, Sklar LA, Steinkamp JA (1995) Simultaneous dual-frequency phase-sensitive flow cytometric measurements for rapid identification of heterogeneous fluorescence decays in fluorochrome-labeled cells and particles. Cytometry A 21(4):318–328
41. Keij JF, Steinkamp JA (1998) Flow cytometric characterization and classification of multiple dual-color fluorescent microspheres using fluorescence lifetime. Cytometry A 33(3):318–323
42. Sailer BL, Nastasi AJ, Valdez JG, Steinkamp JA, Crissman HA (1998) Interactions of intercalating fluorochromes with DNA analyzed by conventional and fluorescence lifetime flow cytometry utilizing deuterium oxide. Cytometry A 25(2):164–172
43. Jenkins PL, Freyer JP, Naivar MS, Arteaga A, Houston JP (2011) Flow cytometric separation of spectrally overlapping fluorophores using multifrequency fluorescence lifetime analysis. In: SPIE BiOS., 2011. International Society for Optics and Photonics, pp 790216–790218
44. Stringari C, Cinquin A, Cinquin O, Digman MA, Donovan PJ, Gratton E (2011) Phasor approach to fluorescence lifetime microscopy distinguishes different metabolic states of germ cells in a live tissue. Proc Natl Acad Sci U S A 108(33):13582–13587. doi:10.1073/pnas.1108161108
45. Colyer RA, Lee C, Gratton E (2008) A novel fluorescence lifetime imaging system that optimizes photon efficiency. Microsc Res Tech 71 (3):201–213. doi:10.1002/jemt.20540
46. Dean KM, Davis LM, Lubbeck JL, Manna P, Palmer AE, Jimenez R (2014) Microfluidic flow cytometer for multiparametric screening of fluorophore photophysics. Opt Soc Am:1–3
47. Li W, Vacca G, Castillo M, Houston KD, Houston JP (2014) Fluorescence lifetime excitation cytometry by kinetic dithering. Electrophoresis 35(12–13):1846–1854
48. Lu Y, Lu J, Zhao J, Cusido J, Raymo FM, Yuan J, Yang S, Leif RC, Huo Y, Piper JA (2014) On-the-fly decoding luminescence lifetimes in the microsecond region for lanthanide-encoded suspension arrays. Nat Commun 5:3741
49. Lu Y, Zhao J, Zhang R, Liu Y, Liu D, Goldys EM, Yang X, Xi P, Sunna A, Lu J (2014) Tunable lifetime multiplexing using luminescent nanocrystals. Nat Photonics 8(1):32–36
50. Ding M, Chen D, Ma D, Liu P, Song K, Lu H, Ji Z (2015) Tuning the upconversion luminescence lifetimes of KYb2F7: Ho3+ nanocrystals for optical multiplexing. Chem Phys Chem 16 (18):3784–3789
51. Cao R, Naivar MA, Wilder M, Houston JP (2014) Expanding the potential of standard flow cytometry by extracting fluorescence lifetimes from cytometric pulse shifts. Cytometry A 85(12):999–1010
52. Deka C, Steinkamp JA (1996) Time-resolved fluorescence-decay measurement and analysis on single cells by flow cytometry. Appl Opt 35 (22):4481–4489
53. Steinkamp JA, Keij JF (1998) Fluorescence lifetime measurement of free and cell/particle-bound fluorophore by phase-sensitive flow cytometry. In: BiOS'98 international biomedical optics symposium. International Society for Optics and Photonics, pp 154–161
54. Steinkamp JA, Lehnert NM, Keij JF, Lehnert BE (1999) Enhanced immunofluorescence measurement resolution of surface antigens on highly autofluorescent, glutaraldehyde-fixed cells analyzed by phase-sensitive flow cytometry. Cytometry A 37(4):275–283
55. Tirri ME, Wahlroos R, Meltola NJ, Toivonen J, Hänninen PE (2006) Effect of polystyrene microsphere surface to fluorescence lifetime under two-photon excitation. J Fluoresc 16 (6):809–816
56. Jin D, Connally R, Piper J (2007) Practical time-gated luminescence flow cytometry. I: Concepts. Cytometry A 71(10):783–796
57. Jones T, Jenkins P, Houston J (2010) Resolving multiple fluorescence decays from single cytometric events. In: Biomedical optics. Optical Society of America, p BTuD113p
58. Lu Y, Xi P, Piper JA, Huo Y, Jin D (2012) Time-gated orthogonal scanning automated microscopy (OSAM) for high-speed cell detection and analysis. Sci Rep 2:837
59. Buschke DG, Resto P, Schumacher N, Cox B, Tallavajhula A, Vivekanandan A, Eliceiri KW, Williams JC, Ogle BM (2012) Microfluidic sorting of microtissues. Biomicrofluidics 6 (1):014116
60. Dahal E, Cao R, Jenkins P, Houston JP (2014) High-throughput measurement of the long excited-state lifetime of quantum dots in flow cytometry. In: SPIE BiOS. International Society for Optics and Photonics, pp 89470S–89478
61. Léonard J, Dumas N, Caussé J, Maillot S, Giannakopoulou N, Barre S, Uhring W

(2014) High-throughput time-correlated single photon counting. Lab Chip 14 (22):4338–4343

62. Bene L, Szöllősi J (2014) À la Fizeau in flow: Pulse shape-assisted fluorescence lifetime. Cytometry A 85(12):991–994
63. Dean KM, Davis LM, Lubbeck JL, Manna P, Friis P, Palmer AE, Jimenez R (2015) High-speed multiparameter photophysical analyses of fluorophore libraries. Anal Chem 87 (10):5026–5030
64. Suzuki M, Sakata I, Sakai T, Tomioka H, Nishigaki K, Tramier M (2015) A high-throughput direct FRET-based assay for analyzing apoptotic proteases using flow cytometry and fluorescence-lifetime measurements. Anal Biochem 491:10
65. Sailer BL, Steinkamp JL, Crissman HA (1998) Flow cytometric lifetime analysis of DNA-binding probes. Eur J Histochem 48:19–27
66. Yang Z, Shcherbakova D, Verkhusha V, Houston J (2016) Developing a time-resolved flow cytometer for fluorescence lifetime measurements of near-infrared fluorescent proteins. In: Conference on lasers and electro-optics CLEO 2016, San Jose, CA. Optical Society of America
67. Hinde E, Digman MA, Welch C, Hahn KM, Gratton E (2012) Biosensor Förster resonance energy transfer detection by the phasor approach to fluorescence lifetime imaging microscopy. Microsc Res Tech 75 (3):271–281. doi:10.1002/jemt.21054
68. Chigaev A, Buranda T, Dwyer DC, Prossnitz ER, Sklar LA (2003) FRET detection of cellular α4-integrin conformational activation. Biophys J 85(6):3951–3962. doi:10.1016/S0006-3495(03)74809-7
69. Chigaev A, Smagley Y, Haynes MK, Ursu O, Bologa CG, Halip L, Oprea T, Waller A, Carter MB, Zhang Y (2015) FRET detection of lymphocyte function-associated antigen-1 conformational extension. Mol Biol Cell 26(1):43–54
70. Chigaev A, Blenc AM, Braaten JV, Kumaraswamy N, Kepley CL, Andrews RP, Oliver JM, Edwards BS, Prossnitz ER, Larson RS (2001) Real time analysis of the affinity regulation of α4-integrin the physiologically activated receptor is intermediate in affinity between resting and Mn2+ or antibody activation. J Biol Chem 276(52):48670–48678
71. Lakowicz JR, Szmacinski H, Nowaczyk K, Johnson ML (1992) Fluorescence lifetime imaging of free and protein-bound NADH. Proc Natl Acad Sci U S A 89(4):1271–1275

Chapter 19

Overview of Lasers for Flow Cytometry

William G. Telford

Abstract

Lasers are critical elements of all flow cytometers. Instrument capabilities are dictated by the wavelengths and characteristics of its laser sources. In this chapter, we review the lasers available for flow cytometry, and provide guidance in choosing laser wavelengths and characteristics to best match the analytical needs of biomedical research laboratories.

Key words Flow cytometry, Laser, Diode, Diode-pumped solid state

1 Introduction

Lasers are the primary light sources in virtually all flow cytometers. Flow cytometers require powerful, highly shaped, and focused light sources, both for the resolution of forward and side light scatter, and for the excitation of the multitude of fluorescent probes used to determine cell identity, status, and physiology [1]. The first practical laser sources fortuitously preceded the development of the earliest flow cytometers by only a few years. While the earliest flow cytometers relied on lamp sources, the highly coherent nature of laser light has made it an ideal source for flow cytometric analysis.

The earliest commercial flow cytometer systems developed in the late 1970s and early 1980s were usually equipped with a single laser source, almost always a powerful, water-cooled gas laser. The blue-green or cyan 488 nm laser line, generated by water-cooled argon-ion lasers, became and remains the primary laser wavelength both for scatter measurement and fluorochrome excitation. Fluorescein, a low molecular weight fluorochrome that can be readily conjugated to antibodies and other proteins, is well-excited at this wavelength. Blue-green 488 nm excitation and fluorescein remain the most common excitation/emission pair in most flow cytometric techniques. The subsequent development of the naturally occurring phycobiliprotein phycoerythrin (PE) as a fluorescent probe increased the number of fluorescent parameters to two [2];

Teresa S. Hawley and Robert G. Hawley (eds.), *Flow Cytometry Protocols*, Methods in Molecular Biology, vol. 1678, DOI 10.1007/978-1-4939-7346-0_19,

the subsequent development of PE tandem dyes (PE-Cy5, PE-Cy5.5, and PE-Cy7) increased this number even further, allowing more than one fluorescent probe to be analyzed simultaneously.

While cyan 488 nm was and remains the primary wavelength used in flow cytometry, even the earliest instruments were not limited to this laser line. Water-cooled gas lasers can produce multiple laser lines depending on their dichroic properties of their Brewster mirrors, and can be modified to produce other wavelengths. Argon-ion lasers can generate ultraviolet (351 and 357 nm), green (514 nm), and blue (457 nm) at sufficient power levels. Krypton-ion lasers, frequently installed on early cytometers, can produce wavelengths in the ultraviolet (361, 365 nm), violet (405, 407, and 415 nm), green (523 and 530 nm), yellow (568 nm), and red (641 and 647 nm). Early flow cytometers could therefore take advantage of other fluorochromes not excited at 488 nm. Rhodamine, sulforhodamine, and Texas Red were all low molecular weight fluorochromes that could be excited with green or yellow laser sources from argon- or krypton-ion lasers [3]. Ultraviolet excited DNA dyes including DAPI and the Hoechst dyes saw the wide use for DNA content analysis and even chromosome analysis using the ultraviolet lines from gas lasers. The red lines from a krypton-ion source could excite Cy5, a low molecular weight red-excited fluorochrome. Red helium-neon (HeNe) lasers were air-cooled and could also analyze red-excited fluorochromes [4, 5]. More sophisticated flow cytometers could be equipped with two lasers, allowing simultaneous excitation with two spatially separated laser wavelengths [5, 6].

The late1980s and early 1990s ushered in significant improvements in laser technology, which were soon introduced into commercial flow cytometers. Early gas lasers were typically large, requiring water cooling. The first air-cooled argon-ion lasers were introduced; these were much smaller than their water-cooled counterparts, requiring only air cooling and lower power requirements [7]. This allowed the development of smaller flow cytometers that did not require extensive facility modifications. These smaller lasers were less powerful, but still excellent fluorescence sensitivity when combined with high-efficiency light collection optics. The first commercially practical solid state lasers were also introduced into flow cytometers. Red laser diodes were frequently included as a second laser source on many systems, allowing excitation of Cy5 and the phycobiliprotein allophycocyanin (APC), its tandem dyes and other red excited fluorochromes [8, 9]. Three- and four-color flow cytometry could now be routinely performed on small benchtop cytometers. More sophisticated cell sorters could now analyze five to eight fluorochromes simultaneously [10].

The late 1990s and the early 2000s continued the trend toward more excitation wavelengths in flow cytometry. Small, relatively inexpensive violet laser diodes were added as a third laser source

in many systems [11, 12]. Low molecular weight fluorochromes like Cascade Blue and Pacific Blue that previously required the violet laser lines from a water-cooled krypton-ion source could now be used on smaller benchtop instruments [13]. In addition to increasing the total number of simultaneous fluorochromes, this increase in available laser wavelengths was dramatically increasing the analysis flexibility of cytometers; many fluorescent probes, both old and new, were now accessible to cytometric analysis.

In the last 10 years, the laser wavelengths available for flow cytometry have increased even further. Solid state laser technology has advanced to the point that virtually any visible laser line can be generated. Green and yellow laser lines, previously generated only by gas lasers, were now available from diode-pumped solid laser sources in the form of green 532 nm and yellow 561 nm sources. These laser lines have been used extensively for both better excitation of PE and its tandem dyes, and to excite a wide variety of newly available red fluorescent proteins like DsRed and mCherry [14, 15]. Green and yellow laser sources have joined blue-green, red, and violet sources as standard equipment on many commercial systems. Violet lasers have become especially important for high-dimensional multicolor analysis with the development of quantum dots and the Brilliant Violet polymer fluorochromes [16–18]. Blue (440–460 nm) and orange (592–594 nm) lasers are often included in more advanced systems for fluorescent protein excitation [19–21]. Ultraviolet laser light, traditionally a difficult and expensive wavelength to produce from gas sources, is now available from smaller solid state sources [22, 23]. In addition to allowing the use of DNA-binding dyes like DAPI, it has achieved great importance for excitation of the newly available Brilliant Ultraviolet polymer fluorochromes. Near Infrared (NIR) lasers are starting to be introduced into commercial systems as well.

Nowadays, commercial flow cytometers are often equipped with three or four laser sources. Advanced custom systems can be equipped with ten or more different laser wavelengths. This selection has given us unprecedented capability and flexibility in fluorochrome detection. However, it has also made the selection of appropriate laser sources for a new system more challenging. In this chapter, we will discuss the laser technology and wavelengths available for cytometry, and provide guidelines for choosing wavelengths in a multicolor system. The field is fortunate in that many cytometer manufacturers have embraced the introduction of multiple and novel laser sources in their instrument platforms. However, it is the responsibility of the end user to choose laser sources applicable to their research objectives. This chapter will provide guidance in reaching this goal.

2 Laser and Cytometer Terminology

The following laser and cytometer characteristics should be understood when choosing laser sources for a new cytometer system. The design of the cytometer (cuvette versus stream-in-air, spatially separated versus collinear intercepts, etc.) will dictate the laser types and configurations that can be accommodated. While the instrument manufacturer will manage these issues, it is important for the end user to be aware of these constraints when designing their cytometer optical configuration.

2.1 Cuvette Versus Stream-in-Air

Almost all flow cytometers require a fluid delivery system to pass cells through a laser source and "interrogate" the resulting scatter and fluorescent signals. This stream is composed of an internal core stream (containing the cells) and a cylindrical outer sheath stream that encompasses the cells and hydrodynamically focuses them in the core stream. This hydrodynamic focusing confines the cells to a very narrow core, and ensures optimal alignment between the sample stream and the laser beam.

Most benchtop flow cytometers use a quartz cuvette to confine the sheath and core streams. The laser is focused on the stream contained within the cuvette, and light collection optics can be gel coupled at a 90° angle to the laser beam for efficient fluorescence signal collection. These so-called *cuvette cytometers* are by far the most dominant design in modern flow cytometry. Almost all cuvette systems use hydrodynamic focusing, although a small number use narrow capillaries and other methods to achieve stream alignment.

Flow cytometers equipped for fluorescence-activated cell sorting (FACS) usually require an open stream unconfined by a cuvette. Stream and cell interrogation therefore takes place in the open air following the ejection of the sheath and core stream through a nozzle. After ejection, the stream is charged, droplets are generated, and the droplets are sorted using electrically charged plates. These cytometers are referred to as *stream-in-air* or *jet-in-air* cytometers. At this writing, the BD Biosciences Influx and the Beckman-Coulter MoFlo Astrios cell sorters both utilize stream-in-air interrogation, as do smaller cell sorters like the Sony Biotechnology SH800 and the Bio-Rad S6. The BD Biosciences FACSAria series (I, II, and III) use a hybrid cuvette system for cell interrogation, followed by ejection of the stream for stream charging, droplet generation, and separation. For the purposes of this chapter, FACSAria series systems are considered cuvette-based.

2.2 Spatial Separation Versus Collinear Laser Beams

Cytometers with more than one laser need a mechanism to allow stream and cell interrogation by multiple laser beams. Most commercial cytometers use spatially and temporally separated laser beams to achieve this. A primary laser (usually the 488 nm source)

is the first beam encountered by the cell stream. The subsequent beams are focused on points in the stream "after" the primary, with collection optics appropriate for each laser source aligned to each stream intercept. The time delay between each laser is calculated, and the cell data for each intercept correlated. Many modern cytometers use a light collection "pinhole" aligned with each beam to collect scatter and fluorescence signals, with fiber optic collection of signals. Advanced systems can have seven or more laser intercepts and signal collection fibers.

A few commercial cytometers use collinear lasers, with the laser beams aligned to a single point on the sample stream. While this design is simpler, older systems that utilized this approach could not collect many fluorescent parameters due to laser light impinging on fluorescent detectors with similar wavelength ranges. For example, a collinear red HeNe laser would impinge on the PE-Cy5 detector intended for cyan 488 nm excitation. This problem could be avoided in spatially separated systems due to the separation of different signal paths. Newer collinear systems utilize modulated lasers, timed to fire in the picosecond repetition range and temporally synchronized with detector activation. So, the downstream detectors will only be active for 488 nm excited fluorochromes when the 488 nm laser is active. This approach is used for multilaser flow cytometry in the BD Biosciences Accuri/Accuri Plus and EMD Millipore Guava cytometer systems.

2.3 Gas Versus Solid State

In the 1980s and 1990s, virtually all lasers integrated into flow cytometers were gas lasers. As discussed above, water-cooled argon-ion lasers were used to produce the primary 488 nm line. Krypton-ion lasers were often installed on more advanced cell sorters, and produced a variety of laser lines. These water-cooled lasers could generate high power levels, up to several hundred milliwatts for some laser lines. Air-cooled 488 nm lasers largely replaced water-cooled systems in smaller cuvette cytometers in the 1990s, although their power output was lower (usually 10–30 mW). Air-cooled krypton-ion lasers were inefficient at low power levels and were rarely seen on flow cytometers. Helium-neon (HeNe) lasers have also been integrated into many flow cytometers, mainly to generate the important red 633 nm laser line. HeNe lasers were available in green (543 nm), yellow (592 nm), and orange (612 nm) lines as well, although at far lower power levels than the red emission. These other HeNe lasers were only infrequently used as flow cytometric laser sources [23]. Interestingly, HeNe lasers are the one gas laser type still being manufactured and in use today; their good beam characteristics, stability, and long life have extended their usefulness in some types of instrumentation.

Gas lasers have been largely replaced by solid state laser sources. No flow cytometers are now built with argon- or krypton-ion lasers, although legacy instruments with air-cooled argon-ion

488 nm lasers and red HeNe lasers are still in use. Solid state lasers fall into two main categories. These include *laser diodes*, or *direct diodes*, which use a semiconductor sandwich construction to produce a single laser line in a single step, and *diode-pumped solid state (DPSS) lasers*, which use an infrared laser to "pump" a solid state medium, generating the final laser output in at least two steps. This output is then often frequency doubled, tripled, or quadrupled to further adjust the output wavelength. Direct diodes produce a useful but limited number of wavelengths, the most common being violet, red, and near infrared. Blue 440–450 nm, cyan 488 nm, and green (up to 523 nm) direct diodes are also now available and are starting to see use in flow cytometry. DPSS laser produces a wide and increasing variety of laser lines, including ultraviolet, blue, cyan, green, yellow, and red. DPSS lasers are more expensive than direct diodes but can now be designed with virtually any wavelength output. However, the number of wavelengths available from direct diodes is also increasing, at a lower cost.

2.4 Beam Quality

Flow cytometers require lasers with good beam quality, particularly in the areas of *beam profile, low noise*, *collimation*, and *life expectancy*. Laser beams can be *single mode* (usually a single circular spot) or *multimode,* with a complex multi-peak beam pattern. Flow cytometers almost always require a single mode beam with a TEM_{00} beam pattern. This beam profile is recognizable as a round beam spot with a Gaussian distribution on the profile. Multimode lasers are more powerful but with complex beam profiles, and are usually not suitable for flow cytometry without significant beam shaping. Most flow cytometers are equipped with beam focusing and shaping optics that will reshape a circular beam into an elliptical profile. These downstream shaping optics include circular beam expanders and anamorphic prism pairs. A horizontal ellipse is an ideal final beam shape flow cell interception, since it will more uniformly illuminate a cell even if it is not perfectly aligned in the fluid stream. Almost all lasers designed for flow cytometry will have circular beam profiles of $M^2 = 1.2$ or less prior to downstream beam shaping. Gas lasers typically have excellent Gaussian beam profiles; DPSS laser similarly produces very uniform beams. Direct diodes intrinsically have more non-uniform beams, although better laser cavity designs and post-laser optics have improved their profiles dramatically. Some lasers, particularly diodes designed for cytometry, have internal optics that deliver an elliptical beam with less need for downstream instrument focusing or shaping optics.

Lasers for flow cytometry also need to have low *RMS noise levels* as measured in the kilohertz to megahertz range. Laser noise translates as power instability, and can be from a variety of sources, including the lasing medium, electronics, and power supply. RMS noise levels should be less than 0.5%; high-quality lasers often have

noise levels significantly less than this. Laser noise will be apparent in applications requiring very high resolution, such as DNA content analysis, but is less critical for immunophenotyping and other applications with broad signal distributions. Instrument manufacturers will typically attempt to limit the noise "budget" of a multilaser instrument to less than 1%. With modern low noise lasers, this is usually not a problem.

Laser collimation reflects the divergence of the beam once it leaves the laser. Most lasers built for flow cytometry are built to be well-collimated at least several meters post-output. This is sufficient for most commercial systems, which then rely on focusing and shaping optics to further modify the beam shape. Again, laser manufacturers for flow cytometers usually meet or exceed these requirements.

Modern direct diodes can be expected to have an operational lifetime of at least 5000 h, and sometimes much more. DPSS lasers typically function for at least 10,000 h. This is in contrast to earlier gas lasers, where lifetimes of a few thousand hours were exceptional.

Keep in mind that many inexpensive laser sources have very poor profile, noise, collimation, and life expectancy characteristics. Many inexpensive lasers are actually multimode units, which complex beam characteristics unsuitable for flow cytometry. As with most things, laser cost is directly proportional to quality!

2.5 Free Space Versus Fiber-Coupled Laser Delivery

Almost all older cytometers "deliver" the laser beam to the stream in free space, using prisms, mirrors, and lenses to steer and focus the beam on the stream. Many modern cytometers use *single mode fiber optics* to transmit the laser beam to the cuvette or cell stream. This approach has many advantages. It eliminates the need to steer a beam to the stream, improving alignment stability and reducing the safety issue of an open laser beam. The laser can be aligned simply by adjusting the position of the fiber output. A malfunctioning laser can be easily replaced with only minimum disruption of laser alignment. A single mode fiber can also "clean up" an imperfect beam profile by occluding the outer edge of the beam, with some power loss. The BD Biosciences FACSAria series and the Beckman-Coulter MoFlo Astrios systems both use fiber delivery systems.

However, fiber delivery has its problems. Fiber delivery loses some laser power in the coupling process; this loss can be significant, especially in the ultraviolet and violet range, and with diode lasers with non-Gaussian beam characteristics. Fiber optics can also degrade with time, especially with long-term exposure to short wavelength violet and ultraviolet lasers. Single mode fiber optics are also expensive. Many modern cytometers, including the BD Biosciences Fortessa series, the Beckman-Coulter Gallios/Navios and CytoFLEX systems, and the ACEA Biosciences NovoCyte instruments, still rely on free space laser beam delivery to the sample

stream. These systems usually use a series of damage-resistant longpass dichroics to reflect, merge, and steer multiple laser beams to the flow cell or stream.

For cytometers that use free space laser installations, mirrors and dichroics are necessary to steer the laser beams to the flow cell. 100% mirrors for beam steering and alignment should be of high quality. In the case of ultraviolet lasers, specially coated mirrors for UV light are necessary. Enhanced aluminum mirrors may be necessary for ultraviolet sources below 350 nm. For beam merging, dichroic mirrors (usually longpass) with high damage resistance are required. The LaserMUX mirror series from Semrock (Rochester, NY) is a good example of laser dichroics that allow multiple beams to be merged.

2.6 Continuous Wave Versus Quasi-CW

Most lasers used in flow cytometry are continuous wave, or CW; they are not modulated or pulsed, and are always "on." This is usually essential for cell interrogation, where the "dwell time" for a cell in the laser beam may be less than 1 μs. Most modulated lasers pulse in the kilohertz repetition rate with picosecond to femtosecond pulse durations, too infrequent for uniform cell illumination. However, lasers with rapid repetition rates (10 MHz or greater) with picoseconds pulse intervals will illuminate the stream with sufficient repetition and power to give good excitation. These quasi-CW laser sources do appear on flow cytometers, particularly in the ultraviolet range.

An exception to the utility of lasers with lower repetition rates is in cytometers designed to operate with laser modulation, such as the EMD Millipore Guava cytometers and the BD Accuri described above.

2.7 Package Size or Form Factor

Lasers are available in all shapes and sizes depending on the manufacturer. Solid state laser packages usually include much more than the laser itself; cooling systems, driver and power electronics, and beam shaping optics are often integrated into the laser package. While sizes and shapes vary, several standard form factors appear to have been adopted by the industry. So-called "lipstick" laser diodes are roughly 12 mm in diameter, a specification that seems to be adhered to by many manufacturers. A circular laser module package (the IQ unit) popularized by Power Technology, Inc. (Alexander, AR, USA) with an approximate diameter of 44 mm has been adopted by several manufacturers where a larger cylindrical unit can be accommodated. Coherent Laser (Mountain View, CA, USA) has produced lasers in the Sapphire, CUBE, and OBIS form factors, all widely adopted by the industry. Many cytometer manufacturers have adopted these form factors in their instrument designs. Fortunately, their wide usage allows a selection of manufacturers when choosing a laser module.

2.8 Laser Coherence and Wavelength Stability

Laser coherence refers to the width of the laser wavelength, with highly coherent lasers having a very restricted wavelength value. High coherence is not strictly necessary for lasers in flow cytometry; a wavelength bandwidth of 1 nm or less is adequate, and is readily supplied by most lasers sold for flow cytometers.

Laser diodes can emit low levels of light at slightly lower or higher wavelengths than the specified value, both as coherent laser light and as non-coherent diode "glow." To ensure that this light does not impinge on downstream optics, a "clean-up" filter is often installed in front of the laser. This optic is a very narrow bandpass filter that allows the only transmission of the specified wavelength. A 640/8 nm bandpass filter is typical for red laser diodes. Violet laser diodes are often equipped with a 405/10 nm filter, and NUVLD 375 nm laser diodes with a 375/6 nm filter. Diode laser wavelength is also somewhat temperature-dependent, with changes in operating temperature causing small shifts in emission wavelength. Direct diodes are usually equipped with Peltier cooling devices to maintain the constant temperature around the diode.

3 Laser Wavelengths

All laser tests in this paper were carried out on a BD LSR II (BD Biosciences, San Jose, CA, USA) specially equipped for laser testing. For comparisons between lasers, power was matched between lasers whenever possible. The downstream detection optics and PMTs were the same for all laser comparisons, such that the laser was the only variable.

3.1 Cyan 488 nm: The Primary Laser Source

With very few exceptions, blue-green or cyan 488 nm module occupies the primary position in most flow cytometers. They are used for forward and side scatter measurement, and to excite fluorescein and fluorescein-derived fluorochromes, fluorescent proteins including Green Fluorescent Protein (GFP), as well as phycoerythrin (PE) and its tandem dyes. Some smaller, less expensive cytometers use only a 488 nm source, but this limits these systems to only three to five fluorescent probes maximum.

Virtually all modern 488 nm sources are diode-pumped solid state (DPSS) units [30]. The 488 nm laser line is also now available as a direct diode laser, although these modules are typically lower in power. DPSS 488 nm lasers span a wide power range from low (10–20 mW) to high (up to 1 W). Most cuvette-based flow cytometers use 488 nm lasers in the 20–100 mW range, although a few custom systems can be equipped with higher power units. A 50 or 100 mW 488 nm laser is quite adequate for most cuvette-based instruments. Stream-in-air cytometers are typically equipped with units in the 100–200 mW range. Water-cooled argon-ion lasers emitting at 488 nm are no longer manufactured, and are now

only seen on older large cell sorter systems. Air-cooled argon-ion lasers are still seen on older legacy systems like the BD Biosciences FACSCaliburs and the Beckman-Coulter XL and FC500 series, but are no longer being installed on newer instruments.

Cytometer systems with green-to-yellow lasers for PE and PE tandem excitation (see Green and Yellow Lasers, below) use the 488 nm laser line only for scatter and fluorescein excitation. However, the red phycobiliproteins PerCP and its tandem dye PerCP-Cy5.5 are not well excited with green and yellow lasers and still require a 488 nm laser. Brilliant Blue 515 is a polymer dye developed by BD Sirigin from the same class of probes as the Brilliant Violet dyes; it is intended as a fluorescein replacement and is also excited at 488 nm. A series of Brilliant Blue dyes extending from the green to the red will be released in the near future, and will also require 488 nm excitation. At this writing, Brilliant Blue 630, 667, 700, and 796 have been used in high-dimensional panel development (Mario Roederer, personal communication) but are not yet commercially available. The wavelength designations of these dyes may change once then are officially released.

3.2 Red Lasers

The earliest red laser lines on flow cytometers were generated by water-cooled krypton-ion lasers, which could produce laser lines at 641 and 647 nm. These lines could excite the monomeric cyanin dye Cy5, as well as the widely used phycobiliprotein allophycocyanin. However, these lines were very close to the emission range of both of these dyes (666–675 nm), making the design of a filter for these short Stokes shift fluorescent probes difficult.

The red HeNe laser emitting at 633 nm (or more precisely at 632.8 nm) then became the dominant laser source for red-excited fluorochromes and the most common second laser on flow cytometers [5, 8]. Its shorter wavelength made it a nearly ideal laser source for these probes, allowing the excitation of APC, the APC tandem dye APC-Cy5.5 (or Alexa Fluor 700) and APC-Cy7, giving three additional fluorescent parameters. However, red HeNe lasers were not very powerful; small units (typically about 0.7 m in length) only produced up to about 25 mW in total output. Larger HeNe lasers (about 1.5 m in length) could produce up to 35 mW, but this was the practical power limit for this laser source. Nevertheless, red HeNe lasers were widely employed in many cytometers, giving access to red-excited fluorochromes and increasing the total number of fluorescent parameters.

The advent of inexpensive red laser diodes in the 1990s offered a smaller and more powerful alternative to red HeNe lasers [6, 7, 9]. Red laser diodes typically emit in the 638–645 nm range, with the average at 642–643 nm. These direct diodes were far cheaper than HeNe sources and much smaller; “lipstick” red diodes remain standard equipment on many cytometers, with power outputs in the 20–30 mW range. Red diodes in larger form factors (including

the Power Technology IQ and Coherent CUBE and OBIS form factors) are also available at power levels up to several hundred milliwatts. Typically, red excitation from 20 to 50 mW is adequate for most applications, particularly on cuvette instruments. Stream-in-air cytometer users may opt for a 50–100 mW source. As diode sources, red laser diodes are prone to non-uniform beam profiles, but this has improved in recent years. Red diode lasers are often equipped with a narrow bandpass filter such as 640/8 nm to "clean up" stray emission outside the primary wavelength and reduce laser-associated detector background.

While red laser diodes are economical and widely used, they share the same problem as the early krypton-ion sources, namely being very close to the emission ranges of Cy5, Alexa Fluor 647 and APC. This requires a detection filter that is well-blocked for the red laser, or with bandpass specifications enough to evade it entirely. These filter modifications can reduce instrument sensitivity. This problem is shown in Fig. 1, where a low fluorescence APC bead array (Bangs Laboratory PE MESF microspheres, Polysciences, Warrington, PA, USA) was analyzed on flow cytometers equipped with a traditional HeNe 633 nm laser, or a typical red laser diode emitting at 642 nm. The APC filters used were a typical 660/20 nm bandpass, or a longer 675/25 nm filter to improve exclusion of the red laser light. The red 642 nm laser light strongly impinged on the filter, increasing the fluorescence background and strongly reducing sensitivity for the dimmest populations. Inserting a 640/8 nm "clean-up" filter in front of the laser only partially fixed the problem. Most commercial instruments will attempt to use well-blocked bandpass filter in the APC position. Nevertheless, when using a red laser diode, the user should always monitor sensitivity in this detector and change the detection filter when necessary.

A possible solution to this problem is to return to a shorter red laser more akin to the HeNe 633 nm wavelength. Several DPSS lasers are available in the 620 and 628 nm range which make more ideal excitation sources for short Stokes shift fluorescent probes like Cy5, Alexa Fluor 647, and APC. Figure 2 shows Bangs APC bead detection using shorter red 620 and 628 nm laser sources (MPB Communications, Quebec, Canada). While useful, this "short red" laser technology remains expensive for smaller benchtop instrumentation. However, a new generation of red laser diodes that emit in the 632–633 nm range is now available. Once translated into laser diodes, these "short red" lasers will make better alternatives to traditional red laser diodes.

3.3 Violet Lasers

Water-cooled krypton-ion lasers on older cytometers could generate violet laser lines at approximately 407, 413, and 415 nm [24]. These lines were optimal for exciting several low molecular weight fluorochromes that could be easily conjugated and antibodies, including Cascade Blue and Pacific Blue [10]. Widespread use of

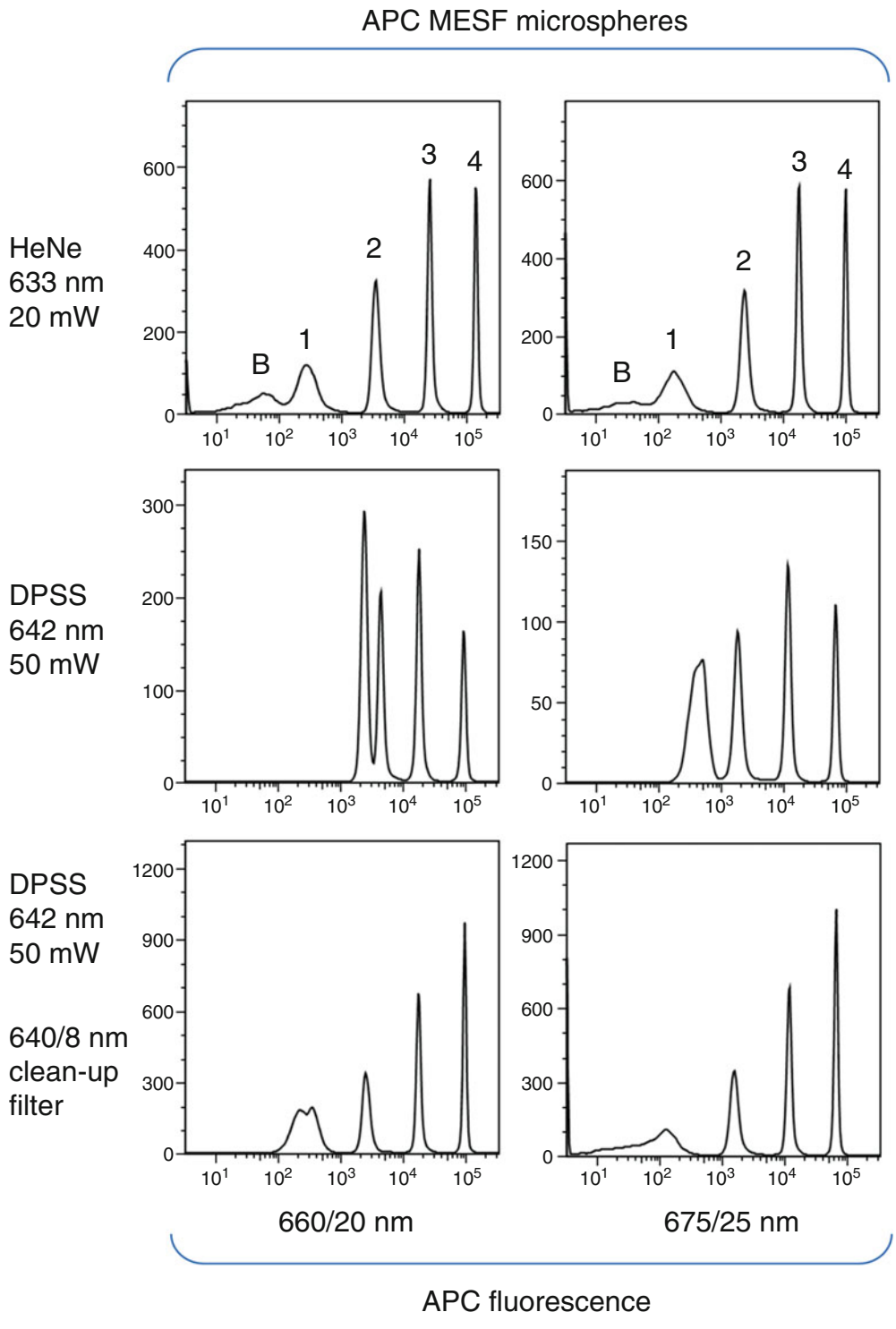

Fig. 1 Red lasers. Analysis of APC microsphere mixture, with four populations coupled to varying levels of APC (labeled 1, 2, 3, and 4) plus background (*B*) (Bangs Laboratories APC MESF microspheres, Polysciences, Warrington, PA, USA). This microsphere mixture was excited with the following lasers: a HeNe 633 nm at 20 mW (*top row*), a DPSS 642 nm at 50 mW with no clean-up filter (*middle row*), and the same laser with a 640/8 nm clean-up filter (*bottom row*). Microspheres were detected through two different bandpass filter (660/20 and 675/25 nm). The background signal is elevated with the 642 nm, and the dim microsphere resolution lost even with a clean-up filter

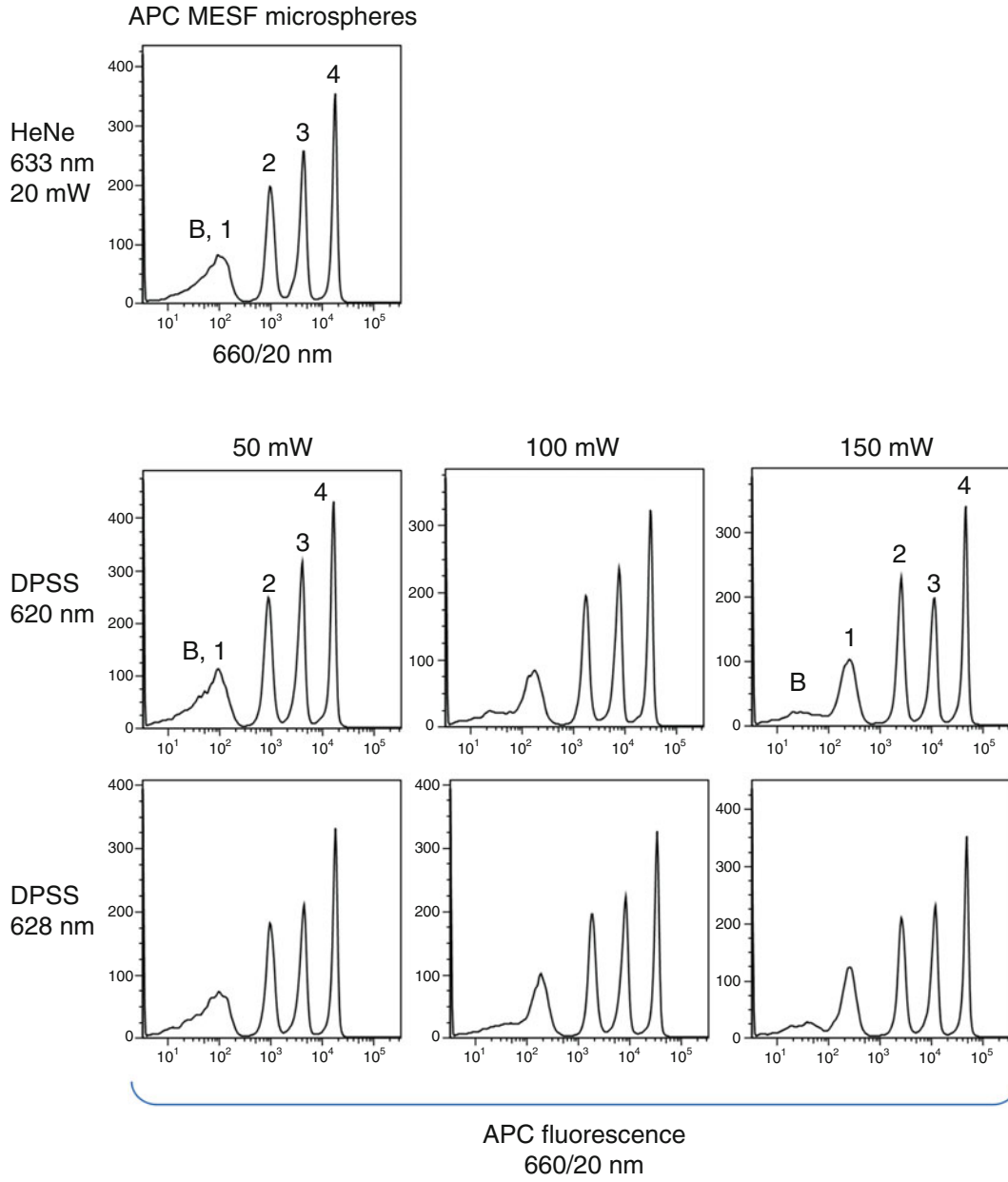

Fig. 2 Short red lasers. Analysis of APC microsphere mixture, with four populations coupled to varying levels of APC (labeled 1, 2, 3, and 4) plus background (*B*) (Bangs Laboratories APC MESF microspheres, Polysciences, Warrington, PA, USA). This microsphere mixture was excited with the following lasers: a HeNe 633 nm at 20 mW (*top histogram*), a DPSS 620 nm at 50 mW (*middle row*), and a DPSS 628 nm laser at 50 mW (*bottom row*). The 620 and 628 nm lasers were tested at 50, 100, and 150 mW (*left*, *middle*, and *right columns*)

these fluorochromes was not possible, however, until the development of violet laser diodes in the mid-1990s [25]. Violet laser diodes emit in the 395–415 nm range, with an average wavelength of approximately 407 nm. Howard Shapiro first demonstrated their

use in flow cytometry in 1999, and they have since become standard equipment on many instruments, usually in combination with a cyan 488 nm and a red laser source [11, 12]. The development of violet-excited quantum nanoparticles (Qdots) as fluorescent probes greatly increased the utility of this wavelength. Up to seven Qdots with emissions ranging from 525 to 800 nm allowed a substantial expansion of the number of fluorescent markers that could be simultaneously analyzed [16, 17]. In combination with a cyan 488 nm source (five fluorescent parameters) and a red source (three fluorescent parameters), the addition of a violet source theoretically allowed 15 color analysis [17].

While bright, Qdots have ultimately proven to be difficult to conjugate to proteins, and therefore impractical for most flow cytometry applications. They have been largely replaced by the Brilliant Violet series of polymer dyes development by Sirigin. A series of seven Brilliant Violet dyes are now available with emission properties spanning from blue to the near infrared, including BV421, BV510, BV570, BV605, BV650, BV711, and BV785 [18]. They can be easily conjugated to proteins and are now essential reagents in high-dimensional flow cytometry panels. A cytometer equipped with three lasers and seven violet detectors can therefore potentially analyze 16 fluorescent parameters simultaneously. Violet-excited viability probes and DNA binding dyes have also been developed. The expressible GFP mutant Cyan Fluorescent Protein (CFP) is also well-excited with violet lasers; many violet-excited fluorescent proteins with improved expression and brightness characteristics are now available [13, 26].

While not as inexpensive as red diodes, the cost of violet laser diodes has decreased to the point where many commercial systems can be equipped with one. Cytometers are now often equipped with five to seven detectors aligned to their violet sources to accommodate a large number of available Brilliant Violet dyes. Like their red counterparts, violet laser diodes are available in several standard form factors, with power levels ranging from 20 to 200 mW and higher [26]. Most fluorochromes and fluorescent proteins can be well-excited with diodes in the 50–100 mW range, although higher power levels have been shown to improve Brilliant Violet dye and cyan fluorescent protein sensitivity somewhat (P. Chattopadhyay and M. Roederer, personal communication).

3.4 Green to Yellow Lasers

A cyan 488 nm, red ~640 nm, and a violet ~405 nm laser combination (the so-called laser "triad") is a powerful combination that gives both excitation flexibility and the capacity to do true high-dimensional flow cytometry. Nevertheless, several additional laser wavelengths have been found to add important functionality to multi-laser cytometer systems. DPSS 532 (green), 550–553 nm (green-yellow), and 561 nm (yellow) lasers have become common fixtures on many commercial systems, as a fourth laser source along

with the standard triad [14, 15]. There are several important advantages in adding a green or yellow laser to a multi-laser cytometer. First, phycoerythrin (PE) and its tandem dyes are adequately but not optimally excited at 488 nm. PE has a complex excitation profile, with the maximum excitation peak at approximately 554 nm. Green 532 nm and yellow 561 nm lasers both excite PE and its tandem dyes to a higher degree than a 488 nm laser source. This is shown in Fig. 3, where a mixture of unlabeled and PE-labeled microspheres with varying levels of probe (Bangs PE MESF microspheres) have been excited and analyzed with 488, 532, 553, and 561 nm laser sources. The red and black values on each histogram refer to the staining index (SI) for the dimmest (population 1) and second-dimmest (population 2) fractions of beads, respectively. The green, green-yellow, and yellow lasers show at least threefold sensitivity improvement over 488 nm excitation. While this is likely due to improved PE excitation, it may also be the result of lower cellular autofluorescence with green to yellow excitation.

A common configuration now used on many advanced commercial systems is to retain the 488 nm laser for scatter and fluorescein excitation, but include a spatially separated green-to-yellow laser source for PE and PE tandem excitation. Green 532 nm and yellow 561 nm lasers were the first widely available green and yellow DPSS lasers and saw considerable early use for this purpose. Intermediate green-yellow lasers were developed later, but are now available on commercial systems as well [27]. Green-yellow lasers ranging from 550 to 553 nm suitable for flow cytometry are now available from several manufacturers. Unlike green 532 nm and yellow 561 nm lasers, there has been some manufacturer variability with regard to wavelength for green-yellow lasers. The first commercially available modules in this range applicable for flow cytometry were a 550 nm unit (formerly Zekotec, now Inversion Fiber JSC, Novosibirsk, Russia) and a 555 nm module NTT (Tokyo, Japan). The unit used in this chapter was a 553 nm module from Oxxius (Lannion, France). The most common commercial unit installed on cytometers is a 552 nm module from Coherent Laser (Mountain View, CA, USA), available in several form factors including the OBIS module.

One advantage of using a green-yellow source is its improved spectral distance from the fluorescein and PE detection bandwidths. Green 532 nm lasers emit very close to the fluorescein emission range, requiring special filter precautions to exclude laser light from the detector. The same is true of yellow 561 nm lasers and the PE emission range. The green-yellow 550–553 nm lasers avoid both ranges, making downstream detection optic design simpler [27].

A second important application for these laser wavelengths is the excitation of red fluorescent proteins. DsRed, the first identified

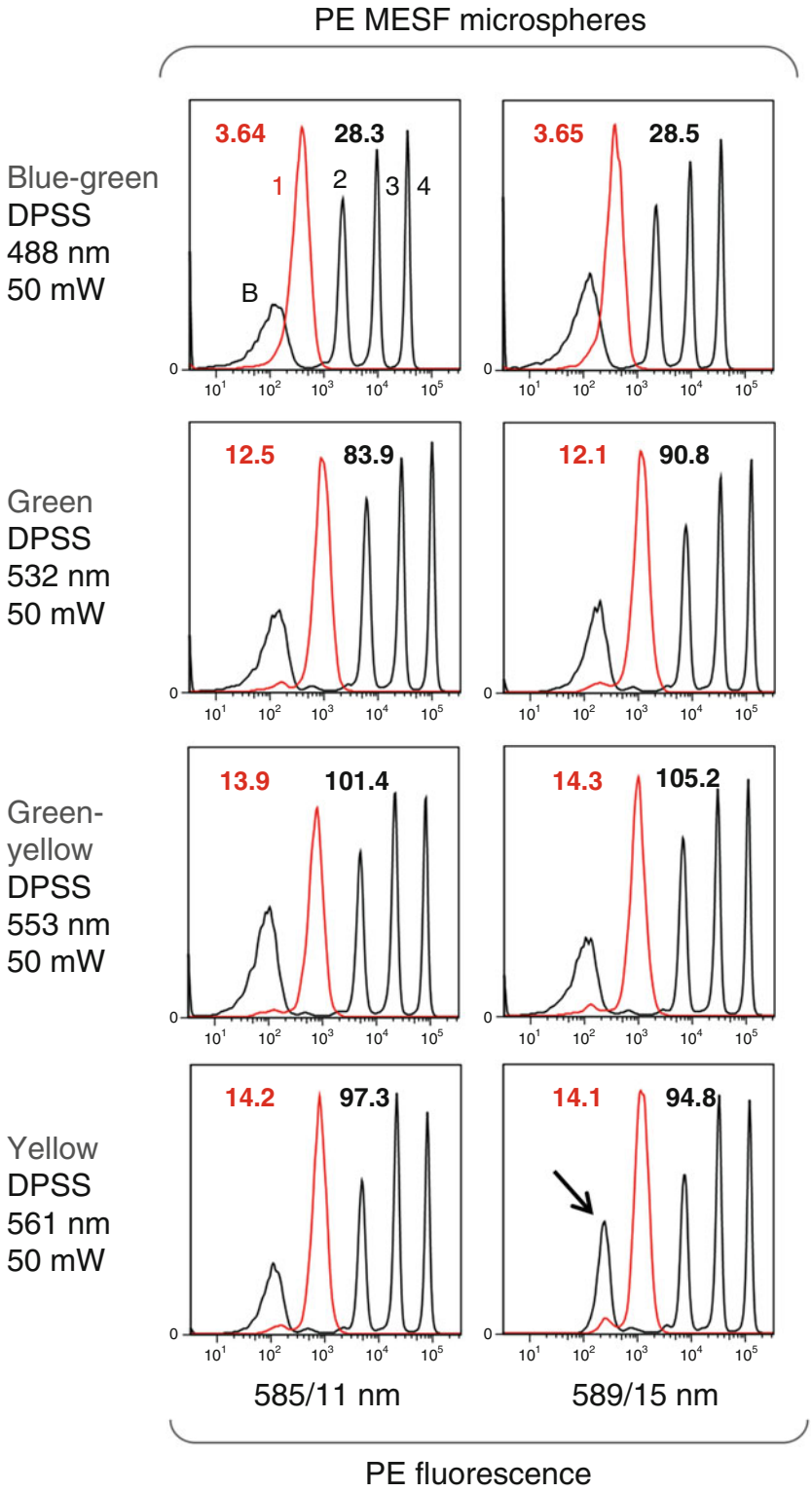

Fig. 3 Green to yellow lasers for PE detection. Analysis of PE microsphere mixture, with four populations coupled to varying levels of PE (labeled 1, 2, 3, and 4) plus background (*B*) (Bangs Laboratories PE MESF microspheres, Polysciences, Warrington, PA, USA). The dimmest population (1) is shown in red. The following lasers were tested: a DPSS 488 nm at 50 mW (*top row*), a DPSS 532 nm at 50 mW (*second row*), a DPSS 553 nm at 50 mW (*third row*), and a DPSS 561 nm at 50 mW (*bottom row*). Staining indices (Sis), an indicator of fluorescence signal strength, are shown in each histogram (red for population 1, black for population 2)

red fluorescent protein, is sub-optimally excited at 488 nm [28]. The excitation maximum for DsRed is approximately 552 nm, suggesting that a green or yellow laser would provide better excitation. This is shown in Fig. 4a, where Sp2/0 cells expressing DsRed show considerably better excitation with power-matched 532, 553, and 561 nm laser sources compared to 488 nm. Dozens of red fluorescent proteins have since been isolated or derived, all ideally requiring green to yellow lasers for optimal excitation [29]. Figure 4b also shows analysis of a mixture of six fluorescent microsphere populations labeled with varying levels of the fluorescent protein mCherry, possessing an even longer excitation maxima of 587 nm. The 488 nm source can only resolve the brightest population of microspheres (not shown); the 532, 553, and 561 nm sources can resolve increasingly dim populations. Increasing the power level from 50 to 150 mW also improved dim microsphere resolution. Green to yellow laser sources are critical tools for analyzing this important class of expressible fluorescent proteins.

Finally, using a distinct laser source to excite PE, PE tandems or red fluorescent proteins can reduce the level of fluorescent compensation in multicolor experiments [14]. Figure 5 shows analysis of cells expressing GFP and labeled simultaneously with PE. The left column shows cells excited with a single 488 nm laser; the right column shows cells excited with spatially separated 488 and 553 nm lasers. With single laser excitation, the spectral overlap of GFP into the PE detector is considerable, requiring almost 16% compensation to subtract the spillover. With excitation by spatially separated dual lasers, the 488 nm laser still excites both probes, but the 553 nm laser only excites PE and not GFP. As a result, the spillover of GFP into the PE detector is almost zero. Using spatially separated lasers to excite individual fluorochromes is an excellent way to reduce spillover; the use of green to yellow lasers in addition to cyan 488 nm is a good example of this.

3.5 Ultraviolet Lasers

Ultraviolet (UV) excitation has traditionally been a difficult and expensive wavelength to provide for flow cytometry [24, 30]. Many large early cell sorters had water-cooled argon- and krypton-ion lasers that could generate UV laser lines in the 351–365 nm range. This allowed the development of a small but important group of applications for flow cytometry. The UV-excited DNA binding dyes DAPI, Hoechst 33258, and Hoechst 33342 saw the early use for DNA cell cycle analysis. DAPI does not bind to RNA, and was thus an excellent probe for high-resolution DNA content analysis. Hoechst 33342 is cell permeable and could be used for cell cycle analysis where cell viability is required. The fluorescent ratiometric calcium chelator indo-1 was and remains the best reagents for intracellular calcium flux in lymphocytes, and requires a UV laser. While these reagents saw considerable use on large cell

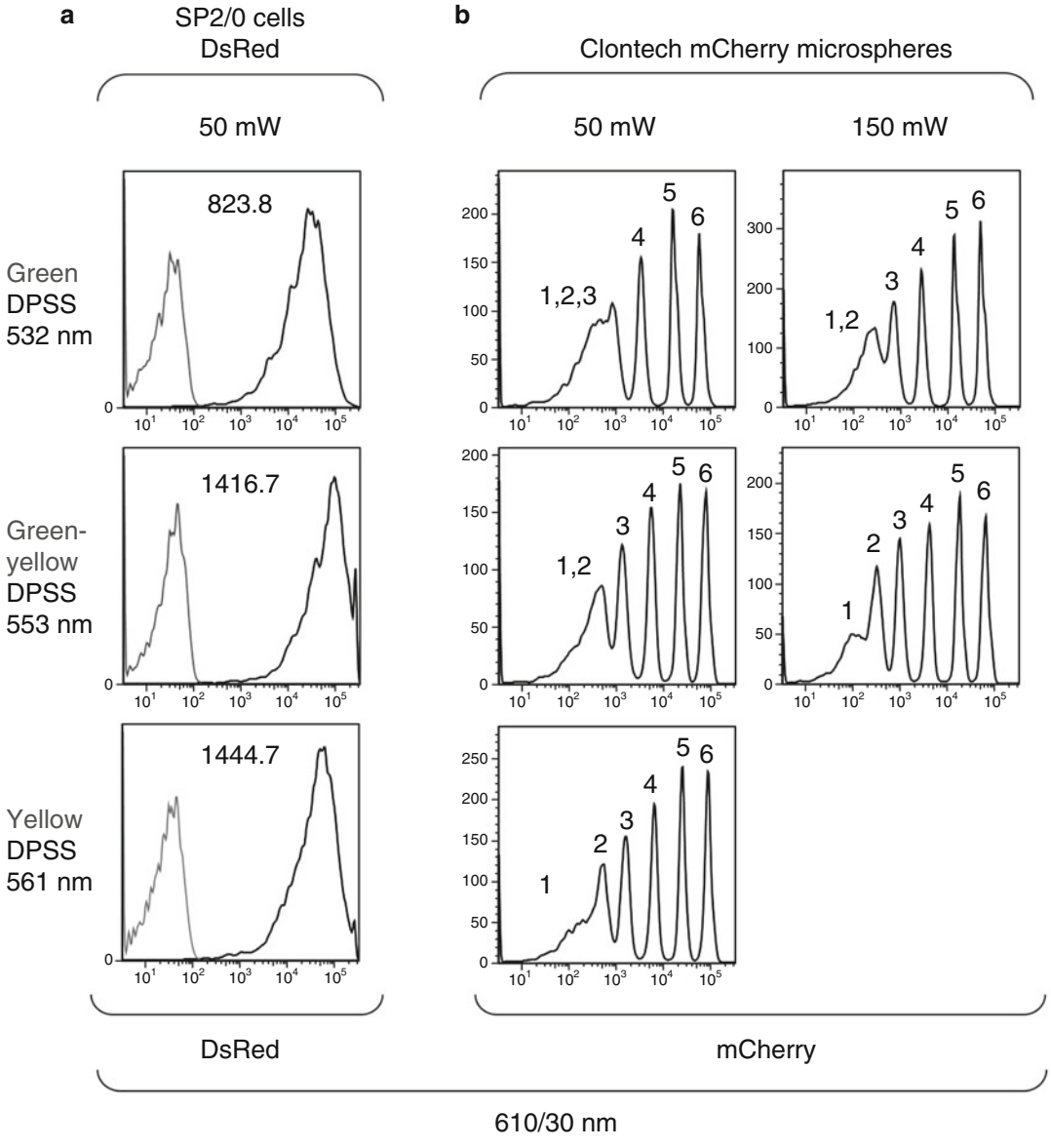

Fig. 4 Green to yellow lasers for DsRed and mCherry detection. (**a**) Analysis of Sp2/0 cells expressing DsRed. Black peaks, DsRed expressing cells; grey peaks, wild-type cells with no DsRed expression. Staining indices (Sis) for each analysis are shown. (**b**) Analysis of mCherry microsphere mixture, with six populations coupled to varying levels of mCherry (labeled 1, 2, 3, 4, 5, and 6) (mCherry Flow Cytometer Calibration Beads, Takara Bio USA/Clontech Laboratories, Kusatsu Shiga, Japan). The following lasers were tested: A DPSS 532 nm (*top row*), a DPSS 553 nm (*middle row*), and a DPSS 561 nm (*bottom row*). Power levels for DsRed analysis were matched at 50 mW. Power levels for mCherry microspheres were set at 50 mW (*middle column*) or 150 mW (*right column*)

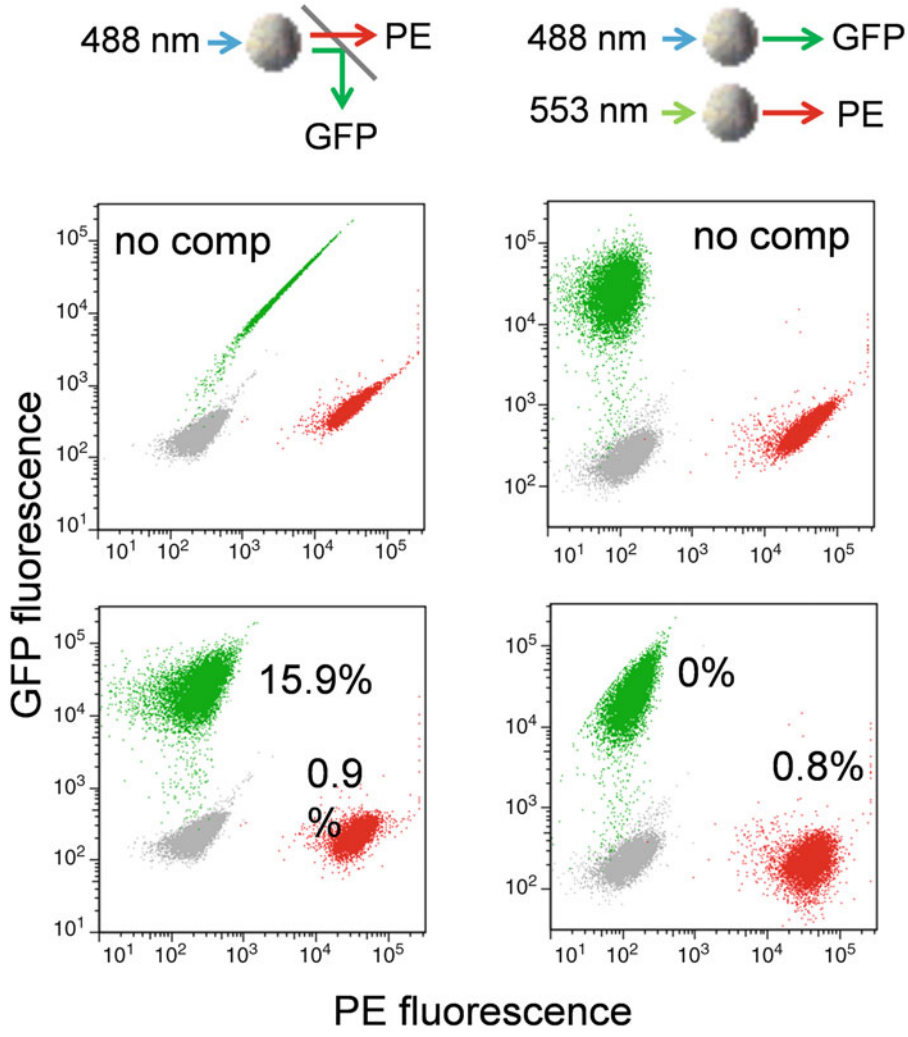

Fig. 5 Green to yellow lasers for improved compensation. Simultaneous analysis of Sp2/0 cells expressing enhanced GFP (GFP) and labeled for the surface antigen CD90 using a PE conjugated antibody (PE). Cells were analyzed using a single cyan 488 nm laser source (*left column*), or spatially separated 488 nm and green-yellow 553 nm lasers (*right column*). Data are shown uncompensated (*top row*), or compensated using automated software-based spillover analysis (*bottom row*). Compensation values are shown on the respective dotplots. Grey dots, unlabeled cells; green dots, GFP expressing cells; red dots, PE labeled cells

sorters, the high maintenance requirements and cost of large gas lasers made their use difficult and expensive.

UV laser line generation by gas lasers is not efficient, and air-cooled argon lasers could not produce sufficient UV power for benchtop cytometers. Air-cooled helium-cadmium (HeCad) lasers emitting at 325 nm saw infrequent use on benchtop cytometers, but their short lifetimes and high noise levels limited their usefulness [31, 32]. Almost all flow cytometers now rely on frequency-doubled Nd:YVO_4 solid state UV lasers emitting at 355 nm [24].

These lasers are smaller and much easier to use than their water-cooled gas predecessors, although their cost remains high. Nevertheless, the importance of UV lasers for flow cytometry continues to increase. Stem cell analysis by measuring efflux of Hoechst 33342 (the Hoechst side population or SP technique) has increased the need for UV laser sources [22, 33, 34]. More important is the development of the Brilliant Ultraviolet (BUV) series of polymer dyes, using the same technology as the Brilliant Violet (BV) series. Six BUV dyes have been developed by BD Sirigin ranging from the near UV to the near Infrared (BUV395, BUV496, BUV563, BUV661, BUV737, and BUV805). The BUV dyes are spectrally compatible with the BV dyes and have pushed the theoretical number of simultaneous fluorescent markers to over 20. The BUV dye series has made a UV source as important as a violet for high-dimensional flow cytometry.

Frequency doubled Nd:YVO_4 solid state UV lasers are generally available at power levels ranging from 20 to over 150 mW [24, 30]. More powerful units are also available (i.e., the Newport Spectra Physics Vanguard series at 350 mW), although these are more powerful than typically required for flow cytometry. Solid state UV lasers are often quasi-CW, with repetition rates at 20 MHz or higher, making them useable for flow cytometry. More modern solid state UV sources are often CW. Cuvette cytometers are usually equipped with 20–50 mW units, while stream-in-air typically use 100–150 mW. However, small Nd:YVO_4 lasers are now available with lower UV power levels but in form factors more compatible with smaller instruments. The Cobolt Zouk (Uppsala, Sweden) and the Coherent OBIS 355 nm laser units range from 10 to 20 mW yet are still suitable for many UV applications [24]. Figure 6a shows an InSpeck Blue microsphere mixture (Thermo Fisher Scientific) with seven bead populations labeled with descending levels of a UV-excited fluorochrome. Resolution of even the dimmest bead populations is similar between 10 and 20 mW laser modules. Hoechst SP analysis of stem cells in mouse bone marrow in Fig. 6b also showed nearly identical results between the two power levels. While this power level is not suitable for stream-in-air instruments, it appears adequate for cuvette cytometers.

While frequency-doubled Nd:YVO_4 355 nm lasers are the most common choice for UV excitation, they remain very expensive. A more cost-effective option is the near-UV direct diodes (NUVLDs) [22, 23, 35]. With similar semiconductor chemistry to the violet diode, these lasers range from 370 to 380 nm, with an average of 375 nm. They range in power from 10 to 50 mW. They can be used in place of 355 nm laser sources for flow cytometry with a few caveats. First, their slightly longer wavelength does not allow excitation of the calcium probe indo-1; the calcium-bound emission for indo-1 peaks at about 395 nm, too close to the laser emission.

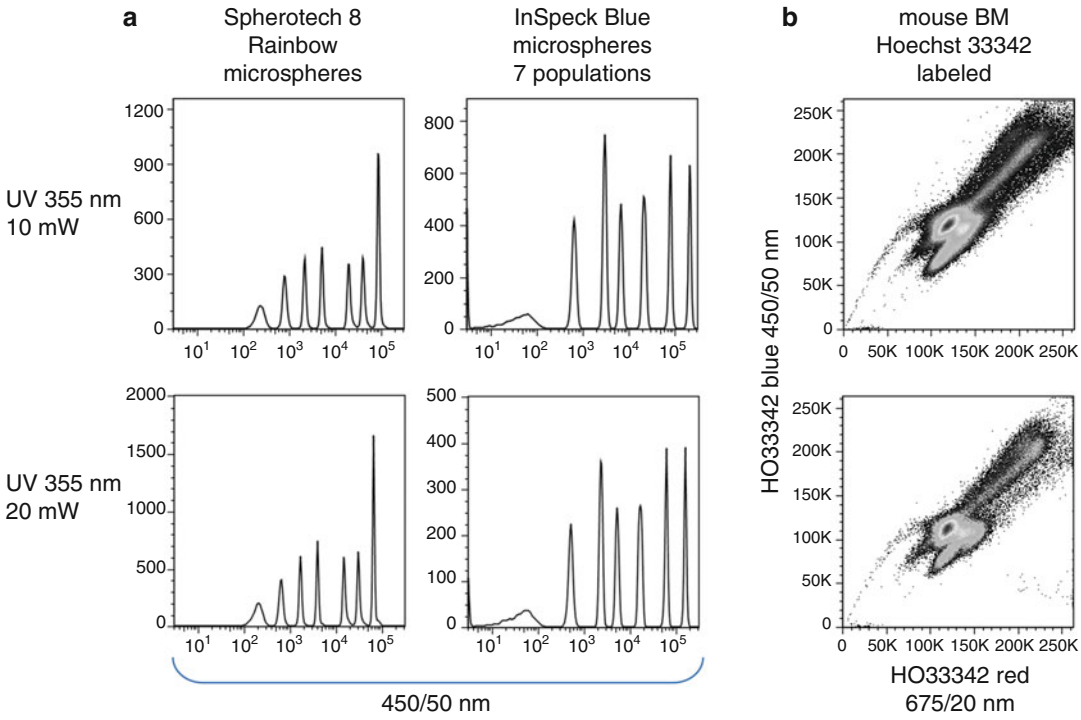

Fig. 6 Low power UV 355 nm lasers. (**a**) Analysis of a Spherotech eight Rainbow microsphere mixture, eight populations (*left column*) or an InSpeck Blue microsphere mixture, seven populations (Thermo Fisher) (*middle column*). The two brightest Spherotech eight peaks are superimposed and cannot be separated using UV excitation. (**b**) Analysis of mouse bone marrow labeled with Hoechst 33342 at 5 μg/ml for 90 minutes at 37 °C for Hoechst side population (SP) analysis of stem cells (*right column*). The following lasers were tested: a DPSS UV 355 nm laser at 10 mW (*top row*), and a DPSS UV 355 nm laser emitting at 20 mW (*bottom row*)

NUVLDs can excite BUV395, but a slightly longer filter than the usual 386/23 nm bandpass is required [36]. Otherwise, NUVLDs at 375 nm show similar excitation efficiency for other UV excited probes [36]. Analysis of the same InSpeck Blue microsphere mixture in Fig. 6a is shown for both 355 nm and NUVLD 375 nm sources in Fig. 7a. Even at reduced power output (16 mW), the NUVLD discrimination of the dimmest bead populations is similar to the 355 nm source. Hoechst SP analysis of mouse bone marrow is also similar for both laser sources (Fig. 7b). Similarly, excitation of the BUV dyes is similar for both laser wavelengths; a three-color panel of mouse splenocytes labeled with BUV496, BUV563, and BUV661 conjugated antibodies is shown with 355 and NUVLD 375 nm sources, with little difference between the two (Fig. 8). A NUVLD 375 nm source is therefore applicable where cost restrictions preclude a more expensive 355 nm source.

As DPSS technology progresses, other solid state UV sources should also become available. At this writing, a DPSS 320 nm source was under development. This wavelength is similar to the HeCad emission and should be applicable to flow cytometry.

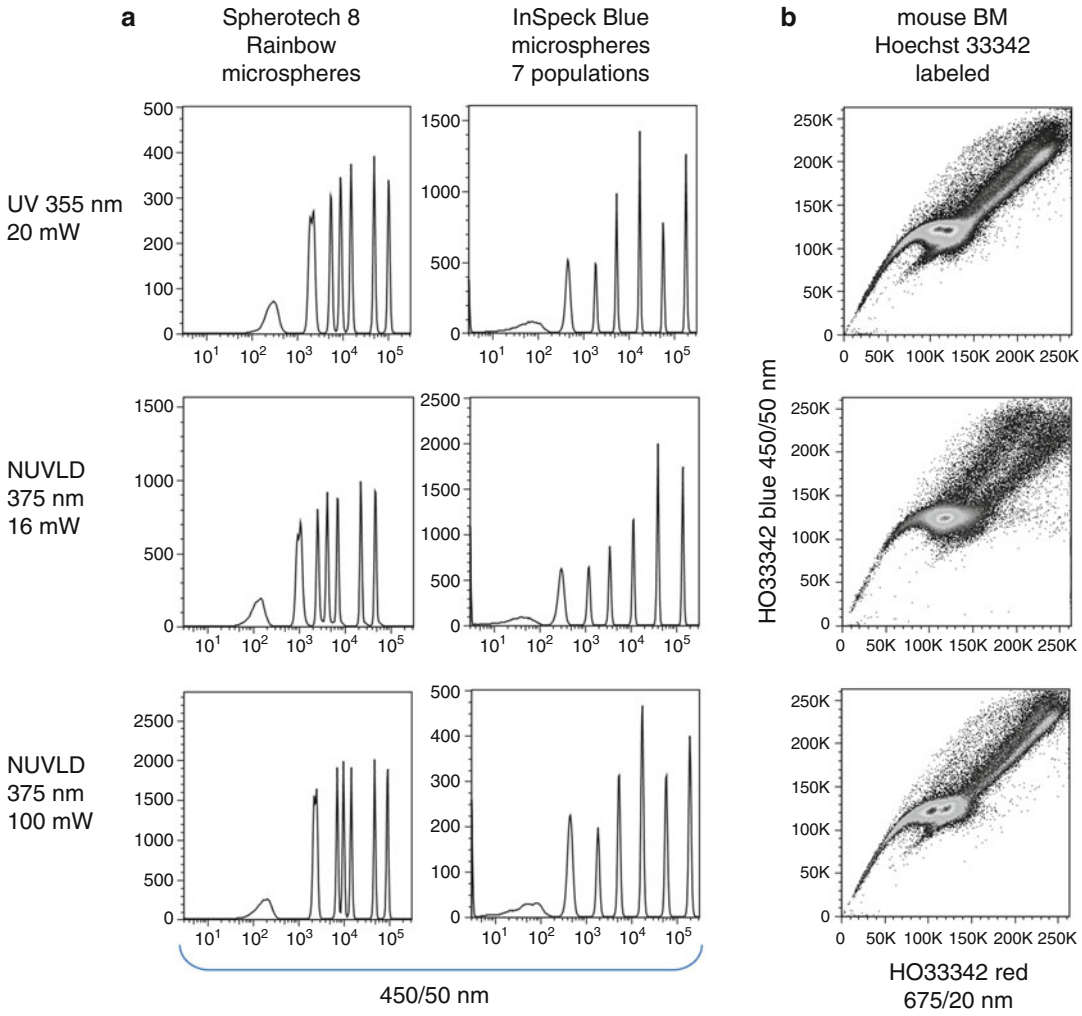

Fig. 7 NUVLD 375 nm laser. (**a**) Analysis of a Spherotech eight Rainbow microsphere mixture, eight populations (left column) or an InSpeck Blue microsphere mixture, seven populations (Thermo Fisher)(middle column). (**b**) Analysis of mouse bone marrow labeled with Hoechst 33342 at 5 μg/ml for 90 minutes at 37 °C for Hoechst side population (SP) analysis of stem cells (*right column*). The following lasers were tested: a DPSS UV 355 nm laser at 20 mW (*top row*), a NUVLD 375 nm at 16 mW (*middle row*), and a NUVLD 375 nm at 100 mW (*bottom row*)

3.6 Blue Lasers

An "essential" laser package for high-dimensional flow cytometry therefore consists of a cyan 488, red and violet sources, with the possible addition of a green to yellow, and a UV for additional fluorochromes. This combination of five lasers can potentially excite up to 28 fluorochromes simultaneously, making it adequate for most applications. However, some additional niche lasers can add flexibility to a multi-laser system, and provide additional functionality for specialized applications.

Blue laser diodes are also similar in semiconductor chemistry to violet diodes, and emit in the 440–450 nm range. DPSS blue lasers

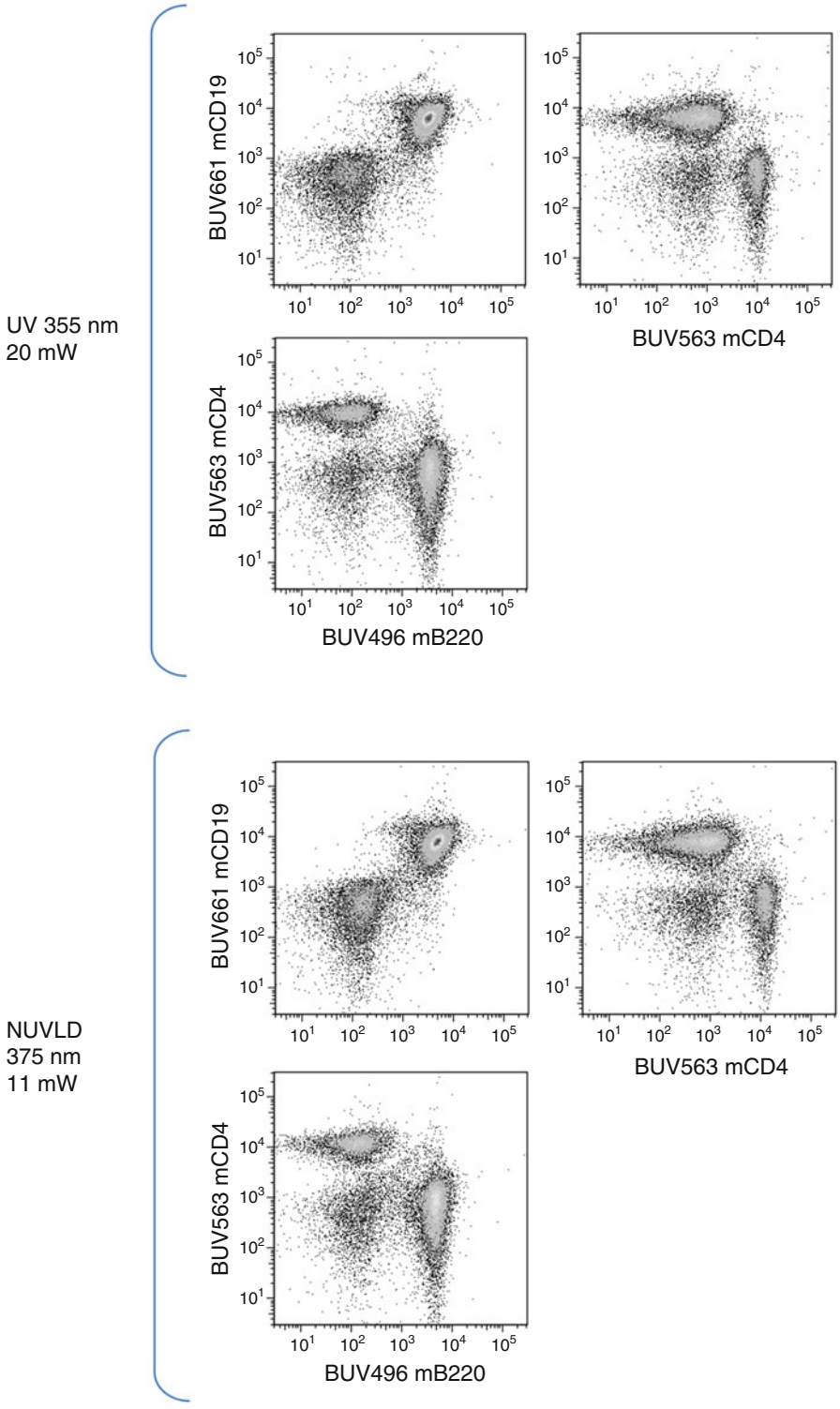

Fig. 8 NUVLD 375 nm laser. Analysis of mouse splenocytes labeled with BUV496 anti-mouse B220, BUV563 anti-mouse CD4, and BUV661 anti-mouse CD19. Data are displayed as two parameter dotplots for all fluorochrome combinations. The following lasers were tested: a DPSS UV 355 nm laser at 20 mW (*top dotplots*) and a NUVLD 375 nm at 11 mW (*bottom dotplots*)

are also available at wavelengths between 450 and 460 nm at power levels ranging from 10 to several hundred milliwatts. DPSS blue lasers are also available at 457 nm (the same as an original argon-ion blue line) and 460 nm. DPSS units are more powerful, and can be considerably more expensive.

One important application of flow cytometry is improved excitation of enhanced Cyan Fluorescent Protein (ECFP) and other cyan FPs. Although CFP can be excited with a violet laser, its excitation maximum is actually 437 nm; early work with argon-ion lasers emitting at 457 nm showed that this wavelength gave good CFP excitation [37]. Similarly, blue laser diodes give substantially better excitation of this expressible FP [36]. This is shown in Fig. 9a, where Sp2/0 cells expressing ECFP were analyzed with either violet or blue laser diodes. Blue laser excitation improved the SI by at least three-fold.

Blue laser diodes are also essential for exciting longer wavelength cyan fluorescent proteins like AmCyan, which are even less well excited using violet sources. Figure 9b shows detection of AmCyan labeling with both violet and blue laser sources. The subpopulation of mouse splenocytes labeled with AmCyan was undetectable with a violet laser source, but could be discriminated using the blue source. With both ECFP and AmCyan, increasing the laser power level from 50 to 100 mW increased sensitivity (Fig. 9).

Another application for blue lasers is better discrimination of simultaneous EGFP and enhanced Yellow Fluorescent Protein (EYFP) expression. Simultaneous detection of GFP and YFP is traditionally carried out using a single 488 nm laser to excite both probes. The high degree of spectral overlap between GFP and YFP makes this discrimination difficult. Very high levels of compensation are usually required to subtract YFP fluorescence from the GFP signal, even with optical filters specially designed for simultaneous GFP/YFP discrimination. One solution to this problem is similar to the GFP/PE discrimination method illustrated in Fig. 5 namely excitation of GFP and YFP using different spatially separated lasers. Blue diode lasers excite GFP nearly as well as cyan 488 nm lasers; Fig. 10a shows analysis of acGFP microsphere array similar to the mCherry array shown in Fig. 4b, a bead mixture with populations coupled to decreasing amounts of the fluorescent protein. The blue diode laser source discriminated the dimmest populations nearly as well as the cyan 488 nm source. However, the blue diode source poorly excited YFP expressing cells. Excitation of GFP with the blue diode and YFP with a spatially separated 488 nm source therefore caused a dramatic decrease in the YFP spectral overlap into the GFP detector (Fig.10b). Again, careful choice of spatially separated lasers allowed improvements to be made not only in instrument sensitivity but also in reduced spectral overlap.

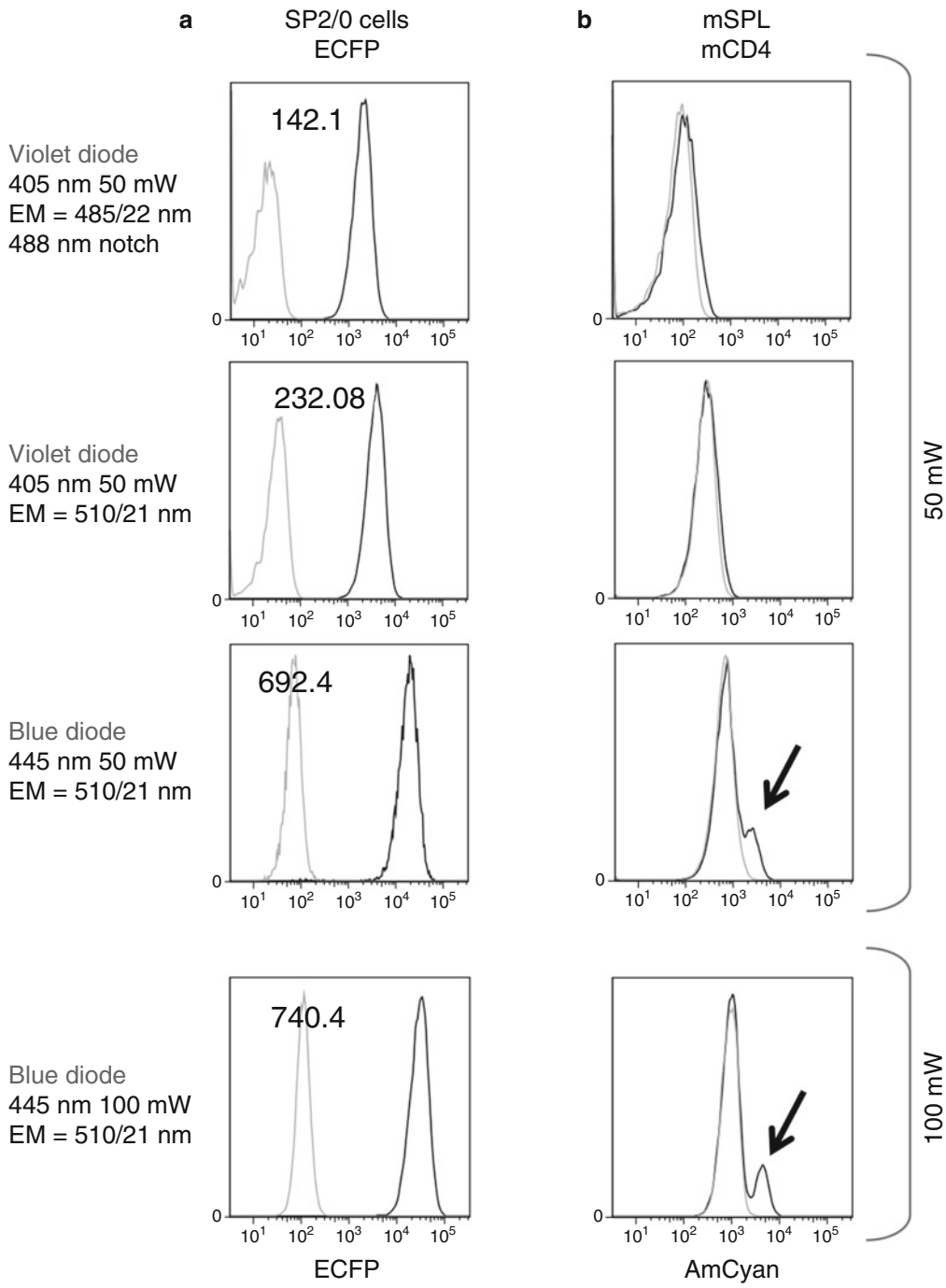

Fig. 9 Blue lasers for cyan fluorescent protein detection. (**a**) Analysis of Sp2/0 cells expressing enhanced Cyan Fluorescent Protein (CFP). Black peaks, CFP expressing cells; grey peaks, wild-type cells with no CFP expression. Staining indices (Sis) for each analysis are shown. (**b**) Analysis of mouse splenocytes labeled with AmCyan conjugated antibody against mouse CD4. The following lasers were tested: Blue peaks, AmCyan-labeled cells; grey peaks, cells with no AmCyan labeling. The following lasers and detection filters were tested: a violet laser diode 405 nm at 50 mW, using a 485/22 nm detection filter with 488 nm notch (*top row*); a violet laser diode 405 nm at 50 mW with a 510/21 nm detection filter (*second row*); a blue laser diode 445 nm at 50 mW with a 510/21 nm detection filter (*third row*); a blue laser diode 445 nm at 100 mW with a 510/21 nm detection filter (*bottom row*)

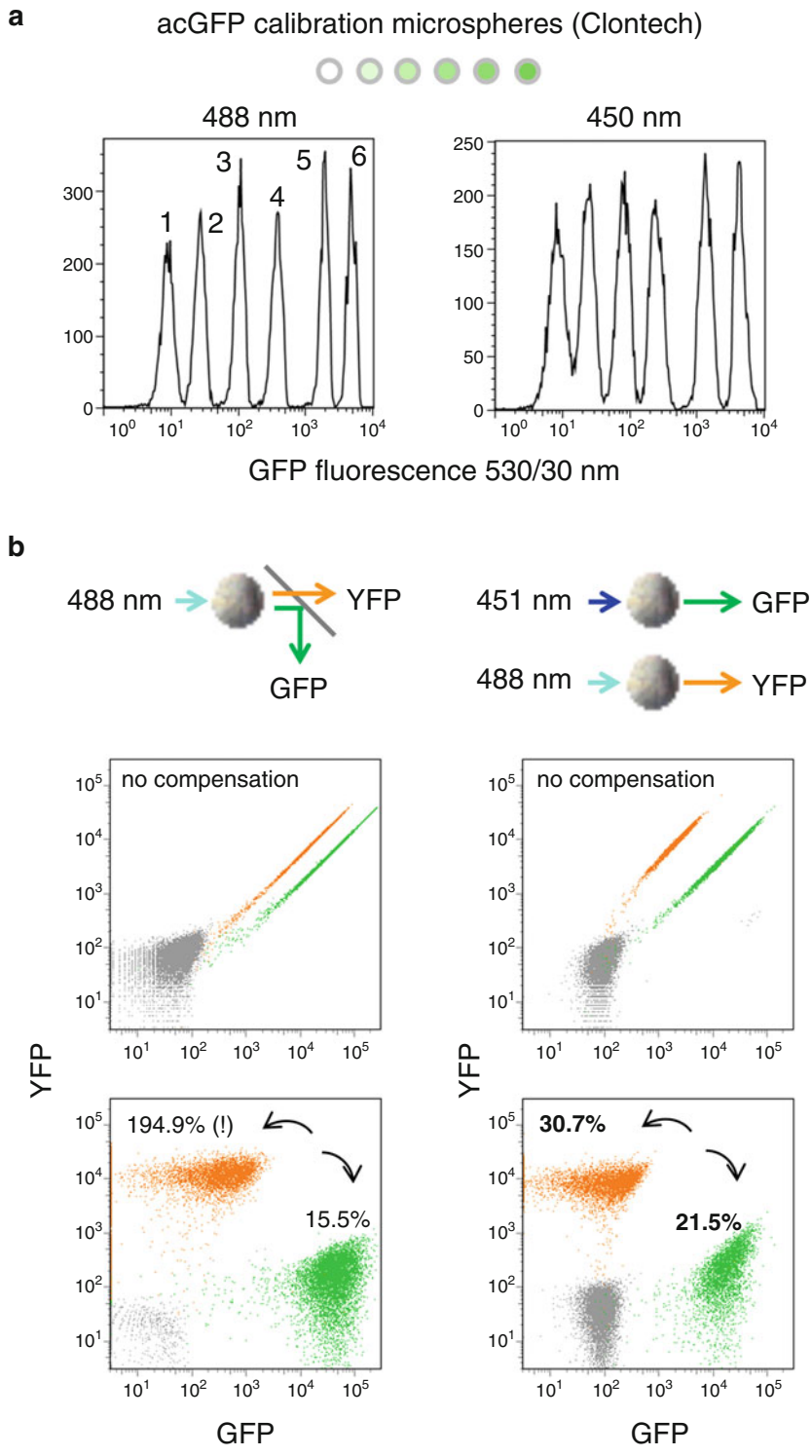

Fig. 10 Blue lasers for GFP/YFP discrimination. (**a**) Analysis of acGFP microsphere mixture, with six populations coupled to varying levels of acGFP (labeled 1, 2, 3, 4, 5, and 6) (acGFP Flow Cytometer Calibration Beads, Takara Bio USA/Clontech Laboratories, Kusatsu Shiga, Japan). (**b**) Simultaneous analysis of Sp2/0 cells expressing enhanced GFP (GFP) or enhanced YFP (YFP). Cells were analyzed using a single cyan 488 nm laser source (*left column*), or spatially separated 451 nm blue and cyan 488 nm lasers (*right column*). Data are shown uncompensated (*top row*), or compensated using automated software-based spillover analysis (*bottom row*). Compensation values are shown on the respective dotplots. Grey dots, unlabeled cells; green dots, GFP expressing cells; orange dots, YFP expressing cells

Since the above two applications would make simultaneous use of a blue and violet laser diode either difficult or unnecessary, most users will not require spatially separated blue and violet lasers. The blue and violet laser diodes can interrogate at the same time delay and/or pinhole, and be switched on or off separately.

3.7 Orange Lasers

Orange lasers (generally in the 592–594 nm range) have seen limited but definite use in flow cytometry. This laser wavelength range has until recently been difficult to generate. Dye head lasers have been historically used to generate laser wavelengths in the 590–600 nm range, using a powerful water-cooled argon-ion laser emitting at 488 or 514.5 nm, pumping a dye head running the laser dye rhodamine 6G [3]. This configuration was large and difficult to maintain, and could be accommodated only on large cell sorters. The attraction of this laser wavelength was its ability to excite certain longer wavelength fluorochromes, including sulforhodamine and Texas Red, often in combination with fluorescein. An orange 594 nm laser line can also be generated by a yellow HeNe laser; however, a maximum of only ~4 mW of laser power can be produced by yellow HeNe lasers, a marginal power level for flow cytometry [23].

Orange 592–594 nm lasers are now available from frequency-doubled DPSS sources by several mechanisms, and several manufacturers now produce lasers suitable for flow cytometry. While still not common on flow cytometes, orange lasers do have several interesting applications. They excite longer wavelength red fluorescent proteins, including mPlum, mKate, E2 Crimson, and mNeptune with greater efficiency than yellow 561 nm sources [19, 20]. Orange lasers can also replace red lasers for the excitation of APC and its tandems [24]. An orange 594 nm laser source can excite APC nearly as well as a red laser (Fig. 11a), allowing substitution. Exciting APC, APC-Cy5.5 (or Alexa Fluor 700), and APC-Cy7 in this manner allows the addition of a fourth fluorochrome, Texas Red, or Alexa Fluor 594 to this combination, giving an additional fluorochrome in this group. This is shown in Fig. 11, where combinations of either Texas red, APC and APC-Cy7, or APC, Alexa Fluor 700 and APC-Cy7 are well-excited using an orange laser source. Only Alexa Fluor 700 (a common third fluorochrome used with red lasers) is less well-excited with orange lasers compared to red. Orange lasers are available as options on several advanced flow cytometry systems.

3.8 Near Infrared (NIR) Lasers

Commercially available lasers now cover virtually the entire visible spectrum, with fluorescent probes available that require these wavelengths. Nevertheless, the near infrared (NIR) range (defined here as approximately 660–780 nm) remains underutilized, with only a handful of fluorescent probes available with excitation values in this range. However, some probes are available, and the importance of

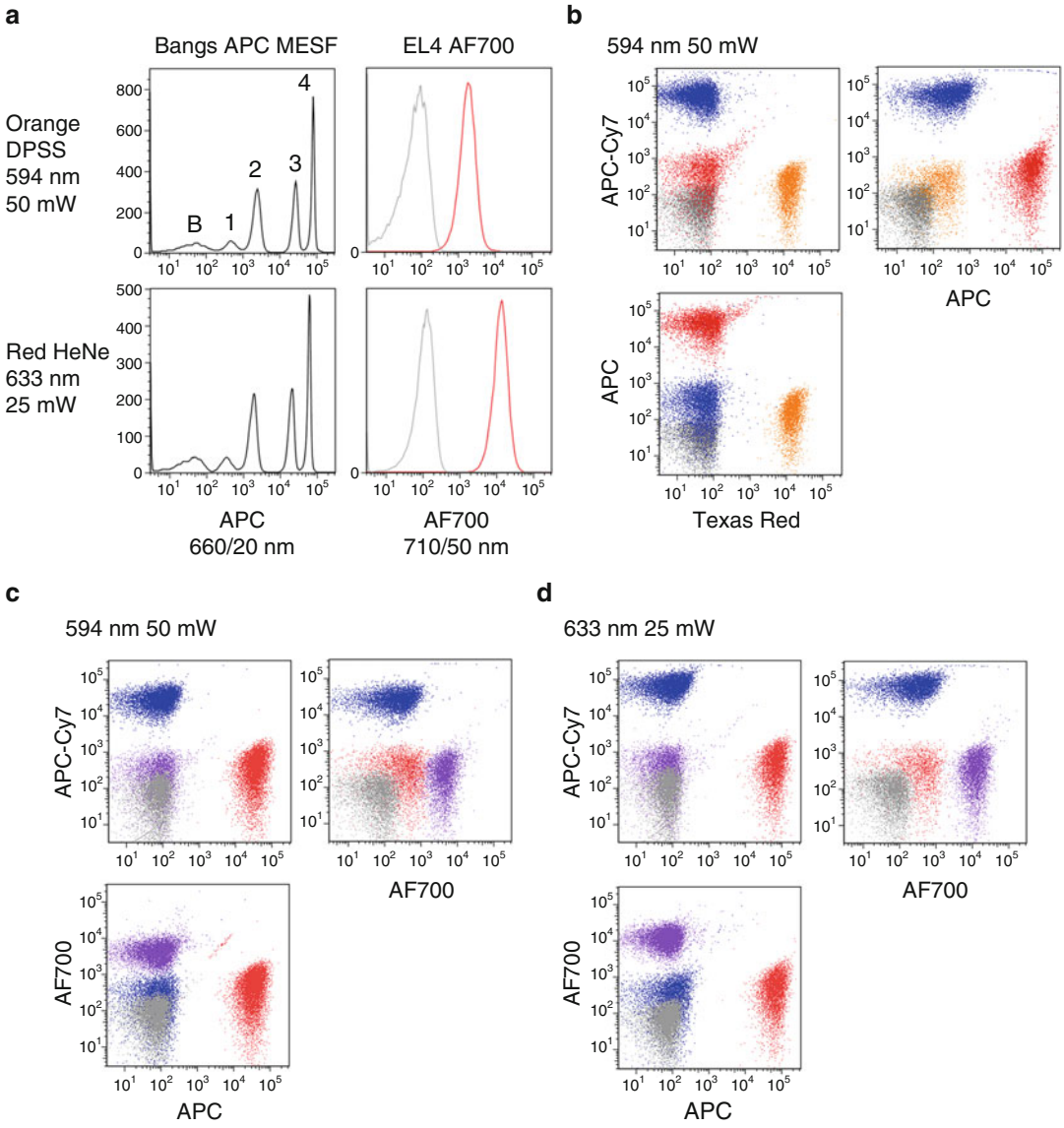

Fig. 11 Orange lasers. (**a**, *left column*) Analysis of APC microsphere mixture, with four populations coupled to varying levels of APC (labeled 1, 2, 3, and 4) plus background (*B*). (**a**, *right column*) EL4 mouse lymphoma cells labeled with anti-mouse CD44 conjugated with Alexa Fluor 700. The following lasers were tested: a DPSS 594 nm at 50 mW (*top row*), or a HeNe 633 nm at 25 mW (*bottom row*). (**b**) EL4 mouse lymphoma cells labeled with Texas Red anti-mouse CD44, APC anti-mouse CD44, or APC-Cy7 anti-mouse CD44, and analyzed with a DPSS 594 nm laser at 50 mW. (**c**) EL4 mouse lymphoma cells labeled with APC anti-mouse CD44, Alexa Fluor 700 anti-mouse CD44, or APC-Cy7 anti-mouse CD44, and analyzed with a DPSS 594 nm laser at 50 mW. (**d**) EL4 mouse lymphoma cells labeled with APC anti-mouse CD44, Alexa Fluor 700 anti-mouse CD44, or APC-Cy7 anti-mouse CD44, and analyzed with a HeNe 633 nm laser at 25 mW. Grey dots, no label; orange dots, Texas Red; red dots, APC; violet dots, Alexa Fluor 700; blue dots, APC-Cy7

NIR probes in confocal microscopy makes this a fertile area for innovation. Almost all lasers in the NIR range are direct diodes, with modules available that emit at 660, 685, 705, 730, and 785 nm [38]. All of these laser wavelengths have been used for flow cytometry, and several are available as options on commercial instruments. Modern flow cytometers are also starting to incorporate detectors more sensitive to NIR fluorescence, including specialized photomultiplier tubes and avalanche photodiodes (APDs) [39].

While the current probe selection is not vast, NIR probes developed for imaging applications have been applied to flow cytometry. The long-wavelength Alexa Fluor dyes (Thermo Fisher) include Alexa Fluor 660, Alexa Fluor 680, Alexa Fluor 700, Alexa Fluor 750, and Alexa Fluor 790. The excitation properties of these probes are illustrated in Fig. 12, where HeNe 633 nm and NIR diodes emitting at 660, 685, 705, and 730 nm were used for excitation. Alexa Fluor 660 and Alexa Fluor 700 are both reasonably well excited using traditional red sources, and Alexa Fluor 700 is often included with APC and APC-Cy7 for three-color labeling using a red laser. However, a 660 nm diode gives improved sensitivity for both probes. The longer Alexa Fluor dyes require a longer wavelength NIR laser. Common NIR tracking dyes like indocyanine green have also seen use in flow cytometry and also require these longer laser wavelengths. The NIR is one of the last unexploited spectral regions for new fluorochrome development; it is likely that new fluorescent probes will be developed here to expand the current palette of simultaneous immunophenotyping fluorochromes.

3.9 Unusual Laser Wavelengths

The most common laser wavelengths for flow cytometry are listed above. Some unusual laser wavelengths are listed below; while these see little use in flow cytometry, they may be available as options in some advanced systems and may be useful for specialized applications.

1. Violet 420–425 nm: This violet laser has similar semiconductor chemistry to violet 405 and blue 450 nm diodes. Like the blue diodes, it gives improved excitation of cyan fluorescent proteins. Its overlap with the Brilliant Violet 421 nm emission range has limited its use in flow cytometry.
2. Green 505, 515, 520, and 523 nm: These short wavelength green lasers are problematic for flow cytometers due to their overlap with the fluorescein emission range. However, they provide excellent excitation of yellow fluorescent proteins. The green 514 nm corresponds to the 514.5 nm line previously available from argon-ion sources. The direct diode 520 and 523 nm sources are increments in the anticipated development

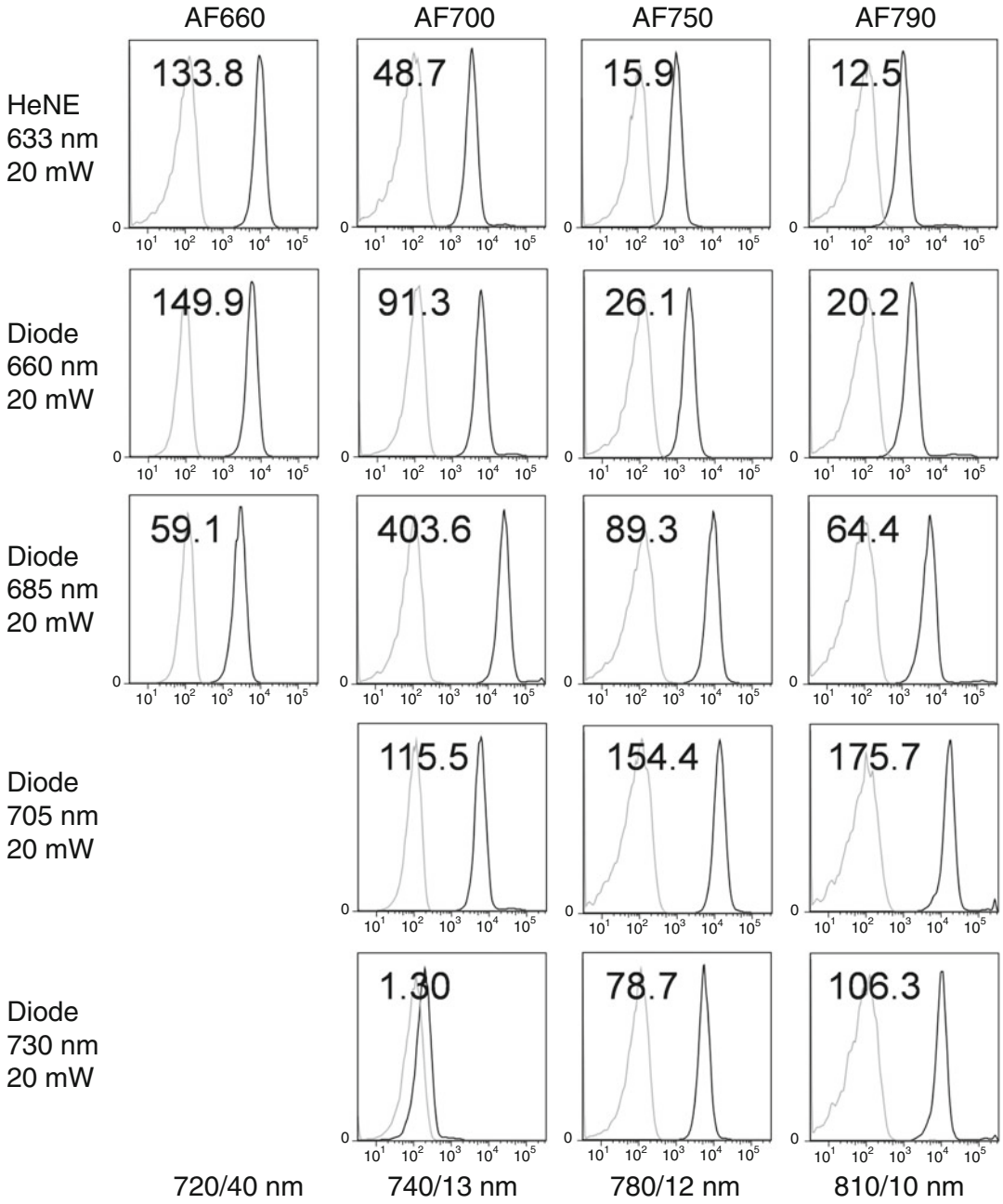

Fig. 12 NIR lasers. Analysis of EL4 mouse lymphoma cells labeled with Alexa Fluor 660, Alexa Fluor 700, Alexa Fluor 750, or Alexa Fluor 790 conjugated antibodies against mouse CD44 (*left* to *right columns*). Excitation with a red HeNe 633 nm at 20 mW (*top row*), a NIR laser diode 660 nm at 20 mW (*second row*), a NIR laser diode 685 nm at 20 mW (*third row*), a NIR laser diode 705 nm at 20 mW (*fourth row*), and a NIR laser diode 730 nm at 20 mW (*bottom row*). Black peaks, labeled cells; grey peaks, unlabeled cells

of a direct diode 532 nm source that may replace more expensive DPSS 532 nm lasers.

3. Yellow 568, 570, and 580 nm: Solid state lasers at these wavelengths are available. The 568 nm laser corresponds to the krypton-ion 568 nm laser line and sees use in fluorescence microscopy. These lines are close to the PE emission range and thus see little use in flow cytometry.
4. Orange 607 nm: This DPSS laser can be used to excite very long red fluorescent proteins, or APC and its tandems. Since it overlaps with the Texas Red emission range, however, it sees little use in flow cytometry.

3.10 Laser Combinations

Based on the above descriptions, it is now possible to assemble appropriate groups of lasers for both simultaneous analyses of many fluorescent parameters, and to maximize excitation flexibility for a broad range of fluorochrome types. The field of flow cytometry benefits from a solid base of instrument suppliers that offer both number and flexibility in laser integration into commercial systems. A few such systems are listed below in the order of complexity and capability. All of these configurations and others are available from multiple manufacturers.

1. Cyan 488 nm and red ~640 nm: This basic configuration was introduced by the BD Biosciences FACSCalibur, and remains a common configuration for low-cost four color systems like the BD Biosciences Accuri and the handyem HPC-150. In theory, up to nine color analyses should be possible using FITC, PE, and PE tandem dyes, and APC and APC tandem dyes.
2. Cyan 488 nm and violet 405 nm: This basic configuration is less common than 488 nm and red, but can take advantage of the Brilliant Violet fluorochrome array.
3. Cyan 488 nm, red ~640 nm, and violet 405 nm: This three-laser "triad" is the most common multi-laser configuration now available, and is provided by many manufacturers. Up to 16 fluorescent parameters can theoretically be excited using this combination.
4. Cyan 488 nm, red ~640 nm, violet 405 nm, and green-to-yellow 532–561 nm: The addition of a fourth green-to-yellow laser gives improved excitation of PE and its tandems, as well as access to the red fluorescent proteins. While it alone does not increase the total number of simultaneous fluorochromes available, the soon-to-be-released Brilliant Blue dye series excited with the 488 nm laser will increase the total number of fluorescent probes to beyond 16.
5. Cyan 488 nm, red ~640 nm, violet 405 nm, green-to-yellow 532–561 nm, and ultraviolet: The addition of an ultraviolet

laser allows excitation of up to six Brilliant Ultraviolet dyes, increasing simultaneous fluorochrome capability dramatically. This five laser combination will likely become the standard for high-dimensional flow cytometry.

6. Blue and orange lasers can be added to the last combination: Since the functionality of these sources overlaps, blue and orange lasers can be aligned to the same intercepts (in spatially separated systems) as violet and red sources, respectively.

References

1. Shapiro HM (2003) How flow cytometers work. In: Practical flow cytometry, 4th edn. John Wiley & Sons, New York, NY, pp 124–149
2. Oi VT, Glazer AN, Stryer L (1982) Fluorescent phycobiliprotein conjugates for analyses of cells and molecules. J Cell Biol 93(3):981–986
3. Titus JA, Haugland R, Sharrow SO, Segal DM (1982) Texas red, a hydrophilic, red-emitting fluorophore for use with fluorescein in dual parameter flow microfluorometric and fluorescence microscopic studies. J Immunol Methods 50(2):193–204
4. Shapiro HM, Stephens S (1986) Flow cytometry of DNA content using oxazine 750 or related laser dyes with 633 nm excitation. Cytometry 7(1):107–110. doi:10.1002/cyto.990070118
5. Hoffman RA, Reinhardt BN, Stevens FE (1987) Two-color immunofluorescence using a red helium neon laser. Cytometry Suppl 1:103
6. Shapiro HM (1993) Trends and developments in flow cytometry instrumentation. Ann N Y Acad Sci 677:155–166
7. Shapiro HM (1986) The little laser that could: applications of low power lasers in clinical flow cytometry. Ann N Y Acad Sci 468:18–27
8. Loken MR, Keij JF, Kelley KA (1987) Comparison of helium-neon and dye lasers for the excitation of allophycocyanin. Cytometry 8 (1):96–100. doi:10.1002/cyto.990080114
9. Doornbos RM, De Grooth BG, Kraan YM, Van Der Poel CJ, Greve J (1994) Visible diode lasers can be used for flow cytometric immunofluorescence and DNA analysis. Cytometry 15(3):267–271. doi:10.1002/cyto.990150312
10. Roederer M (2002) Multiparameter FACS analysis. Curr Protoc Immunol. Chapter 5: Unit 5.8. doi:10.1002/0471142735.im0508s49
11. Shapiro HM, Perlmutter NG (2001) Violet laser diodes as light sources for cytometry. Cytometry 44(2):133–136
12. Hoffman RA (2002) Multicolor immunofluorescence flow cytometry using 400 nm laser diode excitation. Cytometry Suppl 11:124
13. Telford WG, Hawley TS, Hawley RG (2003) Analysis of violet-excited fluorochromes by flow cytometry using a violet laser diode. Cytometry A 54(1):48–55. doi:10.1002/cyto.a.10046
14. Telford WG, Murga M, Hawley TS, Hawley RG, Packard BZ, Komoriya A, Hass R, Hubert C (2005) DPSS yellow-green 561 nm lasers for improved fluorochrome detection by flow cytometry. Cytometry A 68:36–44
15. Perfetto SP, Roederer M (2007) Increased immunofluorescence sensitivity using 532 nm laser excitation. Cytometry A 71(2):73–79. doi:10.1002/cyto.a.20358
16. Chattopadhyay PK, Price DA, Harper TF, Betts MR, Yu J, Gostick E, Perfetto SP, Goepfert P, Koup RA, De Rosa SC, Bruchez MP, Roederer M (2006) Quantum dot semiconductor nanocrystals for immunophenotyping by polychromatic flow cytometry. Nat Med 12 (8):972–977. doi:10.1038/nm1371
17. Chattopadhyay PK, Yu J, Roederer M (2007) Application of quantum dots to multicolor flow cytometry. Methods Mol Biol 374:175–184. doi:10.1385/1-59745-369-2:175
18. Chattopadhyay PK, Gaylord B, Palmer A, Jiang N, Raven MA, Lewis G, Reuter MA, Nur-ur Rahman AK, Price DA, Betts MR, Roederer M (2012) Brilliant violet fluorophores: a new class of ultrabright fluorescent compounds for immunofluorescence experiments. Cytometry A 81(6):456–466. doi:10.1002/cyto.a.22043
19. Kapoor V, Subach FV, Kozlov VG, Grudinin A, Verkhusha VV, Telford WG (2007) New lasers for flow cytometry: filling the gaps. Nat Methods 4(9):678–679. doi:10.1038/nmeth0907-678

20. Kapoor V, Karpov V, Linton C, Subach FV, Verkhusha VV, Telford WG (2008) Solid state yellow and orange lasers for flow cytometry. Cytometry A 73(6):570–577. doi:10.1002/cyto.a.20563
21. Telford WG, Hawley TS, Subach F, Verkhusha VV, Hawley RG (2012) Flow cytometry of fluorescent proteins. Methods 57 (3):318–330. doi:10.1016/j.ymeth.2012.01.003
22. Telford WG, Frolova EG (2004) Discrimination of the Hoechst side population in mouse bone marrow with violet and near-ultraviolet laser diodes. Cytometry A 57(1):45–52. doi:10.1002/cyto.a.10109
23. Telford WG (2004) Small lasers in flow cytometry. In: Hawley TS, Hawley RG (eds) Flow cytometry protocols, Methods in molecular biology, vol 263. Humana Press, London, UK, pp 399–418. doi:10.1385/1-59259-773-4:399
24. Telford WG (2011) Lasers in flow cytometry. In: Darzykiewicz Z et al (eds) Methods in cell biology, vol 102. Academic Press, New York, NY, pp 375–409. doi:10.1016/B978-0-12-374912-3.00015-8
25. Nakamura S, Fasol G (1997) The blue laser diode. GaN based light emitters and lasers. Springer-Verlag, Berlin, Heidelberg. doi:10.1007/978-3-662-03462-0
26. Telford WG, Kapoor V, Jackson J, Burgess W, Buller G, Hawley TS, Hawley RG (2006) Violet laser diodes in flow cytometry: an update. Cytometry A 69:1153–1160
27. Telford WG, Babin SA, Khorev SV, Rowe SH (2009) Green fiber lasers: an alternative to traditional DPSS green lasers for flow cytometry. Cytometry A 75(12):1031–1039. doi:10.1002/cyto.a.20790
28. Matz MV, Fradkov AF, Labas YA, Savitsky AP, Zaraisky AG, Markelov ML, Lukyanov SA (1999) Fluorescent proteins from nonbioluminescent Anthozoa species. Nat Biotechnol 17 (10):969–973. doi:10.1038/13657
29. Shaner NC, Campbell RE, Steinbach PA, Giepmans BN, Palmer AE, Tsien RY (2004) Improved monomeric red, orange and yellow fluorescent proteins derived from Discosoma sp. red fluorescent protein. Nat Biotechnol 22 (12):1567–1572. doi:10.1038/nbt1037
30. Shapiro HM, Telford WG (2016) Lasers for flow cytometry: current and future trends. In: Robinson JP, Darzynkiewicz Z, Dobrucki J, Hoffman RA, Nolan JP, Orfao A, Rabinovitch PS, Telford WG (eds) Current protocols in cytometry. John Wiley and Sons, New York, NY
31. Snow C, Cram LS (1993) The suitability of air-cooled helium cadmium (HeCd) lasers for two color analysis and sorting of human chromosomes. Cytometry Suppl 6:20
32. Frey T, Houck DW, Shenker BJ, Hoffman RA (1994) Bivariate flow karyotyping with air-cooled lasers. Cytometry 16(2):169–174. doi:10.1002/cyto.990160211
33. Goodell MA, Brose K, Paradis G, Conner AS, Mulligan RC (1996) Isolation and functional properties of murine hematopoietic stem cells that are replicating in vivo. J Exp Med 183 (4):1797–1806
34. Cabana R, Frolova EG, Kapoor V, Thomas RA, Krishan A, Telford WG (2006) The minimal instrumentation requirements for Hoechst side population analysis: stem cell analysis on low-cost flow cytometry platforms. Stem Cells 24(11):2573–2581. doi:10.1634/stemcells.2006-0266
35. Telford WG (2004) Analysis of UV-excited fluorochromes by flow cytometry using near-ultraviolet laser diodes. Cytometry A 61 (1):9–17. doi:10.1002/cyto.a.20032
36. Telford WG (2015) Near-ultraviolet laser diodes for brilliant ultraviolet fluorophore excitation. Cytometry A 87(12):1127–1137. doi:10.1002/cyto.a.22686
37. Beavis AJ, Kalejta RF (1999) Simultaneous analysis of the cyan, yellow and green fluorescent proteins by flow cytometry using single-laser excitation at 458 nm. Cytometry 37 (1):68–73
38. Telford WG (2015) Near infrared lasers in flow cytometry. Methods 82:12–20. doi:10.1016/j.ymeth.2015.03.010
39. Lawrence WG, Varadi G, Entine G, Podniesinski E, Wallace PK (2008) Enhanced red and near infrared detection in flow cytometry using avalanche photodiodes. Cytometry A 73 (8):767–776. doi:10.1002/cyto.a.20595

Chapter 20

Flow Cytometry: The Glass Is Half Empty

Howard M. Shapiro

Abstract

In hopes of broadening the reader's perspective, this closing chapter discusses what flow cytometry cannot do; hence, the glass is half empty. Alternative methods using affordable and sustainable simple imaging cytometers are presented.

Key words CD4 counters, HIV, Imaging cytometers, TB bacteria, Malaria parasites

CYTO 2015 in Glasgow concluded with a Hooke Lecture exemplifying flow cytometry at its best; it began with a Special Lecture that took us where flow cannot go. The talk was given by Eric Betzig, who shared the 2014 Nobel Prize in Chemistry with Stefan Hell and William Moerner for "Super-Resolved Fluorescence Microscopy." The trio of physicists devised several different methods to circumvent the conventional Abbe resolution limit of optical microscopy, permitting visualization of single fluorophore molecules in "dense media" such as biological tissues.

The Royal Swedish Academy's "Scientific Background" on the Prize notes: "...[In 1976, Tomas] Hirschfeld [1] used polyethyleneimine to tag antibodies ([gamma] globulin with a large number of fluorophores 980-100 per protein molecule). He then used TIRF [Total Internal Reflection Fluorescence] microscopy at ambient temperatures to observe the diffusion as well as the mechanically driven movement of the multi-labeled molecules through a small volume illuminated by an Ar laser. These results, obtained with near-field excitation and far-field detection microscopy, defined the beginning of the long and arduous road to reach single fluorophore detection in dense media."

That the first light on that "long and arduous road" was shed by an ISAC luminary is fitting. Tomas Hirschfeld, a Uruguayan analytical chemist and polymath, who was Chief Scientist at Block Engineering and later moved to Lawrence Livermore National Laboratory, conceived Block's multibeam flow cytometers in the

Teresa S. Hawley and Robert G. Hawley (eds.), *Flow Cytometry Protocols*, Methods in Molecular Biology, vol. 1678, DOI 10.1007/978-1-4939-7346-0_20,

early 1970s as well as the single laser flow and imaging systems used later in that decade to characterize single virions. He was a founding member of the original Society for Analytical Cytology in 1978, but unfortunately did not live to see his 1985 prediction that "the combination of sensor-based instrumentation and microminiaturization will make possible distributed measurement by allowing point-of-use measurements by nonexperts" [2] realized, having left us far too soon in 1986. Having been exposed to some simple but very impressive flying model airplanes Tomas built, I can only guess what he would now be doing with drones.

"Measurements by nonexperts" are one reason for which the flow cytometry glass can be considered half empty, rather than half full. None of us who have been in the field since its infancy started out as experts, so our own lack of knowledge sometimes prevented us from carefully considering all hypotheses that might explain a novel result. Case in point: in the early days of flow cytometric cell membrane potential measurement, it was assumed that cells with high membrane potentials would take up more fluorescent dye than cells with low or no membrane potential. We were unaware that certain blood cells, such as stem cells and activated lymphocytes, might express efflux pumps which would pump dye out. The first few papers in the literature report that cells with pumps have low membrane potentials; nobody bothered to send in corrections.

Flow cytometers designed for clinical applications are meant to be used by nonexperts. Hematology counters have software that prints out counts of blood cells without operators having to define gates. Surprisingly, however, the 400-cell visual count remains the standard for differential white cell counts ("diffs") after many decades. Almost all flow cytometric hematology counters produce higher monocyte counts than would be reported by a trained observer; it has long been known that the Giemsa and Wright stains used for visual diffs do not enable good differentiation of small monocytes from lymphocytes. There have been at least two combinations of dyes and monoclonal antibodies proposed which have been shown to give the "ground truth" about the cell sample but neither has yet dethroned the old standard. The hematologists and hematopathologists rightly are more concerned with such problems as the detection of residual disease in leukemias and lymphomas than with differential counts, but they have been dawdling for decades.

The first generation of automated differential counters, which reached the market in the early 1970s, were essentially automated microscopes that examined conventionally stained slides. Although a flow cytometric counter using more precise cytochemical staining appeared a few years later, it was slow in gaining acceptance. The appearance of monoclonal antibody reagents around 1980 and their quickly established utility in hematology research quickly shifted the balance toward flow cytometric differential counters,

which now are dominant. Such instruments typically measure only one or two fluorescence parameters. The clinicians interested in more serious immunological analyses use modern multilaser instruments measuring ten or more fluorescence parameters, and requiring interaction with highly trained operators. The two populations of cytometer users have become increasingly separated.

On the positive side, the proliferation of monoclonals forced the immunology community to organize to standardize them, developing the CD antigen nomenclature, now including hundreds of antibodies, most available from many manufacturers and with many labels. The identification of AIDS in the early 1980s was accomplished using monoclonal antibodies before the CD designations were established and without benefit of flow cytometry. Even before HIV was identified as the pathogen, it became obvious that the disease was accompanied by a severe depletion of what are now known as CD4-positive T cells, levels of which provided the best indicator of prognosis and, later, of response to therapy. Users and manufacturers of flow cytometers together made a huge contribution to global public health by perfecting and standardizing both flow cytometric methods of counting these cells and quality assurance programs worldwide.

As was inevitable, science has marched on. Highly effective antiretroviral therapy began to emerge in the 1990s, and tests for direct detection of viral load have continued to become more practical and affordable. The World Health Organization recommended in September 2015 that routine CD4 counting be discontinued, with all patients newly diagnosed with HIV being placed on therapy and followed with viral load measurements. Ironically, by the time the recommendation was made, two imaging-based CD4 counting instruments had reached the market. In their present guise, these appear to be "one trick ponies"; it is not clear how readily either of them could be repurposed to meet other needs for infectious disease diagnostics in resource-poor areas. Paradoxically, there are still people out there, ostensibly with expertise in biomedical engineering and electro-optics, getting paid to develop automated point-of-care hematology counters using the old stains. This is only slightly less silly than bleeding onto your mobile phone camera and sending a "cellfie" of undiluted unstained blood to "the cloud" for analysis, a notion which has also attracted funding.

What the 2014 chemistry Nobel winners are doing certainly qualifies as cytometry. Many of the fluorophores they use are commonly used both in flow and in more conventional image cytometry. Tomas Hirschfeld's work toward single-molecule detection was done using flow cytometers with relatively conventional optical geometry, but with very small observation volumes and flow rates greatly reduced compared to standard flow cytometers. Detection of fluorescence of single molecules of organic dyes in such apparatus was reported within a few years of Tomas's death. More

recently, sophisticated imaging techniques have outperformed flow cytometry.

The cytometer that had been used for the single virion scatter work done decades ago was optimized to detect small scatter signals; flow was observed in a water-immersed system with core diameters and beam sizes of only a few μm, and side scatter signals were collected by a single photon counting avalanche diode detector. Most flow cytometers now in use would require some modification to achieve the level of performance possible with what Tomas called the "immunometer," which almost certainly could have detected phycoerythrin molecules.

The recent literature contains numerous examples of attempts to measure microvesicles and other submicron particles with conventional flow cytometers in which the only signals which triggered the electronics came from aggregates of particles; this can happen when fluorescence signals are used for triggering as well as when scatter signals are used. Most commercial flow cytometers were designed to work with eukaryotic cells; some modifications have been made that let them deal with microorganisms that are about 1/1000 that size, but for viruses and vesicles, some redesign in the direction of what is now being used for single fluorophore work might be appropriate. Unfortunately, bad cytometry still happens to good journals.

I wrote extensively in my chapter in the previous version of this volume about the ability of small, inexpensive widefield imaging cytometers to do many of the tasks for which flow cytometers are now used in research and clinical laboratories [3]. I became interested in the possibility of building such an apparatus around 2000 when I was asked to consider building inexpensive diode laser source flow cytometers for use in counting CD4-positive T cells in HIV/AIDS patients in resource-poor countries. It was my feeling then that even if flow cytometers cost a nickel, they would be too complex to be operated sustainably in many places where the disease was taking its greatest toll.

The digital cameras which could be used in imaging devices have continued to drop in price and increase in quality since 2000, and microprocessor systems have progressed in the same directions. In 2000, the visible and UV light emitting diodes (LEDs) available were not sufficiently powerful to be used for fluorescence excitation, they are now more than adequate and cost less. The developers of the blue LED were awarded the 2014 Nobel Prize in physics; I have said many times that the benefits to global health from cytometers using these devices will probably be greater than those from super-resolution microscopy.

My philosophy has always been that affordable and sustainable simple imaging cytometers could be built as "platform technology," usable for multiple assays in the same way as are general-purpose flow cytometers. Having been assured over 40 years ago,

when "flow cytometry" was given its name, that nobody would ever need three beams or four fluorescence parameters, I am gratified to find that a modern "entry level" flow cytometer for an institution or corporation has at least three beams and at least six fluorescence parameters. I believe, however, that many of the assays most necessary and practical for infectious disease diagnosis in resource-poor areas could be done with a 4- to 6-parameter imaging instrument.

After I started working on inexpensive CD4 counters in 2000, I was approached by people interested in whether the same imaging technology could be used for TB and malaria, for both of which standard microscopic diagnoses are done from slides. During the past 10 years, I have become familiar with both the literature on research and treatment of both diseases and with the communities of people involved. Although I had some funding from NIH to work on TB and on CD4, I never succeeded in getting either the conventional funding sources or the industry interested in my approach to malaria. I know many of the relatively few people who have attempted to do cytometry of TB bacteria and malaria parasites; a few of us have collaborated in malaria, which was discussed in my previous chapter in this volume, and on TB, the latter at a lower level because of biosafety issues.

In terms of accessibility of samples from TB and malaria patients, the United States is a resource-poor country. My colleagues and I have a good idea of what cellular parameters of the pathogens need to be examined to diagnose malaria or TB. We have looked at cultured malaria, even at some that has been flown from Australia to the United States (I will take the Fifth on whether it was declared). Some species of malaria, however, including the less common ones, cannot be cultured, and are typically found in relatively inaccessible places in Africa and Asia. It would be nearly impossible to get viable organisms in patient samples from there to the U.S., to which they are very likely to be denied entry. There should be many fewer problems getting slides of TB and malaria because they are much less sensitive to ambient conditions in transit and because preparation procedures at the point of origin eliminate the possibility of contagion.

The combination of parameters that need to be measured to distinguish parasites by species and growth stage to diagnose malaria or characterize it for other purposes is difficult to set up on most commercial flow cytometers. It would be impractical to build a special instrument, even a ruggedized and miniaturized one, and drag it from continent to continent looking for rare malaria species in living patients. The parameters in question, however, can easily be measured in a relatively cheap and simple imaging cytometer. Most of the people with whom I collaborate would be more than happy to send me slides if I would send them a cytometer. It would take a much shorter time to optimize diagnostic algorithms if we had more instruments.

TB has got its own set of problems. For one thing, even if I had access to the BSL4 lab in Boston, I would not be thrilled with the prospect of dealing with extensively drug-resistant (XDR) TB. Many of the more things we are doing with that organism need to be done with live bacteria. Colleagues in Africa are equipped with a fancy enough flow cytometer to do the work, and, unfortunately, with a steady supply of patients who have both XDR TB and HIV/AIDS. These patients have relatively few bacteria in their sputum, and even immunocompetent patients with active TB have an average of only a few hundred organisms per milliliter of sputum. The generation time of *Mycobacterium tuberculosis* (Mtb) is about 18 h. Researchers working on bacteria isolated from TB patients spend weeks growing enough organisms to run in the flow cytometer.

Classical culture-based diagnosis and determination of antimicrobial susceptibility of Mtb typically does not produce definitive results for 1–2 months; many HIV/AIDS patients with XDR TB will deteriorate significantly and may die in this interval. Molecular methods are used for rapid diagnosis but, although they can detect TB genes and drug-resistant genes within hours, cannot indicate whether the organisms in a sample are alive. That determination can be done definitively within a few generation times by imaging cytometry of small numbers of organisms using probes and methods that are already well established. Results for TB would be obtained in a few days; applied to the more common, more rapidly growing bacteria encountered in most infections, imaging can yield results in hours. My colleagues and I established this in studies done for a microbiologic diagnostics company decades ago [4], using a flow cytometer that would fit in an attaché case and cost under $10,000; the complexity of the process was what ultimately resulted in a decision not to proceed.

While cytometry people have continued to advocate the use of flow and laser scanning cytometry for microbiology over the years, the level of interest within microbiologic diagnostics companies has remained low, although a 2013 publication [5] suggested flow cytometry might be of interest. The major obstacle to its use in 1990 remains today; most cell-based susceptibility tests require multiple aliquots of sample, and, even if these are prepared in multiwell plates and presented to the flow cytometer by an automated handler, the instrument must process all objects in a well one by one. Colony formation, past a certain point, may halt processing, but even if flow remains uninterrupted, analysis times quickly become unacceptably long. As I suggested long ago, "...it may eventually be possible to speed up operation by incorporating several cytometers into a single system for microbiological analysis." I was then optimistically anticipating advances in flow cytometry based on early successes with "flow-on-a-chip," which has not met early expectations; I could now make a list of imaging

components that would allow several wells to be read simultaneously and would in total cost less than a good PMT.

By 1983, I had managed to simplify the design of a multibeam, multiparameter flow cytometer to the point where it could be built by people who had modest mechanical skills, some knowledge of computers and electronics, and some familiarity with the flow cytometers and sorters that had been sold up to that time. At least a few dozen people built flow cytometers from the plans that later appeared in early editions of *Practical Flow Cytometry*; I also sold inexpensive PC interfaces and software. Some of those systems, none of which ever had anything like a service call, are still running a third of a century later. I can still knock a three-beam, 8-parameter system together in a few days, but I have not done any flow cytometry in my lab for several years now, because I either cannot get or cannot run the malaria and TB samples essential for what I am now trying to learn. I now design and do experiments with colleagues in Africa, Asia, and Australia, relying heavily on Skype.

Existing manufacturers apparently have not figured out how to make the simple imaging instruments that I think are needed in resource-poor countries fit into their business plans.

The electro-optical components are not terribly expensive, but they are small and my aging fingers do not get them together as easily as they used to. Microprocessors and open source software are both amazingly complex compared to the early PCs, and it is hard to get the "experts" calibrated, but I and my colleagues have been working on it.

My new company, a nonprofit called One World Cytometry, Inc., which I call a "finishup," is attempting to design a general-purpose imaging system made from open-source, readily available hardware and software components and provide plans to anyone who wants to use them, starting with my overseas colleagues working on malaria and TB. I am reasonably sure that groups of people working where the diseases have their greatest impact will figure out how to build sustainable businesses that will make and maintain the apparatus and provide training and consumables. Make no mistake about it, cytometry at this level will save lives.

My father broke a line of generations of rabbis to go to medical school; there are now three generations of doctors in the family. As I have gotten older, I seem to revert more frequently to the ways of my ancestors. The real Bible orders us to share the corners of our fields with those less fortunate. Having preached my sermon, I will now pass the plate.

References

1. Hirschfeld T (1976) Optical microscopic observation of single small molecules. Appl Opt 15 (12):2965–2966. doi:10.1364/AO.15.002965

2. Hirschfeld T (1985) Instrumentation in the next decade. Science 230(4723):286–291. doi:10.1126/science.230.4723.286

3. Shapiro HM (2011) The cytometric future: it ain't necessarily flow! Methods Mol Biol 699:471–482. doi:10.1007/978-1-61737-950-5_23
4. Shapiro HM (1990) Flow cytometry in laboratory microbiology: new directions. Am Soc Microbiol News 56:584–588
5. van Belkum A, Dunne WM Jr (2013) Next-generation antimicrobial susceptibility testing. J Clin Microbiol 51(7):2018–2024. doi:10.1128/JCM.00313-13

INDEX

Teresa S. Hawley and Robert G. Hawley (eds.), *Flow Cytometry Protocols*, Methods in Molecular Biology, vol. 1678, DOI 10.1007/978-1-4939-7346-0, © Springer Science+Business Media LLC 2018

H

I

L

M

N

P

Q

R

V